MOLECULAR MECHANISMS OF MYOPATHIES

by

Massimiliano Memo

Thesis submitted for the degree of

Doctor of Philosophy

Myocardial Function
National Heart and Lung Institute
Faculty of Medicine
Imperial College London

February 2012

Abstract

This study was aimed at the investigation of the mechanisms by which mutations on proteins of the thin filaments could lead to cardiac and skeletal muscle diseases. The contractile properties of reconstituted thin filaments were assessed using the quantitative *in vitro* motility assay.

The cardiac disease investigated was the dilated cardiomyopathy (DCM). Pilot work on 2 mutants indicated that, contrarily to what was believed in the past, the molecular phenotype generated by mutations on thin filament proteins linked to the disease was not a reduced absolute Ca^{2+}-sensitivity and cross-bridge turnover rate, but an uncoupling between the phosphorylation level of troponin I and the Ca^{2+}-sensitivity. In this thesis I will present the confirmation of the hypothesis with 7 DCM causing mutations. At least one mutation on each of the thin filaments subunits was tested and they all shared that molecular phenotype despite differences in the absolute Ca^{2+}-sensitivity.

Mutations on β- and γ-tropomyosin linked to 3 skeletal muscle diseases, Nemaline myopathy, Cap disease and congenital fibre type disproportion (CFTD), were taken into consideration. Some of these mutations were also reported to cause more than one of these diseases. The β-tropomyosin mutations indicated that there is not a clear correlation between molecular phenotype and disease, as different modifications of the contractile properties seem to lead to the same disease. One of the β-tropomyosin mutations (ΔK7), though, as another mutation on skeletal actin (K326N) that was investigated, showed a new hypercontractile phenotype connected to a gain-of-function molecular phenotype, which led to a change in the clinical diagnosis. The

experiments performed with the γ-tropomyosin mutants encountered many technical issues but indicated that a common phenotype of decreased Ca^{2+}-sensitivity might be connected to CFTD, observation supported also by a β-tropomyosin mutant connected only to that disease.

Declaration of originality

The work presented in this thesis is my own unless otherwise stated.

Table of Contents

Abstract **2**

Declaration of originality **4**

List of figures **13**

List of tables **20**

List of Abbreviations **25**

Acknowledgments **27**

1 Introduction **28**

1.1 Muscle Structure **28**

1.1.1 The Sarcomere 28

1.1.2 The Thick Filament 31

1.1.2.1 Myosin Structure and Function 31

1.1.2.2 Myosin Light Chains 33

1.1.3 The Thin Filament 34

1.1.3.1 Actin 34

1.1.3.2 Tropomyosin 36

1.1.3.3 Troponin Complex 39

1.1.3.4 Troponin C 40

1.1.3.5 Troponin I 41

1.1.3.6 Troponin T 44

1.1.4 Skeletal Muscle 46

1.1.4.1 The Skeletal Muscle and Myocyte Structure 47

1.1.5 The Cardiovascular System and the Heart 49

1.1.5.1 The Heart Structure 50
1.1.5.2 The Cardiac Cycle 52
1.1.5.3 The Cardiac Myocyte 53
1.2 Muscle Contraction 54
1.2.1 Action Potential and Propagation of the Electric Impulse in Skeletal and Cardiac Muscle 54
1.2.2 Excitation-Contraction Coupling 56
1.2.3 The Sliding Filament Theory and the Cross-Bridge Cycle 58
1.3 Muscle Regulation 61
1.3.1 The Thin Filament Switch 61
1.3.1.1 Troponin Complex Structure 61
1.3.1.2 The Three State Model 64
1.3.2 β-adrenergic Regulation of the Cardiac Output 66
1.3.2.1 Phosphorylation of Cardiac Troponin I by PKA 68
1.4 Dilated Cardiomyopathy (DCM) 70
1.5 Skeletal Muscle Diseases 72
1.5.1 Nemaline Myopathy 72
1.5.2 Cap Disease 75
1.5.3 Congenital Fibre Type Disproportion (CFTD) 77
1.5.4 Evidences of Overlap between these Skeletal Muscle Pathologies 79
1.6 Context and Aim of this Study 81
1.6.1 The *In Vitro* Motility Assay 81
1.6.2 Dilated Cardiomyopathy Studies 82
1.6.3 Congenital Myopathies Studies 83
1.6.4 Aims of the Thesis 83
2 Materials and Methods 85
2.1 Sources of Sample Proteins 85

2.1.1 Human and Mouse Heart Samples 85
2.1.1.1 Donor Human Hearts 85
2.1.1.2 Failing Human Hearts 85
2.1.1.3 Dilated Cardiomyopathy (DCM) Human Hearts 86
2.1.1.4 DCM Mouse Hearts 87
2.1.2 Baculovirus Expression System 88
2.1.2.1 DCM α-tropomyosin Mutants 89
2.1.2.2 Nemaline Myopathy and Cap Disease β-tropomyosin Mutants 89
2.1.2.3 Congenital Fibre Type Disproportion (CFTD) γ-tropomyosin Mutants 90
2.1.3 Human Skeletal Muscle Biopsies 91
2.2 Protein Preparation from Tissue 91
2.2.1 Preparation of Motor Protein 91
2.2.1.1 Fast Skeletal Myosin Preparation from Rabbit Skeletal Muscle 91
2.2.1.2 Preparation of Heavy Meromyosin for the IVMA 93
2.2.1.3 Affinity Precipitation of HMM 95
2.2.2 Preparation of F-actin 96
2.2.2.1 Acetone Powder Preparation from Rabbit Skeletal Muscle 96
2.2.2.2 F-actin Preparation from Acetone Powder 97
2.2.2.3 F-actin Isolation from Transgenic Mouse Heart 98
2.2.2.4 F-actin Isolation from Human Skeletal Muscle Biopsy 100
2.2.3 Purification of the Troponin Complex 101
2.2.3.1 Human and Mouse Cardiac Troponin Preparation 101
2.2.3.2 Preparation of Rabbit Skeletal Muscle Troponin 104
2.2.4 Purification of Tropomyosin 104
2.2.4.1 Preparation of Human Cardiac Tropomyosin 104
2.2.4.2 Tropomyosin Preparation from Baculovirus/*sf9* Cell Pellets 104
2.2.5 Purification of α-actinin 106
2.3 Manipulation of Troponin Phosphorylation 106
2.3.1 Protein Kinase A Treatment of Human Cardiac Troponin 106

2.3.2 Dephosphorylation of Troponin 107

2.4 Analysis of Protein 108

2.4.1 Determination of Protein Concentration 108

2.4.1.1 The Bradford Assay 108

2.4.1.2 The Lowry Assay 109

2.4.2 Sodium Dodecylsulphate Polyacrylamide Gel Electrophoresis (SDS-PAGE) 109

2.4.2.1 Sample Preparation 109

2.4.2.2 The Pharmacia System 109

2.4.2.3 The Mini PROTEAN System 110

2.4.2.4 Phosphate Affinity SDS-PAGE 110

2.4.3 Protein Staining 112

2.4.3.1 Coomassie Blue 112

2.4.3.2 Pro-Q Diamond Phosphoprotein Stain 112

2.4.4 Western Blot Analysis 114

2.4.5 Densitometric Analysis 115

2.5 *In Vitro* Motility Assay 116

2.5.1 Buffers for IVMA 116

2.5.2 Fluorescent Labelling of F-actin 117

2.5.3 Preparation of the IVMA Flow Cell 117

2.5.4 Reconstitution of Thin Filaments 118

2.5.5 Loading Protocol for Flow Cells 119

2.5.6 Preparation of Ca^{2+} -EGTA Buffers 121

2.5.7 Experimental Strategy IVMA Experiments 122

2.5.8 Standard Weekly Protocol of *In Vitro* Motility Experiments 123

2.5.9 Recording Apparatus 124

2.5.9.1 Temperature Control of the IVMA 126

2.5.9.2 Analysis of Filament Movement 126

2.5.9.3 Acquisition of a Sequence of Images 127

2.5.10 Analysis of Filament Movement....129
2.5.10.1 Computer Hardware....129
2.5.10.2 Software Calibration....129
2.5.10.3 Automatic Filament Tracking....130
2.5.10.4 Production and Statistical Analysis of a Ca^{2+}-concentration Titration....133

3 Completion of a Study on DCM Mutants Leading to a Hypothesis on the Molecular Mechanism Generating the Disease....137

3.1 General Introduction....137

3.2 Functional Investigation of DCM Mutant Troponin C Gly159Asp and Actin Glu361Gly....139

3.2.1 Introduction....139
3.2.2 Location of the TnC G159D and Actin E361G Mutations....139
3.2.3 *In Vitro* Motility Analysis....140
3.2.3.1 Effects of Human Cardiac Tropomyosin and Donor or TnC G159D Troponin on Rabbit Skeletal Muscle Actin Filament Motility....140
3.2.3.2 Effects of TnC G159D Troponin on the Thin Filaments Ca^{2+}-sensitivity Compared to Donor Human Cardiac Troponin....141
3.2.3.3 Effects of Troponin I Dephosphorylation on the Ca^{2+}-Sensitivity of G159D Thin Filaments....144
3.2.3.4 Thin Filament E361G and Non-Transgenic Actin Motility....151
3.2.3.5 Effects of Donor Human Cardiac Troponin and Tropomyosin on Non Transgenic and E361G Thin Filament Actin Motility at High and Low Ca^{2+}....152
3.2.3.6 Effects of E361G Actin on the Thin Filament Ca^{2+}-sensitivity Compared to Non-Transgenic mouse heart actin....153
3.2.3.7 Effects of Cardiac Troponin Dephosphorylation on the Ca^{2+}-Sensitivity of E361G Thin Filaments....158

3.3 Discussion....160

3.3.1 IVMA Advantages and Limitations....160

3.3.2 Troponin C G159D and Actin E361G Purification and activity....162

3.3.3 IVMA Results Leading to the "Uncoupling Hypothesis"....165

3.3.4 Proving the Uncoupling Hypothesis....167

4 Testing The Uncoupling Hypothesis with Five Different Mutations....168

4.1 Functional Investigation of DCM Mutant Troponin I Lys36Gln from Human Sample....168

4.1.1 Introduction on TnI K36Q....168

4.1.2 Manipulation of TnI K36Q Phosphorylation....169

4.1.3 Ca^{2+} Concentration Titrations....170

4.1.3.1 Comparison of K36Q Troponin (Native Phosphorylation or PKA Treated) with Donor Human Cardiac Troponin....170

4.1.3.2 Effects of Troponin I Dephosphorylation on the Ca^{2+}-Sensitivity of K36Q Thin Filaments 176

4.2 Functional Investigation of DCM Mutant Troponin T Arg141Trp (R141W) and ΔLys210 (ΔK210) from Transgenic Mouse Samples....184

4.2.1 Introduction on Cardiac TnT R141W....184

4.2.2 *In Vitro* Motility Analysis for Transgenic R141W Troponin....186

4.2.2.1 Effects of R141W Troponin on the Thin Filament Ca^{2+}-sensitivity Compared to Non-Transgenic Troponin....186

4.2.2.2 Effects of Troponin I Dephosphorylation on the Ca^{2+}-Sensitivity of R141W Thin Filaments....189

4.2.3 Introduction on Cardiac TnT ΔK210....194

4.2.4 *In Vitro* Motility Analysis for Transgenic ΔK210 Troponin....195

4.2.4.1 Effects of ΔK210 Troponin, Homo- and Heterozygous, on the Thin Filaments Ca^{2+}-sensitivity Compared to Non-Transgenic Troponin....196

4.2.4.2 Effects of Troponin I Dephosphorylation on the Ca^{2+}-Sensitivity of ΔK210 Thin Filaments, Homo- and Heterozygous....201

4.2.5 Control Experiments with Mouse Donor Troponin....209

4.3 Functional Investigation of DCM Mutant α-tropomyosin Glu40Lys (E40K) and Glu54Lys (E54K) from Baculovirus/*sf*9 Recombinant Samples 211

4.3.1 Introduction on E40K and E54K α-tropomyosin 211

4.3.2 *In Vitro* Motility Analysis for Recombinant E40K and E54K α-tropomyosin 213

4.3.2.1 Effects of Recombinant E40K α-tropomyosin on the Thin Filaments Ca^{2+}-sensitivity Compared to Wild-Type α-tropomyosin 213

4.3.2.2 Effects of Recombinant E54K α-tropomyosin on the Thin Filaments Ca^{2+}-sensitivity Compared to Wild-Type α-tropomyosin 216

4.3.2.3 Effects of Troponin I Dephosphorylation on the Ca^{2+}-Sensitivity of E40K and E54K Thin Filaments 218

4.4 Dose Dependency of Mutant Protein to Produce the Uncoupling Phenotype 233

4.5 Discussion 236

4.5.1 Concentration of DCM Mutant Proteins in the Experimental Samples 236

4.5.2 DCM Molecular Phenotype 237

4.5.3 A Potential Structural Mechanism Inducing DCM 243

4.5.4 Physiological Consequences of the Uncoupling 244

5 Functional Investigation of β- and γ-tropomyosin Mutants Leading to the Development of Nemaline Myopathy, Cap Disease and Congenital Fibre Type Disproportion 245

5.1 Introduction on the β- and γ-tropomyosin Mutants Linked to Nemaline Myopathy (NM), Cap Disease (CD) and Congenital Fibre type Disproportion (CFTD) 245

5.1.1 Six β-tropomyosin Mutants 245

5.1.2 Five γ-tropomyosin Mutants 248

5.2 *In Vitro* Motility Analysis of β-tropomyosin Mutants linked to Nemaline Myopathy and Cap Disease 249

5.2.1 Effects of the ΔK7 Mutation on Thin Filament Motility 250

5.2.2 Effects of the E41K and E117K Mutation on Thin Filaments Motility 258

5.2.3 Effects of the ΔK49, ΔE139 and Q147P Mutation on Thin Filament Motility 263

5.3 Effects of γ-tropomyosin Mutations on thin Filaments Motility 269

5.4 Discussion 277

5.4.1 Guidelines to the Investigation 277

5.4.2 The β-tropomyosin Mutants 278

5.4.3 The γ-tropomyosin Mutants.....283

6 Hypercontractile Nemaline Myopathy: a Novel Disease Caused by a Skeletal Muscle α-actin Mutation.....285

6.1 Introduction on K326N α-actin..... 285

6.2 K326N actin *In Vitro* Motility Analysis..... 286

6.2.1 The Opposite Phenotype: Actin D292V 295

6.3 Discussion 297

6.3.1 A Novel Molecular Phenotype 297

6.3.2 Structural Insights.....299

7 General Discussion.....302

7.1 DCM as a Result of Uncoupling Between Troponin I Phosphorylation and the Thin Filament Ca^{2+}-sensitivity..... 302

7.2 The Hypercontractile Phenotype..... 306

7.3 Tropomyosin Mutations and Skeletal Muscle Myopathy: An Undefined Situation 311

7.4 Future Work 313

Bibliography.....345

List of figures

Figure 1.1: The sarcomere 30

Figure 1.2: Schematic representation of myosin II 32

Figure 1.3: Ribbon structure of myosin S-1 33

Figure 1.4: The thin filament 34

Figure 1.5: Actin from globular to filament 36

Figure 1.6: Sequence alignement of *TPM1*, *TPM2* and *TPM3* 37

Figure 1.7: Tropomyosin coiled-coil, the heptapeptide repeat and the end-to-end polymerisation 39

Figure 1.8: Structure of troponin C 41

Figure 1.9: cTn core structure with and without Ser22/23 phosphorylation 44

Figure 1.10: Troponin T and its interactions 46

Figure 1.11: Structure of the skeletal muscle 49

Figure 1.12: Anatomy of the heart 51

Figure 1.13: Pressure and volume changes during the cardiac cycle 53

Figure 1.14: Diagram showing the direction of depolarisation in the heart 55

Figure 1.15: Ca^{2+} flux in the cardiac myocyte 57

Figure 1.16: Scheme for the actomyosin cross-bridge cycle 60

Figure 1.17: The core domain of the troponin complex 62

Figure 1.18: The proposed thin filament switch 63

Figure 1.19: The three state model of regulation 64

Figure 1.20: The three positions assumed by tropomyosin on the actin filaments corresponding to the three different states 66

Figure 1.21: β-adrenergic signalling pathway 68

Figure 1.22: Normal v DCM heart 70

Figure 1.23: Nemaline myopathy histology 73

Figure 1.24: Cap disease histology 76

Figure 1.25: CFTD histology 77

Figure 2.1: Myosin and HMM purification SDS-PAGE gel 94

Figure 2.2: Schematic representation of the affinity precipitation of HMM 96

Figure 2.3: Actin NTg and E361G purification SDS-PAGE gel 100

Figure 2.4: SDS-PAGE gel of troponin elution steps 103

Figure 2.5: SDS-PAGE gel of baculovirus/*sf9* tropomyosin purification steps 106

Figure 2.6: Calibration curve for the Bradford assay 108

Figure 2.7: Phosphate affinity SDS-PAGE examples 111

Figure 2.8: Example of mini gel stained with Pro-Q Diamond 113

Figure 2.9: GeneTools densitometric analysis screenshot 116

Figure 2.10: Construction of flow cell 118

Figure 2.11: Flow cell loading protocol 120

Figure 2.12: Schematic diagram of the visualisation and recording apparatus 125

Figure 2.13: Sequential flow diagram of the process of image acquisition 127

Figure 2.14: Graph showing optimal time interval against filament velocity 128

Figure 2.15: Calibration of the IVMA image analysis software 129

Figure 2.16: Sequential flow diagram of automatic filament tracking 132

Figure 2.17: Multiple histograms are used to build a Ca^{2+}-concentration titration curve 133

Figure 2.18: Normal distribution of the EC_{50} ratio of donor / failing heart troponin 135

Figure 3.1: *In vitro* motility measurements comparing donor and G159D troponin 141

Figure 3.2: Ca^{2+} concentration titration comparing thin filaments containing human donor and G159D troponin 143

Figure 3.3: Ca^{2+} concentration titration comparing thin filaments containing phosphorylated and dephosphorylated G159D troponin 146

Figure 3.4: Ca^{2+} concentration titrations comparing thin filaments containing phosphorylated and dephosphorylated human donor troponin 147

Figure 3.5: Ca^{2+} concentration titration comparing thin filaments containing dephosphorylated G159D and donor troponin 150

Figure 3.6: *In vitro* motility measurements comparing NTg and E361G actin 153

Figure 3.7: Ca^{2+} concentration titration comparing thin filaments containing non-transgenic and E361G actin 155

Figure 3.8: Ca^{2+} concentration titration comparing E361G actin thin filaments containing phosphorylated and dephosphorylated troponin 159

Figure 3.9: MALDI-MS spectra of troponin C G159D 163

Figure 3.10: 2D electrophoresis of transgenic mouse cardiac actin E361G 164

Figure 4.1: Pedigree of the K36Q TnI patient's family 168

Figure 4.2: Ca^{2+} concentration titration comparing thin filaments containing human donor and untreated K36Q troponin 172

Figure 4.3: Ca^{2+} concentration titration comparing thin filaments containing human donor and PKA treated K36Q troponin 174

Figure 4.4: Ca^{2+} concentration titration comparing thin filaments containing natively phosphorylated and dephosphorylated K36Q troponin 177

Figure 4.5: Ca^{2+} concentration titration comparing thin filaments containing natively PKA treated and dephosphorylated K36Q troponin 179

Figure 4.6: Ca^{2+} concentration titration comparing thin filaments containing dephosphorylated K36Q and dephosphorylated donor troponin 182

Figure 4.7: Pedigree of the R141W TnT family 184

Figure 4.8: WT and transgenic cTnT R141W mouse hearts and sections 186

Figure 4.9: Ca^{2+} concentration titration comparing thin filaments containing non-transgenic and R141W mouse troponin 188

Figure 4.10: Ca^{2+} concentration titration comparing thin filaments containing natively phosphorylated and dephosphorylated R141W troponin 190

Figure 4.11: Ca^{2+} concentration titration comparing thin filaments containing dephosphorylated R141W and dephosphorylated non-transgenic troponin 192

Figure 4.12: Pedigrees of the ΔK210 TnT families 194

Figure 4.13: Ca^{2+} concentration titration comparing thin filaments containing non-transgenic and homozygous ΔK210 mouse troponin 197

Figure 4.14: Ca^{2+} concentration titration comparing thin filaments containing non-transgenic and heterozygous ΔK210 mouse troponin 199

Figure 4.15: Ca^{2+} concentration titration comparing thin filaments containing natively phosphorylated and dephosphorylated homozygous ΔK210 troponin 202

Figure 4.16: Ca^{2+} concentration titration comparing thin filaments containing natively phosphorylated and dephosphorylated heterozygous ΔK210 troponin 204

Figure 4.17: Ca^{2+} concentration titration comparing thin filaments containing dephosphorylated homozygous ΔK210 and dephosphorylated non-transgenic troponin 206

Figure 4.18: Ca^{2+} concentration titration comparing thin filaments containing dephosphorylated heterozygous ΔK210 and dephosphorylated non-transgenic troponin 208

Figure 4.19: Ca^{2+} concentration titrations comparing thin filaments containing phosphorylated and dephosphorylated mouse donor troponin 210

Figure 4.20: Pedigrees of E40K and E54K *TPM1* families 211

Figure 4.21: Ca^{2+} concentration titration comparing thin filaments containing human natively phosphorylated cardiac troponin and either wild-type or E40K recombinant tropomyosin. 215

Figure 4.22: Ca^{2+} concentration titration comparing thin filaments containing human natively phosphorylated cardiac troponin and either wild-type or E54K recombinant tropomyosin. 217

Figure 4.23: Ca^{2+} concentration titration comparing thin filaments containing rabbit skeletal troponin and either wild-type or E40K recombinant tropomyosin 219

Figure 4.24: Ca^{2+} concentration titration comparing thin filaments containing rabbit skeletal troponin and either wild-type or E54K recombinant tropomyosin 220

Figure 4.25: Ca^{2+} concentration titration comparing thin filaments containing human cardiac donor or failing heart troponin and either wild-type or E40K recombinant tropomyosin 221

Figure 4.26: Ca^{2+} concentration titration comparing thin filaments containing natively phosphorylated or dephosphorylated human cardiac troponin and recombinant E40K tropomyosin 223

Figure 4.27: Ca^{2+} concentration titration comparing thin filaments containing natively phosphorylated or dephosphorylated human cardiac troponin and recombinant E54K tropomyosin 226

Figure 4.28: Ca^{2+} concentration titration comparing thin filaments containing dephosphorylated human cardiac troponin and either wild-type or E40K recombinant tropomyosin 229

Figure 4.29: Ca^{2+} concentration titration comparing thin filaments containing dephosphorylated human cardiac troponin and either wild-type or E54K recombinant tropomyosin 231

Figure 4.30: EC_{50} ratio P / dP troponin for thin filaments reconstituted with different E40K / WT ratios of α-tropomyosin 235

Figure 4.31: Ca^{2+}-dependent speed increase for thin filaments reconstituted with combinations of proteins from different sources 240

Figure 4.32: Percentage motile EC_{50} ratios mutant / WT when troponin is natively phosphorylated 241

Figure 4.33: Percentage motile EC_{50} ratios for donor and mutant thin filaments comparing phosphorylated and dephosphorylated troponin 242

Figure 5.1: Positions of the β- and γ-tropomyosin mutations on the molecule 248

Figure 5.2: Percentage motile bar graph in high and low Ca^{2+} for recombinant WT and ΔE139 β-tropomyosin with and without β-tropomyosin mixed in buffer C and D 250

Figure 5.3: Recombinant β-tropomyosin titration WT v ΔK7 252

Figure 5.4: Ca^{2+}-concentration titration of recombinant human β-tropomyosin WT v 100% ΔK7 reconstituted in thin filaments with rabbit skeletal muscle troponin and actin 253

Figure 5.5: Ca^{2+}-concentration titration of recombinant human β-tropomyosin WT v 50% ΔK7 reconstituted in thin filaments with rabbit skeletal muscle troponin and actin 255

Figure 5.6: Ca^{2+}-concentration titration of recombinant human β-tropomyosin WT v E41K reconstituted in thin filaments with rabbit skeletal muscle troponin and actin 259

Figure 5.7: Recombinant β-tropomyosin titration WT v E41K 260

Figure 5.8: Switch off effect on the percentage motile of E41K β-tropomyosin highly concentrated at 3.9 μM Ca^{2+} 261

Figure 5.9: Ca^{2+}-concentration titration of recombinant human β-tropomyosin WT v E117K reconstituted in thin filaments with rabbit skeletal muscle troponin and actin 262

Figure 5.10: Ca^{2+}-concentration titration of recombinant human β-tropomyosin WT v ΔK49 reconstituted in thin filaments with rabbit skeletal muscle troponin and actin 264

Figure 5.11: Ca^{2+}-concentration titration of recombinant human β-tropomyosin WT v ΔE139 reconstituted in thin filaments with rabbit skeletal muscle troponin and actin 266

Figure 5.12: Ca^{2+}-concentration titration of recombinant human β-tropomyosin WT v Q147P reconstituted in thin filaments with rabbit skeletal muscle troponin and actin.....268
Figure 5.13: SDS-PAGE gel of pure γ-tropomyosin WT and mutants.....270
Figure 5.14: Recombinant wild-type TPM1 v TPM3 titration 271
Figure 5.15: Ca^{2+}-concentration titration of recombinant human γ-tropomyosin wild-type v mutant reconstituted in thin filaments with rabbit skeletal muscle troponin and actin 273
Figure 5.16: Position of ΔK7 in the end-to-end tropomyosin interaction.....279
Figure 6.1: 2D electrophoresis of actin purified from K326N patient's biopsy.....285
Figure 6.2: β-tropomyosin titration comparing human donor skeletal actin and K326N skeletal actin.....288
Figure 6.3: Ca^{2+} concentration titrations comparing thin filaments containing donor and K326N human skeletal actin.....290
Figure 6.4: α-actinin titration comparing the isometric force properties of donor and K326N skeletal human actin.....293
Figure 6.5: *In vitro* motility measurements comparing skeletal muscle donor and D292V actin, with β-tropomyosin and rabbit skeletal muscle troponin.....296
Figure 6.6: Muscle biopsy from the quadriceps.....298
Figure 6.7: Structural model showing the contact between actin K326 and tropomyosin E181 when the actin-tropomyosin complex is in the "closed" state 301
Figure 7.1: Ribbon structures of the N-terminus of cTnC and the N-terminal extension of cTnI when phosphorylated and unphosphorylated 305
Figure 7.2: Force generation and Ca^{2+}-sensitivity of single myofibres dissected from ΔK7 patient muscle biopsy.....308
Figure 7.3: Structural model showing the contact between actin D25 and tropomyosin K6 when the actin-tropomyosin complex is in the "closed" state 310

List of tables

Table 2.1: Clinical details of all the human donor and failing heart samples studied 86

Table 2.2: DCM explanted heart patients details 87

Table 2.3: DCM transgenic mice details 88

Table 2.4: Summary of the mutants expressed with the baculovirus/*sf9* system and initial diagnosis 90

Table 2.5: Preparation of the Ca^{2+}-EGTA buffers 121

Table 3.1: Ca^{2+}-sensitivity data for G159D v donor troponin thin filaments sliding speed . 144

Table 3.2: Ca^{2+}-sensitivity data for G159D v donor troponin thin filaments percentage motile 144

Table 3.3: Ca^{2+}-sensitivity data for the sliding speed of thin filaments reconstituted with G159D phosphorylated v G159D dephosphorylated troponin 145

Table 3.4: Ca^{2+}-sensitivity data for the percentage motile of thin filaments reconstituted with G159D phosphorylated v G159D dephosphorylated troponin 145

Table 3.5: Ca^{2+}-sensitivity data for thin filaments reconstituted with human donor troponin phosphorylated v dephosphorylated 148

Table 3.6: Ca^{2+}-sensitivity data for sliding speed of dephosphorylated G159D v dephosphorylated donor thin filaments 149

Table 3.7: Ca^{2+}-sensitivity data for percentage motile of dephosphorylated G159D v dephosphorylated donor thin filaments 149

Table 3.8: Comparison of motility of non-transgenic and E361G thin filament actin 152

Table 3.9: Ca^{2+}-sensitivity data for E361G v Non-Transgenic actin thin filaments 157

Table 3.10: Ca^{2+}-sensitivity data for E361G actin thin filaments natively phosphorylated human cardiac troponin v dephosphorylated human cardiac troponin 158

Table 4.1: Ca^{2+}-sensitivity data for untreated K36Q v donor troponin thin filament sliding speed 171

Table 4.2: Ca^{2+}-sensitivity data for untreated K36Q v donor troponin thin filament percentage motile 171

Table 4.3: Ca^{2+}-sensitivity data for PKA treated K36Q v donor troponin thin filament sliding speed 175

Table 4.4: Ca^{2+}-sensitivity data for PKA treated K36Q v donor troponin thin filament percentage motile 175

Table 4.5: Ca^{2+}-sensitivity data for the sliding speed of thin filaments reconstituted with K36Q natively phosphorylated v K36Q dephosphorylated troponin 178

Table 4.6: Ca^{2+}-sensitivity data for the percentage motile of thin filaments reconstituted with K36Q natively phosphorylated v K36Q dephosphorylated troponin 178

Table 4.7: Ca^{2+}-sensitivity data for the sliding speed of thin filaments reconstituted with PKA treated K36Q v K36Q dephosphorylated troponin 180

Table 4.8: Ca^{2+}-sensitivity data for the percentage motile of thin filaments reconstituted with PKA treated K36Q v K36Q dephosphorylated troponin 180

Table 4.9: Ca^{2+}-sensitivity data for sliding speed of dephosphorylated K36Q v dephosphorylated donor thin filaments 183

Table 4.10: Ca^{2+}-sensitivity data for percentage motile of dephosphorylated K36Q v dephosphorylated donor thin filaments 183

Table 4.11: Ca^{2+}-sensitivity data for R141W v non-transgenic mouse natively phosphorylated troponin thin filaments 187

Table 4.12: Ca^{2+}-sensitivity data for the sliding speed of thin filaments reconstituted with R141W natively phosphorylated v R141W dephosphorylated mouse troponin 191

Table 4.13: Ca^{2+}-sensitivity data for the percentage motile of thin filaments reconstituted with R141W natively phosphorylated v R141W dephosphorylated mouse troponin.....191
Table 4.14: Ca^{2+}-sensitivity data for thin filaments reconstituted with mouse dephosphorylated troponin, non-transgenic v R141W 193
Table 4.15: Ca^{2+}-sensitivity data for homozygous ΔK210 v non-transgenic mouse natively phosphorylated troponin thin filaments 198
Table 4.16: Ca^{2+}-sensitivity data for heterozygous ΔK210 v non-transgenic mouse natively phosphorylated troponin thin filaments sliding speed 200
Table 4.17: Ca^{2+}-sensitivity data for heterozygous ΔK210 v non-transgenic mouse natively phosphorylated troponin thin filaments percentage motile.....200
Table 4.18: Ca^{2+}-sensitivity data for the sliding speed of thin filaments reconstituted with homozygous ΔK210 troponin, natively phosphorylated v dephosphorylated 203
Table 4.19: Ca^{2+}-sensitivity data for the percentage motile of thin filaments reconstituted with homozygous ΔK210 troponin, natively phosphorylated v dephosphorylated 203
Table 4.20: Ca^{2+}-sensitivity data for thin filaments reconstituted with heterozygous ΔK210 troponin, natively phosphorylated v dephosphorylated.....205
Table 4.21: Ca^{2+}-sensitivity data for thin filaments reconstituted with dephosphorylated troponin, non-transgenic v homozygous ΔK210 207
Table 4.22: Ca^{2+}-sensitivity data for thin filaments reconstituted with dephosphorylated troponin, non-transgenic v heterozygous ΔK210.....209
Table 4.23: Ca^{2+}-sensitivity data for thin filaments reconstituted with mouse donor troponin phosphorylated v dephosphorylated 209
Table 4.24: Ca^{2+}-sensitivity data for wild-type v E40K recombinant tropomyosin with natively phosphorylated human cardiac troponin thin filaments.....214

Table 4.25: Ca^{2+}-sensitivity data for wild-type v E54K recombinant tropomyosin with natively phosphorylated human cardiac troponin thin filaments 216
Table 4.26: Ca^{2+}-sensitivity data for the sliding speed of thin filaments reconstituted with recombinant E40K tropomyosin and human cardiac troponin, phosphorylated v dephosphorylated 224
Table 4.27: Ca^{2+}-sensitivity data for the percentage motile of thin filaments reconstituted with recombinant E40K tropomyosin and human cardiac troponin, phosphorylated v dephosphorylated 224
Table 4.28: Ca^{2+}-sensitivity data for the sliding speed of thin filaments reconstituted with recombinant E54K tropomyosin and human cardiac troponin, phosphorylated v dephosphorylated 227
Table 4.29: Ca^{2+}-sensitivity data for the percentage motile of thin filaments reconstituted with recombinant E54K tropomyosin and human cardiac troponin, phosphorylated v dephosphorylated 227
Table 4.30: Ca^{2+}-sensitivity data for the sliding speed of thin filaments reconstituted with dephosphorylated human cardiac troponin, wild type v E40K recombinant tropomyosin 230
Table 4.31: Ca^{2+}-sensitivity data for the percentage motile of thin filaments reconstituted with dephosphorylated human cardiac troponin, wild type v E40K recombinant tropomyosin 230
Table 4.32: Ca^{2+}-sensitivity data of thin filaments reconstituted with dephosphorylated human cardiac troponin, wild type v E54K recombinant tropomyosin 232
Table 4.33: Ca^{2+}-sensitivity data for titrations performed with different α-tropomyosin E40K / WT ratios and troponin phosphorylated v dephosphorylated 234
Table 4.34: MS data for reporter peptides measured by MALDI-TOF/TOF, used to quantitate TnI K36Q and TnT ΔK210 237

Table 4.35: DCM mutations data summary 238

Table 5.1: Ca^{2+}-sensitivity data for recombinant β-tropomyosin WT v 100% ΔK7 thin filaments 254

Table 5.2: Ca^{2+}-sensitivity data for recombinant β-tropomyosin WT v 50% ΔK7 thin filaments motile velocity 257

Table 5.3: Ca^{2+}-sensitivity data for recombinant β-tropomyosin WT v 50% ΔK7 thin filaments percentage motile 257

Table 5.4: Ca^{2+}-sensitivity data for recombinant β-tropomyosin WT v E117K thin filaments 263

Table 5.5: Ca^{2+}-sensitivity data for recombinant β-tropomyosin WT v ΔK49 thin filaments 265

Table 5.6: Ca^{2+}-sensitivity data for recombinant β-tropomyosin WT v ΔE139 thin filaments 267

Table 5.7: Ca^{2+}-sensitivity data for thin filaments reconstituted with rabbit skeletal muscle troponin and recombinant wild-type v 5 mutant γ-tropomyosins 276

Table 6.1: Comparison of motility of donor and K326N thin filament actin 287

Table 6.2: Ca^{2+}-sensitivity data for donor v K326N skeletal actin thin filaments motile velocity 291

Table 6.3: Ca^{2+}-sensitivity data for donor v K326N skeletal actin thin filaments percentage motile 291

Table 7.1: Examples of gain-of-function mutations in thin filaments proteins 309

Table 7.2: Summary of the findings on β- and γ-tropomyosin 311

List of Abbreviations

ϕ	Tetramethyl Rhodamine Isothiocyanate (TRITC) -phalloidin
ACEX	Actin extraction buffer
ACTA1	Skeletal actin
ACTC	Cardiac actin gene
ADP	Adenosine diphosphate
ATP	Adenosine triphosphate
BSA	Bovine serum albumin
cAMP	Cyclic adenosine monophosphate
CD	Cap disease
CFTD	Congenital fibre type disproportion
DCM	Dilated cardiomyopathy
DTT	1,4-Dithiothreitol
E-64	L-trans-epoxysuccinyl-leucylamide-(4-guanido)- butane
ECL	Enhanced chemiluminescence reagents
EDTA	Ethylenediamine tetraacetic acid
EGTA	Ethylene glycol-bis (2-amino-ethylether), N,N,N’,N’-tetraacetic acid
ELC	Essential light chain
F-actin	Filamentous actin
G-actin	Monomeric actin
HCM	Hypertrophic cardiomyopathy
HMM	Heavy meromyosin
IVMA	*In vitro* motility assay
LMM	Light meromyosin
MHC	Myosin heavy chain
MOPS	3-(N-Morpholino) propanesulphonic acid

MyBP-C	Myosin binding protein-C
NM	Nemaline myopathy
NTg	Non-transgenic
PAGE	Polyacrylamide gel electrophoresis
PBS	Phosphate buffered saline
pCa	-log[Ca^{2+}]
Pi	Inorganic phosphate
PIPES	Piperazine-N,N'-bis (2-ethanesulphonic acid)
PKA	Protein kinase A
PLB	Phospholamban
PMSF	Phenylmethylsulfonylfluoride
RLC	Regulatory light chain
S1	Myosin subfragment 1
SDS	Sodium dodecyl sulphate
SERCA	Sarcoplasmic/Endoplasmic reticulum Ca^{2+}-ATPase
SR	Sarcoplasmic reticulum
Tg	Transgenic
Tm	Tropomyosin
Tn	Troponin
TnC	Troponin C
TnI	Troponin I
TnT	Troponin T
Tris	Tris (hydroxymethyl) amino-methane
Triton-X-100	Polyethylene glycol tert-octylphenyl ether
Tween 20	Polyoxyethylenesorbitan monolaurate
WT	Wild type

Acknowledgments

I would like to thank my main supervisor, Professor Steven Martson, firstly for having handed me this exciting project, but especially for his wise guidance and the great knowledge he tried to transfer me. A particular thank goes also to Dr. Andrew Messer, who helped me throughout the project and the writing with solid enthusiasm. Mr O'Neal Copeland for his assistance in the lab, but also for the long chats. Dr Christopher Bayliss for sharing the darkness with me both physically and morally. Mr Ross Wilkinson for some office and football fun. Dr Judy Leung for her happy presence in the lab. I would also like to thank people that unfortunately made a shorter appearance in my work life: Miss Gaelle Kikonda, Dr Helen Paur, Dr Clare Gallon, Miss Christina Rowlands, Dr Weihua Song.

I would like to mention my deepest gratitude to the British Heart Foundation for funding me and my project very generously. I would like to thank also all the collaborators providing me with samples. Specifically these are: Prof. Cris dos Remedios for the donor, failing and DCM (K36Q TnI) heart samples; Dr Lianfeng Zhang for the R141W TnT transgenic mouse hearts; Prof. Sachio Morimoto for the ΔK210 TnT transgenic mouse hearts; Dr Kristen Nowak for the α- and γ-tropomyosin baculovirus/*sf9* pellets; Prof. Carina Wallgren-Pettersson for the β-tropomyosin baculovirus/*sf9* pellets; Prof. Nigel Laing for the K326N skeletal actin human muscle biopsy; Dr Nigel Clarke for the D292V skeletal actin human muscle biopsy.

Finally I would like to thank my two families. First, my Italian family, including friends, but especially my parents, Daniele and Federica, who have always been exceptional in giving me the greatest love and support, second my London family, all the people coming and going, which accompanied me across this adventure with its ups and its downs, but never doubting that I could make it. Out of the bunch I would like to thank the old friend Gattone, the rediscovered friend Spritzada, and my 'amorsito' Edna.

1 Introduction

1.1 Muscle Structure

Vertebrates have three distinct muscle types: smooth muscle, skeletal muscle and cardiac muscle. Skeletal and cardiac muscle are called striated muscles for the highly ordered and regularly repeated pattern of bands constituting its fibres. Skeletal muscle can be further divided into slow and fast forms. The characteristics of the skeletal muscle will be discussed in a section dedicated to it (see 1.1.4). Cardiac muscle, instead, is a type of striated muscle present only in the heart. It differs in many respects from the skeletal muscle and also its particular features will be discussed in another section (see 1.1.5). What both kind of muscle share is the basic molecular unit, the sarcomere, and the way its basic function of contracting gets regulated.

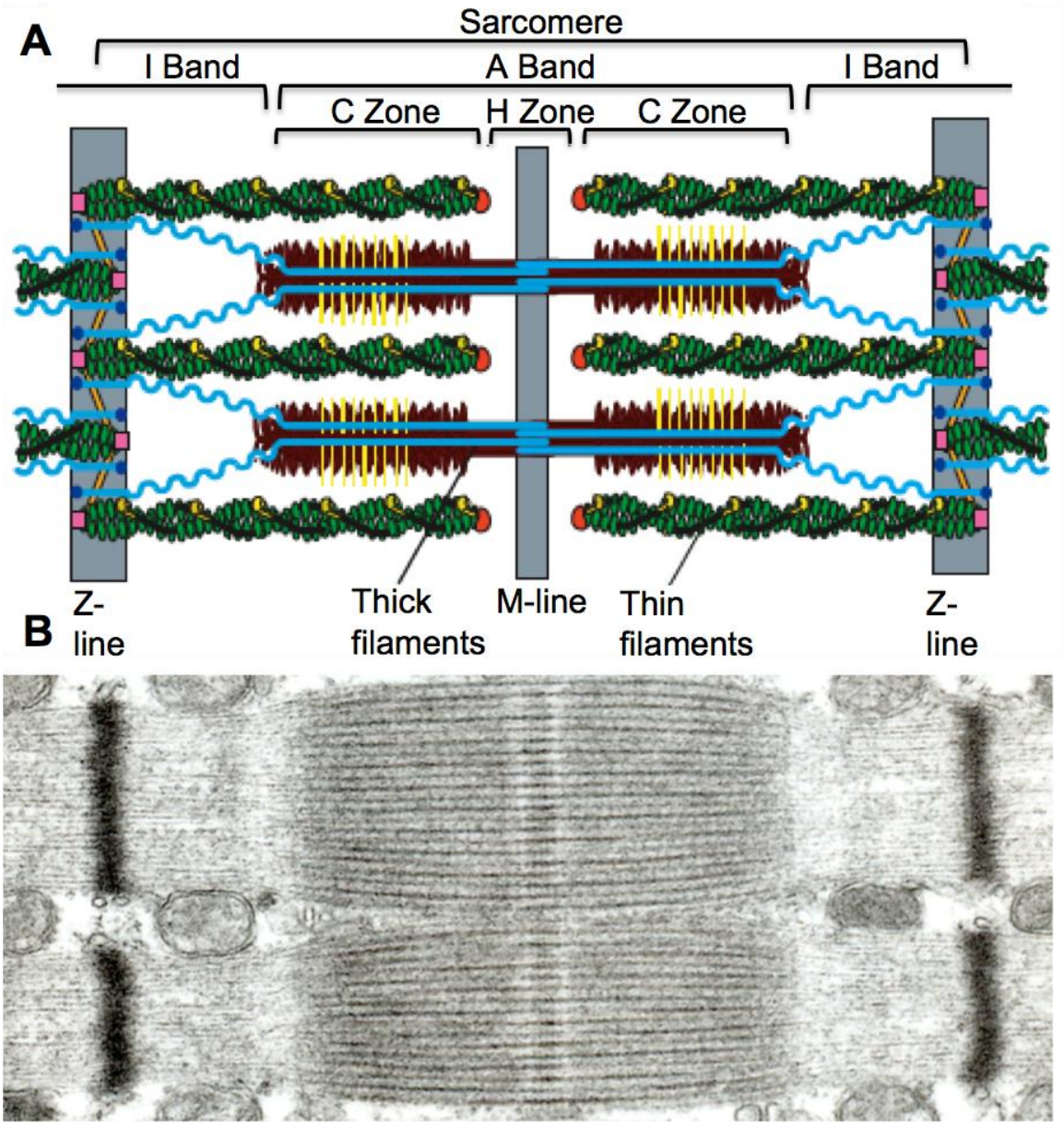
1.1.1 The Sarcomere

The sarcomere (Figure 1.1) is the base contractile unit that gets repeated in series to form a myofibril, which, in turn, repeated in parallel will form the striated muscle cell, the myocyte. The main structural features of the sarcomere are the M line, the midpoint of the thick filament containing the protein myomesin, which cross-links the thick filament to maintain their regular structure, and the Z line, where the actin filaments interact with α-actinin. The Z-line makes contacts with T-tubules (see 1.1.4.1) and costameres, contains proteins involved in signalling and also separates different sarcomere units. The dense region where the thick filament is present is termed the anisotropic or “A” band, and, within this, the C zone is the region where cross-bridge formation occurs, and the H zone contains naked thick filaments primarily consisting of polymerised myosin rods. The less dense region, where only thin

filaments are present, is termed the isotropic or “I” band. The contraction and relaxation of cardiac muscle is due to the sliding of the thin filaments over the thick filaments (see 1.2.3), such that the width of the A band remains constant during contraction, whilst the I band shortens (Huxley and Niedergerke, 1954, Huxley and Hanson, 1954).

The sarcomere also contains many other proteins taking part in assembly, in maintenance of structural integrity and in the regulation of contractile activity. In the thick filament these are the regulatory and essential light chains (see 1.1.2.2), titin, spanning from the Z-line to the M-line and being responsible for the passive tension, and myosin binding protein-C, present in the C zone. In the thin filaments, the regulatory proteins are tropomyosin and the troponin complex (troponin C, I and T), which will be discussed in detail below. Many other thin filament-associated proteins exist (e.g. nebulin and tropomodulin) but they won't be discussed in detail being superfluous to the aim of this study.

Figure 1.1: The sarcomere



A) Schematic diagram of a sarcomere. Thin filaments are composed of actin (green), troponin (dark yellow), tropomyosin filaments (black lines). Thin filaments in muscle sarcomeres are anchored at the Z-disk by the cross-linking protein α -actinin (gold) and are capped by CapZ (pink squares). The thin-filament pointed ends terminate within the A band, and are capped by tropomodulin (bright red). Thick filaments are represented with myosin (red), myosin-binding-protein C (MyBP-C; yellow transverse lines). One titin molecule spans half of the sarcomere (light-blue). Figure adapted from (Gregorio and Antin, 2000).
B) Electronmicroscopic photograph of the ultrastructural organization of sarcomeres in parallel (Ottenheijm et al., 2008).

1.1.2 The Thick Filament

1.1.2.1 Myosin Structure and Function

The major constituent of the thick filament is the molecular motor protein, myosin. The class of myosin found in muscle is myosin II. Myosin II consists of two heavy chains (~200 kDa each) and four light chains (~20 kDa each) (Gordon et al., 2000).There are six genes in mammals encoding for fast skeletal muscle myosin (*MYH-1, -2, -3, -4, -8, -13*). The isoforms MyHC-2A and -2X are coded respectively by the genes *MYH-2* and *-1* and are expressed in human fast-twitch fibres (Schiaffino and Reggiani, 2011). There are two isoforms of cardiac myosin heavy chain (α and β) encoded by two genes (*MYH6* and *MYH7*) on chromosome 14 (Jaenicke et al., 1990), the β-MHC is the predominant form found in human adult ventricles, only 5% is represented by α-myosin. The β-MHC is also expressed in the slow-twitch skeletal muscle fibres. Myosin light chains can be either regulatory (RLC) or essential (ELC) and each heavy chain is associated with one of each kind of light chain.

Myosin heavy chain can be divided into three domains:

1) Subfragment 1 (S-1). This is the catalytic domain that contains the nucleotide binding site responsible for acto-myosin ATPase activity and the actin binding site.

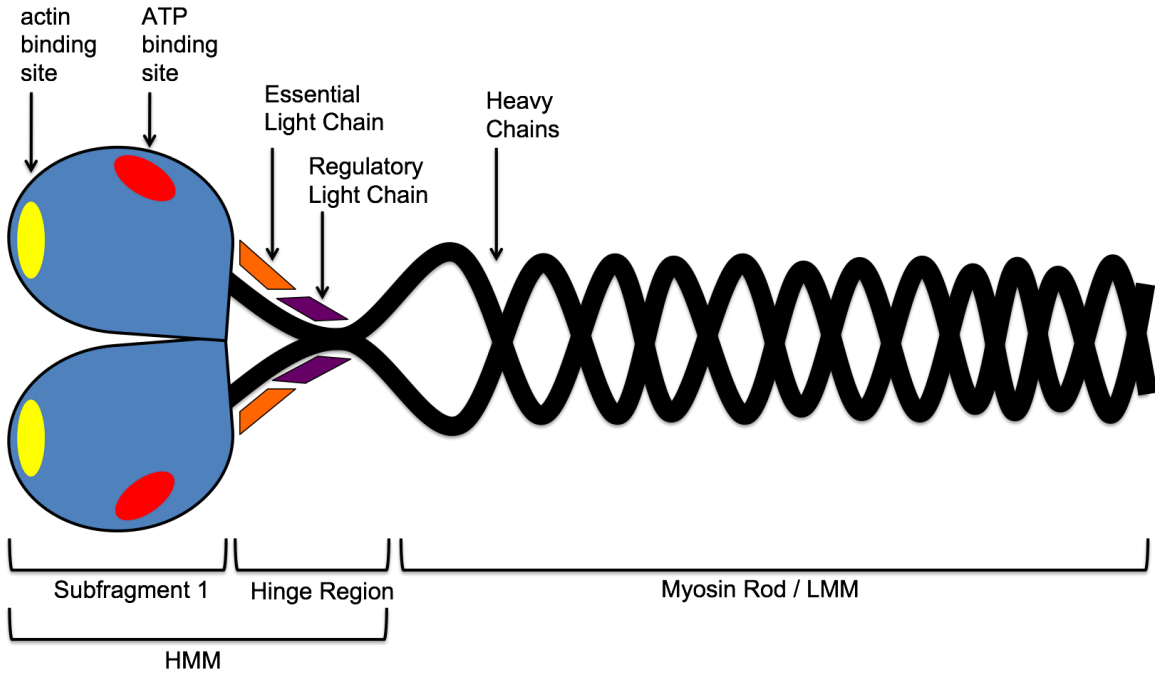
2) The hinge region that contains the lever arm. By changing in conformation it produces the cross bridge movement. Both essential and regulatory light chains bind in this region.

3) The myosin rod. It consists of an elongated α-helix, approximately 130 nm long. It dimerises with the second heavy chain to generate the complete myosin molecule but also polymerises with other myosins to form the thick filament.

If digested with chymotrypsin at high KCl concentrations, myosin gets cut in two fragments: heavy mero-myosin (HMM), which contains the globular head and the hinge region, and light

mero-myosin (LMM). If digested with at low salt concentrations, two different fragments get separated instead: S1 and rod; the latter containing the neck and LMM domains (Weeds and Taylor, 1975). Myosin and its subdomains are schematically represented in Figure 1.2.

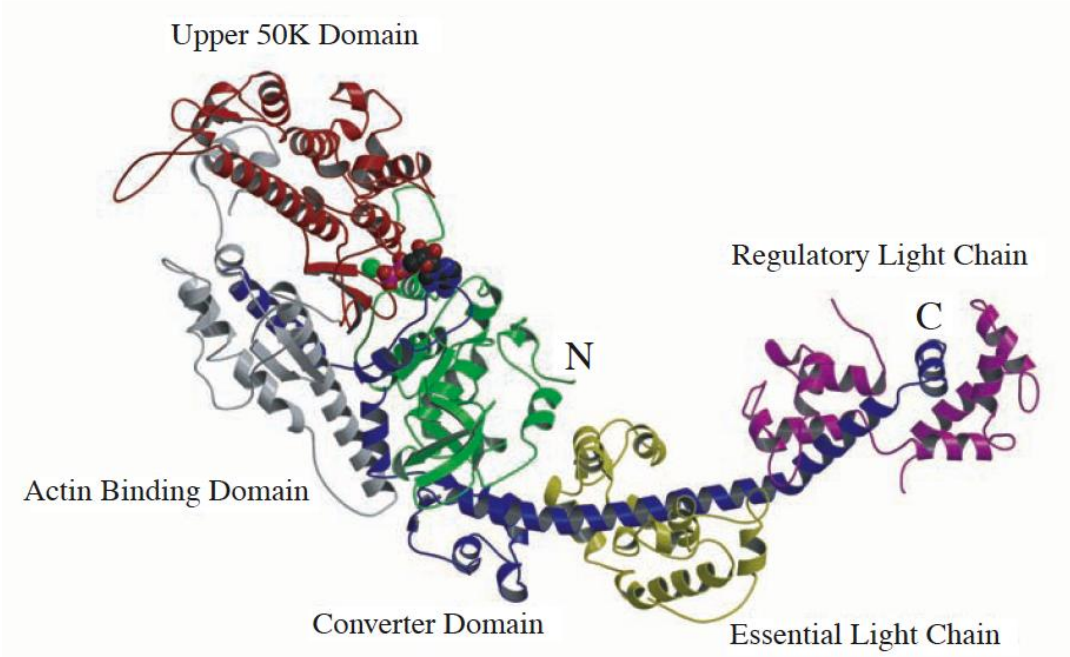
Figure 1.2: Schematic representation of myosin II



Myosin transduces the energy released from the hydrolysis of ATP into kinetic energy via the cross-bridge cycle. The myosin head binds to F-actin and its movement results in the translocation of the F-actin. The movement of F-actin on both sides of the A-band pulls the Z-disks towards each other, shortening the sarcomere. The first X-ray crystal structure of myosin (Rayment et al., 1993) showed the S-1 fragment of chicken skeletal muscle myosin (Figure 1.3). It highlighted the structural basis of the S-1 domain: a 7-stranded anti-parallel β-sheet. It could be further divided into three regions: the N-terminal 25 K (Da) domain, the middle 50 K domain and the C-terminal 20 K domain (Geeves and Holmes, 1999). The ATP binding site consists of a P-loop motif flanked by two switch motifs (SW 1 & 2) similar to

those found in G-proteins (Smith and Rayment, 1996, Sprang, 1997, Squire and Parry, 2005). Other important structural features are the relay helix, the SH helix, the converter domain and the lever arm. The converter domain forms a socket for the lever arm. The lever arm is an extended α-helical structure which binds two light chains and links to the highly ordered C-terminal tail (Geeves and Holmes, 2005).

Figure 1.3: Ribbon structure of myosin S-1



Ribbon structure of myosin S-1. Different regions are labelled and coloured differentially. The proteolytic fragments: the 25K N-terminal region in green; the 50K domain spans two subdomains, the upper and the lower or actin binding, respectively in red and gray; the 20K domain C-terminal in blue. The regulatory light chain is coloured magenta and the essential light chain in yellow (Geeves and Holmes, 1999).

1.1.2.2 Myosin Light Chains

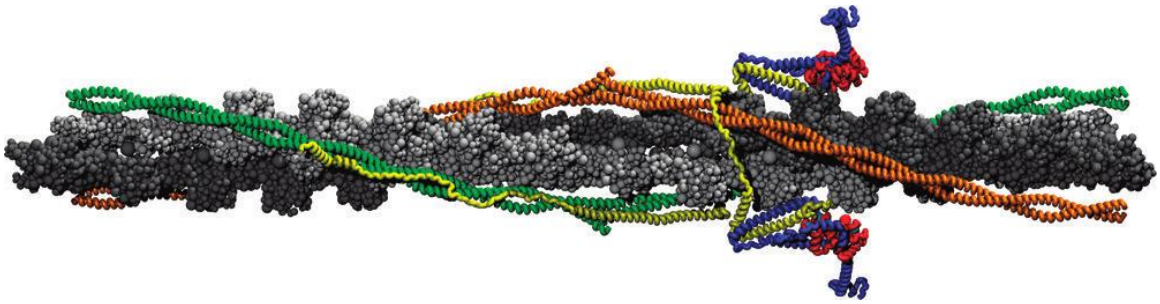
The essential light chain (ELC) and the regulatory light chain (RLC) bind to the 'neck' of the myosin head region. Both are EF-hand proteins, able to bind divalent cations, but the ELC has an N-terminal 30 amino acid residue extension, rich in prolines and alanines, which extends to interact with actin (Trayer et al., 1987), slowing the kinetics of cross-bridge

cycling (Schaub et al., 1998, Timson et al., 1998). It may be needed to position actin and myosin correctly and form cross-bridges (Sweeney, 1995). The main structural features of both light chains are a pair of helix-loop-helix structures in a dumbbell-like shape (Xie et al., 1994). The ELC binds to the N-terminal portion of the neck and the RLC binds around the C-terminal part with minimal contact between the light chains (Xie et al., 1994). Both the light chains bind myosin on IQ motifs, which are binding sites for EF-hand proteins, via C-terminal domain interactions (Xie et al., 1994). The RLC can be phosphorylated by calmodulin-dependent myosin light chain kinase at its N-terminus, resulting in an increase in Ca^{2+}-sensitivity at sub-maximal Ca^{2+} activation levels (Sweeney et al., 1993). In striated muscle therefore, these proteins could act to modulate the acto-myosin interaction.

1.1.3 The Thin Filament

The thin filament is mainly composed of F-actin, tropomyosin and troponin (Figure 1.4).

Figure 1.4: The thin filament



Representation of the human thin filament. Actin filament in grey/silver; tropomyosin in orange/green; troponin T in yellow; troponin I in blue and troponin C in red. (Manning et al., 2011)

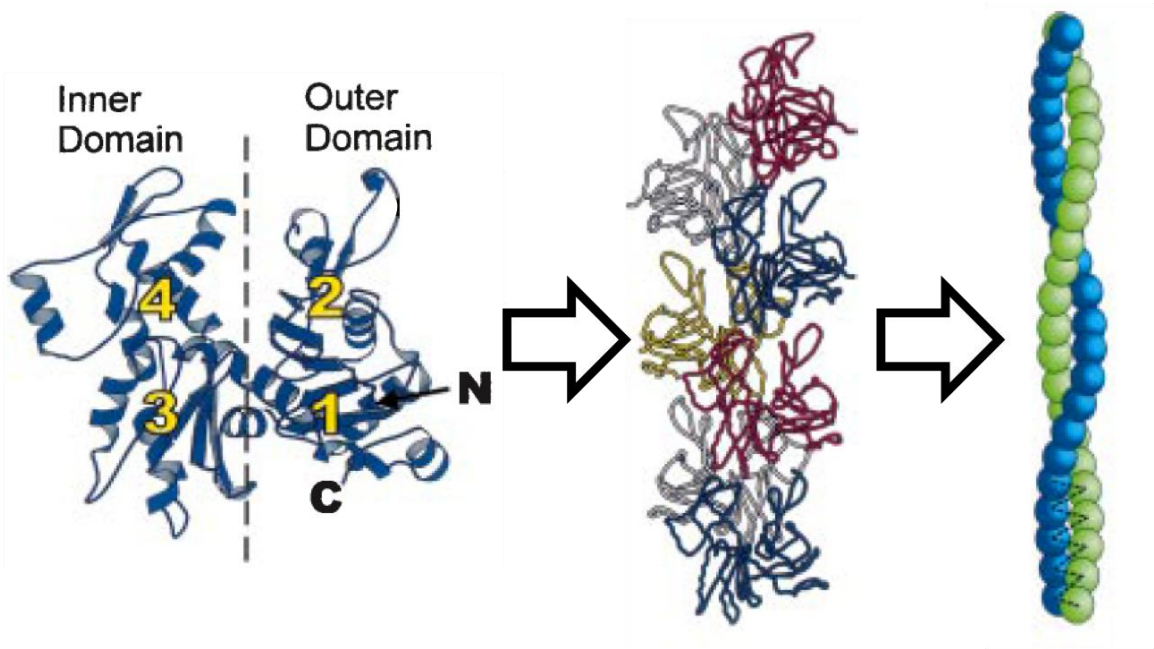
1.1.3.1 Actin

Actin is a protein ubiquitous in the eukaryotes with an impressive level of conservation. Actin exists in globular (G-actin) and filamentous (F-actin) forms (Figure 1.5). The actin monomer is a single polypeptide 375 residues long, it binds ATP and a divalent cation (dos

Remedios and Moens, 1995). An actin monomer consists of two domains called large (inner) and small (outer) separated by a cleft which contains both the nucleotide and the divalent ion binding site (Hodgkinson, 2000). These two main domains can each be divided into two subdomains to a total of four: the outer domain includes subdomains 1 and 2, the inner domain includes subdomains 3 and 4. G-actin polymerises to form F-actin, in the presence of divalent cations and ATP, through domains 3 and 4 of the monomer, which interface with the same domains of other monomers. They can contact 4 other monomers in the helix (dos Remedios and Moens, 1995). ATP gets hydrolysed following polymerisation (Korn et al., 1987). Domains 1 and 2 are quite exposed and form the main myosin binding sites. Electron microscopy has shown that the structure of F-actin is a double helix with 13 actin molecules every full turn (Holmes et al., 1990).

Actin is the major constituent of sarcomeric thin filaments. In skeletal muscle thin filaments get to the exact length of 1.05 μm determined by the giant filament protein nebulin (600-900 kDa) which regulates actin's polymerisation (Horowits, 2006, Pfuhl et al., 1994). Nebulin is expressed also in cardiac muscle, but there its concentration is not high enough to precisely regulate the length of the thin filaments (Kazmierski et al., 2003). Nebulette and N-RAP are smaller alternative isoforms of nebulin, which are expressed in the myocardium and result in greater variability in cardiac thin filament length (Burgoyne et al., 2008). Actin polymerization in the cardiac muscle is mainly regulated by capping proteins like tropomodulin (Weber et al., 1994). F-actin is a polar molecule with a barbed (+) end and a pointed (-) end. The barbed end docks the thin filaments through the binding of α-actinin in the Z-disk, whereas tropomodulin caps them at the pointed end.

Figure 1.5: Actin from globular to filament



On the left, ribbon structure of globular monomeric actin, with the 4 subdomains indicated by numbers and a dashed line separating the inner from the outer domain. In the middle, the atomic model of 7 actin monomers, representing the unit of the thin filaments. On the right, three turns of a right-handed actin filament. Figure adapted from Hodgkinson (2000).

1.1.3.2 Tropomyosin

Tropomyosin (Tm) is another highly conserved protein, ubiquitous in the eukaryotes, but not in the kingdom of plants. It is necessary for the regulation of the thin filament and gives cooperativity to the system. Four genes, *TPM1-4*, encode respectively α, β, γ (sequence alignment of these three in Figure 1.6) and δ tropomyosin, each of which has tissue-specific alternatively spliced variants to a total of 20 variants (Gunning et al., 2005). In the heart the predominant form of tropomyosin is α-Tm, accounting for 97-99% of the total. In skeletal muscle α-, β- and γ-Tm are expressed instead, but in different ratios depending on the fibre type. β-Tm is expressed less in fast-twitch type 2 fibres (~ 30%) and more in slow-twitch type 1 fibres (~ 65%). α-Tm is more expressed in type 2 fibres, while γ-Tm is present only in

type 1 fibres (Perry, 2001). Tropomyosin forms both homodimer and heterodimers *in vivo*. When α-Tm or γ-Tm are in presence of β-Tm, the heterodimer is the preferred form (Bronson and Schachat, 1982). Tropomyosin dimers form a left handed parallel coiled coil structure made entirely of α-helix (Mason and Arndt, 2004).

Figure 1.6: Sequence alignement of *TPM1*, *TPM2* and *TPM3*

```
TPM1_HUMAN      MDAIKKKMQMLKLDKENALDRAEQAEADKKAAEDRSKQLEDELVSLQKKLKGTEDELDKY 60
TPM3_HUMAN      MEAIKKKMQMLKLDKENALDRAEQAEAEQKQAEERSKQLEDELAAMQKKLKGTEDELDKY 60
TPM2_HUMAN      MDAIKKKMQMLKLDKENAIDRAEQAEADKKQAEDRCKQLEEEQQALQKKLKGTEDEVEKY 60
                *:****************:********:** **:*.****:*  ::**********::**

TPM1_HUMAN      SEALKDAQEKLELAEKKATDAEADVASLNRRIQLVEEELDRAQERLATALQKLEEAEKAA 120
TPM3_HUMAN      SEALKDAQEKLELAEKKAADAEAEVASLNRRIQLVEEELDRAQERLATALQKLEEAEKAA 120
TPM2_HUMAN      SESVKEAQEKLEQAEKKATDAEADVASLNRRIQLVEEELDRAQERLATALQKLEEAEKAA 120
                **::*:****** *****:****:************************************

TPM1_HUMAN      DESERGMKVIESRAQKDEEKMEIQEIQLKEAKHIAEDADRKYEEVARKLVIIESDLERAE 180
TPM3_HUMAN      DESERGMKVIENRALKDEEKMELQEIQLKEAKHIAEEADRKYEEVARKLVIIEGDLERTE 180
TPM2_HUMAN      DESERGMKVIENRAMKDEEKMELQEMQLKEAKHIAEDSDRKYEEVARKLVILEGELERSE 180
                **********.** *******:**:**********::*************:*.:***:*

TPM1_HUMAN      ERAELSEGKCAELEEELKTVTNNLKSLEAQAEKYSQKEDRYEEEIKVLSDKLKEAETRAE 240
TPM3_HUMAN      ERAELAESKCSELEEELKNVTNNLKSLEAQAEKYSQKEDKYEEEIKILTDKLKEAETRAE 240
TPM2_HUMAN      ERAEVAESKCGDLEEELKIVTNNLKSLEAQADKYSTKEDKYEEEIKLLEEKLKEAETRAE 240
                ****::*.**.:****** ************:*** ***:******:* :**********

TPM1_HUMAN      FAERSVTKLEKSIDDLEDELYAQKLKYKAISEELDHALNDMTSI 284
TPM3_HUMAN      FAERSVAKLEKTIDDLEDELYAQKLKYKAISEELDHALNDMTSI 284
TPM2_HUMAN      FAERSVAKLEKTIDDLEDEVYAQKMKYKAISEELDNALNDITSL 284
                ******:****:*******:****:**********:****:**:
```

The three tropomyosin isoforms share great homology, even more marked between *TPM1* and *TPM3*. Alignment obtained with Clustal V.

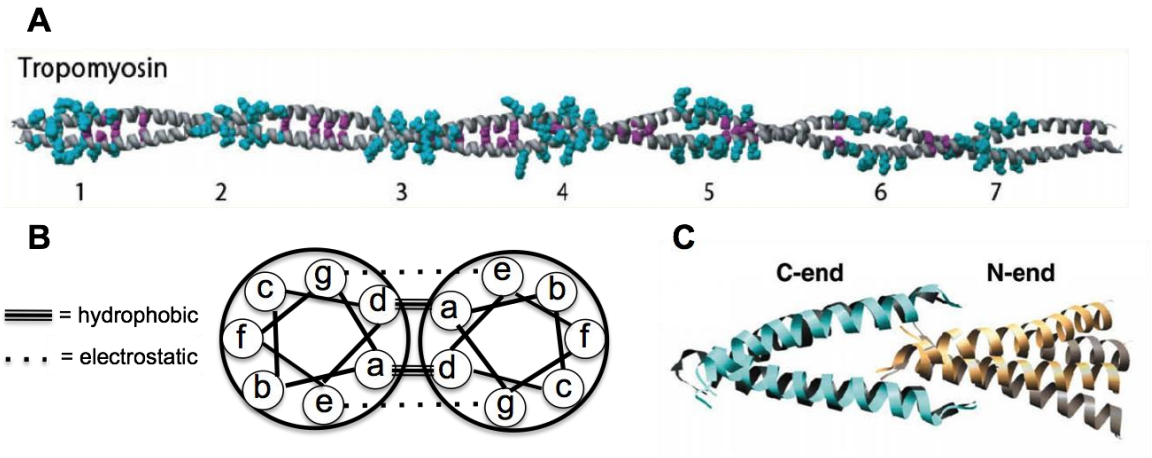
The structure of a coiled-coil tropomyosin dimer contains seven pseudo repeats, which correspond to seven actin binding sites, one for each actin monomer in a regulatory unit. These repeats are made of two subzones made of repeats of a 19 amino acid motif each containing α- and β-bands (Hitchcock-DeGregori and Singh, 2010). The alpha band is thought to be important for the interactions of tropomyosin with actin in the 'closed' or 'blocked' states, whereas the beta band interacts with actin in the 'open' state (Holthauzen et al., 2004). The three states and the mechanism involved in the switch will be discussed in detail in section 1.3. Each tropomyosin dimer forms head-to-tail overlapping interactions

(Figure 1.7 C) with nine amino acids on adjacent dimers to form a continuous polymer along the F-actin filament, which stabilises its otherwise weak interaction with actin (Greenfield et al., 2006). N-terminal acetylation is of extreme importance for the affinity between the C- and N-terminus of two dimers, but also for the formation of the ternary complex with troponin T (Palm et al., 2003). This interaction is thought to be essential for cooperative regulation of tropomyosin and to enable prompt switching of tropomyosin binding along the whole thin filament following activation via Ca^{2+} binding to the troponin complex. Tropomyosin's orientation on actin is with the N-terminus towards the pointed end of the filament, therefore, where actin is capped by tropomodulin, it needs to contact tropomyosin to be effective (Kostyukova et al., 2007).

Tropomyosin has a repeated pattern of seven amino acids, heptapeptide, which is a characteristic of α-helical coiled coil molecules (Figure 1.7 B). Positions 'a' and 'd' of the heptad are usually small hydrophobic residues, which are important for the dimerisation. Positions 'e' and 'g' are usually charged residues which form inter-chain salt bridges between the monomers to stabilise the dimerisation of the molecule (Phillips et al., 1986). The coiled-coil structure of tropomyosin is not completely pure, irregular interruptions of hydrophobic interactions, Ala clusters in particular (Figure 1.7 A), allow the tropomyosin to bend and thus wrap around the actin filament for the length of seven actin monomers (Hitchcock-DeGregori and Singh, 2010). Individual interaction between tropomyosin and actin monomers are relatively weak (K_d 0.1-1 mM) as the majority of interactions are electrostatic (Lehman and Craig, 2008). What allows the strong interaction between the two filaments is the summation of many weak interactions between filamentous tropomyosin and actin. But having weak local interactions is necessary for muscle regulation: they allow the tropomyosin filament to shift between different positions on the actin filament, and consequently let myosin interact

with actin in a Ca^{2+}-regulated fashion (Li et al., 2011). The mechanism of shifting between positions on actin by tropomyosin has not yet been well described but a rolling model and a sliding model have been proposed (Lehman and Craig, 2008). Tropomyosin is overall semirigid, and this seems like an important property for the assembly on the actin filament and for its action as a cooperative unit in transducing the Ca^{2+}-regulation to the thin filaments (Li et al., 2010).

Figure 1.7: Tropomyosin coiled-coil, the heptapeptide repeat and the end-to-end polymerisation



A) Structure of striated muscle tropomyosin. The α-helical coiled coil in grey, in magenta the Ala clusters and in cyan the consensus residues in proposed actin binding sites. B) The heptapeptide repeat in a cross section of the molecule. In evidence are the bonding interactions between molecules: g-e salt bridges and d-a hydrophobic interactions. A and C are taken from Hitchcock-DeGregori and Singh (2010).

1.1.3.3 Troponin Complex

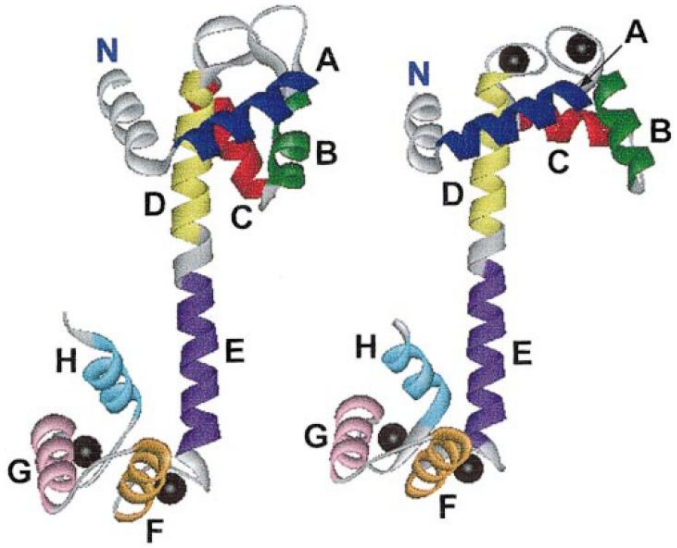
Troponin is the Ca^{2+}-sensitive protein, which regulates the switch between open and closed/blocked states of the thin filament. In cooperation with tropomyosin it allows myosin to bind actin only in certain conditions and therefore regulates muscle contraction. Troponin is composed of three subunits, troponin C (TnC), troponin I (TnI) and troponin T (TnT). Each of these subunits has multiple isoforms which are expressed with tissue specificity. A total of eight genes encoding for troponin subunits have been identified: 3 for TnI, 3 for TnT and 2

for TnC (Barton et al., 1997). Troponin C is the Ca^{2+} binding subunit. Troponin I is the inhibitory subunit. Troponin T is the backbone of the troponin complex, and also binds to tropomyosin.

1.1.3.4 Troponin C

Troponin C (TnC) has a molecular mass of around 18 kDa and is coded by *TNNC1*, which is expressed in slow-twitch skeletal and cardiac muscle, and *TNNC2*, expressed in fast skeletal muscle (Townsend et al., 1997a, Townsend et al., 1997b). TnC is attached to the thin filament through the interactions with TnI and TnT. It is dumb-bell shaped and composed of two globular regions for each of the termini, N and C, separated by a linker linear chain of hydrophobic amino acids (Herzberg and James, 1985). Each of these globular regions contains an EF-hand motif, which acts as the binding site for a divalent cation (either Ca^{2+} or Mg^{2+}) and is composed of an α-helix-loop-α-helix structure (Kawasaki et al., 1998). These sites are numbered from I-IV starting from the N-terminus. In skeletal muscle sites I & II are described as Ca^{2+} specific sites, as these selectively bind Ca^{2+} ($K_{Ca} \sim 10^5\ M^{-1}$) and can bind/unbind following its intracellular oscillations. Sites III & IV are just structural sites as binding of a divalent ion strengthens the interaction with TnT and TnI, these sites bind Ca^{2+} ions with even higher affinity ($K_{Ca} \sim 10^7\ M^{-1}$), but have enough affinity for Mg^{2+} to be constantly saturated in physiological conditions (Gordon et al., 2000). Site I of cardiac TnC cannot bind a divalent ion as several amino acid are replaced in the coordinating site (van Eerd and Takahashi, 1975). Site II ($K_{Ca} = 1.2 \times 10^6\ M^{-1}$) is the only site where Ca^{2+} can exchange under physiological conditions and in the time course of a heart beat (Kobayashi and Solaro, 2005).

Figure 1.8: Structure of troponin C



On the left, ribbon representation of the crystal structure of turkey TnC with Ca^{2+} (solid circles) bound to the 2 C-terminal binding sites. On the right, ribbon representation of rabbit skeletal muscle TnC with Ca^{2+} bound to all of the 4 binding sites. Notably the spatial arrangement of the helices changes at the N-terminus when Ca^{2+} is bound. (Gordon et al., 2000)

1.1.3.5 Troponin I

Troponin I (TnI) is the inhibitory subunit. The TnI subunit is responsible for the majority of actin binding and can bind to actin in the absence of the other troponin subunits, inhibiting acto-myosin ATPase activity (Greaser and Gergely, 1973). Inhibition is enhanced by tropomyosin.

There are three isoforms of TnI in humans, slow skeletal coded by the *TNNI1* gene, fast skeletal coded by the *TNNI2* gene and cardiac coded by the *TNNI3* gene. The three proteins are highly conserved between isoforms. The most important difference is an N-terminal extension of 31 amino acids in the cardiac isoform but not in the two skeletal isoforms. This contains two phosphorylation sites important for the response to the β-adrenergic stimulation of the heart (Barton et al., 1997).

The structure of cardiac TnI can be divided into 6 functional regions:

1) a N-terminal extension, unique to cardiac TnI.

2) the region binding to the C-lobe of TnC.

3) the region that binds to a C-terminal section of TnT forming half a coiled-coil.

4) the first actin-binding region (containing the inhibitory peptide).

5) a regulatory region.

6) the second actin-binding region at the C-terminus (Kobayashi and Solaro, 2005).

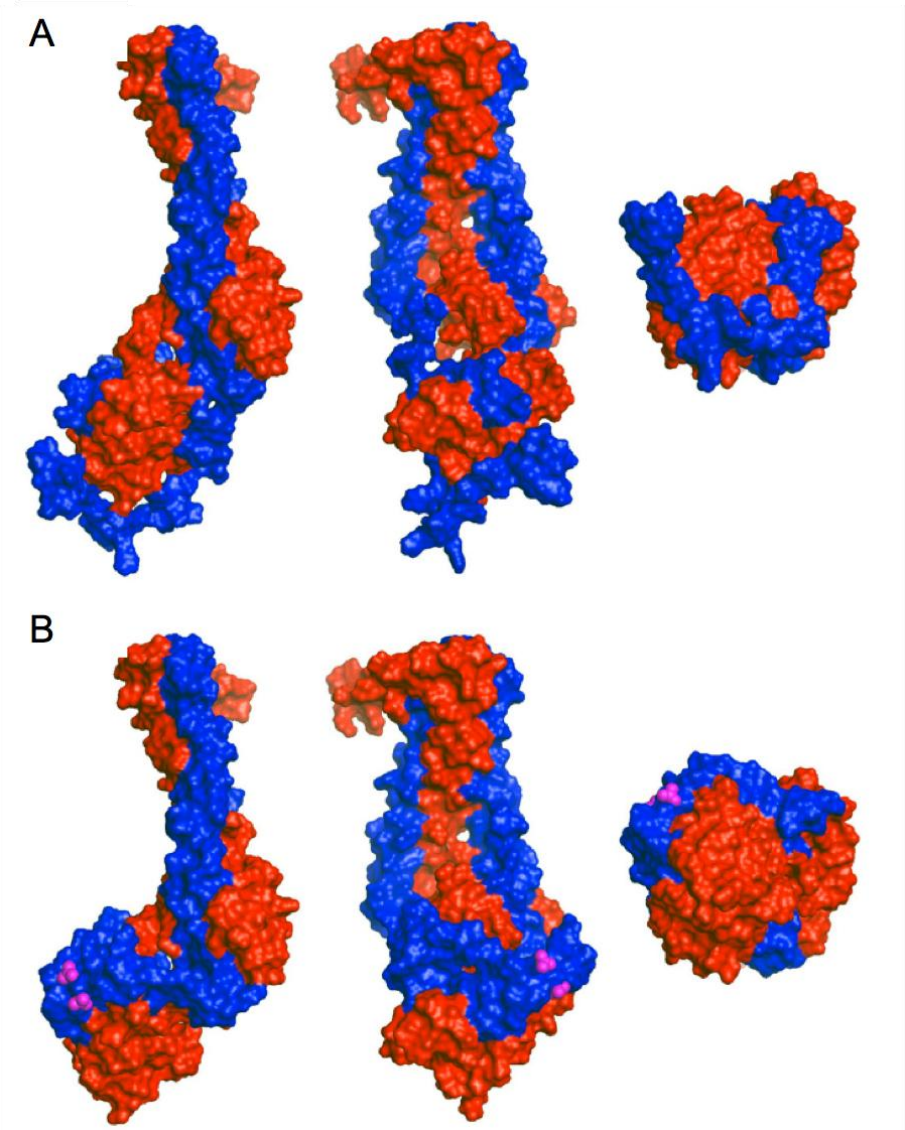
The first actin-binding region, which is highly conserved between isoforms, contains a sequence known as the inhibitory peptide, comprising residues 96-116 in rabbit fast skeletal muscle, which alone could inhibit myosin ATPase activity (Perry, 1999). TnI can alone inhibit the ATPase activity of myosin with a maximum inhibition at 1:1 ratio to actin. But in thin filaments the optimal ratio observed in the presence of tropomyosin is 7:1 actin:TnI, which indicates that tropomyosin facilitates a periodic distribution of troponin on actin and at the same time amplifies the regulatory property of TnI giving cooperativity to the system (Kobayashi and Solaro, 2005). Also the C-terminal actin binding region of TnI, seems to be important for the regulation of the thin filament (Takeda et al., 2003).

The N-terminal extension of cardiac TnI is composed of 31 amino acids (Sadayappan et al., 2008). The N-terminal comprises three regions; an acidic N-terminal region, an extended rigid polyproline helix and a C-terminal helix containing the bisphosphorylation site (Solaro et al., 2008). The bisphosphorylation site consists of two serine residues (22/23), these are the only residues phosphorylated by PKA in physiological conditions, which is under control of cAMP and ultimately β-adrenergic receptors on the cardiomyocyte surface (Ayaz-Guner et al., 2009, Messer et al., 2009). Phosphorylation of TnI by PKA decreases the sensitivity to Ca^{2+} of muscle contraction (Solaro et al., 2008). Phosphorylation of TnI changes the affinity of the TnC subunit for Ca^{2+} by increasing the rate of Ca^{2+} dissociation 2-3 fold (Robertson et al., 1982) (see 1.3.2.1). Other putative TnI phosphorylation sites are serine 31, 43/45 & 77,

threonine 145 and serine 149 (Layland et al., 2005, Solaro and van der Velden, 2010), but they do not get phosphorylated by PKA *in vivo* (Marston and Walker, 2009, Ayaz-Guner et al., 2009).

The N-terminal extension of cardiac TnI can assume two different conformations one when unphosphorylated and one with Ser 22/23 phosphorylated (Figure 1.9). When these residues are unphosphorylated the N-terminal extension can make contacts, through its basic residues between positions 20 and 32, with the acidic residues on the N-lobe of cardiac TnC increasing the overall Ca^{2+} affinity at site-II of TnC. The presence of the phosphate groups in positions 22/23 would destabilise these interactions moving the N-terminus extension of cardiac TnI away, an especially acidic N-terminal region which seems to be directly involved in the increased Ca^{2+} affinity (Howarth et al., 2007).

Figure 1.9: cTn core structure with and without Ser22/23 phosphorylation



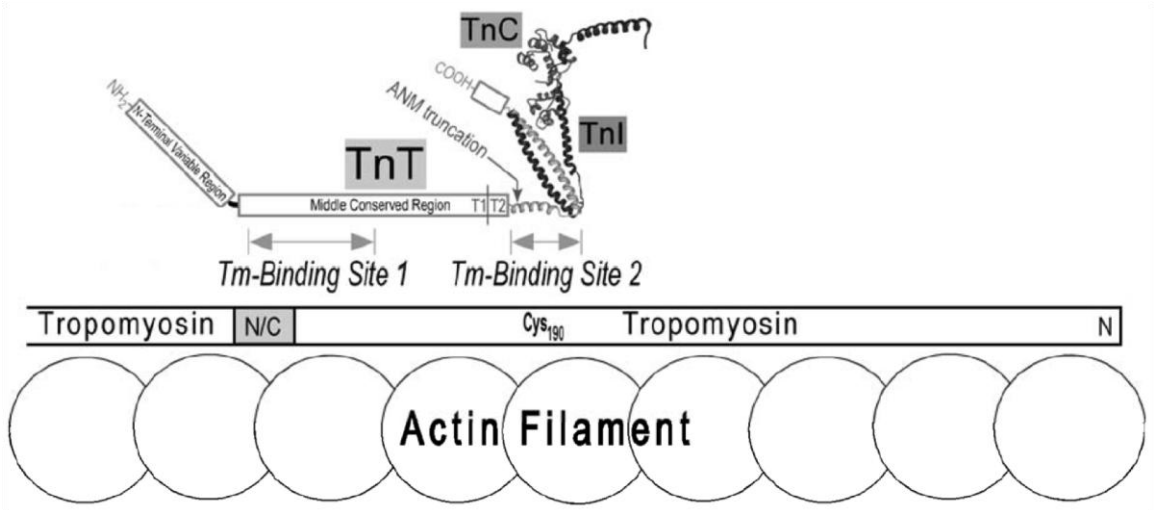
Three orthogonal views of the cardiac troponin core complex. cTnI (residues 1-161) is shown in blue, whereas cTnC and cTnT (residues 202-270) are in red. A) cTnI unphosphorylated, B) cTnI phosphorylated, with the phosphoryl groups at Ser22/23 in magenta. It is visible how the N-terminal regulatory domain shifts in a different position after the phosphorylation. (Howarth et al., 2007)

1.1.3.6 Troponin T

Troponin T (TnT) is crucial for the regulation of muscle contraction, it has been described as the glue that holds the regulatory system together (Tobacman, 1996). The cardiac isoform is encoded from the *TNNT2* gene, this gene produces many proteins by alternative splicing, which are expressed in different ratios in foetal and adult heart, but also in failing heart. The

main isoform in the adult human heart is a protein of 288 amino acids, weighing approximately 34 kDa named T3 by Anderson *et al.* (1991). None of the cardiac isoforms are present in adult skeletal muscle where the main isoform for the fast fibres is expressed from the *TNNT3* gene, has 258 amino acids and is 32 kDa due to a shorter tail domain at the N terminus. *TNNT1* codes for the slow skeletal muscle isoform (Barton et al., 1997). TnT is a rod shaped protein that, by interacting with tropomyosin, keeps the troponin complex docked to the thin filament (Figure 1.10). The structure of TnT is divided in two, also proteolytically separate, domains: the α-helical tail at the N-terminus, TnT-T1 (residues 1-158), and a globular head at the C-terminus, TnT-T2 (residues 159-258 fast skeletal TnT). Within the T1 region is an N-terminal acidic sequence of ~15 residues and a Tm binding domain located towards the C-terminus (Perry, 1998). T1 is associated with the overlap region between adjacent tropomyosin dimers in an antiparallel fashion and this association is not sensitive to $[Ca^{2+}]$. The T2 region interacts with the two other troponin subunits (TnC and TnI) and tropomyosin (Perry, 1998). The interaction between the T2 region and tropomyosin is sensitive to $[Ca^{2+}]$ (Takeda et al., 2003). Troponin T is thought to be responsible for the transduction of conformational changes in troponin C and I when Ca^{2+} binds the troponin core domain to the tropomyosin. This happens through its Ca^{2+} dependant binding to it at the T2 region and the Ca^{2+} independent binding of the T1 region over the tropomyosin head-to-tail joint (Li et al., 2004).

Figure 1.10: Troponin T and its interactions



Thin filament structure with schematic representation of actin and tropomyosin, TnT partially schematic and partially in ribbon representation in complex with TnI and TnC in the core domain. The division between T1 and T2 is represented by a vertical line. The two tropomyosin binding sites, one at the head-to-tail junction and one in the proximity of Cys190 are indicated. Adapted from Jin and Chong (2010).

1.1.4 Skeletal Muscle

What supports and moves the bones composing the skeleton of an organism is an intricate system of skeletal muscles. They make up fifty percent of the total body weight and there are 640 individually named skeletal muscles in the human body. The primary function of a skeletal muscle is to produce movement by contracting, but they also serve other functions like maintain the posture and body position, support soft tissues, guard body entrances and exits and maintain body temperature. Usually a skeletal muscle links two bones across its connecting joint made of collagen, known as a tendon, but it can also be indirectly connected. Skeletal muscles are organs mainly composed of myocytes, a very specialised kind of cell developed from the fusion of embryonic myoblasts. The structure of the myocyte will be described in detail below. Skeletal muscles are voluntary muscles, under the control of the somatic nervous system. A skeletal muscle contains not only myocytes, but also blood vessels, nerves and connective tissue.

1.1.4.1 The Skeletal Muscle and Myocyte Structure

A representation of the structure of the skeletal muscle is shown in Figure 1.11. The skeletal muscle is enclosed in the epimysium. This is a dense layer of collagen fibers connected to the deep fascia, and it separates the muscle from surrounding tissue and organs. Inside this envelope, the skeletal muscle is organised in fascicles, which are bundles of muscle fibers. The fascicles are separated between each other by the perimysium, which like the epimysium is mainly composed of collagen and elastic fibers, but contains also blood vessels, supplying nutrients and oxygen to the muscle or removing metabolic waste, and nerves to transmit the action potentials of the central nervous system and control contraction. Branches of these blood vessels and nerves will reach each fascicle together creating an extensive network. Each fascicle is then made of single muscle fibres. These are surrounded by a delicate connective tissue known as endomysium, which interconnects them. Finally, scattered between these single fibres are the satellite cells, which are embryonic stem cells necessary to repair the muscle in case of damage. Perimysium and endomysium blend into one another in the areas of contact and at each end of the muscle they will blend together with the epimysium as well to form the tendon (or aponeurosis). The tendon will extend further than the muscle to reach the bone where it terminates mixing into the bone matrix and therefore providing a strong dock to the muscle to pull the bone and generate movement.

Skeletal muscle fibers are single, multinucleated, and enormous cells. They may contain hundreds of nuclei inside the same cell membrane, called sarcolemma. This feature comes to be very important when the fast metabolic turnover of enzymes and structural proteins in the muscles is considered, thus having many scattered centres of protein production in the different districts speeds up the supply process. They have a small diameter but they span the length of the entire muscle. The fact of having such long and multinucleated cells is a

consequence of the fusion of myoblasts during development: each myoblast fused contributes with a nucleus.

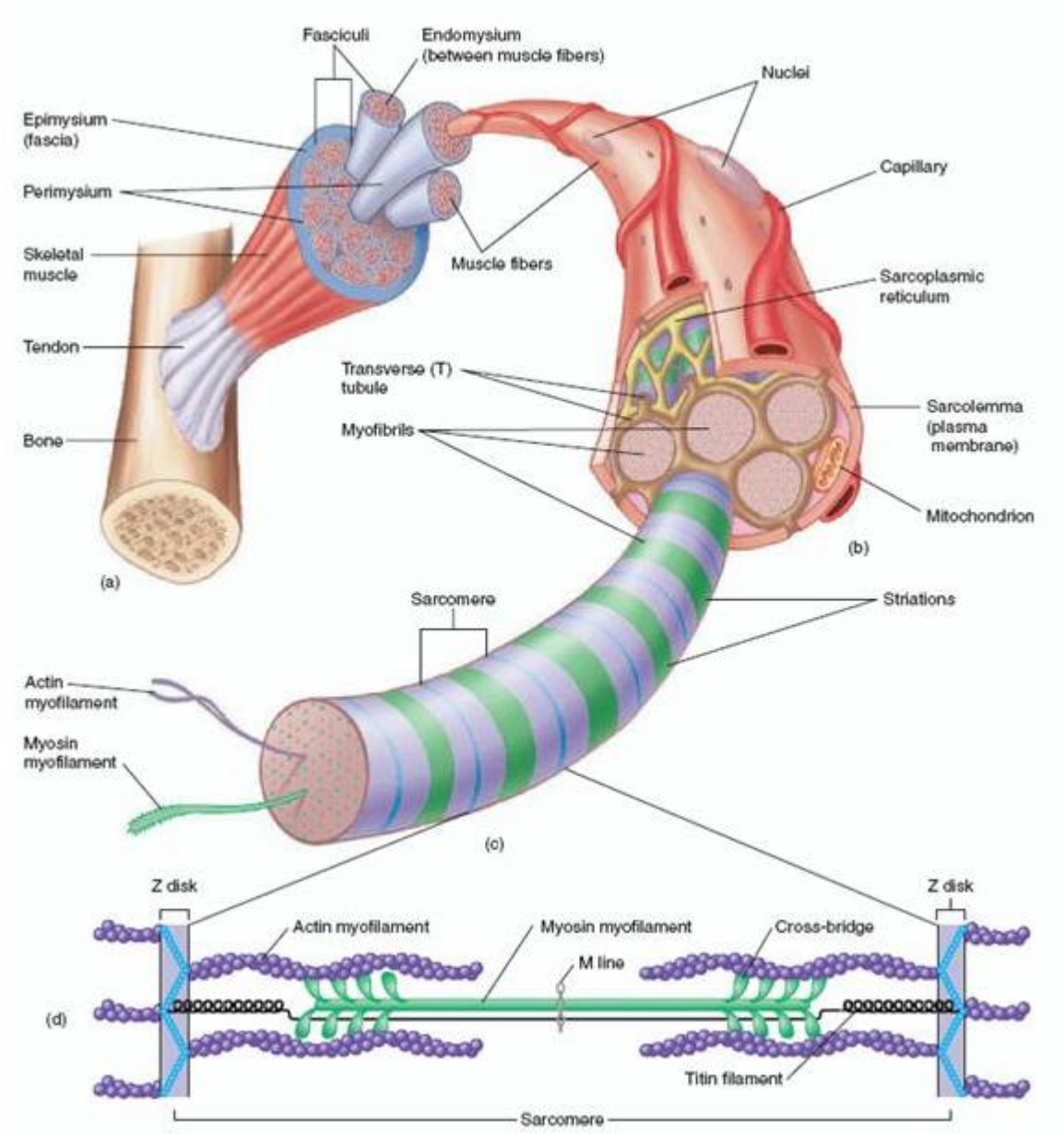
Inside the muscle fiber there are hundreds to thousands of myofibrils. These are cylindrical structures made of bundles of myofilaments: thin and thick filaments. These are responsible for the contraction of the muscle and are made of a series of contractile units called sarcomeres (see 1.1.1).

The sarcolemma surrounds the sarcoplasm (cytoplasm of a muscle fiber) and has structures called transverse tubules (T-tubules), which are contiguous to it and penetrate the sarcoplasm at right angles to the cell surface. These T-tubules are filled with extracellular fluid and have the same general properties of the sarcolemma, but are full of L-type Ca^{2+} channels which are essential to trigger muscle contraction as explained later (see 1.2.2). The T-tubules are the structures that allow the electrical impulses to travel inside the muscle fiber and therefore obtain fast activation. T-tubules surround the myofibrils in close proximity to the Z-discs of the sarcomeres.

Inside the sarcoplasm the main organelle is the sarcoplasmic reticulum, a muscle specialised version of the endoplasmic reticulum, which is the most important Ca^{2+} storage of the myocyte. The sarcoplasmic reticulum is associated with the T-tubules and also encircles a myofibril to form a tubular network around each myofibril. Where the sarcoplasmic reticulum interacts with the T-tubules it is organised in large terminal cisternae.

All along the muscle fibers are scattered a huge number of mitochondria and granules of glycogen to meet the energetic needs of the myocyte.

Figure 1.11: Structure of the skeletal muscle



Taken from http://www.shoppingtrolley.net/skeletal%20muscle.shtml

1.1.5 The Cardiovascular System and the Heart

The cardiovascular system is a necessary transport system for the delivery of oxygen and nutrients, hormones and heat to different districts of the body and at the same time the removal of carbon dioxide and excretory products. This system is composed of two major

circulatory systems: the pulmonary system, pumping blood from the right side of the heart to the lungs and finally back to the left side of the heart, and the systemic system, which pumps blood from the left side of the heart to the rest of the body, to end on the right side of the heart.

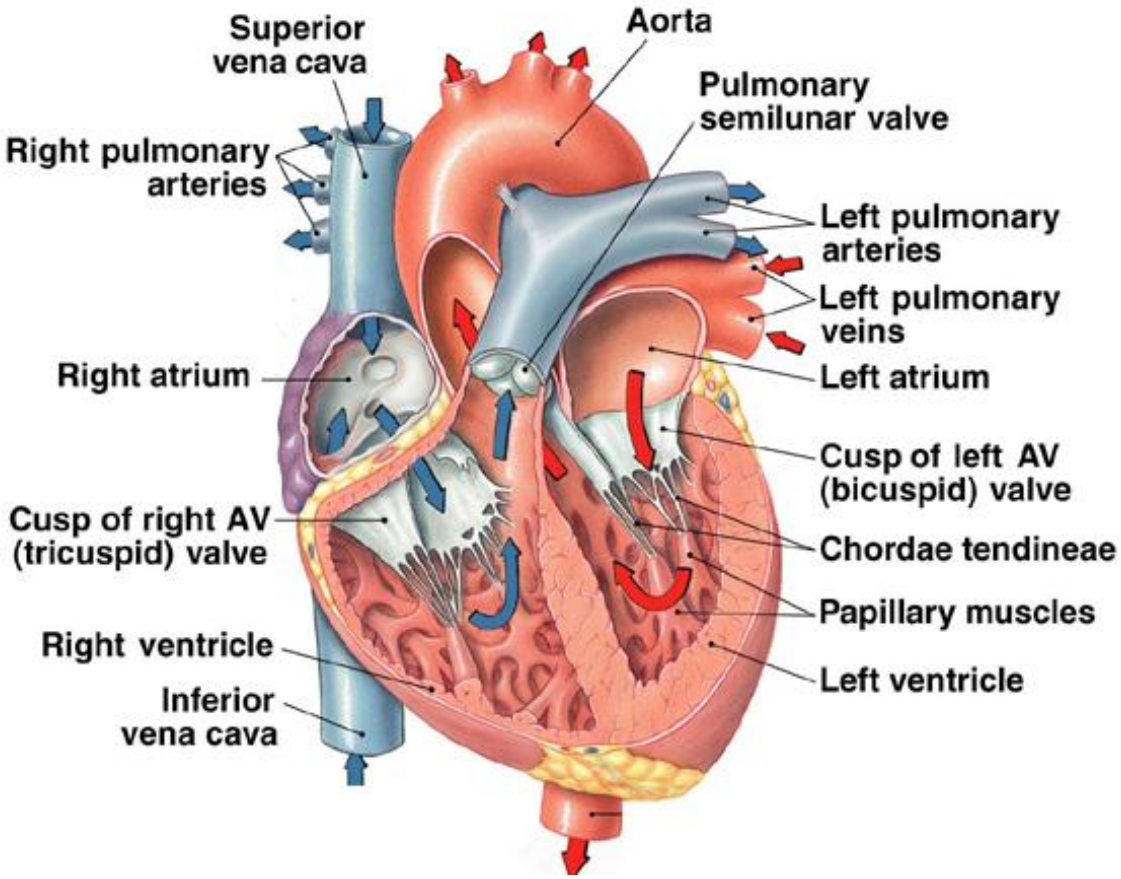
The first understanding of the heart and circulation was established by Harvey (1578-1657) who described the circulation of blood as a result of the pumping action of the heart. The heart is, in fact, an organ consisting of two muscular mechanical pumps, the right and left ventricles, which are filled from respective atria present on the same side of the heart, and responsible for respectively the pulmonary and systemic circulations.

The rate and force of its contraction and relaxation is regulated dynamically in response to the changing metabolic and circulatory needs of the body during different stages of development, exercise and disease.

1.1.5.1 The Heart Structure

The heart is divided by a partition, called septum, into two halves, each of which is divided into an upper chamber, atrium, and a lower chamber, ventricle. The chambers on each side are separated by valves, which direct the blood flow one way by preventing backflow. The tricuspid valve is on the right-hand side and the mitral is on the left-hand side. To avoid backflow to the left and right ventricles the semilunar valves are present respectively in the aorta and pulmonary artery. The anatomy of the heart is shown in Figure 1.12.

Figure 1.12: Anatomy of the heart



Taken from http://www.colorado.edu/intphys/Class/IPHY3430-200/image/14-7.jpg

The mass of the heart is mainly made up of cardiomyocytes, which are the specialised cells containing the contractile apparatus required for the contraction and therefore pumping of blood. But 70% of the total number of cells of the heart consists of fibroblasts, smooth muscle cells, epithelial and endothelial cells (Katz, 2006).

The heart is contained within the pericardial sac, which consists of an outer fibrous layer and the serous pericardium. The serous pericardium consists of two layers separated by the pericardial cavity, which contains a small amount of lubricating fluid. These two layers are the parietal layer, which is associated to the fibrous outer layer, and the visceral layer, which is part of the epicardium and is made of connective tissue covered by epithelium and protects

the external side of the heart. Inside the epicardium is the myocardium, the muscular layer producing the force by contraction. The cardiomyocytes are arranged in the myocardium in laminars or fibres composed of four to six myocytes and separated from one another mainly by collagen (LeGrice et al., 1995). Finally the myocardium is separated from the inner space of the chambers by the endocardium, a layer made of epithelial tissue and connective tissue. It is continuous with the inner lining of the blood vessels and covers the whole of the cavities including the heart valves.

1.1.5.2 The Cardiac Cycle

The cardiac cycle is the sequence of events that occurs when the heart beats and by which it pumps blood through the peripheral circulation. It basically consists of two phases: systole, which concerns the contraction of the ventricles, and diastole, which concerns the relaxation of the ventricles. The cardiac cycle can, then, be divided in four main stages:

A) Ventricular filling

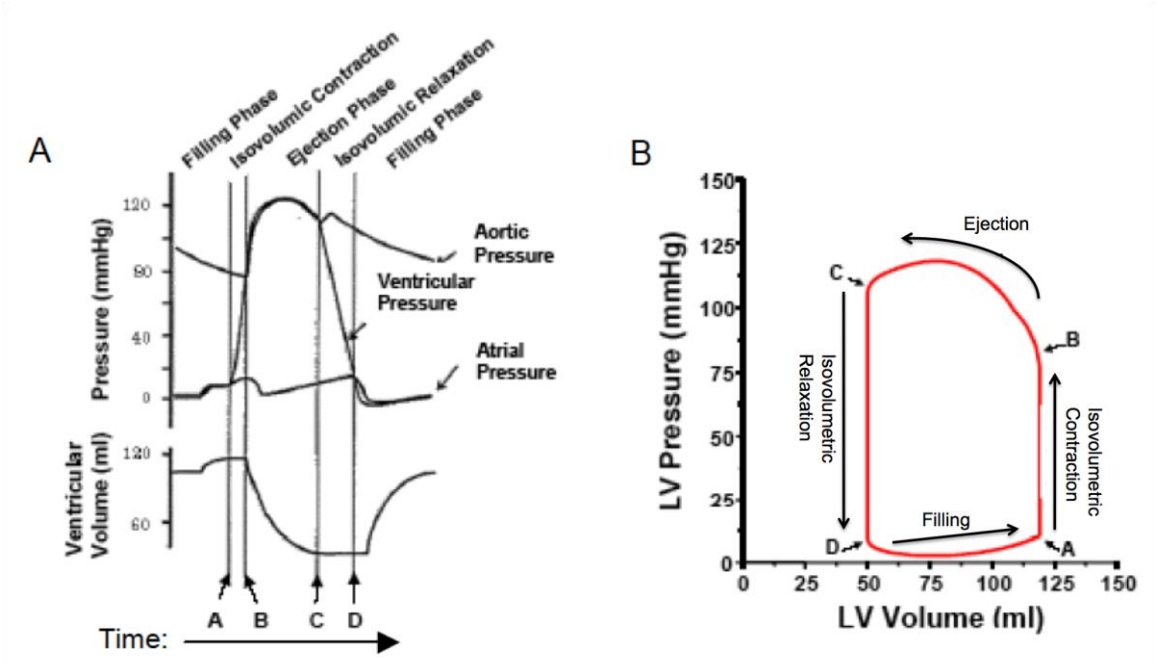
B) Isovolumetric contraction

C) Ejection

D) Isovolumetric relaxation

As shown in Figure 1.13, stage A is at the end of the diastole and represents the end-diastolic pressure and maximum end-diastolic volume. When the ventricle begins to contract (A-B), the left ventricular pressure (LVP) increases, but the left ventricular volume (LVV) remains the same. When the LVP exceeds the aortic diastolic pressure, the ejection phase (C) takes place. The LVV is reduced at roughly constant LVP. Pressure then decreases as the ventricle begins to relax. Stage D is reached and when the LVP is smaller than the left atrial pressure (LAP) the valve between chambers will open, allowing the blood to fill the ventricle once again.

Figure 1.13: Pressure and volume changes during the cardiac cycle



A) Plot of left ventricular volume (LVV). left ventricular pressure (LVP), left atrial pressure (LAP) and aortic pressure as a function of time. B) A 'pressure-volume' loop for one cardiac cycle, the cycle proceeds in an anti-clockwise direction. (Lionel, 2005)

1.1.5.3 The Cardiac Myocyte

Cardiomyocytes have a similar striated pattern to skeletal muscle cells but are smaller, irregularly branched and roughly cylindrical measuring 10-20 μm wide by 50-150 μm long (Kocica et al., 2006). Cardiomyocytes are mechanically and electrically associated with their neighbouring cells through intercalated discs, but also mechanically to the extracellular matrix. Like all cells, there is a potential difference across the plasma membrane of a cardiomyocyte. The membrane potential at rest is around -80 mV to -90 mV. The triggered opening of specific membrane ion channels cause this membrane potential to depolarise. The intercalated disc is an area of association of the plasma membranes from two adjacent cardiomyocytes, these contain two forms of cell junctions. Gap junctions allow the passing of an electrical or chemical signal between adjoining cells and thus facilitate the synchronous

spread of depolarisation through the heart. Desmosomes link the intermediate filaments of bordering cells bolting them together. Each individual myocyte makes contact with approximately 10 other myocytes. Typically myofibrils comprise 47% and mitochondria 36% of the total cell volume of a cardiomyocyte, the remainder consists of cytosol 11.5%, sarcoplasmic reticulum 3.5% and nucleus 2% (Page, 1978). Mitochondria supply the energy for contraction to the myofibrils and to the ion pumps for the maintenance of the ion gradients.

Each myofibril is roughly cylindrical (2-3 μm in diameter), stretches the length of the cell and is anchored at each end of the cell in a fascia adherens junction.

1.2 Muscle Contraction

1.2.1 Action Potential and Propagation of the Electric Impulse in Skeletal and Cardiac Muscle

Both skeletal and cardiac muscle experience a depolarisation of the membrane potential following an action potential from -85 to +20 mV, which activates the voltage gated ion channels and lets Ca^{2+} ions to cross the membrane and trigger a process that will ultimately lead to muscle contraction.

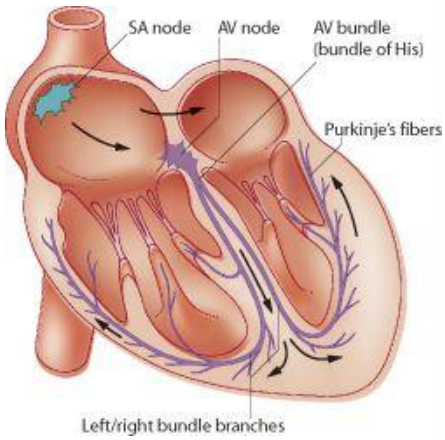
For skeletal muscle cells, the action potential comes from a motor neuron's axon innervating the muscle, reaching a neuromuscular junction midway along the muscle fiber. Here the action potential will get to the synaptic terminal and it will trigger the release of the neurotransmitter acetylcholine from vesicles stored there into the synaptic cleft. Here the acetylcholine will bind on the receptors placed on the sarcolemma's side of the cleft, known as the motor end plate, which will cause the influx of Na^{+} ions with consequent

depolarisation of the sarcolemma. This new action potential will propagate all along the fiber and inside it through the T-tubules.

The initial stimulus for the heart to contract, arises at the cardiac pacemaker, the sinoatrial (SA) node at the top of the right atrium. The action potential originated by constantly and spontaneously depolarising cells in this region spreads to the atrioventricular (AV) node along fibrous tissue (annulus fibrosus that electrically isolates the atria from the ventricles) with a small delay that allows the atria to contract first and fill the ventricles with blood. The depolarisation through the atrioventricular bundle, that goes across the annulus fibrosus, will eventually reach the Purkinje fibres, which facilitate ventricular contraction by distributing the depolarisation over the ventricles. A diagram showing the direction of the depolarising wave is shown in Figure 1.14.

Sympathetic and parasympathetic nervous systems control the rate and frequency of cardiac contraction through respectively catecholamines (adrenalin, noradrenalin) to upregulate heart beat, and acetylcholine to slow the heart rate through the pathway of the muscarinic receptors.

Figure 1.14: Diagram showing the direction of depolarisation in the heart



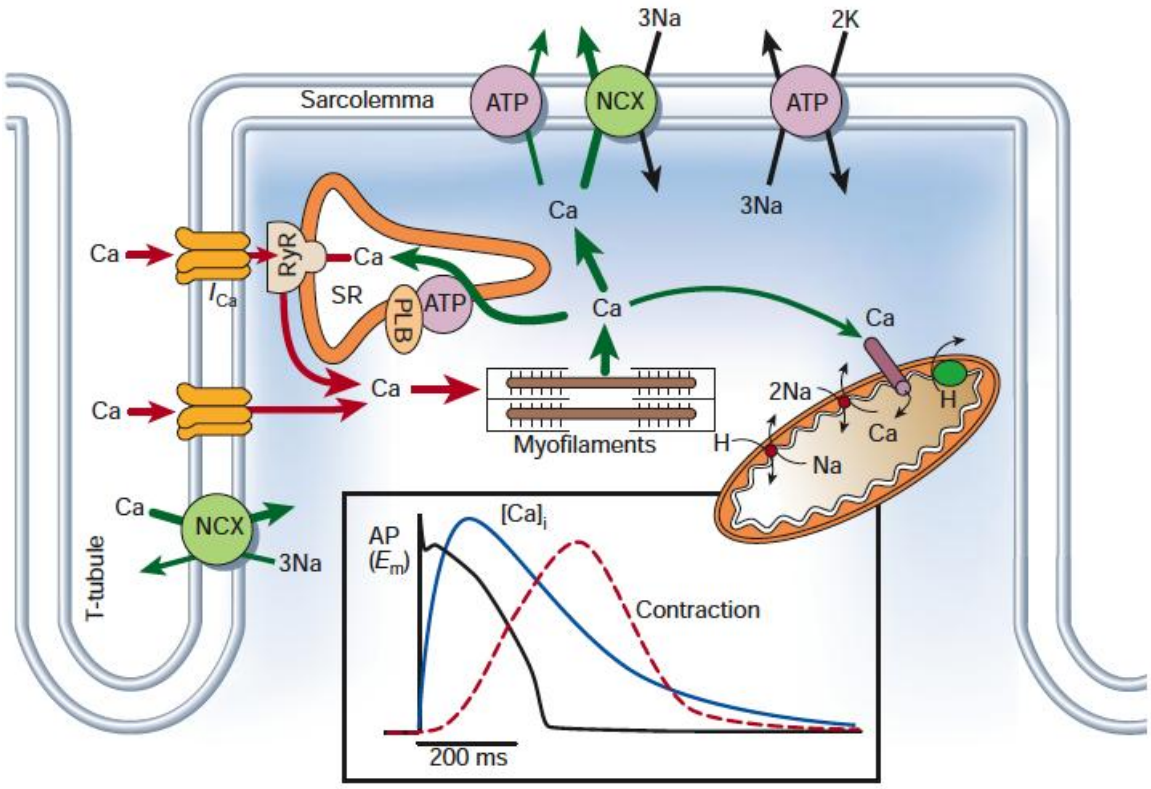
(Cunningham, 2002)

1.2.2 Excitation-Contraction Coupling

The general molecular mechanism by which the excitation of the myocyte is coupled to the muscle contraction has been shown to be very similar between skeletal and cardiac muscle, although the single proteins taking part in the process may change isoforms between muscle types or developmental stage and therefore give different kinetics to the process.

An array of T-tubules carries the wave of depolarisation from the surface into the centre of the myocytes, where it causes L-type Ca^{2+} channels to open and in consequence a small influx of extracellular Ca^{2+} into the cell. This will trigger a large release of Ca^{2+} from the sarcoplasmic reticulum, via the ryanodine receptor, through a process called Ca^{2+} induced Ca^{2+} release. Key for this process to take place successfully is the proximity of the T-tubule and sarcoplasmic reticulum terminal cisternae, which allows the co-localisation of the two types of Ca^{2+}-channels (20-25 L-type Ca^{2+} channels and over 100 ryanodine receptors) and therefore a large release of Ca^{2+}. This will in turn trigger the contraction in the cardiomyocytes. The transduction of the electrical signal to mechanical work is described as excitation-contraction coupling. L-type Ca^{2+}-channels are negatively regulated by the binding of Ca^{2+} to calmodulin, which in turn binds a regulatory region of the channel closing it.

Figure 1.15: Ca^{2+} flux in the cardiac myocyte



Ca^{2+} enters the cytosol via the sodium-calcium exchanger, the L-type Ca^{2+}-channels and mostly the ryanodine receptor. It is then mostly taken back up into the sarcoplasmic reticulum through the SERCA ATPase, controlled by phospholamban, but it is also removed by sarcolemmal pumps and the mitochondrial Ca^{2+} uniport. The diagram also show the time course of the E-C coupling. (Bers, 2002)

Of extreme importance to this process is the movement of Ca^{2+} ions (Figure 1.15). The influx and efflux of Ca^{2+} ions into the sarcomeric cytosol controls the duration and force produced by the myocyte. Most of the sarcoplasmic Ca^{2+} is taken back into the same storage that released it earlier, the sarcoplasmic reticulum, and there it stays until the next cycle starts. The major player in the reuptake is a Ca^{2+} pump called SERCA (Sarco-Endoplasmic Reticulum Ca^{2+} ATPase). Different isoforms of SERCA are expressed in different ratios for different types of muscle. SERCA is located on protrusions of the sarcoplasmic reticulum, which follow the length of the myofibril away from the terminal cisternae located at the Z-disc. In this way the reuptake of Ca^{2+} can be faster from the sarcomere following contraction.

Troponin is the Ca^{2+}-binding element of the thin filaments that switches on the contractile apparatus and regulates it, sensing the differences in Ca^{2+}-concentration. As a consequence, any change or modification to the ability of troponin to sense the cytosolic [Ca^{2+}] are important and may be involved in the development of contractile dysfunction.

1.2.3 The Sliding Filament Theory and the Cross-Bridge Cycle

In the sarcomere the thick and thin filaments are arranged in parallel and interdigitated. When muscle shortens thick and thin filaments slide past each other, they do not modify their own length but the total length of the sarcomere changes. It has been demonstrated that the production of force is proportional to the amount of filament overlap. This is because the number of myosin heads that can form generating cross-bridges depends upon the degree of filament overlap.

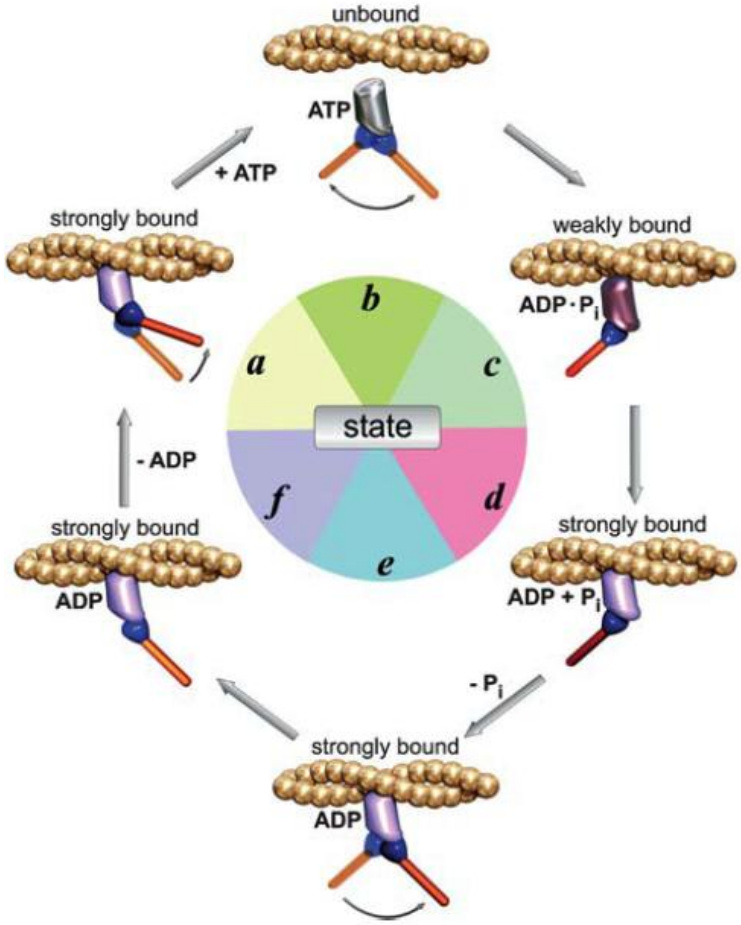
Myosin is a motor protein that uses energy liberated by ATP hydrolysis to power muscle contraction. The myosin ATPase activity is activated by actin and inhibited by ADP and Pi. The theory of the cross bridge cycle (Huxley, 1957) states that muscle kinetics can be explained by the sum of individual force generators. Work completed by Lymn and Taylor elucidated how myosin, as an enzyme, uses ATP hydrolysis to power the cross bridge cycle, summarised as the Lymn-Taylor cycle (Lymn and Taylor, 1971). Throughout the cycle the myosin head can exist in two conformations only described as the 90° (up) and 45° (down) corresponding to the two positions of the lever arm. By convention, the cycle begins with the cross-bridge in rigor, the head is in the down position bound to the actin molecule and in the absence of a bound ATP molecule. During the next step a nucleotide binds and this induces a fast dissociation of actin and causes a conformational change resulting in the myosin head moving from the down to the up conformation. The third step sees the bound nucleotide getting hydrolysed. After which the myosin.ADP.Pi will rebind to actin. The binding of actin

allows the release of the products of hydrolysis (Pi and ADP). As Pi is released the power stroke occurs where the myosin head (bound to the actin) returns to its original down conformation, thus moving (pulling) the actin along by ~10 nm in this process (Spudich, 2001, Holmes, 1997). The actomyosin will then release the ADP and finish the cycle in the rigor state once again. The cross-bridge cycle is represented in Figure 1.16.

These cross-bridges are the independent force generating elements and the total force produced by a muscle is a function of the number of cross-bridges able to interact with the thin filaments. The speed of shortening reflects the average cross-bridge cycling rate.

The isometric force produced by a muscle depends upon the sarcomere length. It is optimal when the overlap is such that all the myosin cross-bridges can interact with actin (usually between 2 and 2.25 μm). If longer or shorter than the optimum length range, the tension developed during contraction will decrease (Sonnenblick and Skelton, 1974). In the heart, the sarcomere length is generally shorter than the skeletal average. Preload stretches the sarcomere to 2.1 μm at the end of diastole and it contracts to around 1.6 μm during systole. The increase in stretch during diastole produces an increase in the force generated in the next contraction. This is responsible in part for Starling's law of the heart, which states that ventricular stroke volume varies directly with changes in end-diastolic ventricular volume. In dilated cardiomyopathy (DCM), sarcomeres may be stretched more than 2-3 μm and this could cause a reduced generation of force when contracting (Sugden, 2003).

Figure 1.16: Scheme for the actomyosin cross-bridge cycle



Mechanochemical scheme for the actomyosin cross-bridge cycle. The state 'a' represents the rigor complex with no nucleotide attached. When ATP binds (b), it makes the complex dissociate rapidly and the lever arm to change position (up). ATP gets hydrolysed and the complex binds actin again. The interaction is weak at the beginning (c) and then gets stronger (d). This induces the dissociation of P_i and the power stroke (e), which brings the lever arm in the down position. When the tail swing is completed (f) ADP can be released to return in the rigor state (a) and start a new cycle. (Geeves et al., 2005)

1.3 Muscle Regulation

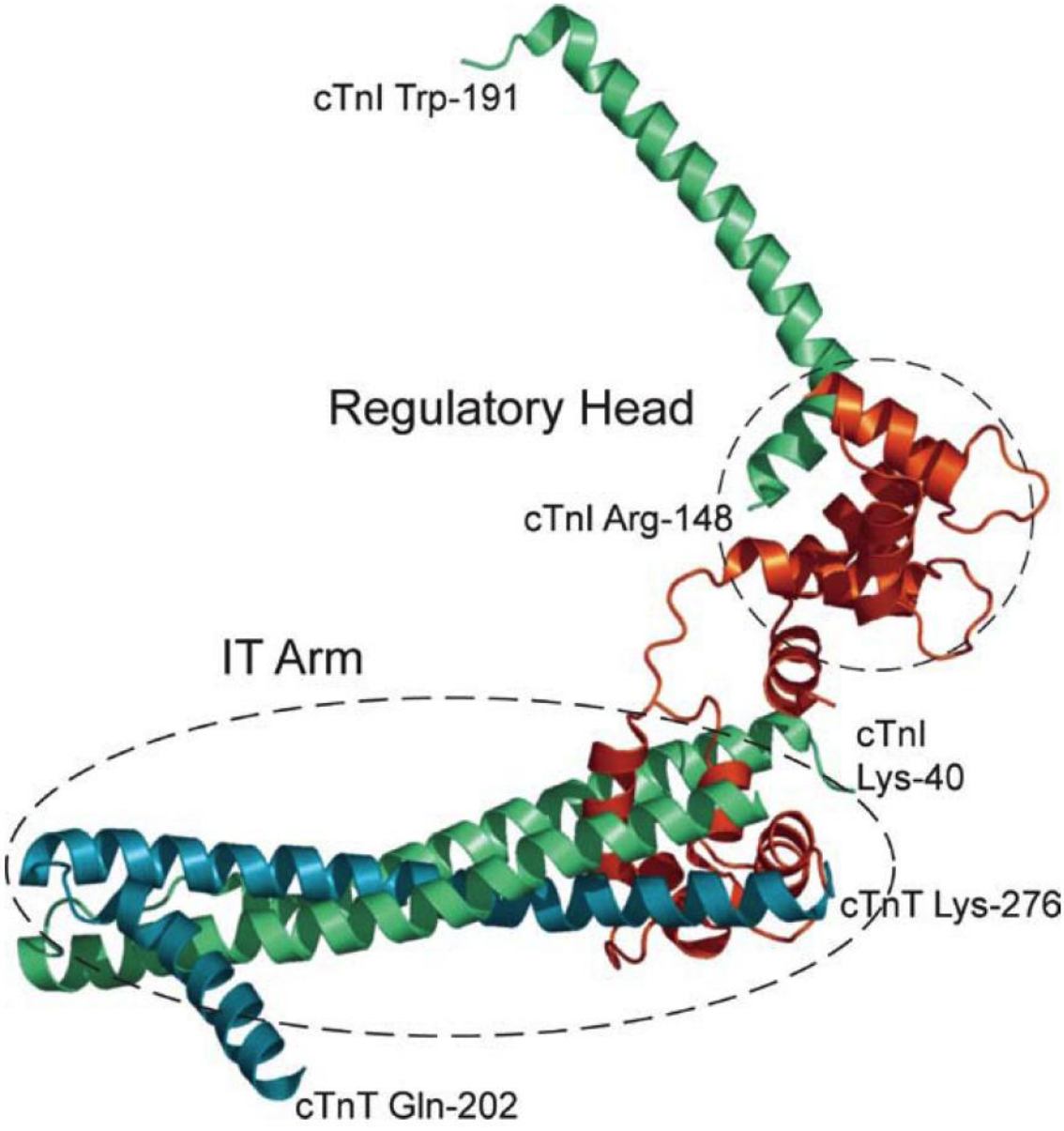
1.3.1 The Thin Filament Switch

The troponin complex represents the regulatory switch of the thin filaments between different activation/inactivation states. The 3D structures of the complex in all the different states and including all of the different regions of the ternary complex are yet to be obtained and the mechanism of switch is not fully understood, but in the last two decades several experiments have been able to give valuable information to build a model.

1.3.1.1 Troponin Complex Structure

The troponin complex can be divided in two regions: the Tn core domain (Figure 1.17) and the extended structure of TnT-T1, which binds tropomyosin laterally at the joint between two dimers in the polymer (Perry, 1998). The core domain is structured with the bilobed TnC attached to a multi-stranded W-shaped TnI-TnT arm (IT arm), which does not seem to modify its shape in relation to Ca^{2+} oscillations, and a C-terminal regulatory sequence of TnI, which could modify its orientation depending on the presence of Ca^{2+} (Vinogradova et al., 2005). The IT arm seems to make contacts with tropomyosin through a second binding site on TnT-T2 (Perry, 1998).

Figure 1.17: The core domain of the troponin complex

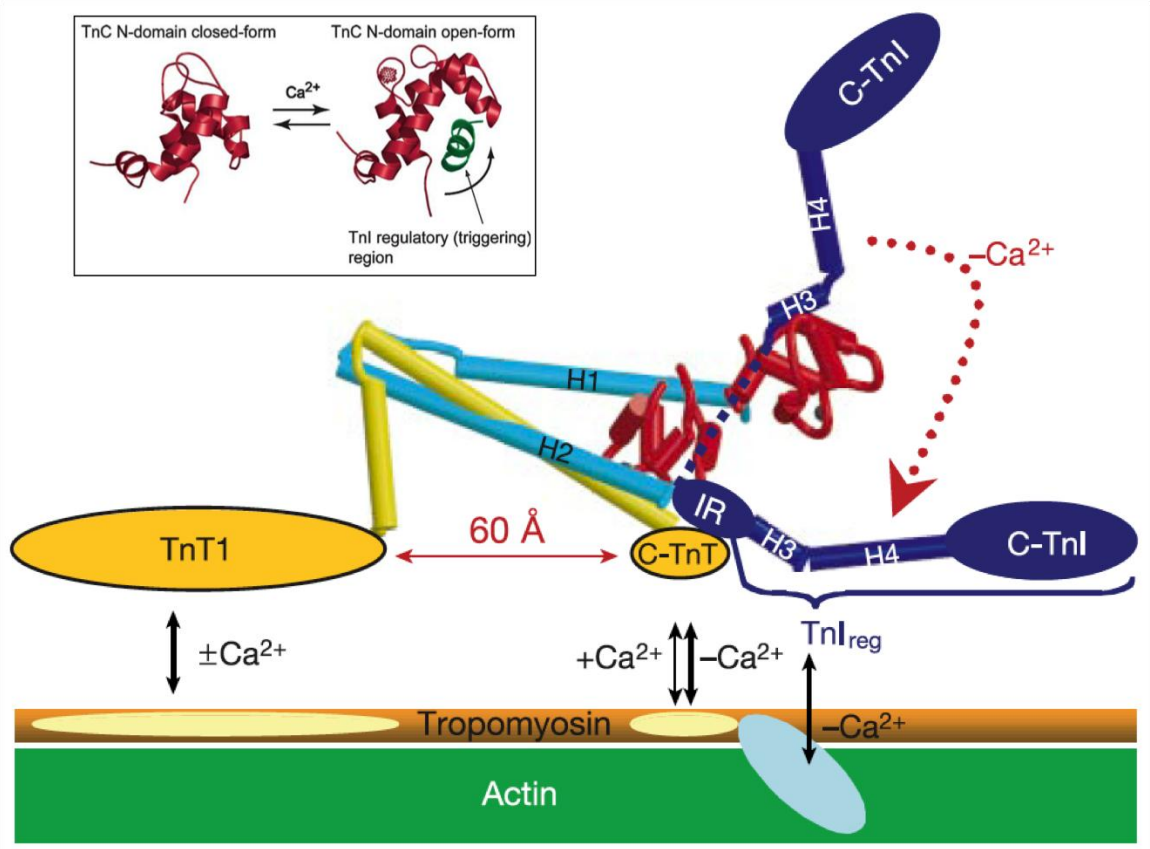


Ribbon model of the crystal structure of the troponin complex when Ca^{2+}-saturated. TnC in orange; TnT in blue; TnI in green. (Kobayashi and Solaro, 2005)

The proposed activation model wants the C-terminal regulatory sequence of TnI, which is composed of two actin binding sites separated by a "switch segment", to be able to bind actin in the absence of Ca^{2+}, thus blocking the access to the actin binding sites to myosin. When

Ca^{2+} binds to the N-terminal lobe of TnC, these EF-hands will open a hydrophobic cavity where the switch segment can bind (Figure 1.18), removing the block from the actin surface (Mercier et al., 2003). When this happens it seems also that the conformational changes induced by Ca^{2+} binding get transduced through TnT to tropomyosin, triggering its movement to a different sterical position on the actin's groove (see 1.3.1.2), and giving cooperativity to the system (Xu et al., 1999, Maytum et al., 1999).

Figure 1.18: The proposed thin filament switch



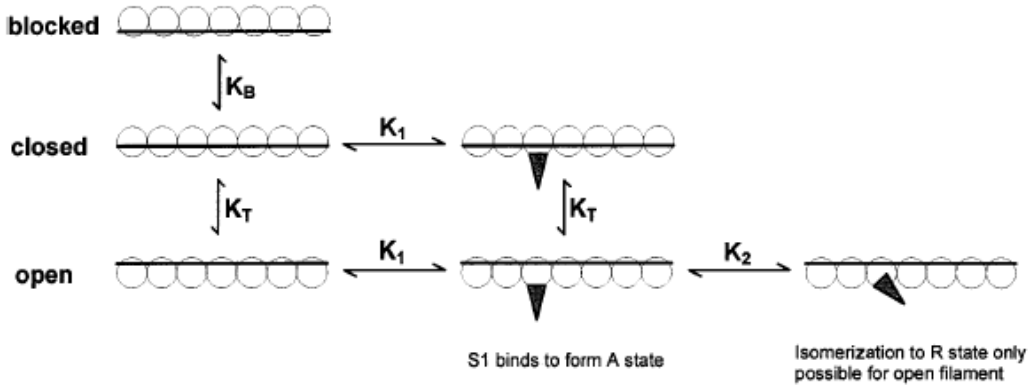
In the proposed model of thin filament activation, TnI acts as the thin filament's switch. Its regulatory C-terminal region can either interact directly with actin, inhibiting the cross-bridge cycle, or interact with TnC when Ca^{2+} binds it. In the detail square is represented the structure of the N-lobe of TnC with and without Ca^{2+} bound. When Ca^{2+} binds it triggers a conformational change that opens a hydrophobic pocket on TnC where the regulatory region of TnI can bind (in green). (Takeda et al., 2003, Kobayashi and Solaro, 2005)

1.3.1.2 The Three State Model

In the early 80s it was hypothesized that the regulation exerted by tropomyosin and troponin on the thin filaments, could be described by a two-state model of regulation (Hill et al., 1980, Hill et al., 1983). In this model, the thin filament equilibrium was oscillating between an open and a closed position, with Ca^{2+} and myosin S-1 as the factors influencing this equilibrium towards the open state.

Later in the 90s the model was redesigned on evidence given by mathematical modelling and kinetic studies, further proved by structural data, which proposed a three state model, adding the 'blocked' state to the possible conformations (McKillop and Geeves, 1993, Vibert et al., 1997, Maytum et al., 1999, Lehman et al., 2000).

Figure 1.19: The three state model of regulation



One structural unit of thin filaments is represented by 7 circles (actin) and one line (tropomyosin). Myosin is represented by the triangle. (Maytum et al., 1999)

This model describes the dynamic equilibrium between the 3 states this way (Figure 1.19):

1) The 3 states can be occupied only when both troponin and tropomyosin are present. Plain actin would always be in an 'open' state, and actin-tropomyosin would present only two states, 'open' and 'closed'.

2) Myosin S-1 can bind the thin filament in two different ways, weak (attached, A-state) when it binds the filament in the 'closed' state, or strong (rigor, R-state) when it isomerises with the thin filament in the 'open' state. The R-state is the only one in which the ATPase activity of myosin S-1 can work.

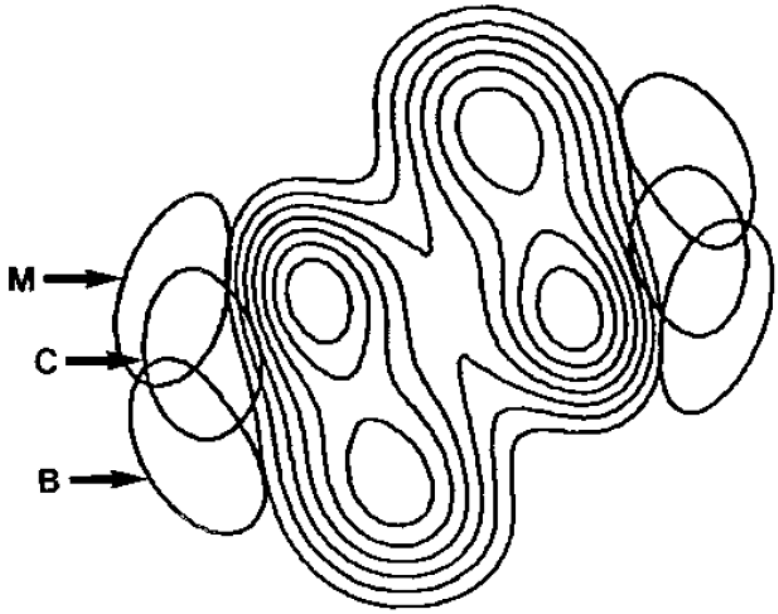
3) The 'blocked' state is the most populated in the absence of Ca^{2+}, which indeed blocks the cross-bridge cycle. This is achieved through the inhibiting action of Tn and in particular TnI's direct binding to actin and tropomyosin's constrained position given by troponin (see 1.3.1.1). Myosin S-1 cannot possibly bind in this state.

4) The presence of Ca^{2+} releases tropomyosin and TnI from the inhibiting positions, thus the thin filament is now able to change the equilibrium towards 'closed' and 'open' states. In both of these myosin S-1 can bind weakly (K_1), but its binding shifts the equilibrium towards the 'open' state (or 'myosin induced' state, regulated by K_T). In these conditions it can isomerise to the R-state (K_2) and allow the cross-bridge cycle to begin.

Evidence also suggests that the cooperative unit is larger than 1, which would mean 7 actin monomers, for each activated troponin. This means that the regulation is transmitted through the head-to-tail interactions of tropomyosin to other regulatory units on the side.

When these premises are applied to physiology of the muscle, where the concentration of myosin S-1 is fixed and high, the equilibrium in the presence of Ca^{2+} will be shifted towards the open state, allowing contraction. The three positions occupied by tropomyosin on the actin filament are represented in Figure 1.20.

Figure 1.20: The three positions assumed by tropomyosin on the actin filaments corresponding to the three different states



The relative positions of tropomyosin on the actin filament in the three different activation states. B: blocked; C: closed; M: myosin induced (open). (Lehman et al., 2000)

1.3.2 β-adrenergic Regulation of the Cardiac Output

While in skeletal muscles the modulation of contraction mainly relies on the strength and duration of the nerve impulses from the motor neurones at the neuromuscular junction, the cardiac muscle, which is controlled by the autonomous pacemaker activity, can be modulated by the sympathetic nervous system, through the release of adrenalin and noradrenalin.

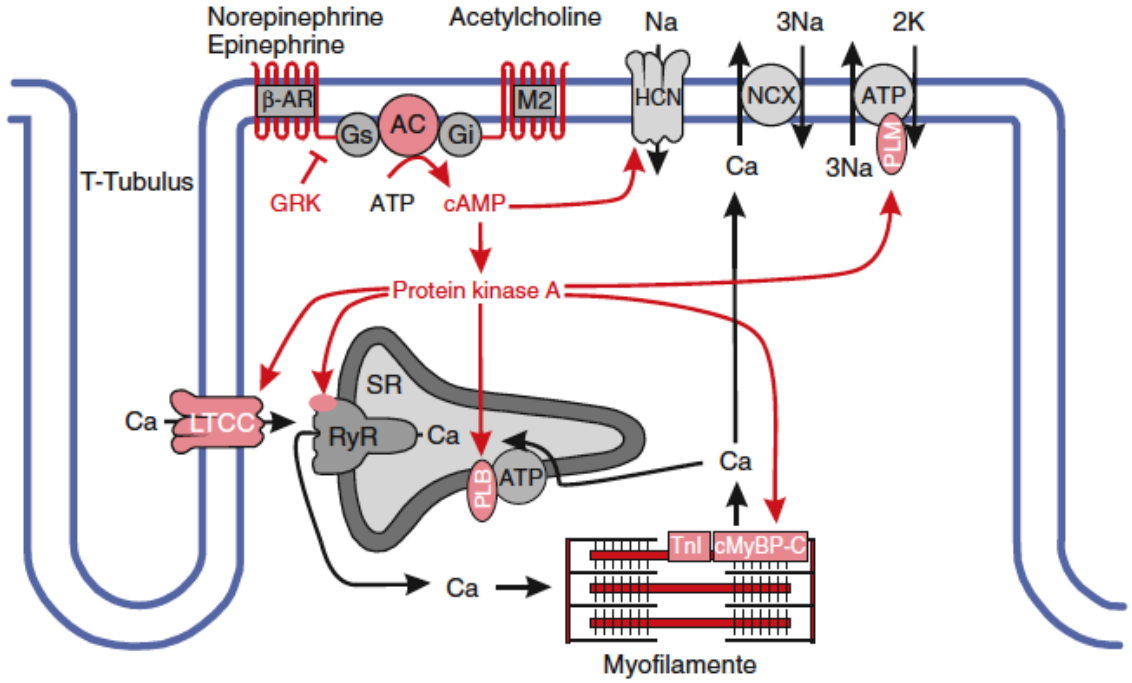
Cardiac output is defined as the amount of blood pumped out of the left ventricle in a given time. This might need to be modulated during the life of an adult human to satisfy the demand of blood requested by different activities.

From the resting condition, the heart can increase the beat-rate (chronotropy), the strength with which it pumps (inotropy) and the rate at which the heart relaxes (lusitropy).

The inotropic pathway is triggered by the hormone adrenaline and the neurotransmitter noradrenaline, which are secreted respectively by the adrenal glands in the bloodstream and

by the post-ganglionic synapses of the sympathetic nervous system. Both of these bind to β-adrenergic receptors (G-protein coupled receptors), present in the plasma membrane of cardiomyocytes, by stimulating its Gsα subunit to associate and activate the membrane associated enzyme adenyl cyclase. Activated adenyl cyclase catalyses the conversion of ATP into cyclic-AMP (cAMP). cAMP can bind and activate a number of targets including protein kinase A (PKA), which, in turn, phosphorylates a number of targets obtaining increased contraction and relaxation (Figure 1.21). The phosphorylated targets include the TnI subunit of troponin, phospholamban (PLB), myosin binding protein C (MyBP-C), L-type Ca^{2+}-channel and the ryanodine receptor (El-Armouche and Eschenhagen, 2009). PLB is a protein that binds the Ca^{2+} pump SERCA on the sarcoplasmic reticulum when unphosphorylated preventing ATPase activity and Ca^{2+} translocation. When Ca^{2+} concentrations increase however, Ca^{2+} binding to SERCA squeezes the PLB out of its binding site and inhibition is terminated (Toyoshima et al., 2003). Phosphorylation of PLB by PKA promotes the formation of homopentamers of dissociated PLB, these pentamers are no longer able to bind and therefore inhibit SERCA ATPase which will pump Ca^{2+} out of the cytosol faster (MacLennan and Kranias, 2003). MyBP-C phosphorylation would dissociate it from the myosin head allowing its incorporation into the contractile cycle (Flashman et al., 2004). PKA is believed to increase the open probability of ryanodine receptors (Bers, 2002). The effect of phosphorylation of TnI results in a decrease of TnC Ca^{2+}-sensitivity and therefore a faster kinetic of dissociation of Ca^{2+} from the thin filaments and faster relaxation. Since this effect is of key importance for this thesis, it will be discussed in detail below. Additionally PKA affects genes involved in energy metabolism and can increase the production of ATP. The increased Ca^{2+} release and faster kinetics cause an increase in the rate and magnitude of force generation and relaxation by the contractile apparatus.

Figure 1.21: β-adrenergic signalling pathway



Following β-adrenergic stimulation of the heart, PKA gets activated and phosphorylates a number of target proteins to obtain inotropy and lusitropy. Phosphorylation of proteins involved in the influx of Ca^{2+} like L-type Ca^{2+} channel and ryanodine receptor will obtain inotropy, whereas phosphorylation of cTnI on Ser22/23 will increase the rate of dissociation of Ca^{2+} from troponin, obtaining lusitropy. In the picture the phosphorylation targets are coloured in pink. (El-Armouche and Eschenhagen, 2009)

1.3.2.1 Phosphorylation of Cardiac Troponin I by PKA

Phosphorylation of cardiac troponin I occurs at residues Ser 22/23 (Metzger and Westfall, 2004, Solaro and Rarick, 1998), inside a 31 amino acid N-terminal domain absent in any other isoform (Sadayappan et al., 2008). A number of studies investigated the physiological effect of Ser 22/23 phosphorylation by PKA and they have shown that it reduces myofilament Ca^{2+}-sensitivity, increases the cross-bridge cycling rate and enhances unloaded shortening velocity (Hoh et al., 1988, Saeki et al., 1990, Fentzke et al., 1999, Kentish et al., 2001, Herron et al., 2001). To increase the heart rate it is crucial that TnC dissociates faster from Ca^{2+} to let the muscle relax faster. However, in the cardiomyocytes TnI is usually

phosphorylated to around 1.6 mols P_i / mol TnI, with around 50% occupancy of Ser22/23 (Messer et al., 2009). PKA treated non-failing donor cardiomyocytes show a minor decrease in the Ca^{2+} sensitivity of isometric force (van der Velden et al., 2003). Similarly, Messer *et al.* reported that the Ca^{2+} sensitivity of thin filaments containing human non-failing donor troponin was increased upon dephosphorylation of TnI by phosphatase treatment (Messer et al., 2007). These functional studies indicate that cardiomyocyte contractile properties can be modified by alterations in TnI phosphorylation and be responsible for fine regulation of the cardiac output.

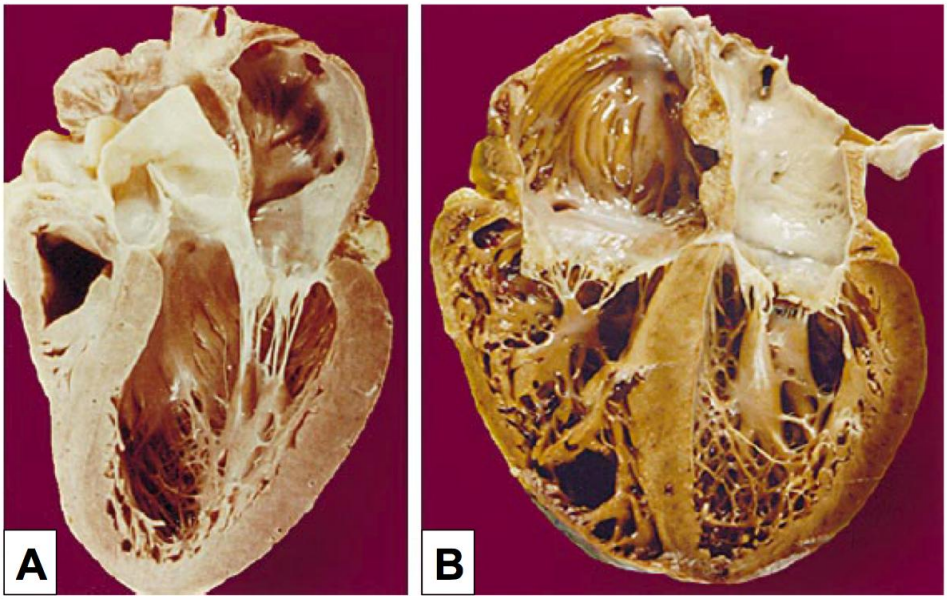
Studies made on failing heart proved its abnormal contractile properties, a decreased rate of maximally activated cross-bridge cycling and a decrease in contraction and relaxation rate, but also an increase in the Ca^{2+} sensitivity and reduced responsiveness to β-adrenergic stimulation. These could altogether reduce the rate of relaxation in diastole, leaving it incomplete and so decrease the work output in systole, till heart failure is reached (Houser and Margulies, 2003, Pagani et al., 1988, Wolff et al., 1996, Alpert et al., 2002).

Studies of human heart muscle by *in vitro* motility assay reported that changes in troponin function alone could alone be causing contractile abnormalities in failing heart muscle (Messer et al., 2007). What was different between non-failing and failing troponin was the very low level of phosphorylation in the failing heart. Ca^{2+}-sensitivity and maximum velocity were shown to correlate with the level of TnI phosphorylation.

1.4 Dilated Cardiomyopathy (DCM)

Dilated cardiomyopathy (DCM) is a disease clinically characterised mainly by left ventricular dilation, and systolic dysfunction, with a reduction of the ejection fraction (< 50%). It is estimated to affect 36.5 in 100,000 individuals (Cohn et al., 1997).

Figure 1.22: Normal v DCM heart



A) A section of a normal heart. B) A section of a DCM heart. Adapted from Seidman and Seidman (2001).

The ventricular wall thickness is normal or reduced, which could mask an increase in its mass, but the ventricular cavity increases in size (Figure 1.22), creating more space for the blood to clot at the apices adding the risk of thrombus and in the worst case a potential thromboembolic event. DCM can lead to heart failure, sudden death and only 50% of the patients survive 5 years after initial diagnosis. So far, only heart transplantation has been successful enough in prolonging the life expectancy of the patients.

Histologically the myocytes increase their length and the nuclear size, because of DNA synthesis. They can become polyploid and the number of myofibrils can decrease. They

appear empty and vacuolated on histology. Myocytes diminish in number because of apoptosis and necrosis, with increases in interstitial fibrosis that can surround and isolate individual myocytes. Also macrophages and T lymphocytes can increase in number in the interstitial spaces. The degree of all these phenotypical features changes from case to case (Davies, 2000).

The possible causes of DCM are multiple. It can be triggered by other diseases like coronary artery disease, viral myocarditis, thyroid disease, or by immunologic processes, or even by toxins, like alcohol *in primis*, but in many cases it can not be directly linked to the etiological factor. In those circumstances it is referred to as 'idiopathic DCM' (IDC) and at this stage it is still the most common diagnosis. Familial dilated cardiomyopathy (FDC) is conventionally defined by the same clinical criteria of IDC, but in at least two closely related members of a family, and it can account for 20 - 35% of the IDC cases.

To date, mutations in more than 40 genes have been linked to the genesis of the disease, most of which are autosomal, but there are also 2 X-linked, and the number is very likely to grow. The genetic cause is identified only in 30 - 35% of cases of FDC. The inheritance is mostly autosomal dominant, nevertheless recessive and X-linked have been described (Hershberger and Siegfried, 2011).

While another cardiomyopathy, hypertrophic cardiomyopathy, is mainly a genetic disease of the sarcomere proteins (in 50 - 75% of familial cases a mutation can be identified and are mostly located on myosin heavy chain or myosin-binding protein C), FDC has been linked to mutations in several different components of different compartments and pathways. Some of these are the nuclear envelope, the mitochondrion, the sarcoplasmic reticulum and the Z-disc. The first gene mutant to be identified was a component of the cytoskeleton, dystrophin (Muntoni et al., 1993, Towbin et al., 1993), while the first mutant gene coding for a

component of the sarcomere was *ACTC* (Olson et al., 1998). Then, almost every protein of the sarcomere presented mutations that could be linked to DCM. It is notable that mutations in proteins of thin or thick filaments are associated with 'pure' DCM, with no additional phenotypes (Kamisago et al., 2000, Mogensen et al., 2004).

This thesis will present the investigation made on 7 different mutations of thin filament proteins (at least one on each subunit of the basic regulatory machinery), in the effort of finding a common molecular phenotype that could trigger DCM. These are actin E361G (Olson et al., 1998), troponin I K36Q (Carballo et al., 2009), troponin C G159D (Mogensen et al., 2004), troponin T R141W (Li et al., 2001), troponin T ΔK210 (Kamisago et al., 2000), tropomyosin E40K and E54K (Olson et al., 2001). The characteristics of each mutation will be discussed when taken into consideration in Chapters 3 and 4.

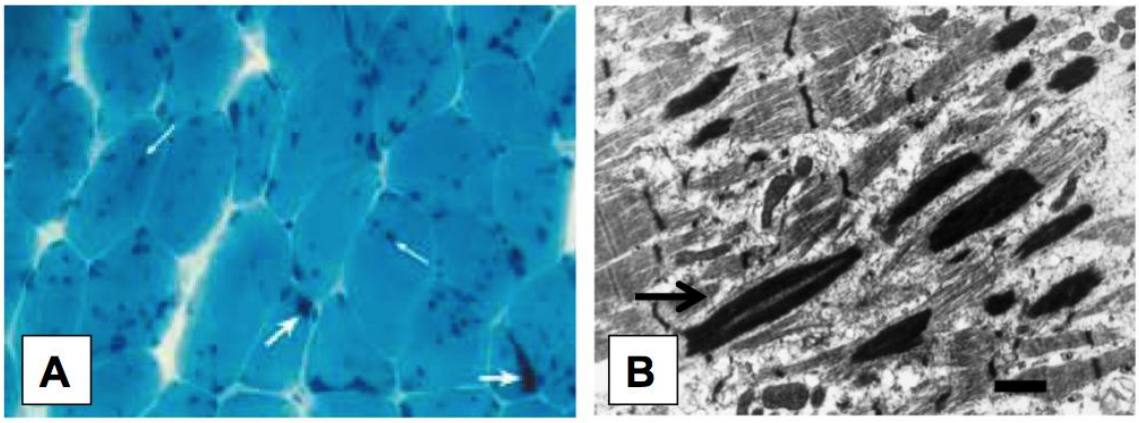
1.5 Skeletal Muscle Diseases

1.5.1 Nemaline Myopathy

Nemaline Myopathy (NM) was first described by Shy and Conen in two different reports in 1963 (Shy et al., 1963, Conen et al., 1963). It is a skeletal muscle disease with high variability in severity and age of onset, but characterised by general muscle weakness, hypotonia and nemaline bodies in the myocytes. These are a structural abnormality of the muscle fibres visible after histochemical staining (Gomori trichrome method, Figure 1.23). They are the only visible histological abnormality and they look like threads/rods protruding from the Z-line and are composed primarily of actin filaments and α-actinin (Wallgren-Pettersson et al., 1995). There are six forms of NM, classified by onset and severity of motor and respiratory involvement: severe congenital (neonatal) form (16% of all individuals with

NM); Amish NM, intermediate congenital form (20%); typical congenital form (46%); childhood-onset form (13%); and adult-onset (late-onset) form (4%) (North, 2010).

Figure 1.23: Nemaline myopathy histology



A) Gomori trichrome-stained transverse section of skeletal muscle biopsy of a nemaline myopathy patient. Rods appear in every fibre as darkly staining bodies all across the cytoplasm (small arrows), or underneath the sarcolemma (large arrows), (Sanoudou and Beggs, 2001). B) Electron micrograph (scale bar = 1 μm) showing typical nemaline rods developing from the Z-line and disrupting the normal sarcomeric architecture (Wattanasirichaigoon et al., 2002).

Muscle weakness is usually most severe in the face, the neck flexors, and the proximal limb muscles, but it can also involve the distal ones. When it has congenital onset the face is usually elongated and expressionless, the palate arched, and the tongue small. Many patients cannot lift their head from supine position, have hyperlordotic spine and respiratory capacity restricted, with risk of nocturnal hypoxia or sudden respiratory failure. Cardiac contractility and intelligence are usually normal (North et al., 1997).

The distribution of nemaline rods can be considered quite random, but they tend to cluster under the sarcolemma and around the nuclei, with a variable presence in different fibres, although in some patients they are present only in type I fibres. The rods themselves measure 1-7 μm in length and 0.3-2 μm in width, with a surrounding layer of desmin. They are considered as deriving from the lateral expansion of Z-disks because on EM they are in

structural continuity with them, the structure resembling the lattice pattern of the Z-disk and the rods are made mainly of the same component α-actinin (North et al., 1997). The nemaline bodies are not specific only to NM, but have been reported in combination to other conditions such as HIV infection, in these cases the onset of the myopathy is late and it is referred to as 'Sporadic Late-onset Nemaline Myopathy' (SLONM), even though SLONM can be congenital NM and it is not clear how often patients are HIV-positive (Rowland, 2011). Predominance of fibre type I is a common feature of NM, with extreme cases of patients with only fibre type I. Fibre type I predominance and atrophy seems to get more severe with age. Fibrosis was seen in some biopsies.

NM is inherited in an autosomal dominant, or autosomal recessive way, but mostly with single occurrence in one family that could be a heterozygous dominant or a homozygous recessive individual (North, 2010). To date, seven different genes have been linked to the genesis of the disease: nebulin (*NEB*) (Pelin et al., 1999), α-actin (*ACTA1*) (Nowak et al., 1999), slow skeletal muscle troponin T (*TNNT1*) (Johnston et al., 2000), cofilin-2 (*CFL2*) (Agrawal et al., 2007), *KBTBD13* (Sambuughin et al., 2010) and, most importantly for this thesis γ-tropomyosin (*TPM3*) (Laing et al., 1995) and β-tropomyosin (*TPM2*) (Donner et al., 2002).

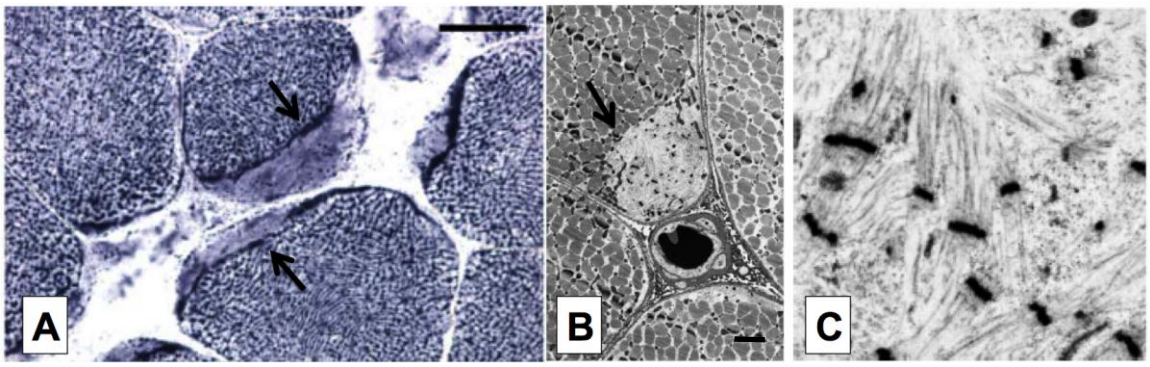
The first mutant identified in time in *TPM3* has been M9R in a large family (Laing et al., 1995). This is also the most studied mutant and with different methods and recombinant sources (*E.coli* and baculovirus/*sf9*) it has been proved to have a much lower affinity for actin that the wild-type (Moraczewska et al., 2000, Akkari et al., 2002). It was also shown that it could be integrated into sarcomeres, that it could destabilise the head-to-tail tropomyosin interaction and the binding of tropomodulin, because of its position at the N-terminus and that it also down-regulates the presence of β-tropomyosin, shifting the preferential dimer to

γγ (Ilkovski et al., 2008, Corbett et al., 2005). The γγ dimer is also supposed to reduce the Ca^{2+}-sensitivity of the thin filaments. The *TPM3* mutant R167H has been described in two studies on two unrelated families (Durling et al., 2002, Penisson-Besnier et al., 2007). In β-tropomyosin the identified mutants leading to Nemaline myopathy have been E117K and Q147P, although at closer scrutiny the biopsy of the first one did not show any Nemaline rods after being diagnosed with this disease (Donner et al., 2002).

1.5.2 Cap Disease

Cap disease was presented as an independent congenital myopathy in two different reports describing 4 different patients with the same symptoms and morphological features (Fidzianska et al., 1981, Fidzianska, 2002). They were all reported with muscle hypotonia, non-progressive or slowly progressive muscle weakness, skeletal dysmorphy and respiratory insufficiency since childhood. What differentiates it from other myopathies are cap-like structures at the periphery of the muscle fibres underneath the sarcolemma (Figure 1.24 A and B). But the first genetic evidence of a mutation linked to the disease was provided only recently by Lehtokari *et al.* (Lehtokari et al., 2007) with a deletion in β-tropomyosin (ΔE139); later this was found in another unrelated family with similar features, except for a reduced presence of cap structures (Clarke et al., 2009). In the second report it was also proven that the mutant tropomyosin was able to assemble in the thin filaments.

Figure 1.24: Cap disease histology



A) Light microscopy of a skeletal muscle biopsy of a cap disease patient stained with NADH-TR. The black arrows indicate the peripheral sub-sarcolemmal cap structures (scale bar = 100 µm). B) Electron microscopy of the same biopsy showing a cap structure (black arrow; scale bar = 2.5 µm). C) Magnification of the cap structure shown in B (15 µm x side). It consists of unorganised myofibrils with lack of thick filaments and enlarged Z-lines. Adapted from Cuisset *et al.* (2006).

The cap-like structure seems to be made of disoriented and disorganised myofibrils with a lack of thick filaments and Z-disk abnormalities (Figure 1.24 C), like rod formations. Z-lines look thickened even in regularly assembled sarcomeres. In the caps have been reported to be localised mainly desmin, troponin T, nebulin, actin, α-actinin, tropomyosin, myotilin and SERCA2, with rare occasions of myosin and vimentin. Cap disease patients show also a quite consistent fibre type disproportion, with many more hypotrophic type I fibres and few hypertonic type II fibres (Lehtokari et al., 2007).

Later four other β-tropomyosin mutations have been identified and linked to cap disease, ΔK49, G53dup, N202K, E41K (Ohlsson et al., 2008, Tajsharghi et al., 2007). Another report on E41K gave the first insight on the functional properties of cap disease related mutations suggesting a negative effect on contractile properties, with a decrease in Ca^{2+}-sensitivity and contracting speed in skinned muscle fibres (Ochala et al., 2008).

Also two mutations in the *TPM3* gene, R167C and R167H, have been associated with cap disease in two different reports, and a mutation in the *ACTA1* gene, M47V, proving the

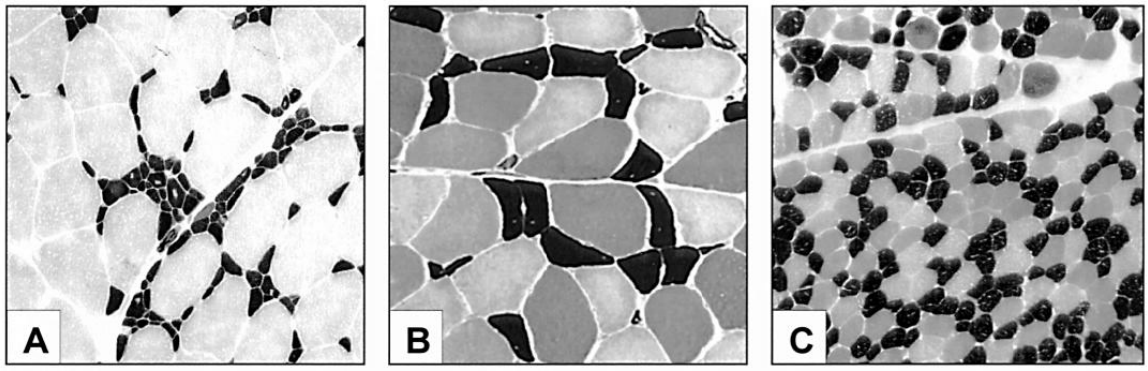
genetic heterogeneity of the disease (Ohlsson et al., 2009, De Paula et al., 2009, Hung et al., 2009). It is notable that only thin filament proteins have been linked to the disease and a characteristic irregular and coarse-meshed intermyofibrillary network with jagged Z-lines has been described as a common feature (Ohlsson et al., 2008). Some of these γ- and β-tropomyosin mutants have also been linked with other diseases (see 1.5.4).

One important observation made on different cap disease patients is that the onset can be neonatal or infant, with the neonatal form being more severe, showing caps in 70 - 75% of the fibres and leading to premature death, whereas the infant form is milder, with caps in only 10 - 30% of the muscle fibres and a better prognosis (Fidzianska, 2002, De Paula et al., 2009, Hung et al., 2009). This could be related to the expression of the mutant protein in different developmental stages.

1.5.3 Congenital Fibre Type Disproportion (CFTD)

Congenital fibre type disproportion (CFTD) is a term coined by Brooke in 1973, after describing 12 patients with the same abnormalities on muscle biopsy that was seen in several other patients earlier in the 1960s and early 1970s (Brooke, 1973).

Figure 1.25: CFTD histology



Muscle biopsies stained with ATPase of patients with varying degrees of fibre size disproportion associated with CFTD. Type 1 fibres are dark, type 2A are pale and 2B are intermediate. (Clarke and North, 2003)

The main diagnostic feature of CFTD is a marked hypotrophy of type I skeletal muscle fibres, resulting in them being at least 50% smaller than type II fibres, which will be either normal or hypertrophic (Figure 1.25). CFTD shows all the clinical features of a congenital myopathy, with hypotonia and generalised muscle weakness at birth or within the first year of life, failure to thrive, multiple joint contractures, scoliosis, long thin face and high arched palate, ptosis and inheritability along the family line. Around 30% of the patients show respiratory involvement with possibility of respiratory failure. The main histological feature, though, is shared with many other congenital neuromuscular and muscular pathologies, as seen for cases of Nemaline myopathy and Cap disease (see 1.5.1 and 1.5.2). So, to be used as a diagnosis, CFTD can be considered when the other possible diseases can be excluded (Clarke and North, 2003).

The prognosis is quite variable with some patients remaining non-ambulatory throughout life, and others developing the ability to walk. For most patients the weakness is static or it improves, for only 10% it is progressive.

The first three cases for which a genetic cause could be highlighted were reported by Laing *et al*. and they were all mutants of *ACTA1*: D292V, L221P, P332S (Laing et al., 2004). They presented considerable fibre type disproportion and no other pathological markers, but they all died at very young age. The mutations do not cluster together but they lie on the region were tropomyosin is supposed to shift in the open state of the thin filaments, suggesting a common pathogenic mechanism. Further studies were done on samples from two of these patients, D292V and P332S, and they showed that the sarcomere structure in the original tissue was well organised, that the mutant protein accounts for 50 and 25% of the total respectively and that D292V in the *in vitro* motility assay had a dominant negative effect on

the motility of the thin filaments switching them off in the presence of tropomyosin, without the chance of being rescued by troponin (Clarke et al., 2007).

Subsequently, a X-linked case of CFTD and one due to a recessive selenoprotein N mutation were reported (Clarke et al., 2005, Clarke et al., 2006).

A more relevant study in the context of this thesis was then published with the description of five new *TPM3* mutations with typical CFTD: L100M, R167C, R167G, K168E, R245G (Clarke et al., 2008). In that study another *TPM3* mutation was considered, R167H, which in two different patients of the same family showed both nemaline myopathy and CFTD phenotypes, and was already been described as nemaline myopathy causing in two different reports from two different family pedigrees (Durling et al., 2002, Penisson-Besnier et al., 2007). The matter of the possible relationships between nemaline myopathy, cap disease and CFTD will be described in the next paragraph (1.5.4).

Another report added two other *TPM3* mutation relevant to this thesis, A4V and R91P (Lawlor et al., 2010), and another broadened the genetic heterogeneity of the disease to recessive mutations on *RYR1*, although they could be also misinterpretations of core myopathy mutations (Clarke et al., 2010).

1.5.4 Evidences of Overlap between these Skeletal Muscle Pathologies

With several studies made along a few decades timeframe, it became evident that congenital myopathies often share some characteristic traits and that sometimes there is a genetic overlap between different diseases. In this context it has been seen that hypotrophic type I fibres, which could become the majority of the fibres in the muscle, if not the exclusive fibres, is a characteristic of many diseases, like Nemaline myopathy, cap disease, core myopathy, distal arthrogryposis, and also the main feature of CFTD.

Sometimes, though, biopsies performed at a young age show only fibre type size disproportion, leading to a diagnosis of CFTD, but if performed again later they could show nemaline rods or cap structures (De Paula et al., 2009, Tajsharghi et al., 2007).

The picture becomes even more complicated when it is considered that in histology the presence of both nemaline rods and cap structures has never been observed on the same biopsy sample or in biopsies from two different muscles in the same patient. However with several single mutations the possibility of generating either one of the structures in different patients both within the same family or in different ones has been observed.

One example is given by β-tropomyosin E41K, where cap-like structures were found in one patient at 26 years old, while its mother, with the same clinical symptoms, did not show any aberrant structure in a biopsy performed when 32 years old, but showed cap structures with nemaline bodies inside in a second biopsy at 57 years (Tajsharghi et al., 2007). This was the first evidence of the close relation between Nemaline myopathy and cap disease, which was already been hypothesized since a report on three patients, two siblings of related parents and a half-cousin, showing cap-structures in the case of the siblings and nemaline bodies in the cousin (Cuisset et al., 2006).

Two *TPM3* mutants are further proving this overlap of the diseases. They are both on R167, which is considered a mutation hotspot. It is a very conserved residue, between isoforms and species (till Zebrafish), which is important in actin binding (Brown et al., 2005). *TPM3* R167C has been described for the first time as CFTD linked by Clarke *et al.* with two biopsies at age 6 and 19 on one patient, but then in two different studies it was linked to the cap disease with a biopsy on one patient at 18 years old and on the other at 3 years old (Clarke et al., 2008, Ohlsson et al., 2009, Waddell et al., 2010). These findings also exclude as simplistic the possible objection that the caps will form over time with some mutants.

Probably the best example showing disease overlap is *TPM3* R167H. This was initially described as causing nemaline myopathy in two separate studies (Durling et al., 2002, Penisson-Besnier et al., 2007). A third added the possibility of CFTD as the daughter presented nemaline rods age 20, while the father only fibre type disproportion at 56 (Clarke et al., 2008). A recent study on an 11 year old patient diagnosed CFTD (Munot et al., 2010), but more importantly a previous one linked the mutation with cap disease (De Paula et al., 2009).

The reason for the variable formation of protein inclusions is still uncertain, as it is the variability in fibre type and size. It has been proposed that the formation of nemaline rods or cap structures is due to some other genetic factor, but maybe also a problem of age and muscle sampled (Ohlsson et al., 2009, Cuisset et al., 2006). For what regards the type I fibre predominance and hypotrophy it has been proposed that it might be a compensatory mechanism to conserve energy, by converting the fibres to lower energetic requiring or even by altering their maturation (Ilkovski et al., 2008).

1.6 Context and Aim of this Study

1.6.1 The *In Vitro* Motility Assay

The main technique employed for this thesis has been the quantitative *in vitro* motility assay (IVMA). This is a reductionist approach able to screen functional properties of the basic contractile proteins *in vitro*. All the subunits of the thin filaments (actin, troponin, tropomyosin) get purified separately, potentially from different sources of tissue according to the aim of the experiment, and, then, reconstituted *in vitro*. These thin filaments will then be observed, thanks to a fluorescent label, moving on a bed of immobilized heavy meromyosin.

Parameters like the density of attached filaments, their velocity and the percentage of them moving, will be taken into consideration for functional evaluations. This technique involves the real-time screening of two different reconstitutions, which will share the exact same experimental conditions except for one protein, allowing the comparison between a wild-type against mutant protein. Any functional difference could therefore highlight a molecular phenotype derived directly from the mutation.

It has been established that Ca^{2+} regulates the percentage of filaments moving, corresponding to the fraction of filaments in the open vs closed/blocked states. Ca^{2+} also controls the sliding speed, but, as it will be shown, this depends also on the origin of the proteins involved and their conditions at the moment of the experiment, generating difficulties in the evaluation of the data (Fraser and Marston, 1995, Marston, 2003).

1.6.2 Dilated Cardiomyopathy Studies

The IVMA was used in the past to investigate DCM mutations, but the studies were made using recombinant *Escherichia coli* expressed proteins (Mirza et al., 2005, Mirza et al., 2007). These proteins were easy to produce and use, but were lacking the post-translational modifications observed *in vivo.*

More recently in our lab Dr. E. Dyer started using more physiological proteins in the IVMA, which were purified from human or animal tissue. This way the phosphorylation status of the proteins used in the assay could be taken into consideration and especially that of troponin I, which is meant to finely regulate the Ca^{2+}-sensitivity of the thin filament and is connected to the lusitropic response of the β-adrenergic stimulation (see section 1.3.2.1).

This pilot work led to the formulation of a hypothesis: DCM could be caused by an uncoupling between the Ca^{2+}-sensitivity of the thin filament and the phosphorylation level of troponin I.

This work of thesis completed the pilot work made on E361G actin and G159D troponin C, further developing and proving the hypothesis by investigating five other mutations on thin filament proteins: one in troponin I, two in troponin T and two in α-tropomyosin.

1.6.3 Congenital Myopathies Studies

As described in section 1.5, Nemaline myopathy, Cap disease and CFTD are congenital myopathies characterized by different specific histological features, but presenting large genetic and phenotypical overlap. The molecular mechanism at the base of these diseases remains largely unknown and only little work, confined to *ACTA1* mutations (Feng and Marston, 2009), has been done to understand the functional properties of mutants leading to them. There are no functional studies on tropomyosin mutations.

The aim of this thesis has been that of screening the functional properties of six β- and five γ-tropomyosin mutants that have been linked previously to one or more of these diseases and evaluate the possibility a common molecular behaviour exists.

Furthermore a novel actin mutation (K326N) presenting Nemaline myopathy features, but a novel hypercontractile phenotype, has been investigated and compared to another actin mutation (D292V) presenting the opposite molecular phenotype.

1.6.4 Aims of the Thesis

The overall aim of this thesis was to investigate how mutations in the proteins of the thin filaments cause inherited myopathies in both cardiac and skeletal muscle. Both congenital skeletal muscle myopathy and familial DCM have been associated with loss of function (Feng and Marston, 2009, Mirza et al., 2005, Chang and Potter, 2005, Marston, 2011). I studied 7 mutations connected to dilated cardiomyopathy and 13 mutations identified as associated with one or more of the skeletal muscle diseases, Nemaline myopathy, Cap disease

and congenital fibre type disproportion (CFTD), in the effort to underline any similarity between their functional properties. This would have allowed me to formulate a hypothesis on potential common principles in inherited myopathies. In addition during the course of this study, two mutations (*ACTA1* K326N and *TPM2* ΔK7) were discovered to cause a novel gain of function molecular phenotype.

All of the mutations taken into consideration have relatively mild effects, meaning that they are compatible with life, at least till early infancy. Some of them showed severe chronic effects and made necessary drastic medical procedure, like heart transplantation at the age of 3 and 15 years old for respectively the TnC G159D and TnI K36Q patients. Most of the skeletal muscle disease related mutants had mild effects and many patients remained ambulatory till middle age. Only the skeletal actin K326N mutation caused death of the patient in less than a year, but it had a very different sort of phenotype with gain-of-function, rather than loss-of-function.

A deeper knowledge about the functional deficiencies introduced by mutations in the contractile apparatus might help in the diagnosis of the diseases, which are at present based on physiological and histological criteria, and direct future development of treatments for patients affected. It can moreover give insights on the structure-function relationships in the thin filament proteins and on the mechanisms regulating the whole system.

2 Materials and Methods

2.1 Sources of Sample Proteins

2.1.1 Human and Mouse Heart Samples

2.1.1.1 Donor Human Hearts

All donor human heart samples were supplied by Prof. C Dos Remedios, University of Sydney, Australia. Ethical approval was obtained from The Brompton, Harefield & NHLI, London and St. Vincent's Hospital, Sydney. The investigation conformed with the principles outlined in the Declaration of Helsinki (World Medical Association, 1996). Non-failing adult myocardium was obtained from subjects who were in first place assessed as potential heart donors but then no suitable recipient was found or the heart was deemed unusable for other reasons. The donors had no history of cardiac disease, a normal cardiac examination, a normal admission ECG and normal ventricular function on transthoracic echocardiography performed within 24 hours of heart explantation. These criteria were set to exclude any potential donor hearts with myocardial dysfunction or damage. Immediately following explantation, the ventricular wall was cut up into 1g segments and frozen in liquid nitrogen and stored for later analysis. Clinical details are shown in Table 2.1.

2.1.1.2 Failing Human Hearts

The failing heart sample used in this study (Table 2.1) also originated from St. Vincents's Hospital, Sydney and was collected and stored as described for donor heart. The source of

failing heart tissue was a patient presenting end-stage heart failure (NYHA class III or IV, ejection fraction of < 20%). Sample collection and storage procedures were the same as those described for donor human hearts 2.1.1.1.

Table 2.1: Clinical details of all the human donor and failing heart samples studied

SAMPLE		Diagnosis	Operation	Gender	Age	NYHA Class	LVEF on ECHO
Donor	N7	-	Donor	Female	45	-	-
	N10	SAH	Donor	Female	48	-	-
	N11	SAH	Donor	Male	55	-	-
	NE	HBI	Donor	Male	29	-	-
	NG	Aneurism	Donor	Male	53	-	-
	NH	SAH	Donor	Female	48	-	-
	NI	SAH	Donor	Female	42	-	-
	NL	Aneurism	Donor	Female	42	-	-
Failing	FC	IDCM	OCT	Male	30	III	10-15%

LVEF = left ventricular ejection fraction; Donor = heart transplant donor after brain stem death; SAH = subarachnoid haemorrhage; HBI = Hypoxic brain injury; IDCM = idiopathic DCM; OCT = orthotopic cardiac transplantation.

2.1.1.3 Dilated Cardiomyopathy (DCM) Human Hearts

The heart tissue sample used in this study presenting the missense mutation Lys36Gln (K36Q) in cardiac troponin I was collected and then kindly provided to us by Prof. C Dos Remedios (University of Sydney, Australia). The heart tissue belonged to a patient who underwent heart transplantation for deterioration of severe DCM. The mutation was first identified and described in Oxford from a sample belonging to the transplanted heart of this patient (Carballo et al., 2009). Clinical details of this patient are in Table 2.2.

The missense mutation Gly159Asp (G159D) in cardiac troponin C is associated with DCM (Mogensen et al., 2004). A cardiac muscle sample from the transplanted heart of a patient belonging to the original family in which the mutation was isolated was collected by Dr

Adam Jacques from Great Ormond Street Hospital. The clinical features of the patient are described by Kaski *el al.* (2007) and summarised in Table 2.2.

Table 2.2: DCM explanted heart patients details

Mutation	Age	Clinical Features	Cardiac Parameters	Family History
TnC G159D (autosomal dominant)	3 y.o.	Increased cardiothoracic ratio, pulmonary oedema, respiratory distress, bradycardia, respiratory arrest, 4 chambers dilation, poor biventricular systolic function,	LVED 54 mm LVES 50 mm LVEF 20%	Yes
TnI K36Q (autosomal dominant)	15 y.o.	Congestive heart failure, biventricular dilation, anisocytosis with occasional brick shaped nuclei, prominent myocytolysis, patchy interstitial fibrosiscentered on thickened endocardium	LVED 70 mm LVES 57 mm LVEF 15-20%	Yes

LVED = left ventricular end diastolic diameter; LVES = left ventricular end systolic diameter; LVEF = left ventricular ejection fraction

2.1.1.4 DCM Mouse Hearts

The mutation Arg141Trp (R141W) in cardiac troponin T was isolated through a study on a large family (Li et al., 2001). A transgenic mouse model was then produced by Dr L. Zhang (Peking Union Medical College, China), who provided us with 3 frozen hearts of this transgenic line and some non-transgenic littermates hearts for comparison. In his study he described the development of DCM phenotype in mice (Table 2.3) as a result of the presence of the mutant troponin T (Juan et al., 2008).

Another mutation on human cardiac troponin T, the deletion of the residue Lys210 (ΔK210), was linked to DCM (Kamisago et al., 2000) through a study on two unrelated families. For this mutation a knock-in mouse model was generated, and we studied hearts from homozygous and heterozygous knock-in mice. Both of them developed DCM (Table 2.3)

phenotypes with an increased severity for the homozygous (Du et al., 2007). Prof. S. Morimoto (Kyushu University Graduate School of Medicine, Japan) kindly provided us with a collection of hearts of both disease models and the non-transgenic littermates for comparisons.

The gene coding for cardiac actin (*ACTC*) is highly conserved intra- and inter-specifically and therefore the mutation Glu361Gly (E361G), which cosegregates with idiopathic DCM, is very likely to cause the disease (Olson et al., 1998). Transgenic mice overexpressing actin E361G in the heart (Table 2.3) were created and characterised in our lab (Song et al., 2010).

Table 2.3: DCM transgenic mice details

Mutation	Expression Level %	Mouse phenotype	Mice Cardiac Parameters	
α-actin E361G (autosomal dominant)	50	No overt sign of cardiac abnormality at 4/6 months	/	
TnT ΔK210 (autosomal dominant)	40	Enlarged hearts, interstitial fibrosis, increased apoptosis, high incidence of sudden death	4/5 months	
			WT LVED = 3.38 mm LVES = 1.95 mm LVEF = 80.3%	LVED = 4.12 mm LVES = 3.14 mm LVEF = 53.6%
	100			LVED = 5.23 mm LVES = 4.50 mm LVEF = 34.7%
TnT R141W (autosomal dominant)	60	Heart dilation, mural thrombi, moderate incidence of immature death, thinner ventricle wall, interstitial fibrosis, elongated and lysed myofibrils	4 months	
			WT LVED = 3.6 mm LVES = 2.4 mm LVEF = 62.7%	LVED = 4.6 mm LVES = 3.8 mm LVEF = 37.7%

LVED = left ventricular end diastolic diameter; LVES = left ventricular end systolic diameter; LVEF = left ventricular ejection fraction.

2.1.2 Baculovirus Expression System

Recombinant α-, β- and γ-tropomyosin were produced with the baculovirus/*sf9* system. This recombinant expression system uses eukaryotic insect cells (*Spodoptera frugiperda*, *sf9*), thus providing eukaryotic post-translational modifications, especially N-terminal acetylation,

which has been highlighted as essential for proper tropomyosin head-to-tail assembly along the actin filament (Urbancikova and Hitchcock DeGregori, 1994). All mutants used are summarised in Table 2.4.

2.1.2.1 DCM α-tropomyosin Mutants

Two α-tropomyosin (*TPM1* gene) DCM linked mutants were taken into consideration in this study. Glu40Lys (E40K) and Glu54Lys (E54K) α-tropomyosin were identified as aetiological cause of DCM through a study conducted on two small families (Olson et al., 2001). Baculovirus/*sf9* pellets of cells containing either one of these mutations, or the wild type for comparison, were supplied by Dr. K. Nowak, University of Western Australia, Nedlands, Australia.

2.1.2.2 Nemaline Myopathy and Cap Disease β-tropomyosin Mutants

The functional properties of six different β-tropomyosin (*TPM2* gene) mutants, which have been linked to nemaline myopathy or cap disease, will be described in this thesis. These β-tropomyosin mutants are ΔLys7 (ΔK7; data not published yet) and Gln147Pro [Q147P (Donner et al., 2002)] for nemaline myopathy, ΔLys49 [ΔK49 (Ohlsson et al., 2008)] and ΔGlu139 [ΔE139 (Lehtokari et al., 2007)] for cap disease, Glu41Lys [E41K (Tajsharghi et al., 2007)] which was described as presenting features of both diseases and Glu117Lys (E117K) at first diagnosed as nemaline myopathy but then at close scrutiny found not to show verifiable nemaline bodies (Donner et al., 2002).

All the baculovirus/*sf9* cell pellets of these mutants, and the wild type for comparison, were provided to us by Prof. C. Wallgren-Pettersson, University of Helsinki, Finland.

2.1.2.3 Congenital Fibre Type Disproportion (CFTD) γ-tropomyosin Mutants

Five mutations on the gene *TPM3* (γ-tropomyosin) were taken into consideration to screen the possible functional differences with the wild type leading to CFTD. These mutants were Ala4Val (A4V) and Arg91Leu (R91L) which have been described by Lawlor *et al.* (Lawlor et al., 2010), and Leu100Met (L100M), Arg167His (R167H) and Arg167Cys (R167C) which have been fully described by Clarke *et al.* (Clarke et al., 2008). The *TPM3* mutants R167C and R167H have been described also as the genetic cause of cap disease the first and cap disease and nemaline myopathy the second (see section 1.5.4).

All of the baculovirus/*sf9* γ-tropomyosin cell pellets were supplied by Dr. K. Nowak, University of Western Australia, Nedlands, Australia.

Table 2.4: Summary of the mutants expressed with the baculovirus/*sf9* system and initial diagnosis

Protein	Disease	Mutation
α-tropomyosin	DCM	E40K
		E54K
β-tropomyosin	NEMALINE MYOPATHY	ΔK7
		Q147P
	Similar to NM	E117K
	CAP DISEASE	ΔK49
		ΔE139
	NM and CD features	E41K
γ-tropomyosin	CFTD	A4V
		R91L
		L100M
	CFTD and CD	R167C
	CFTD, NM and CD	R167H

NM= nemaline myopathy; CD=cap disease; CFTD= congenital fibre type disproportion

2.1.3 Human Skeletal Muscle Biopsies

A biopsy from a patient with nemaline rods and an atypical clinical presentation of stiff muscle was used in this study. A novel Lys326Asn (K326N) mutation on skeletal muscle α-actin gene (*ACTA1*) was identified. C. Sewry (UCL Institute of Child Health, UK) provided us with a biopsy from the quadriceps muscle, which was frozen in liquid nitrogen.
Another skeletal muscle biopsy was investigated in this study. The patient was diagnosed with CFTD and presented a point mutation on skeletal muscle α-actin (*ACTA1* gene). The mutation D292V had already been studied in this lab (Clarke et al., 2007). The biopsy was kindly provided by Dr. N. Clarke as -80° C frozen thick tissue section (Sydney).

2.2 Protein Preparation from Tissue

2.2.1 Preparation of Motor Protein

2.2.1.1 Fast Skeletal Myosin Preparation from Rabbit Skeletal Muscle

The *in vitro* motility assay (IVMA) is a functional assay that over the period of this study required a relatively large amount of heavy meromyosin (HMM), a soluble fragment of myosin. Rabbit back muscle was used as source of skeletal muscle myosin, prepared by the method of Margossian and Lowey (1982). The protocol ran over two days and all steps were carried out at 4° C.

Day 1: Immediately after the rabbit was sacrificed, the back muscle was excised and cooled on ice for 1 hour. The muscle was then skinned and diced before being twice minced in a pre-

cooled meat grinder. The minced muscle was then weighed resulting in an average of around 300 g of minced muscle obtained from one rabbit. Myosin was extracted from this in three volumes of myosin extraction buffer, containing 300 mM KCl, 150 mM Potassium phosphate (50 mM K_2HPO_4 / 100 mM KH_2PO_4), 20 mM EDTA, 5 mM $MgCl_2$, 1 mM ATP and 5 mM DTT pH 6.5 and 2 μg/ml of each protease inhibitor (E-64, chymostatin, leupeptin & pepstatin A), for exactly 10 minutes with occasional stirring. The extract was centrifuged at 25,000 x g (13,000 rpm, Sorvall Evolution RC, SLA-1500 rotor) for 5 minutes. The pellets were saved for F-actin preparation through the acetone powder method (see section 2.2.2.1). The supernatant was filtered through glass wool into a 25 litre plastic bin and diluted gradually with 12 volumes of cold distilled H_2O. Crude myosin was allowed to precipitate with no agitation. After 3 hours sedimentation the supernatant was easily siphoned off without disturbing the sediment. The myosin was then pelleted by centrifugation at 25,000 x g (13,000 rpm, Sorvall Evolution RC, SLA-3000 rotor) for 6 minutes. The resulting pellet was resuspended with 3 M KCl at the ratio of 220 ml per kg of starting muscle. Once dissolved, the myosin solution was dialysed overnight against another buffer containing 600 mM KCl, 25 mM potassium phosphate (8 mM K_2HPO_4 / 17 mM KH_2PO_4), 10 mM EDTA and 2 mM DTT, pH 6.5 and 2 μg/ml of each protease inhibitor (E-64, chymostatin, leupeptin & pepstatin A).

Day 2: The dialysate was gradually diluted two-fold with cold distilled H_2O and stirred for 30 minutes, to allow any actomyosin still present to precipitate. It was then centrifuged at 50,000 x g (20,000 rpm, Sorvall Evolution RC, SS-34 rotor) for 1 hour. The resulting supernatant was diluted eight-fold with cold distilled H_2O to precipitate the myosin. The myosin was then pelleted by centrifugation at 25,000 x g (13,000 rpm, Sorvall Evolution RC, SLA-1500 rotor)

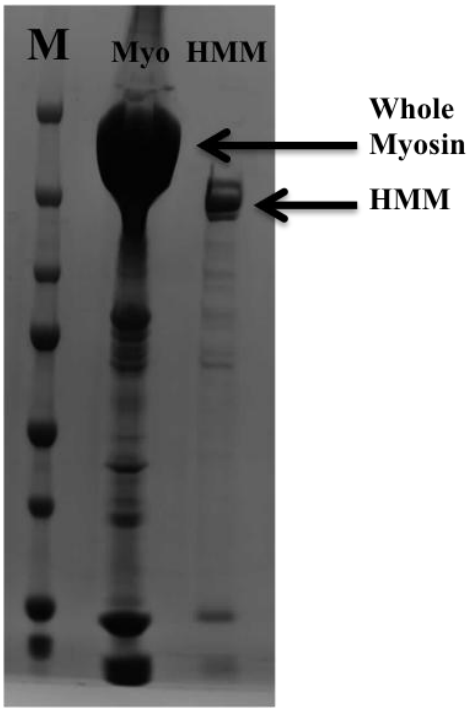
for 10 minutes. This pellet was then weighed and resuspended in 1/4 weight/volume of 4 M KCl. Finally the dissolved myosin was centrifuged at 146,000 x g (45,000 rpm, Sorvall Discovery 90SE, T-865 rotor) for 1 hour and the supernatant retained. After which the final product was preserved by dropping 100µl aliquots directly into liquid nitrogen to form myosin pellets, which were then stored in liquid nitrogen for future use for about one year (Figure 2.1). The concentration of the myosin obtained was usually in the range of 30-60 mg/ml.

2.2.1.2 Preparation of Heavy Meromyosin for the IVMA

Heavy Meromyosin (HMM) is an enzymatically shortened version of myosin consisting of sub-fragment 1, part of the rod and the two light chains (Weeds and Taylor, 1975). This form of myosin, without the majority of the long hydrophobic C-terminal rod, is required as the immobilized motor protein in the IVMA. The protocol is based on the method of Okamoto (Okamoto and Sekine, 1985, Fraser and Marston, 1995). A myosin pellet (see 2.2.1.1) was thawed from liquid nitrogen on ice and diluted with HMM buffer A (HA) (0.1 mM $NaHCO_3$, 0.1 mM EGTA, 2 mM DTT, pH 7.4). The thawed myosin was diluted to about 1.9 mg/ml in 1.5 ml of buffer HA and mixed thoroughly, this homogenate was incubated at 4° C for 20 minutes. The myosin was pelleted by centrifugation at 21,100 x g (14,800 rpm, Thermo Scientific Heraecus Fresco 21) for 10 minutes at 4° C. The supernatant was discarded and the pellet dissolved gently in 100 µl of HMM buffer B (HB) (1 M KCl, 20 mM imidazole, 4 mM $MgCl_2$ 2 mM DTT, pH 7) and incubated at 4° C for 10 minutes. The total volume was then made up to 200 µl with the addition of buffer HA and incubated in an Eppendorf thermomixer at 25° C for ten minutes. The myosin was then cleaved by incubation with 7.5 µl of 0.4 mg/ml TLCK treated α-chymotrypsin (Sigma type VII, C-3142) for 9 minutes at

25° C. The digestion was stopped by the addition of 2.7 ml of chilled buffer HA containing additional 3 mM $MgCl_2$ and 0.1 mM phenylmethylsulfonyl fluoride (PMSF). The mixture was incubated at 4° C for 30 minutes and then centrifuged at 337,000 x g (100,000 rpm. Sorvall MC-120SE, S100-AT6 rotor) for 20 minutes at 4° C. The supernatant contained pure HMM which was stored at 4° C for use with the IVMA (Figure 2.1). HMM prepared by this method could be used for up to five days. The concentration was determined by Bradford assay (see section 2.4.1.1). The range of concentrations usually obtained and suitable for use in the IVMA was 0.3-0.7 mg/ml.

Figure 2.1: Myosin and HMM purification SDS-PAGE gel

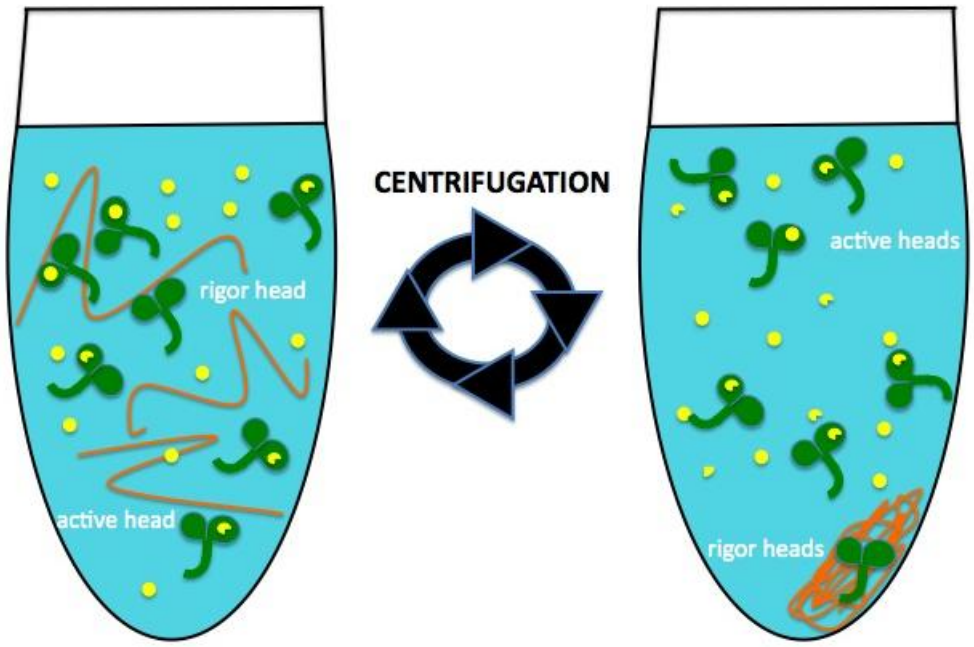


M = marker; Myo = myosin pellet; HMM = HMM after cleavage

2.2.1.3 Affinity Precipitation of HMM

In the *in vitro* motility assay filament movement is prevented by the presence of more than 1% HMM "rigor heads". These "rigor heads" show irreversible, ATP insensitive binding and hence lead to a lower fraction of the filaments being motile. The product of the HMM preparation (see 2.2.1.2) was pure HMM, but not necessarily fully functional HMM. To minimise the presence of "rigor heads", HMM preparations were treated with F-actin in the presence of ATP (Kron and Spudich 1986, Fraser and Marston 1995) prior to use in the motility assay (see Figure 2.2). Skeletal muscle HMM was mixed with F-actin and Mg^{2+}-ATP to final concentrations of 200 μg/ml, 150 μg/ml and 1 mM respectively in motility buffer A (see section 2.5.1) and incubated on ice for 10 minutes. The mixture was centrifuged at 337,000 x g (100,000 rpm, Sorvall MC-120SE, S100-AT6 rotor) for 15 minutes at 4° C to pellet the F-actin and associated rigor heads. This leaves pure and functional HMM in the supernatant which when stored on ice could be used for 4-5 hours in the motility assay, before rigor heads returned and interfered with the assay.

Figure 2.2: Schematic representation of the affinity precipitation of HMM



ATP represented by yellow dots; ADP+Pi represented by 3/4 of a yellow dot; actin represented by orange lines; HMM in green.

2.2.2 Preparation of F-actin

2.2.2.1 Acetone Powder Preparation from Rabbit Skeletal Muscle

To prepare skeletal muscle F-actin, skeletal muscle acetone powder was made by treating the pellet obtained from the initial myosin extraction (section 2.2.1.1) with a series of washes, before being dried to form the acetone powder. This protocol is based on the methods of Straub (1942). In each step, the muscle residue was dispersed by manual homogenising and then filtered through a nylon mesh and squeezed to drain liquid. The weighed pellet was washed as follows:

1) 10 volumes of cold dH_2O for 5 minutes at 4° C, repeated twice.
2) 4 volumes of 0.4% $NaHCO_3$, for 45 minutes at room temperature with stirring.
3) 2 volumes of 1 mM Tris-HCl pH 8.5, for 5 minutes at 4° C, repeated twice.

4) 4 volumes of acetone, for 10 minutes at 4° C, repeated four times.

Following the final acetone wash the residual pellet was dried to a powder in a fume hood overnight and then stored at –20° C until used.

2.2.2.2 F-actin Preparation from Acetone Powder

The method for preparation of F-actin from acetone powder is based on the Spudich method (Spudich and Watt, 1971) with an additional step of a S300 gel filtration column. A sample of about 2.5 g of acetone powder (see section 2.2.2.1) was removed from the -20° C storage and allowed to warm to 4° C. The acetone powder was then dissolved in 50 ml of G-actin buffer (2 mM Tris-HCl, 0.2 mM ATP, 0.1 mM $CaCl_2$, 1 mM NaN_3, 500 nM DTT, pH 8.0) and stirred for 30 minutes at 4° C. The solution was centrifuged at 15,000 x g (18,000 rpm, Sorvall Evolution RC, SS-34 rotor) for 20 minutes at 4° C. The pellet was re-extracted in an additional 15 ml of G-actin buffer and centrifuged as before. The supernatants were combined and filtered through glass wool into a measuring cylinder. G-actin polymerization was obtained with the addition of 0.1 volume of 10x KME buffer, (0.5 M KCl, 100 mM Tris-HCl, 25 mM $MgCl_2$, 10 mM EGTA, 10 mM NaN_3, pH 8.0) and gentle mixing, by sealing the measuring cylinder with parafilm™ and inverting it slowly several times. It was then incubated in a water bath at 30° C for 45 minutes. The KCl concentration was then adjusted to 0.8 M by the addition of 0.34 volumes of 3 M KCl. This solution was mixed at room temperature for 20 minutes by intermittent inversion of the resealed measuring cylinder. The resulting F-actin, free of troponin and tropomyosin, was pelleted by centrifugation at 146,000 x g (45,000 rpm, Sorvall Discovery 90SE, T-865 rotor) for 1.5 hours at 4° C. The supernatant was discarded, the pellets rinsed in distilled H_2O and then dissolved in 12-13 ml of G-actin buffer for a final concentration of 5-6 mg/ml. The dissolved actin was then homogenized using a Dounce homogeniser before being dialysed against G-actin buffer for 48 hours, the

reduction in the concentration of KCl caused the actin to depolymerise. The dialysate was centrifuged at 146,000 x g (45,000 rpm, Sorvall Discovery 90SE, T-865 rotor) for 1.5 hours at 4° C.

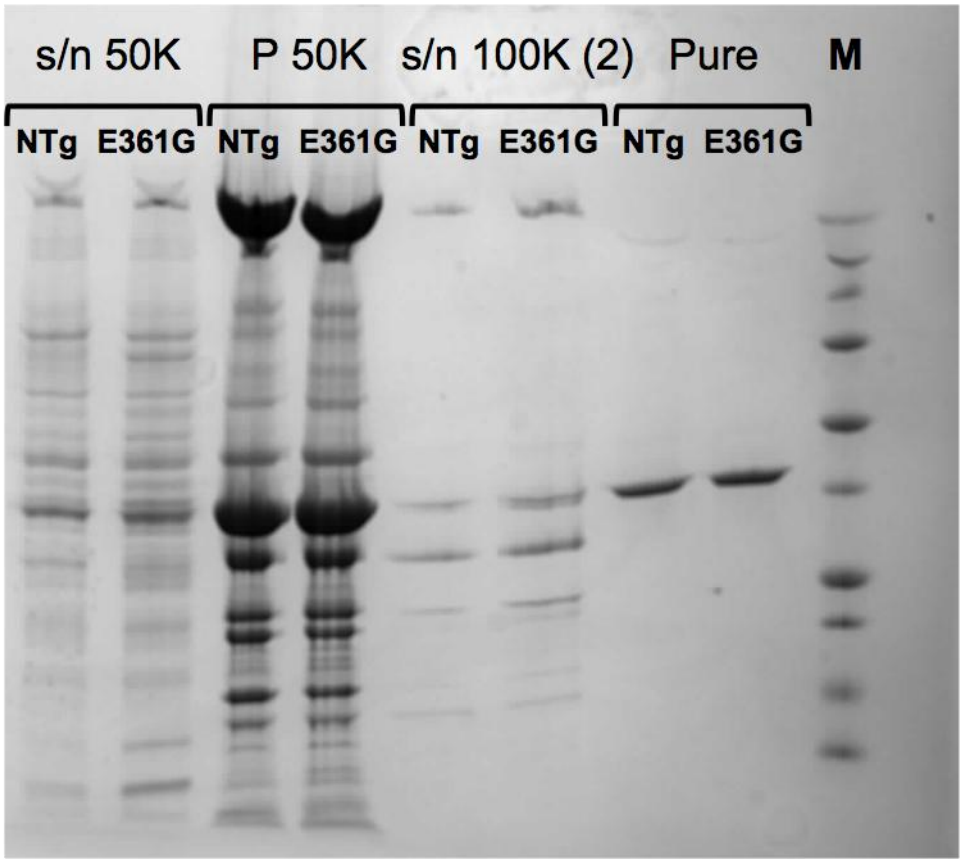
The G-actin supernatant was filtered through glass wool and loaded onto a 2.5 x 90 cm Sephacryl S300 gel filtration column, which had previously been equilibriated with 1.5 l of G-actin buffer. This was run overnight at a flow rate of 50 ml/hour with fractions being collected every 6 minutes. A single peak was recorded on the Pharmacia U.V. monitor II system. Fractions producing the peak were checked by measuring their optical density (absorbance) at 290 nm in a quartz cuvette. Any fractions that gave a reading of higher than 0.35 were pooled together. The G-actin was polymerized for the final time by the addition of 0.1 volumes of 10x KME buffer at 30° C for 45 minutes and centrifuged at 146,000 x g (45,000 rpm, Sorvall Discovery 90SE, T-865 rotor) for 1.5 hours at 4° C as before. The supernatant was discarded and the F-actin pellets were dissolved in ATPase buffer (100 mM KCl, 5 mM PIPES-K_2, 2.5 mM $MgCl_2$, 1 mM DTT, 10 mM NaN_3, pH 7.3) at around 10 mg/ml. This was stored for up to a month at 4° C for experimental use.

2.2.2.3 F-actin Isolation from Transgenic Mouse Heart

F-actin was isolated simultaneously from 5-7 week-old mutant (actin E361G, see section 2.1.1.4) and non-transgenic littermates mouse hearts. Since E361G F-actin was deficient in the mutation when extracted via an acetone powder method (see section 2.2.2.1) it was deduced that the monomeric form is unstable and aggregates in certain conditions. We therefore used a method of purification developed by Dr E. Dyer (Song et al., 2010). It preserved the 50% mutant actin content, as proved through 2DE (see section 3.3.2).

One heart (50-100 mg) was pulverised in a liquid nitrogen cooled percussion mortar and homogenised in a 10x volume of wash buffer containing 20 mM Pi, 0.1 M NaCl, 5 mM $MgCl_2$, 0.5 mM EGTA, 5 mM DTT with 2 μg/ml of each of the protease inhibitors (E-64, chymostatin, leupeptin & pepstatin A), pH7.0. Samples were spun at 21,100 x g (14,800 rpm, Thermo Scientific Heraeus Fresco 21) for 3 minutes at 4° C. This washing step was repeated 4 times and the pellet was then extracted twice in 1.5 volume of thin filament extraction buffer (5 mM Mg-ATP and 1.5 μM blebbistatin in wash buffer) and centrifuged at 21,100 x g (14,800 rpm, Thermo Scientific Heraeus Fresco 21) for 3 minutes at 4° C. The supernatants were combined and centrifuged at 111,700 x g (50,000 rpm, Sorvall RCM120SE, S100-AT6) for 5 minutes at 4° C. Again the supernatant was retained and subjected to a further centrifugation of 446,800 x g (100,000 rpm, Sorvall RCM120SE, RCM-120 rotor) for 25 minutes at 4° C. The pellet, containing thin filaments, was resuspended in 1.5 volume of 'actin resuspension buffer' (20 mM Pi, 0.1 M NaCl, 5 mM $MgCl_2$ and 1 mM ATP, pH 6.0) and dialysed for 3 hours at 4° C. A 2 minutes spin at 21,100 x g (14,800 rpm, Thermo Scientific Heraeus Fresco 21) at 4° C removed the remaining myosin. 3 M KCl stock was added to the supernatant to a final concentration of 0.8 M to dissociate actin from troponin-tropomyosin. 150 nM TRITC-phalloidin was also added. The actin solution was centrifuged at 446,800 x g (100,000 rpm, Sorvall RCM120SE, S100-AT6 rotor) for 25 minutes at 4° C. Finally the pellet containing the F-actin was resuspended in 50 μl of 'ACEX buffer' (2 mM Tris-HCl, 0.2 mM $CaCl_2$, 0.2 mM ATP, 1 mM DTT, pH 8.0) overnight at 4° C. The F-actin was then labelled with TRITC-phalloidin for IVMA investigation (see section 2.5.2). An SDS-PAGE gel with some of the purification steps is shown in Figure 2.3.

Figure 2.3: Actin NTg and E361G purification SDS-PAGE gel



s/n = supernatant; 50K = 50.000 rpm; P = pellet; 100K = 100.000 rpm; M = marker; NTg = non-transgenic. '(2)' indicates that it was the second 100.000 rpm centrifugation.

2.2.2.4 F-actin Isolation from Human Skeletal Muscle Biopsy

Muscle acetone powder was made in parallel from several 30 µm-thick cryosections (6 mg total) of frozen muscle from a biopsy of a patient carrying an actin mutation (either K326N or D292V, see section 2.1.3) and a control age matched frozen biopsy, as described previously (D'Amico et al., 2006, Marston et al., 2004, Razzaq et al., 1999).

The muscle was washed in 0.5 ml of York modified glycerol (20 mM Pi, 50% glycerol, 0.5% Triton X-100, 2 mM $MgCl_2$, 1 mM DTT, 1 mM NaN_3, pH 7.0) and then spun for 2 min at 21,100 x g (14,800 rpm, Thermo Scientific Heraeus Fresco 21). The pellet was extracted in 500 µl of high salt buffer (20 mM Pi, 800 mM KCl, pH 7.0) at room temperature for 2 min. After centrifuging again, the pellet was washed twice with deionized water (1 ml and then 0.5

ml) to remove salt, and dehydrated using 50 and then 100% ice-cold acetone, followed by air-drying at room temperature for around 15 min.

Monomeric actin was extracted from the acetone powder with 2 consecutive 30 µl aliquots of ACEX (2 mM Tris-HCl, 0.2 mM $CaCl_2$, 0.2 mM ATP, 1 mM DTT, pH 8.0) for 25 minutes, with 5 minutes sonication at the start of each extraction, then centrifugation for 20 minutes at 21,100 x g (14,800 rpm, Thermo Scientific Heraeus Fresco 21). The G-actin containing supernatant was sedimented at 446,800 x g (100,000 rpm, Sorvall RCM120SE, S100-AT6 rotor) for 20 minutes to remove aggregated actin. The extracted G-actin was polymerized by adding 1/10 volume of a buffer containing 500 mM KCl, 20 mM $MgCl_2$ and TRITC-phalloidin to 200 nM (from 33 µM stock), and incubating for 2 hours at room temperature. F-actin was isolated by sedimentation at 446,800 x g for 20 minutes at 4° C. Actin concentration was about 1 µM.

2.2.3 Purification of the Troponin Complex

2.2.3.1 Human and Mouse Cardiac Troponin Preparation

Troponin was purified from human and mouse cardiac tissue by the method of Messer (Messer et al., 2007). The desired tissue sample was removed from storage in liquid nitrogen. One mouse heart (around 100 mg) or 100-150 mg of human heart tissue was immediately pulverized in a percussion motor, which was cooled with liquid nitrogen. After pulverisation the tissue sample was washed and manually homogenized with a micropestle in 1.5 ml of 'myofibril wash buffer' (5 mM NaH_2PO_4, 5 mM Na_2HPO_4, 0.1 M NaCl, 5 mM $MgCl_2$, 0.5 mM EGTA, 0.1% Triton X-100, 5 mM DTT, pH 7, and 2 µg/ml of the protease inhibitors E-64, chymostatin, leupeptin and pepstatin A). The homogenate was then centrifuged at 21,100

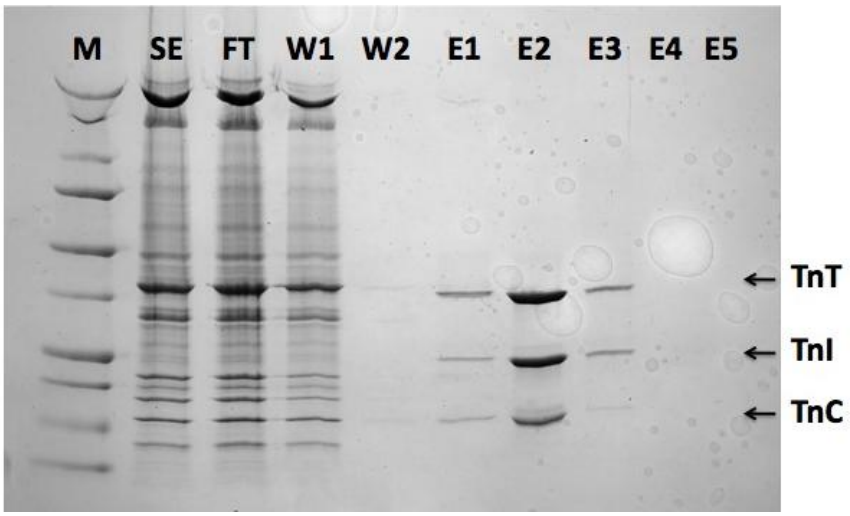
x g (14,800 rpm, Thermo Scientific Heraeus Fresco 21) for 3 minutes at 4° C. The pellet was kept, resuspended and pelleted in the same fashion a further three times.

The myofilament proteins present in the pellet were dissolved in 5 volumes of 'troponin extraction buffer' (0.7 M LiCl, 25 mM Tris, 5 mM EGTA , 0.1 mM $CaCl_2$, 5 mM DTT, pH 7.5 and 2 μg/ml of each protease inhibitor). The mixture was homogenized with a micropestle and then mixed on a rotating wheel for 25 minutes at 4° C. After which the homogenate was centrifuged at 21,100 x g (14,800 rpm, Thermo Scientific Heraeus Fresco 21) for 3 minutes at 4° C. The supernatant was retained and kept at 4° C, while the pellet underwent three subsequent extractions stages spending 20, 15 and 10 minutes on the rotating wheel respectively. The supernatant was added to the pool of supernatant at the end of each stage. After the final extraction the pooled supernatant was centrifuged at 337,000 x g (100,000 rpm, Sorvall RCM-120SE, S100-AT6 rotor) for 20 minutes at 4° C. After this step the supernatant was saved and it was referred to as the 'spun extract'.

The troponin was purified from the spun extract by affinity column chromatography. The affinity column consisted of 0.6 ml of CNBr Sepharose CL-4B conjugated with a monoclonal anti-troponin I antibody (14G5) gift from N. Gusev and A. Katrukha (Katrukha et al., 1995). The matrix was equilibrated in 4.5 ml of troponin extraction buffer prior to the addition of spun extract. After adding the spun extract to the column it was mixed for 15 minutes on the rotating wheel at 4°C. Eight 2 ml tubes were setup and labelled: flow through (FT), wash 1 & 2 (W1&2), and elution fraction 1-5 (E1-5). In each of the elution fractions tubes 50 μl of 1 M MOPS pH 8 was aliquoted, this was to neutralize the low pH of the elution buffer. After 15 minutes on the rotating wheel the liquid phase of the column was completely eluted into the FT 2 ml tube. The column matrix was then washed twice with 0.8 ml of troponin extraction buffer (W1&2). Finally the troponin was eluted with 0.4 ml of elution buffer (0.1 M glycine,

5 mM DTT pH 2 and protease inhibitors) added five times sequentially (E1-5). The elution fraction in which the troponin was present was determined by SDS-PAGE (see section 2.4.2). Samples were taken from each stage of the column elution process, 20 µl of each stage was mixed with 20 µl of 2x SDS Sample buffer (see Figure 2.4). The troponin usually eluted in fraction E2, and sporadically in E1. Therefore, immediately after elution these 2 samples were put into dialysis against 'troponin dialysis buffer' (1 M KCl, 10 mM MES, 0.1 mM $CaCl_2$, 5 mM DTT, pH 6 with protease inhibitors). These samples were dialysed overnight at 4° C. The following day the elution fraction which contained the troponin was kept and the other discarded. The troponin was then centrifuged at 21,100 x g (14,800 rpm, Thermo Scientific Heraeus Fresco 21) for 3 minutes at 4° C. The supernatant was kept and stored at 4° C for use with the IVMA. The final concentration was determined by Lowry assay (see section 2.4.1.2), this was normally in the range of 5-10 µM and around 400 µl was normally obtained. Troponin purified from both human and mouse heart was active for 2 days.

Figure 2.4: SDS-PAGE gel of troponin elution steps



M=molecular weight marker; SE= spun extract; FT= flow through; W1-2= wash one-two; E1-5= elution fractions one to five. As visible troponin was eluted mainly in fraction E2 and presented each of the 3 subunits.

2.2.3.2 Preparation of Rabbit Skeletal Muscle Troponin

Rabbit skeletal muscle troponin was purified from an ethanol-ether powder as human cardiac tropomyosin (see section 2.2.4.1), by the method of Potter (Potter, 1982), but the starting material was 300 g of rabbit skeletal back muscle. The preparation was completed by O'Neal Copeland. The yield was of about 60 mg every 100 g of ethanol-ether powder.

2.2.4 Purification of Tropomyosin

2.2.4.1 Preparation of Human Cardiac Tropomyosin

Human cardiac tropomyosin was prepared by O'Neal Copeland following a method based on that of Eisenberg and Kielley (Eisenberg and Kielley, 1974) and described by Knott *et al*. (Knott et al., 2002). An ethanol-ether powder was prepared from 30 g of human cardiac muscle from which the tropomyosin was extracted and purified. The yield was of 5-10 mg of tropomyosin from 2-3 grams of ethanol-ether powder.

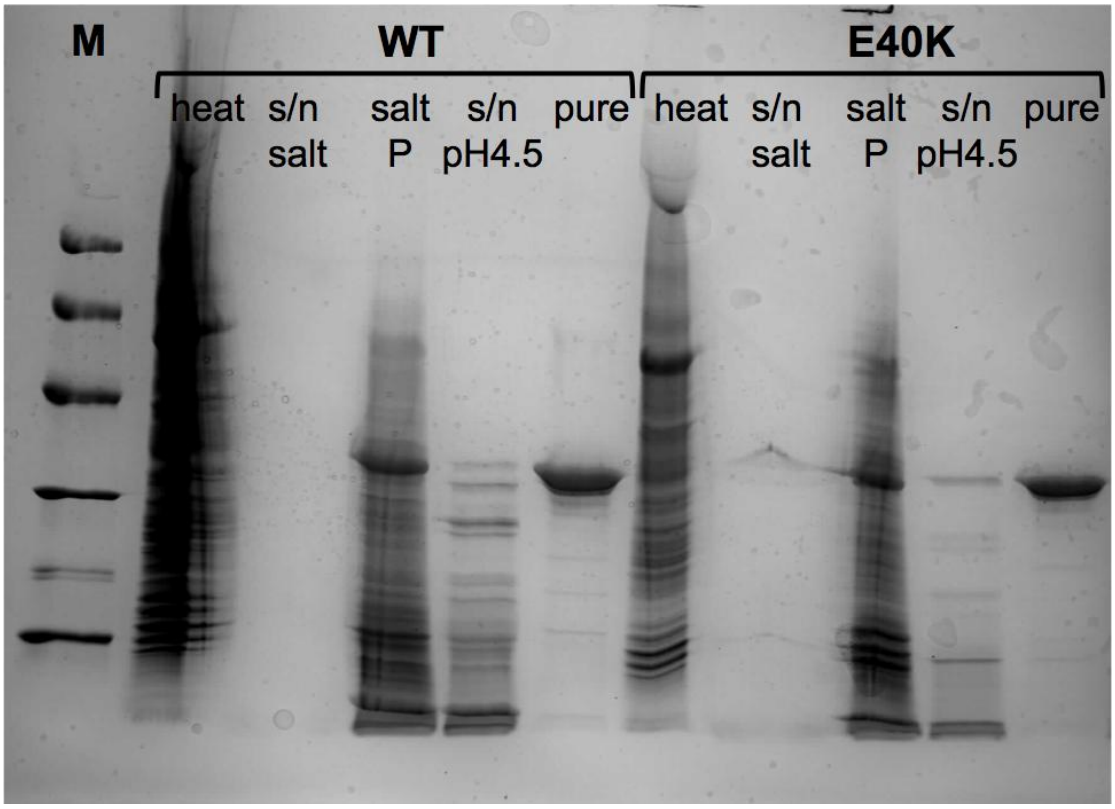
2.2.4.2 Tropomyosin Preparation from Baculovirus/*sf9* Cell Pellets

Recombinant tropomyosin expressed with the baculovirus/*sf9* system was purified with a protocol based on that by Akkari *et al.* (2002).

A baculovirus/*sf9* cell pellet was removed from storage in liquid nitrogen and thawed at room temperature. Tropomyosin was extracted twice with 5 volume/volume of a buffer containing 1 M NaCl, 50 mM imidazole (pH 7.0), 0.5 mM $MgCl_2$, 1 mM EDTA, 1 mM EGTA, 0.1 mM PMSF, 5 mM DTT and 2 μg/ml of the protease inhibitors (E-64, chymostatin, leupeptin and pepstatin A). The mixture was homogenized with an electric homogeniser (Heidolph, DIAX 900), then mixed on a rotating wheel for 10 minutes at 4° C and spun at 27,100 x g (30,000 rpm, Sorvall RCM-120SE, S100-AT6 rotor) for 10 minutes at 4° C. Supernatant was kept and then put in a water bath for 10 minutes at around 100° C. This was then spun again at

21,100 x g (14,800 rpm, Thermo Scientific Heraeus Fresco 21) for 10 minutes at 4° C. The supernatant was saved and tropomyosin was precipitated by adding 70% weight/volume ammonium sulphate to the solution. This was spun again at 21,100 x g (14,800 rpm, Thermo Scientific Heraeus Fresco 21), the supernatant was discarded, while the pellet was collected and dissolved in a buffer containing 0.4 M NaCl, 5 mM PIPES pH 7.1, 5 mM DTT and protease inhibitors. The sample was dialysed overnight at 4° C in the same buffer. The following day the sample was spun at 21,100 x g and then the supernatant was dialysed at 4° C in a buffer containing 50 mM NaH_2PO_4 pH 4.5, 1 M NaCl, 5 mM DTT and protease inhibitors for 5-7 hours. The low pH makes tropomyosin precipitate once again. The sample was spun at 21,100 x g for 10 minutes at 4° C and the pellet was resuspended in 0.5-1 ml of a buffer containing 1 M NaCl, 5 mM PIPES pH 7.1, 5 mM DTT and protease inhibitors. The sample was dialysed overnight in the same buffer at 4° C. The sample obtained the following day was referred to as ‘crude tropomyosin’ and it was spun once more for 10 minutes at 21,100 x g at 4° C. The supernatant contained ‘pure tropomyosin’ whose purity was determined by SDS-PAGE (see section 2.4.2). Samples were taken from each stage of the purification process for screening. The usual yield was 1-2 mg/ml of cell pellet. An SDS-PAGE gel with some of the purification steps is shown in Figure 2.5.

Figure 2.5: SDS-PAGE gel of baculovirus/*sf9* tropomyosin purification steps



M = marker; heat = water bath 100° C; s/n = supernatant; salt = salting out.

2.2.5 Purification of α-actinin

α-actinin was prepared by Prof. S. Marston from chicken gizzard as described by Bing *et al.* (2000) based on the method by Craig *et al.* (1982).

2.3 Manipulation of Troponin Phosphorylation

2.3.1 Protein Kinase A Treatment of Human Cardiac Troponin

The troponin I (TnI) phosphorylation level on the human heart sample carrying the TnI K36Q mutation proved to be lower than the average donor level. Therefore in order to investigate the relationship between thin filament Ca^{2+}-sensitivity and constituent TnI phosphorylation it was desirable to be able to increase the level of TnI phosphorylation. Mutant troponin was

taken after the column separation (see section 2.2.3.1) and dialysed against 'phosphorylation buffer B' (0.5 M KCl, 50 mM MOPS pH 7.0, 20 mM NaF, 1 mM DTT and 10 mM $MgCl_2$) for 4 hours at 4° C. The PKA catalytic subunit from bovine pancreas (Sigma, P2645-400) was then prepared by making a 2,000 units/ml solution by dissolving the PKA in 'phosphorylation buffer A' (same as phosphorylation buffer B but with no KCl). The PKA treatment reaction mixture consisted of 400 μl of purified troponin, 32 μl of PKA (2,000 units/ml), 9 μl of Mg^{2+}-ATP (100 mM) and 9 μl of phosphorylation buffer B. The control reaction mixture consisted of 400 μl of purified troponin and 50 μl of phosphorylation buffer B. These mixtures were added to a 1.5 ml eppendorf and incubated overnight at 4° C on a rotating wheel. Finally, they were centrifuged at 21,100 x g (14,800 rpm, Thermo Scientific Heraeus Fresco 21) for 5 minutes at 4° C to remove any insoluble material. The supernatant, which contained phosphorylated troponin, was collected and stored at 4° C.

2.3.2 Dephosphorylation of Troponin

Throughout the study of DCM mutations one of the key parameters to evaluate the functional differences between wild-type and mutant thin filaments, has been the response to inotropic stimulation. A complete dephosphorylation was therefore necessary to evaluate the response in Ca^{2+}-sensitivity to TnI phosphorylation.

Before the overnight dialysis step (see section 2.2.3.1), troponin can be dephosphorylated by incubating with 90 U/ml Shrimp Alkaline Phosphatase (SIGMA P9088). The extracted troponin was mixed with the phosphatase and dialysed overnight at 4° C against the troponin dialysis buffer. The dialysate was centrifuged at 21,100 x g (14,800 rpm, Thermo Scientific Heraeus Fresco 21) for 10 minutes at 4° C to remove any insoluble material. The supernatant contained dephosphorylated troponin.

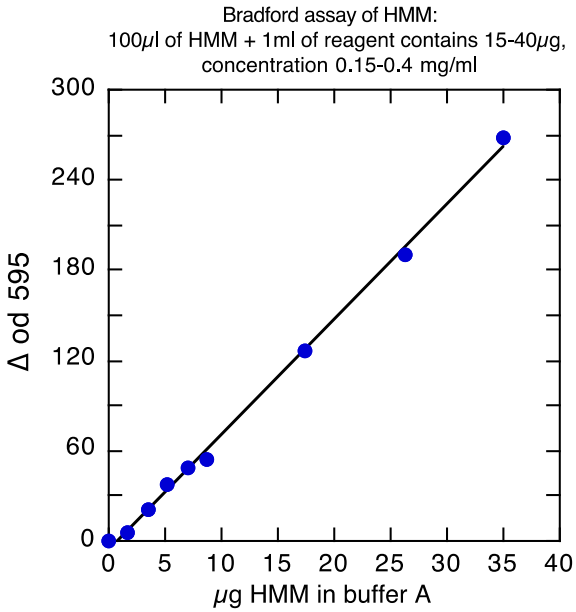
2.4 Analysis of Protein

2.4.1 Determination of Protein Concentration

2.4.1.1 The Bradford Assay

The Bradford assay was used to rapidly determine the concentration of the HMM preparation as it was expected to be relatively constant (Bradford, 1976). 100 µl of HMM were mixed thoroughly and incubated with 1ml of Bradford reagent (Sigma, B6916) for 5 minutes at room temperature. A blank, consisting of just 1ml of Bradford reagent, was also incubated for the same time. The absorbance of the solution was measured at 595 nm, after zeroing the spectrophotometer using the blank. The concentration was determined using the previously established calibration curve (see Figure 2.6).

Figure 2.6: Calibration curve for the Bradford assay



2.4.1.2 The Lowry Assay

The Lowry assay was used for solutions where the protein concentration was relatively low (Lowry et al., 1951), which was the case for most of the proteins used in this thesis with the exception of HMM. To start, Lowry solution A was prepared which consisted of 48 ml of 2% Na_2CO_3, 1ml of 0.5% $CuSO_4$ and 1 ml of 1% NaK tartrate. Aliquots of 5 µl, 10 µl and 15 µl of the protein solution (1-2 mg/ml) were taken and made up to 500 µl with NaOH, to which 5 ml of Lowry solution A was added. This mixture was vortexed and incubated at room temperature for 10 minutes. Following this 500 µl of Lowry solution B (1 part Folin and Ciocalteu's reagent to 1 part distilled H_2O) was added and the mixture vortexed and incubated at room temperature for 30 minutes. Finally the absorbance of each aliquot was measured at 700 nm, and the protein concentration determined from a previously established calibration curve.

2.4.2 Sodium Dodecylsulphate Polyacrylamide Gel Electrophoresis (SDS-PAGE)

2.4.2.1 Sample Preparation

Protein solutions were diluted 1:1 (v/v) with '2x SDS sample buffer' (125 mM Tris-HCl, 10% Sodium dodecylsulphate (SDS), 130 mM DTT, 0.05% bromophenol blue, pH 6.8). The samples were then heated at about 95° C for 3 minutes.

2.4.2.2 The Pharmacia System

Two forms of discontinuous SDS PAGE were used during this study: the Pharmacia system and the mini PROTEAN system. The Pharmacia system was used preferentially, as the set-up time was shorter. However, the Excel gels were more difficult to handle when the backing

they are attached to was removed, which was needed to visualise proteins with a fluorescent stain. In these cases, mini PROTEAN gels, which were more robust, were used instead.
For the Pharmacia system, precast gels on plastic backings (Excelgel-SDS 8-18% gradient, Pharmacia LKB) were orientated on the pre-cooled horizontal plate of a Multiphor II (Pharmacia LKB) electrophoresis system. Polyacrylamide anodic and cathodic buffer strips were placed horizontal and parallel at the top and bottom edges of the gel. Loading strips, consisting of precut pieces of filter paper 5 mm x 10 mm, were placed approximately 5 mm apart adjacent to the cathodic buffer strip. Up to 20 µl of prepared samples were pipetted into the loading strips in a predetermined order. Electrophoresis of a full gel was completed at 50 mA/ 600 V/ 30 W (a half gel was run at 25 mA/ 600 V/ 15 W) for 80 minutes at 10° C.

2.4.2.3 The Mini PROTEAN System

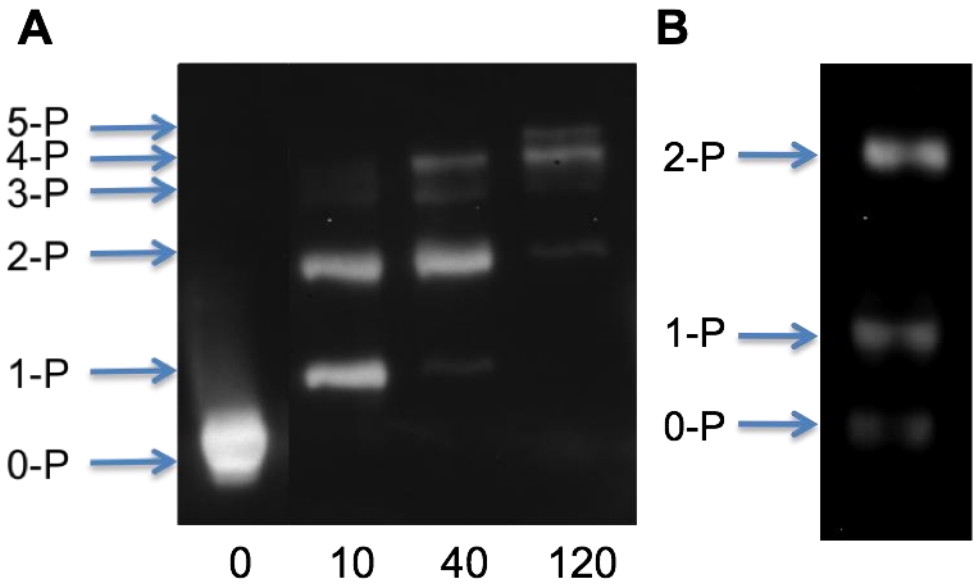
The mini PROTEAN tetra system (BioRad laboratories) was run with a 12% resolving/ 4% stacker polyacrylamide gel (37.5:1 acrylamide:bisacrylamide ratio). Electrophoresis was completed at 25 mA/ 200 V for 90 minutes in standard ‘Laemmli running buffer’ (25 mM Tris-Base, 192 mM glycine, 0.1% SDS) (Laemmli, 1970).

2.4.2.4 Phosphate Affinity SDS-PAGE

Phosphate affinity SDS-PAGE is a relatively novel technique invented by Kinoshita *et al.* (Kinoshita et al., 2006, Kinoshita-Kikuta et al., 2007), which separates the phospho-species of a protein by retarding them relative to phosphate content (Figure 2.7). This technique has been used to investigate the phosphorylation site distribution of cardiac troponin I in human heart muscle (Messer et al., 2009).The advantage of phosphate affinity SDS-PAGE is that you can determine the amount of phosphate per amount of protein without the need for an internal (radioactive) standard. In this study phosphate affinity SDS-PAGE was used to

determine the level of TnI phosphorylation. For this technique phos-tag pendent moieties (NARD Institute, Hyogo, Japan) are included in the ingredients of the polyacrylamide gel (Kinoshita et al., 2006, Kinoshita-Kikuta et al., 2007). The gel was composed of 10% resolving (+50 μM Mn-Phos-tag acrylamide)/ 4% stacker polyacrylamide gel (29:1 acrylamide:bisacrylamide ratio). The phos-tag gels were electrophoresed (25 mA/ 200 V for 90 minutes) and Western blotted (see 2.4.4.).

Figure 2.7: Phosphate affinity SDS-PAGE examples



A) This example is from the study by Messer *et al* who treated recombinant TnI with PKA at 30°C for 120 minutes. Samples were taken at time points 0 minutes, 10 minutes, 40 minutes and 120 minutes, run onto a phosphate-affinity mini gel and then Western blotted with the anti-TnI antibody (14G5). The different phosphospecies of TnI: unphosphorylated (0-P), mono-phosphorylated (1-P), bis-phosphorylated (2-P), tris-phosphorylated (3-P), tetra kis-phosphorylated (4-P) and penta kis-phosphorylated (5-P). This image was taken from the study by Messer *et al* (2009). B) Another Western blot of phosphate-affinity mini gel. This is an example of Tn purified from human sample (NE). It can be observed how only three phosphospecies of TnI are present and the different ratios present *in vivo*.

2.4.3 Protein Staining

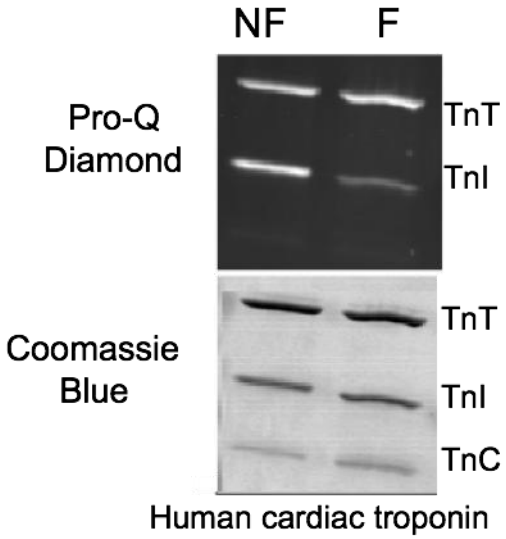
2.4.3.1 Coomassie Blue

Coomassie blue staining solution (800 ml) was made up from 2 PhastGel™Blue R tablets (GE Healthcare, 17-0518-01) dissolved in 60% methanol for 30 minutes and then diluted 1:1 with 20% acetic acid. Upon completion of electrophoresis the gel was immersed in fixing solution (50% methanol, 10% acetic acid) for 20 minutes with agitation at room temperature. The gel was then immersed in ~100 ml Coomassie Blue staining solution for 20 minutes with agitation at room temperature. The gel was then destained by immersion in 'destain solution' (25% methanol, 8% acetic acid) with agitation for 1 hour or until satisfactorily destained at room temperature. Coomassie blue staining solution was also used after Pro-Q Diamond stain (2.4.3.2) for which the same staining protocol was used but without the initial fix steps.

2.4.3.2 Pro-Q Diamond Phosphoprotein Stain

Pro-Q Diamond phosphoprotein gel stain (Invitrogen - Molecular Probes, P33300) is a fluorescent stain that is specific for proteins with phosphate moieties bound to threonine, serine and tyrosine residues (Steinberg et al., 2003, Schulenberg et al., 2003). It was a useful tool for analysing the phosphorylation profile of different myofilament proteins together or individually (Figure 2.8). Pro-Q Diamond phosphoprotein gel stain (Pro-Q Diamond) has also been shown to bind in a linear fashion for the amount of phosphate moieties present, therefore facilitating the quantitative measurement of changes in the level of phosphorylation of troponin I (Messer et al., 2007).

Figure 2.8: Example of mini gel stained with Pro-Q Diamond



A mini gel loaded with pure human non-failing (NF) and failing (F) heart troponin stained with Pro-Q Diamond (upper) and Coomassie blue (lower). As the TnT and TnI subunits have a degree of phosphorylation these are stained in both gels, TnC is not phosphorylated and thus does not appear with Pro-Q Diamond stain. It is also noticeable the sensitivity of the technique since it shows the difference in phosphorylation of TnI between non-failing and failing heart samples, as alredy reported by Messer *et al*. (2007).

After completion of electrophoresis the gel was immersed in 100 ml of freshly made Pro-Q Diamond fixing solution (50% methanol, 10% acetic acid) with agitation for 30 minutes at room temperature. The Pro-Q Diamond fixing solution was then replaced with another fresh 100 ml of the same solution, in which the gel was immersed overnight with agitation. The following day the gel was washed three times in 100 ml of distilled H_2O for 10 minutes. The gel was immersed in 60 ml of Pro-Q Diamond stain for 90 minutes in complete darkness. All remaining steps were completed in total darkness to prevent light contamination. The gel was then destained by three, 30 minute, washes with 90 ml of Pro-Q Diamond phosphoprotein gel destaining solution (Invitrogen, P-33311) and washed twice for 5 minutes in distilled H_2O. All immersion steps were completed with gentle agitation. If the gel was an Excelgel the backing was removed and the gel was not agitated. A digital image of the gel was then

visualised, using the U.V. transiluminator settings, by a cooled CCD camera based gel imager (G:Box Chemi XT16, Syngene) (G:BOX). After an image had been obtained the gel was then stained with a total protein stain, Coomassie Blue.

2.4.4 Western Blot Analysis

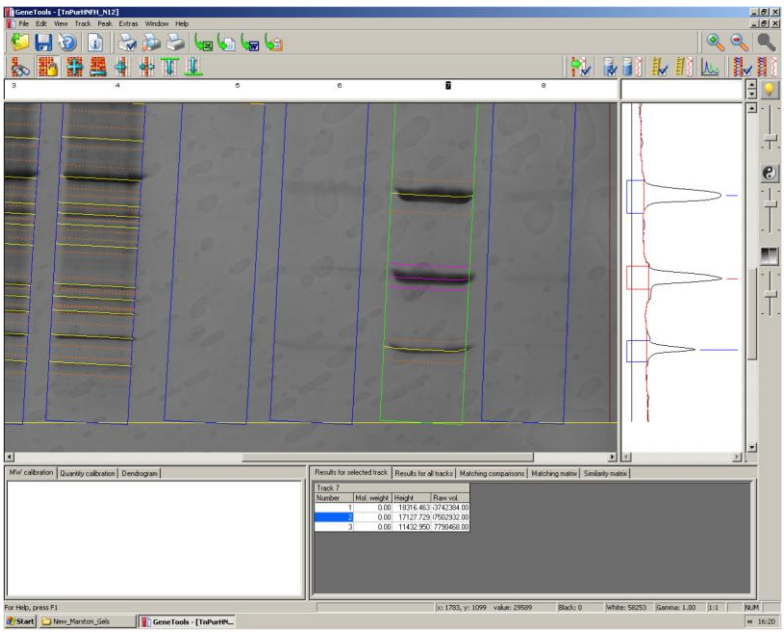
Protein samples were separated by SDS-PAGE (see 2.4.2.3). The gel was then immersed in pre-chilled 'transfer buffer' (25 mM Tris-Base, 192 mM glycine, 20% methanol) for 10 minutes. Polyvinylidene fluoride (PVDF) Transfer membrane (Hybond-P, GE Healthcare) was soaked in methanol for 10 seconds, washed in distilled water for 5 minutes and equilibriated with transfer buffer for 10 minutes. A wet western blot method was used and the blotting sandwich was made by putting the blotting apparatus in a container filled with transfer buffer with the cathodic side down. A pad was applied to this side, followed by a piece of filter paper, the gel, the PVDF membrane, then again a piece of filter paper and finally another pad. Everything was well soaked in transfer buffer and the sandwich was closed by clipping it with the anodic side of the blotting apparatus. The proteins were then transferred from the gel to the PVDF membrane for 1 hour at 100 V, 350 mA in the presence of transfer buffer using the Mini Trans-Blot cell (BioRad). After transfer, the PVDF membrane was immersed in PBS-Tween (PBS, 0.1% TWEEN-20) for 10 minutes. The PVDF membrane was then blocked in 50 ml of PBS-Tween-Milk (PBS, 0.1% TWEEN-20, 1% dried skimmed milk powder) to prevent non-specific binding of the antibody to the PVDF membrane. The protein of interest was probed using a specific primary antibody. One primary antibody was used in this study: anti-TnI (14G5) (1/2,000). The antibody was diluted in 10 ml of PBS-Tween-Milk and the PVDF membrane was immersed in this overnight at 4° C with agitation.

The following day the PVDF membrane was rinsed briefly three times in PBS-Tween, and then washed for 5 minutes, 3 times, in PBS-Tween. The secondary antibody was then added. This study used anti-mouse IgG, horseradish peroxidase linked whole antibody (from sheep) (GE Healthcare, NXA931), which was diluted 1/10,000 in 10 ml of PBS-Tween-Milk. The PVDF membrane was immersed in this for 1 hour. The PVDF membrane was then rinsed briefly three times in PBS-Tween, and then washed for 5 minutes, three times, in PBS-Tween. The proteins were then visualised using the ECL Plus Western Blotting Detection system (GE Healthcare, RPN2132) and the chemiluminscence was detected by a cooled CCD camera based gel imager (G:BOX Chemi XT16, Syngene). All immersion steps were completed at room temperature with agitation unless otherwise stated.

2.4.5 Densitometric Analysis

Digital images of gels and Western blots were visualised with a cooled CCD camera based gel imager (G:BOX Chemi XT16, Syngene) and GeneSnap (version 7.05, Synoptics Ltd) software. Exposure time for gels stained with Coomassie Blue was 80 ms, for Pro-Q Diamond phosphoprotein gel stain it was 1 and 2 minutes, for Western blots it was 10 and 30 seconds, then 1, 2 and 5 minutes. Protein bands were analysed by scanning densitometry using GeneTools (version 4.00, Synoptics Ltd, Figure 2.9) software (Messer et al., 2009, Copeland et al., 2010).

Figure 2.9: GeneTools densitometric analysis screenshot



Example of a GeneTools screenshot with the analysis of a troponin purification gel stained with Coomassie Blue. In detail is the analysis of the three troponin bands.

2.5 *In Vitro* Motility Assay

2.5.1 Buffers for IVMA

The basic buffer for IVMA is 'motility buffer A' (50 mM KCl, 25 mM imidazole, 4 mM $MgCl_2$, 1 mM EDTA, 5 mM DTT, pH 7.4). Alongside motility buffer A, motility buffers B, C & D are required for the IVMA. Buffer B consists of 4 ml of buffer A and 12 µl of 22.5% BSA. Buffer C consisted of 425 µl of cold distilled H_2O, 26 µl of catalase (Sigma, C3515) stock (26 mg/ml), 26 µl of glucose oxidase (Sigma, G6641) stock (19 mg/ml), 20 µl of glucose stock (100 mg/ml), 3 µl of 22.5% BSA and 500 µl of 1% methylcellulose dissolved in motility buffer 2A. Buffer D was almost identical but contained 415 µl of distilled H_2O and an addition of 10 µl of 100 mM Mg^{2+}-ATP.

2.5.2 Fluorescent Labelling of F-actin

F-actin was labelled with TRITC-phalloidin (ϕ) (Sigma, P1951), for visualisation under a fluorescence microscope. To label F-actin, 36 μl of the 33 μM TRITC-phalloidin was added to 438 μl of motility buffer A and vortex mixed. Stock F-actin was diluted to 1 mg/ml in motility buffer A and 20 μl were added to the aforementioned solution. The tube was then wrapped in aluminium foil and incubated for 16-18 hours at 4° C before use. Labelled actin was useable for 4 weeks after which another batch was prepared.

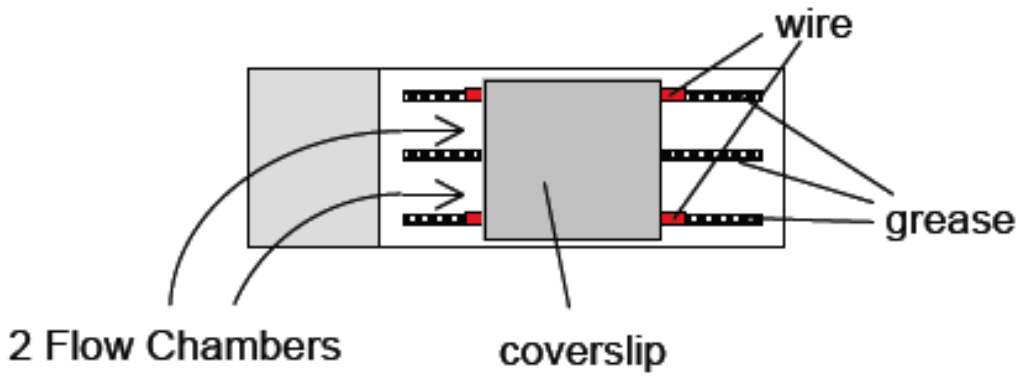
Actin prepared from biopsy was labelled during the purification, as explained in 2.2.2.4.

2.5.3 Preparation of the IVMA Flow Cell

Flow cells were constructed for the IVMA. All solutions and flow cells had to be kept dry by storage in a dessicator cabinet (Nalgene, 5317-0120). These consisted of a microscope slide (Sigma, S8400) and a coverslip (VWR, 631-0125), which were adhered by silicon grease (BDH, 63608 2B). The coverslips were given a siliconised coating by immersing and drawing backwards and forward in a solution of 40 ml of chloroform (Sigma, 496189) with 0.2% dichloromethylsilane (Fluka, 39909) for 1 minute, before slowly being withdraw. This was performed in a fume hood where the coverslips were left to dry for 30 minutes. The result of this process was to produce clean coverslips with a hydrophobic surface to which the motor protein (HMM) would adhere. Subsequent to the cell coating the microscope slides were lined with three parallel longitudinal rows of silicon grease at the top, middle and bottom of the slide. Half way along the top and bottom rows of grease a 2-3 cm piece of lacquered copper wire (100 μm diameter) was placed. To complete construction a siliconised coverslip was placed across all three rows of silicon grease (see Figure 2.10). The internal

volume of each channel of the flow cell is approximately 50 µl. Flow cells were prepared at least one day before they were used in the IVMA experiments.

Figure 2.10: Construction of flow cell



2.5.4 Reconstitution of Thin Filaments

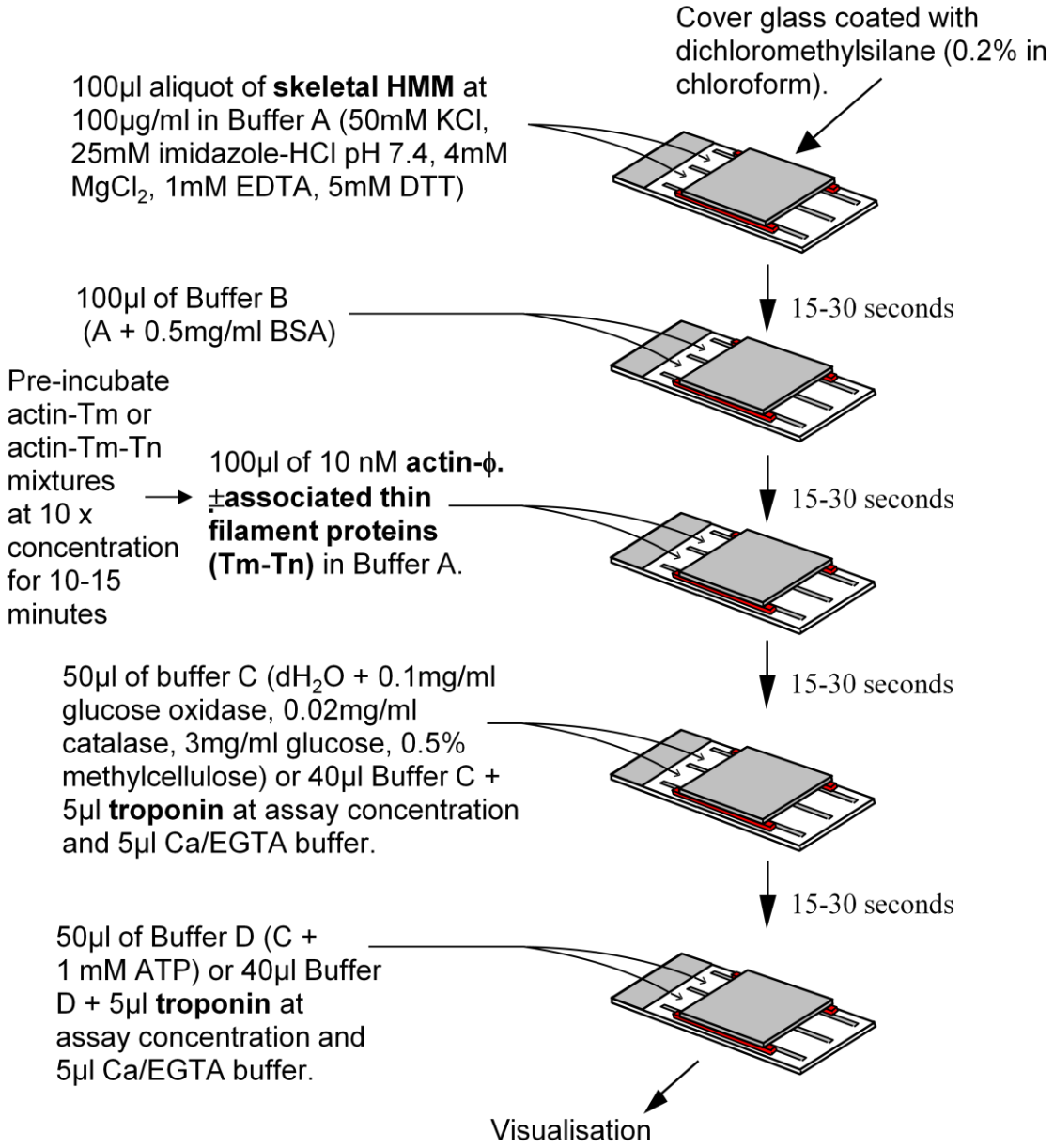
Stock solutions of 2 µM tropomyosin and troponin were made up with motility buffer A and kept on ice with the TRITC-phalloidin labelled actin (ϕ -actin, 100 nM). Thin filament solutions were prepared with the appropriate components added at ten-fold the required concentration for IVMA analysis. The motility buffer A was added first, followed by tropomyosin and troponin. This was thoroughly mixed before the ϕ- actin was added and mixed. These were incubated at 4° C for 15 minutes before ten-fold dilution in motility buffer A immediately before being loaded into the flow cells. Actin (plain actin) and actin and tropomyosin (A-Tm) were also analysed by this method. The final concentration of actin was around 1 nM.

2.5.5 Loading Protocol for Flow Cells

The flow cell was set at an angle of 30° with the frosted end of the microscope slide at the zenith. The protocol for loading the flow cell is illustrated in Figure 2.11. Each step is separated by a 30 s gap. First 100 μl of affinity precipitated HMM was loaded to each side of the flow cell followed by100 μl of Buffer B. 100 μl of reconstituted thin filament were then loaded. Lastly 50 μl of motility buffers C & D were loaded sequentially. Buffers C&D contained the free radical scavenging system to inhibit photobleaching and methylcellulose to keep the filaments pushed towards the coverslip.

If complete thin filaments were being examined then buffers C & D were modified to contain a Ca^{2+}-EGTA buffer and troponin. The troponin was diluted in motility buffer A to the same concentration as in the 10-fold thin filament incubation. It was then diluted 10-fold by addition of 5 μl to 40 μl of buffers C & D. 5 μl of a Ca^{2+}-EGTA buffer were also added. The stock solutions and final Ca^{2+} concentrations in buffers C & D are shown in Table 2.5. The troponin was added in motility buffers C & D to prevent partial dissociation of troponin from the reconstituted thin filaments which may have occurred due to the low protein concentration of the final solutions.

Figure 2.11: Flow cell loading protocol



2.5.6 Preparation of Ca^{2+} -EGTA Buffers

Ca^{2+} concentrations were varied by the incorporation of Ca^{2+}-EGTA buffers into IVMA buffers C & D as previously stated. Ca^{2+}-EGTA buffers were prepared by adapting the method of McGuigan *et al.* (1991). Buffers of different [Ca^{2+}] were made by mixing an EGTA buffer (50 mM KCl, 25 mM Imidazole pH 7.4, 50 mM EGTA, 1 mM EDTA, 4 mM $MgCl_2$, 95 mM KOH, 1.43 mM HCl, 8mM NaCl, pH adjusted using concentrated HCl) and a Ca-EGTA buffer (50 mM KCl, 25 mM Imidazole pH 7.4, 50 mM EGTA, 50 mM $CaCl_2$, 1 mM EDTA, 4 mM $MgCl_2$, 8 mM NaCl, pH adjusted using 1M KOH) at appropriate ratios to obtain Ca-EGTA buffers ranging from 1 nM to 3.9 µM. The free [Ca^{2+}] values were determined using the Maxchelator computer programme (see Table 2.5).

Table 2.5: Preparation of the Ca^{2+}-EGTA buffers

Solution Name	Volume of 50mM EGTA buffer added (ml)	Volume of 50mM Ca/EGTA buffer added (ml)	Ratio	pCa	Free [Ca^{2+}]
A	47	0.5	94/1	9.00	1.00×10^{-9}
C	40	4	10/1	8.14	7.24×10^{-9}
D	40	10	4/1	7.74	1.82×10^{-8}
E	30	15	2/1	7.43	3.72×10^{-8}
F	25	17.5	1/0.7	7.24	5.75×10^{-8}
G	25	25	1/1	7.13	7.41×10^{-8}
H	20	30	1/1.5	6.95	1.12×10^{-7}
I	15	30	1/2	6.84	1.45×10^{-7}
J	10	30	1/3	6.64	2.29×10^{-7}
K	10	40	1/4	6.52	3.02×10^{-7}
L	8	40	1/5	6.42	3.80×10^{-7}
M	7	42	1/6	6.34	4.57×10^{-7}
N	6	42	1/7	6.28	5.25×10^{-7}
P	5	40	1/8	6.23	5.89×10^{-7}
Q	5	45	1/9	6.18	6.61×10^{-7}
R	2	40	1/20	5.88	1.32×10^{-6}
S	1.5	45	1/30	5.75	1.79×10^{-6}
T	0	50	-/1	5.43	3.9×10^{-6}

2.5.7 Experimental Strategy IVMA Experiments

The *in vitro* motility assay was used to investigate the [Ca^{2+}] dependent effect on regulation of thin filaments reconstituted from proteins from different origins. To reduce the variability that may occur during preparation, test and control proteins were prepared simultaneously. All the experiments in this study were performed at 28° C.

The first stage of any IVMA experiment was to confirm that the basic assay was functioning adequately. A flow cell was set up loaded with plain actin (10 nM). The experiments were automatically tracked (see 2.5.10.3) and motile parameters analysed. To continue both the mean sliding speed had to be above 2 μm/s and the fraction motile had to be above 80%. If one or both did not meet these criteria there was a problem with either the surface of the flow cell, the quality of affinity precipitated HMM or one of the buffers. On the occasions when this occurred, the problem was either identified by ruling out the other options or alternatively every component was replaced. The initial experiment could either involve both sides of the cell containing plain actin, or with one side with plain actin and the other with actin-tropomyosin (A-Tm). If an A-Tm mixture was used then the concentration of tropomyosin generally used was 60 nM. Previously the presence of tropomyosin in the absence of troponin was shown to have a positive effect on motile parameters, however during most of the experiments completed in this study this effect was not detected.

The majority of experiments completed for this study analysed fully reconstituted thin filaments, with actin-tropomyosin-troponin mixtures. The main method was to compare two sets of thin filaments over a range of Ca^{2+} concentrations (6-10 points between 1 nM and 3.7 μM). The output from these results was a Ca^{2+} concentration titration, which could be plotted and fitted with the Hill equation (see 2.5.10.4). By fitting the data with the Hill equation two

parameters could be determined, the EC_{50} value, this is the value at which 50% of the thin filaments were activated. The second parameter is the Hill Coefficient, this is related to the steepness of the fitted curve, and is an indication of system cooperativitity.

Before the Ca^{2+} concentration titration curve could be undertaken a troponin titration for both sets of thin filaments was completed at high (3.7 μM) and low (1 nM) Ca^{2+} concentrations. Generally troponin was titrated at 1-4 points between 10 and 100 nM depending upon functionality of the protein. The tropomyosin concentration was generally 60 nM. These data were automatically tracked and analysed. A troponin concentration that gave similarly good activation at high [Ca^{2+}] (fraction motile > 80%, sliding speed > 2.0 μm/s) and good inhibition at low [Ca^{2+}] (fraction motile < 20%) was selected for each set of thin filaments. Once this had been completed a Ca^{2+} concentration curve could be performed.

2.5.8 Standard Weekly Protocol of *In Vitro* Motility Experiments

A standard week of *in vitro* motility experiments with cardiac troponin was organised like this:

- Monday: preparation of fresh HMM and stock buffers
- Tuesday: preparation of cardiac human (or mouse) troponin from frozen tissue
- Wednesday & Thursday: affinity precipitation of HMM and *in vitro* motility assay experiments
- Friday: data analysis

The preparation of HMM and troponin are two long processes that could not be arranged in just one working day. One full *in vitro* motility assay experiment then lasts for around 3 to 5 hours, meaning that most of the time only 2 complete experiments could be achieved in one

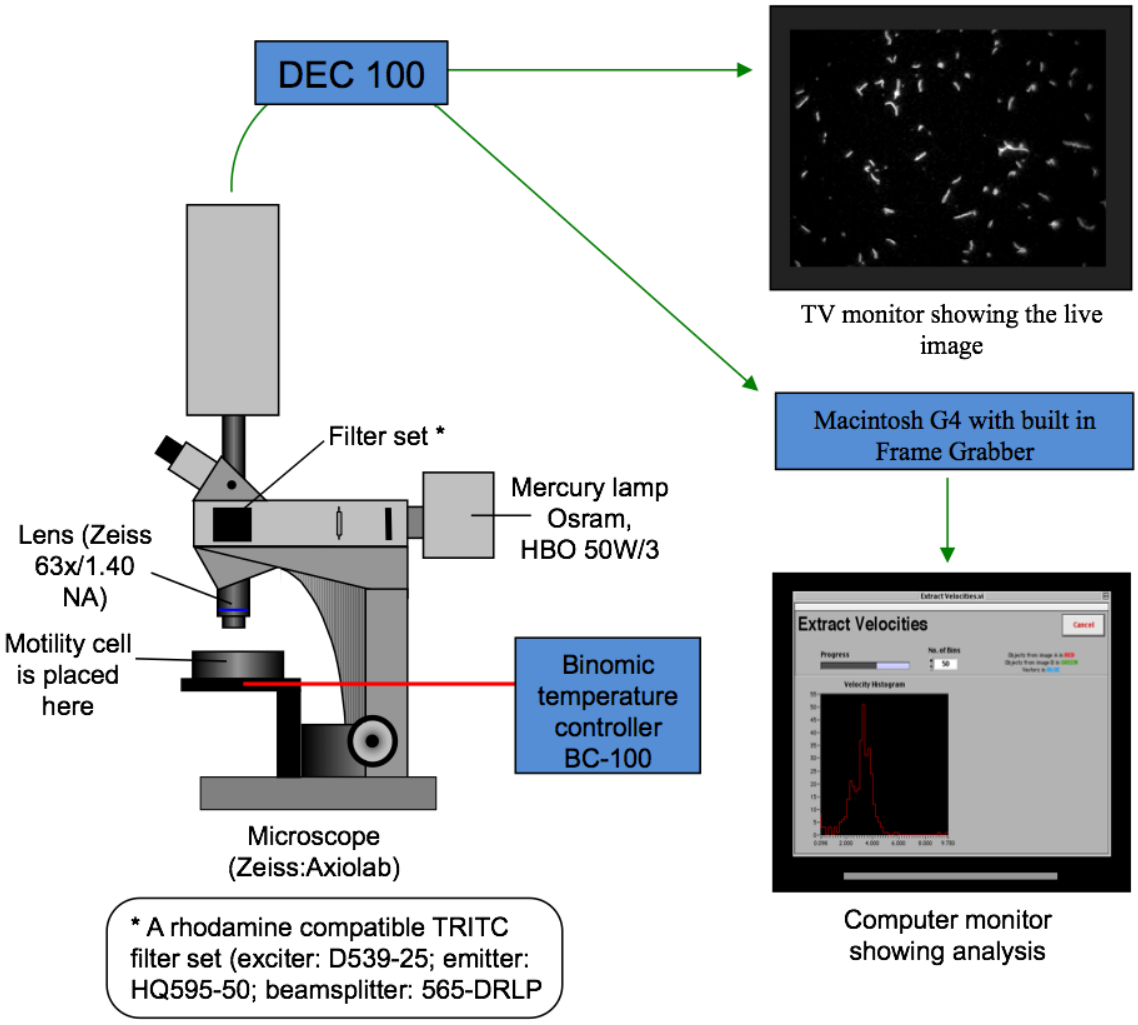
day. Because of the labile nature of purified cardiac troponin it could not be purified in advance and then stored in the freezer. It had to be always freshly prepared and used within 2 days from the purification, or else it would lose its ability to regulate thin filaments. Furthermore, often the purification would fail to achieve active troponin, wasting 2 or sometimes 3 days of work. For all of these reasons most of the cardiac work has been performed in collaboration with Dr. A. Messer, leading parallel titrations with the same material and in the same conditions, and therefore making the most out of the lifetime of purified troponin.

These issues were not the case of rabbit skeletal muscle troponin, which was on the contrary very stable and could be stored in the - 80° C freezer. Once defrosted it preserved good activity for up to 3 days. All the work presented in this thesis made with skeletal muscle troponin was made by me alone.

2.5.9 Recording Apparatus

The movement of thin filament over the immobilised bed of HMM was visualised by the fluorescently labelled actin. The microscope and recording apparatus was setup as illustrated in Figure 2.12.

Figure 2.12: Schematic diagram of the visualisation and recording apparatus



The flow cell was placed in the metal temperature control chamber on the stage of the Zeiss Axiolab microscope, with a Zeiss 63x / 1.40 NA PlanApochromat objective lens (44 07 60-03) fitted with an epifluorescence illuminator (Zeiss, 39 26 42-9901) containing a 50 W mercury high pressure arc lamp (Osram, HBO 50W/3), and a rhodamine compatible filter set (Chrome technology, emission: HQ 595-50, excitation: D539-25, dichroic: 565-DRLP special). The microscope was connected through a C-mount (45 61 05), to a highly sensitive video camera (Hamamatsu C2400), which in turn was linked through a Time Base Corrector (DEC100) to both a television monitor and a Macintosh G4. A drop of immersion oil, type A (Cargille laboratories, 16482) was placed on the coverslip of the flow cell and the image of the fluorescently labelled actin filaments were brought into focus on the television screen.

2.5.9.1 Temperature Control of the IVMA

The temperature at which IVMA experiments were performed was controlled using a Bionomic Controller BC-100 (20/20 Technology Inc.) This controller sets and maintains the temperature of a metal heating platform onto which a flow cell is placed. All IVMA experiments were completed at 28° C.

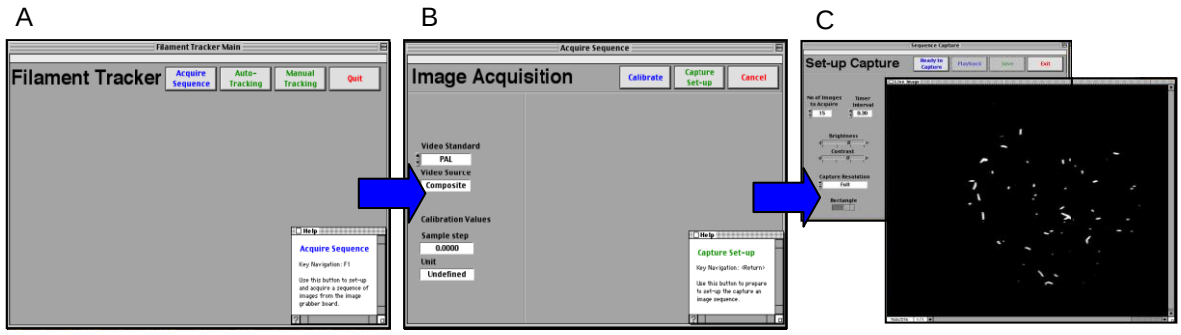
2.5.9.2 Analysis of Filament Movement

To complete quantitative analysis of filament movement, bespoke computer software had been designed and provided by ME Electronics (Reading, UK) for use on a Macintosh computer with Operating System 9 (Marston et al., 1996). The name of the software package was ‘Filament Tracker 2.0.3’, this was run using LabVIEW-3.1.1 Run-Time image analysis application (National Instruments Corp.). The software completes two tasks: the first was to digitise a series of filament images; the second was the image analysis function. This determines the movement of each filament by comparing sequential images.

2.5.9.3 Acquisition of a Sequence of Images

To record images using the Filament Tracker 2.0.3 the following command sequence was followed (see Figure 2.13). The first step was to select the 'Acquire Sequence' in the tracking panel (Figure 2.13 A). Next the 'Capture Set-up' was selected (Figure 2.13 B). This would open the 'Capture Setup' screen where the live image from the microscope could be viewed in the image window. Also displayed were four parameters that could be adjusted for optimal image acquisition. Two of these parameters were the 'contrast' and 'brightness', which along with setting on the microscope and camera could be adjusted to improve the quality of the image. The number of images acquired and the time interval between image acquisition could also be adjusted. The setting for the number of images acquired depended on the density of the filaments in the microscope field. The aim was to record 250-500 filament vectors which usually meant 10-16 images were acquired (Marston et al., 1996).

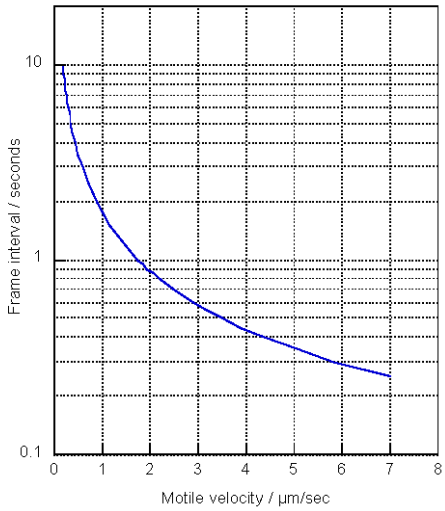
Figure 2.13: Sequential flow diagram of the process of image acquisition



The time interval was dependant on filament sliding speed, and was set to allow filaments to move 1.6-1.8 μm between image acquisitions The distance had previously been determined to facilitate the most accurate results from the tracker software (Marston et al., 1996). A

calibration curve for filament velocity and frame interval is shown below (Figure 2.14). Once set, time intervals were kept constant during a set of measurements.

Figure 2.14: Graph showing optimal time interval against filament velocity



Once all parameters were maximally optimised a sequence of images could be obtained. To do this, the 'Ready to Capture' option was selected, followed by 'Start Capture'. For any given experiment once the optimum parameters had been selected they were kept constant. For each side of each cell, 4 sequences were recorded from randomly selected areas of the flow cell. Image files were saved into a predetermined data file. Each cell side was designated a letter. A record was kept linking the image files to the experiment completed on each specific cell side.

2.5.10 Analysis of Filament Movement

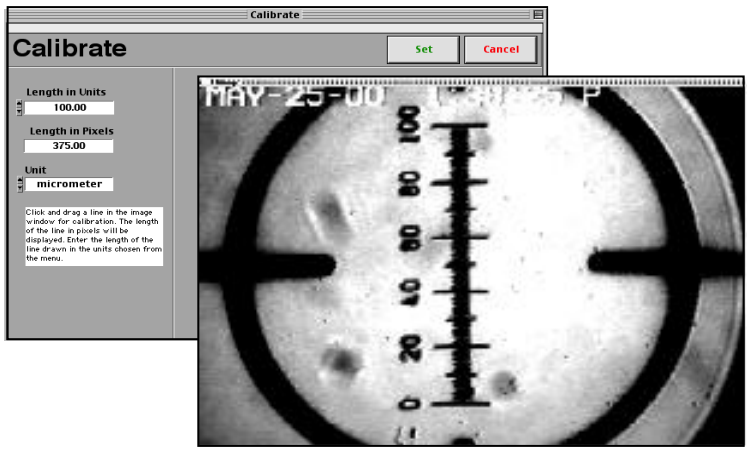
2.5.10.1 Computer Hardware

Image digitization and filament movement was performed on a single hardware unit containing integrated software. Computing hardware was a Macintosh G4 computer with a PCI Neotech frame grabber.

2.5.10.2 Software Calibration

A 100 μm microscope graticule was visualized using the transmission lamp filter system on the microscope setup. In ‘tracker’ the options ‘acquire image’ and ‘calibrate’ were selected from the main on screen options. Using the mouse-controlled cursor, a line was drawn across the graticule image (shown in Figure 2.15) and the appropriate length entered to calibrate the software for subsequent IVMA experiments.

Figure 2.15: Calibration of the IVMA image analysis software



A 100 micron graticule as it appears under a transmission microscope.

2.5.10.3 Automatic Filament Tracking

Image files of filament movement were analysed using the automatic-tracking segment of the tracker programme. Auto tracking was selected from the main ‘Filament tracker’ panel, from there the desired set of images were loaded. In the ‘Pre-process’ panel filaments that fulfilled the set criteria were displayed and highlighted as green objects on the original black and white image. Selection of the ‘Change Settings’ command allowed the adjustment of the movement analysis parameters. The maximum velocity cut-off was set at 8 μm/s, this is 2.5x mean velocity, (as vectors designated with larger velocities were probably due to errors in the vector tracking). Finally, the selection sensitivity was set to discriminate objects from noise. When these setting had been optimised the ‘Extract Velocities’ command was selected (Figure 2.16 A)

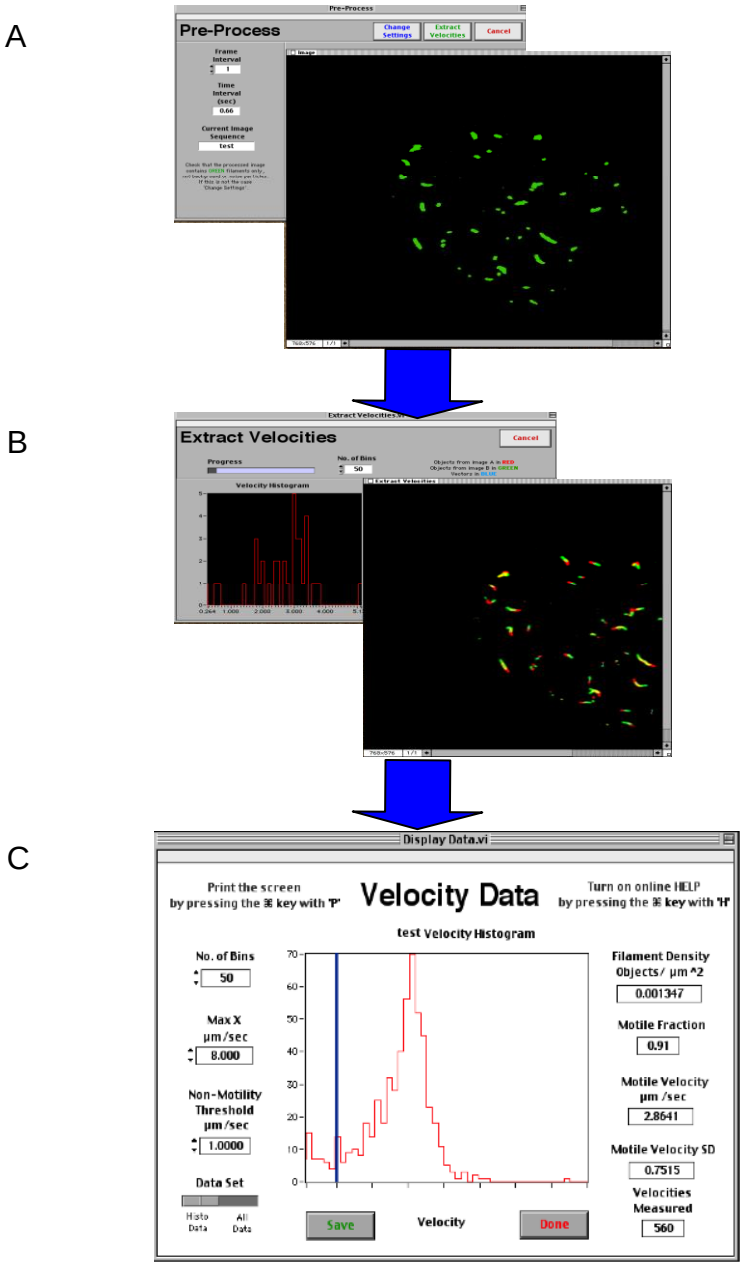
Usually settings only needed to be changed at the beginning of each day's experiments. As the tracking progresses two images are superimposed over each other on a screen similar to the live image screen. In the first image the filaments are coloured green and in the second the filaments are coloured red (Figure 2.16 B). Therefore any filaments present in the same position in both images will appear yellow. White lines connecting two filaments represent the vectors of filament movement.

After sequential tracking of all of the images is complete a histogram will appear (Figure 2.16 C). On the left hand side three parameters to further optimise tracking can be set: the number of bins (e.g. size of velocity channels); maximum velocity, and the velocity, which defines the threshold between non-motile and motile filaments. This velocity is a visually selected value deemed to separate motile and non-motile fractions, since quantitative analysis

has shown that curve-fitting produces the same result as direct observation (Marston et al., 1996). Even at low Ca^{2+} or ATP concentrations not all the filaments will be remain static. One weakness of the tracker program is that it cannot distinguish between linear movement and oscillatory movement around a fixed point. Some filaments may move with a Brownian motion and other filaments may 'wobble' if only in the 'weak' binding state with myosin. By reviewing the results from a set of thin filaments in a high Ca^{2+} concentration in the presence of ATP a value for this threshold is selected. For consistency this value must remain constant for the entire data set. This was normally set at 1 (μm/s).

The calculated parameters: filament density, motile fraction, motile velocity, standard deviation of velocities and velocities measures are displayed on the right hand side. These values are manually recorded and linked to the experiment they represent. It was assumed the sliding speeds were distributed as a single Gaussian distribution, based on the initial setup of this system (Marston et al., 1996), Thus mean values and standard deviation were calculated by the software. If the standard deviation was > 0.5X mean sliding speed this data was discarded.

Figure 2.16: Sequential flow diagram of automatic filament tracking

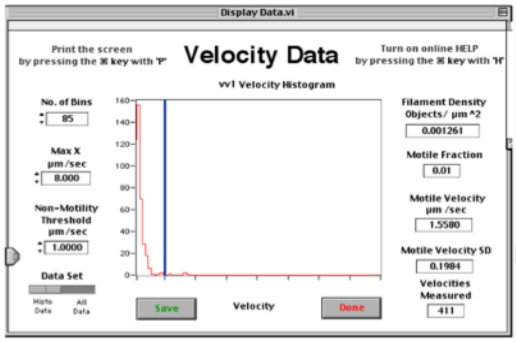


In the foreground of panel A) Filaments are coloured green, B) two sets are overlayed showing filaments from the first (sequential) acquisition (green), filaments from the second acquisition (red), those that have not moved are therefore coloured yellow. Panel C shows an example of the final histogram.

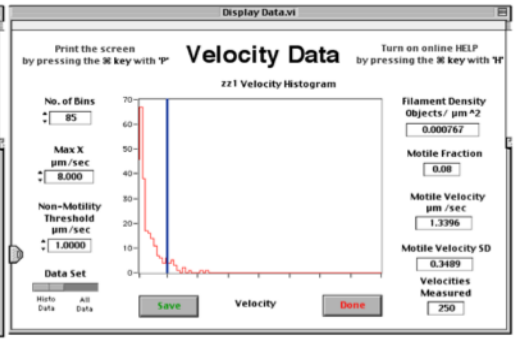
2.5.10.4 Production and Statistical Analysis of a Ca^{2+}-concentration Titration

Figure 2.17: Multiple histograms are used to build a Ca^{2+}-concentration titration curve

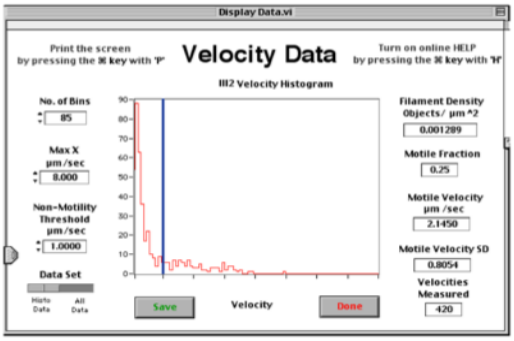
1 nM



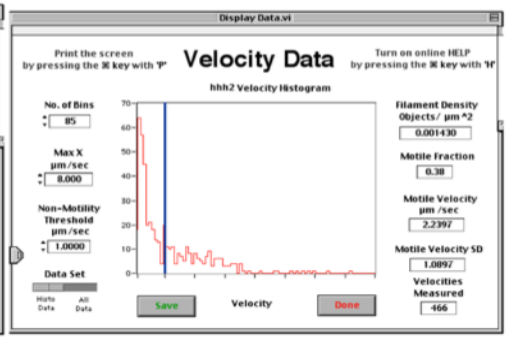
37.2 nM



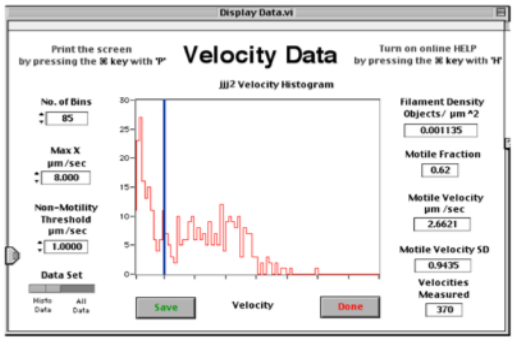
74.1 nM



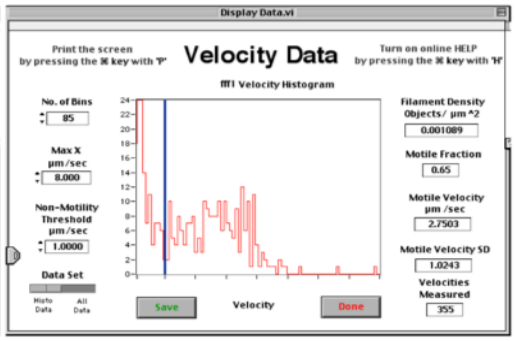
145 nM



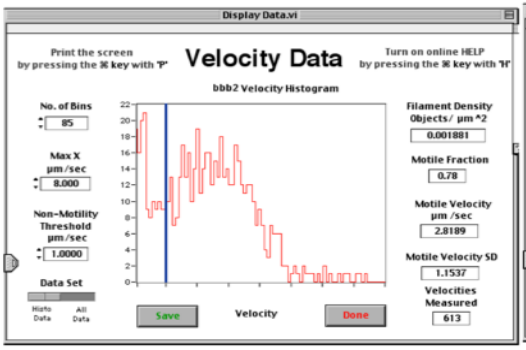
229 nM

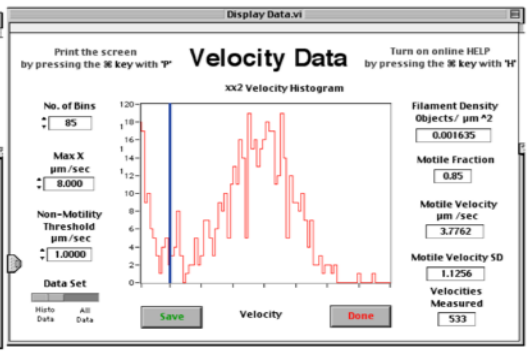


380 nM



525 nM





3.72 µM

To produce a Ca^{2+}-concentration titration, measurements were completed on the same incubation of thin filaments (actin-Tm-Tn) over a range of Ca^{2+}-concentrations from 1 nM to 3.7 μM. Figure 2.17 is composed of histograms from measurements at eight different [Ca^{2+}]. This demonstrates how the fraction of filaments moving and the sliding speed increases with the increase in [Ca^{2+}] and how this is measured by the tracker software. It should be noted that for the experiments in this thesis four measurements were completed at each [Ca^{2+}] point, therefore there are four histograms per [Ca^{2+}] point from areas of the flow cell chosen at random. Data from obviously defective areas (low or zero motility) were discarded. The mean fraction motile values from these measurements were then plotted and fitted with the Hill equation. The fraction motile was fitted to a 4-parameter Hill Equation using KaleidaGraph (Synergy Software). In some cases a and/or b were fixed at reasonable values to obtain a 3 or 2-parameter fit.

Hill Equation:

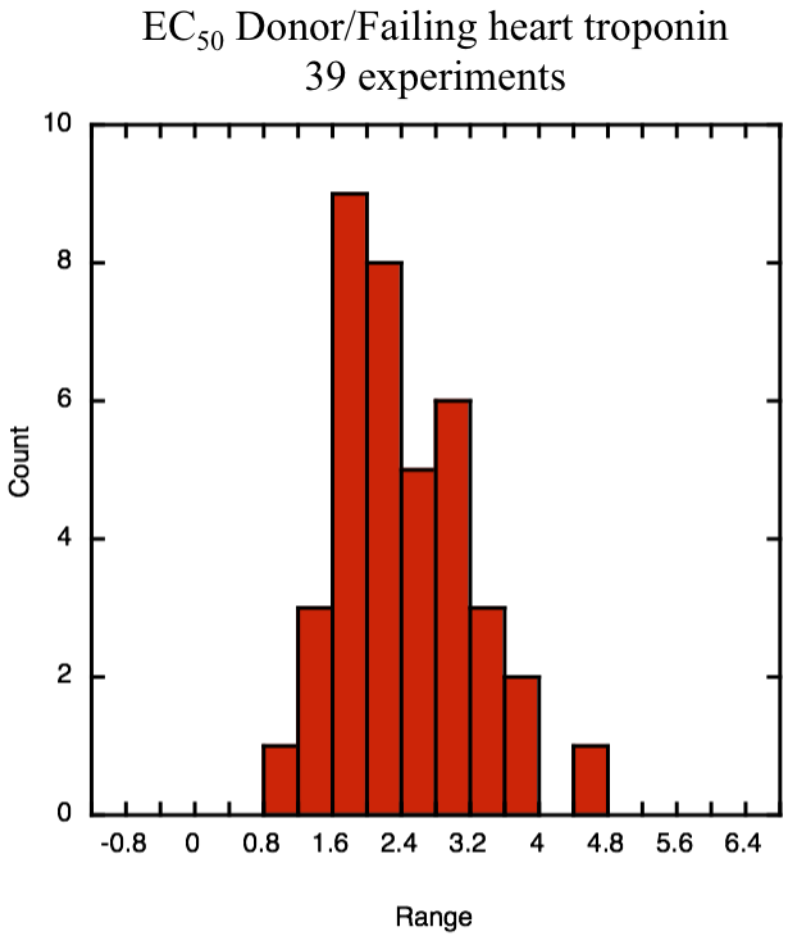
$$X = a + \frac{b[Ca^{2+}]^{\eta}}{(k^{\eta} + [Ca^{2+}]^{\eta})}$$

a = min value
b = max-min value
k = EC_{50}
η = hill co-efficient

Two parameters were obtained by fitting this equation to the data, the EC_{50} which was used as a measure of thin filament Ca^{2+}-sensitivity and the Hill co-efficient (η), which is an indicator of cooperativity. EC_{50} was used as the measure of Ca^{2+}-sensitivity as the graphs were plotted with the x-axis as Molar [Ca^{2+}] instead of pCa50, this was only because of laboratory convention, but analysis of curve fits to [Ca^{2+}] and pCa show little difference so

both of these would have been acceptable (Walker et al., 2010). Mean data values are shown alongside standard deviation of the mean unless otherwise stated. Data was compared for statistical significance using the Student t-test where $p < 0.05$ was classed as significant. The Student t-test is the best method for significance tests on small populations, such as in this thesis (< 10 replicates) provided the distribution of the EC_{50} parameter is normal.

Figure 2.18: Normal distribution of the EC_{50} ratio of donor / failing heart troponin



The extensive measurements by Dr. Messer have established that this is true for the IVMA system used here (Messer et al., 2007). He considered 39 paired measurements of EC_{50} in donor and failing hearts using the same methods as in this thesis. It showed that the

distribution of the ratio is roughly normal (Figure 2.18), justifying use of the t-test to determine whether the effect of the mutation is significant. It should be noted that these experiments used 5 donor samples and 5 failing samples in various combinations and thus establish that the variability in the measurements is not due to variability between muscle samples, but rather variability between troponin preparations and the assay.

3 Completion of a Study on DCM Mutants Leading to a Hypothesis on the Molecular Mechanism Generating the Disease

3.1 General Introduction

Mutations causing DCM have been found in 33 different genes. Many of the proteins coded by these genes are components of the contractile apparatus. Within the sarcomere, in particular, all of the cardiac thin filaments subunits presented mutations which have been linked with the genesis of the pathology (Hershberger and Siegfried, 2011, Chang and Potter, 2005, Marston, 2011).

The next two chapters will describe the functional investigation of seven different mutations localised, at least one, on every subunit of the cardiac thin filaments through the well-established and versatile method of the *in vitro* motility assay (IVMA). The two main parameters measured with this assay are the percentage motile and motile velocity, which can give indications on the thin filament switching, cooperativity and cross-bridge cycling rate. The key feature of the assay is the real-time comparison of two different samples, which will share every experimental condition during the assay, except for one different thin filament component, in order to evaluate any functional difference generated by that component itself. This feature allowed us to screen for small functional differences between wild-type and mutant proteins, but also between the same protein isoform with different levels of a post-translational modification, like phosphorylation.

The phosphorylation of troponin I (TnI) is a downstream effect of β-adrenergic stimulation of the heart, as part of the lusitropic response (Bers, 2001, Layland et al., 2005). The level of

TnI phosphorylation has been shown to modify the Ca^{2+}-sensitivity of the thin filament. This has been thoroughly investigated using a number of techniques (Kentish et al., 2001, van der Velden et al., 2003, Layland et al., 2005, Hamdani et al., 2008), including the IVMA (Messer et al., 2007).

Initial investigation of the DCM mutations in thin filament proteins through the IVMA were conducted using recombinant proteins expressed in *E. coli* and all produced a phenotype presenting lower Ca^{2+}-sensitivity and maximum sliding speed (Mirza et al., 2005, Mirza et al., 2007). Further studies were made more recently, using more physiological sources such as human patient and donor heart samples, or transgenic mice and littermate hearts to purify the proteins. They were made respectively on the troponin C (TnC) Gly159Asp (G159D) and actin Glu361Gly (E361G) mutants. In these studies the proteins were presenting physiological post-translational modifications and therefore their phosphorylation could be taken into account and manipulated. The results obtained lead to the hypothesis that the etiology of the disease was to be found in an uncoupling between TnI phosphorylation and the Ca^{2+}-sensitivity of the thin filaments, as described in E. Dyer's thesis, whose results were too few to achieve significance. The study presented in this chapter took over from that pilot work by repeating the experiments enough to achieve significance with the same two mutant samples. To confirm this hypothesis the next chapter will scrutinize its validity with 5 more mutants and the same physiological experimental setup. Because of the short lifetime of cardiac troponin and the long time required to perform *in vitro* motility experiments most of the work on all of these cardiac mutants was made in simultaneous collaboration with Dr. A. Messer on two identical IVMA set-ups. This was done to maximise the experimental output from scarce tissue resources (see section 2.5.8).

3.2 Functional Investigation of DCM Mutant Troponin C Gly159Asp and Actin Glu361Gly

3.2.1 Introduction

The missense mutation Gly159Asp (G159D) on cardiac TnC was first described by Mogensen *et al.* in a study considering 235 patients with idiopathic DCM (Mogensen et al., 2004). We obtained a cardiac muscle sample from a transplanted heart belonging to a patient that was a member of the original family in which the TnC G159D mutation was isolated. This patient's clinical details were described by Kaski *et al.*(Kaski et al., 2007).
Actin Glu361Gly (E361G) was first described by Olson *et al.* in a family in which the mutation was cosegregating with DCM phenotype in several members (Olson et al., 1998). We produced in our lab a transgenic mouse model carrying the mutation and expressing it at around 50% of the total actin in the heart.

3.2.2 Location of the TnC G159D and Actin E361G Mutations

Human cardiac troponin is composed of two domains: the regulatory head and the TnI-TnT arm. The G159D mutation is located within the C-terminal lobe of cardiac TnC (Biesiadecki et al., 2007), which is considered a structural rather than a regulatory site [reviewed in (Kobayashi and Solaro, 2005)]. Nevertheless it has been shown by NMR analysis that the N-terminal domain of TnI makes contact with the C-terminal domain of TnC at a site close to the G159D (Finley et al., 1999).

The E361G mutation is located in subdomain 1 of the actin monomer and occupies a proposed α-actinin binding site. It also produces the loss of a charge on the surface with

substitution of a small non-polar amino acid, but it is in a region unlikely to be involved directly with actin polymerisation.

3.2.3 *In Vitro* Motility Analysis

3.2.3.1 Effects of Human Cardiac Tropomyosin and Donor or TnC G159D Troponin on Rabbit Skeletal Muscle Actin Filament Motility

Results described in this paragraph are shown in Figure 3.1.

Rabbit skeletal muscle actin alone from 2 different purifications was tested 13 times in the *in vitro* motility assay prior to experiments with mutant troponin C G159D with average motile velocity of 2.51 ± 0.05 μm/sec and 79.9 ± 1.8% motility. Addition of 60 nM human cardiac tropomyosin resulted in a 5% speed increase to 2.64 ± 0.08 μm/sec and a 1% increase in the percentage motile to 80.7 ± 2.2%.

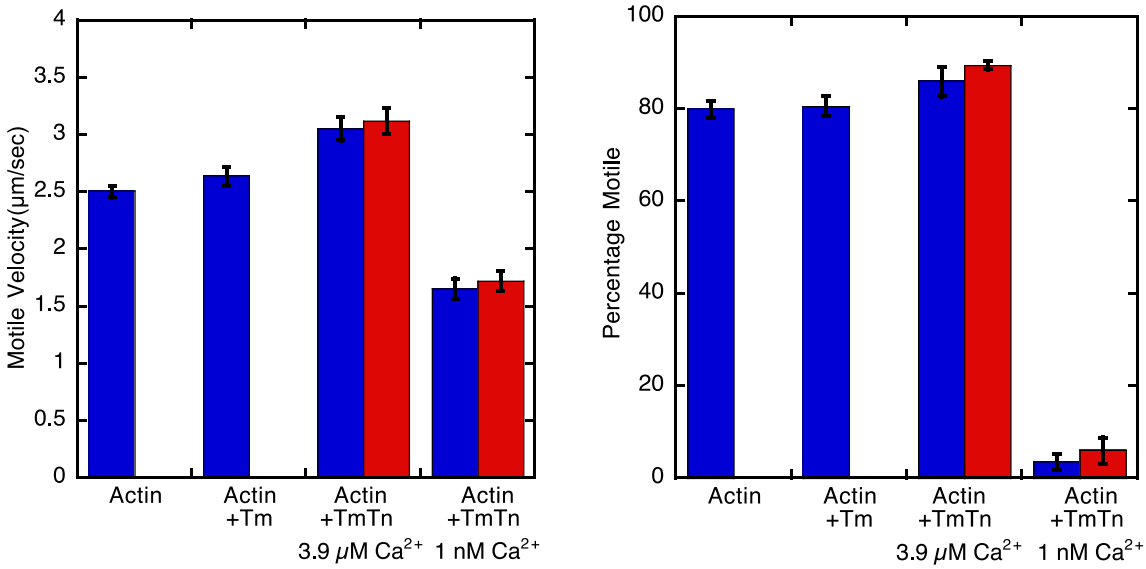
Thin filaments were then assembled using rabbit skeletal muscle actin, human cardiac tropomyosin and donor or TnC G159D troponin. Actin was always 10 nM and tropomyosin 60 nM, troponin was titrated at 30 or 60 nM, and the lowest concentration consistent with good Ca^{2+} regulation was used.

It was observed that in the presence of donor human troponin in low Ca^{2+} (1 nM Ca^{2+}) thin filaments were switching off with percentage motile falling to 3.6 ± 1.66% and velocity to 1.66 ± 0.09 μm/sec. When reconstituted with G159D troponin thin filaments showed a very similar behaviour in 1 nM Ca^{2+}, with motility dropping to 6 ± 2.9% and sliding speed 1.72 ± 0.09 μm/sec. The velocities were 37% and 35% slower than actin-tropomyosin, respectively for donor and G159D troponin reconstitutions. There was no significant difference between donor and G159D troponin in terms of the percentage motile ($p = 0.19$) or the sliding speed

(p = 0.74), which indicates that both troponins could inhibit actin filaments to a similar degree.

In high Ca^{2+} (3.9 μM Ca^{2+}), donor and G159D increased the sliding speed of respectively 16% and 18%, with an increase in the percentage motile of respectively 7% and 11%. These differences were not significant in sliding speed (p = 0.87) or percentage motile (p = 0.94).

Figure 3.1: *In vitro* motility measurements comparing donor and G159D troponin



Blue bars, WT thin filaments; red bars, G159D troponin. Means and S.E. were made on sets of 5-13 measurements. Two troponin purifications were used. In presence of troponin, filaments were Ca^{2+} regulated.

3.2.3.2 Effects of TnC G159D Troponin on the Thin Filaments Ca^{2+}-sensitivity Compared to Donor Human Cardiac Troponin

Thin filaments were reconstituted with rabbit skeletal muscle actin 10 nM, human cardiac tropomyosin 60 nM and troponin 60 nM, donor or G159D. The phosphorylation level of G159D troponin was on average 1.53 ± 0.05 mols P_i / mol TnI, which matches the donor human troponin average of 1.6 mols P_i / mol TnI.

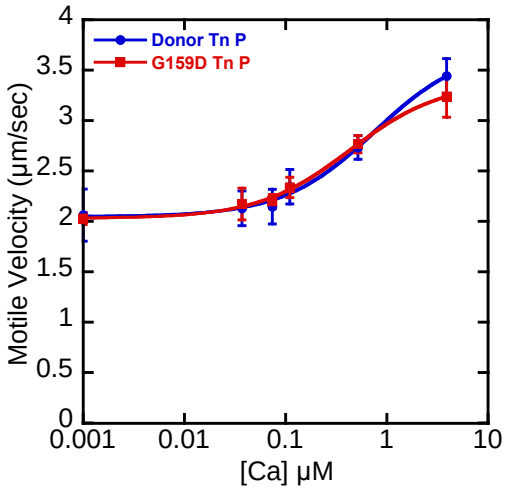
Two complete Ca^{2+} titrations were performed comparing thin filaments reconstituted with donor or G159D troponin (shown in Figure 3.2).

As summarised in Table 3.1 there seems to be no difference in the maximum sliding speed reached by the filaments or in the percentage of its increase between low and high Ca^{2+} concentration. EC_{50} values indicate a higher Ca^{2+}-sensitivity for the mutant troponin.

The percentage motile (Table 3.2) shows similar values in high Ca^{2+}, but the filaments reconstituted with the mutation showed higher cooperativity with a 133% larger Hill coefficient. G159D filaments also show a shift of the percentage motile EC_{50} towards higher Ca^{2+}-sensitivity, with an EC_{50} G159D / donor ratio of 0.81 ± 0.11.

Figure 3.2: Ca^{2+} concentration titration comparing thin filaments containing human donor and G159D troponin

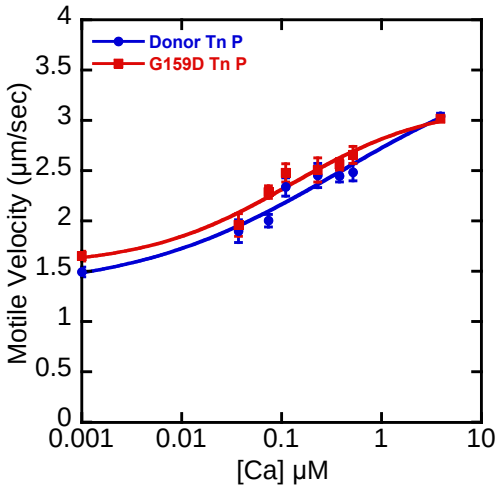
1



	Value	Error
Hill Coefficient	1	/
EC_{50}	0.75	0.36

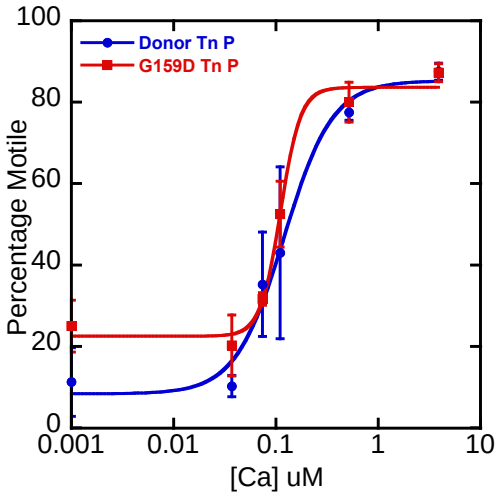
	Value	Error
Hill Coefficient	1	/
EC_{50}	0.43	0.09

2



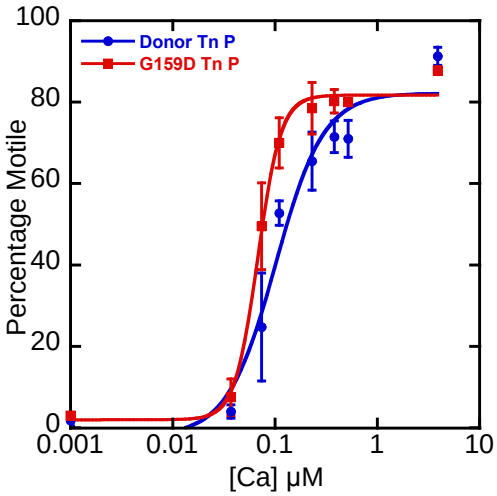
	Value	Error
Hill Coefficient	1	/
EC_{50}	0.39	0.82

	Value	Error
Hill Coefficient	1	/
EC_{50}	0.12	0.08



	Value	Error
Hill Coefficient	1.83	0.73
EC_{50}	0.12	0.03

	Value	Error
Hill Coefficient	4.42	1.86
EC_{50}	0.11	0.01



	Value	Error
Hill Coefficient	1.8	0.67
EC_{50}	0.1	0.02

	Value	Error
Hill Coefficient	3.87	0.77
EC_{50}	0.07	0.01

Table 3.1: Ca^{2+}-sensitivity data for G159D v donor troponin thin filaments sliding speed

Tn G159D ANALYSIS	EC_{50} Sliding speed, µM		EC_{50} mutant/ EC_{50} Donor	Ca^{2+} activation of sliding speed (%)		Maximum sliding speed (µm/sec)	
EXP N	Donor	G159D		Donor	G159D	Donor	G159D
1	0.61±0.11	0.54±0.09	0.89	62	52	3.41	3.23
2	0.39±0.82	0.12±0.08	0.31	101	88	3.02	3
MEAN±SE	0.5±0.11	0.33±0.21	0.6±0.29	82±20	70±18	3.22±0.2	3.12±0.12

Table 3.2: Ca^{2+}-sensitivity data for G159D v donor troponin thin filaments percentage motile

Tn G159D ANALYSIS	EC_{50} Percentage motility, µM		EC_{50} mutant/ EC_{50} Donor	Hill coefficient n		% Motile 3.9 µM Ca^{2+}	
EXP N	Donor	G159D		Donor	G159D	Donor	G159D
1	0.12±0.03	0.11±0.01	0.92	1.8	4.4	85	84
2	0.1±0.02	0.07±0.01	0.7	1.8	3.9	90	88
MEAN±SE	0.11±0.01	0.09±0.02	0.81±0.11	1.8	4.2±0.3	88±1	86±2

3.2.3.3 Effects of Troponin I Dephosphorylation on the Ca^{2+}-Sensitivity of G159D Thin Filaments

To investigate the effect of the G159D mutation on the regulation provided by troponin I phosphorylation, both G159D and donor troponin purifications were divided in two samples, one of each starting material, and was then thoroughly dephosphorylated (see section 2.3.2). Pro-Q Diamond stained gels indicated that the phosphorylation level of donor TnI after the dephosphorylation procedure was 2.3 ± 0.1% of the untreated and the level of G159D TnI was 8 ± 0.1%.

The first experiment screening the influence of the G159D mutation in relation to different phosphorylation states used thin filaments reconstituted using 10 nM rabbit skeletal muscle actin, 60 nM tropomyosin and 60 nM G159D troponin, phosphorylated or dephosphorylated. Two complete Ca^{2+} titrations were performed comparing the two post-translational states of the mutant (Figure 3.3 and details in Table 3.3 and Table 3.4). The percentage motile parameters were all very similar. In particular there was not a great difference in the Ca^{2+}-sensitivity due to dephosphorylation of troponin I, with an average EC_{50} ratio phosphorylated / dephosphorylated of 1.11 ± 0.11. The sliding speed EC_{50} does not show a well defined direction of shift.

Table 3.3: Ca^{2+}-sensitivity data for the sliding speed of thin filaments reconstituted with G159D phosphorylated v G159D dephosphorylated troponin

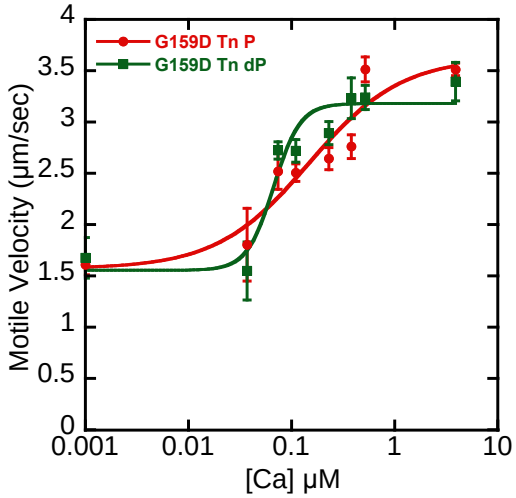
Tn G159D ANALYSIS	EC_{50} Sliding speed, µM		EC_{50} P/ EC_{50} dP	Ca^{2+} activation of sliding speed (%)		Maximum sliding speed (µm/sec)	
EXP N	G159D P	G159D dP		P	dP	P	dP
1	0.15±0.09	0.07±0.01	2.14	130	125	3.63	3.5
2	0.17±0.05	0.21±0.07	0.81	52	68	2.83	2.86
MEAN±SE	0.16±0.01	0.14±0.07	1.48±0.67	91±39	97±29	3.23±0.4	3.18±0.32

Table 3.4: Ca^{2+}-sensitivity data for the percentage motile of thin filaments reconstituted with G159D phosphorylated v G159D dephosphorylated troponin

Tn G159D ANALYSIS	EC_{50} Percentage motility, µM		EC_{50} P/ EC_{50} dP	Hill coefficient n		% Motile 3.9 µM Ca^{2+}	
EXP N	G159D P	G159D dP		P	dP	P	dP
1	0.06±0.02	0.06±0.01	1	8.3	8.8	77	84
2	0.11±0.03	0.09±0.02	1.22	1.9	2.4	87	86
MEAN±SE	0.09±0.03	0.08±0.02	1.11±0.11	5.1±3.2	5.6±3.2	82±5	85±1

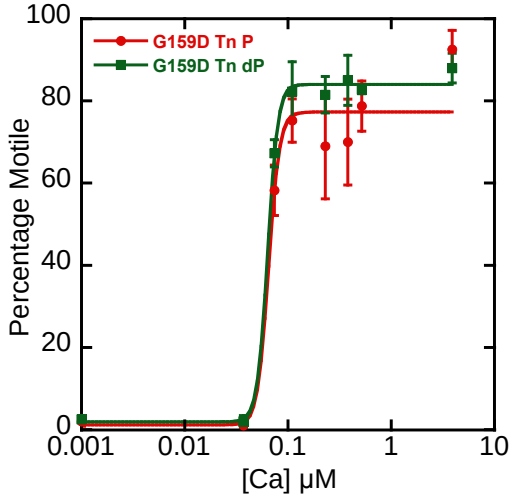
Figure 3.3: Ca^{2+} concentration titration comparing thin filaments containing phosphorylated and dephosphorylated G159D troponin

1



	Value	Error
Hill Coefficient	1	/
EC_{50}	0.15	0.09

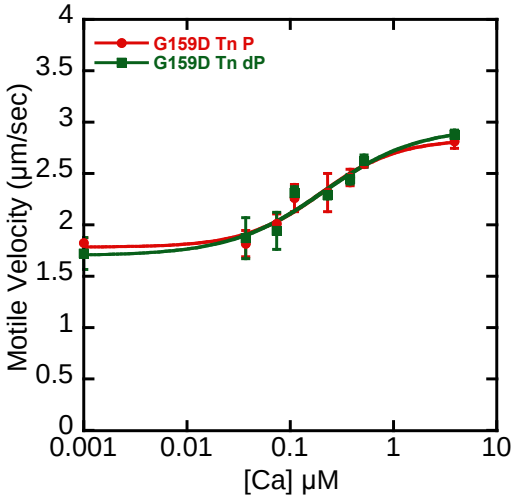
	Value	Error
Hill Coefficient	3.37	2.12
EC_{50}	0.07	0.01



	Value	Error
Hill Coefficient	8.28	19.42
EC_{50}	0.06	0.02

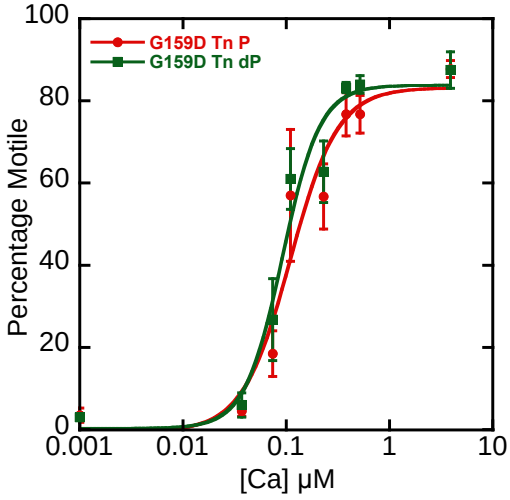
	Value	Error
Hill Coefficient	8.8	6.27
EC_{50}	0.06	0.01

2



	Value	Error
Hill Coefficient	1.18	0.34
EC_{50}	0.2	0.06

	Value	Error
Hill Coefficient	0.95	0.34
EC_{50}	0.21	0.09

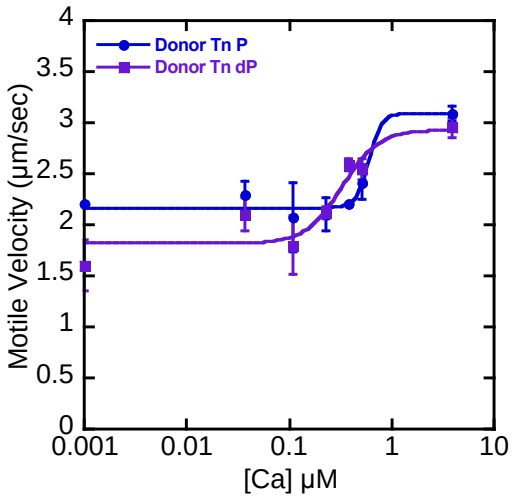


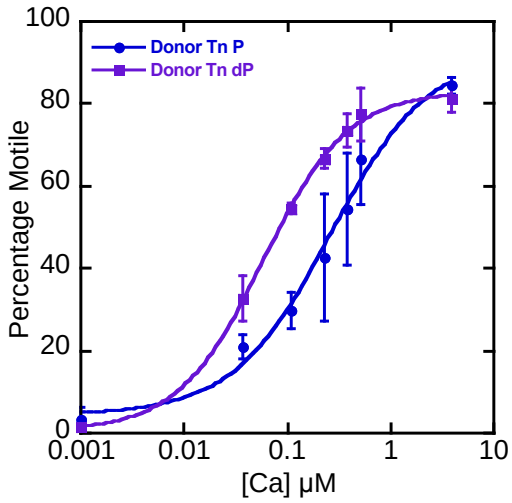
	Value	Error
Hill Coefficient	1.88	0.85
EC_{50}	0.11	0.03

	Value	Error
Hill Coefficient	2.39	1
EC_{50}	0.09	0.02

Figure 3.4: Ca^{2+} concentration titrations comparing thin filaments containing phosphorylated and dephosphorylated human donor troponin

2

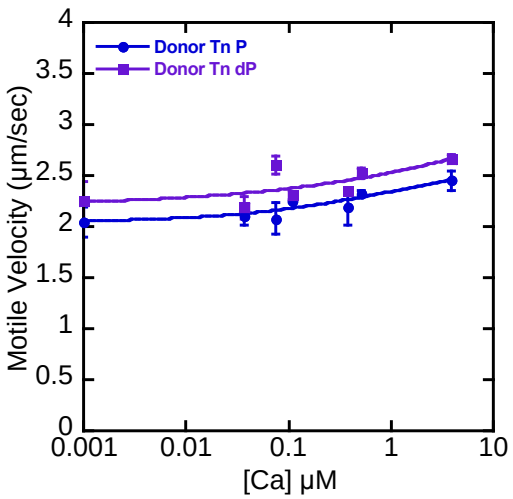


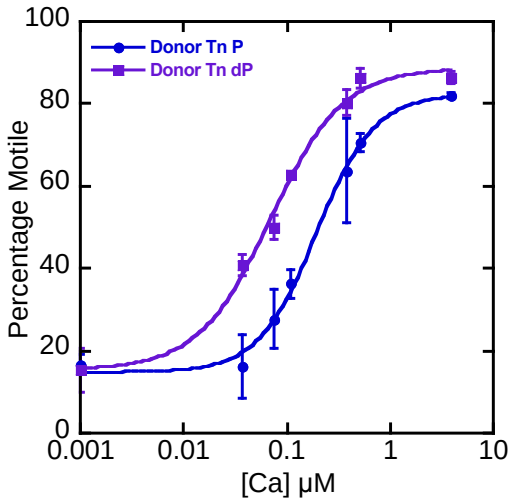


	Value	Error
Hill Coefficient	1.02	0.23
EC_{50}	0.26	0.07

	Value	Error
Hill Coefficient	1.06	0.08
EC_{50}	0.06	0.01

3





	Value	Error
Hill Coefficient	1.56	0.19
EC_{50}	0.19	0.02

	Value	Error
Hill Coefficient	1.24	0.25
EC_{50}	0.07	0.01

Since a large number of experiments in the past proved that the dephosphorylation of TnI was increasing the Ca^{2+}-sensitivity of the thin filaments in IVMA, only three control experiments were performed comparing donor troponin phosphorylated and dephosphorylated (Figure 3.4 shows experiments 2 and 3, experiment 1 is in APPENDIX; data in Table 3.5). These comparisons gave further evidence of the Ca^{2+}-sensitivity regulation given by the phosphorylation of TnI for donor troponin, with an EC_{50} ratio of phosphorylated / dephosphorylated of 2.93 ± 0.75 for the percentage motile. Most of the parameters are similar, but the average EC_{50} for the percentage motile statistically shows a significant difference (paired p = 0.03; unpaired p = 0.02).

Table 3.5: Ca^{2+}-sensitivity data for thin filaments reconstituted with human donor troponin phosphorylated v dephosphorylated

human Tn Donor ANALYSIS	EC_{50} Percentage motility, µM		EC_{50} P / EC_{50} dP	Hill coefficient n		% Motile 3.9 µM Ca^{2+}		Ca^{2+} activation of sliding speed (%)		Maximum sliding speed (µm/sec)	
EXP N	Donor P	Donor dP		P	dP	P	dP	P	dP	P	dP
1	0.28±0.12	0.16±0.03	1.75	1.39	4.45	74	77	67	46	2.85	2.99
2	0.26±0.07	0.06±0.01	4.33	1.02	1.06	85	81	40	83	3.09	2.95
3	0.19±0.02	0.07±0.01	2.71	1.56	1.24	82	86	20	19	2.45	2.67
MEAN±SE	0.24±0.03	0.1±0.03	2.93±0.75	1.32± 0.16	2.25± 1.1	80±3	81±3	42±14	49±19	2.8±0.19	2.87±0.1
Student's t-test (paired)	p=0.03		single group, p=0.12 (compared with one)								
(unpaired)	p=0.02										

A final comparison was made using thin filaments reconstituted with donor or G159D troponin both dephosphorylated. Two Ca^{2+} titrations were recorded, which are shown in Figure 3.5.

Again there is not any evident difference in the maximum sliding speed reached by the filaments or in the Ca^{2+} dependent increase of the sliding speed. The sliding speed EC_{50} indicates still a higher Ca^{2+}-sensitivity for the G159D filaments (Table 3.6).

For the percentage motile parameter dephosphorylated G159D filaments showed a 67% higher Hill coefficient relative to the dephosphorylated donor and a higher Ca^{2+}-sensitivity with EC_{50} ratio G159D / Donor = 0.7 ± 0.13 (Table 3.7).

Table 3.6: Ca^{2+}-sensitivity data for sliding speed of dephosphorylated G159D v dephosphorylated donor thin filaments

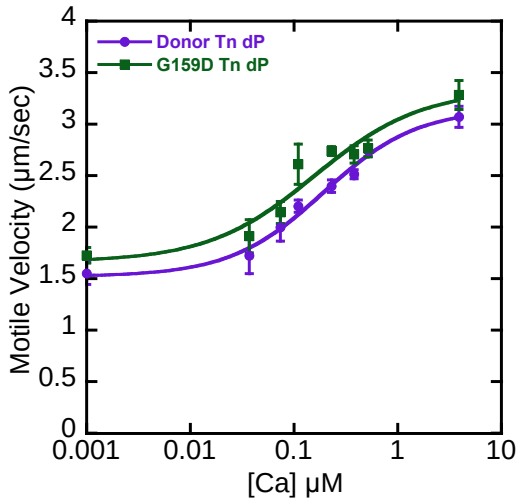
Tn G159D ANALYSIS	EC_{50} Sliding speed, µM		EC_{50} mutant/ EC_{50} Donor	Ca^{2+} activation of sliding speed (%)		Maximum sliding speed (µm/sec)	
EXP N	Donor dP	G159D dP		Donor dP	G159D dP	Donor dP	G159D dP
1	0.19±0.04	0.16±0.09	0.84	100	100	3.15	3.33
2	0.18±0.05	0.09±0.02	0.5	104	127	2.93	2.91
MEAN±SE	0.19±0.01	0.13±0.04	0.67±0.17	102±2	114±14	3.04±0.11	3.12±0.21

Table 3.7: Ca^{2+}-sensitivity data for percentage motile of dephosphorylated G159D v dephosphorylated donor thin filaments

Tn G159D ANALYSIS	EC_{50} Percentage motility, µM		EC_{50} mutant/ EC_{50} Donor	Hill coefficient n		% Motile 3.9 µM Ca^{2+}	
EXP N	Donor dP	G159D dP		Donor dP	G159D dP	Donor dP	G159D dP
1	0.14±0.02	0.08±0.01	0.57	1.7	3.8	92	87
2	0.12±0.02	0.1±0.01	0.83	2.2	2.7	89	89
MEAN±SE	0.13±0.01	0.09±0.01	0.7±0.13	2±0.3	3.3±0.6	91±2	88±1

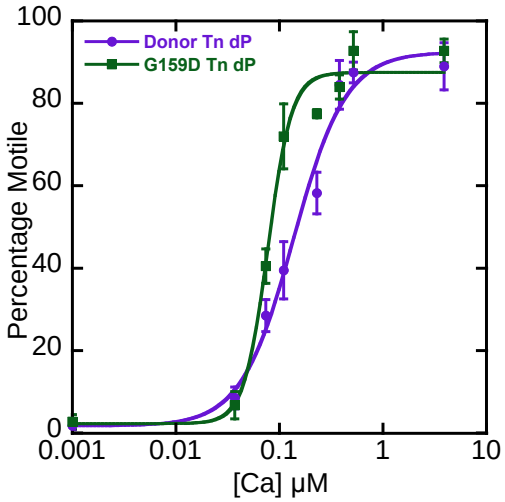
Figure 3.5: Ca^{2+} concentration titration comparing thin filaments containing dephosphorylated G159D and donor troponin

1



	Value	Error
Hill Coefficient	1	/
EC_{50}	0.19	0.04

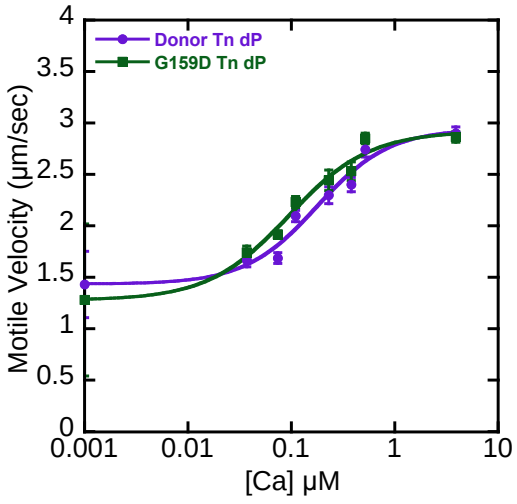
	Value	Error
Hill Coefficient	1	/
EC_{50}	0.16	0.09



	Value	Error
Hill Coefficient	1.71	0.34
EC_{50}	0.14	0.02

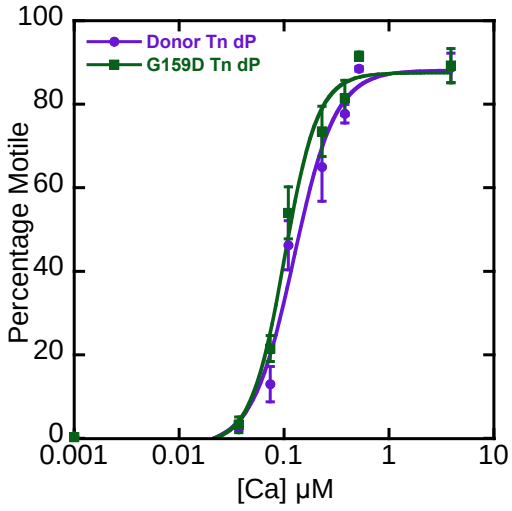
	Value	Error
Hill Coefficient	3.8	1.19
EC_{50}	0.08	0.01

2



	Value	Error
Hill Coefficient	1.24	0.34
EC_{50}	0.18	0.05

	Value	Error
Hill Coefficient	1.12	0.26
EC_{50}	0.09	0.02



	Value	Error
Hill Coefficient	2.19	0.58
EC_{50}	0.12	0.02

	Value	Error
Hill Coefficient	2.72	0.7
EC_{50}	0.1	0.01

3.2.3.4 Thin Filament E361G and Non-Transgenic Actin Motility

Mouse cardiac actin was purified through the method developed by Dr E. Dyer (see section 2.2.2.3), who observed the loss in mutant protein when actin was purified by the standard acetone powder method. The mutant monomer, in fact, is less stable than the wild-type actin and therefore would aggregate before polymerisation. On the contrary the newly developed method secured the purification of the mutant E361G actin at the same physiological ratios seen in myofibrils, as proved by 2-D electrophoresis (see section 3.3.2).

Purified mutant actin contained around 50% E361G actin and it was compared in the IVMA with wild-type actin purified from non-transgenic littermate mouse hearts. Four different parallel purifications were performed and plain wild-type actin was compared 11 times with the mutant actin showing that, on average the mutant was only 2% faster than the wild-type with a percentage motile 3% higher (Table 3.8). Neither of the parameters, though, were statistically significant in both paired and unpaired student t-test.

Table 3.8: Comparison of motility of non-transgenic and E361G thin filament actin

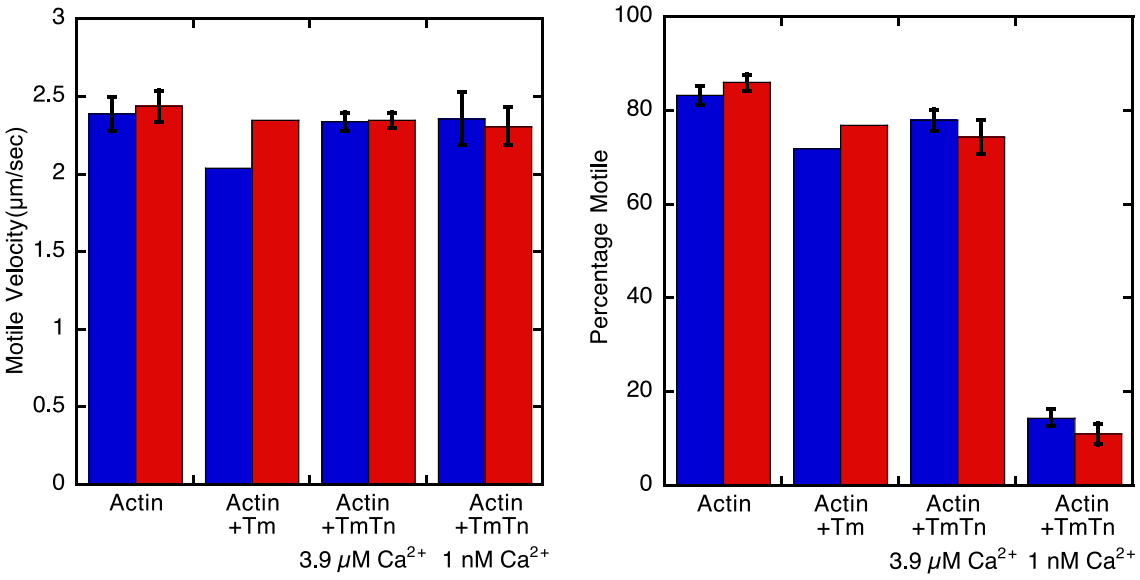
Preparation	Sliding Speed (µm/sec)		Percentage Motile	
	NTg	E361G	NTg	E361G
1	2.11±0.09	2.08±0.09	86.3±3.3	77.8±6.7
	2.96±0.04	3.26±0.08	88.3±2.1	94.3±2.2
	2.28±0.16	2.39±0.08	83.5±2.4	89±4
	2.21±0.13	2.27±0.05	85.5±2.5	89±2.7
	1.95±0.13	2.27±0.14	71.5±9	90.3±4.9
2	2.57±0.07	2.65±0.06	92.5±4.1	94.8±1.3
3	2.1±0.05	2.24±0.14	84.8±6.2	81±7
	2.9±0.13	2.71±0.07	88.3±2.2	86.5±1
	2.22±0.11	2.06±0.06	80±1.4	78.8±3.3
4	2.8±0.07	2.55±0.12	85.5±7.2	83.5±1.3
	2.14±0.08	2.33±0.09	71.3±11.3	80.8±8.3
MEAN±SE N=11	2.39±0.11	2.44±0.1	83.4±2	86±1.8
t-test p value	paired=0.39 unpaired=0.73		paired=0.28 unpaired=0.36	

3.2.3.5 Effects of Donor Human Cardiac Troponin and Tropomyosin on Non Transgenic and E361G Thin Filament Actin Motility at High and Low Ca^{2+}

Thin filaments were reconstituted using tropomyosin and troponin isolated from donor human heart, and mouse cardiac actin, non-transgenic or E361G. Actin was always 10 nM, while tropomyosin was always used at 60 nM. Troponin was titrated between 20-60 nM to find optimal switch off in low Ca^{2+} buffer (1 nM) and switch on in high Ca^{2+} buffer (3.9 µM). Only one measurement was recorded with actin and tropomyosin alone, which is coupled with the very first plain actin measurement. It did not show a peculiar behaviour and it maintained similar values to those of plain actin.

With the addition of troponin the filaments became Ca^{2+}-sensitive and in activating conditions over 70% of the filaments were motile, whilst in relaxing Ca^{2+} concentrations the percentage motile dropped to less than 15%. The velocity of the filaments did not seem to show any statistical difference either between high and low Ca^{2+} concentrations, or with that of plain actin (Figure 3.6).

Figure 3.6: *In vitro* motility measurements comparing NTg and E361G actin



Blue bars, NTg actin; red bars, E361G actin. Means and S.E. were made on sets of 3-8 measurements, using 4 pairs of mouse hearts. Only Actin+Tm represents a single measurement and has no error bar. No significant difference was observed on any velocity. In presence of troponin, filaments were Ca^{2+} regulated.

3.2.3.6 Effects of E361G Actin on the Thin Filament Ca^{2+}-sensitivity Compared to Non-Transgenic mouse heart actin

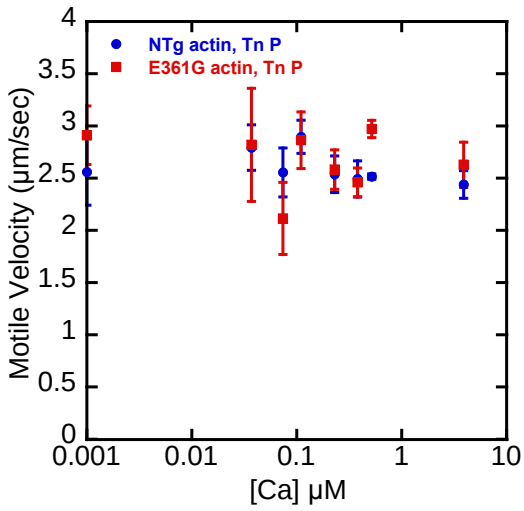
Thin filaments were reconstituted with mouse cardiac actin, non-transgenic or E361G, and tropomyosin and troponin purified from donor human heart. Human cardiac troponin I is usually phosphorylated at around 1.6 mols P_i/mol TnI. The Ca^{2+}-sensitivity of sliding and

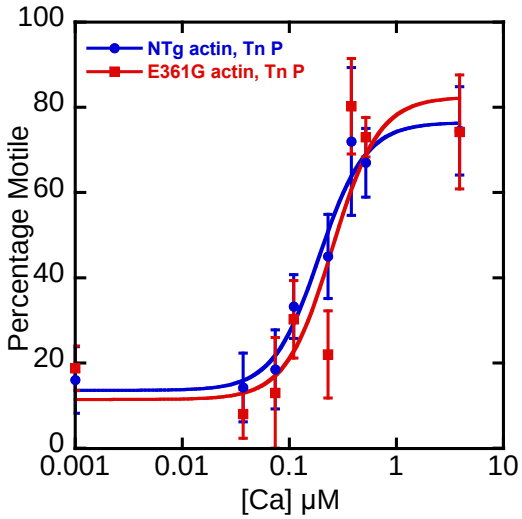
percentage motile were measured with actin from two paired non-transgenic and E361G preparations.

After reconstituting the thin filaments, it was verified that they responded to Ca^{2+} regulation and thereafter they were titrated at different Ca^{2+} concentrations. Three complete titrations were recorded, and are shown in Figure 3.7.

Figure 3.7: Ca^{2+} concentration titration comparing thin filaments containing non-transgenic and E361G actin

1

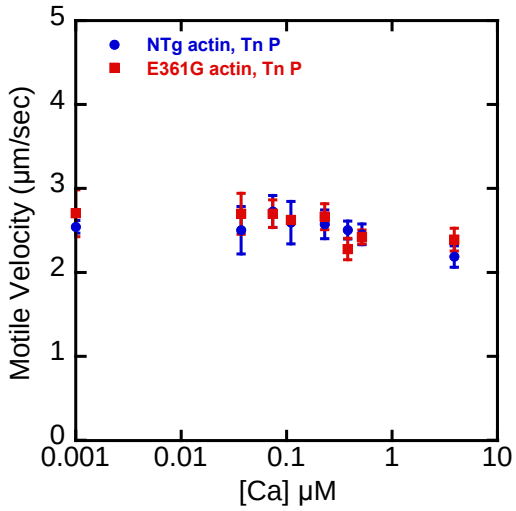


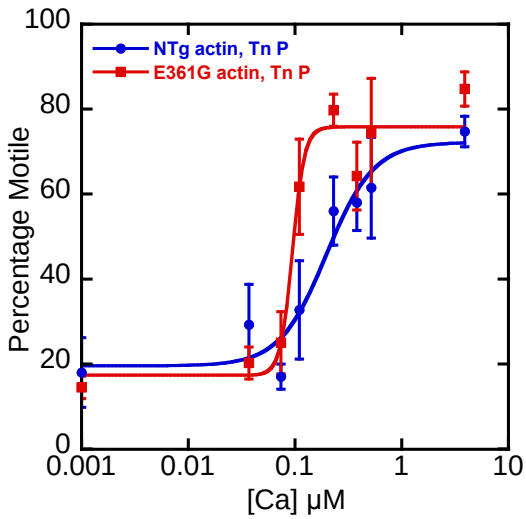


	Value	Error
Hill Coefficient	2	/
EC_{50}	0.19	0.04

	Value	Error
Hill Coefficient	2	/
EC_{50}	0.25	0.11

2

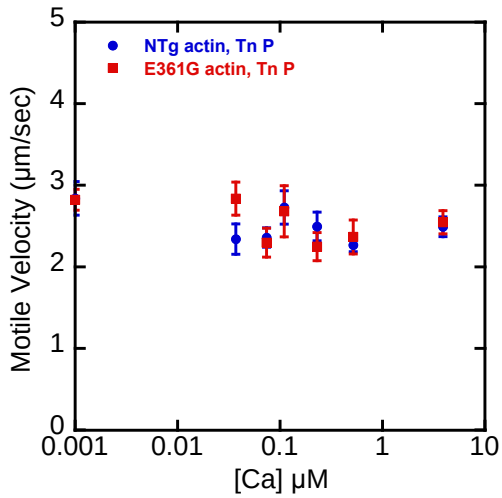


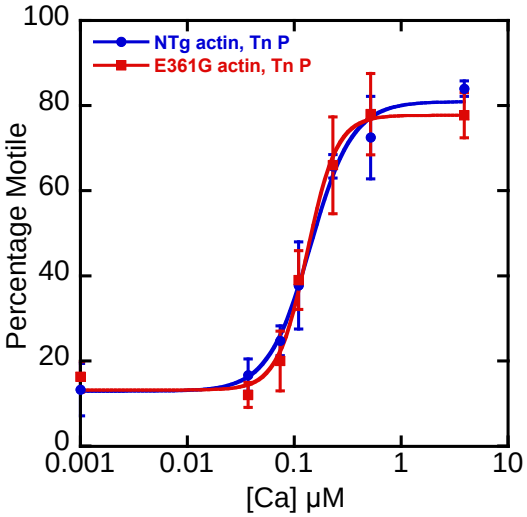


	Value	Error
Hill Coefficient	1.97	0.88
EC_{50}	0.2	0.06

	Value	Error
Hill Coefficient	7.69	3.9
EC_{50}	0.09	0.01

3





	Value	Error
Hill Coefficient	2.2	0.41
EC_{50}	0.14	0.01

	Value	Error
Hill Coefficient	3.11	0.59
EC_{50}	0.13	0.01

Tracking of E361G and non-transgenic sliding speeds produced large variability in the Ca^{2+}-sensitivity plots and did not show Ca^{2+} regulation, therefore no accurate fit has been possible and the points have simply been plotted.

Table 3.9: Ca^{2+}-sensitivity data for E361G v Non-Transgenic actin thin filaments

actin E361G ANALYSIS	EC_{50} Percentage motility, µM		EC_{50} mutant / EC_{50} NTg	Hill coefficient n		% Motile 3.9 µM Ca^{2+}		Ca^{2+} activation of sliding speed (%)		Maximum sliding speed (µm/sec)	
EXP N	NTg	E361G		NTg	E361G	NTg	E361G	NTg	E361G	NTg	E361G
1	0.19±0.04	0.25±0.11	1.32	2	2	75	74	0	0	2.89	2.97
2	0.20±0.06	0.09±0.01	0.45	2	7.69	75	85	0	0	2.73	2.7
3	0.14±0.01	0.13±0.01	0.93	2.2	3.11	84	78	0	0	2.84	2.84
MEAN±SE	0.18±0.02	0.16±0.05	0.9±0.25	2.07± 0.07	4.27± 1.74	78±3	79±3	0	0	2.82±0.05	2.84±0.08
Student's t-test (paired)	p=0.72		single group, p=0.73 (compared with one)								
(unpaired)	p=0.73										

The parameters observed in the three experiments are summarised in Table 3.9.

The maximum sliding speed was on average very similar and there was no Ca^{2+}-dependent activation of the thin filaments. Also the percentage of motile filaments in high Ca^{2+} was on average almost the same, while E361G actin thin filaments showed a higher Hill coefficient, suggesting a higher cooperativity.

The percentage of motile filaments across the titration could be accurately fitted to the Hill Equation, giving information about the Ca^{2+}-sensitivity. Although the Ca^{2+}-curves showed variability in individual experiments, the average number shows great similarity in the EC_{50} value. Statistical analysis confirms that there was no significant difference between the percentage motile EC_{50} values of E361G and non-transgenic thin filaments (three values is the minimum for a significance test; paired $p = 0.72$, unpaired $p = 0.73$), nor between the ratio of those values compared to 1 ($p = 0.73$).

3.2.3.7 Effects of Cardiac Troponin Dephosphorylation on the Ca^{2+}-Sensitivity of E361G Thin Filaments

Complete dephosphorylation of TnI was obtained following the protocol reported in 2.3.2. Two experiments were performed comparing thin filaments reconstituted with E361G actin, human cardiac tropomyosin and human cardiac troponin either natively phosphorylated or thoroughly dephosphorylated (Figure 3.8). These experiments would show the direct effect of phosphorylation on the thin filaments Ca^{2+}-sensitivity, which is expected to be decreasing with increasing phosphorylation.

Table 3.10: Ca^{2+}-sensitivity data for E361G actin thin filaments natively phosphorylated human cardiac troponin v dephosphorylated human cardiac troponin

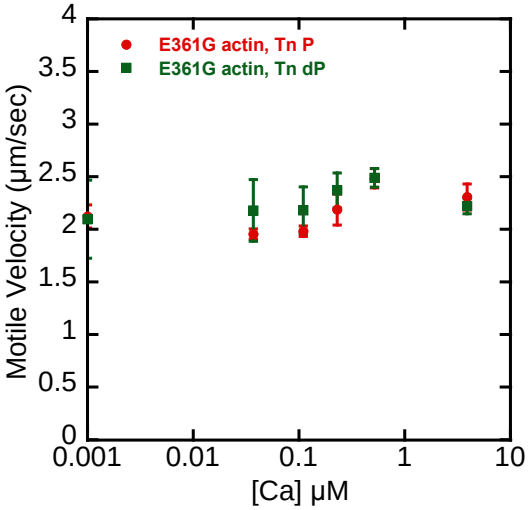
actin E361G ANALYSIS	EC_{50} Percentage motility, µM		EC_{50} P / EC_{50} dP	Hill coefficient n		% Motile 3.9 µM Ca^{2+}		Ca^{2+} activation of sliding speed (%)		Maximum sliding speed (µm/sec)	
EXP N	E361G P	E361G dP		P	dP	P	dP	P	dP	P	dP
1	0.14±0.02	0.17±0.01	0.82	4	3.25	70	74	9	6	2.49	2.49
2	0.15±0.05	0.14±0.05	1.07	1.16	1	82	82	0	1	2.67	2.77
MEAN±SE	0.15±0.01	0.16±0.02	0.95±0.13	2.58± 1.42	2.13± 1.13	76±6	78±4	4.5±4.5	3.5±2.5	2.58±0.09	2.63±0.14

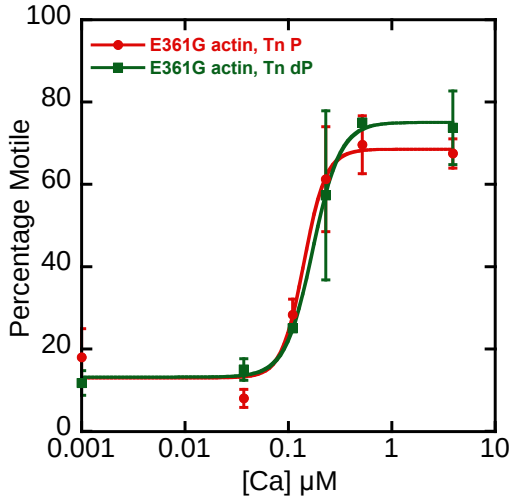
The thin filaments again did not show much Ca^{2+}-regulation of the sliding speed and showed no significant difference in the maximum velocities or percentage motile in 3.9 µM Ca^{2+} due to different phosphorylation levels of troponin, but the velocity seems to increase a bit earlier with dephosphorylated troponin.

The EC_{50} values of percentage motile do not show much difference and the phosphorylated / dephosphorylated ratios are on average very close to one. The Hill coefficient is very similar as well (Table 3.10).

Figure 3.8: Ca^{2+} concentration titration comparing E361G actin thin filaments containing phosphorylated and dephosphorylated troponin

1

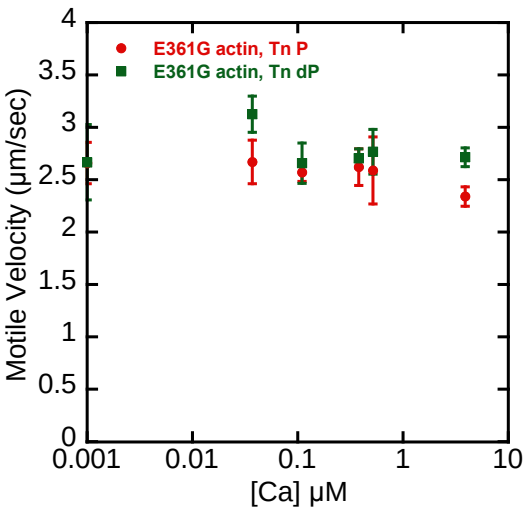


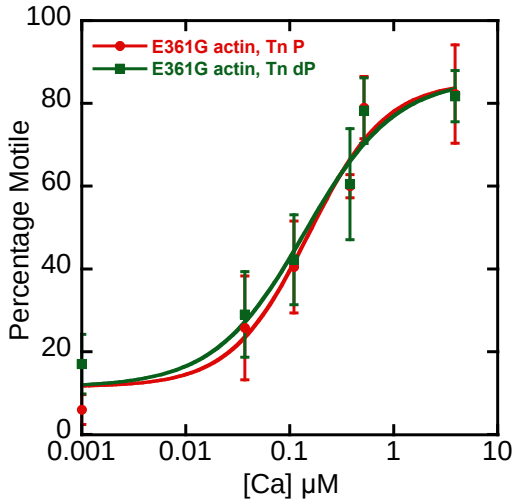


	Value	Error
Hill Coefficient	4.01	1.58
EC_{50}	0.14	0.02

	Value	Error
Hill Coefficient	3.25	0.41
EC_{50}	0.17	0.01

2





	Value	Error
Hill Coefficient	1.16	0.37
EC_{50}	0.15	0.05

	Value	Error
Hill Coefficient	1	0.32
EC_{50}	0.14	0.05

3.3 Discussion

3.3.1 IVMA Advantages and Limitations

The IVMA is a very versatile technique, which allows real-time comparison of the functional properties of a pair of reconstituted thin filaments with just one component different.

The technique we used substitutes the more widely adopted nitrocellulose surface with a silicone coated glass as the substrate for attaching HMM (Marston, 2003). The difference is mainly produced by the friction generated by the nitrocellulose, which, acting as a load, completely stops all the thin filaments in low Ca^{2+} concentration. With increasing Ca^{2+} concentrations, then, it allows them all to speed up increasingly, until maximum velocity is reached in high Ca^{2+} concentration. With a siliconised surface, instead, two populations of moving thin filaments will always exist, corresponding to a two state system. One population will be stopping and the other one moving, corresponding respectively to populations in the closed/blocked state and in the open state (Fraser and Marston, 1995, Sundberg et al., 2003). The moving population, even in low Ca^{2+} concentrations has a motile velocity, which, most of the time, exceeds 2 μm/sec. It has been observed that by adding just tropomyosin to plain actin, the motile velocity usually increases, and the same happens by adding troponin to actin-tropomyosin in activating Ca^{2+} buffer. This should correlate to a larger cooperativity acquired by the system.

In this context the percentage motile represents the ratio of thin filaments split between the two activation states as a function of the Ca^{2+} concentration and can be fitted through the Hill equation. The main criteria considered to compare the two fitted curves obtained are the EC_{50}, which gives information on the Ca^{2+}-sensitivity, and the Hill coefficient, which gives

information on the cooperativity of the system. IVMA has been demonstrated to achieve reproducible data in single experiments when comparing two reconstitutions in the same motility cell, using the same batches of purified proteins with only one element differing. Between two different experiments considering thin filaments reconstituted with the same kind of proteins, in fact, analysis of the data showed the same trend, but sometimes the absolute value of the parameters changed slightly. This is a consequence of using either a protein from the same purification at different times or the same kind of protein but from two different preparations, which would therefore change slightly its concentration and activity. Since human and mouse cardiac troponin is unstable, the preparations have a limited life-time and are variable. In the single experiment only one protein differs between the two reconstitutions, whereas everything else is used in the exact same concentrations and from the same purification batch; this enables the attribution of the differences to action of the different protein.

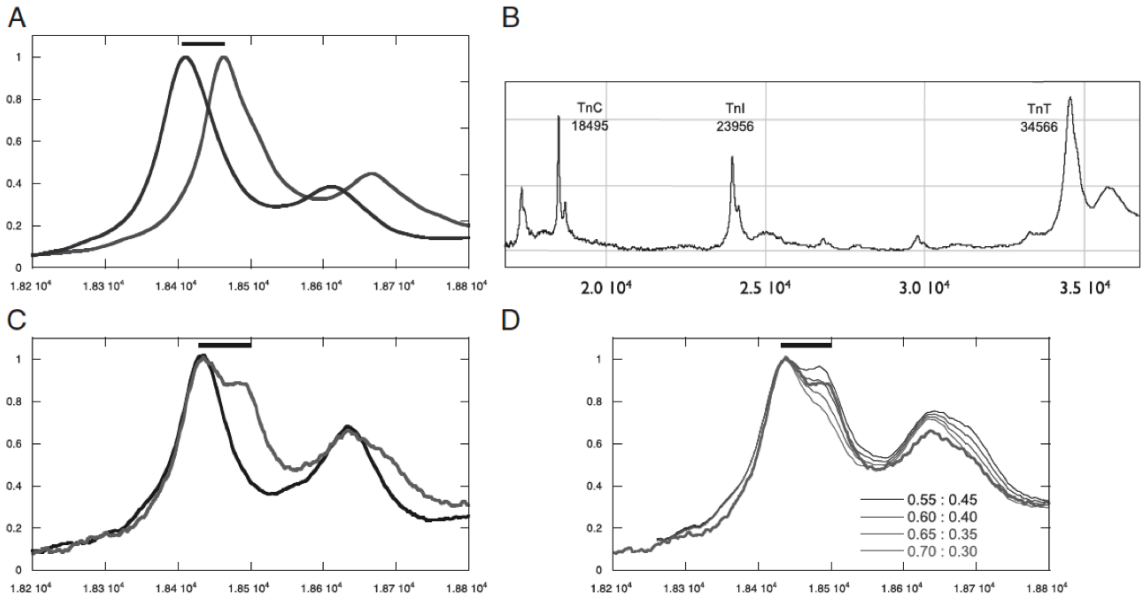
The motile velocity increased in a similar Ca^{2+}-dependent manner to the percentage motile and could therefore produce information on the same parameters. But this has proved to be much less consistent, so it cannot always be taken into account. While for the percentage motile the increase of motile filaments just depends on the Ca^{2+}-dependent switch between states, the motile velocity is a function of the cross-bridge cycling rate, but with additional contributing factors. The motile velocity is influenced by the rate of cross-bridge turnover, which in turn depends on every component of the acto-myosin, in particular myosin and troponin T (Bing et al., 1997). It is also influenced by the viscous drag of the siliconised surface, which sometimes can be inhomogeneous. In some circumstances the motile velocity is independent of Ca^{2+} (e.g. with actin made directly from thin filaments, as seen for E361G and the NTg actin) and it also seems to be species dependant as human troponin produces a

larger Ca^{2+}-dependent increase of the motile velocity than the mouse troponin (see section 4.5.2). Because of these difficulties sometimes this data could not be considered. When the Ca^{2+}-dependent velocity change was large enough data could be analysed for this parameter and values could be obtained for the maximum speed reached or the percentage of increase in the velocity between low and high Ca^{2+} concentrations. When also the Ca^{2+}-sensitivity could be considered I found that comparison of velocity and percentage motile always produced the same values.

3.3.2 Troponin C G159D and Actin E361G Purification and activity

Troponin from the explanted heart tissue of the TnC G159D patient was purified, just like the donor troponin, by affinity chromatography. The presence and concentration of the mutant TnC was then tested through matrix-assisted laser desorption/ionization mass spectrometry (MALDI-MS) experiments done by Dr D. Ward, Birmingham. Analysing the peaks generated, it was evident that the purified troponin from the patient heart sample had an additional peak at approximately the distance expected for a 58 Da increase in molecular weight (Figure 3.9 A-B-C). An estimation of the fraction of mutant TnC was obtained by comparison with spectra obtained with recombinant proteins mixed in different ratios. The best fitting was obtained with 45% mutant protein (Figure 3.9 D). Furthermore Fourier transform ion cyclotron resonance mass spectroscopy, confirmed the presence of two peaks differing by the expected 58 Da in mass and in the 60% and 40% ratio.

Figure 3.9: MALDI-MS spectra of troponin C G159D



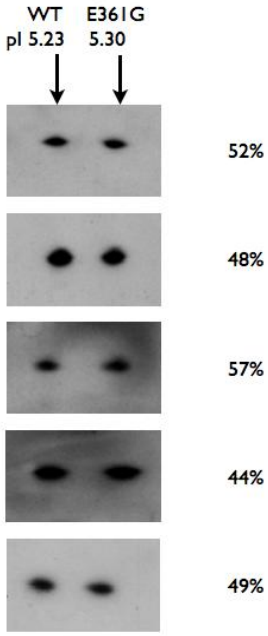
A) Matrix-assisted laser desorption/ionization mass spectrometry (MALDI-MS) spectra of recombinant troponin C. Normalized peak signal intensity is plotted against mass to charge (m/z) ratio. Overlaid spectra of recombinant WT and G159D cTnC. Black bar indicates the 58 Da shift expected for the mutation. B) Spectrum of the whole human troponin. C) Spectrum of the cTnC component of the G159D purified troponin with overlaid in black the normalised peak of the donor heart troponin. D) Comparison of the G159D cTnC human cardiac troponin (thick line) with synthetic spectra overlaid containing different concentrations of mutant G159D cTnC (Dyer et al., 2009).

Myofibrils were also screened for any difference in composition or phosphorylation from the donor heart sample but they were indistinguishable. When thin filaments were reconstituted *in vitro* with G159D troponin they showed Ca^{2+} regulation with a very similar behaviour to that of donor troponin, both in percentage motile and motile velocity, thus confirming the activity of G159D containing troponin.

In the case of *ACTC* E361G, a transgenic mouse line was produced in our lab by Dr D. Wells and Dr W. Song. 2D electrophoresis analysis, performed by Dr E. Dyer and Dr J. Leung, was able to detect two actin bands since the mutation shifted the pI of the protein by substituting a negatively charged residue with a neutral one. The mutation was stably expressed to 50% of the total actin in the cardiomyocytes (Figure 3.10) of the mice up to 18 months of age, which

is the oldest age used to perform experiments. Myofibrillar composition and their phosphorylation were indistinguishable from that of non-transgenic mice. When E361G actin was used in the IVMA it did not seem to have any peculiarity compared to the NTg actin in the motile properties whether alone, or in the presence of tropomyosin. When the thin filaments were fully reconstituted by adding troponin, it showed good regulation by Ca^{2+}.

Figure 3.10: 2D electrophoresis of transgenic mouse cardiac actin E361G



2D electrophoresis of whole mouse heart homogenate. Actin is detected in western blots with anti-sarcomeric actin antibody 5C5. Results from 5 different 5-week old PCR-positive mice are shown. The E361G mutant actin migrates at a higher pI than wild-type. The amount of mutant actin, determined by densitometry, is indicated (Song et al., 2010).

3.3.3 IVMA Results Leading to the "Uncoupling Hypothesis"

The results obtained with troponin C G159D and actin E361G were combined to those recoded by Dr E. Dyer (my own are highlighted in green):

TnC G159D

Tn G159D ANALYSIS	EC_{50} Percentage motility, µM		EC_{50} mutant / EC_{50} Donor
EXP N	Donor	G159D	
1	0.044±0.002	0.010±0.013	0.23
2	0.201±0.080	0.025±0.009	0.12
3	0.177±0.029	0.112±0.019	0.63
4	0.180±0.10	0.140±0.11	0.77
5	0.120±0.02	0.110±0.008	0.91
6	0.101±0.022	0.067±0.004	0.66
MEAN±SE	0.137±0.060	0.077±0.009	0.55±0.13 p=0.017

Tn G159D ANALYSIS	EC_{50} Percentage motility, µM		EC_{50} P / EC_{50} dP
EXP N	G159D P	G159D dP	
1	0.036±0.014	0.033±0.009	1.09
2	0.019±0.005	0.018±0.003	1.05
3	0.033±0.018	0.021±0.010	1.57
4	0.065±0.021	0.063±0.007	1.03
5	0.109±0.030	0.092±0.016	1.18
MEAN±SE	0.052±0.036	0.045±0.032	1.18±0.09 p=0.0003

Tn G159D ANALYSIS	EC_{50} Percentage motility, µM		EC_{50} mutant / EC_{50} Donor
EXP N	Donor dP	G159D dP	
1	0.132±0.041	0.064±0.031	0.48
2	0.137±0.021	0.077±0.006	0.56
3	0.124±0.018	0.100±0.009	0.80
MEAN±SE	0.131±0.009	0.080±0.018	0.61±0.09 p=0.024

actin E361G

actin E361G ANALYSIS	EC_{50} Percentage motility, µM		EC_{50} mutant / EC_{50} NTg
EXP N	NTg	E361G	
1	0.143±0.045	0.107±0.028	0.747
2	0.261±0.039	0.242±0.001	0.927
3	0.039±0.025	0.031±0.016	0.795
4	0.070±0.022	0.090±0.098	1.285
5	0.143±0.193	0.114±0.606	0.797
6	0.045±0.014	0.052±0.018	1.156
7	0.190±0.04	0.250±0.11	1.32
8	0.200±0.06	0.090±0.01	0.45
9	0.140±0.01	0.130±0.01	0.93
MEAN±SE	0.137±0.025	0.123±0.025	0.934±0.09 p=0.5

actin E361G ANALYSIS	EC_{50} Percentage motility, µM		EC_{50} P / EC_{50} dP
EXP N	E361G P	E361G dP	
1	0.309±0.091	0.331±0.087	0.93
2	0.604±0.160	0.623±0.073	0.97
3	0.153±0.046	0.120±0.045	1.28
4	0.335±0.058	0.358±0.058	0.94
5	0.140±0.02	0.170±0.01	0.82
6	0.150±0.05	0.140±0.05	1.07
MEAN±SE	0.282±0.073	0.290±0.078	1.0±0.065 p=0.98

The object of this chapter was to repeat preliminary work of Dr E. Dyer with these two DCM mutations. I was able to obtain the same results with both G159D and E361G, which confirm the initial findings, therefore the datasets have been combined. The final outcome is that, with

natively phosphorylated troponin, G159D thin filaments have a higher Ca^{2+}-sensitivity than donor thin filaments (ratio of EC_{50} 0.55 ± 0.13), which differs from what was seen with this mutation when expressed recombinantly, whereas E361G thin filaments have the same Ca^{2+}-sensitivity of non-transgenic thin filaments. Thus the hypothesis of having a lower Ca^{2+}-sensitivity in thin filaments as the cause of DCM is not supported. The new hypothesis supported by the data shown in this chapter is that DCM is the result of an uncoupling between TnI phosphorylation and the thin filament Ca^{2+}-sensitivity.

The absence of a response to PKA phosphorylation on TnI, which is supposed to decrease the Ca^{2+}-sensitivity of the thin filaments, would impair the rapid relaxation (lusitropy) of the heart muscle, an essential consequence of the β-adrenergic stimulation for increasing the heart rate and the contractile force (inotropy). In the long run, the uncoupling produced by these mutations could reduce the cardiac reserve and produce cardiac dysfunction under stress, terminating in the DCM phenotype.

The phenotype shown by the E361G mice, though, when investigated *in vivo*, did not show DCM, with the only indication of a potentially dilated heart given by a 15% higher left ventricle internal diameter. The pathology induced by E361G in the human patients anyway was reported to be only mild (Olson et al., 2001), therefore it could have been compensated by other changes, but, most importantly, the mice were not put through any sort of stress, which could have in this case prevented the manifestation of the phenotype. In the case of the G159D mutation, the higher Ca^{2+}-sensitivity manifested by the thin filaments could correlate with the more severe phenotype. Another indication of the possible *in vivo* uncoupling was given by acute dobutamine stimulation experiments, where the response of E361G mice was significantly lower than the NTg's in the increase of the heart rate, ejection fraction and cardiac output (Song et al., 2010).

3.3.4 Proving the Uncoupling Hypothesis

The work presented above gave clear indications on the value of using proteins coming from human donor and patients' tissue when available, or from transgenic mouse models, but most importantly proteins should present the key post-translational modifications that have been showed to influence the outcome of the experiments so much.

The IVMA, as well, has proved to be an extremely useful tool, since it enables the reproduction of a situation very close to the physiological scenario and it also allows the use of proteins whose phosphorylation status was manipulated. This is still a limit of techniques using skinned myofibres, were no direct dephosphorylation is possible and therefore native troponin is exchanged with recombinant troponin (Kooij et al., 2010).

The work presented in the next chapter follows the same guidelines. It will test the possibility that the uncoupling hypothesis corresponds to a general rule followed by other mutations that lead to DCM. Five mutations will be investigated, placed on different subunits of the thin filaments in respect to the two discussed above. The first will be a mutation on TnI: K36Q. This will be purified from human heart tissue belonging to a patient whose heart was transplanted.

Two mutants on TnT will then be taken into consideration: R141W and ΔK210. Both of these were purified from transgenic mouse model developing DCM.

Finally, two α-tropomyosin mutants, expressed in eukaryotic recombinant cells with the baculovirus/*sf9* system, are going to be analysed: E40K and E54K. With E40K an experiment was also performed testing the dose-dependency of the phenotype.

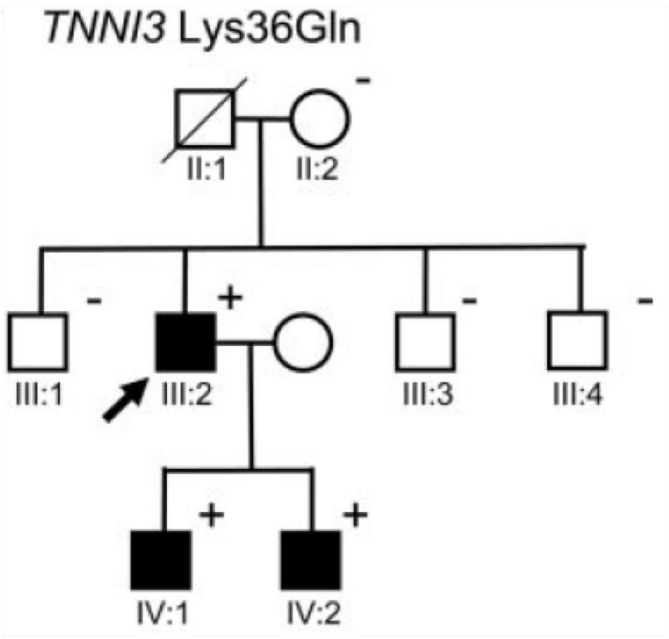
4 Testing The Uncoupling Hypothesis with Five Different Mutations

4.1 Functional Investigation of DCM Mutant Troponin I Lys36Gln from Human Sample

4.1.1 Introduction on TnI K36Q

K36Q together with N185K was reported as a DCM causing mutation in the first study giving evidence of TnI as a disease linked gene (Carballo et al., 2009). In that case, 94 probands were screened for a TnI mutation with these two autosomal dominant missense mutations identified.

Figure 4.1: Pedigree of the K36Q TnI patient's family



Square = male; circle = female; '+' = presence of the mutation; '-' = absence of the mutation; black filling = person affected; slanted bars = deceased; bold arrow indicates the proband. (Carballo et al., 2009)

The TnI K36Q patient was diagnosed with severe DCM at age 15 and had to undergo heart transplantation 2 months later, following a rapid deterioration. The explanted heart had globular shape and biventricular dilatation. Left ventricular histology showed moderate anisocytosis with occasional enlarged brick-shaped nuclei, prominent myocytolysis, patchy interstitial fibrosis centered on a thickened endocardium with occasional trapped inflammatory cells.

Both sons of the proband were shown to carry the mutation and one had only a mild DCM phenotype, while the other had severe DCM and had an early cardiac transplantation at the age of 6 (Figure 4.1). The parents of the proband were both asymptomatic, the mother did not carry the mutation and the father died at 50 and could not be tested. All the siblings did not carry the mutation and did not show signs of cardiac disease. Haplotype studies demonstrated that the chromosome was inherited from the father.

The position of the mutation is very near the 31 amino acid long N-terminal regulatory extension of cardiac TnI and is the first of an extremely conserved cluster of three arginines. The substitution of a positively charged amino acid for a non-charged glutamine, in a conserved region of the protein just outside a region important for the β-adrenergic modulation of the Ca^{2+}-sensitivity, makes this mutant a perfect candidate for testing the hypothesis of an uncoupling between TnI phosphorylation and Ca^{2+}-sensitivity.

4.1.2 Manipulation of TnI K36Q Phosphorylation

Phosphate affinity SDS-PAGE gels of parallel purifications of human donor troponin and TnI K36Q troponin from human patient heart sample showed low phosphorylation of TnI K36Q troponin. The average phosphorylation level for the human donor sample was 1.64 ± 0.25 mols P_i / mol TnI (n = 4), which perfectly fits with the average measured for all of the donor sample tested so far with phos-tag (Messer et al., 2009). The mutant TnI, on the contrary, in

two different purifications showed an average phosphorylation of just 0.33 ± 0.14 mols P_i / mol TnI. Having this rather low level of phosphorylation we proceeded not only by dephosphorylating TnI thoroughly, but also to increase phosphorylation to donor's levels by phosphorylating it with PKA (see section 2.3.1). The average of four different dephosphorylations was 0.09 ± 0.01 mols P_i / mol TnI, while the average for two different PKA treatments was 1.31 ± 0.01 mols P_i / mol TnI. IVMA has been performed comparing Ca^{2+}-sensitivity with different combinations of these three phosphorylation states both between each other and with phosphorylated and unphosphorylated donor. Dephosphorylated donor troponin had 0.12 ± 0.07 mols P_i / mol TnI (n = 4).

4.1.3 Ca^{2+} Concentration Titrations

Every experiment described in the following sections was performed using thin filaments reconstituted with rabbit skeletal muscle actin 10 nM, human cardiac tropomyosin 60 nM and donor or K36Q troponin 60 nM. The Ca^{2+} titrations were all recorded after Ca^{2+} regulation of the thin filaments was observed to be efficient and similar for the two reconstitutions.

4.1.3.1 Comparison of K36Q Troponin (Native Phosphorylation or PKA Treated) with Donor Human Cardiac Troponin

As described in the previous paragraph the starting phosphorylation level of the two troponin samples was different. Two Ca^{2+} titrations (Figure 4.2) were performed with two different troponin preparations to screen the possible differences given by the presence of the mutation and the low phosphorylation of TnI, which in normal conditions would imply a shift towards a higher Ca^{2+} sensitivity for the thin filaments.

What is visible from the titrations is that the velocities (Table 4.1) start and finish at the same levels. In experiment 1 they increase very similarly, whereas in experiment 2, the mutant shows a lower Ca^{2+} sensitivity (EC_{50} ratio K36Q / donor = 2.5).

Table 4.1: Ca^{2+}-sensitivity data for untreated K36Q v donor troponin thin filament sliding speed

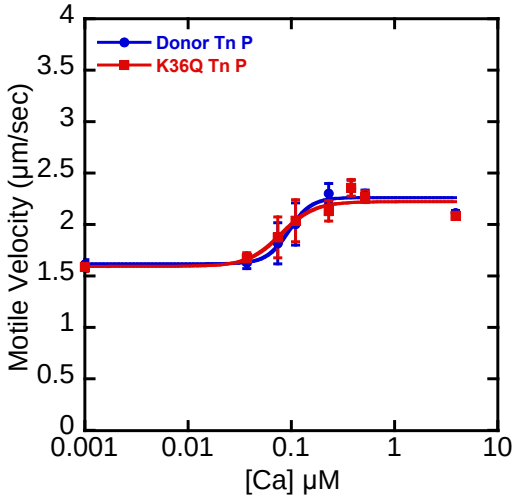
Tn K36Q ANALYSIS	EC_{50} Sliding speed, µM		EC_{50} mutant/ EC_{50} Donor	Ca^{2+} activation of sliding speed (%)		Maximum sliding speed (µm/sec)	
EXP N	Donor	K36Q		Donor	K36Q	Donor	K36Q
1	0.09±0.01	0.08±0.02	0.89	46	49	2.35	2.36
2	0.06±0.02	0.15±0.02	2.5	69	60	2.52	2.47
MEAN±SE	0.08±0.02	0.12±0.04	1.7±0.81	58±12	55±6	2.44±0.09	2.42±0.06

Table 4.2: Ca^{2+}-sensitivity data for untreated K36Q v donor troponin thin filament percentage motile

Tn K36Q ANALYSIS	EC_{50} Percentage motility, µM		EC_{50} mutant / EC_{50} Donor	Hill coefficient n		% Motile 3.9 µM Ca^{2+}	
EXP N	Donor	K36Q		Donor	K36Q	Donor	K36Q
1	0.13±0.01	0.24±0.04	1.85	1.48	2.22	85	84
2	0.16±0.03	0.39±0.04	2.6	1.1	3.04	91	89
MEAN±SE	0.15±0.02	0.32±0.08	2.23±0.38	1.29±0.19	2.63±0.41	88±3	87±3

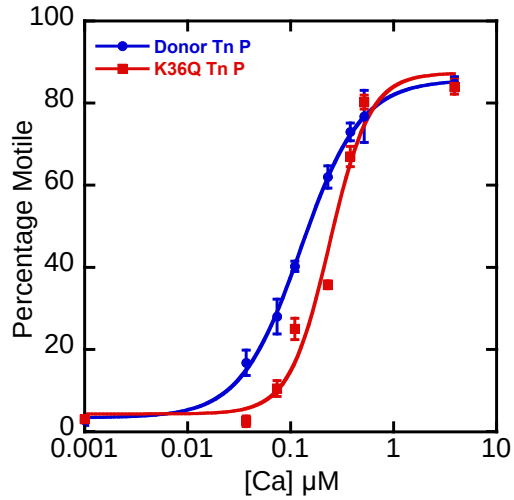
Figure 4.2: Ca^{2+} concentration titration comparing thin filaments containing human donor and untreated K36Q troponin

1



	Value	Error
Hill COefficient	4.01	2.53
EC_{50}	0.09	0.01

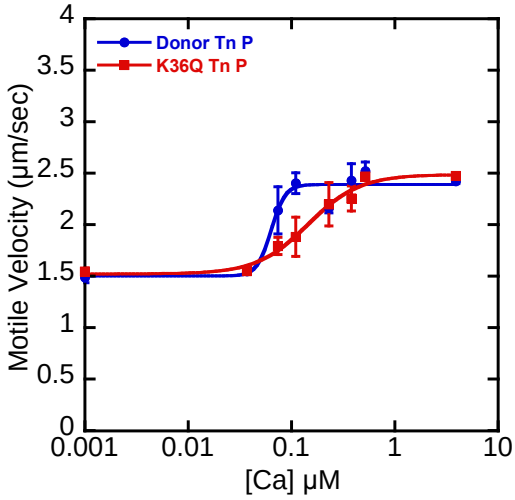
	Value	Error
Hill COefficient	2.73	1.86
EC_{50}	0.08	0.02



	Value	Error
Hill Coefficient	1.48	0.07
EC_{50}	0.13	0.01

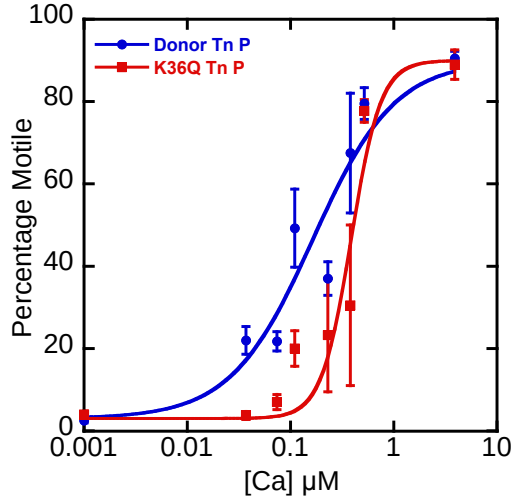
	Value	Error
Hill Coefficient	2.22	0.62
EC_{50}	0.24	0.04

2



	Value	Error
Hill Coefficient	6.39	8.49
EC_{50}	0.06	0.02

	Value	Error
Hill Coefficient	1.74	0.38
EC_{50}	0.15	0.02



	Value	Error
Hill Coefficient	1.1	0.29
EC_{50}	0.16	0.03

	Value	Error
Hill Coefficient	3.04	1.21
EC_{50}	0.39	0.04

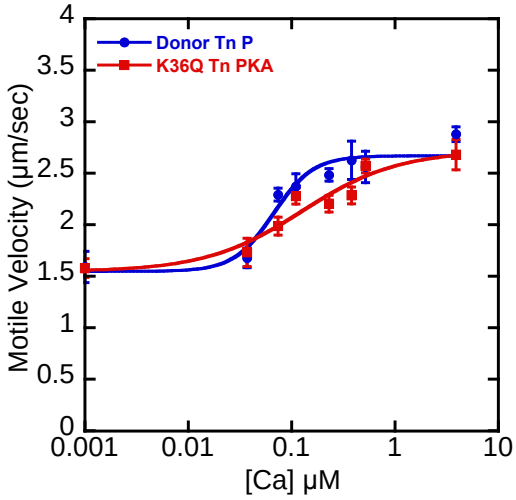
The percentage motile has a much better defined phenotype (Table 4.2). High and low Ca^{2+} points are very similar, but the mutant, despite the lower phosphorylation of TnI, shows a much lower Ca^{2+} sensitivity (EC_{50} ratio K36Q / donor = 2.23 ± 0.38). K36Q troponin also presents a larger Hill Coefficient.

K36Q was then treated with PKA to achieve a phosphorylation of the same order of that shown by the donor troponin. As described in 4.1.2, the phosphorylation reached by the mutant after the PKA treatment was 80% of that of the donor, compared with the initial 20% of the untreated sample. Four Ca^{2+} titrations were performed with the PKA treated sample in parallel to the donor untreated troponin (experiments 3 and 4 are shown in Figure 4.3, experiments 1 and 2 are shown in APPENDIX). These experiments were performed using two different troponin preparations: the first for experiments 1, 2, and 3, the second for experiment 4. The data extracted from these experiments (summarised in Table 4.3 and Table 4.4) are very similar to those shown by the comparison between untreated K36Q and donor troponin.

Although one of the velocity plots (experiment 1) could not be fitted for the high variability of the measurements, the others showed a lower Ca^{2+}-sensitivity for the mutant troponin (EC_{50} ratio K36Q / donor = 1.94 ± 0.4), although it gets statistical significance only with the unpaired student t-test ($p = 0.043$). The percentage motile showed a lower Ca^{2+}-sensitivity, which was significantly different in the paired student t-test ($p = 0.009$), consequently the EC_{50} ratio K36Q / donor was also significantly different from 1 ($p = 0.004$). The Hill Coefficient was again higher for K36Q troponin in the percentage motile parameter.

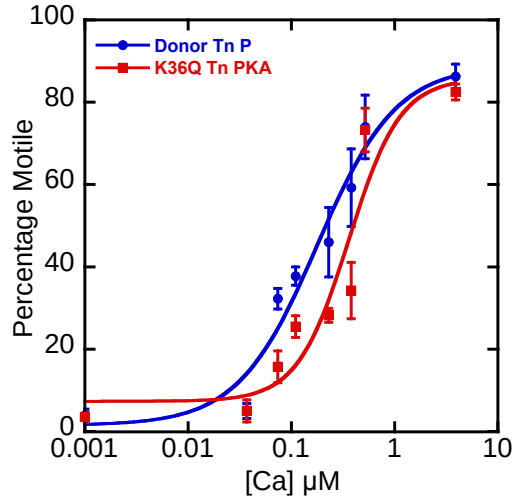
Figure 4.3: Ca^{2+} concentration titration comparing thin filaments containing human donor and PKA treated K36Q troponin

3



	Value	Error
Hill Coefficient	2.27	1.13
EC_{50}	0.07	0.02

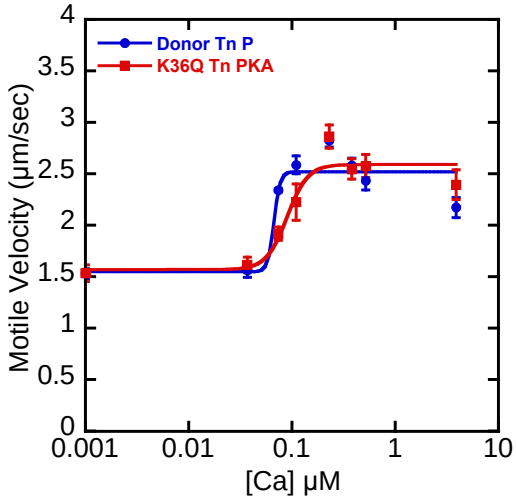
	Value	Error
Hill Coefficient	1	/
EC_{50}	0.13	0.07



	Value	Error
Hill COefficient	1.14	0.34
EC_{50}	0.18	0.06

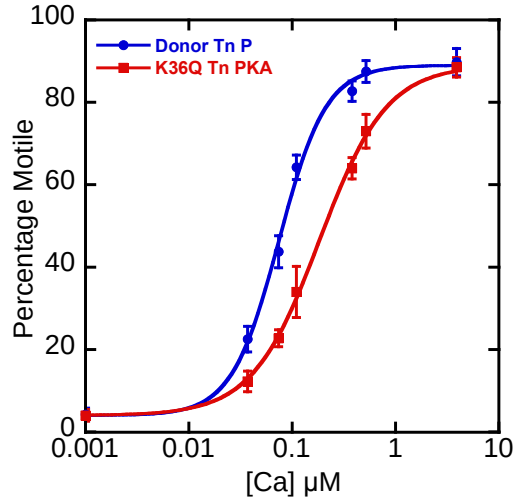
	Value	Error
Hill Coefficient	1.75	1.07
EC_{50}	0.36	0.12

4



	Value	Error
Hill Coefficient	14.82	1045.9
EC_{50}	0.07	0.47

	Value	Error
Hill Coefficient	4.34	3.17
EC_{50}	0.09	0.02



	Value	Error
Hill Coefficient	1.9	0.15
EC_{50}	0.07	0.01

	Value	Error
Hill Coefficient	1.34	0.04
EC_{50}	0.18	0.01

Table 4.3: Ca^{2+}-sensitivity data for PKA treated K36Q v donor troponin thin filament sliding speed

Tn PKA K36Q ANALYSIS	EC_{50} Sliding speed, µM		EC_{50} mutant/ EC_{50} Donor	Ca^{2+} activation of sliding speed (%)		Maximum sliding speed (µm/sec)	
EXP N	Donor	K36Q PKA		Donor	PKA	Donor	PKA
1	/	/	/	28	46	2.5	2.72
2	0.06±0.02	0.16±0.11	2.67	95	86	2.92	2.84
3	0.07±0.02	0.13±0.07	1.86	104	70	2.88	2.68
4	0.07±0.47	0.09±0.02	1.29	69	69	2.59	2.58
MEAN±SE	0.07±0.01	0.13±0.02	1.94±0.4	74±17	68±8	2.72±0.1	2.71±0.05
Student's t-test (paired)	p=0.122		single group, p=0.143 (compared with one)				
(unpaired)	p=0.043						

Table 4.4: Ca^{2+}-sensitivity data for PKA treated K36Q v donor troponin thin filament percentage motile

Tn PKA K36Q ANALYSIS	EC_{50} Percentage motility, µM		EC_{50} mutant / EC_{50} Donor	Hill coefficient n		% Motile 3.9 µM Ca^{2+}	
EXP N	Donor	K36Q PKA		Donor	PKA	Donor	PKA
1	0.29±0.11	0.55±0.01	1.9	1.18	3.1	78	87
2	0.17±0.04	0.36±0.06	2.12	1.38	3.06	85	86
3	0.18±0.06	0.36±0.12	2	1.14	1.75	86	83
4	0.07±0.01	0.18±0.01	2.57	1.9	1.34	90	89
MEAN±SE	0.18±0.04	0.36±0.08	2.15±0.15	1.4±0.17	2.31±0.45	85±2	86±1
Student's t-test (paired)	p=0.009		single group, p=0.004 (compared with one)				
(unpaired)	p=0.08						

4.1.3.2 Effects of Troponin I Dephosphorylation on the Ca^{2+}-Sensitivity of K36Q Thin Filaments

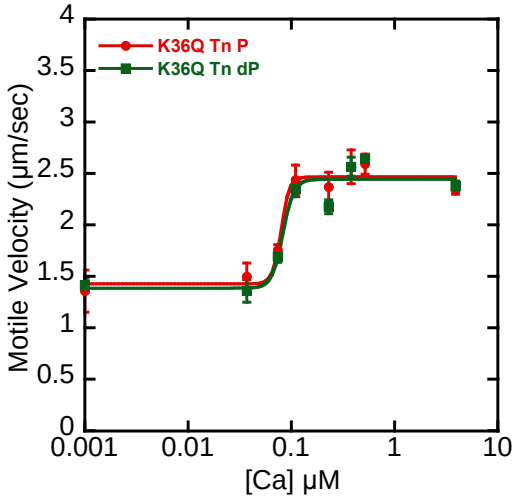
Thoroughly dephosphorylated K36Q troponin was compared with both natively phosphorylated K36Q troponin and PKA treated K36Q troponin. Three experiments were performed for each comparison.

When the natively phosphorylated K36Q troponin was compared to the dephosphorylated K36Q troponin in IVMA it showed almost perfectly superimposable curves for each experiment (experiments 1 and 3 are shown in Figure 4.4, experiment 2 in APPENDIX; all the measured parameters are in Table 4.5 and Table 4.6). There was not a significant difference between any of the parameters measured for EC_{50} of the motile velocity (paired p = 0.184, unpaired p = 0.116) or percentage motile (paired p = 0.742, unpaired p = 0.915). These experiments were performed using two different troponin preparation: the first for experiments 1 and 2, the second for experiment 3.

Very similarly, PKA treated K36Q troponin compared to dephosphorylated K36Q troponin produced curves with almost identical parameters with no statistical difference between them in both motile velocity and percentage motile. These are summarised in Table 4.7 and Table 4.8; experiments 2 and 3 are shown in Figure 4.5. The other titration is shown in the APPENDIX. The motile velocity plot for Ca^{2+} titration 1 was not taken into consideration due to the very small Ca^{2+} induced increase in the sliding speed. These experiments were performed using two different troponin preparations: the first for experiments 1 and 2, the second for experiment 3.

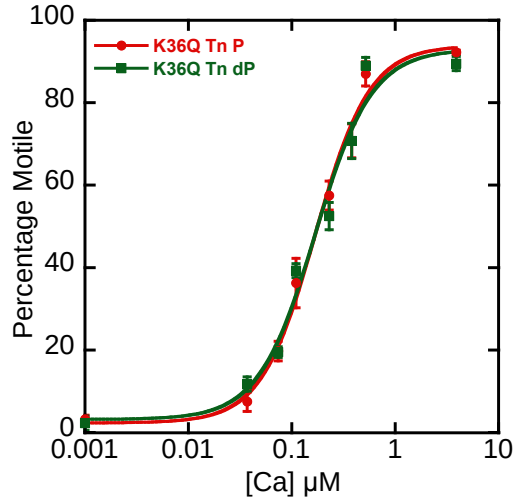
Figure 4.4: Ca^{2+} concentration titration comparing thin filaments containing natively phosphorylated and dephosphorylated K36Q troponin

1



	Value	Error
Hill Coefficient	10.74	11.55
EC_{50}	0.08	0.01

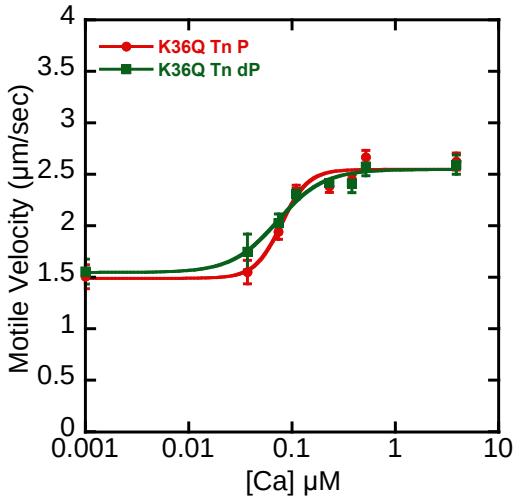
	Value	Error
Hill Coefficient	8.16	6.26
EC_{50}	0.08	0.01



	Value	Error
Hill COefficient	1.65	0.24
EC_{50}	0.17	0.02

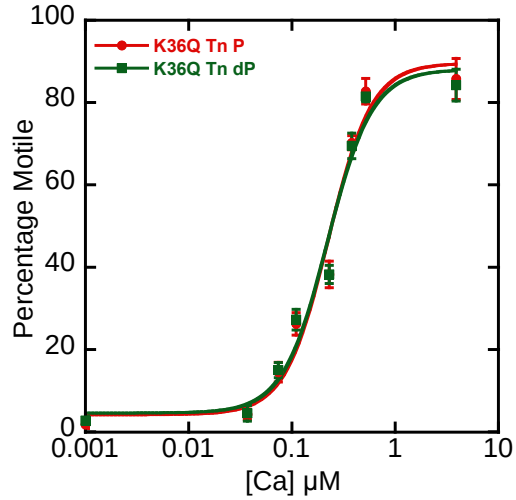
	Value	Error
Hill Coefficient	1.59	0.37
EC_{50}	0.17	0.03

3



	Value	Error
Hill Coefficient	3.38	1.55
EC_{50}	0.08	0.01

	Value	Error
Hill Coefficient	1.96	0.53
EC_{50}	0.07	0.01



	Value	Error
Hill Coefficient	2.06	0.56
EC_{50}	0.23	0.04

	Value	Error
Hill Coefficient	2.02	0.56
EC_{50}	0.22	0.04

Table 4.5: Ca^{2+}-sensitivity data for the sliding speed of thin filaments reconstituted with K36Q natively phosphorylated v K36Q dephosphorylated troponin

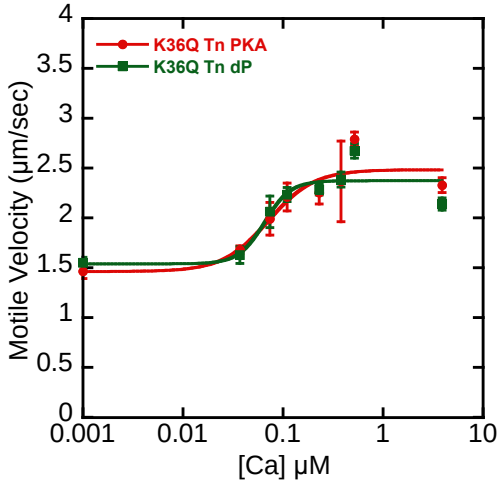
Tn K36Q ANALYSIS	EC_{50} Sliding speed, µM		EC_{50} P/ EC_{50} dP	Ca^{2+} activation of sliding speed (%)		Maximum sliding speed (µm/sec)	
EXP N	K36Q P	K36Q dP		P	dP	P	dP
1	0.08±0.01	0.08±0.01	1	90	96	2.56	2.64
2	0.08±0.01	0.07±0.01	1.14	94	130	2.91	2.88
3	0.08±0.01	0.07±0.01	1.14	77	67	2.66	2.59
MEAN±SE	0.08	0.07±0.01	1.09±0.05	87±5	98±18	2.71±0.1	2.7±0.09
Student's t-test (paired)	p=0.184		single group, p=0.184 (compared with one)				
(unpaired)	p=0.116						

Table 4.6: Ca^{2+}-sensitivity data for the percentage motile of thin filaments reconstituted with K36Q natively phosphorylated v K36Q dephosphorylated troponin

Tn K36Q ANALYSIS	EC_{50} Percentage motility, µM		EC_{50} P / EC_{50} dP	Hill coefficient n		% Motile 3.9 µM Ca^{2+}	
EXP N	K36Q P	K36Q dP		P	dP	P	dP
1	0.17±0.02	0.17±0.03	1	1.65	1.59	92	90
2	0.15±0.01	0.17±0.02	0.88	1.68	1.59	91	96
3	0.23±2.06	0.22±0.04	1.05	2.06	2.02	86	84
MEAN±SE	0.18±0.02	0.19±0.02	0.98±0.05	1.8±0.13	1.73±0.14	90±2	90±3
Student's t-test (paired)	p=0.742		single group, p=0.689 (compared with one)				
(unpaired)	p=0.915						

Figure 4.5: Ca^{2+} concentration titration comparing thin filaments containing natively PKA treated and dephosphorylated K36Q troponin

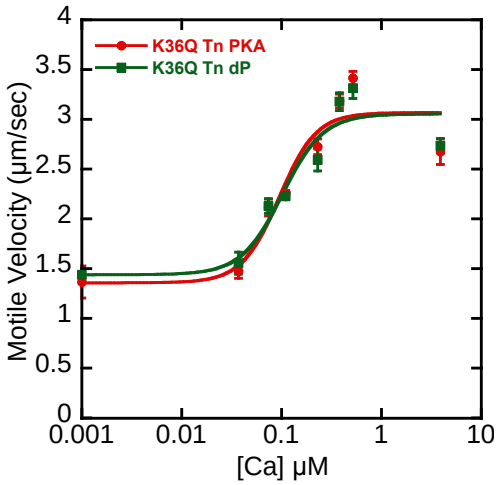
2



	Value	Error
Hill Coefficient	1.9	1.34
EC_{50}	0.07	0.03

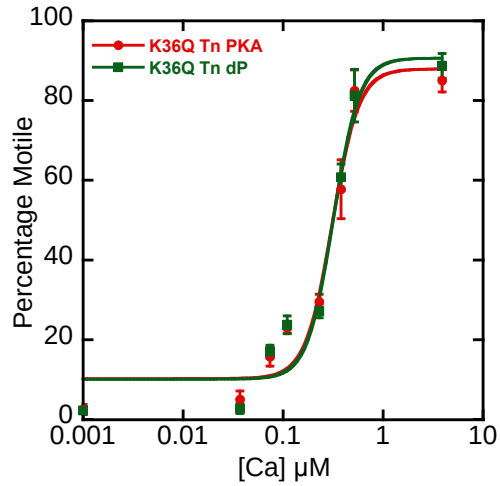
	Value	Error
Hill Coefficient	3.37	3.04
EC_{50}	0.07	0.02

3



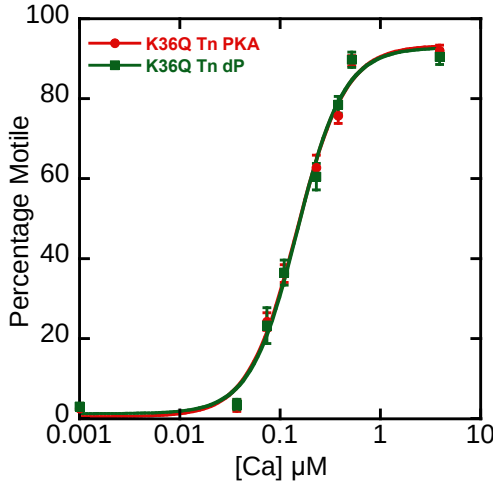
	Value	Error
Hill Coefficient	2.32	1.63
EC_{50}	0.09	0.03

	Value	Error
Hill Coefficient	2.12	1.38
EC_{50}	0.1	0.03



	Value	Error
Hill Coefficient	3.29	1.25
EC_{50}	0.31	0.04

	Value	Error
Hill Coefficient	3.35	1.28
EC_{50}	0.32	0.04



	Value	Error
Hill Coefficient	1.79	0.26
EC_{50}	0.15	0.02

	Value	Error
Hill Coefficient	1.86	0.29
EC_{50}	0.15	0.02

Table 4.7: Ca^{2+}-sensitivity data for the sliding speed of thin filaments reconstituted with PKA treated K36Q v K36Q dephosphorylated troponin

Tn PKA K36Q ANALYSIS	EC_{50} Sliding speed, µM		EC_{50} P/ EC_{50} dP	Ca^{2+} activation of sliding speed (%)		Maximum sliding speed (µm/sec)	
EXP N	K36Q PKA	K36Q dP		PKA	dP	PKA	dP
1	/	/	/	33	20	2.79	2.47
2	0.07±0.03	0.07±0.02	1	91	72	2.79	2.67
3	0.09±0.03	0.1±0.03	0.9	149	130	3.42	3.41
MEAN±SE	0.08±0.01	0.09±0.02	0.95±0.05	91±33	74±32	3±0.21	2.85±0.29

Table 4.8: Ca^{2+}-sensitivity data for the percentage motile of thin filaments reconstituted with PKA treated K36Q v K36Q dephosphorylated troponin

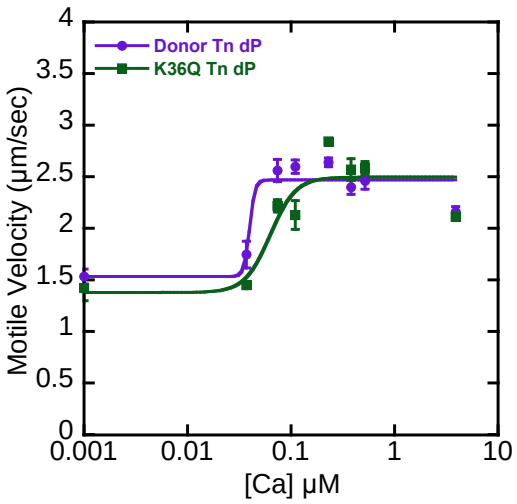
Tn PKA K36Q ANALYSIS	EC_{50} Percentage motility, µM		EC_{50} PKA / EC_{50} dP	Hill coefficient n		% Motile 3.9 µM Ca^{2+}	
EXP N	K36Q PKA	K36Q dP		PKA	dP	PKA	dP
1	0.24±0.02	0.25±0.03	0.96	4.44	3.14	77	77
2	0.31±0.04	0.32±0.04	0.97	3.29	3.35	85	89
3	0.15±0.02	0.15±0.02	1	1.79	1.86	92	91
MEAN±SE	0.23±0.05	0.24±0.05	0.98±0.01	3.17± 0.77	2.78± 0.47	85±4	86±4
Student's t-test (paired)	p=0.184		single group, p=0.192 (compared with one)				
(unpaired)	p=0.926						

Dephosphorylated K36Q was also compared to dephosphorylated donor troponin in three experiments: 1 and 3 are shown in Figure 4.6, 2 is shown in APPENDIX; all the measured parameters are summarised in Table 4.9 and Table 4.10. For these experiments only one troponin preparation was used.

The EC_{50} shows a fairly large variability between different experiments, which prevents any consideration on unpaired data. Nevertheless paired values clearly show that the measured Ca^{2+}-sensitivity for both motile velocity and percentage motile is lower for the mutant protein. The n-numbers were too low to achieve statistical significance. The other parameters were all similar between donor and mutant thin filaments. Experiment 2 motile velocity plot could not be fitted for the high variability of the measurements.

Figure 4.6: Ca^{2+} concentration titration comparing thin filaments containing dephosphorylated K36Q and dephosphorylated donor troponin

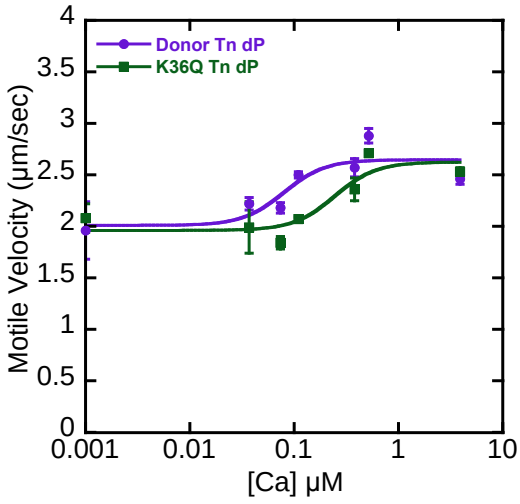
1



	Value	Error
Hill Coefficient	16.69	10661
EC_{50}	0.04	1.82

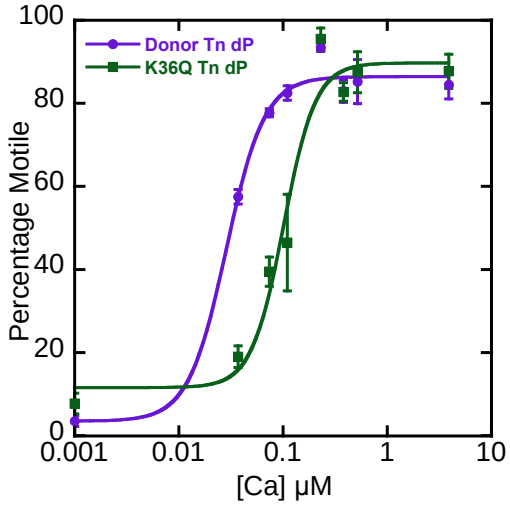
	Value	Error
Hill Coefficient	3.56	3.69
EC_{50}	0.06	0.02

3



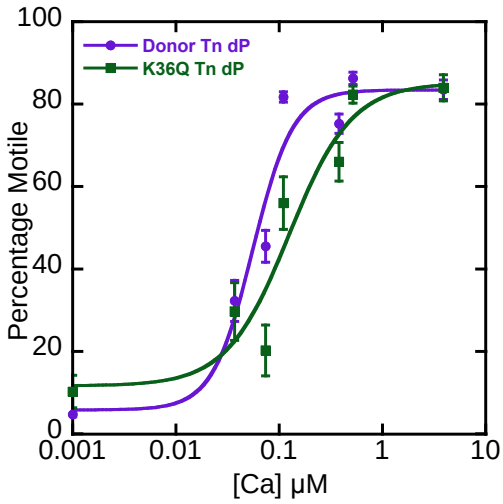
	Value	Error
Hill Coefficient	2.2	3
EC_{50}	0.08	0.04

	Value	Error
Hill Coefficient	2.2	/
EC_{50}	0.25	0.14



	Value	Error
Hill Coefficient	2.37	0.92
EC_{50}	0.03	0.01

	Value	Error
Hill Coefficient	2.82	1.35
EC_{50}	0.1	0.02



	Value	Error
Hill Coefficient	2.24	1.12
EC_{50}	0.06	0.01

	Value	Error
Hill COefficient	1.44	0.89
EC_{50}	0.13	0.07

Table 4.9: Ca^{2+}-sensitivity data for sliding speed of dephosphorylated K36Q v dephosphorylated donor thin filaments

Tn K36Q ANALYSIS	EC_{50} Sliding speed, µM		EC_{50} mutant/ EC_{50} Donor	Ca^{2+} activation of sliding speed (%)		Maximum sliding speed (µm/sec)	
EXP N	Donor dP	K36Q dP		Donor dP	K36Q dP	Donor dP	K36Q dP
1	0.04±1.82	0.06±0.02	1.5	73	100	2.64	2.84
2	/	/	/	21	45	2.51	2.57
3	0.08±0.04	0.25±0.14	3.13	47	36	2.88	2.71
MEAN±SE	0.06±0.02	0.16±0.1	2.32± 0.82	47±15	60±20	2.68±0.11	2.71±0.08

Table 4.10: Ca^{2+}-sensitivity data for percentage motile of dephosphorylated K36Q v dephosphorylated donor thin filaments

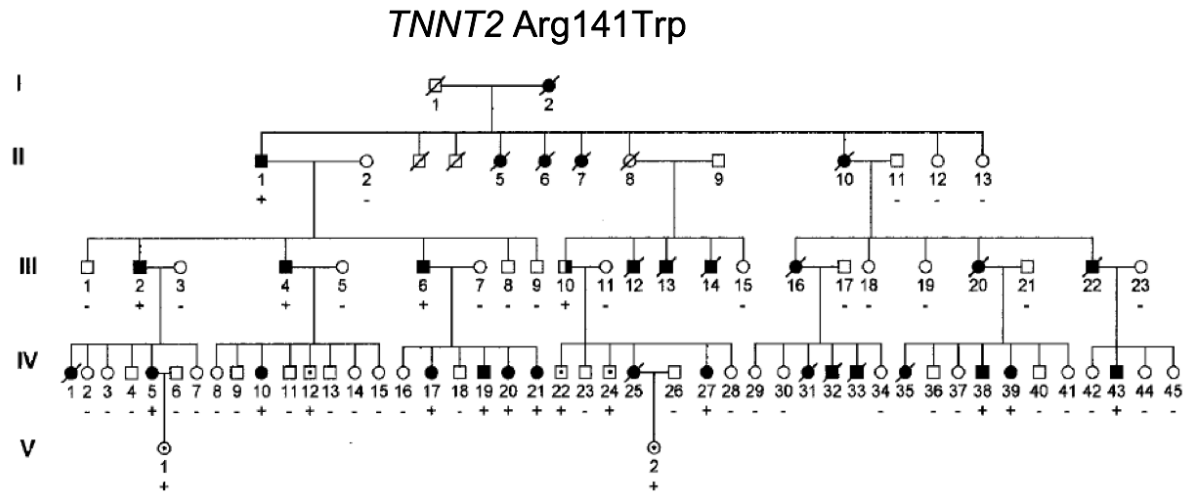
Tn K36Q ANALYSIS	EC_{50} Percentage motility, µM		EC_{50} Mutant / EC_{50} Donor	Hill coefficient n		% Motile 3.9 µM Ca^{2+}	
EXP N	Donor dP	K36Q dP		Donor dP	K36Q dP	Donor dP	K36Q dP
1	0.03±0.01	0.1±0.02	3.33	2.37	2.82	85	88
2	0.2±0.04	0.36±0.09	1.8	1	1	84	87
3	0.06±0.01	0.13±0.07	2.17	2.24	1.44	84	84
MEAN±SE	0.1±0.05	0.2±0.08	2.43±0.46	1.87±0.44	1.75±0.55	84±0.33	86±1.2
Student's t-test (paired)	p=0.079		single group, p=0.0897 (compared with one)				
(unpaired)	p=0.36						

4.2 Functional Investigation of DCM Mutant Troponin T Arg141Trp (R141W) and ΔLys210 (ΔK210) from Transgenic Mouse Samples

4.2.1 Introduction on Cardiac TnT R141W

The *TNNT2* R141W mutation was identified through a study made on five generations of a very large family (85 members), after linkage studies on that family had already identified the locus (Li et al., 2001, Durand et al., 1995). Tests could be performed on 72 living members of this family (Figure 4.7), out of which the mutation was found in 20, with 14 affected by DCM, 1 borderline and 5 not showing the phenotype. None of the other family members showed any symptoms of DCM, indicating that the disease cosegregates with the mutation, which has a moderately high penetrance.

Figure 4.7: Pedigree of the R141W TnT family



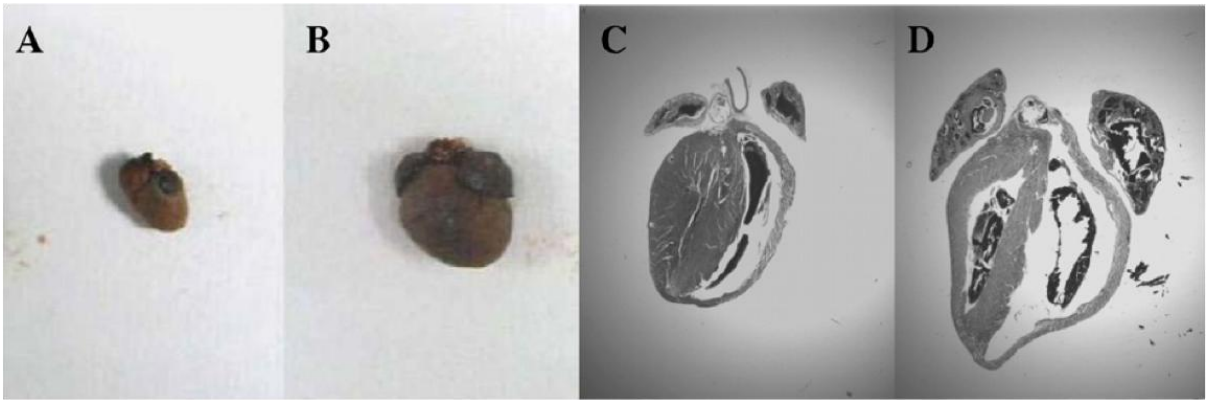
Square = male; circle = female; '+' = presence of the mutation; '-' = absence of the mutation; black filling = affected individual; half filled = borderline individual; dots = mutation carriers; slanted bars = deceased. (Li et al., 2001)

In general the clinical features shown by the members of the family were the onset of the cardiac symptoms in the second decade of life with progression of the disease to overt heart failure between 30 and 50. They all had classical DCM features of depressed contractile function and ventricular dilatation. There was no documented history of sudden cardiac death, but 17 individuals died of heart failure, some of them at a young age.

The amino acid is highly conserved between TnT isoforms in human and in other species, up to *C.elegans*. It changes a basic amino acid to a polar one and it resides in the TnT-T1 domain, which is supposed to make contacts with tropomyosin.

A transgenic mouse model for this mutation was generated by Dr L. Zhang's lab (Juan et al., 2008). This mouse expressed human cardiac TnT R141W in the heart and incorporated it in the sarcomere, as proved by immunohistochemistry. It also developed DCM phenotype, with a thinner ventricular wall and enlarged chambers (Figure 4.8). Interstitial fibrosis was seen with histology and also elongated and lysed myofibrils. Ejection fraction percentage was decreased, as was the fractional shortening, proving systolic dysfunction. After 4 months premature death of several mice was recorded. All of these observations brought to the conclusion that the human TnT R141W mutation is causative for DCM in mouse and it is therefore a good experimental model. In the next section I am going to describe the functional observation made with troponin purified from hearts belonging to these mice.

Figure 4.8: WT and transgenic cTnT R141W mouse hearts and sections



Mice sacrificed were 4 months old. A) WT heart; B) Transgenic cTnT R141W heart; C) Section of WT heart stained with H&E and observed under a stereoscope; D) same as 'C', but with transgenic cTnT R141W heart. The dilation in the transgenic heart is visible. (Juan et al., 2008)

4.2.2 *In Vitro* Motility Analysis for Transgenic R141W Troponin

Every experiment described in the following sections was performed using thin filaments reconstituted with rabbit skeletal muscle actin 10 nM, human cardiac tropomyosin 60 nM and troponin, 60 or 80 nM, purified from R141W transgenic mice or non-transgenic littermates.

4.2.2.1 Effects of R141W Troponin on the Thin Filament Ca^{2+}-sensitivity Compared to Non-Transgenic Troponin

Three different experiments were performed with one preparation of troponin (Figure 4.9 shows 1 and 2 and APPENDIX shows 3, parameters measured are shown in Table 4.11). NTg troponin was phosphorylated to 1.3 ± 0.01 mols P_i / mol TnI and R141W to 1.15 ± 0.07 mols P_i / mol TnI, with only 12% difference between them.

They all show a consistent difference in the Ca^{2+}-sensitivity in the percentage motile, with average EC_{50} ratio mutant / NTg of 4.19 ± 1.59. This lower Ca^{2+}-sensitivity gets statistical significance only in the unpaired student t-test ($p = 0.012$) because of the low number of experiments. In experiment 3 the percentage motile in high Ca^{2+} is 22% lower for the mutant

filaments, but it is equal to that of the non-transgenic filaments in experiments 1 and 2. The Hill coefficient does not seem to be much different between the tested filaments.

The motile velocity could not be fitted in experiment 2. In experiment 3 it increases faster and gets to a 19% higher maximum in the non-transgenic compared to the mutant filaments. Nevertheless the non-transgenic filaments could not be fitted properly to the Hill equation.

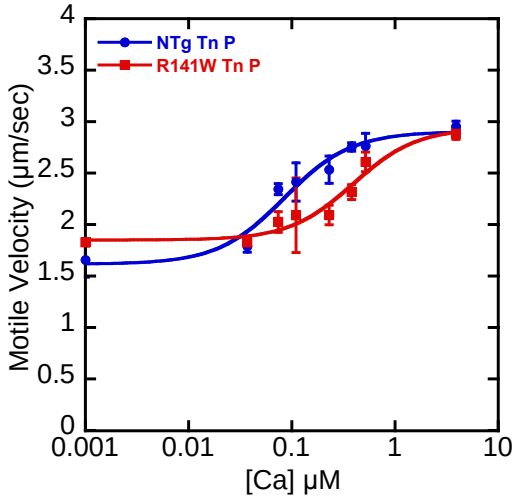
Experiment 1 could get both filaments to fit in Ca^{2+}-curves and the EC_{50} mutant / NTg ratio is 4.88, which further indicates a lower Ca^{2+}-sensitivity for the mutant.

Table 4.11: Ca^{2+}-sensitivity data for R141W v non-transgenic mouse natively phosphorylated troponin thin filaments

Tn R141W ANALYSIS	EC_{50} Percentage motility, µM		EC_{50} mutant / EC_{50} NTg	Hill coefficient n		% Motile 3.9 µM Ca^{2+}		Ca^{2+} activation of sliding speed (%)		Maximum sliding speed (µm/sec)	
EXP N	NTg	R141W		NTg	R141W	NTg	R141W	NTg	R141W	NTg	R141W
1	0.07±0.01	0.25±0.05	3.57	2.28	1.6	92	89	79	57	2.95	2.88
2	0.05±0.02	0.36±0.03	7.2	1	1.24	85	88	57	23	2.85	3.09
3	0.14±0.03	0.25±0.03	1.79	1.31	1.36	93	73	91	65	3.07	2.59
MEAN±SE	0.09±0.03	0.29±0.04	4.19±1.59	1.53± 0.39	1.4± 0.11	90±3	83±5	76±10	48±13	2.96±0.06	2.85±0.14
Student's t-test (paired)	p=0.076		single group, p=0.183 (compared with one)					p=0.016			
(unpaired)	p=0.012							p=0.17			

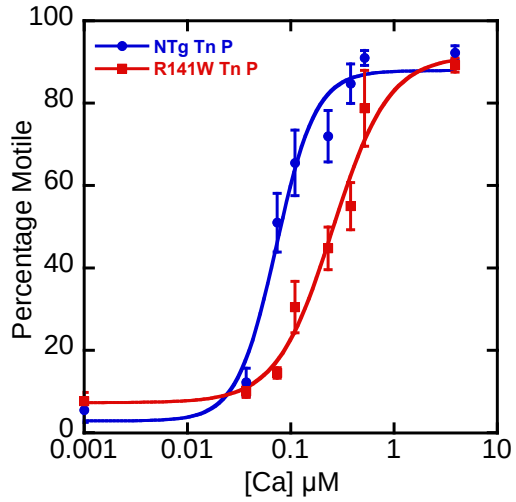
Figure 4.9: Ca^{2+} concentration titration comparing thin filaments containing non-transgenic and R141W mouse troponin

1



	Value	Error
Hill Coefficient	1.34	0.46
EC_{50}	0.08	0.02

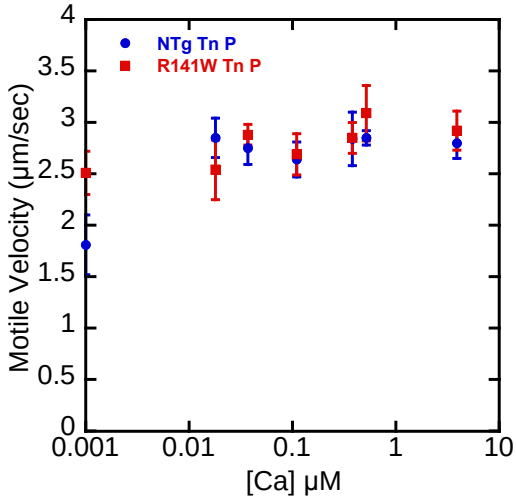
	Value	Error
Hill Coefficient	1.41	0.61
EC_{50}	0.39	0.11

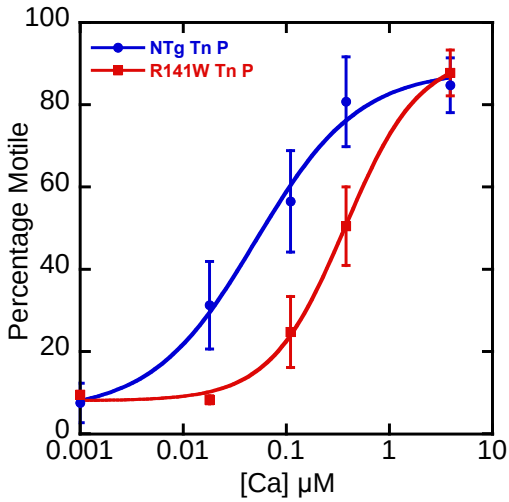


	Value	Error
Hill Coefficient	2.28	0.7
EC_{50}	0.07	0.01

	Value	Error
Hill Coefficient	1.6	0.41
EC_{50}	0.25	0.05

2





	Value	Error
Hill Coefficient	1	/
EC_{50}	0.05	0.02

	Value	Error
Hill Coefficient	1.24	0.23
EC_{50}	0.36	0.03

4.2.2.2 Effects of Troponin I Dephosphorylation on the Ca^{2+}-Sensitivity of R141W Thin Filaments

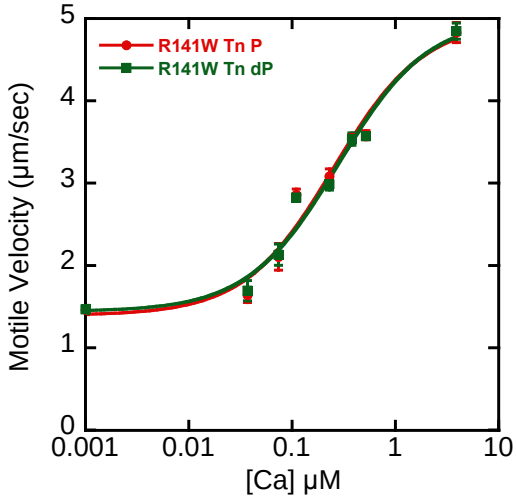
The phosphorylation level of R141W TnI after phosphatase treatment dropped to 0.19 mols P_i / mol TnI, 17% of the average untreated phosphorylation level. The NTg TnI phosphorylation after treatment was 0.12 mols P_i / mol TnI, 9% of the starting value.

Three experiments were performed with one troponin preparation, comparing thin filaments reconstituted with R141W in the two different phosphorylation states. Experiment 1 and 3 are shown in Figure 4.10, experiment 2 in APPENDIX, and all the parameters measured are summarised in Table 4.12 and Table 4.13.

Percentage motile parameters were all very similar with average EC_{50} ratio P / dP of 0.95 ± 0.06, indicating that TnI phosphorylation fails to modulate the thin filaments Ca^{2+} sensitivity. Motile velocity parameters show extremely similar curves for experiment 1 and 3, while the values of experiment 2 could not be fitted.

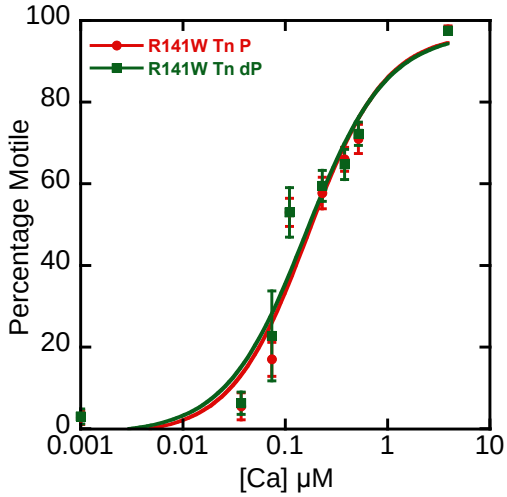
Figure 4.10: Ca^{2+} concentration titration comparing thin filaments containing natively phosphorylated and dephosphorylated R141W troponin

1



	Value	Error
Hill Coefficient	1	/
EC_{50}	0.25	0.07

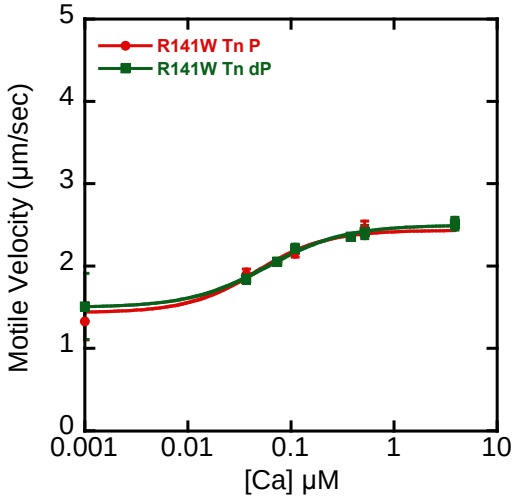
	Value	Error
Hill Coefficient	1	/
EC_{50}	0.28	0.07



	Value	Error
Hill Coefficient	1.15	0.45
EC_{50}	0.17	0.07

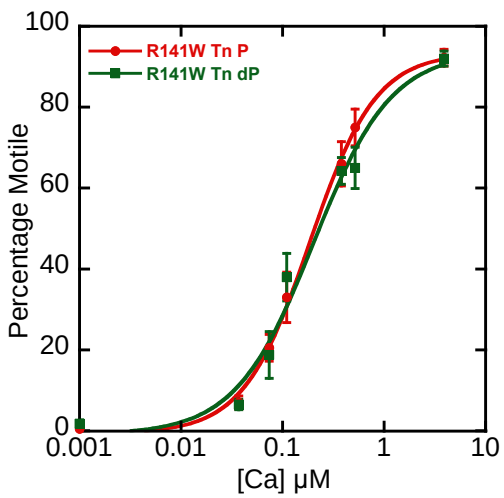
	Value	Error
Hill Coefficient	1.11	0.4
EC_{50}	0.16	0.06

3



	Value	Error
Hill Coefficient	1.29	0.4
EC_{50}	0.05	0.01

	Value	Error
Hill Coefficient	1.16	0.13
EC_{50}	0.06	0.01



	Value	Error
Hill Coefficient	1.33	0.1
EC_{50}	0.18	0.01

	Value	Error
Hill Coefficient	1.13	0.27
EC_{50}	0.2	0.06

Table 4.12: Ca^{2+}-sensitivity data for the sliding speed of thin filaments reconstituted with R141W natively phosphorylated v R141W dephosphorylated mouse troponin

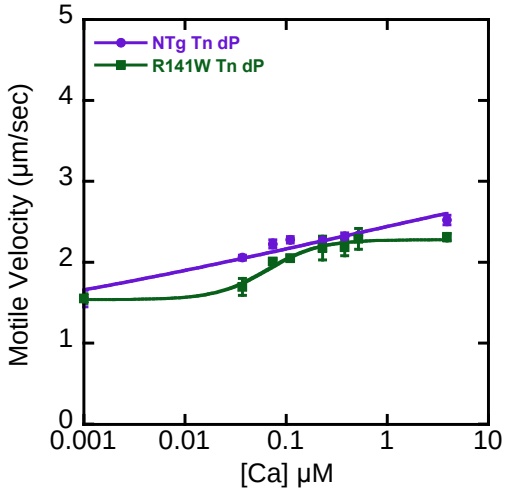
Tn R141W ANALYSIS	EC_{50} Sliding speed, µM		EC_{50} P/ EC_{50} dP	Ca^{2+} activation of sliding speed (%)		Maximum sliding speed (µm/sec)	
EXP N	R141W P	R141W dP		P	dP	P	dP
1	0.25±0.07	0.28±0.07	0.89	233	230	4.83	4.85
2	/	/	/	40	44	3	3.18
3	0.05±0.01	0.06±0.01	0.83	89	67	2.51	2.52
MEAN±SE	0.15±0.1	0.17±0.11	0.86±0.03	121±58	114± 59	3.45±0.71	3.52±0.69

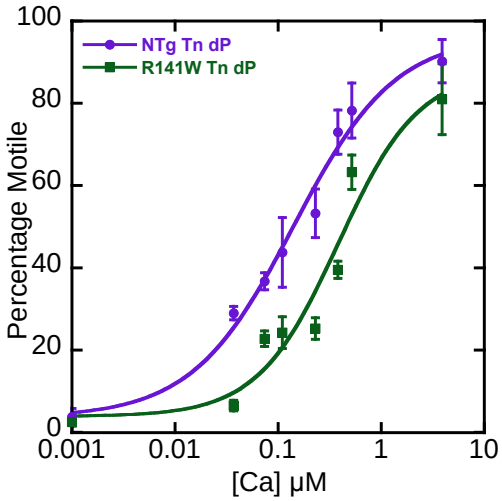
Table 4.13: Ca^{2+}-sensitivity data for the percentage motile of thin filaments reconstituted with R141W natively phosphorylated v R141W dephosphorylated mouse troponin

Tn R141W ANALYSIS	EC_{50} Percentage motility, µM		EC_{50} P / EC_{50} dP	Hill coefficient n		% Motile 3.9 µM Ca^{2+}	
EXP N	R141W P	R141W dP		P	dP	P	dP
1	0.17±0.07	0.16±0.06	1.06	1.15	1.11	98	98
2	0.16±0.08	0.18±0.1	0.89	1.02	1.19	78	80
3	0.18±0.01	0.2±0.06	0.9	1.33	1.13	92	92
MEAN±SE	0.17±0.01	0.18±0.01	0.95±0.06	1.17±0.09	1.14± 0.02	89±6	90±5
Student's t-test (paired)	p=0.42		single group, p=0.46 (compared with one)				
(unpaired)	p=0.48						

Figure 4.11: Ca^{2+} concentration titration comparing thin filaments containing dephosphorylated R141W and dephosphorylated non-transgenic troponin

1

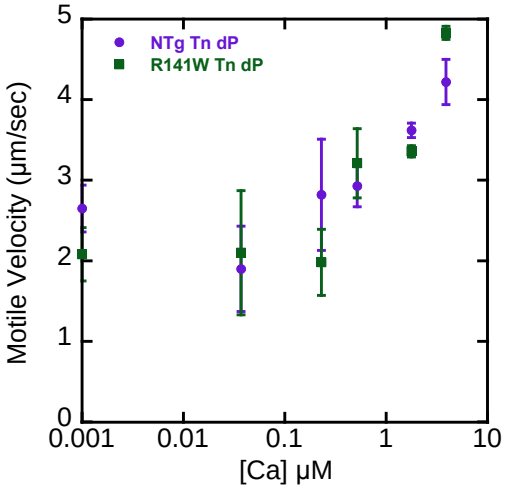


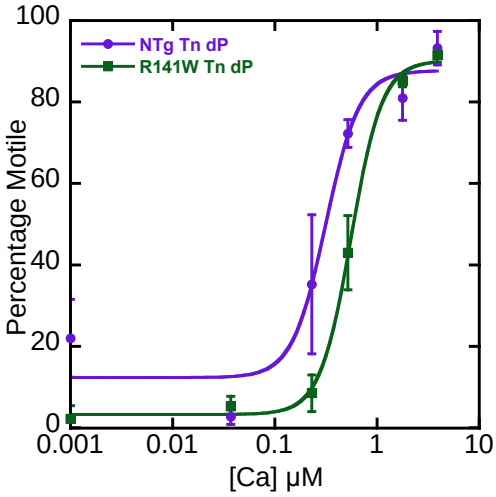


	Value	Error
Hill Coefficient	1	/
EC_{50}	0.14	0.04

	Value	Error
Hill Coefficient	1.11	0.53
EC_{50}	0.38	0.17

2





	Value	Error
Hill Coefficient	2.66	1.58
EC_{50}	0.32	0.08

	Value	Error
Hill Coefficient	2.85	0.55
EC_{50}	0.55	0.03

Table 4.14: Ca^{2+}-sensitivity data for thin filaments reconstituted with mouse dephosphorylated troponin, non-transgenic v R141W

Tn R141W ANALYSIS	EC_{50} Percentage motility, µM		EC_{50} Mutant / EC_{50} NTg	Hill coefficient n		% Motile 3.9 µM Ca^{2+}		Ca^{2+} activation of sliding speed (%)		Maximum sliding speed (µm/sec)	
EXP N	NTg dP	R141W dP		NTg dP	R141W dP	NTg dP	R141W dP	NTg dP	R141W dP	NTg dP	R141W dP
1	0.14±0.04	0.38±0.17	2.71	1	1.11	90	81	63	49	2.52	2.31
2	0.32±0.08	0.55±0.03	1.79	2.66	2.85	93	92	122	144	4.22	4.83
3	0.15±0.2	0.87±0.61	5.8	1	1.04	96	95	14	17	2.46	2.47
MEAN±SE	0.2±0.06	0.6±0.14	3.41±1.23	1.55± 0.55	1.67± 0.59	93±2	89±4	66±31	70±38	3.07±0.58	3.2±0.81
Student's t-test (paired)	p=0.13		single group, p=0.189 (compared with one)								
(unpaired)	p=0.063										

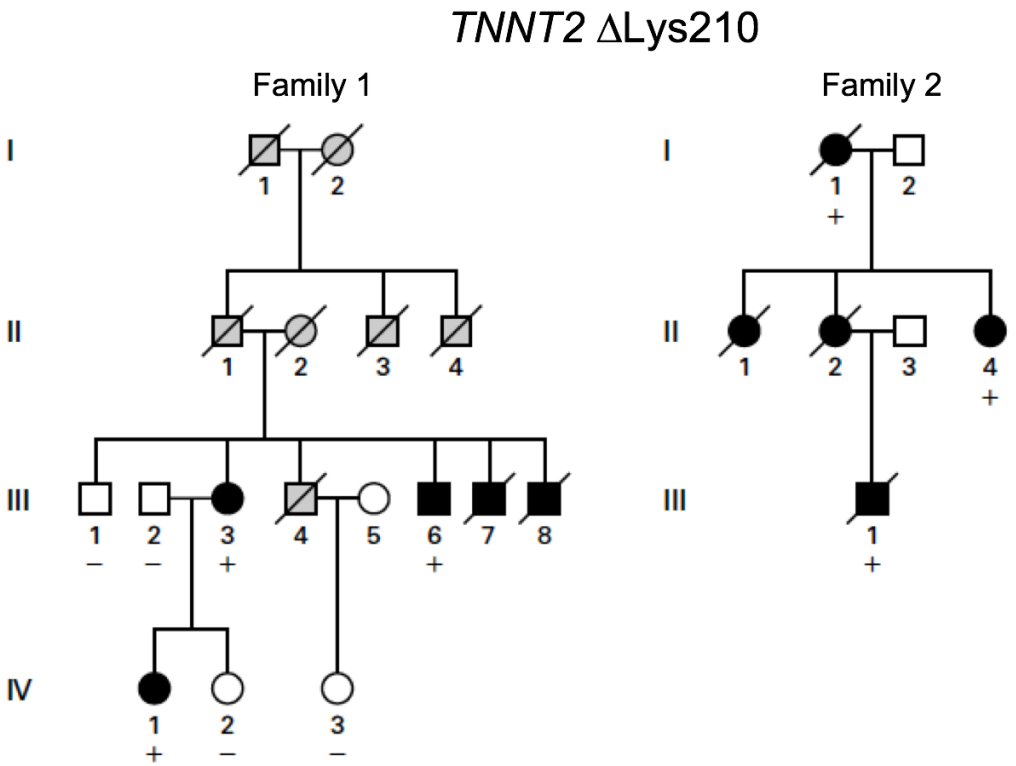
Dephosphorylated R141W troponin was then compared to dephosphorylated NTg troponin three times using one troponin preparation. Experiment 1 and 2 are shown in Figure 4.11, experiment 3 in APPENDIX, and all the parameters measured are summarised in Table 4.14. Just like the untreated troponin experiments, these percentage motile graphs show a lower Ca^{2+}-sensitivity for R141W thin filaments (EC_{50} ratio R141W / NTg = 3.41 ± 1.23), but because of the reduced dataset, statistical significance was not reached.

The motile velocity could not be fitted properly in any of the experiments. The only indication is given by experiment 1, in which the NTg filaments seem to have a slight increase of speed compared to the R141W filaments at low Ca^{2+} concentrations.

4.2.3 Introduction on Cardiac TnT ΔK210

Cardiac TnT ΔK210 was the first mutation to be linked to DCM out of the 7 known on the gene *TNNT2* (Kamisago et al., 2000). It was identified within a study that found this same mutation in two unrelated families, while screening the sequences of sarcomeric proteins. Apparently the mutation arose independently in the two families and cosegregated with the disease. All the carriers show marked ventricular dilatation and dysfunction, with a pure DCM phenotype. In one of the families sudden death was recorded for 2 infants and 3 young adults, whereas in the other family 3 heart failure deaths occurred before 20 years of age. The pedigrees of the two families indicate a complete penetrance with severe phenotype (Figure 4.12).

Figure 4.12: Pedigrees of the ΔK210 TnT families



Square = male; circle = female; '+' = presence of the mutation; '-' = absence of the mutation; black filling = affected individual; shaded = unknown clinical status; slanted bars = deceased. Adapted from Kamisago *et al.* (2000).

The mutation is positioned at the end of a very conserved 4 Lys cluster. A lysine in that position is present also in the human slow skeletal muscle isoform, while in the fast skeletal muscle isoform it is replaced by another basic amino acid (arginine). Lys210 is in the TnT-T2 domain, located close to the globular core of troponin.

Du *et al.* used embryonic stem cell technology to produce knock-in mice with human cardiac TnT ΔK210 replacing the endogenous TNNT2 gene (Du et al., 2007). Both the heterozygous and the homozygous knock-in mouse were studied. The mice presented enlarged hearts, with increased fibrosis and cardiomyocyte apoptosis. Systolic dysfunction was observed as well as a high incidence of sudden death. It seemed that the DCM phenotype development was dose dependent, with the homozygous mice having more marked characteristics. Hearts of mice produced in this original study have been used in this thesis as a source of troponin, and are particularly interesting for the possibility of assessing potential differences given by the dosage of mutant protein.

4.2.4 *In Vitro* Motility Analysis for Transgenic ΔK210 Troponin

Every experiment described in the following sections was performed using thin filaments reconstituted with rabbit skeletal muscle actin 10 nM, human cardiac tropomyosin 60 nM and troponin, between 30 and 80 nM depending on the optimal conditions, purified from non-transgenic littermates or ΔK210 transgenic mice. I studied both heterozygous and homozygous mice.

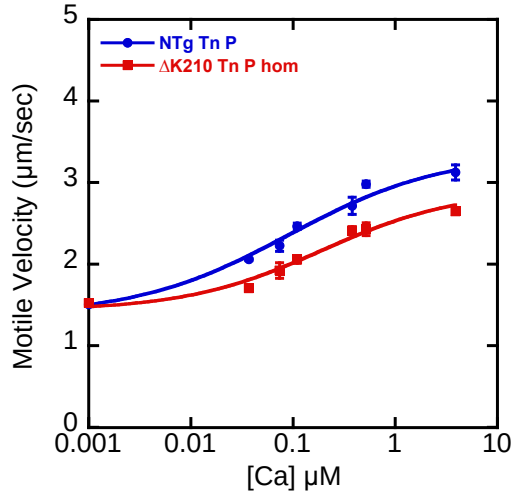
4.2.4.1 Effects of ΔK210 Troponin, Homo- and Heterozygous, on the Thin Filaments Ca^{2+}-sensitivity Compared to Non-Transgenic Troponin

Thin filaments reconstituted with homozygous natively phosphorylated ΔK210 troponin (1.06 ± 0.06 mols P_i / mol TnI) were compared with thin filaments reconstituted with natively phosphorylated NTg troponin (1.03 ± 0.12 mols P_i / mol TnI) six times, using one troponin preparation. Experiments 1 and 5 are shown in Figure 4.13, the others are in APPENDIX, all the data is shown in Table 4.15.

Most of the motile velocity data could not be fitted properly due to the variability of the measurements. Experiments 2 and 5 seemed to show a larger increase of the NTg filaments velocity with increasing Ca^{2+} concentration compared to the ΔK210 filaments. In experiment 1, the only one that could be fitted properly, the EC_{50} ratio ΔK210 / NTg is 2.11, indicating a lower Ca^{2+} sensitivity for the mutant filaments.

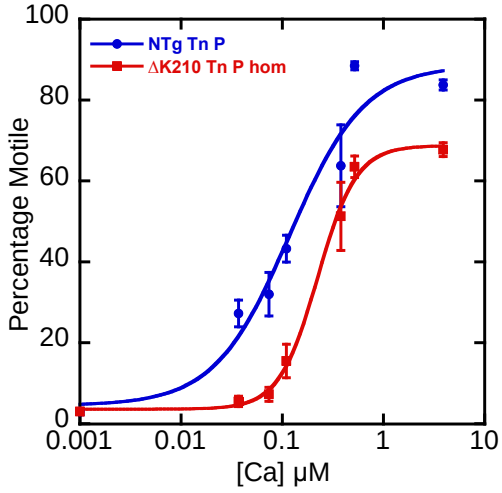
Figure 4.13: Ca^{2+} concentration titration comparing thin filaments containing non-transgenic and homozygous ΔK210 mouse troponin

1



	Value	Error
Hill Coefficient	0.58	0.28
EC_{50}	0.09	0.05

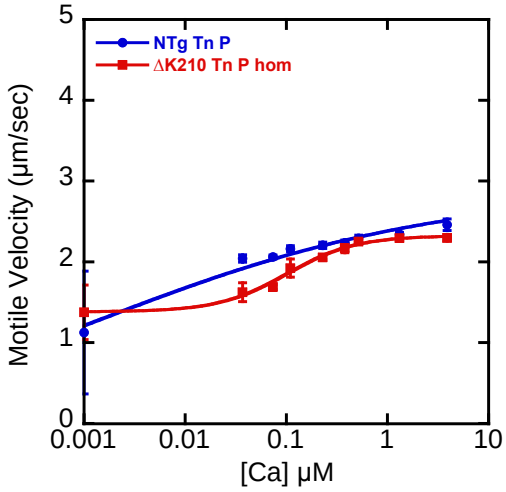
	Value	Error
Hill Coefficient	0.65	0.28
EC_{50}	0.19	0.13

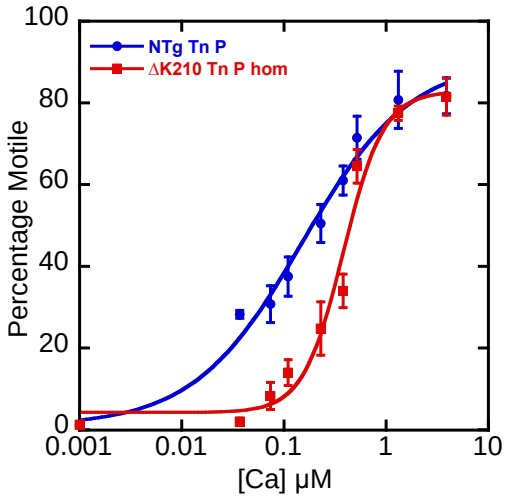


	Value	Error
Hill Coefficient	1.18	0.5
EC_{50}	0.12	0.05

	Value	Error
Hill Coefficient	2.28	0.31
EC_{50}	0.22	0.02

5





	Value	Error
Hill Coefficient	1	/
EC_{50}	0.15	0.04

	Value	Error
Hill Coefficient	2.21	0.69
EC_{50}	0.38	0.05

Table 4.15: Ca^{2+}-sensitivity data for homozygous ΔK210 v non-transgenic mouse natively phosphorylated troponin thin filaments

Tn ΔK210hom ANALYSIS	EC_{50} Percentage motility, μM		EC_{50} Mutant / EC_{50} NTg	Hill coefficient n		% Motile 3.9 μM Ca^{2+}		Ca^{2+} activation of sliding speed (%)		Maximum sliding speed (μm/sec)	
EXP N	NTg	ΔK210		NTg	ΔK210	NTg	ΔK210	NTg	ΔK210	NTg	ΔK210
1	0.12±0.05	0.22±0.02	1.83	1	2.8	84	68	107	74	3.13	2.65
2	0.35±0.19	0.78±0.17	2.23	1	1.5	92	89	154	145	4	3.53
3	0.22±0.05	0.67±0.09	3.05	1	1	94	91	136	111	3.59	3.95
4	0.13±0.02	0.29±0.09	2.23	2.18	4.87	76	80	47	89	2.69	2.96
5	0.15±0.04	0.38±0.05	2.53	1	2.21	82	82	119	67	2.46	2.3
6	0.3±0.05	0.36±0.03	1.2	2.57	4.16	87	87	16	26	2.63	2.57
MEAN±SE	0.21±0.04	0.45±0.09	2.18±0.26	1.46± 0.29	2.76± 0.62	86±3	83±3	97±22	85±17	3.08±0.25	2.76±0.62
Student's t-test (paired)	p=0.017		single group, p=0.006 (compared with one)								
(unpaired)	p=0.037										

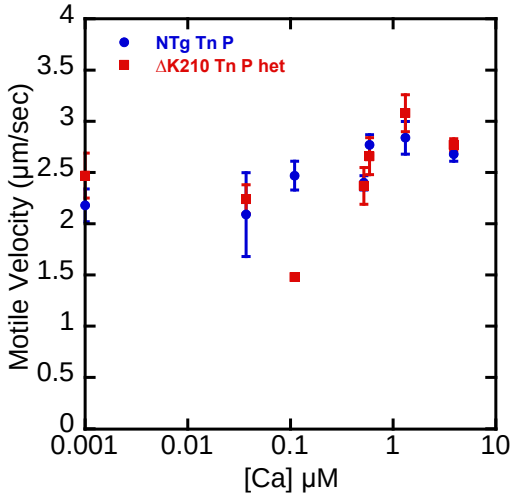
The percentage motile shows a significantly lower Ca^{2+} sensitivity for the mutant (paired p = 0.017, unpaired p = 0.037, EC_{50} ratio compared to 1, p = 0.006). The Hill coefficient is higher for ΔK210 filaments, while only in experiment 1 the maximum percentage motile reached by ΔK210 filaments is considerably lower than that of NTg filaments.

Thin filaments reconstituted with heterozygous natively phosphorylated ΔK210 troponin (1.15 ± 0.04 mols P_i / mol TnI) were compared 4 times with NTg filaments, using 2 different preparations. Experiments 2 and 3 are shown in Figure 4.14, 1 and 4 in APPENDIX, and all data is summarised in Table 4.16 and Table 4.17.

The motile velocity plots could be fitted for experiments 3 and 4 and indicates again a lower Ca^{2+}-sensitivity for ΔK210 filaments. The maximum sliding speed this time is slightly higher (4%) for ΔK210 filaments.

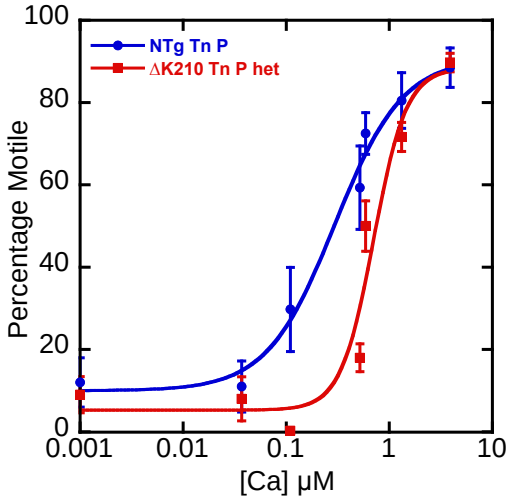
Figure 4.14: Ca^{2+} concentration titration comparing thin filaments containing non-transgenic and heterozygous ΔK210 mouse troponin

2



	Value	Error
Hill Coefficient	6.94	10.41
EC_{50}	0.06	0.02

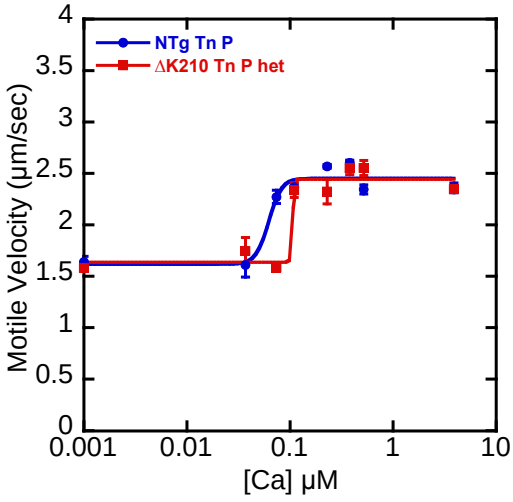
	Value	Error
Hill Coefficient	52.95	9.68e+7
EC_{50}	0.11	6881.2

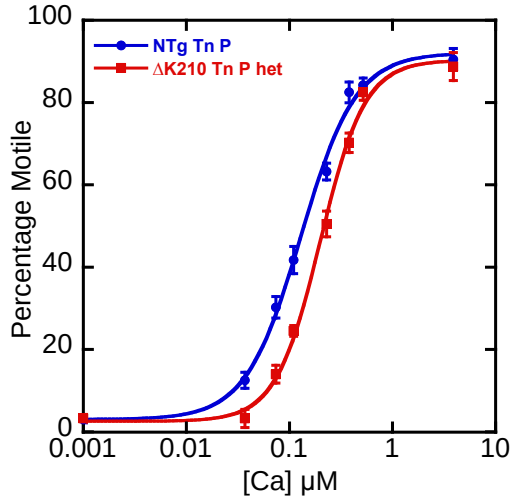


	Value	Error
Hill Coefficient	1.32	0.33
EC_{50}	0.3	0.07

	Value	Error
Hill Coefficient	2.74	1.73
EC_{50}	0.71	0.17

3





	Value	Error
Hill Coefficient	1.63	0.17
EC_{50}	0.13	0.01

	Value	Error
Hill Coefficient	2	0.19
EC_{50}	0.2	0.01

Table 4.16: Ca^{2+}-sensitivity data for heterozygous ΔK210 v non-transgenic mouse natively phosphorylated troponin thin filaments sliding speed

Tn ΔK210het ANALYSIS	EC_{50} Sliding speed, μM		EC_{50} mutant/ EC_{50} NTg	Ca^{2+} activation of sliding speed (%)		Maximum sliding speed (μm/sec)	
EXP N	NTg	ΔK210		NTg	ΔK210	NTg	ΔK210
1	/	/	/	74	68	2.52	2.63
2	/	/	/	36	38	2.84	3.08
3	0.06±0.02	0.11±6881	1.83	61	61	2.6	2.55
4	0.09±0.09	0.13±0.04	1.44	72	69	2.67	2.77
MEAN±SE	0.08±0.02	0.12±0.01	1.64±0.2	61±9	59±7	2.66±0.07	2.76±0.12

Table 4.17: Ca^{2+}-sensitivity data for heterozygous ΔK210 v non-transgenic mouse natively phosphorylated troponin thin filaments percentage motile

Tn ΔK210het ANALYSIS	EC_{50} Percentage motility, μM		EC_{50} Mutant / EC_{50} NTg	Hill coefficient n		% Motile 3.9 μM Ca^{2+}	
EXP N	NTg	ΔK210		NTg	ΔK210	NTg	ΔK210
1	0.54±0.03	0.69±0.06	1.28	6	6	74	65
2	0.3±0.07	0.71±0.17	2.37	1.32	2.74	89	90
3	0.13±0.01	0.2±0.01	1.54	1.63	2	91	89
4	0.12±0.01	0.16±0.01	1.33	1.81	2.54	83	83
MEAN±SE	0.27±0.1	0.44±0.15	1.63±0.25	2.69±1.11	3.32±0.91	84±4	82±6
Student's t-test (paired)	p=0.141		single group, p=0.088 (compared with one)				
(unpaired)	p=0.387						

The percentage motility results indicate again a lower Ca^{2+}-sensitivity for ΔK210 filaments compared to NTg filaments (EC_{50} ΔK210 / NTg = 1.63 ± 0.25). However, they are not statistically significant for the inhomogeneity of the data coming from the two different troponin preparations: experiments 1 and 2 have generally lower Ca^{2+}-sensitivities compared to 3 and 4. Hill coefficient is 23% higher for ΔK210 filaments.

4.2.4.2 Effects of Troponin I Dephosphorylation on the Ca^{2+}-Sensitivity of ΔK210 Thin Filaments, Homo- and Heterozygous

Four experiments were performed with homozygous ΔK210 troponin reconstituted thin filaments comparing its phosphorylated and dephosphorylated (0.21 ± 0.08 mols P_i / mol TnI, 20% of the original phosphorylation) states. Two troponin preparations were used for these experiments, the first for experiments 1 and 2 (APPENDIX) and the second for experiments 3 and 4 (Figure 4.15). All data are summarised in Table 4.18 and Table 4.19.

Motile velocity plots 1 and 2 could not be fitted, but they show great similarity between the measurements, just as experiments 3 and 4 in which the curves are almost perfectly superimposable (EC_{50} ratio ΔK210 P / dP = 1).

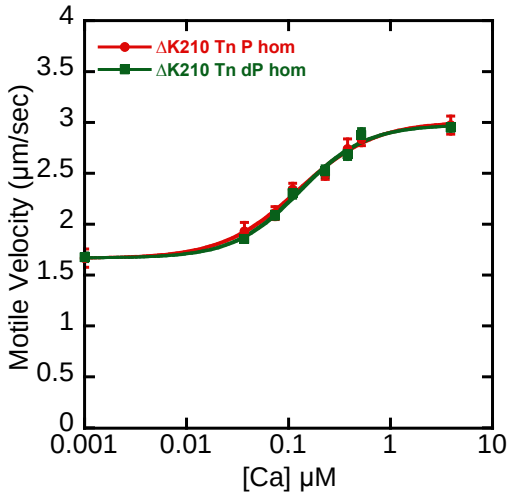
Percentage motile measurements show almost the same Ca^{2+}-sensitivity for ΔK210 phosphorylated and dephosphorylated with EC_{50} ratio ΔK210 P / dP = 0.96 ± 0.09.

Four experiments were performed also with heterozygous ΔK210 filaments comparing the phosphorylated and dephosphorylated (0.23 ± 0.08 mols P_i / mol TnI, 20% of the original phosphorylation) states. A different troponin preparation was used only for experiment 4. Figure 4.16 shows experiments 2 and 3, experiments 1 and 4 are shown in APPENDIX; data are shown in Table 4.20.

Only in experiment 2 could the motile velocity graph be plotted and it shows the same EC_{50} for the two reconstitutions. Also the maximum sliding speed and Ca^{2+}-induced increase in the sliding speed do not present any difference.

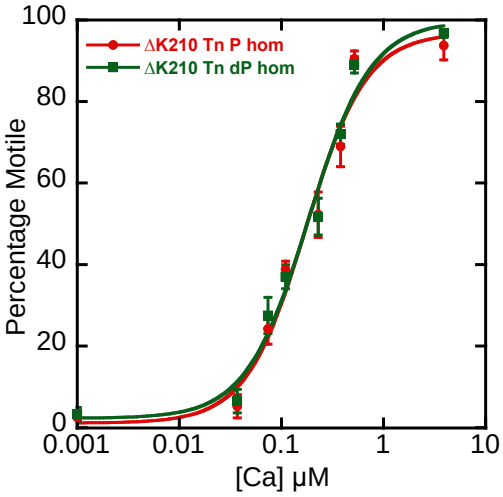
Figure 4.15: Ca^{2+} concentration titration comparing thin filaments containing natively phosphorylated and dephosphorylated homozygous ΔK210 troponin

3



	Value	Error
Hill Coefficient	1.17	0.16
EC_{50}	0.13	0.02

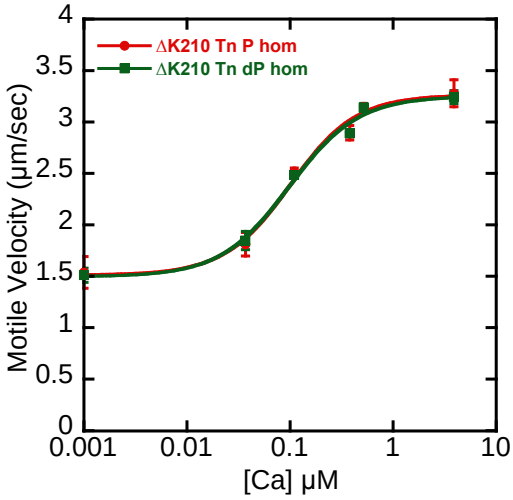
	Value	Error
Hill Coefficient	1.34	0.19
EC_{50}	0.13	0.02



	Value	Error
Hill Coefficient	1.48	0.36
EC_{50}	0.17	0.04

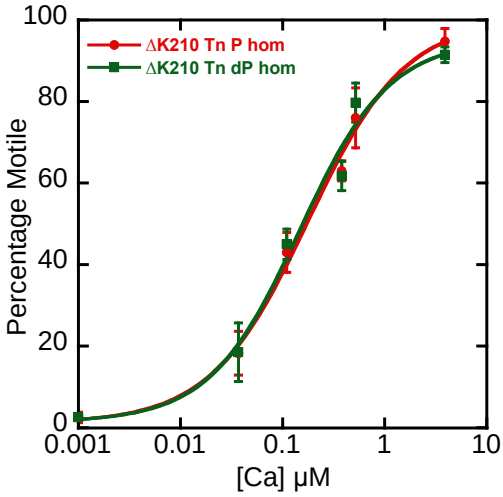
	Value	Error
Hill Coefficient	1.43	0.3
EC_{50}	0.18	0.03

4



	Value	Error
Hill Coefficient	1.36	0.36
EC_{50}	0.1	0.02

	Value	Error
Hill Coefficient	1.3	0.29
EC_{50}	0.1	0.02



	Value	Error
Hill Coefficient	1	/
EC_{50}	0.18	0.04

	Value	Error
Hill Coefficient	1	/
EC_{50}	0.15	0.05

Table 4.18: Ca^{2+}-sensitivity data for the sliding speed of thin filaments reconstituted with homozygous ΔK210 troponin, natively phosphorylated v dephosphorylated

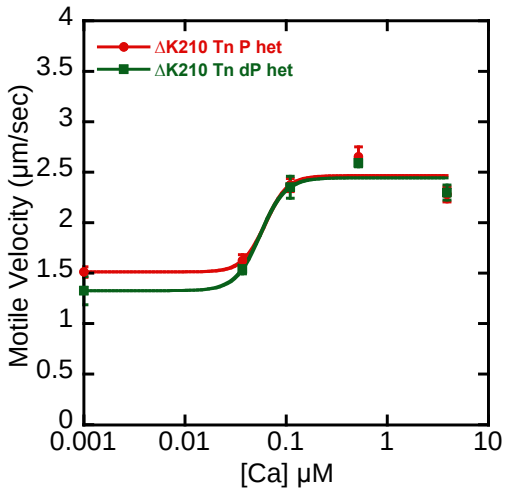
Tn ΔK210hom ANALYSIS	EC_{50} Sliding speed, µM		EC_{50} P/ EC_{50} dP	Ca^{2+} activation of sliding speed (%)		Maximum sliding speed (µm/sec)	
EXP N	ΔK210 P	ΔK210 dP		P	dP	P	dP
1	/	/	/	15	22	2.37	2.35
2	/	/	/	40	34	2.68	2.67
3	0.13±0.02	0.13±0.02	1	78	76	2.97	2.95
4	0.1±0.02	0.1±0.02	1	113	115	3.28	3.24
MEAN±SE	0.12±0.02	0.12±0.02	1	62±22	62±21	2.82±0.19	2.8±0.19

Table 4.19: Ca^{2+}-sensitivity data for the percentage motile of thin filaments reconstituted with homozygous ΔK210 troponin, natively phosphorylated v dephosphorylated

Tn ΔK210hom ANALYSIS	EC_{50} Percentage motility, µM		EC_{50} P / EC_{50} dP	Hill coefficient n		% Motile 3.9 µM Ca^{2+}	
EXP N	ΔK210 P	ΔK210 dP		P	dP	P	dP
1	0.14±0.05	0.18±0.06	0.78	1.44	1.11	84	85
2	0.12±0.03	0.13±0.04	0.92	1	1	89	86
3	0.17±0.04	0.18±0.03	0.94	1.48	1.43	94	97
4	0.18±0.04	0.15±0.05	1.2	1	1	95	92
MEAN±SE	0.15±0.01	0.16±0.01	0.96±0.09	1.23±0.13	1.14± 0.1	91±3	90±3
Student's t-test (paired)	p=0.638		single group, p=0.679 (compared with one)				
(unpaired)	p=0.698						

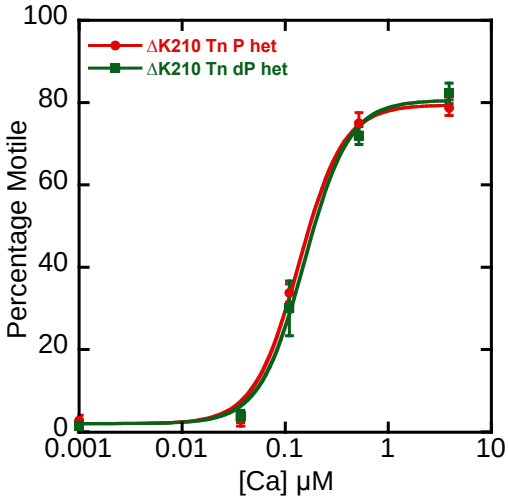
Figure 4.16: Ca^{2+} concentration titration comparing thin filaments containing natively phosphorylated and dephosphorylated heterozygous ΔK210 troponin

2



	Value	Error
Hill Coefficient	3.91	4.58
EC_{50}	0.06	0.04

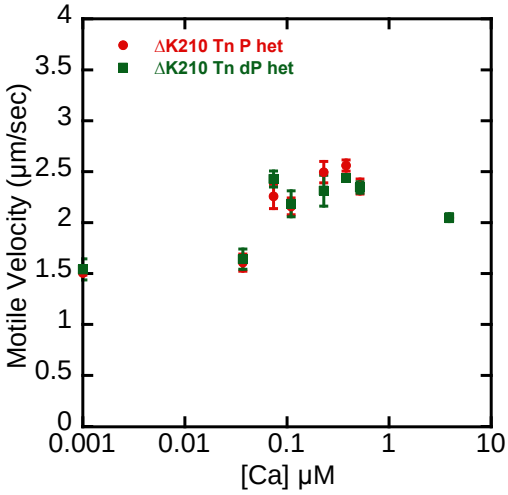
	Value	Error
Hill Coefficient	3.54	2.94
EC_{50}	0.06	0.02

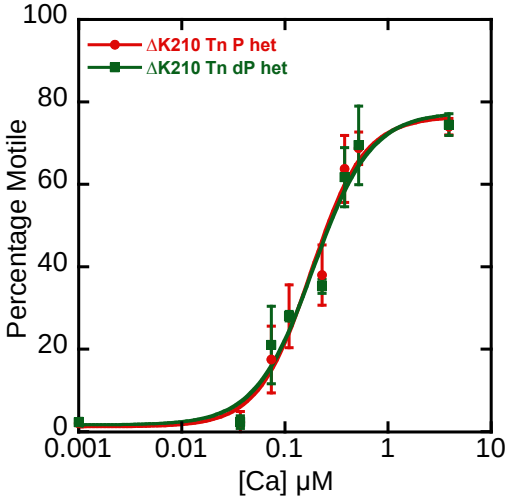


	Value	Error
Hill Coefficient	2	/
EC_{50}	0.14	0.01

	Value	Error
Hill Coefficient	2	/
EC_{50}	0.15	0.01

3





	Value	Error
Hill Coefficient	1.68	0.41
EC_{50}	0.18	0.04

	Value	Error
Hill Coefficient	1.56	0.47
EC_{50}	0.19	0.05

Table 4.20: Ca^{2+}-sensitivity data for thin filaments reconstituted with heterozygous ΔK210 troponin, natively phosphorylated v dephosphorylated

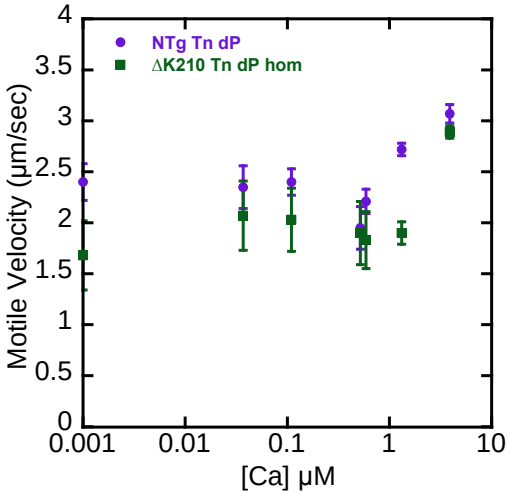
Tn ΔK210het ANALYSIS	EC_{50} Percentage motility, μM		EC_{50} P / EC_{50} dP	Hill coefficient n		% Motile 3.9 μM Ca^{2+}		Ca^{2+} activation of sliding speed (%)		Maximum sliding speed (μm/sec)	
EXP N	ΔK210 P	ΔK210 dP		P	dP	P	dP	P	dP	P	dP
1	0.29±0.04	0.31±0.07	0.94	1.62	1.69	68	67	43	27	2.22	2.25
2	0.14±0.01	0.15±0.01	0.93	2	2	79	82	75	95	2.65	2.59
3	0.18±0.04	0.19±0.05	0.95	1.68	1.56	74	75	70	58	2.56	2.43
4	0.16±0.03	0.16±0.02	1	3.93	3.87	79	76	17	22	2.45	2.36
MEAN±SE	0.19±0.03	0.2±0.04	0.96±0.02	2.31± 0.55	2.28± 0.54	75±3	75±3	51±13	51±17	2.47±0.09	2.41±0.07
Student's t-test (paired)	p=0.092		single group, p=0.063 (compared with one)								
(unpaired)	p=0.846										

For the percentage motile measurements the average Hill coefficient is pretty similar for the two reconstitutions and the EC_{50} ratio ΔK210 / NTg = 0.96 ± 0.02.

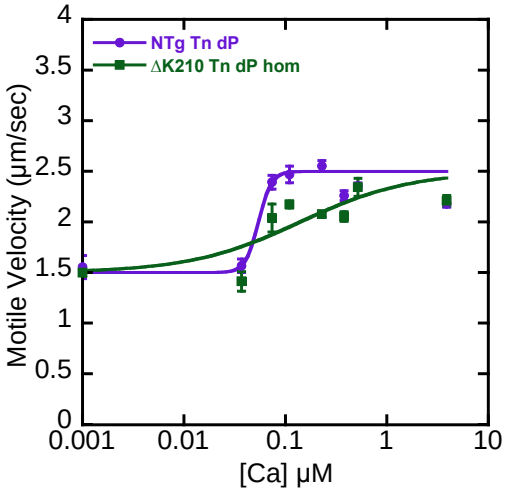
Dephosphorylated homozygous ΔK210 troponin was compared to dephosphorylated NTg troponin (0.18 ± 0.06 mols P_i / mol TnI, 17% of the original phosphorylation) three times with two different troponin preparations (experiments 2 and 3 in Figure 4.17, data in Table 4.21). The first for experiments 1 (shown in APPENDIX) and 2, the second for experiment 3. The first troponin preparation shifted the filaments towards lower Ca^{2+}-sensitivity. The data coming from those indicates that ΔK210 filaments have a lower Ca^{2+}-sensitivity, but for their great variability they could not be averaged with experiment 3, which instead could be fitted to more standard EC_{50}. Nevertheless, experiment 3 shows that ΔK210 filaments are less Ca^{2+}-sensitive both in percentage motile and motile velocity.

Figure 4.17: Ca^{2+} concentration titration comparing thin filaments containing dephosphorylated homozygous ΔK210 and dephosphorylated non-transgenic troponin

2

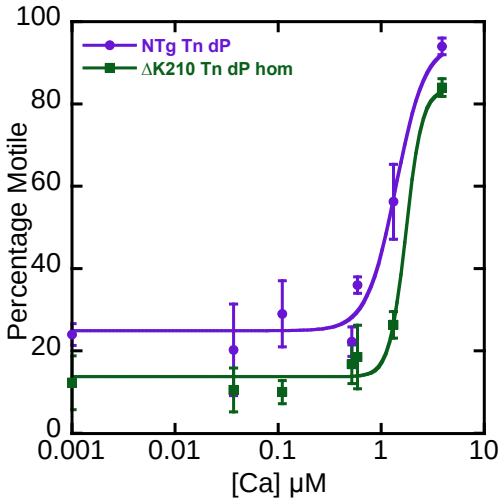


3



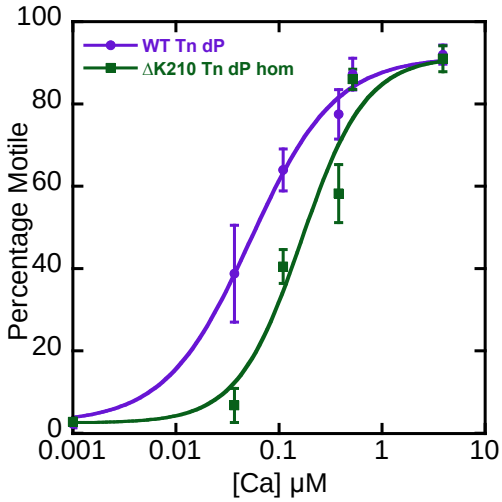
	Value	Error
Hill Coefficient	6.78	4.71
EC_{50}	0.05	0.01

	Value	Error
Hill Coefficient	1	/
EC_{50}	0.14	0.07



	Value	Error
Hill Coefficient	3.07	1.04
EC_{50}	1.39	0.17

	Value	Error
Hill Coefficient	5.48	4.41
EC_{50}	1.73	0.41



	Value	Error
Hill Coefficient	1.05	0.11
EC_{50}	0.05	0.01

	Value	Error
Hill Coefficient	1.39	0.35
EC_{50}	0.17	0.03

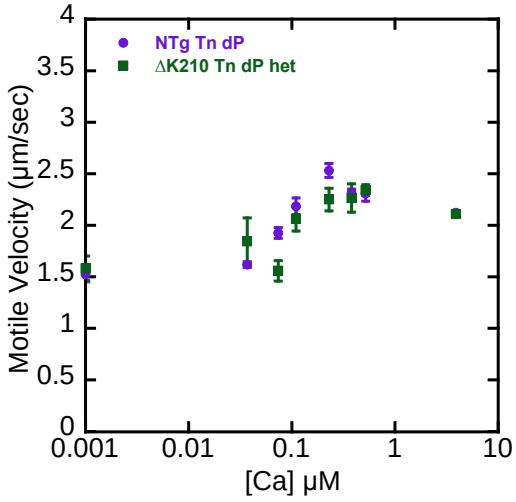
Table 4.21: Ca^{2+}-sensitivity data for thin filaments reconstituted with dephosphorylated troponin, non-transgenic v homozygous ΔK210

Tn ΔK210hom ANALYSIS	EC_{50} Percentage motility, μM		EC_{50} Mutant / EC_{50} NTg	Hill coefficient n		% Motile 3.9 μM Ca^{2+}		Ca^{2+} activation of sliding speed (%)		Maximum sliding speed (μm/sec)	
EXP N	NTg dP	ΔK210 dP		NTg dP	ΔK210 dP	NTg dP	ΔK210 dP	NTg dP	ΔK210 dP	NTg dP	ΔK210 dP
1	0.73±0.08	2.86±96.49	/	1.93	6.02	75	70	33	20	2.56	2.27
2	1.39±0.17	1.73±0.41	1.24	3	5.4	94	84	57	58	3.07	2.89
3	0.05±0.01	0.17±0.03	3.4	1.22	1.34	92	91	40	47	2.18	2.21

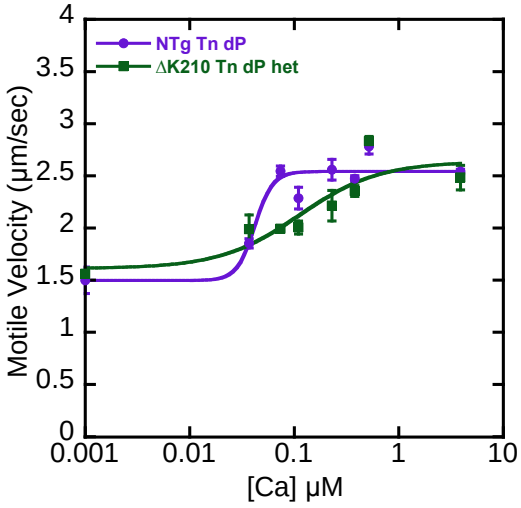
Dephosphorylated heterozygous ΔK210 troponin was compared to dephosphorylated NTg 4 times using two preparations of troponin, the first only for experiment 1. Experiments 2 and 3 are shown in Figure 4.18, 1 and 4 in APPENDIX. Data in Table 4.22. Again motile velocity could be fitted only in experiment 3 and it indicates a lower Ca^{2+}-sensitivity for ΔK210 filaments (EC_{50} ratio ΔK210 / NTg = 2.75). The percentage motile clearly indicates a lower Ca^{2+}-sensitivity which gets significant in the student t-test of EC_{50} ratio compared to 1 (p = 0.01). ΔK210 Hill coefficient is 16% higher than NTg.

Figure 4.18: Ca^{2+} concentration titration comparing thin filaments containing dephosphorylated heterozygous ΔK210 and dephosphorylated non-transgenic troponin

2

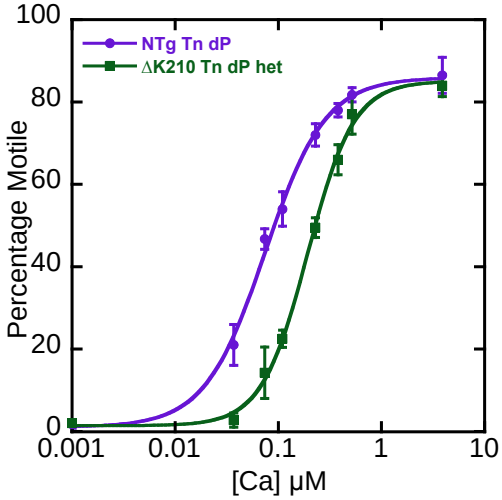


3



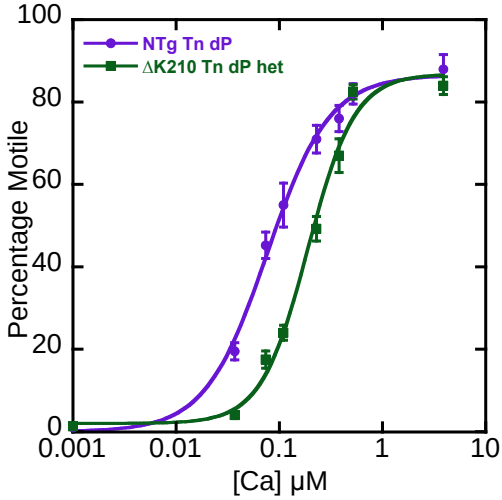
	Value	Error
Hill Coefficient	5.04	5.38
EC_{50}	0.04	0.01

	Value	Error
Hill Coefficient	1.14	0.87
EC_{50}	0.11	0.09



	Value	Error
Hill Coefficient	1.49	0.15
EC_{50}	0.07	0.01

	Value	Error
Hill Coefficient	1.95	0.15
EC_{50}	0.19	0.01



	Value	Error
Hill Coefficient	1.45	0.17
EC_{50}	0.08	0.01

	Value	Error
Hill Coefficient	1.92	0.31
EC_{50}	0.19	0.02

Table 4.22: Ca^{2+}-sensitivity data for thin filaments reconstituted with dephosphorylated troponin, non-transgenic v heterozygous ΔK210

Tn ΔK210het ANALYSIS	EC_{50} Percentage motility, μM		EC_{50} Mutant / EC_{50} NTg	Hill coefficient n		% Motile 3.9 μM Ca^{2+}		Ca^{2+} activation of sliding speed (%)		Maximum sliding speed (μm/sec)	
EXP N	NTg dP	ΔK210 dP		NTg dP	ΔK210 dP	NTg dP	ΔK210 dP	NTg dP	ΔK210 dP	NTg dP	ΔK210 dP
1	0.09±0.01	0.16±0.03	1.78	2.5	2.56	87	84	56	29	3.31	3.17
2	0.07±0.01	0.19±0.01	2.71	1.49	1.95	87	84	66	55	2.53	2.34
3	0.08±0.01	0.19±0.02	2.38	1.45	1.92	88	84	85	81	2.78	2.83
4	0.26±0.07	0.75±0.16	2.88	1	1	80	84	19	15	2.61	2.42
MEAN±SE	0.13±0.05	0.32±0.14	2.44±0.24	1.61± 0.32	1.86± 0.32	86±2	84±0	57±14	45±15	2.81±0.18	2.69±0.19
Student's t-test (paired)	p=0.138		single group, p=0.01 (compared with one)								
(unpaired)	p=0.235										

4.2.5 Control Experiments with Mouse Donor Troponin

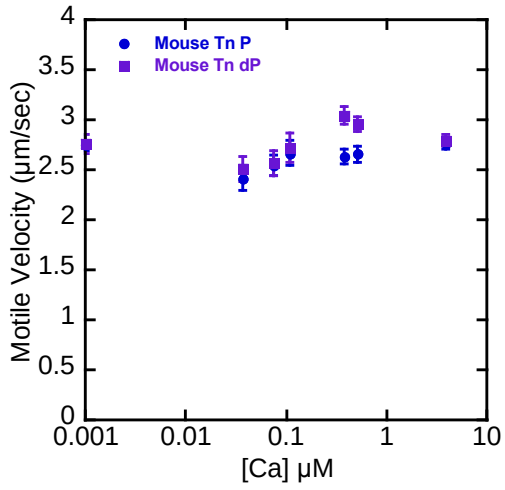
Two control experiments were performed comparing NTg mouse cardiac troponin phosphorylated and dephosphorylated (Figure 4.19, Table 4.23). These were meant to prove that changes in mouse TnI phosphorylation would modulate the Ca^{2+} sensitivity of the thin filaments in IVMA. They showed in fact that most of the motile parameters were extremely similar, while the Ca^{2+}-sensitivity of the dephosphorylated troponin was two times that of the dephosphorylated troponin.

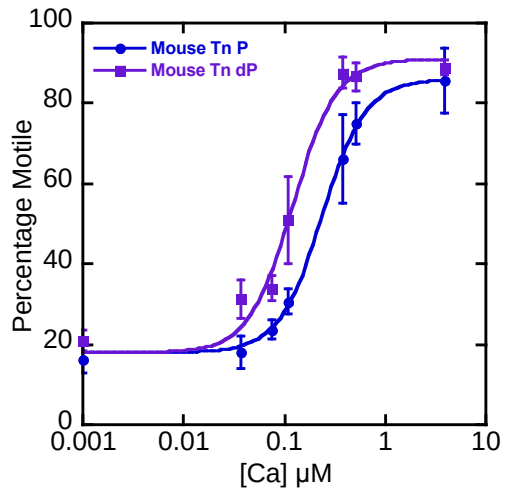
Table 4.23: Ca^{2+}-sensitivity data for thin filaments reconstituted with mouse donor troponin phosphorylated v dephosphorylated

mouse Tn NTg ANALYSIS	EC_{50} Percentage motility, μM		EC_{50} P / EC_{50} dP	Hill coefficient n		% Motile 3.9 μM Ca^{2+}		Ca^{2+} activation of sliding speed (%)		Maximum sliding speed (μm/sec)	
EXP N	NTg P	NTg dP		P	dP	P	dP	P	dP	P	dP
1	0.24±0.01	0.12±0.02	2	2.01	2	86	89	0	0	2.77	2.79
2	0.22±0.02	0.11±0.01	2	2.5	2.47	85	85	10	17	3.08	3.07
MEAN±SE	0.23±0.01	0.12±0.01	2	2.26± 0.25	2.24± 0.24	86±1	87±2	5±5	9±9	2.93±0.16	2.93±0.14

Figure 4.19: Ca^{2+} concentration titrations comparing thin filaments containing phosphorylated and dephosphorylated mouse donor troponin

1

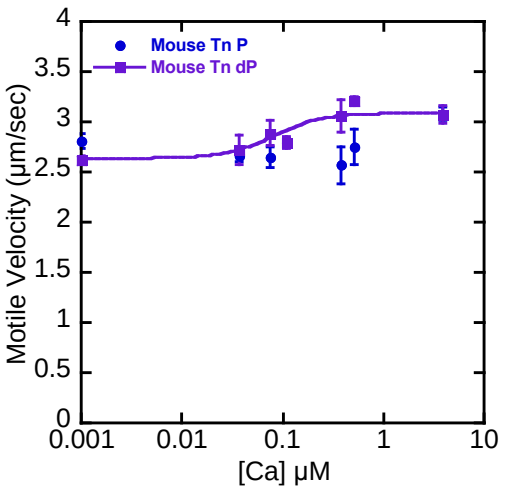


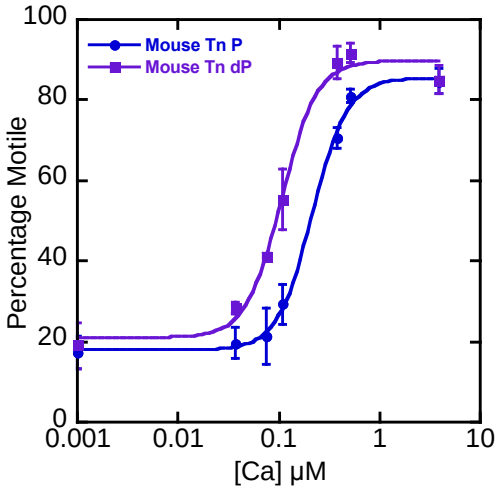


	Value	Error
Hill Coefficient	2.01	0.11
EC_{50}	0.24	0.01

	Value	Error
Hill Coefficient	2	0.5
EC_{50}	0.12	0.02

2





	Value	Error
Hill Coefficient	2.5	0.24
EC_{50}	0.22	0.02

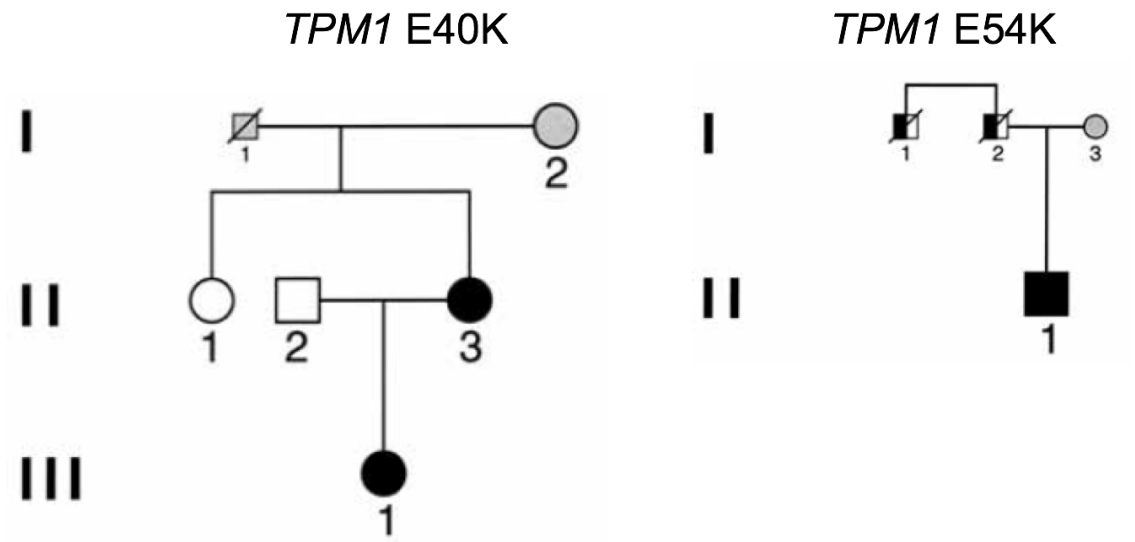
	Value	Error
Hill Coefficient	2.47	0.76
EC_{50}	0.11	0.01

4.3 Functional Investigation of DCM Mutant α-tropomyosin Glu40Lys (E40K) and Glu54Lys (E54K) from Baculovirus/*sf9* Recombinant Samples

4.3.1 Introduction on E40K and E54K α-tropomyosin

Both Glu40Lys (E40K) and Glu54Lys (E54K) α-tropomyosin mutants were identified in a study by Olson *et al.* with a non-positional candidate gene approach, which means that they just screened a large cohort of DCM patients (350 individuals) looking for mutations on the candidate gene *TPM1*. They identified two patients with small pedigrees (Figure 4.20) (Olson et al., 2001).

Figure 4.20: Pedigrees of E40K and E54K *TPM1* families



Square = male; circle = female; black filling = affected individual; half filled = borderline individual; shaded = unknown clinical status; slanted bars = deceased. Adapted from Olson *et al.* (2001).

The patient carrying the E40K mutation was diagnosed with DCM at 3 years old and underwent heart transplantation at 10. Her mother was diagnosed with DCM, but milder and not progressive, and carried the mutation as well, while the grandfather died of myocardial

infarction at 59, but there are not enough clinical details. Histology of the proband's explanted heart showed irregular and fragmented thin filaments, shorter sarcomeres and scalloped sarcolemma.

The patient with the E54K mutation instead was reported as normal on echocardiogram at 17 years old when asymptomatic, but subsequently at 26 presented shortage of breath, oedema and non-sustained ventricular tachycardia. DCM was diagnosed and he died a year later despite aggressive medical therapy. His father and uncle both died of heart failure respectively at 27 and 49.

Both of these mutations are charge swaps from acid to basic amino acids in acidic, very well conserved, regions of the molecule. Both of the mutations occur in the fifth position (e) of the heptapeptide repeat (in fact they are just two modules away), which is a position stabilising the coiled-coil by forming a salt bridge with an amino acid of opposite charge on the other monomer at the seventh position (g). These amino acids have been predicted to be Arg35 for Glu40 and Lys49 for Glu54 (Brown et al., 2001). Thus a localised disruption of the tropomyosin structure could not only interfere with the normal dimerisation but also with other protein interactions, such as with actin.

A transgenic mouse model was produced for E54K and it developed a DCM phenotype, further linking the mutation to the disease (Rajan et al., 2007). In this thesis the two α-tropomyosin mutants have been expressed in the baculovirus/*sf9* system, which, using eukaryotic insect cells, provides the N-terminal acetylation that has been proved to be essential for correct head-to-tail interactions and therefore polymerisation along the actin filament (Palm et al., 2003, Mirza et al., 2007).

4.3.2 *In Vitro* Motility Analysis for Recombinant E40K and E54K α-tropomyosin

Every experiment described in the following sections was performed using thin filaments reconstituted with rabbit skeletal muscle actin 10 nM, human cardiac troponin 60 nM and recombinant α-tropomyosin 60 nM, purified from wild-type, E40K or E54K expressing baculovirus/*sf9* cell pellets.

4.3.2.1 Effects of Recombinant E40K α-tropomyosin on the Thin Filaments Ca^{2+}-sensitivity Compared to Wild-Type α-tropomyosin

Four experiments were performed comparing recombinant E40K and wild-type α-tropomyosin reconstituted with natively phosphorylated human cardiac troponin (1.59 ± 0.15 mols P_i /mol TnI). One preparation of tropomyosin was used for these experiments and three of troponin. Experiments 2 and 4 are shown in Figure 4.21, 1 and 3 in APPENDIX; all data is summarised in Table 4.24.

Only experiment 3 could be plotted properly for the motile velocity and it seems to indicate that the E40K filaments have a slightly higher Ca^{2+}-sensitivity, but the Ca^{2+} dependent increase of the sliding speed is too small to draw a conclusion. In general the wild-type has a 7% higher maximum sliding speed, but does not seem to differ in the Ca^{2+} dependent increase of the sliding speed.

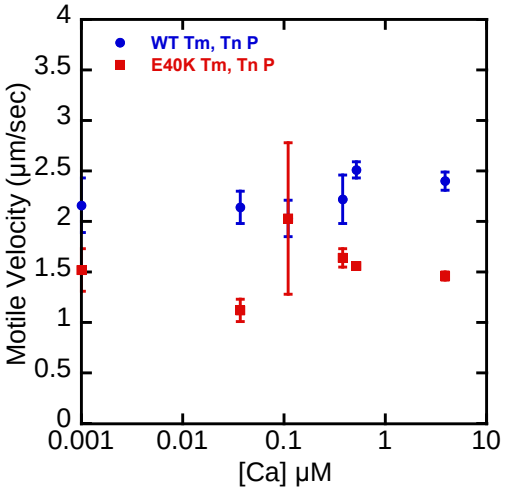
The percentage motile shows a statistically significant decrease in Ca^{2+}-sensitivity with EC_{50} ratio E40K / WT = 2.6 ± 0.38 (paired p = 0.004, unpaired p = 0.0008, single group p = 0.024). The Hill coefficient does not show any significant differences.

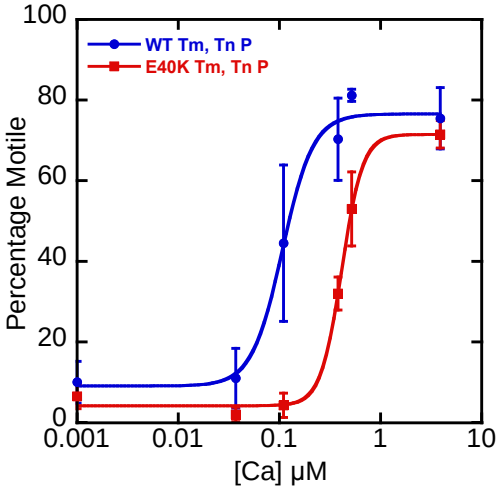
Table 4.24: Ca^{2+}-sensitivity data for wild-type v E40K recombinant tropomyosin with natively phosphorylated human cardiac troponin thin filaments

Tm E40K ANALYSIS	EC_{50} Percentage motility, µM		EC_{50} Mutant / EC_{50} WT	Hill coefficient n		% Motile 3.9 µM Ca^{2+}		Ca^{2+} activation of sliding speed (%)		Maximum sliding speed (µm/sec)	
DATE	WT	E40K		WT	E40K	WT	E40K	WT	E40K	WT	E40K
1	0.13±0.02	0.29±0.14	2.23	1.55	1	92	92	99	38	3.2	3.13
2	0.11±0.01	0.41±0.01	3.73	2.86	4.22	76	72	24	81	2.51	2.03
3	0.18±0.04	0.39±0.09	2.17	1.83	1	82	75	36	46	2.55	2.41
4	0.19±0.04	0.43±0.03	2.26	1.29	1.22	85	88	31	19	2.87	2.74
MEAN±SE	0.15±0.02	0.38±0.03	2.6±0.38	1.88± 0.34	1.86± 0.79	84±3	82±5	48±17	46±13	2.78±0.16	2.58±0.23
Student's t-test (paired)	p=0.004		single group, p=0.024 (compared with one)								
(unpaired)	p=0.0008										

Figure 4.21: Ca^{2+} concentration titration comparing thin filaments containing human natively phosphorylated cardiac troponin and either wild-type or E40K recombinant tropomyosin

2

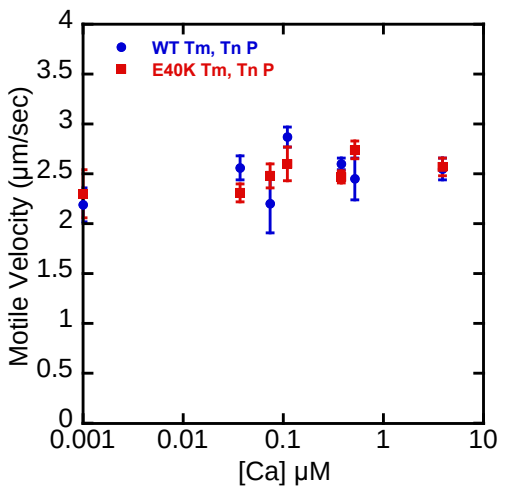


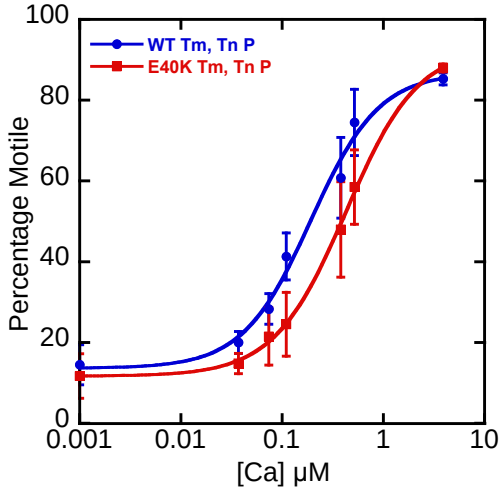


	Value	Error
Hill Coefficient	2.86	1.83
EC_{50}	0.11	0.01

	Value	Error
Hill Coefficient	4.22	0.73
EC_{50}	0.41	0.01

4





	Value	Error
Hill Coefficient	1.29	0.25
EC_{50}	0.19	0.04

	Value	Error
Hill Coefficient	1.22	0.11
EC_{50}	0.43	0.03

4.3.2.2 Effects of Recombinant E54K α-tropomyosin on the Thin Filaments Ca^{2+}-sensitivity Compared to Wild-Type α-tropomyosin

The comparison between thin filaments reconstituted with human cardiac natively phosphorylated troponin and recombinant α-tropomyosin, WT or E54K, was carried out five times, with two different tropomyosin preparations and five different troponin preparations. Experiments 4 and 5 are shown in Figure 4.22, the others in APPENDIX and all data are present in Table 4.25.

Motile velocity graphs could not be plotted due to the high variability in experiments 1, 2 and 3. In Experiment 4 the WT filaments data could not be fitted properly but it gives the indication of being very similar to the E54K filaments curve. Experiment 5, instead, could be plotted and it indicates that the two reconstitutions share the same EC_{50} value.

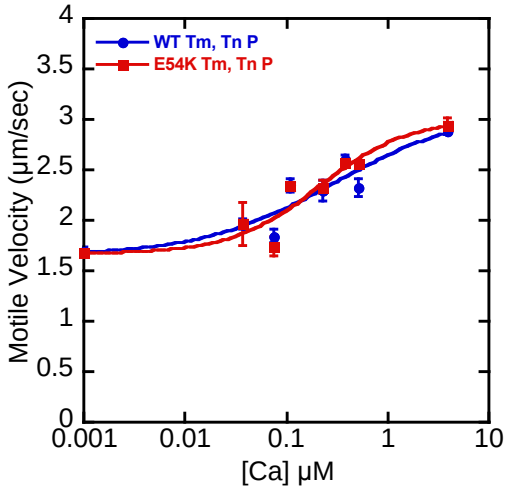
Percentage motile data indicates quite clearly that, differently from E40K, there does not seem to be any change in the Ca^{2+}-sensitivity of the two reconstitutions (EC_{50} ratio E54K / WT =1.01 ± 0.05). Hill coefficient of E54K filaments is 54% larger than that of WT filaments.

Table 4.25: Ca^{2+}-sensitivity data for wild-type v E54K recombinant tropomyosin with natively phosphorylated human cardiac troponin thin filaments

Tm E54K ANALYSIS	EC_{50} Percentage motility, µM		EC_{50} Mutant / EC_{50} WT	Hill coefficient n		% Motile 3.9 µM Ca^{2+}		Ca^{2+} activation of sliding speed (%)		Maximum sliding speed (µm/sec)	
EXP N	WT	E54K		WT	E54K	WT	E54K	WT	E54K	WT	E54K
1	0.1±0.01	0.1±0.01	1	4.4	2.25	80	80	11	44	2.73	2.85
2	0.07±0.03	0.06±0.01	0.86	1.8	6.18	81	74	31	38	3.51	3.41
3	0.09±0.34	0.11±0.01	1.22	3	7.1	75	75	41	19	2.68	2.57
4	0.15±0.06	0.16±0.07	1.07	1	1.1	88	88	69	76	2.88	2.94
5	0.11±0.01	0.1±0.01	0.91	2.22	2.45	93	92	54	59	2.55	2.56
MEAN±SE	0.104±0.01	0.106±0.02	1.01±0.05	2.48± 0.58	3.82± 1.18	83±3	82±4	41±10	47±10	2.87±0.17	2.87±0.16
Student's t-test (paired)	p=0.612		single group, p=0.85 (compared with one)								
(unpaired)	p=0.918										

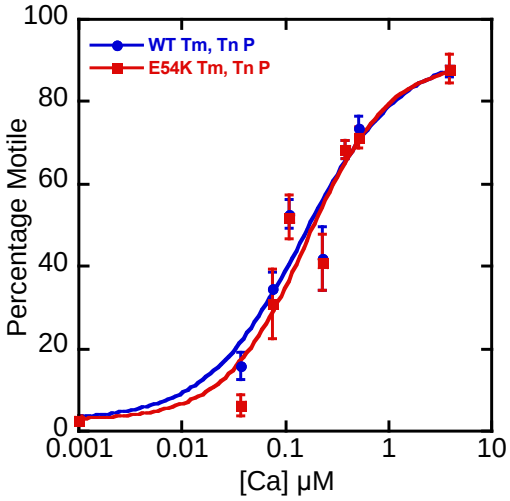
Figure 4.22: Ca^{2+} concentration titration comparing thin filaments containing human natively phosphorylated cardiac troponin and either wild-type or E54K recombinant tropomyosin

4

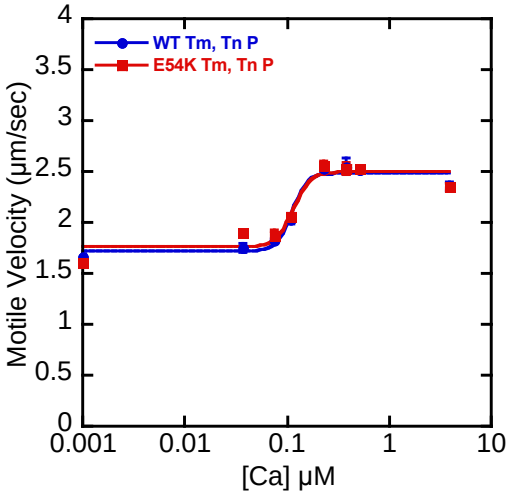


	Value	Error
Hill Coefficient	1	/
EC_{50}	0.15	0.06

	Value	Error
Hill Coefficient	1.1	0.4
EC_{50}	0.16	0.07

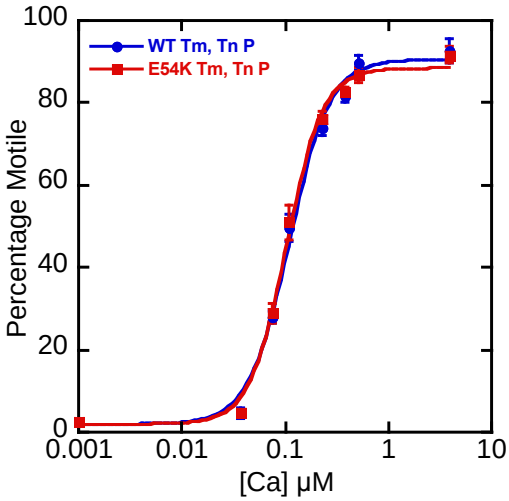


5



	Value	Error
Hill Coefficient	5.83	4.53
EC_{50}	0.11	0.01

	Value	Error
Hill Coefficient	5.21	5.64
EC_{50}	0.11	0.02



	Value	Error
Hill Coefficient	2.22	0.28
EC_{50}	0.11	0.01

	Value	Error
Hill Coefficient	2.45	0.28
EC_{50}	0.1	0.01

4.3.2.3 Effects of Troponin I Dephosphorylation on the Ca^{2+}-Sensitivity of E40K and E54K Thin Filaments

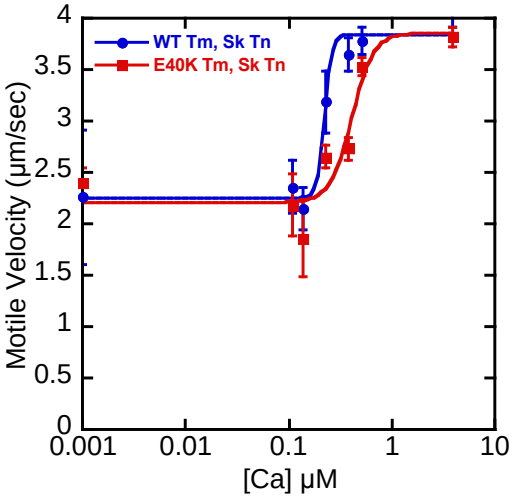
Since this time tropomyosin is the mutant protein and there is also a different phenotype shown by E40K and E54K, a few introductory experiments were performed to assess the properties of the mutant proteins with other isoforms of troponin than the human donor. First the effect of rabbit skeletal troponin was investigated. This troponin does not possess the N-terminal regulatory domain that is phosphorylated by PKA and therefore could mimic a dephosphorylated troponin.

When reconstituted with E40K (Figure 4.23), the Ca^{2+} titration showed a lower Ca^{2+}-sensitivity for both motile velocity (EC_{50} ratio E40K / WT = 1.86) and percentage motile (EC_{50} ratio E40K / WT = 1.53). This agrees with the phenotype seen with phosphorylated troponin, and could be attributable either to a shift of just the WT or a shift of both the reconstitutions to a higher Ca^{2+}-sensitivity.

The case was different for E54K thin filaments (Figure 4.24). When compared to WT filaments, it showed a much larger maximum sliding speed (35%) and Ca^{2+}-induced increase in the sliding speed (83%). The motile velocity seemed also more Ca^{2+}-sensitive for E54K filaments, but a good fit was not achieved to compare EC_{50} values.

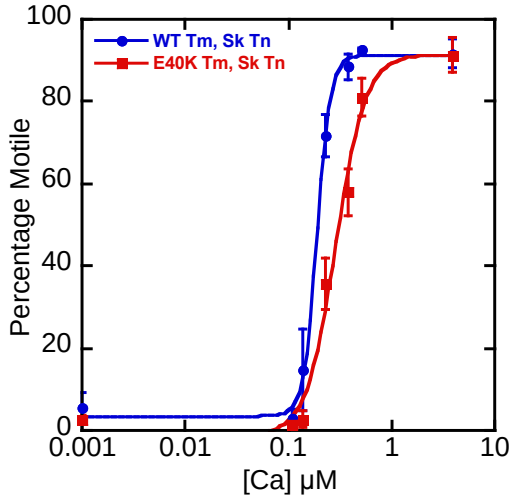
The percentage motile instead showed a lower Ca^{2+}-sensitivity for E54K filaments (EC_{50} ratio E54K / WT = 1.38). This unmasks already a different phenotype from that seen with phosphorylated cardiac troponin.

Figure 4.23: Ca^{2+} concentration titration comparing thin filaments containing rabbit skeletal troponin and either wild-type or E40K recombinant tropomyosin



	Value	Error
Hill Coefficient	12.41	100.63
EC_{50}	0.22	0.05

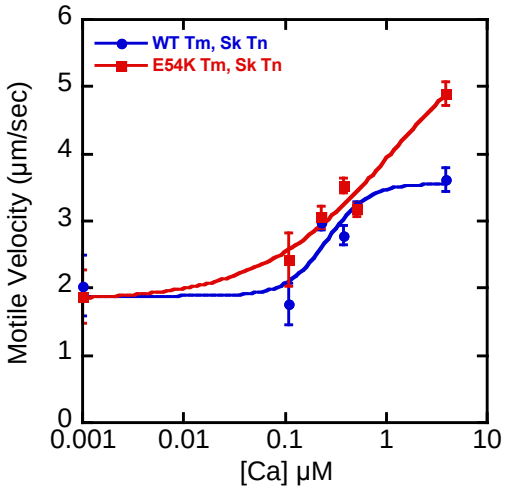
	Value	Error
Hill Coefficient	4.21	3.43
EC_{50}	0.41	0.08

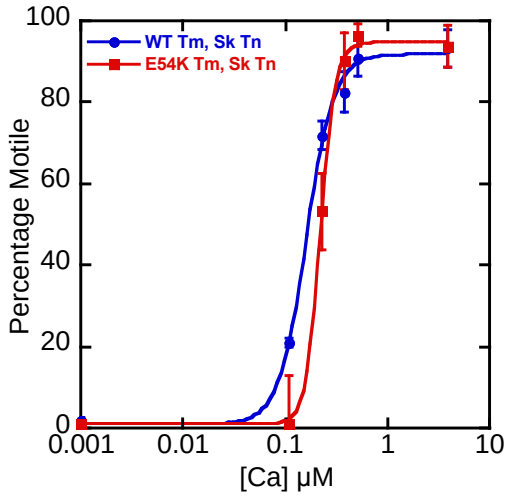


	Value	Error
Hill Coefficient	6.59	0.77
EC_{50}	0.19	0.01

	Value	Error
Hill Coefficient	3.06	0.72
EC_{50}	0.29	0.03

Figure 4.24: Ca^{2+} concentration titration comparing thin filaments containing rabbit skeletal troponin and either wild-type or E54K recombinant tropomyosin

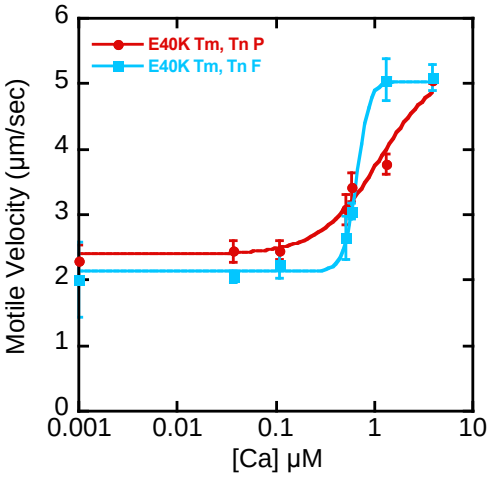


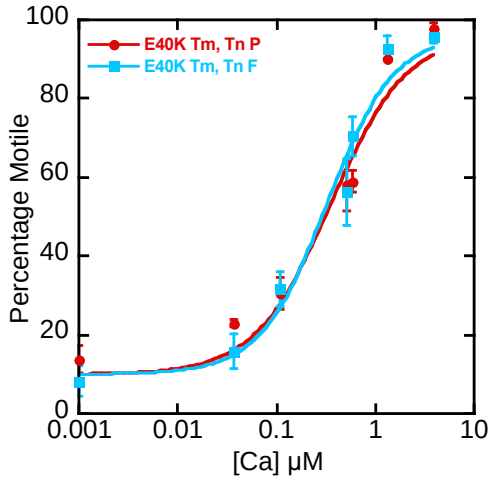


	Value	Error
Hill Coefficient	3.22	0.34
EC_{50}	0.16	0.01

	Value	Error
Hill Coefficient	6	1.07
EC_{50}	0.22	0.01

Figure 4.25: Ca^{2+} concentration titration comparing thin filaments containing human cardiac donor or failing heart troponin and either wild-type or E40K recombinant tropomyosin





	Value	Error
Hill Coefficient	1.14	0.23
EC_{50}	0.35	0.07

	Value	Error
Hill Coefficient	1.28	0.23
EC_{50}	0.32	0.05

A second preliminary experiment was made with E40K tropomyosin reconstituted with donor and failing human heart troponin as shown in Figure 4.25. Failing human heart troponin has been described as having a lower phosphorylation state compared to human donor samples (Messer et al., 2007). This is a way of producing a comparison between phosphorylated and dephosphorylated states of troponin, but without going through the *in vitro* dephosphorylation process.

The motile velocity plot could not be fitted decently enough to get data on the EC_{50}, but Ca^{2+}-induced increase of the sliding speed and maximum sliding speed were equal for thin filaments reconstituted with the two different troponins.

The percentage motile, on the other hand, produced two very similar curves with EC_{50} ratio E40K failing / donor = 0.91.

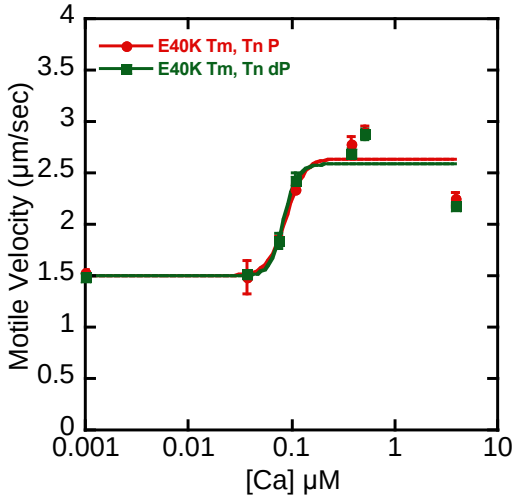
E40K tropomyosin was reconstituted in thin filaments with phosphorylated or dephosphorylated troponin and Ca^{2+} titrated 5 times using 3 different troponin preparations and one tropomyosin preparation. Experiments 2 and 4 are shown in Figure 4.26, while the others are shown in APPENDIX; all data are summarised in Table 4.26 and Table 4.27.

Motile velocity plots could be drawn for experiments 2, 3 and 4. They all showed very similar curves with average EC_{50} ratio P / dP = 1.06 ± 0.09. The dephosphorylated filaments showed higher Ca^{2+}-induced increase of the sliding speed (18%) and maximum sliding speed (5%).

The percentage motile graphs were all perfectly superimposable, with t-test p = 1.

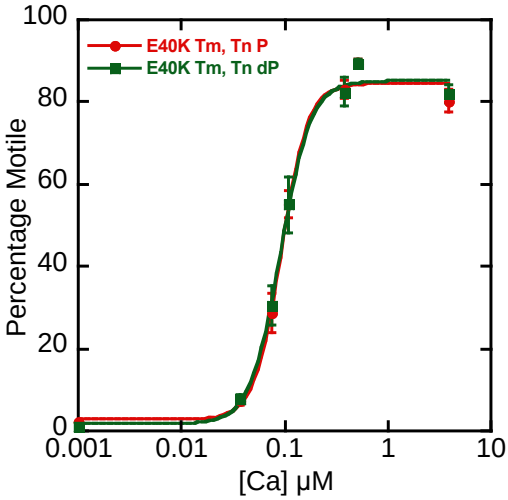
Figure 4.26: Ca^{2+} concentration titration comparing thin filaments containing natively phosphorylated or dephosphorylated human cardiac troponin and recombinant E40K tropomyosin

2



	Value	Error
Hill Coefficient	5.02	4.84
EC_{50}	0.09	0.02

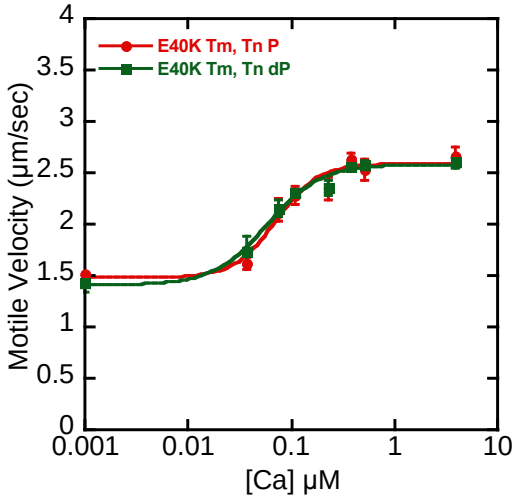
	Value	Error
Hill Coefficient	6.54	7.02
EC_{50}	0.08	0.02



	Value	Error
Hill Coefficient	3.36	0.77
EC_{50}	0.09	0.01

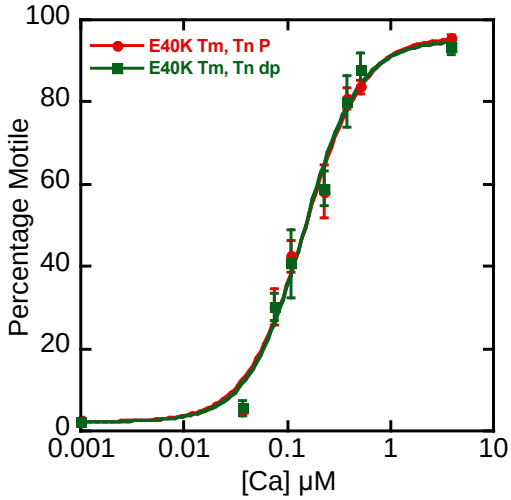
	Value	Error
Hill Coefficient	2.99	0.59
EC_{50}	0.09	0.01

4



	Value	Error
Hill Coefficient	2.11	0.82
EC_{50}	0.07	0.01

	Value	Error
Hill Coefficient	1.69	0.39
EC_{50}	0.06	0.01



	Value	Error
Hill Coefficient	1.53	0.23
EC_{50}	0.15	0.02

	Value	Error
Hill Coefficient	1.61	0.23
EC_{50}	0.15	0.02

Table 4.26: Ca^{2+}-sensitivity data for the sliding speed of thin filaments reconstituted with recombinant E40K tropomyosin and human cardiac troponin, phosphorylated v dephosphorylated

Tm E40K ANALYSIS	EC_{50} Sliding speed, µM		EC_{50} P/ EC_{50} dP	Ca^{2+} activation of sliding speed (%)		Maximum sliding speed (µm/sec)	
EXP N	E40K P	E40K dP		P	dP	P	dP
1	/	/	/	112	182	3.05	3.78
2	0.09±0.02	0.08±0.02	1.13	95	93	2.9	2.88
3	0.08±0.01	0.09±0.01	0.89	53	56	2.38	2.4
4	0.07±0.01	0.06±0.01	1.17	77	83	2.67	2.6
5	/	/	/	19	20	2.7	2.78
MEAN±SE	0.08±0.01	0.08±0.01	1.06±0.09	71±16	87±27	2.74±0.11	2.89±0.24
Student's t-test (paired)	p=0.667		single group, p=0.544 (compared with one)				
(unpaired)	p=0.768						

Table 4.27: Ca^{2+}-sensitivity data for the percentage motile of thin filaments reconstituted with recombinant E40K tropomyosin and human cardiac troponin, phosphorylated v dephosphorylated

Tm E40K ANALYSIS	EC_{50} Percentage motility, µM		EC_{50} P / EC_{50} dP	Hill coefficient n		% Motile 3.9 µM Ca^{2+}	
DATE	E40K P	E40K dP		P	dP	P	dP
1	0.18±0.07	0.18±0.08	1	1	1.19	91	97
2	0.09±0.01	0.09±0.01	1	3.36	2.99	90	90
3	0.14±0.01	0.14±0.02	1	1.79	1.82	87	86
4	0.15±0.02	0.15±0.02	1	1.53	1.61	96	93
5	0.33±0.05	0.33±0.05	1	3.49	3.22	84	86
MEAN±SE	0.18±0.04	0.18±0.04	1	2.23±0.5	2.17±0.4	90±2	90±2
Student's t-test (paired)	p=1		single group, p=1 (compared with one)				
(unpaired)	p=1						

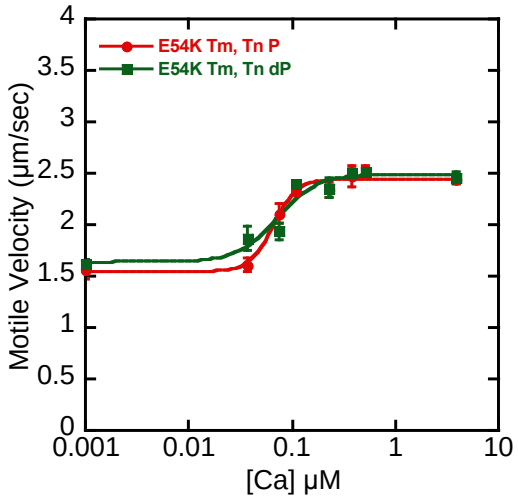
E54K was reconstituted in thin filaments with phosphorylated and dephosphorylated troponin and titrated four times, using one tropomyosin preparation and two troponin preparations. Experiments 1 and 4 are shown in Figure 4.27, while 2 and 3 are shown in APPENDIX; all data are summarised in Table 4.28 and Table 4.29

Motile velocity graphs could be fitted this time for all of the experiments. They all showed very similar curves with average EC_{50} ratio P / dP = 1 ± 0.09. This time phosphorylated filaments showed slightly higher Ca^{2+}-induced increase of the sliding speed (13%).

The percentage motile Ca^{2+} activation graphs were all perfectly superimposable once again, with t-test p = 1.

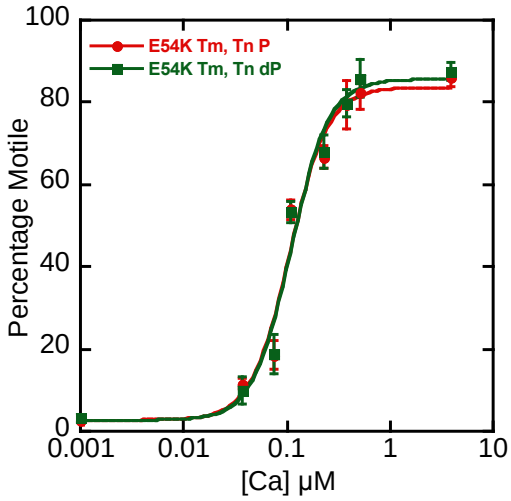
Figure 4.27: Ca^{2+} concentration titration comparing thin filaments containing natively phosphorylated or dephosphorylated human cardiac troponin and recombinant E54K tropomyosin

1



	Value	Error
Hill Coefficient	3.83	1.27
EC_{50}	0.07	0.01

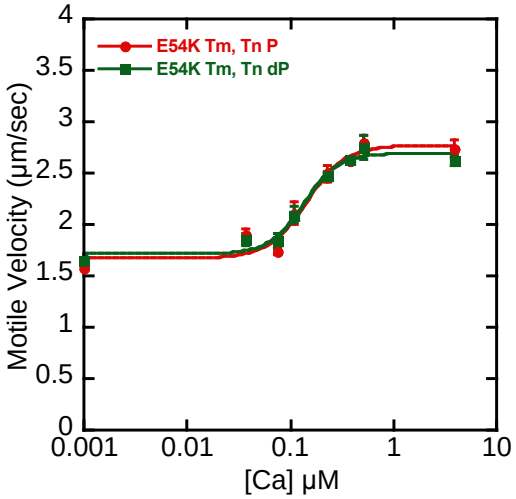
	Value	Error
Hill Coefficient	2.28	1.14
EC_{50}	0.07	0.02



	Value	Error
Hill Coefficient	2.36	0.79
EC_{50}	0.11	0.02

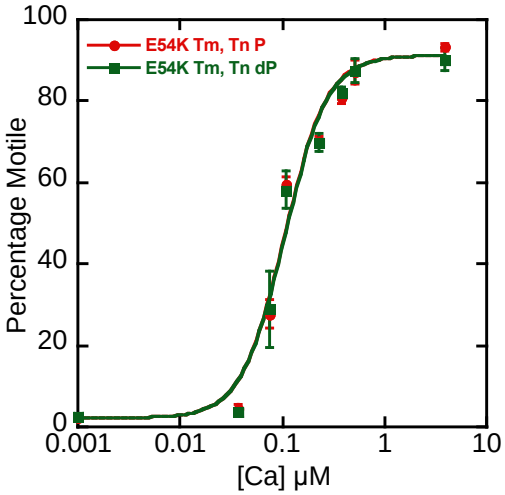
	Value	Error
Hill Coefficient	2.36	0.71
EC_{50}	0.11	0.02

4



	Value	Error
Hill Coefficient	2.31	0.93
EC_{50}	0.14	0.03

	Value	Error
Hill Coefficient	2.64	0.84
EC_{50}	0.14	0.02



	Value	Error
Hill Coefficient	2.07	0.38
EC_{50}	0.105	0.01

	Value	Error
Hill Coefficient	2.06	0.35
EC_{50}	0.105	0.01

Table 4.28: Ca^{2+}-sensitivity data for the sliding speed of thin filaments reconstituted with recombinant E54K tropomyosin and human cardiac troponin, phosphorylated v dephosphorylated

Tm E54K ANALYSIS	EC_{50} Sliding speed, µM		EC_{50} P/ EC_{50} dP	Ca^{2+} activation of sliding speed (%)		Maximum sliding speed (µm/sec)	
EXP N	E54K P	E54K dP		P	dP	P	dP
1	0.07±0.01	0.07±0.02	1	62	56	2.53	2.51
2	0.07±0.01	0.09±0.02	0.78	75	69	2.83	2.8
3	0.12±0.03	0.1±0.01	1.2	69	58	2.7	2.6
4	0.14±0.03	0.14±0.02	1	78	68	2.8	2.75
MEAN±SE	0.1±0.02	0.1±0.01	1±0.09	71±4	63±3	2.72±0.07	2.67±007
Student's t-test (paired)	p=1		single group, p=0.957 (compared with one)	p=0.008			
(unpaired)	p=1			p=0.14			

Table 4.29: Ca^{2+}-sensitivity data for the percentage motile of thin filaments reconstituted with recombinant E54K tropomyosin and human cardiac troponin, phosphorylated v dephosphorylated

Tm E54K ANALYSIS	EC_{50} Percentage motility, µM		EC_{50} P /EC_{50} dP	Hill coefficient n		% Motile 3.9 µM Ca^{2+}	
EXP N	E54K P	E54K dP		P	dP	P	dP
1	0.11±0.02	0.11±0.02	1	2.36	2.36	86	88
2	0.14±0.03	0.14±0.02	1	1.62	1.68	91	89
3	0.1±0.01	0.1±0.01	1	1.94	1.91	94	93
4	0.105±0.01	0.105±0.01	1	2.07	2.06	93	90
MEAN±SE	0.11±0.01	0.11±0.01	1	2±0.15	2±0.14	91±2	90±1
Student's t-test (paired)	p=1		single group, p=1 (compared with one)				
(unpaired)	p=1						

Two final experiments were made comparing E40K or E54K thin filaments reconstituted with dephosphorylated troponin and WT thin filaments with dephosphorylated troponin. Both experiments were repeated 4 times, both using 1 tropomyosin preparation and two troponin preparations.

The E40K tropomyosin experiments 1 and 4 are shown in Figure 4.28, 2 and 3 are shown in APPENDIX, with data shown in Table 4.30 and Table 4.31.

Motile velocity plot number 2 could not be fitted, while all of the others showed the same phenotype of lower Ca^{2+}-sensitivity for E40K (EC_{50} dP ratio E40K/ WT= 2.3 ± 0.15).

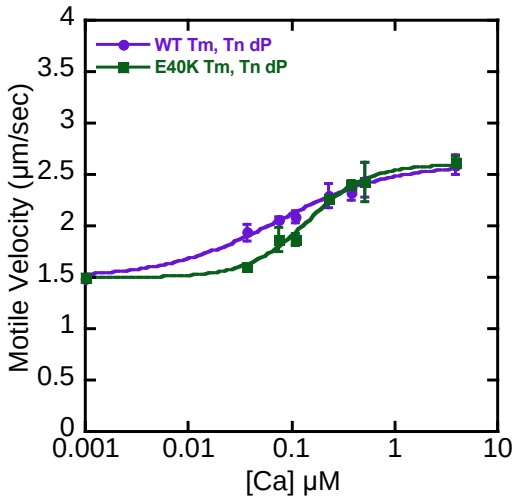
The same phenotype was observed with the percentage motile with EC_{50} dP ratio E40K / WT = 2.63 ± 0.46. The two reconstitutions had statistically different Ca^{2+}-sensitivities with t-test unpaired ($p = 0.037$) and single test compared to 1 for the EC_{50} average ratio ($p = 0.037$). Hill coefficient was larger for E40K filaments (32%).

The E54K tropomyosin experiments 1 and 3 are shown in Figure 4.29, 2 and 4 are shown in APPENDIX, with data shown in Table 4.32.

None of the motile velocity plots could be fitted due to the big variability. The percentage motile graphs indicated higher Ca^{2+}-sensitivity for the WT that gave a statistical difference between the two reconstitutions, with paired t-test $p = 0.009$, unpaired $p = 0.0005$ and single group for EC_{50} average $p = 0.03$.

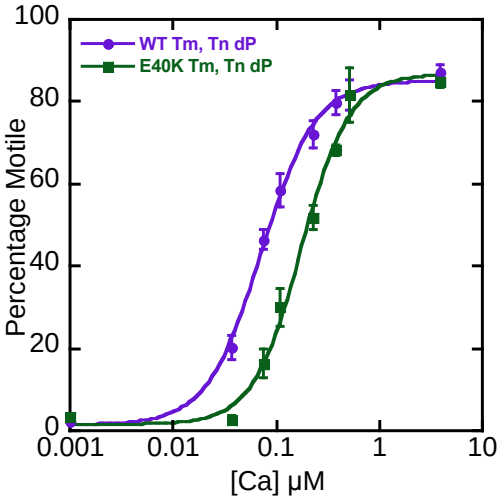
Figure 4.28: Ca^{2+} concentration titration comparing thin filaments containing dephosphorylated human cardiac troponin and either wild-type or E40K recombinant tropomyosin

1



	Value	Error
Hill Coefficient	1	/
EC_{50}	0.07	0.01

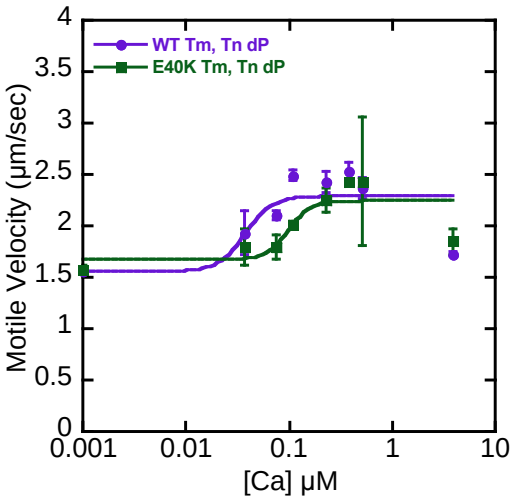
	Value	Error
Hill Coefficient	1.49	0.15
EC_{50}	0.14	0.01



	Value	Error
Hill Coefficient	1.66	0.16
EC_{50}	0.07	0.01

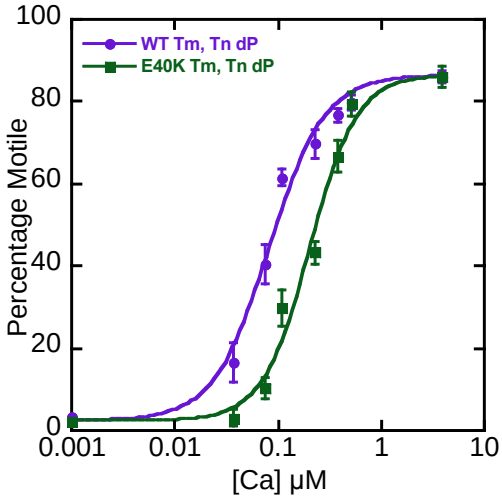
	Value	Error
Hill Coefficient	1.86	0.27
EC_{50}	0.17	0.02

4



	Value	Error
Hill Coefficient	3.28	8.35
EC_{50}	0.04	0.02

	Value	Error
Hill Coefficient	4.16	8.08
EC_{50}	0.1	0.04



	Value	Error
Hill Coefficient	1.62	0.2
EC_{50}	0.08	0.01

	Value	Error
Hill Coefficient	1.91	0.24
EC_{50}	0.2	0.02

Table 4.30: Ca^{2+}-sensitivity data for the sliding speed of thin filaments reconstituted with dephosphorylated human cardiac troponin, wild type v E40K recombinant tropomyosin

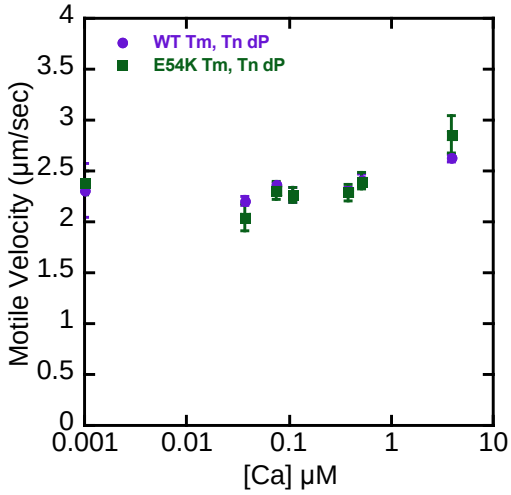
Tm E40K ANALYSIS	EC_{50} Sliding speed, µM		EC_{50} Mutant / EC_{50} WT	Ca^{2+} activation of sliding speed (%)		Maximum sliding speed (µm/sec)	
EXP N	WT dP	E40K dP		WT dP	E40K dP	WT dP	E40K dP
1	0.07±0.01	0.14±0.01	2	74	75	2.59	2.63
2	/	/	/	45	32	2.69	2.5
3	0.05±0.01	0.12±0.04	2.4	71	70	2.61	2.65
4	0.04±0.02	0.1±0.04	2.5	63	55	2.53	2.43
MEAN±SE	0.05±0.01	0.12±0.01	2.3±0.15	63±7	58±10	2.61±0.03	2.55±0.05
Student's t-test (paired)	p=0.002		single group, p=0.014 (compared with one)				
(unpaired)	p=0.01						

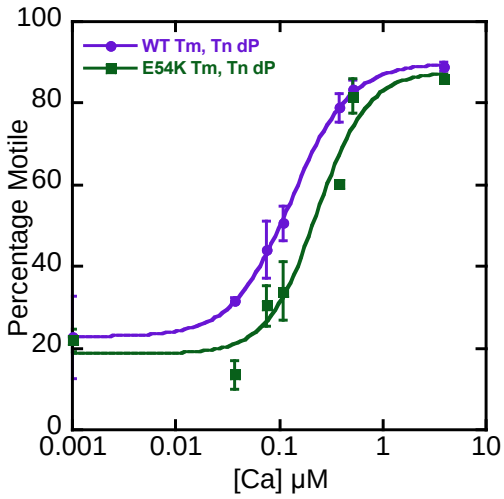
Table 4.31: Ca^{2+}-sensitivity data for the percentage motile of thin filaments reconstituted with dephosphorylated human cardiac troponin, wild type v E40K recombinant tropomyosin

Tm E40K ANALYSIS	EC_{50} Percentage motility, µM		EC_{50} Mutant / EC_{50} WT	Hill coefficient n		% Motile 3.9 µM Ca^{2+}	
DATE	WT dP	E40K dP		WT dP	E40K dP	WT dP	E40K dP
1	0.07±0.01	0.17±0.02	2.43	1.66	1.86	87	85
2	0.09±0.02	0.35±0.07	3.89	1.16	1.94	86	90
3	0.07±0.01	0.12±0.01	1.71	2.12	2.93	91	90
4	0.08±0.01	0.2±0.02	2.5	1.62	1.91	86	86
MEAN±SE	0.08±0.01	0.21±0.05	2.63±0.46	1.64± 0.2	2.16± 0.26	88±1	88±1
Student's t-test (paired)	p=0.06		single group, p=0.037 (compared with one)				
(unpaired)	p=0.037						

Figure 4.29: Ca^{2+} concentration titration comparing thin filaments containing dephosphorylated human cardiac troponin and either wild-type or E54K recombinant tropomyosin

1

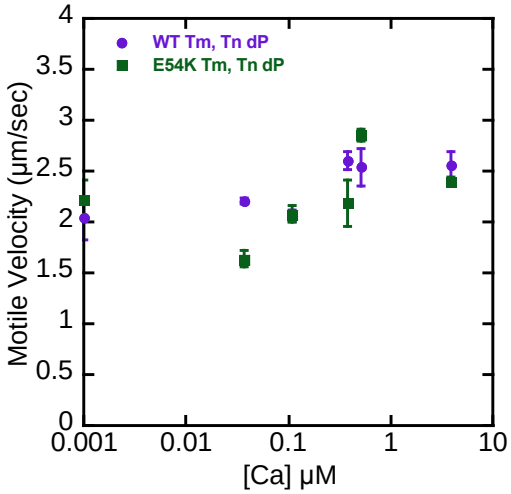


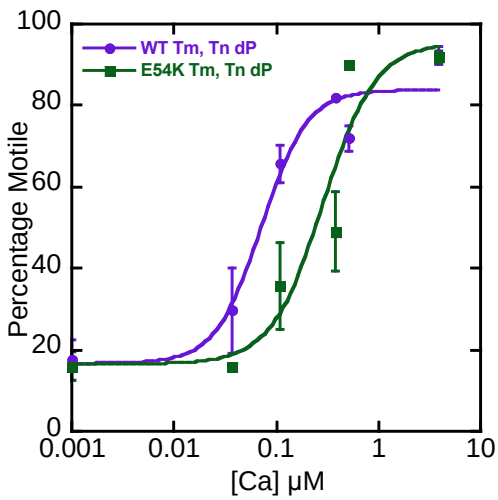


	Value	Error
Hill Coefficient	1.53	0.1
EC_{50}	0.13	0.01

	Value	Error
Hill Coefficient	1.8	0.68
EC_{50}	0.23	0.08

3





	Value	Error
Hill Coefficient	1.95	1.12
EC_{50}	0.07	0.03

	Value	Error
Hill Coefficient	1.71	1.5
EC_{50}	0.29	0.17

Table 4.32: Ca^{2+}-sensitivity data of thin filaments reconstituted with dephosphorylated human cardiac troponin, wild type v E54K recombinant tropomyosin

Tm E54K ANALYSIS	EC_{50} Percentage motility, µM		EC_{50} Mutant / EC_{50} WT	Hill coefficient n		% Motile 3.9 µM Ca^{2+}		Ca^{2+} activation of sliding speed (%)		Maximum sliding speed (µm/sec)	
EXP N	WT dP	E54K dP		WT dP	E54K dP	WT dP	E54K dP	WT dP	E54K dP	WT dP	E54K dP
1	0.13±0.01	0.23±0.08	1.77	1.53	1.8	89	86	19	40	2.63	2.86
2	0.13±0.03	0.29±0.04	2.23	1.44	1.94	89	86	38	66	3	3.05
3	0.07±0.03	0.29±0.17	4.14	1.95	1.71	92	92	28	74	2.61	2.85
4	0.1±0.01	0.23±0.08	2.3	1.79	1.29	90	94	32	66	2.95	3.08
MEAN±SE	0.11±0.01	0.26±0.02	2.44±0.44	1.68± 0.12	1.69± 0.14	90±1	90±2	29±4	62±7	2.8±0.1	2.96±0.06
Student's t-test (paired)	p=0.009		single group, p=0.03 (compared with one)					p=0.009		p=0.036	
(unpaired)	p=0.0005							p=0.009		p=0.22	

4.4 Dose Dependency of Mutant Protein to Produce the Uncoupling Phenotype

One last experiment was performed in order to assess the relationship between the ratio of poison peptide to wild type present in the reconstitution and the extent of the uncoupling generated.

For this experiment the mutant E40K α-tropomyosin was used. It was chosen for several technical reasons: tropomyosin is the most stable protein of the thin filaments; its post-translational modifications do not need to be modified for this experiment; the tropomyosin mutants were the only ones produced recombinantly and therefore 100% mutant α-tropomyosin could be easily mixed with 100% wild-type α-tropomyosin in different ratios; the IVMA experiments made earlier indicated as unlikely any difference in the affinity for actin of E40K compared to wild-type α-tropomyosin, as the behaviour in high and low Ca^{2+} was similar; with phosphorylated troponin, contrarily to E54K, E40K had a different EC_{50} compared to the WT.

To produce the mutant-WT dimer, E40K α-tropomyosin was mixed thoroughly with WT α-tropomyosin and incubated for 20 minutes at 40° C. The samples were then transfered to ice and used to reconstitute thin filaments thereafter. The thin filaments were reconstituted using rabbit skeletal muscle actin 10 nM, human donor cardiac troponin phosphorylated or dephosphorylated 60 nM and the recombinant α-tropomyosin 60 nM. Table 4.33 shows all the data obtained through the Ca^{2+} titrations performed with seven different dilutions of E40K, spanning from 0% to 100% with increases of 12.5% up to 62.5%.

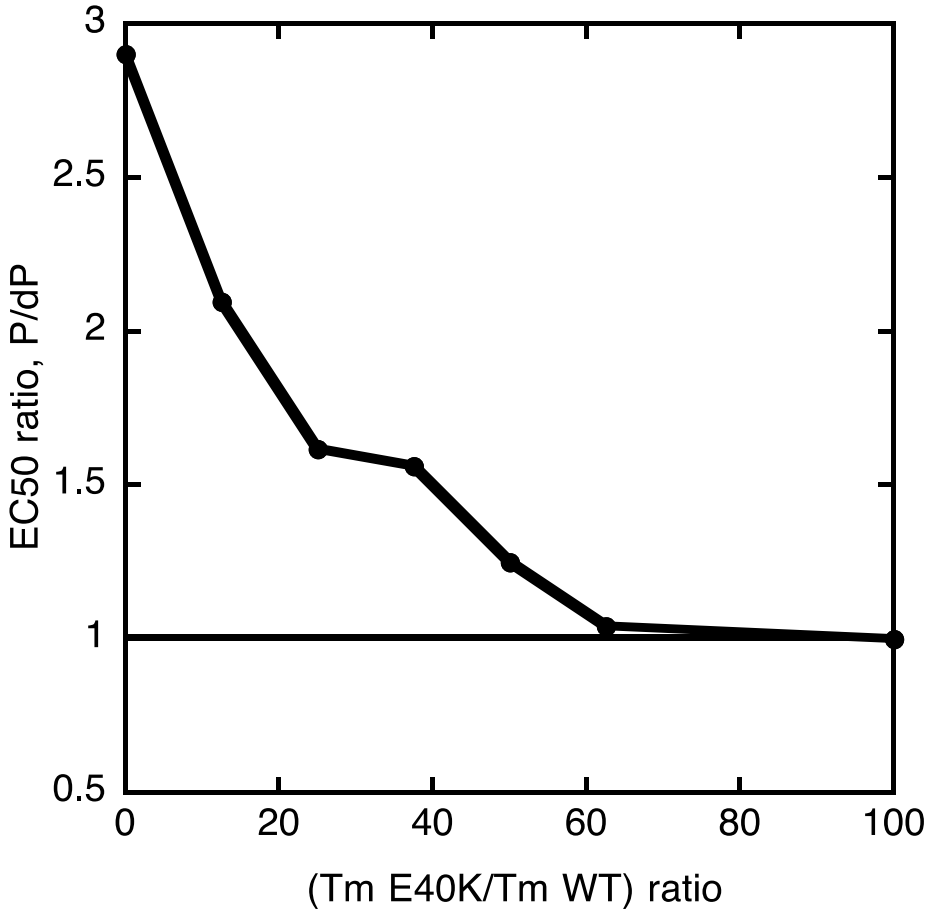
When only WT α-tropomyosin is used to reconstitute thin filaments, the difference in Ca^{2+}-sensitivity produces an EC_{50} ratio P / dP = 2.9. But when the WT α-tropomyosin is mixed

with the E40K this ratio dramatically drops as visible in Figure 4.30. Around the 50% mix of E40K and WT α-tropomyosin the ratio is reduced to 1.25, while when 100% is 1. It is clear that the effect of the mutation is not directly proportional to its presence, on the contrary it seems likely it is able to impair the effect of TnI phosphorylation in very small proportions. There does not seem to be any significant effect on the motile velocity or cooperativity.

Table 4.33: Ca^{2+}-sensitivity data for titrations performed with different α-tropomyosin E40K / WT ratios and troponin phosphorylated v dephosphorylated

E40K DILUTIONS	% of E40K	EC_{50} Percentage motility, µM		EC_{50} ratio P / dP	ΔEC_{50} (P-dP)	Hill coefficient n		% Motile 3.9 µM Ca^{2+}		Ca^{2+} activation of sliding speed, %		Maximum sliding speed (µm/sec)	
Repeats		Tn P	Tn dP			P	dP	P	dP	P	dP	P	dP
Mean (n=5)	100%	0.18	0.18	1	0	2.23	2.17	90	90	71	87	2.74	2.89
n=1	62.5%	0.157± 0.01	0.151± 0.01	1.04	0.006	1.63	1.67	87	85	49	50	2.48	2.5
n=1	50%	0.15± 0.01	0.12± 0.01	1.25	0.03	1.99	2.51	92	93	75	80	2.73	2.85
n=1	37.5%	0.14± 0.01	0.09± 0.01	1.56	0.05	1.86	2.56	88	90	69	64	2.71	2.7
n=1	25%	0.21± 0.04	0.13± 0.03	1.62	0.08	1.77	1.32	86	93	22	23	2.92	3.03
n=1	12.5%	0.21± 0.04	0.1±0.01	2.1	0.11	1.47	1.46	91	92	28	35	3.08	3.37
Mean (n=3)	0%	0.23± 0.11	0.08± 0.03	2.9	0.15	1.66	1.57	88	88	59	47	2.7	2.68

Figure 4.30: EC_{50} ratio P / dP troponin for thin filaments reconstituted with different E40K / WT ratios of α-tropomyosin



4.5 Discussion

4.5.1 Concentration of DCM Mutant Proteins in the Experimental Samples

For these studies on DCM mutations I used mutant human, animal and recombinant proteins. The troponin I and T mutant were purified respectively from human and mouse tissue in which also the wild-type troponin subunit was expressed. It is known that the ratio of wild-type to mutant protein is critical for their function (Mirza et al., 2005, Robinson et al., 2002). To verify the ratio mutant / WT mass spectrometry (MS) and tandem mass spectrometry (MS/MS) were performed by Dr J. Leung and Dr D. Ward on trypsin or Arg-C digestions of the purified samples. The proteases were selected so as to generate reporter peptides ~10 residues long containing the mutation of interest.

Tryptic digestion of TnT from the TnT R141W transgenic mouse produced 10 peptides identified in MS unique to human cTnT and 6 unique to mouse cTnT (Table 4.34). The estimated ratio indicates that around 60% has the human, thus mutant, sequence.

MALDI data collected on peptides cleaved from the human TnI K36Q patient's purified troponin indicated that 93% of the whole TnI is mutant K36Q (Table 4.34). The same sample was also analysed in an Orbitrap spectrometer suggesting that the 86% of the total TnI is K36Q. We therefore considered the actual ratio to be ranging between those two values.

The peptides cleaved by Arg-C on TnT from the TnT ΔK210 mouse are EKKKKILAER and EKKKILAER, corresponding respectively to the WT and mutant TnT. MS analysis indicated that the mutant protein is present at around 40% of the total in the heterozygous animal and 100% in the homozygous animal (Table 4.34).

Table 4.34: MS data for reporter peptides measured by MALDI-TOF/TOF, used to quantitate TnI K36Q and TnT ΔK210

Mutation	Protease	Peptide	Intensity (%)
TnI K36Q	Trypsin	AYATEPHAQK	93
		AYATEPHAK	7
TnT ΔK210 heterozygous	Arg-C	EKKKILAER	42
		EKKKKILAER	58
TnT ΔK210 homozygous	Arg-C	EKKKILAER	100
		EKKKKILAER	-
TnT R141W	Trypsin	10 mutant segments	60
		6 WT segments	40

4.5.2 DCM Molecular Phenotype

In chapter 3 it was highlighted how two mutations in two different proteins, troponin C G159D and actin E361G, shared the molecular phenotype of being insensitive to modulations of TnI phosphorylation, but did not show a common trend in the absolute Ca^{2+}-sensitivity. In this chapter another 5 mutations have been taken into consideration, which summed with the 2 analysed in chapter 3, gives a total of 7 mutations with at least one positioned on each subunit of the thin filaments. Table 4.35 summarises all the experimental details regarding these mutations.

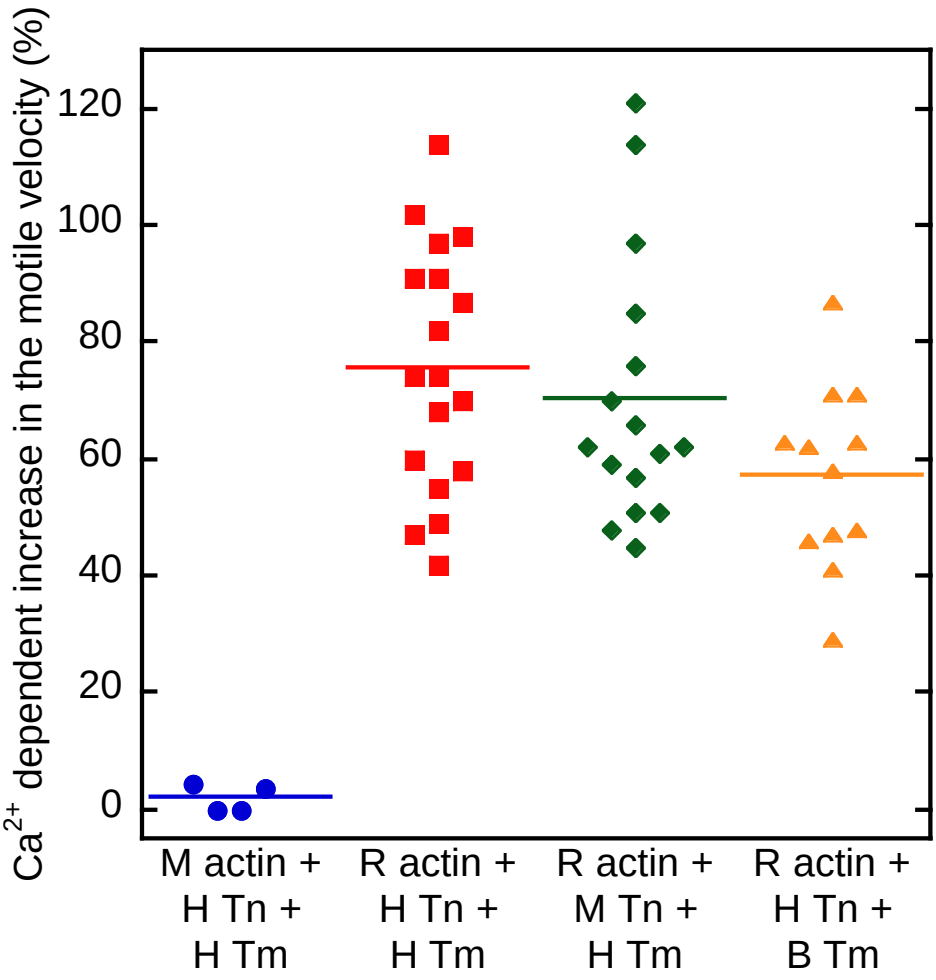
Table 4.35: DCM mutations data summary

Mutation	Source of Tissue	Expression Level %	Motile Velocity Ratio at 3.9 µM Ca^{2+} mutant / WT Native Tn	EC_{50} Ratio mutant / WT Tn P	Mutant EC_{50} Ratio Tn P / dP	Phosphorylation Level Native Troponin mols P_i / mol TnI	Phosphorylation Level Dephosphorylated Troponin mols P_i / mol TnI
TNNI3 **K36Q**	Human Transplant	86-93	1.01±0.03 n=4, p=0.9	2.23±0.38 n=2	0.98±0.05 n=3, p=0.69	Native 0.33±0.14	0.09±0.01
				2.15±0.15 n=4, p=0.004	0.98±0.01 n=3, p=0.19	PKA-trated 1.31±0.01	
TNNT2 **R141W**	TG Mouse	60	0.97±0.07 n=3, p=0.69	4.19±1.59 n=3, p=0.18	0.95±0.06 n=3, p=0.46	1.15±0.07	0.19±0.09
TNNT2 **ΔK210 het**	KI Mouse	40	1.04±0.02 n=4, p=0.18	1.63±0.25 n=4, p=0.09	0.96±0.02 n=4, p=0.06	1.15±0.04	0.23±0.08
TNNT2 **ΔK210 hom**	KI Mouse	100	0.97±0.44 n=6, p=0.57	2.18±0.26 n=6, p=0.01	0.96±0.09 n=4, p=0.68	1.06±0.06	0.21±0.08
TPM1 **E40K**	Baculovirus */sf9*	100	0.92±0.04 n=4, p=0.13	2.6±0.38 n=4, p=0.02	1.00±0.001 n=5, p=1	1.59±0.15	0.09±0.02
TPM1 **E54K**	Baculovirus */sf9*	100	1±0.02 n=5, p=0.99	1.01±0.05 n=5, p=0.85	1.00±0.001 n=4, p=1	1.79±0.04	0.08±0.03
TNNC1 **G159D**	Human Transplant	45	0.97±0.02 n=2	0.55±0.13 n=6, p=0.017	1.18±0.09 n=5, p=0.54	1.53±0.05	0.12±0.01
ACTC **E361G**	TG Mouse	50	1.01±0.01 n=3, p=0.68	0.93±0.09 n=9, p=0.5	1.0±0.07 n=6, p=0.98	1.33±0.09	0.07±0.02
Human donor Tn		100			3.0±0.03 n=7, p=0.003	1.6±0.04	0.12±0.01
Mouse NTg Tn		100			2.0±0.2 n=5, p=0.005	1.3±0.09	0.05±0.02

A first consideration that can be done before analysing the Ca^{2+}-sensitivity of the thin filaments, is that the maximum motile velocity reached by the thin filaments at activating Ca^{2+} concentration was not different between mutant and WT filaments. This result obtained with natively phosphorylated human or mouse troponin is different from what seen with recombinantly expressed troponin, where DCM mutations were inducing a decrease in the motile velocity, and therefore in the cross-bridge turnover rate (Mirza et al., 2005). Also, in relation to what was discussed in section 3.3.1, it was observed that the regulation of the

motile velocity and especially its Ca^{2+}-dependent increase, depends on the nature of the proteins used. As visible in Figure 4.31, the regulation of the motile velocity seems totally absent when actin is purified from a mouse sample directly from thin filaments. This was also noted by Dr E. Dyer in her thesis (and Song *et al*., 2010) and shown to be related to the method by which the actin is isolated. With rabbit or mouse actin, prepared through the acetone powder method, it seems like the average biggest increase is recorded when human proteins are used, followed by thin filaments reconstituted with mouse troponin, and finally by those reconstituted with baculovirus/*sf9* tropomyosin. Thus the change in motile velocity, being very variable as well as dependent both on the preparation and the mutation, is not the most reliable parameter. When the change in motile velocity is small it is not possible to determine the EC_{50} for Ca^{2+} activation and this is why most of the results reported here rely on the EC_{50} of the percentage of motile filaments. Since the large majority of experimental work on thin filaments regulation has used actin isolated from an acetone powder by cycles of polymerisation/depolymerisation, it could be questioned whether the results obtained truly represent the physiological situation.

Figure 4.31: Ca^{2+}-dependent speed increase for thin filaments reconstituted with combinations of proteins from different sources

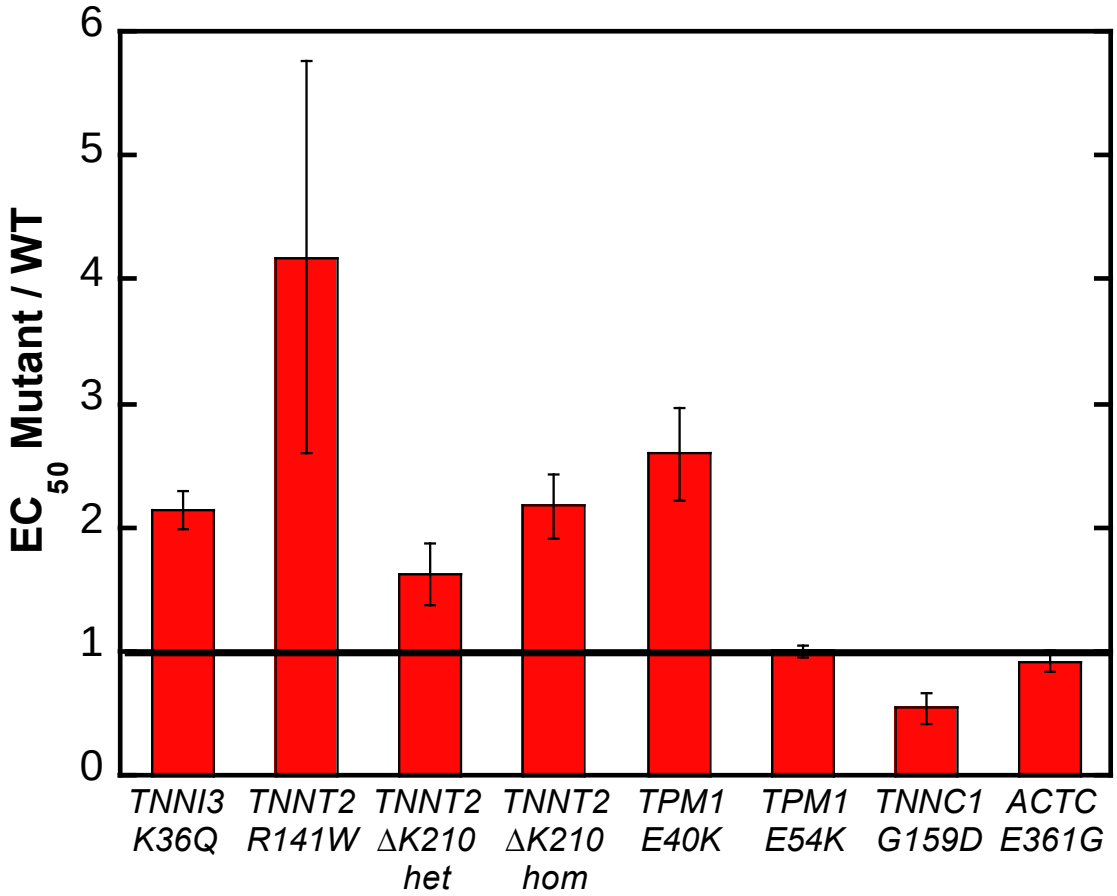


B = baculovirus/*sf*9, H = human, M = mouse direct prep, R = rabbit acetone powder prep

When comparing natively phosphorylated thin filaments reconstituted with WT and mutant proteins, we could observe that, as previously seen in Chapter 3, there is not a consistent trend in the Ca^{2+}-sensitivity relationships. TnI K36Q, TnT ΔK210 homozygous and α-tropomyosin E40K produce a statistically significant decrease in the Ca^{2+}-sensitivity compared to the WT, while TnT ΔK210 heterozygous and TnT R141W also produce a decrease, but without reaching statistical significance. Actin E361G and α-tropomyosin E54K do not seem to produce any difference and TnC G159D increases the Ca^{2+}-sensitivity.

Following the variability of these findings, summarised in Figure 4.32, we propose to rule out the possibility that a common mechanism leading to DCM is triggered by a reduced Ca^{2+}-sensitivity in the thin filaments. Another study further supports this variability and reported an increase in the Ca^{2+}-sensitivity due to α-actin R312H (Debold et al., 2010).

Figure 4.32: Percentage motile EC_{50} ratios mutant / WT when troponin is natively phosphorylated

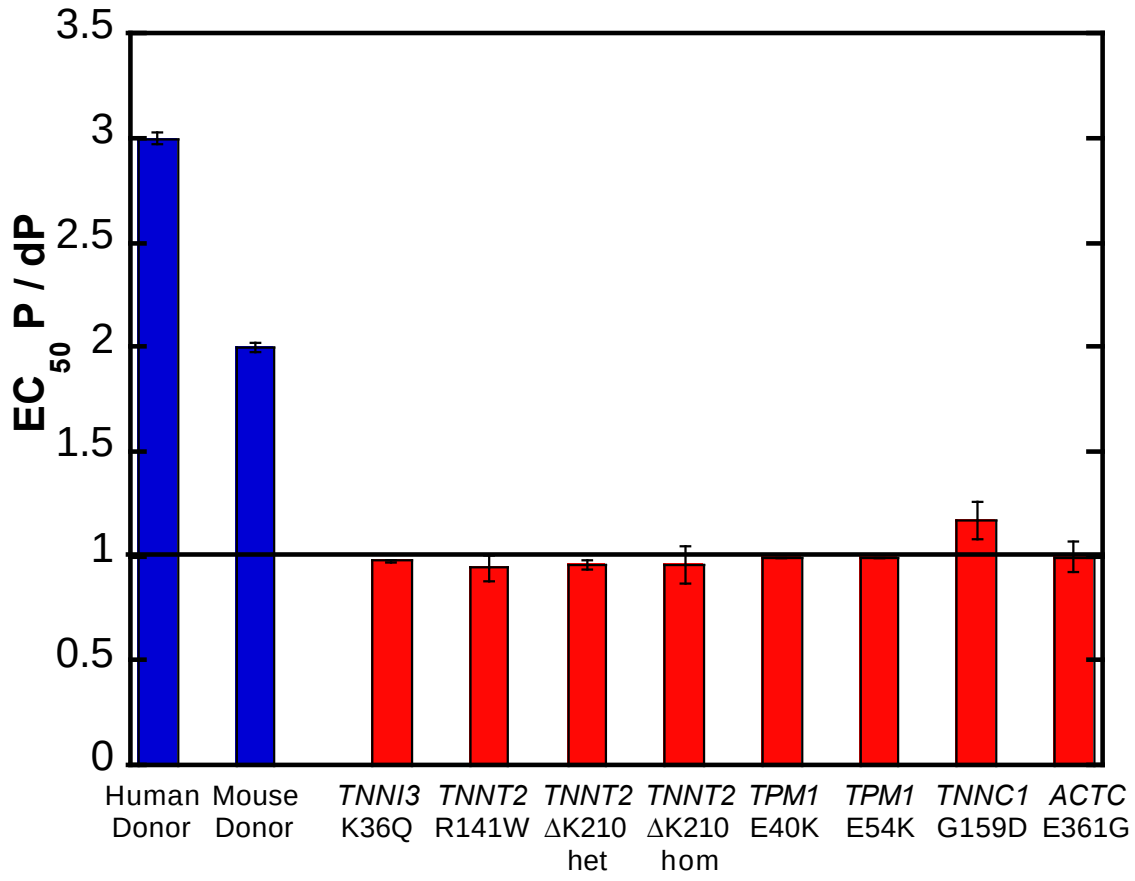


The hypothesis formulated in Chapter 3 proposed that the DCM mutation uncouples the ability of TnI to modulate the Ca^{2+}-sensitivity according to its phosphorylation level.
The N-terminal extension of cTnI can be phosphorylated on serines 22 and 23 by PKA in order to decrease the troponin's affinity to Ca^{2+}.

The results of this chapter all confirm this hypothesis. As visible in Figure 4.33, the normal difference in Ca^{2+}-sensitivity produced by both human and mouse donor cardiac troponin is completely blunted by the presence of a DCM mutation.

For the mutations on cardiac actin and α-tropomyosin we can assume that the uncoupling is a direct consequence of the mutation, as the troponin used was otherwise behaving normally. Another study investigating the functional properties of rare TnC mutants found a reduced or abolished effect on the Ca^{2+}-sensitivity following PKA phosphorylation (Pinto et al., 2011).

Figure 4.33: Percentage motile EC_{50} ratios for donor and mutant thin filaments comparing phosphorylated and dephosphorylated troponin



The dose-dependency experiment demonstrated how even sub-stoichiometric mutant protein in the thin filament can induce the uncoupling. In the case of α-tropomyosin E40K it was seen that with just 12.5% of it in the mix the ratio was reduced to half of that seen with just WT α-tropomyosin, and between 40 to 60% of mutant protein, which corresponds to the ratios measured in human and mouse samples, the uncoupling was almost complete. This indicates how the heterozygous genotype can produce a dominant phenotype in a cooperative multiprotein complex as the thin filament (Fraser and Marston, 1995, Maytum et al., 1999, Lehrer and Geeves, 1998) with a poison peptide in any component of the thin filament allosterically inducing uncoupling.

4.5.3 A Potential Structural Mechanism Inducing DCM

In section 1.3.2.1 I have explained how the N-terminal extension of cardiac troponin I interacts with the N-lobe of cardiac troponin C increasing its affinity for Ca^{2+}, and how PKA phosphorylation on residues 22/23 of this extension determines the breakage of this interaction.

The data presented suggest that most of the mutants induce a lower or equal Ca^{2+}-sensitivity compared to the wild type and that this sensitivity is irresponsive to changes in the phosphorylation level. All this could be the result of a default state induced allosterically by the mutation in which the N-terminal extension of TnI is not able to interact anymore with the N-lobe of TnC, just as if it was consistently phosphorylated. This allosteric mechanism could have variants that induce a higher or lower Ca^{2+}-sensitivity in the thin filaments but still being unresponsive to variation in TnI phosphorylation.

4.5.4 Physiological Consequences of the Uncoupling

The outcome of this molecular mechanism would be an impairment in the ability of the myofiber to relax at a faster rate (lusitropy) when the muscle gets β-adrenergic stimulation. The increased rate of Ca^{2+} dissociation from TnC is in fact regulated by PKA phosphorylation, which in turn is activated as a consequence of β-adrenergic stimulation.

It is very likely that under conditions of stress the uncoupling of these functions would generate contractile dysfunction and, in the long term, DCM due to a reduced cardiac reserve. Many mouse models of DCM mutants, including α-actin E361G, cTnT ΔK210 and α-tropomyosin E54K, showed a significantly reduced response to acute β-adrenergic agonists (Song et al., 2010, Du et al., 2007, Rajan et al., 2007).

It is possible that the absolute change in Ca^{2+}-sensitivity contributes to the development of the DCM phenotype, but it does not seem to be necessary, as the mutations E361G on actin and E54K on α-tropomyosin had the uncoupling as the only abnormality.

We therefore propose that the uncoupling blunts the response to β-adrenergic stimulation in DCM patient hearts, that this reduces the cardiac reserve and that this could be sufficient to cause the DCM phenotype in the long term.

5 Functional Investigation of β- and γ-tropomyosin Mutants Leading to the Development of Nemaline Myopathy, Cap Disease and Congenital Fibre Type Disproportion

5.1 Introduction on the β- and γ-tropomyosin Mutants Linked to Nemaline Myopathy (NM), Cap Disease (CD) and Congenital Fibre type Disproportion (CFTD)

As already described in section 1.5, NM, CD and CFTD are three congenital myopathies with histological markers enabling the diagnosis of each one, but have wide genetic overlap and some mutations have been linked to the development of more than one type of histology.
In this thesis 6 β-tropomyosin and 5 γ-tropomyosin mutants have been investigated through quantitative IVMA (Figure 5.1). To date, most of these mutants have not had any functional work published on them.

5.1.1 Six β-tropomyosin Mutants

ΔK7 β-tropomyosin is a novel (nothing is published on it yet) recurrent autosomal dominant mutation developing nemaline rods in the skeletal myocytes of patients from 5 unrelated families studied by Dr N. Clarke. Three of these families had very likely *de novo* occurrence of the mutation. The patients were diagnosed with Nemaline myopathy for this reason, but the physiological symptoms were quite different from those of a congenital myopathy. They presented prominent muscle weakness in adulthood with onset sometimes in adolescence, but what differentiates them were quite generalised muscle contractures in childhood. Most

patients remained ambulant but often with reduced stamina and myalgias. All patients had normal cardiac function. Muscle biopsy was performed on 7 patients, mostly in mid-adulthood and three frozen muscle biopsies were also available for further analysis. By light and electron microscopy examination, all biopsies showed numerous, small, scattered nemaline bodies in over 50% of muscle fibres, often with sub-sarcolemmal accumulations. Most biopsies showed marked variation in fibre size, a tendency to type 1 fibre atrophy and type 1 fibre predominance (> 55%).

The E41K mutation in β-tropomyosin has been described in a family in which both the mother and her daughter were affected (Tajsharghi et al., 2007). They both had slowly progressive muscle weakness and type 1 fibres uniformity with variability in size, but the daughter presented cap-like structures, whereas the mother in a biopsy when she was 57 had cap-like structures with nemaline rods well visible inside. On a biopsy taken when 32 the mother did not show any inclusions. Functional studies performed on this mutant highlighted a decrease in the speed of contraction in high Ca^{2+}, in the unloaded shortening speed and in the Ca^{2+}-sensitivity (Ochala et al., 2008).

ΔK49 β-tropomyosin was described in a single patient with muscle weakness onset at the age of 8 and with healthy parents and brothers (Ohlsson et al., 2008). Two muscle biopsies were taken when he was 15 and 30, indicating uniformity of type 1 fibres. Only the second one showed cap-like structures. At 42 was still able to deambulate short distances and had normal cardiac function.

ΔE139 was the first β-tropomyosin mutant associated with Cap disease (Lehtokari et al., 2007). It was reported to be a *de novo* mutation in a patient with generalised muscle weakness, hypotonia and many cap-like structures in hypotrophic type 1 fibres, but also few of them in hypertrophic type 2 fibres. The mutation was predicted through a bioinformatical

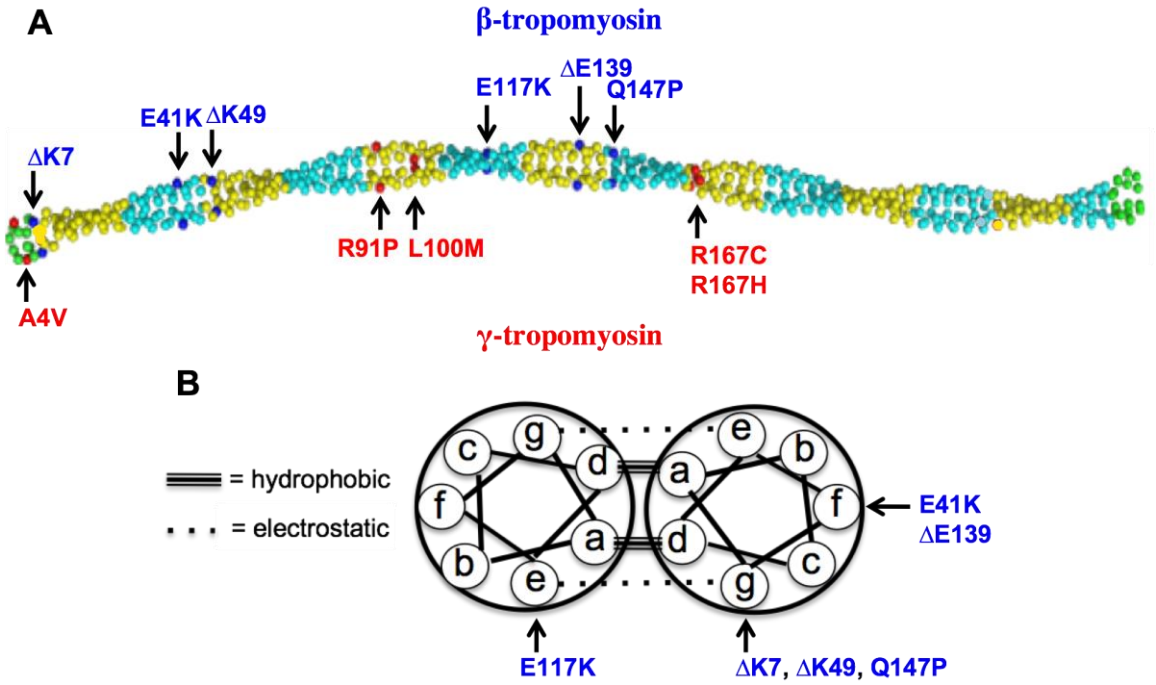
programme to disrupt only locally (~ 15 amino acids) the coiled-coil interactions, thus indicating the other tropomyosin's interactions as more likely to be involved in the genesis of the disease.

Q147P and E117K β-tropomyosin mutants have been described in the same work by Donner *et al.* (2002).

Q147P is a mutation in exon 4 of β-tropomyosin found in a single patient with 7 healthy siblings and parents. She had walking difficulties when 12 and when adult was diagnosed with Nemaline myopathy. Muscle biopsy showed predominance and selective hypotrophy of type 1 fibres with peripheral aggregates of rods.

E117K β-tropomyosin was describe through a study made on a family in which a mother and her son were diagnosed with Nemaline myopathy. None of the parents of the mother were carrying the mutation and were healthy. The son had severe hypotonia at birth, motor milestones delayed and both him and his mother were never able to run. Muscle biopsy at 4 years old, though, never showed Nemaline bodies. It showed increase in number and hypotonia of type 1 fibres, which would indicate CFTD, but as it has been seen with other patients this would not exclude the possibility to develop rods or caps later in age, as much as having them present already in fibres from different muscles.

Figure 5.1: Positions of the β- and γ-tropomyosin mutations on the molecule



A) Positions of the β- (blue) and γ-tropomyosin (red) mutations on the dimer. Residues on the α-zones are in yellow, whereas those in the β-zones are in light-blue. In green are those involved in the end-to-end polymerisation. B) The positions of the β-tropomyosin mutants in the heptad repeat.

5.1.2 Five γ-tropomyosin Mutants

A4V and R91P γ-tropomyosin mutations have been described in a study by Lawlor *et al.* (2010) in which they screened 13 patients diagnosed with CFTD for mutations in *TPM3*. They both presented only a marked type 1 fibre disproportion with no other pathological markers.

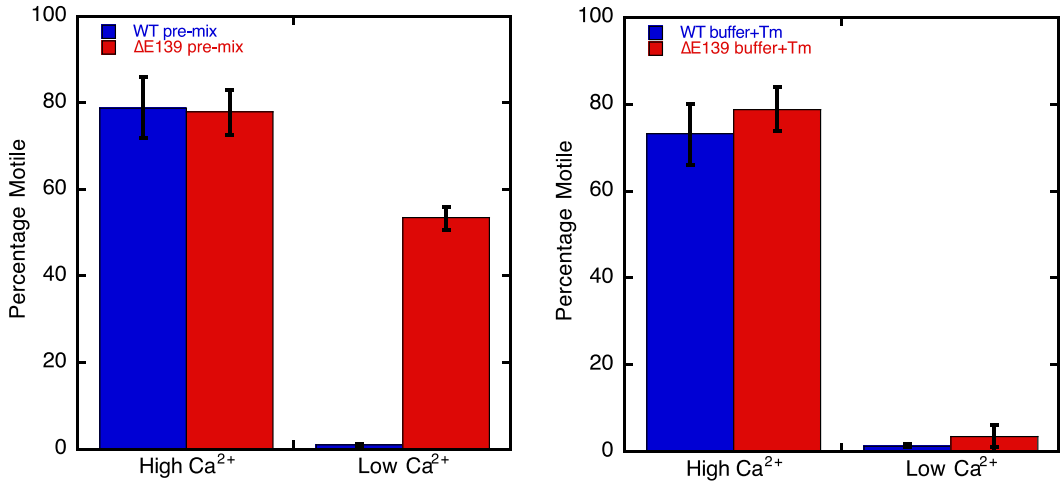
L100M γ-tropomyosins was described as consistently CFTD linked by Clarke *et al.* (2008) with observations made on a big family which did not present any other pathological marker. In the same study R167C and R167H were described as CFTD causing. As already discussed in section 1.5.4, R167 is an hotspot for mutations and both of the mutations above have been linked through different reports to more than one disease: R167C to CFTD and Cap disease (Ohlsson et al., 2009, Waddell et al., 2010), whereas R167H to CFTD, Nemaline myopathy

and Cap disease (Durling et al., 2002, Penisson-Besnier et al., 2007, Munot et al., 2010, De Paula et al., 2009).

5.2 *In Vitro* Motility Analysis of β-tropomyosin Mutants linked to Nemaline Myopathy and Cap Disease

Early stage experiments indicated two different behaviours for two sets of β-tropomyosin mutants. Wild-type β-tropomyosin proved to regulate perfectly at 60 nM, with 15-30 nM rabbit skeletal muscle troponin. E41K and E117K thin filaments showed similar Ca^{2+} regulation to the wild-type, but the other four mutants did not. Thin filaments reconstituted with ΔK7, ΔK49, ΔE139 and Q147P were not regulated in low Ca^{2+}, even when using very high tropomyosin and troponin concentration, such as 90 nM and 60 nM respectively. Higher protein concentrations are not feasible in IVMA since they inhibit filament movement non specifically. It was, therefore, deduced that the issue could be a reduced affinity for actin of these mutants, since troponin was working normally with wild-type β-tropomyosin. Usually Tm is only included in the reconstitution buffer and it remains bound despite the absence of Tm in buffers C and D (Fraser and Marston, 1995). In this case the matter could have been that mutant tropomyosin was washed out of the motility cell when it was infused with buffers C and D (see section 2.5.5). To avoid this, the standard motility cell protocol was amended by adding tropomyosin in the same concentration of the reconstitution in buffers C and D, just as was already done with troponin. This procedure proved to be effective, restoring an acceptable regulation of the filaments (Figure 5.2). All of the experiments presented in this chapter using those mutants were performed with this method.

Figure 5.2: Percentage motile bar graph in high and low Ca^{2+} for recombinant WT and ΔE139 β-tropomyosin with and without β-tropomyosin mixed in buffer C and D



Section 5.2.1 will consider only experiments with ΔK7 because of the peculiar phenotype of muscle contractures during childhood. In section 5.2.2 will be described experiments performed with E41K and E117K as they were the only two mutants with high actin affinity. Section 5.2.3, finally, will report the experiments made using ΔK49, ΔE139 and Q147P as they all showed low affinity.

5.2.1 Effects of the ΔK7 Mutation on Thin Filament Motility

The first set of experiments performed with ΔK7, were a series of three tropomyosin titrations with actin. One of these is shown in Figure 5.3, and none of them showed any difference with wild-type tropomyosin in both motile velocity and percentage motile.

When 100% ΔK7 tropomyosin was reconstituted in thin filaments with rabbit skeletal muscle actin and troponin, it proved to be very difficult to achieve a good switch off in low Ca^{2+} and only two complete Ca^{2+}-titrations were performed out of 12 trials (Figure 5.4, Table 5.1).

ΔK7 tropomyosin was always used at 60 nM and rabbit skeletal muscle troponin at 15-30 nM.

In experiment 1, ΔK7 thin filaments have a much higher Ca^{2+}-sensitivity (EC_{50} ΔK7 / WT = 0.15), but also the percentage motile at 1 nM Ca^{2+} is much higher, which could indicate that the difference in Ca^{2+}-sensitivity is due to incomplete reconstitution of the thin filaments. At 3.9 μM Ca^{2+} the percentage motile is equal. The maximum motile velocity is lower for the mutant and it does not seem to be very influenced by the increasing Ca^{2+} concentration.

Figure 5.3: Recombinant β-tropomyosin titration WT v ΔK7

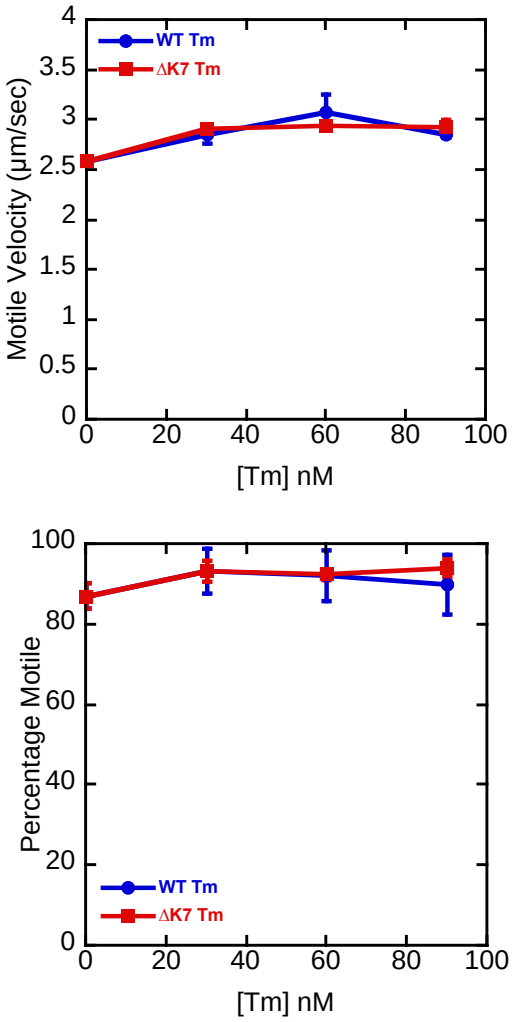
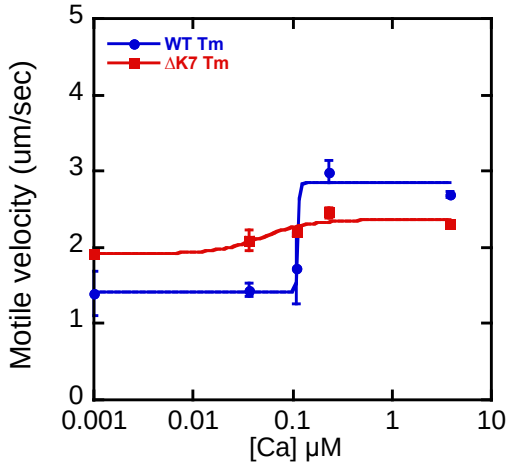
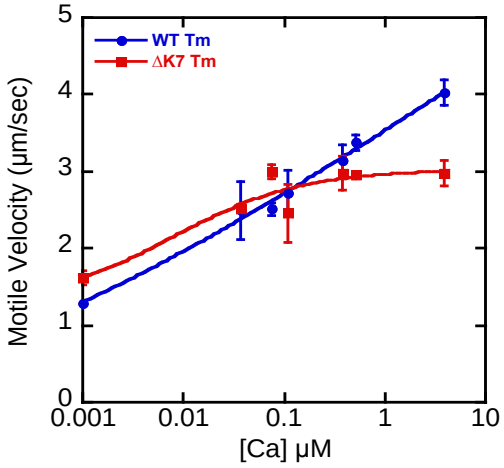


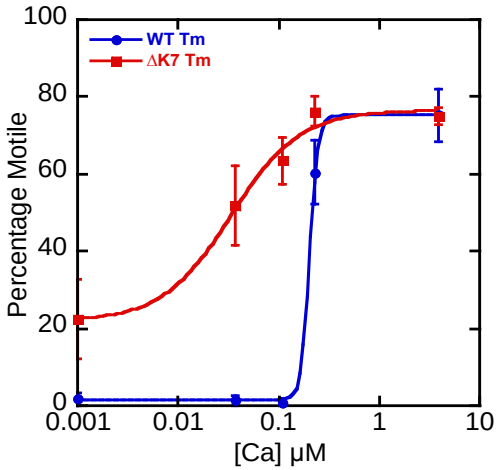
Figure 5.4: Ca^{2+}-concentration titration of recombinant human β-tropomyosin WT v 100% ΔK7 reconstituted in thin filaments with rabbit skeletal muscle troponin and actin

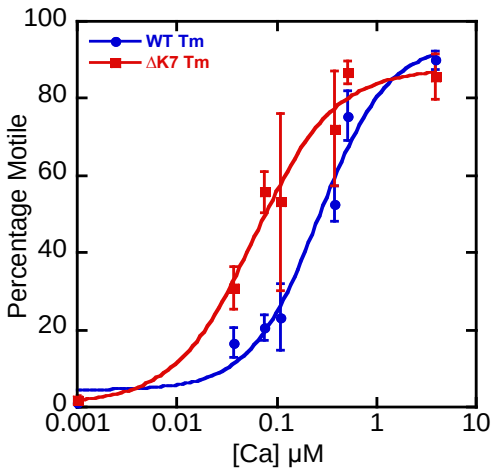
1



2







	Value	Error
Hill Coefficient	10.36	24.65
EC_{50}	0.2	0.06

	Value	Error
Hill Coefficient	1.28	0.75
EC_{50}	0.03	0.01

	Value	Error
Hill Coefficient	1.27	0.39
EC_{50}	0.27	0.08

	Value	Error
Hill Coefficient	1.09	0.42
EC_{50}	0.06	0.02

Table 5.1: Ca^{2+}-sensitivity data for recombinant β-tropomyosin WT v 100% ΔK7 thin filaments

Tm ΔK7 100% ANALYSIS	EC_{50} Percentage motility, µM		EC_{50} mutant / EC_{50} NTg	Hill coefficient n		% Motile 3.9 µM Ca^{2+}		Ca^{2+} activation of sliding speed (%)		Maximum sliding speed (µm/sec)	
EXP N	WT	ΔK7		WT	ΔK7	WT	ΔK7	WT	ΔK7	WT	ΔK7
1	0.2±0.06	0.03±0.01	0.15	(10.36)	1.28	75	75	92	21	2.99	2.45
2	0.27±0.08	0.06±0.02	0.22	1.27	1.09	90	86	212	84	4.03	2.98

Experiment 2 shows the same phenotype of experiment 1 but in this case in 1 nM Ca^{2+} a complete switch off was obtained.

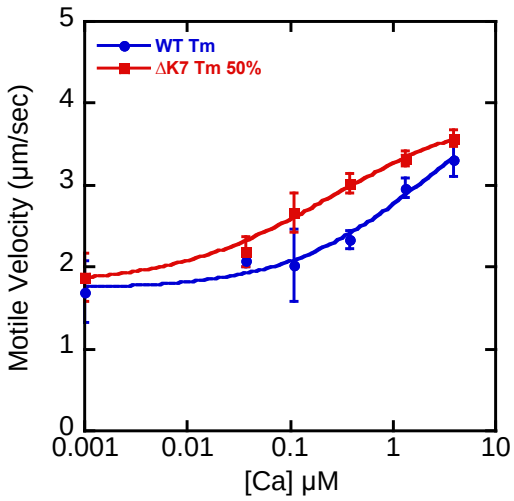
Another set of experiments was performed using a mixture of 50% wild-type and 50% ΔK7, compared with 100% wild-type. This was intended to mimic more the *in vivo* situation and the two proteins were mixed thoroughly for 30 minutes at 35° C before incubating with the other components of the thin filaments to allow the formation of heterodimers as well as homodimers as in the starting sample. The composition could not be checked but it is likely that all of the populations were represented.

Three complete Ca^{2+}-titrations were performed (Figure 5.5 and data in Table 5.2 and Table 5.3). This time the percentage motile at 1 nM Ca^{2+} was always similar or even lower to that of the wild-type, and at 3.9 µM Ca^{2+} it was very similar as well, proving good regulation of the filaments. Again the Ca^{2+}-sensitivity was higher for the mutant, with average EC_{50} ratio ΔK7 / WT = 0.42 ± 0.15. It was not statistically different due to the small n number ($p = 0.06$).

The motile velocity of every experiment was Ca^{2+}-regulated and was more Ca^{2+}-sensitive than the wild-type. The graph of experiment 1 could not give precise information on the Ca^{2+}-sensitivity for the poor fitting, but was showing the same phenotype. The maximum motile velocity of 50% ΔK7 filaments was 10% higher than the wild-type and this was statistically significant (paired, $p = 0.019$).

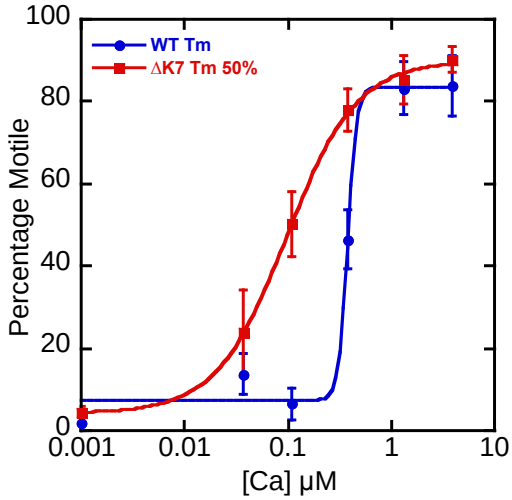
Figure 5.5: Ca^{2+}-concentration titration of recombinant human β-tropomyosin WT v 50% ΔK7 reconstituted in thin filaments with rabbit skeletal muscle troponin and actin

1



	Value	Error
Hill Coefficient	1.42	0.34
EC_{50}	0.06	0.01

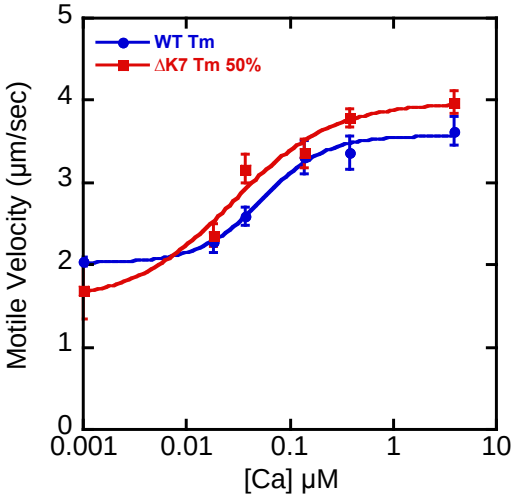
	Value	Error
Hill Coefficient	1	/
EC_{50}	0.03	0.01

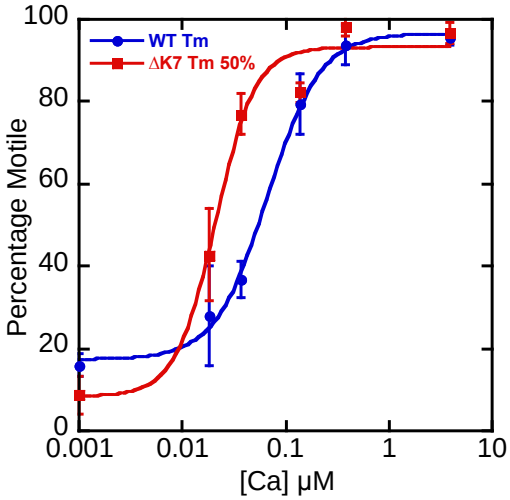


	Value	Error
Hill Coefficient	9.88	12265
EC_{50}	0.38	2.45

	Value	Error
Hill Coefficient	1.28	0.1
EC_{50}	0.1	0.01

2

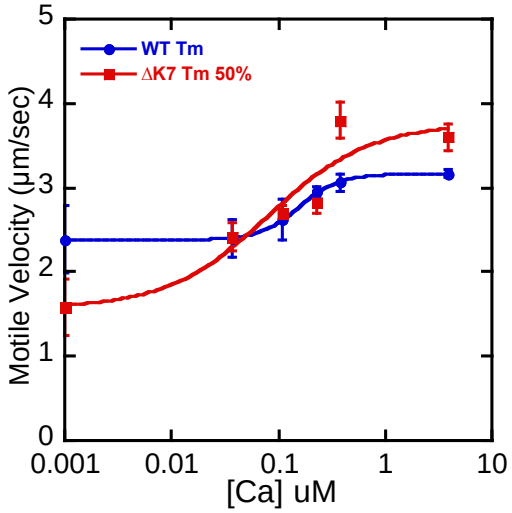




	Value	Error
Hill Coefficient	1.71	0.22
EC_{50}	0.07	0.01

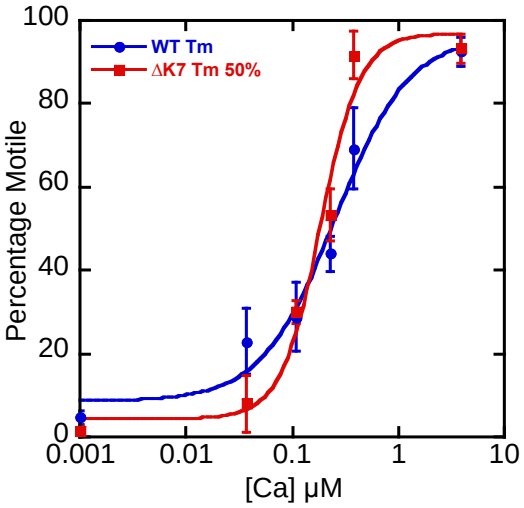
	Value	Error
Hill Coeficient	2.27	1.06
EC_{50}	0.02	0.01

3



	Value	Error
Hill Coefficient	2.34	0.19
EC_{50}	0.16	0.01

	Value	Error
Hill Coefficient	1	/
EC_{50}	0.08	0.08



	Value	Error
Hill Coefficient	1.26	0.57
EC_{50}	0.25	0.08

	Value	Error
Hill Coefficient	2.33	0.93
EC_{50}	0.18	0.04

Table 5.2: Ca^{2+}-sensitivity data for recombinant β-tropomyosin WT v 50% ΔK7 thin filaments motile velocity

Tm ΔK7 50% ANALYSIS	EC_{50} Sliding speed, µM		EC_{50} mutant/ EC_{50} NTg	Ca^{2+} activation of sliding speed (%)		Maximum sliding speed (µm/sec)	
EXP N	WT	ΔK7		WT	ΔK7	WT	ΔK7
1	/	/	/	95	90	3.31	3.57
2	0.06±0.01	0.03±0.01	0.5	78	136	3.63	3.98
3	0.16±0.01	0.08±0.08	0.5	33	128	3.17	3.6
MEAN±SE	0.11±0.05	0.06±0.03	0.5	69±18	118±14	3.37±0.14	3.72±0.13
Student's t-test (paired)						p=0.019	
(unpaired)						p=0.14	

Table 5.3: Ca^{2+}-sensitivity data for recombinant β-tropomyosin WT v 50% ΔK7 thin filaments percentage motile

Tm ΔK7 50% ANALYSIS	EC_{50} Percentage motility, µM		EC_{50} mutant / EC_{50} Donor	Hill coefficient n		% Motile 3.9 µM Ca^{2+}	
EXP N	WT	ΔK7		WT	ΔK7	WT	ΔK7
1	0.38±2.45	0.10±0.01	0.26	(9.88)	1.28	84	90
2	0.07±0.01	0.02±0.01	0.29	1.71	2.27	96	97
3	0.25±0.08	0.18±0.04	0.72	1.26	2.33	93	93
MEAN±SE	0.23±0.09	0.1±0.05	0.42±0.15	1.49±0.23	1.96±0.34	91±4	93±2
Student's t-test (paired)	p=0.21		single group, p=0.06 (compared with one)				
(unpaired)	p=0.26						

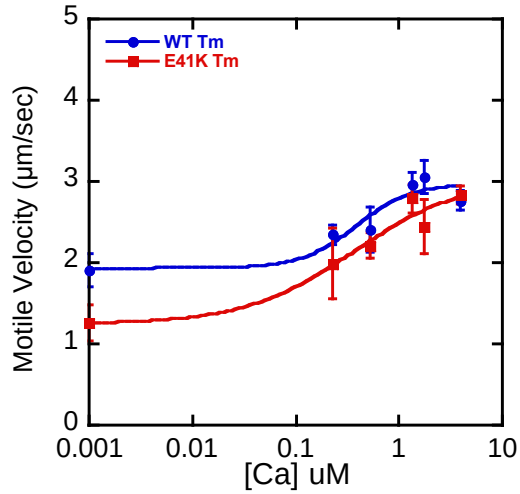
5.2.2 Effects of the E41K and E117K Mutation on Thin Filaments Motility

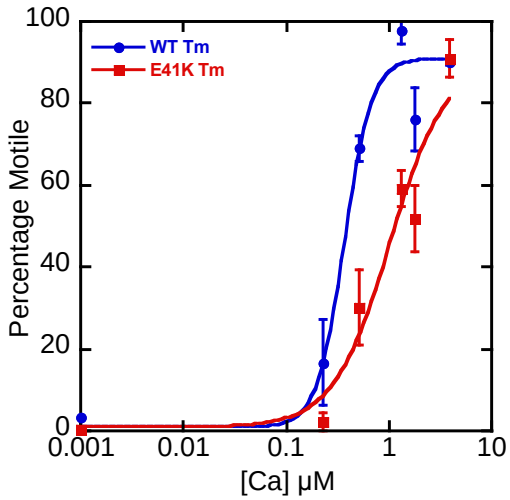
Thin filaments containing the β-tropomyosin mutations E41K and E117K were regulated by Ca^{2+}, causing a complete switch off of their motility at low Ca^{2+} concentration, and did not show any evidence of reduction of the mutant's affinity for actin. In the following experiments, if not differently stated, β-tropomyosin was used at 60 nM and rabbit skeletal muscle troponin at 15-30 nM.

The tropomyosin E41K mutation is an exception as it has been reported to cause the formation of nemaline rods inside the cap structure. Since it bound normally in thin filaments in the *in vitro* motility assay two complete Ca^{2+} titration were recorded (Figure 5.6). The results are very marked in terms of Ca^{2+}-sensitivity. It should be noticed that its switch off at low Ca^{2+} was very good, indicating an intact regulatory system, but the activation in Ca^{2+} had the tendency of being much reduced. The mutation seems to determine a much lower Ca^{2+}-sensitivity for the thin filaments reconstituted with that tropomyosin than when compared with the wild type. This effect was even more highlighted when we raised the tropomyosin concentration higher, to 80nM (Figure 5.8). It was evident that E41K β-tropomyosin containing thin filaments were only partially activated, even at fully activating Ca^{2+}-concentrations. Subsequently to these findings, a tropomyosin titration on plain actin was performed, to screen whether these effects were visible also in the absence of troponin, but as it can be observed in Figure 5.7, there does not seem to be any relevant difference in both motile velocity and percentage motile compared to wild-type β-tropomyosin. Therefore the effect is mediated by troponin.

Figure 5.6: Ca^{2+}-concentration titration of recombinant human β-tropomyosin WT v E41K reconstituted in thin filaments with rabbit skeletal muscle troponin and actin

1

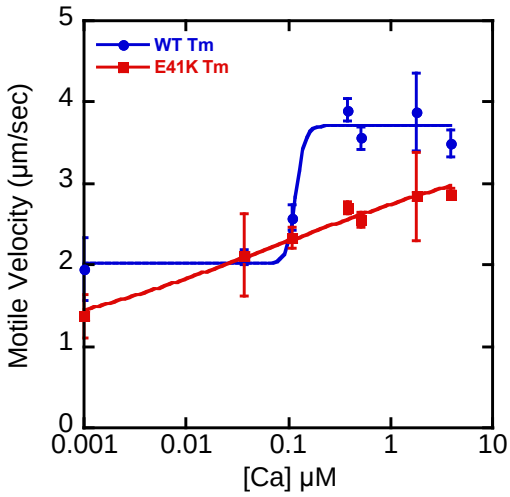


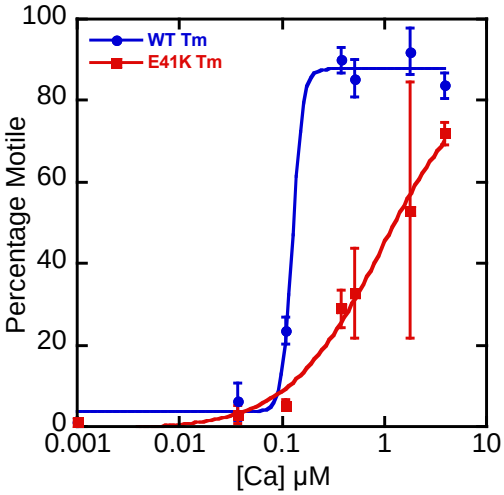


	Value	Error
Hill Coefficient	3.31	0.99
EC_{50}	0.37	0.04

	Value	Error
Hill Coefficient	1.58	0.42
EC_{50}	1.02	0.17

2





	Value	Error
Hill Coefficient	8.61	642.61
EC_{50}	0.13	1.29

Figure 5.7: Recombinant β-tropomyosin titration WT v E41K

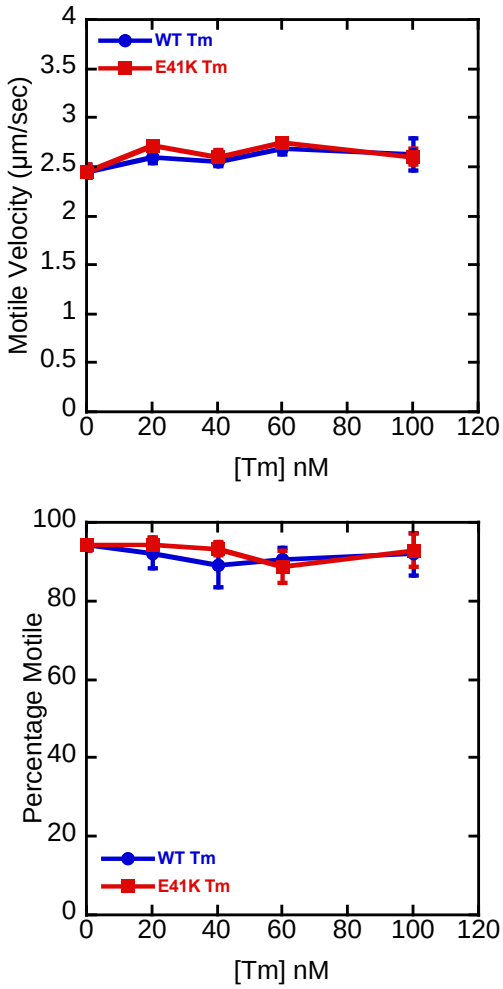
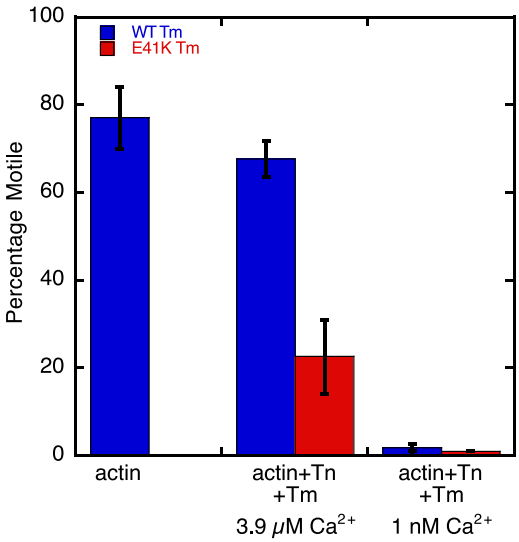


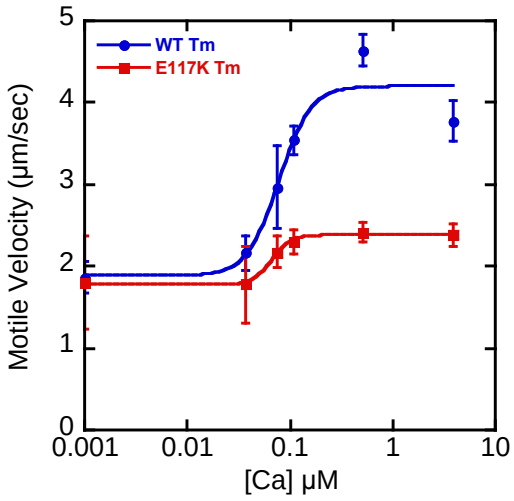
Figure 5.8: Switch off effect on the percentage motile of E41K β-tropomyosin highly concentrated at 3.9 µM Ca^{2+}

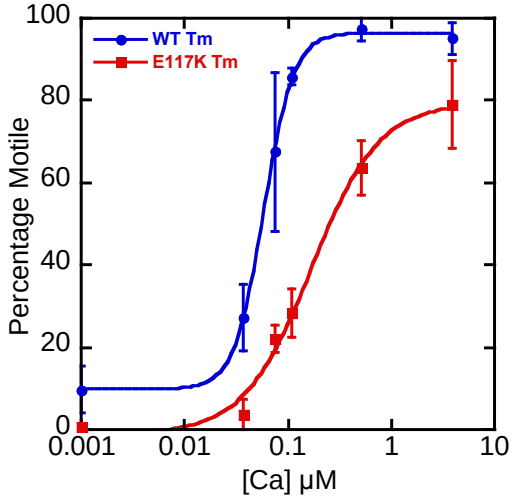


Four Ca^{2+} curves were recorded with E117K tropomyosin (experiment 1 and 4 in Figure 5.9, the others in APPENDIX; data in Table 5.4). In comparison with wild-type thin filaments, motility was generally lower, with less motility at relaxing Ca^{2+} concentration, whilst in high Ca^{2+} it did not reach over 88% motile, while the wild type reached always more than 95% (statistically significant, paired p = 0.007, unpaired p = 0.0005). The motile velocity showed some regulation in the Ca^{2+}-dependent increase of the sliding speed, but it was substantially less than that of the wild type tropomyosin (unpaired p = 0.015). Also the maximum sliding speed was significantly lower (paired p = 0.024, unpaired p = 0.001). In addition, the Ca^{2+}-sensitivity of the percentage motile was much lower (EC_{50} E117K / WT = 2.43 ± 0.35, p = 0.026).

Figure 5.9: Ca^{2+}-concentration titration of recombinant human β-tropomyosin WT v E117K reconstituted in thin filaments with rabbit skeletal muscle troponin and actin

1

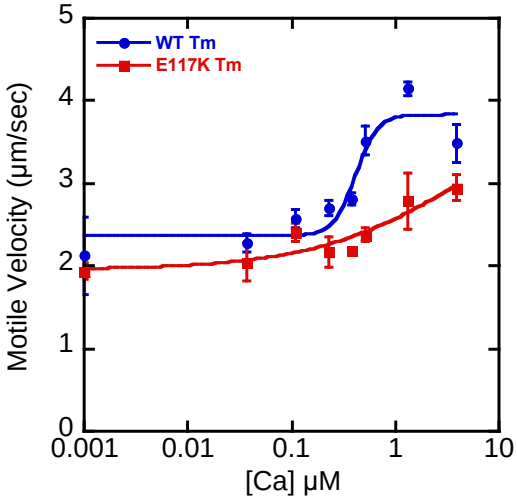


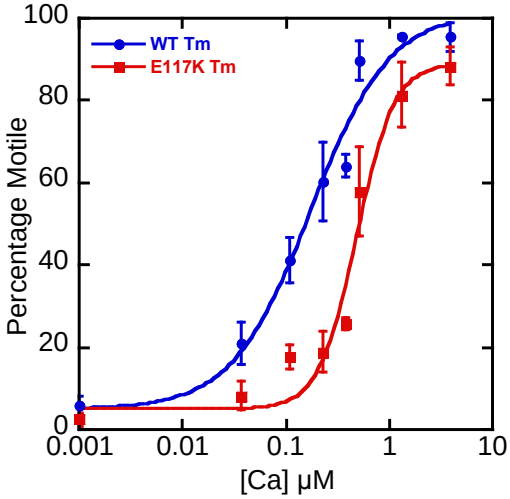


	Value	Error
Hill Coefficient	3.04	0.15
EC_{50}	0.06	0.01

	Value	Error
Hill Coefficient	1.34	0.28
EC_{50}	0.17	0.04

4





	Value	Error
Hill Coefficient	1.15	0.25
EC_{50}	0.18	0.04

	Value	Error
Hill Coefficient	2.4	0.78
EC_{50}	0.48	0.07

Table 5.4: Ca^{2+}-sensitivity data for recombinant β-tropomyosin WT v E117K thin filaments

Tm E117K ANALYSIS	EC_{50} Percentage motility, μM		EC_{50} mutant / EC_{50} NTg	Hill coefficient n		% Motile 3.9 μM Ca^{2+}		Ca^{2+} activation of sliding speed (%)		Maximum sliding speed (μm/sec)	
EXP N	WT	E117K		WT	E117K	WT	E117K	WT	E117K	WT	E117K
1	0.06±0.01	0.17±0.04	2.83	3.04	1.34	95	79	102	32	3.78	2.38
2	0.11±0.01	0.31±0.05	2.82	3.93	5.78	97	79	123	0	4.2	2.39
3	0.1±0.03	0.14±0.02	1.4	1.58	6.71	97	81	128	62	3.79	2.84
4	0.18±0.04	0.48±0.07	2.67	1.15	2.4	96	88	64	52	3.49	2.95
MEAN±SE	0.11±0.02	0.28±0.08	2.43±0.35	2.43± 0.64	4.06± 1.3	96±1	82±2	104±15	37±14	3.82±0.15	2.64±0.15
Student's t-test (paired)	p=0.06		single group, p=0.026 (compared with one)			p=0.007		p=0.058		p=0.024	
(unpaired)	p=0.09					p=0.0005		p=0.015		p=0.001	

5.2.3 Effects of the ΔK49, ΔE139 and Q147P Mutation on Thin Filament Motility

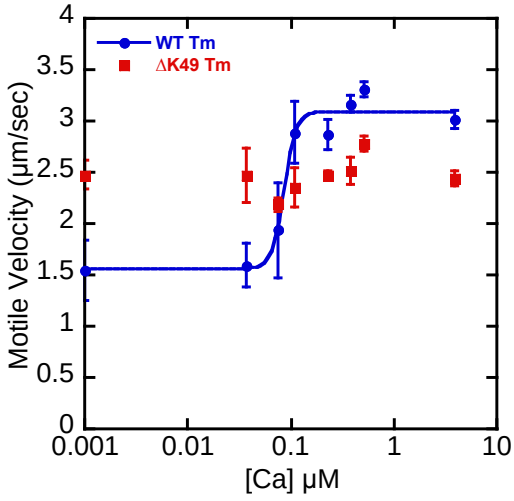
These three mutants all showed a reduced affinity to actin and needed the revised protocol of cell infusion with tropomyosin mixed to buffers C and D to achieve regulation (see section 5.2). In the following experiments the concentration of β-tropomyosin used was 60 nM and that of rabbit skeletal muscle troponin was 15-30 nM.

ΔK49 and ΔE139 are linked to genesis of the Cap Disease. Two complete Ca^{2+}-titrations were performed for both of them; ΔK49 titrations are shown in Figure 5.10, with data in Table 5.5; ΔE139 titrations are shown in Figure 5.11, with data in Table 5.6.

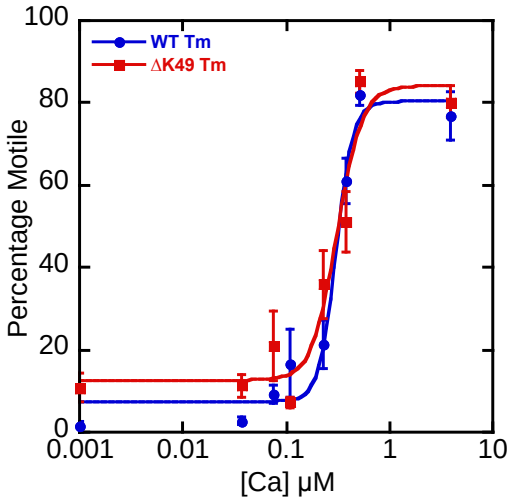
ΔK49 seemed to have a slightly higher Ca^{2+}-sensitivity than the wild-type (EC_{50} ΔK49 / WT = 0.83 ± 0.2), but in one of the two titrations the EC_{50} was actually almost equal to that of the wild-type and in none of the two the ΔK49 thin filaments were switching off to the same level of the wild-type. The maximum sliding speed was 28% lower than the wild-type and in both the titrations was too variable to get a good fitting.

Figure 5.10: Ca^{2+}-concentration titration of recombinant human β-tropomyosin WT v ΔK49 reconstituted in thin filaments with rabbit skeletal muscle troponin and actin

1



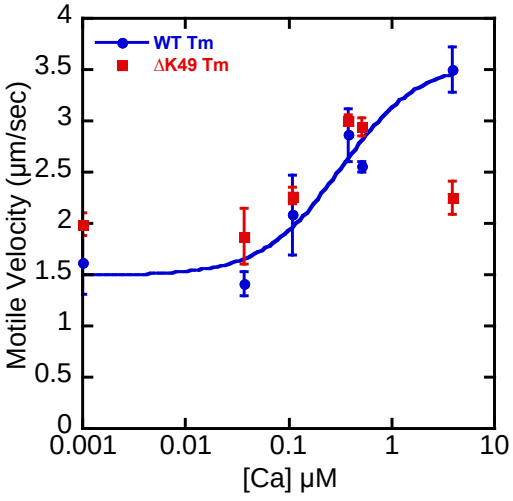
	Value	Error
Hill Coefficient	7.51	2.97
EC_{50}	0.09	0.01



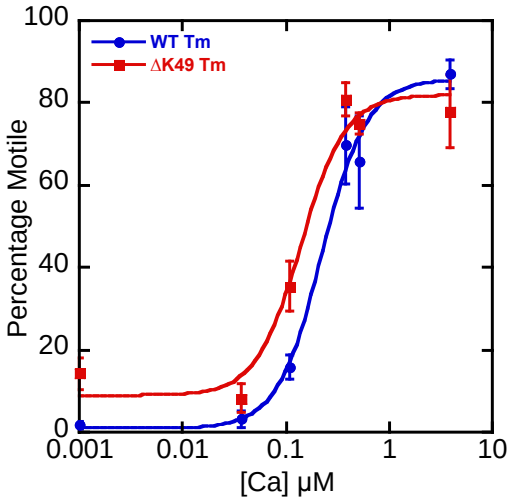
	Value	Error
Hill Coefficient	5.36	1.78
EC_{50}	0.3	0.03

	Value	Error
Hill Coefficient	3.62	1.7
EC_{50}	0.31	0.05

2



	Value	Error
Hill Coefficient	1.14	0.84
EC_{50}	0.32	0.21



	Value	Error
Hill Coefficient	2.03	0.56
EC_{50}	0.22	0.04

	Value	Error
Hill Coefficient	2	/
EC_{50}	0.14	0.03

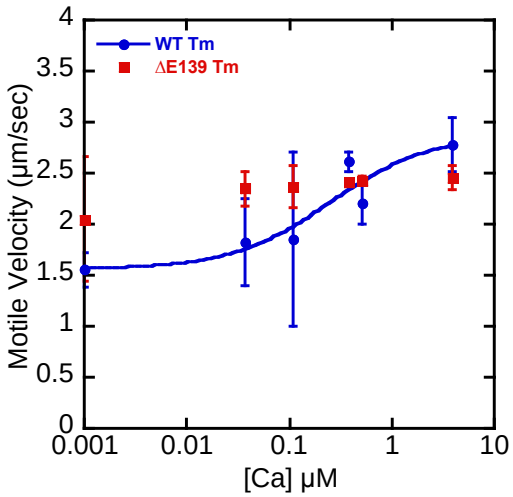
Table 5.5: Ca^{2+}-sensitivity data for recombinant β-tropomyosin WT v ΔK49 thin filaments

Tm ΔK49 ANALYSIS	EC_{50} Percentage motility, μM		EC_{50} mutant / EC_{50} NTg	Hill coefficient n		% Motile 3.9 μM Ca^{2+}		Ca^{2+} activation of sliding speed (%)		Maximum sliding speed (μm/sec)	
EXP N	WT	ΔK49		WT	ΔK49	WT	ΔK49	WT	ΔK49	WT	ΔK49
1	0.3±0.03	0.31±0.05	1.03	5.36	3.62	77	80	96	0	3.02	2.45
2	0.22±0.04	0.14±0.03	0.64	2.03	2	87	78	116	13	3.5	2.25
MEAN±SE	0.26±0.04	0.23±0.09	0.84±0.2	3.7± 1.67	2.81± 0.81	82±5	79±1	106±10	6.5±6.5	3.26±0.24	2.35±0.1

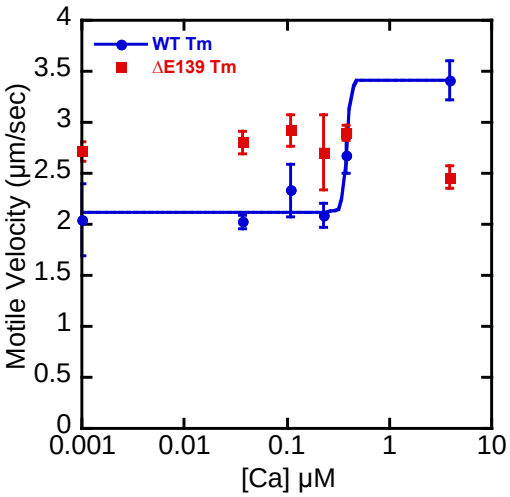
ΔE139 filaments had a similar phenotype, with a higher Ca^{2+}-sensitivity (EC_{50} ΔE139 / WT = 0.66 ± 0.24) and a 21% lower maximum sliding speed. The motile velocity seemed also to be unaltered by the different Ca^{2+} concentrations and could not be fitted with the Hill equation.

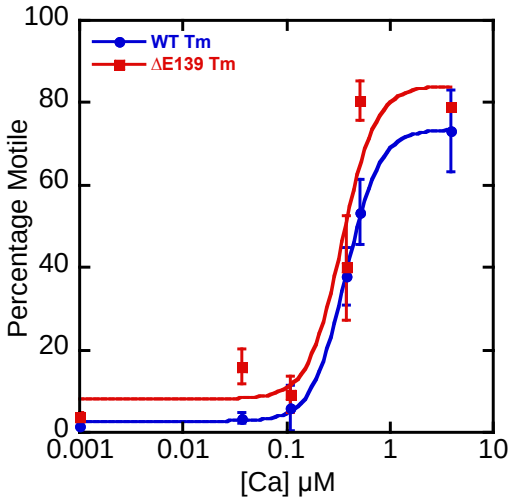
Figure 5.11: Ca^{2+}-concentration titration of recombinant human β-tropomyosin WT v ΔE139 reconstituted in thin filaments with rabbit skeletal muscle troponin and actin

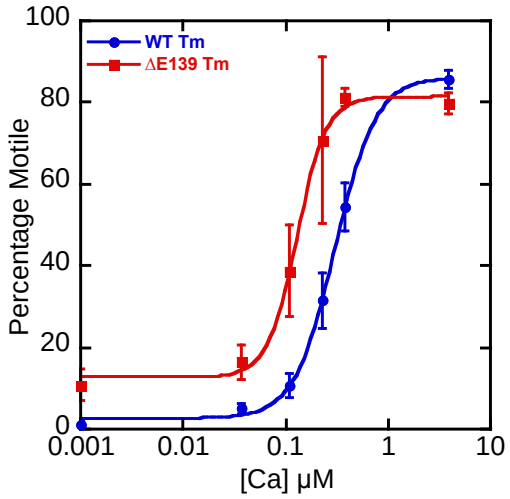
1



2







	Value	Error
Hill Coefficient	2.7	/
EC_{50}	0.38	0.01

	Value	Error
Hill Coefficient	2.7	/
EC_{50}	0.34	0.09

	Value	Error
Hill Coefficient	2.2	0.18
EC_{50}	0.31	0.01

	Value	Error
Hill Coefficient	3.02	0.6
EC_{50}	0.13	0.01

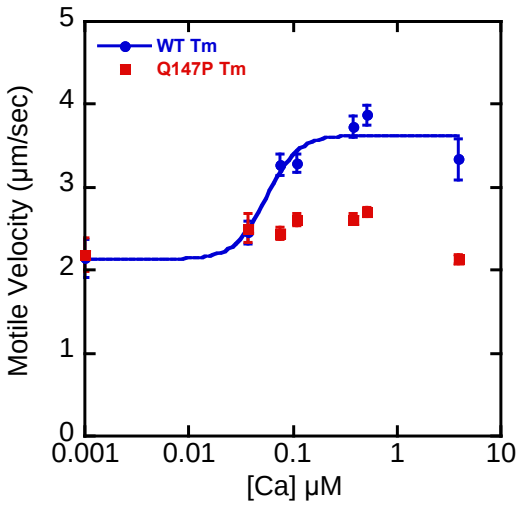
Table 5.6: Ca^{2+}-sensitivity data for recombinant β-tropomyosin WT v ΔE139 thin filaments

Tm ΔE139 ANALYSIS	EC_{50} Percentage motility, μM		EC_{50} mutant / EC_{50} NTg	Hill coefficient n		% Motile 3.9 μM Ca^{2+}		Ca^{2+} activation of sliding speed (%)		Maximum sliding speed (μm/sec)	
EXP N	WT	ΔE139		WT	ΔE139	WT	ΔE139	WT	ΔE139	WT	ΔE139
1	0.38±0.01	0.34±0.09	0.89	2.7	2.7	73	79	78	20	2.78	2.46
2	0.31±0.01	0.13±0.01	0.42	2.2	3.02	86	80	67	0	3.42	2.46
MEAN±SE	0.35±0.04	0.24±0.11	0.66±0.24	2.45± 0.25	2.86± 0.16	80±7	80±1	73±6	10±10	3.1±0.32	2.46

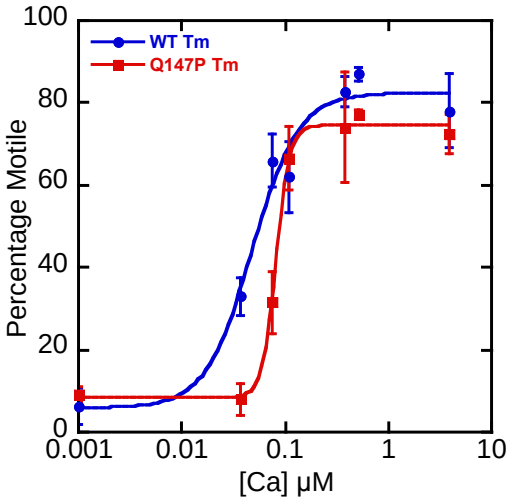
Q147P is a mutation linked to Nemaline myopathy. Only one complete Ca^{2+}-titration could be performed with it, as it was particularly difficult to achieve a switch off.

This titration suggested a lower Ca^{2+}-sensitivity for the mutant protein, with EC_{50} Q147P / WT = 1.6. The maximum sliding speed, even for this mutant, was much lower than the wild-type (36%) and there was no Ca^{2+}-dependent increase in the sliding speed.

Figure 5.12: Ca^{2+}-concentration titration of recombinant human β-tropomyosin WT v Q147P reconstituted in thin filaments with rabbit skeletal muscle troponin and actin



	Value	Error
Hill Coefficient	2.83	1.61
EC_{50}	0.06	0.02



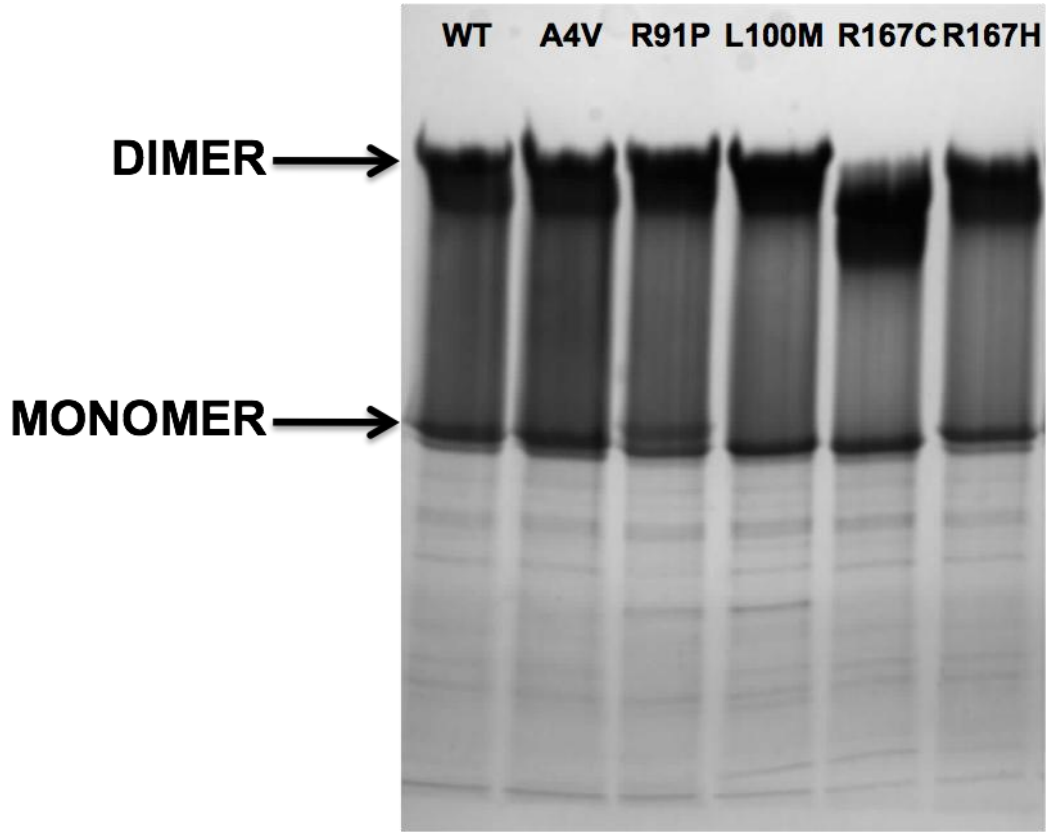
	Value	Error
Hill Coefficient	1.94	0.72
EC_{50}	0.05	0.01

	Value	Error
Hill Coefficient	6.59	0.9
EC_{50}	0.08	0.01

5.3 Effects of γ-tropomyosin Mutations on thin Filaments Motility

Purification of recombinant human γ-tropomyosin expressed with the baculovirus/*sf9* system proved to be different from that obtained with α- and β-tropomyosin. For the latter two, the SDS-PAGE gel lanes of the purified sample was showing just one well defined band, while for γ-tropomyosin it had a smear starting from the molecular weight of the dimer and ending at the molecular weight of the monomer (Figure 5.13). This was the case for the wild-type TPM3 sample and for all of the other mutants, indicating a partial covalent dimerisation of the γ-tropomyosin as it did not denature in monomers when boiled with SDS. Considering the possibility that a disulfide bond was causing the abnormal electrophoretic migration, the γ-tropomyosin sample was left for 1 hour at 50° C in 50 mM DTT. A SDS-PAGE gel run with this sample proved that this treatment had no effect, as the dimer band and the smear were still present and the ratios were maintained.

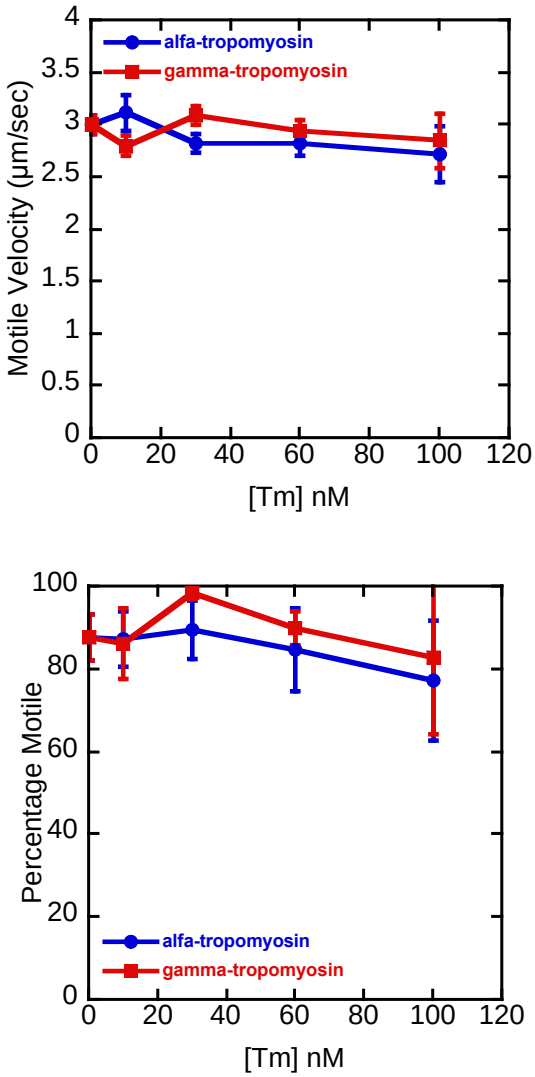
Figure 5.13: SDS-PAGE gel of pure γ-tropomyosin WT and mutants



SDS-PAGE gel of pure γ-tropomyosin WT and mutants. It is evident how the end product is not just monomeric tropomyosin, thus indicating the presence of a covalent bond tying the dimer.

A tropomyosin titration was performed comparing recombinant baculovirus/*sf9* TPM1 and TPM3, reconstituted with 10 nM (Figure 5.14). Except for the 10 μM point, in which α-tropomyosin has the same percentage motile of γ- and 10% more motile velocity, all the other points have 4-9% higher velocity and 6-9% higher percentage for γ-tropomyosin.

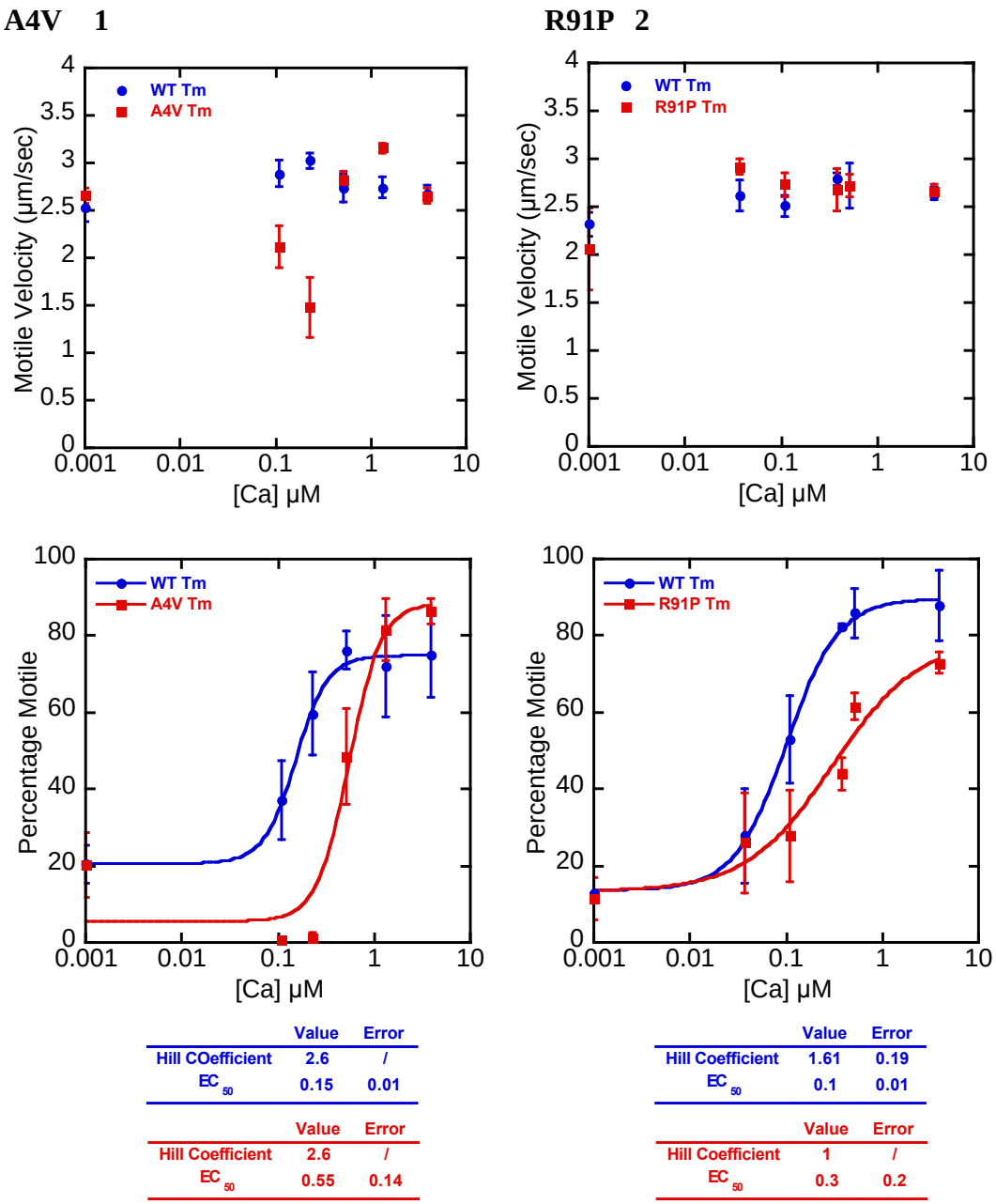
Figure 5.14: Recombinant wild-type TPM1 v TPM3 titration



When reconstituted with skeletal troponin it was very difficult to find optimal conditions of switch off and on for both the wild-type and the mutants. With lower than usual rabbit skeletal muscle troponin, like 15 nM, it was switching all the filaments to the off state, with no switch on at all. At that same concentration of troponin α- and β- tropomyosin would have got perfect regulation, γ-tropomyosin filaments, instead, were unable to move in high Ca^{2+}. Concentrations between 3-10 nM of troponin and 40 nM γ-tropomyosin were used. Furthermore when regulation was achieved it was only temporarily. In fact, the regulation was visible only for the first 1 or 2 minutes after the cell was positioned on the setup. After that time the filaments gradually started moving and losing regulation, getting to almost 100% percentage motile by the third or fourth minute of the experiment.

The experiments showed in Figure 5.15 are one example of Ca^{2+}-titration for each of the 5 mutants investigated in IVMA. All of the experiments performed are summarised in Table 5.7. The recordings were all made from after 30 seconds since positioning of the motility cell on the set up, to warm them up to 28° C, and no later than 2 minutes. This method was intended to keep the recordings inside the timeframe of regulation, but it was probably quite arbitrary. Nevertheless the indication given by this set of 13 experiments is that all of these mutants share a lower Ca^{2+}-sensitivity compared to the wild type. In fact the absolute value for the percentage motile of one of the reconstitutions may vary during the experiment, but it still keeps a constant relationship compared to the other reconstitution. The two sides of the cell, in fact, seemed to lose regulation equally at the same time.

Figure 5.15: Ca^{2+}-concentration titration of recombinant human γ-tropomyosin wild-type v mutant reconstituted in thin filaments with rabbit skeletal muscle troponin and actin



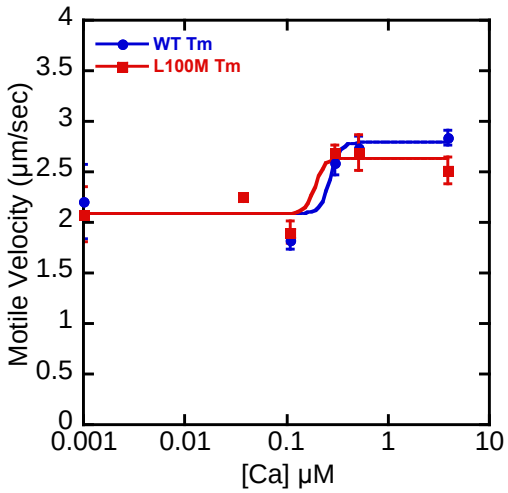
	Value	Error
Hill COefficient	2.6	/
EC_{50}	0.15	0.01

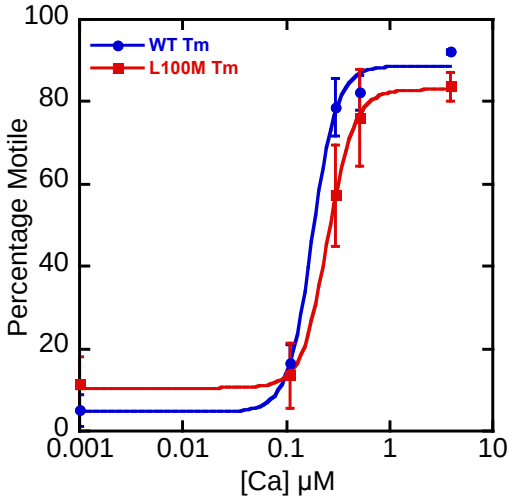
	Value	Error
Hill Coefficient	2.6	/
EC_{50}	0.55	0.14

	Value	Error
Hill Coefficient	1.61	0.19
EC_{50}	0.1	0.01

	Value	Error
Hill Coefficient	1	/
EC_{50}	0.3	0.2

L100M 2

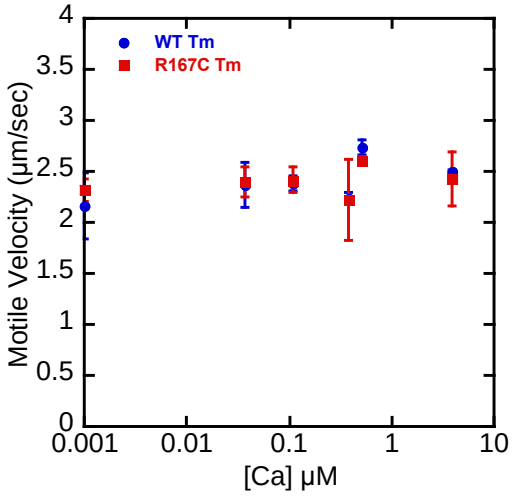


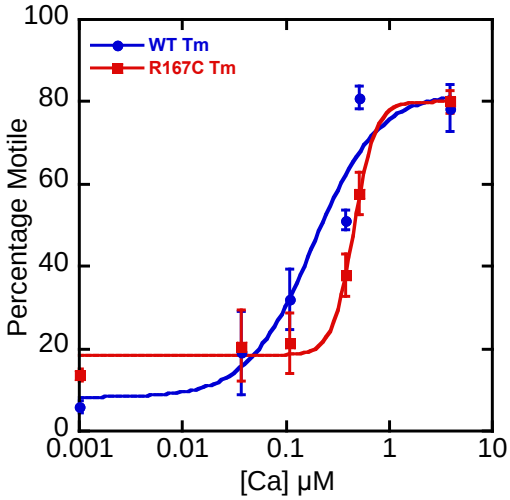


	Value	Error
Hill Coefficient	3.61	1.03
EC_{50}	0.18	0.03

	Value	Error
Hill Coefficient	3.41	0.54
EC_{50}	0.25	0.01

R167C 2

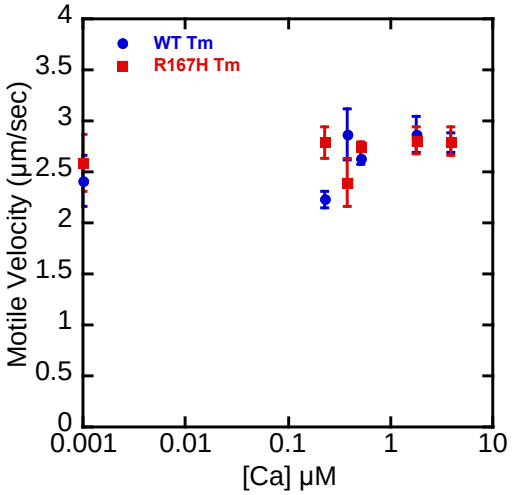


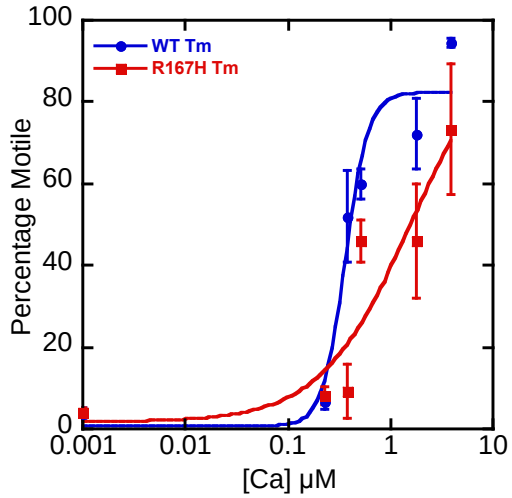


	Value	Error
Hill Coefficient	1.38	0.85
EC_{50}	0.18	0.11

	Value	Error
Hill Coefficient	4.23	1.41
EC_{50}	0.46	0.03

R167H





	Value	Error
Hill Coefficient	3.96	2.55
EC_{50}	0.36	0.07

	Value	Error
Hill Coefficient	1	/
EC_{50}	1.62	6.15

Table 5.7: Ca^{2+}-sensitivity data for thin filaments reconstituted with rabbit skeletal muscle troponin and recombinant wild-type v 5 mutant γ-tropomyosins

γ-Tm ANALYSIS	EC_{50} Percentage motility, μM		EC_{50} mutant / EC_{50} NTg	Hill coefficient n		% Motile 3.9 μM Ca^{2+}		Ca^{2+} activation of sliding speed (%)		Maximum sliding speed (μm/sec)	
EXP N	WT	A4V		WT	A4V	WT	A4V	WT	A4V	WT	A4V
1	0.15±0.01	0.55±0.14	3.67	2.6	2.6	75	87	6	0	2.68	2.65
2	0.24±0.03	0.3±0.06	1.25	1.95	1.76	93	87	18	0	2.46	2.2
3	0.06±0.02	0.09±0.03	1.5	1.3	1.29	80	74	15	7	2.8	2.81
MEAN±SE	0.15±0.05	0.31±0.13	2.14±0.77	1.95± 0.38	1.88± 0.38	83±5	83±4	13±4	2±2	2.65±0.1	2.55±0.18
EXP N	WT	R91P		WT	R91P	WT	R91P	WT	R91P	WT	R91P
1	0.12±0.02	0.53±0.01	4.42	1.98	(13.66)	86	69	14	3	2.53	2.42
2	0.1±0.01	0.3±0.2	3	1.61	1	88	73	14	30	2.64	2.67
3	0.06±0.01	0.31±0.12	5.17	1.29	1.61	79	73	16	33	2.45	2.79
MEAN±SE	0.09±0.02	0.38±0.08	4.19±0.64	1.63± 0.2	1.31± 0.31	84±3	72±1	15±1	22±10	2.54±0.06	2.63±0.11
EXP N	WT	L100M		WT	L100M	WT	L100M	WT	L100M	WT	L100M
1	0.29±0.19	0.35±0.17	1.21	1	1	85	81	14	6	2.45	2.4
2	0.18±0.03	0.25±0.01	1.39	3.61	3.41	92	84	29	21	2.84	2.52
3	0.55±0.01	1.76±0.94	3.2	(25.88)	1.13	89	72	31	8	2.69	2.26
MEAN±SE	0.34±0.11	0.79±0.49	1.93±0.64	2.31± 1.31	1.85± 0.78	89±2	79±4	25±5	12±5	2.66±0.11	2.39±0.08
EXP N	WT	R167C		WT	R167C	WT	R167C	WT	R167C	WT	R167C
1	0.08±0.03	0.17±0.02	2.13	1	1	78	57	19	2	2.47	2.47
2	0.18±0.11	0.46±0.03	2.56	1.38	4.23	79	80	16	5	2.5	2.43
3	0.14±0.04	0.5±0.18	3.57	2.95	1.26	79	76	9	30	2.39	2.66
MEAN±SE	0.13±0.03	0.38±0.1	2.75±0.43	1.78± 0.6	2.16± 1.04	79±1	71±7	15±3	12±9	2.45±0.03	2.52±0.07
EXP N	WT	R167H		WT	R167H	WT	R167H	WT	R167H	WT	R167H
1	0.36±0.07	1.62±6.15	4.5	3.96	1	95	73	15	8	2.79	2.8

5.4 Discussion

5.4.1 Guidelines to the Investigation

The main objective of this study on β- and γ-tropomyosin was to investigate the potential functional abnormalities caused by these mutations and, when gathering up the data, look for a common mechanism that could correlate with the different diseases and histological findings.

All of the mutations considered, both in β- and γ-tropomyosin, were leading to generalised muscle weakness, thus indicating a loss-of-function (with the only exception of ΔK7 that had peculiar symptoms). A decrease in the Ca^{2+}-sensitivity was expected or an even more extreme phenotype like that seen for a CFTD skeletal actin mutant, D292V (see section 6.2.1) (Clarke et al., 2007), which switched the thin filaments off completely at any Ca^{2+} concentration.

Before proceeding into discussing the details of the findings, it must be taken into consideration that most of the experiments presented here, except some made with ΔK7 β-tropomyosin, were performed using pure β- or γ-tropomyosin alone, without mixing them together or mixing β- with α-tropomyosin. This would not reproduce the most significant physiological situation, in which tropomyosin would form both homodimer and, mostly, heterodimer, with the possibility of formation of copolymers of WT and mutant Tm dimers (Bronson and Schachat, 1982). It was intended as a pilot work to define the most extreme phenotype, without any compensation by other isoforms as there is no information about this in the literature. It could have been possible, though, that the phenotype would manifest itself only with the heterodimer. For these reasons, a whole set of experiments performed with mixes of the isoforms, similar to those shown with ΔK7, were planned for this study. The

limited amount of recombinant proteins available prevented them being carried out, but they would still be interesting future work, to increase the understanding of the molecular mechanisms leading to the diseases.

Tropomyosin is the component of the thin filaments that transfers the Ca^{2+}-dependent switch between states, initiated by troponin, towards the 7 actin monomers it interacts with, but also cooperatively to the neighbouring regulatory units through the end-to-end interactions. Mutations on tropomyosin can therefore trigger dysfunctions in many ways, starting from the formation of its own dimer, to any of the interactions with other proteins within the thin filaments.

5.4.2 The β-tropomyosin Mutants

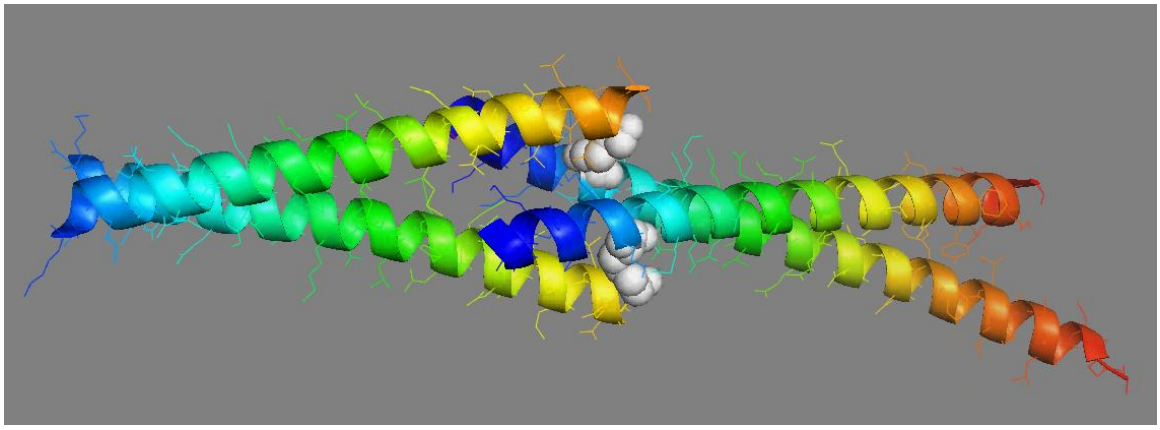
It was noted from early stage experiments that some of the β-tropomyosin mutants did not have the same actin affinity as the WT. ΔK7, ΔK49, ΔE139 and Q147P were unable to switch off the thin filaments properly and needed a modified protocol of infusion in the motility cell. This observation was confirmed by pull-down experiments performed in Dr N. Clarke's lab for ΔK7 and for the latter 3 mutations by actin-binding assays performed by Dr. M Marttila (Marttila et al., 2012).

ΔK7 has been the most thoroughly examined by me in this study. This mutation was linked to Nemaline myopathy because of the presence of many nemaline bodies observed in the histology of all the muscle biopsies taken from the patients, but the cases had very atypical features. It was particularly interesting because the patients were developing weakness in adolescence/mid-adulthood, while in infancy/early-childhood were showing generalised contractures and awkward gaits.

The first thing noted using 100% ΔK7 β-tropomyosin in IVMA, as said, was the lower affinity for actin, which was making it extremely difficult to obtain any regulation of the thin

filaments at the low concentrations used in the IVMA. Since this mutation is so near the N-terminus, molecular modelling was suggesting that it could disrupt the end-to-end polymerisation (Figure 5.16). This region is also supposed to bind actin and TnT (Hitchcock-DeGregori and Singh, 2010), and therefore the mutation can generate impairment in the cooperativity of the system. Only two titrations were performed completely, but the observed phenotype of an increased Ca^{2+}-sensitivity could have been caused by the loss of regulation due to abnormal actin or troponin T binding in a fraction of the filaments during the experiments rather than by different kinetic properties. *In vivo*, though, where the mutant tropomyosin can dimerise with the WT and also the other tropomyosin isoforms, its affinity to actin could be increased.

Figure 5.16: Position of ΔK7 in the end-to-end tropomyosin interaction



This molecular representation of the tropomyosin end-to-end interaction shows how the Lys7 residue is involved in the binding of the C-terminus of another tropomyosin dimer. Its deletion would probably cause a shift in position of the first 4 amino acids, as in position 6 and 5 are present lysines, and would reduce the ability to polymerise. Colours are based on the position with blue on the N-terminus and orange on the C-terminus. Rendering made with Pymol on coordinates from Frye *et al.* (2010).

Results obtained later by Dr C. Ottenheijm on dissected individual myofibres from two frozen biopsies from unrelated patients found a significant increase in the sensitivity of force generation to Ca^{2+}, and a trend for increased maximum force production compared to

controls. It is possible therefore that ΔK7 could form heterodimers with WT tropomyosin, thus allowing for normal end-to-end interaction and actin binding.

These findings encouraged me in trying a 50/50 mixture of ΔK7/WT β-tropomyosin in the IVMA, and this time I noticed that there was good regulation and that my results agreed with those obtained with myofibers, showing an increase of 2.3 fold in the Ca^{2+}-sensitivity and a statistically significant increase in the maximum motile velocity ($p = 0.019$), whereas in the 100% ΔK7 experiments the motile velocity did not show much Ca^{2+} regulation.

This data suggests that the presence of ΔK7 β-tropomyosin does not directly cause muscle weakness in the sarcomere by impairing actin-myosin interactions. They rather seem to correlate with the contractures and gaits seen in childhood, when no muscle weakness was clearly reported. The accumulation of nemaline bodies and the progressive muscle weakness could be due, in the long term, to the reduced actin binding affinity, which could lead to disorganisation within the sarcomere, as will be discussed with the next 3 mutations. This mutation could therefore represent a novel hypercontractile phenotype, later degenerating in Nemaline myopathy. As will be described in Chapter 6 with an *ACTA1* mutation, an increase in the thin filament Ca^{2+}-sensitivity of the same order can generate a hypercontractile phenotype.

Δ**K49** and Δ**E139** were linked only to the formation of cap structures in histology and therefore cap disease. They shorten the α-zone of the second and fourth repeat respectively, which are important for the binding to actin in the 'closed' state. ΔK49 occupies a 'g' position in the heptapeptide repeat, usually forming an ionic bond with the other dimer, while ΔE139 occupies a 'f' position and is supposed to interact directly with actin (Li et al., 2011). These two mutation have been also described to decrease the α-helical content of tropomyosin through circular dichroism experiments (Marttila et al., 2012). In IVMA they both showed an

increase in the Ca^{2+}-sensitivity and the absence of a Ca^{2+}-induced increase of the motile velocity.

Q147P was instead linked to Nemaline myopathy and in IVMA I only achieved one Ca^{2+} titration using it, in which it showed a lower Ca^{2+}-sensitivity contrarily to the previous two mutants, but it also showed the same lack of Ca^{2+} regulation of the motile velocity. The insertion of a proline in a 'g' position, a residue usually never present in coiled coils where it would produce a kink in the helix (East et al., 2010), is expected to impair the formation of a proper coiled coil dimer and the binding to actin. This explains the difficulties in obtaining regulation in IVMA as found by Pronina *et al*. (2007).

From these findings it seems plausible that a deficiency in actin binding by tropomyosin could impair the ability of the thin filaments to assemble. It could lead, then, either to the disorganised myofibril accumulations seen in cap structures, or to the disruption of the sarcomere's structure and to the enlargement of the Z-lines, seen in Nemaline myopathy, if the organisation was lost after a successful assembly in first place. This loss of organisation would produce a weak muscle phenotype, and the Ca^{2+}-sensitivity patterns shown in IVMA would be relevant only if the poison peptide was incorporated in the thin filaments that remained active. Some questions remain to be addressed: will these mutants be able to bind to actin in muscles? Highly likely since the concentration is more than a 1000 times greater in muscles. Would they show more or even less affinity to actin when mixed in heterodimers? They might behave like ΔK7, providing more reliable results when mixed. What would their Ca^{2+}-sensitivity look like then?

E41K and **E117K** β-tropomyosin mutations, instead, showed normal binding to actin. The latter did actually show an increase in actin affinity in the actin binding assay (Marttila et al., 2012). E41K was linked to Cap disease, but with peculiar formation of nemaline rod like

structures within the caps, whereas the E117K patient was diagnosed with Nemaline myopathy, but the histological screening of a muscle biopsy sample gave rather indications of a CFTD phenotype. They both showed a large reduction in the Ca^{2+}-sensitivity and a lower maximum sliding speed, in particular these changes were statistically significant for the E117K mutant, which also showed a statistically significant decrease in the percentage of motile filaments in activating Ca^{2+} concentration and in the Ca^{2+}-induced increase of the motile velocity. The action of E117K could impair the ability of TnT to modulate the motile velocity even though it is not in direct contact with it (Bing et al., 1997). These findings would correlate well with a weak muscle phenotype as they seem to act primarily on the cooperative and allosteric properties of the thin filaments to impair their functions. It is unlikely that the pathogenesis induced by the 2 Cap disease mutants with low affinity for actin corresponds to that of E41K β-tropomyosin, as they show opposite properties. The E41K and E117K β-tropomyosin mutations, showed the expected phenotype as the base of myopathies. E41K mutant has been studied in a muscle biopsy sample. The amount of E41K expressed was not determined, but it was found that the relative expression of α- and β-tropomyosin was altered in the mutant tissue to a larger presence of the β isoform, thus adding another layer of complexity to the situation *in vivo*. Then, it was observed that the mutant muscle had reduced crossbridge turnover rate and Ca^{2+}-sensitivity, in agreement with my results using isolated thin filaments with 100% mutant β-tropomyosin (Ochala et al., 2008, Marston, 2008).

To conclude it seems that different mutations follow different pathways to produce muscle dysfunction and that these do not correlate directly with the molecular phenotype or the histological phenotype shown. This idea is supported also by the fact that the same mutation

can lead to the formation of different pathologic structures within the myofiber in different patients.

5.4.3 The γ-tropomyosin Mutants

The experiments performed with all the γ-tropomyosin mutants were not canonical, as explained in section 5.3. The indications given by the SDS-PAGE gel of their purification were of the presence of some abnormality that was not seen before with the other baculovirus/*sf9* expressed α- and β-tropomyosin. It looked as if some covalent bond was preventing the separation in monomers of the tropomyosin dimer, probably cross-linking at Cys190. Subsequently it was found in our lab that the monomer could be obtained following the treatment of γ-tropomyosin with iodoacetamide to block the -SH groups and the use of high DTT concentrations to prevent cross-links reforming. The need for these extreme conditions would probably modify the normal activity of the thin filament proteins and thus no new experiments were performed.

The covalent modification is likely to be the reason for the difficulties encountered in the IVMA in achieving stable regulation. The impression given in experiments was that for a limited period of time the filaments would behave as expected with two populations, one moving and one stopping, with the percentage of each population being a function of the Ca^{2+} concentration, but as soon as one filament was switching on from the non-motile pool, it was then unable to switch off again, leading to complete loss of regulation in roughly 3 minutes. This loss of regulation was seen for both WT and mutant thin filaments. This behaviour could be due to the supposed covalent modification seen in the SDS-PAGE, which would be expected to introduce more stiffness in the coiled coil and therefore impairing its ability to switch between states of activation. Until the monomers can be efficiently separated in the

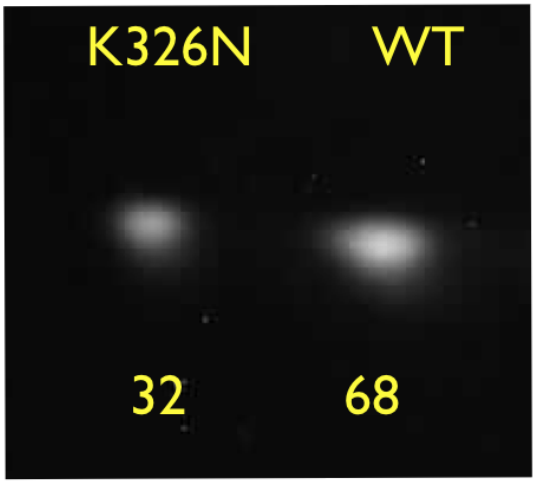
purification and a new set of experiments are performed, the IVMA indications of a lower Ca^{2+}-sensitivity cannot be taken as solid data.

6 Hypercontractile Nemaline Myopathy: a Novel Disease Caused by a Skeletal Muscle α-actin Mutation

6.1 Introduction on K326N α-actin

The mutation K326N on *ACTA1* has been identified and is described in a study in which we directly contributed (Jain et al., 2012, Neurology, in press). Histology carried out on a biopsy of the quadriceps proved the presence of nemaline bodies, leading to the diagnosis of Nemaline myopathy. However the patient's symptoms were the opposite of congenital muscle myopathy. 2D protein electrophoresis showed 32% mutant actin in the biopsy (performed by Dr J. Leung and shown in Figure 6.1).

Figure 6.1: 2D electrophoresis of actin purified from K326N patient's biopsy



The patient was a male child, born from non-consanguineous European parents. At six weeks of age he was hospitalized with apnoeic episodes, probably due to bilateral strangulated

inguinal hernias and an umbilical hernia. Herniotomy was performed, but rigidity and recurrent apnoeas requiring mechanical ventilation continued. The patient was born with no complications, but the mother reported stiffness in the weeks after birth.

When examined he presented very stiff and hypertrophic abdominal and proximal limb muscles and postnatal elbow and knee contractures. Deep tendon reflexes showed brisk contraction and slow relaxation and percussion myotonia could be elicited, although there was no evidence of myotonia. Cardiac assessment was normal. During sleep he showed hypoventilation and carbon dioxide retention.

The underlying stiffness and genetic testing excluded the better known disorders (like hyperekplexia). Pharmacological treatment including phenytoin, carbamazepine, flecainide, baclofen, dantrolene and acetazolamide was ineffective.

He had recurrent episodes of stiffness throughout his life with apnoea, thus he needed invasive and non-invasive ventilation. Despite this he could progress to desaturation, bradycardia and occasionally asystole with resuscitation needed. He died when 9 months old following an asystolic episode.

This is the first case reported where nemaline bodies were associated with stiffness rather than weakness in skeletal muscles.

6.2 K326N actin *In Vitro* Motility Analysis

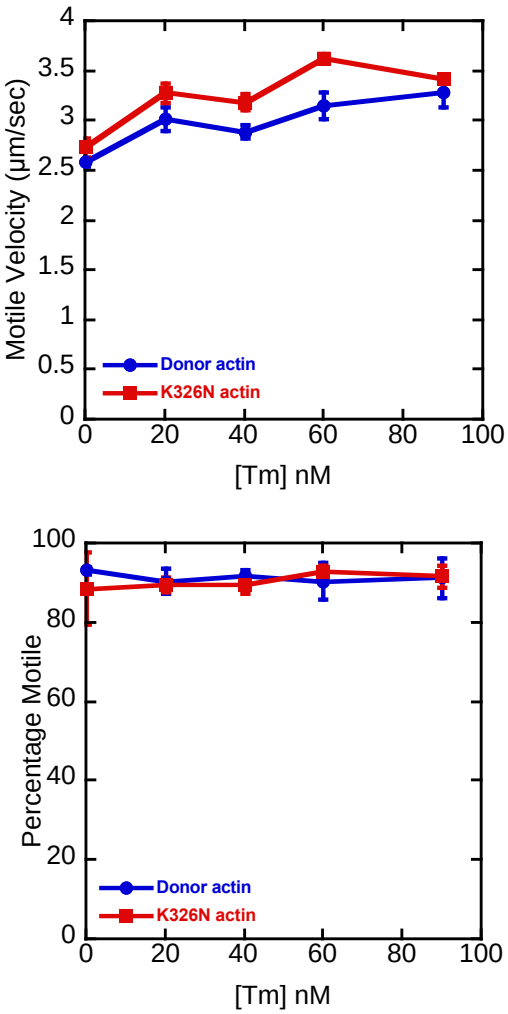
Polymeric actin was extracted from the K326N patient's muscle biopsy (see section 2.2.2.4) and compared with actin from an age-matched biopsy with no actin mutation using the *in vitro* motility assay. The motility of pure actin filaments was very similar for the two actins in both motile velocity and percentage motile (Table 6.1). A β-tropomyosin titration was then performed (Figure 6.2). The β-tropomyosin used was a wild-type recombinant protein

expressed in baculovirus/*sf9* cells, and it was chosen because *TPM2* is the most expressed isoform in human quadriceps skeletal myocytes. The titration shows that there is basically no difference in the percentage motile between donor and K326N actin when reconstituted with β-tropomyosin, but the motile velocity is constantly 5-15% higher for the mutant actin.

Table 6.1: Comparison of motility of donor and K326N thin filament actin

actin	Sliding Speed (μm/sec)		Percentage Motile	
Preparation	Donor	K326N	Donor	K326N
1	2.59±0.04	2.73±0.1	93.3±0.96	88.5±9.1
	2.71±0.13	2.72±0.1	96.3±2.6	95.5±1.9
	2.71±0.19	2.51±0.14	90.2±0.7	89.5±2.2
	3.03±0.07	2.88±0.18	92.3±2.9	81.5±7.7
	2.5±0.09	2.8±0.13	92.8±2.8	92.8±3.6
	3.1±0.05	3.27±0.09	97±1.6	95.8±2.2
	3.2±0.07	3.28±0.02	95.3±2.5	96±0.8
	2.59±0.12	2.76±0.09	93.7±4.7	93.3±1
	2.81±0.06	2.84±0.01	86.3±5.3	86.8±5.1
	2.44±0.15	2.57±0.08	82±7.3	80±9.5
	2.77±0.13	3±0.05	99.3±0.5	96.5±0.6
MEAN±SE N=11	2.77±0.07	2.85±0.08	92.6±1.5	90.6±1.8
t-test p value	paired=0.1 unpaired=0.44		paired=0.07 unpaired=0.39	

Figure 6.2: β-tropomyosin titration comparing human donor skeletal actin and K326N skeletal actin

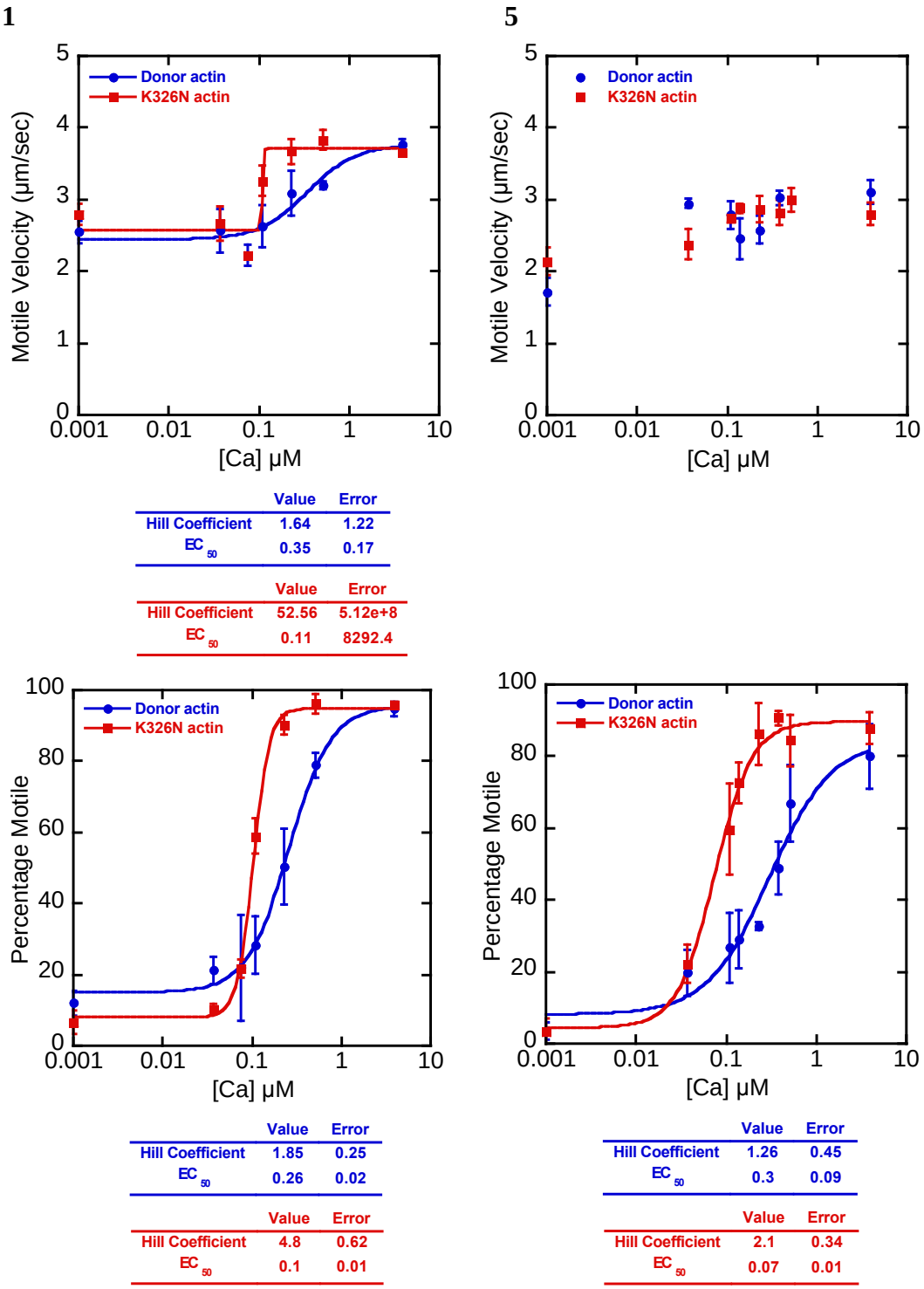


The Ca^{2+}-activation curve was measured six times using just one actin preparation due to the small amount of material provided by the biopsy (experiment 1 and 5 are shown in Figure 6.3, while the rest is in APPENDIX; data is summarised in Table 6.2 and Table 6.3). Actin was always used at 10 nM, β-tropomyosin at 60 nM and troponin was titrated between 20 and 50 nM to find optimal switch off and on conditions.

On average there was a 2.5 fold higher Ca^{2+}-sensitivity (EC_{50} ratio K326N / donor was 0.4 ± 0.05) and 8% higher percentage of filaments motile in high Ca^{2+}. In 5 out of 6 curves the Hill coefficient (n_H) was also greater. If experiment 2 was omitted from the analysis, n_H increased 2.9-fold and this was statistically significant ($p = 0.015$, paired t test).

The motile velocity could be fitted in four experiments. There is no parameter that gets statistical significant difference, but the data indicate again a higher Ca^{2+}-sensitivity for K326N actin (EC_{50} ratio K326N / donor was 0.6 ± 0.15). The maximum sliding speed is 6% higher for K326N actin.

Figure 6.3: Ca^{2+} concentration titrations comparing thin filaments containing donor and K326N human skeletal actin



	Value	Error
Hill Coefficient	1.64	1.22
EC_{50}	0.35	0.17

	Value	Error
Hill Coefficient	52.56	5.12e+8
EC_{50}	0.11	8292.4

	Value	Error
Hill Coefficient	1.85	0.25
EC_{50}	0.26	0.02

	Value	Error
Hill Coefficient	4.8	0.62
EC_{50}	0.1	0.01

	Value	Error
Hill Coefficient	1.26	0.45
EC_{50}	0.3	0.09

	Value	Error
Hill Coefficient	2.1	0.34
EC_{50}	0.07	0.01

Table 6.2: Ca^{2+}-sensitivity data for donor v K326N skeletal actin thin filaments motile velocity

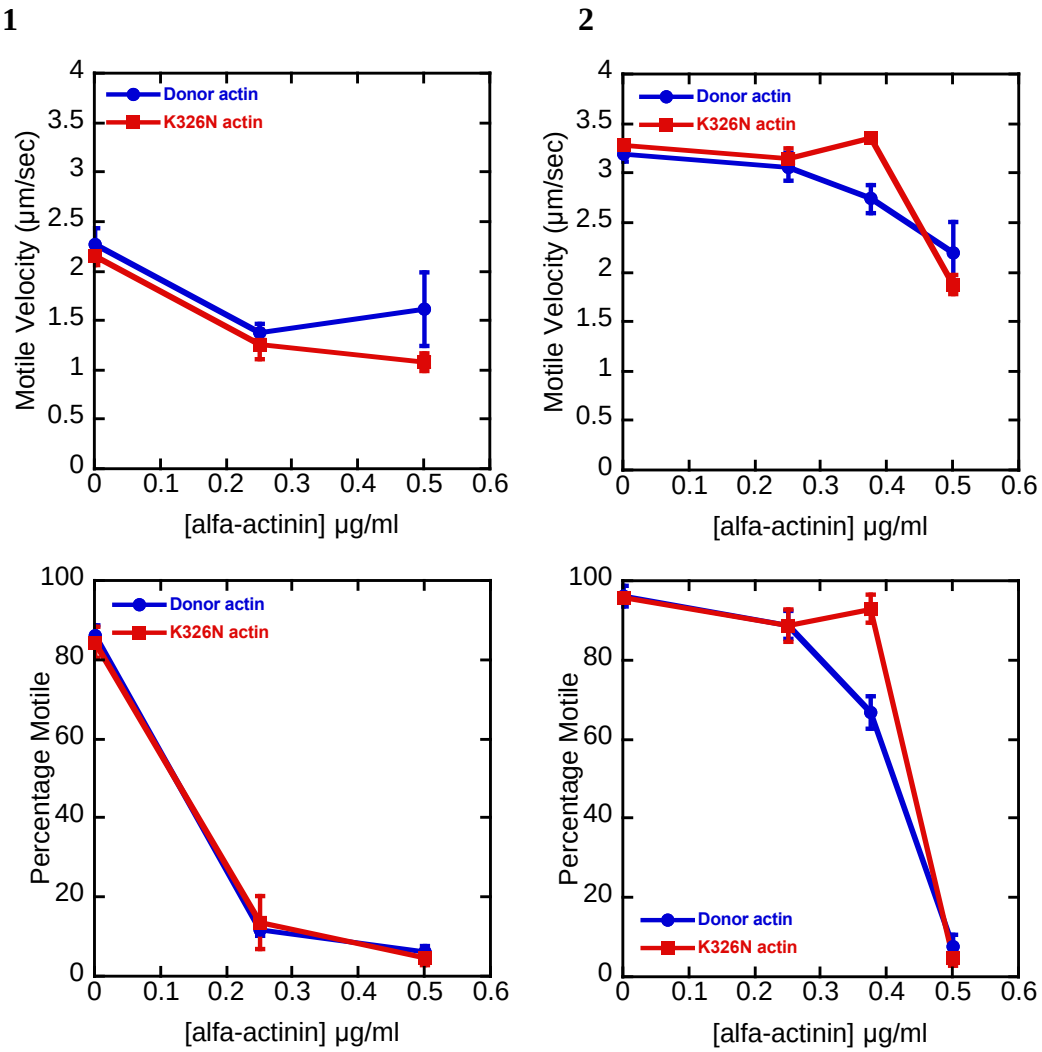
actin K326N ANALYSIS	EC_{50} Sliding speed, µM		EC_{50} mutant/ EC_{50} NTg	Ca^{2+} activation of sliding speed (%)		Maximum sliding speed (µm/sec)	
EXP N	Donor	K326N		Donor	K326N	Donor	K326N
1	0.35±0.17	0.11±8292	0.31	48	31	3.77	3.66
2	0.76±0.38	0.54±0.01	0.71	67	90	3.93	4.68
3	/	/	/	30	34	2.85	3.29
4	0.33±0.09	0.32±0.06	0.97	36	59	3.55	3.87
5	/	/	/	81	31	3.11	2.8
6	0.17±0.2	0.07±0.04	0.41	97	49	3.45	3.49
MEAN±SE	0.4±0.13	0.26±0.11	0.6±0.15	60±11	49±9	3.44±0.17	3.63±0.26
Student's t-test (paired)	p=0.077		single group, p=0.076 (compared with one)	p=0.46		p=0.29	
(unpaired)	p=0.42			p=0.47		p=0.55	

Table 6.3: Ca^{2+}-sensitivity data for donor v K326N skeletal actin thin filaments percentage motile

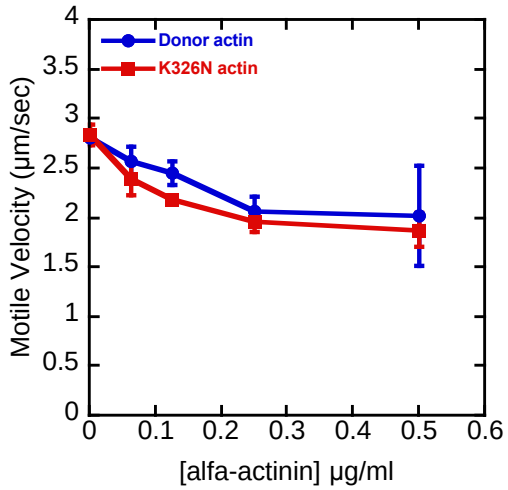
actin K326N ANALYSIS	EC_{50} Percentage motility, µM		EC_{50} mutant / EC_{50} Donor	Hill coefficient n		% Motile 3.9 µM Ca^{2+}	
EXP N	Donor	K326N		Donor	K326N	Donor	K326N
1	0.26±0.02	0.10±0.01	0.38	1.85	4.8	95	96
2	0.53±0.01	0.25±0.07	0.47	5.99	1.19	88	94
3	0.17±0.05	0.09±0.01	0.53	1.51	4.33	80	90
4	0.23±0.01	0.11±0.02	0.48	1.52	6.03	83	96
5	0.3±0.09	0.07±0.01	0.23	1.26	2.10	80	88
6	0.21±0.15	0.07±0.01	0.33	1	2.58	89	94
MEAN±SE	0.28±0.05	0.12±0.03	0.4±0.05	2.19±0.77	3.51±0.75	86±2	93±1
Student's t-test (paired)	p=0.003		single group, p<0.0001 (compared with one)	p=0.37		p=0.008	
(unpaired)	p=0.02			p=0.25		p=0.027	

A final set of experiments was performed in order to compare the isometric force of the actomyosin complex with mutant and donor actin. This was achieved using α-actinin as a load attached to the cover glass, along with the immobilised myosin motor protein, following the method by Bing *et al.* (2000). This protocol applies a small change to the usual loading procedure of the IVMA flow cell: different concentrations of α-actinin were mixed with the solution containing the affinity precipitated HMM before it was loaded to the flow cell. Every other step remained the same. The α-actinin was always titrated in the presence of the usual amount of actin, whereas 50 μg/ml myosin were used in experiment 1, 100 μg/ml myosin, which is the standard IVMA concentration, were used in experiment 2, 3 and 4 (Figure 6.4). In experiment 4 actin was also reconstituted with Tm. The outcome showed that the isometric force does not show any difference between the actin from the control and patient biopsies, with the exception of a wild point in experiment 2 at 0.375 μg/ml of α-actinin, in which probably the mutant side of the cover glass did not get homogeneously coated with the load protein. This can be argued because of the lack of any other different point through the other 3 titrations.

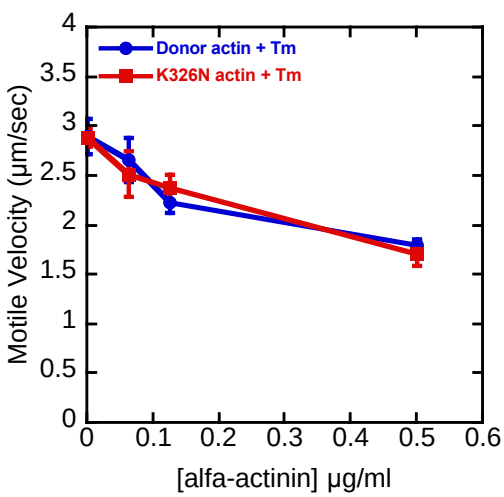
Figure 6.4: α-actinin titration comparing the isometric force properties of donor and K326N skeletal human actin

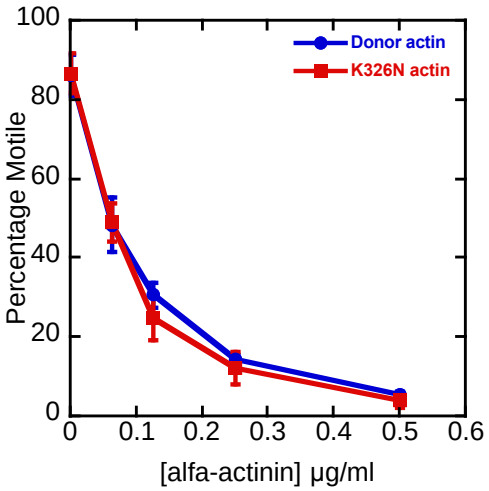


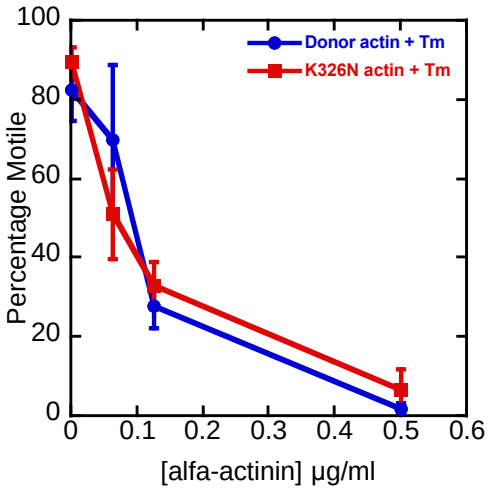
3


Donor actin
K326N actin
Motile Velocity (µm/sec)
[alfa-actinin] µg/ml

4


Donor actin + Tm
K326N actin + Tm
Motile Velocity (µm/sec)
[alfa-actinin] µg/ml


Donor actin
K326N actin
Percentage Motile
[alfa-actinin] µg/ml


Donor actin + Tm
K326N actin + Tm
Percentage Motile
[alfa-actinin] µg/ml

6.2.1 The Opposite Phenotype: Actin D292V

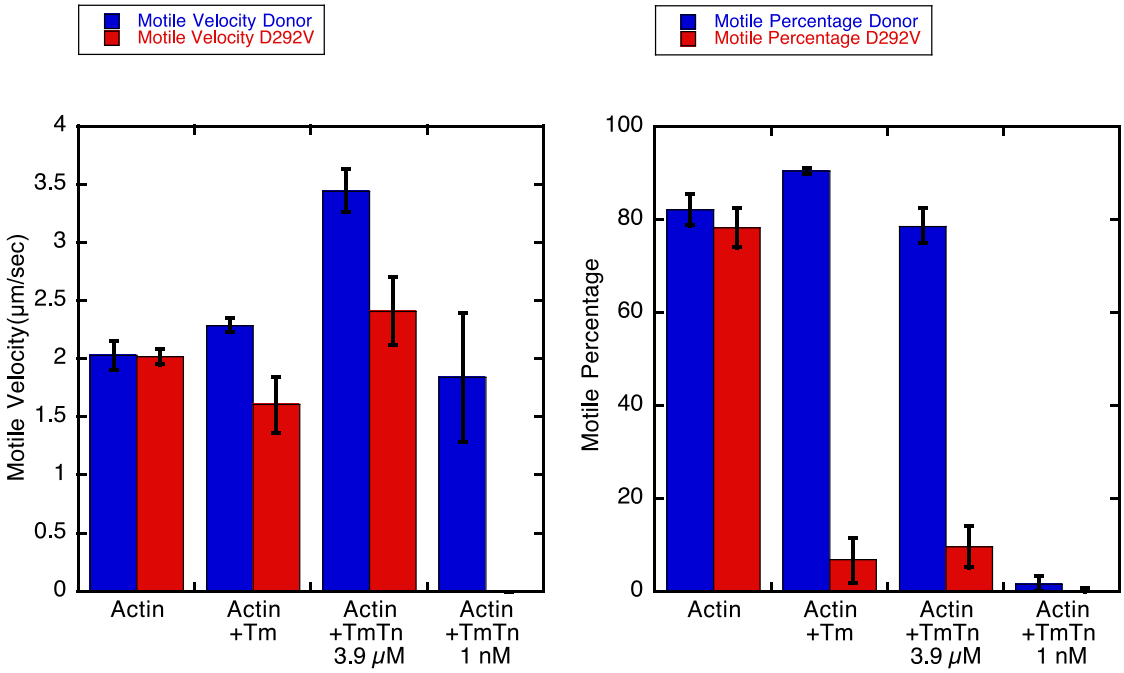
This mutation was previously studied in the lab (Clarke et al., 2007). I have repeated the IVMA measurements with a fresh biopsy sample to compare its function with the K326N actin mutation.

Actin D292V is a CFTD linked mutation sporadically originated in one patient (Laing et al., 2004). He had generalised weakness and hypotonia and required nocturnal ventilation and was fed by gastrostomy. He was basically unable to do big movements, but could lift his forearm. Deep tendon reflexes were all absent and he could make only simple sounds, without closing his jaw. He had a long thin face, high arched palate and scoliosis. He died of respiratory complications when 3.5 years old. Biopsies from quadriceps and deltoid showed the type 1 fiber to be small and interspersed between large type 2 fibres.

Actin D292V was purified from a skeletal muscle biopsy of the original patient. Only one preparation was made through the whole thin filaments method.

Experiments with D292V revealed an extreme phenotype (Figure 6.5). Plain skeletal D292V actin shared the same motile properties of donor skeletal actin, but just by adding tropomyosin it was switching off without any Ca^{2+} buffer added to the motility cell. The motile velocity was just decreased by 20%, while the percentage motile dropped from 78% to 7%. When rabbit skeletal troponin was also reconstituted, the thin filaments motility was not rescued with the 3.9 µM Ca^{2+} buffer.

Figure 6.5: *In vitro* motility measurements comparing skeletal muscle donor and D292V actin, with β-tropomyosin and rabbit skeletal muscle troponin



6.3 Discussion

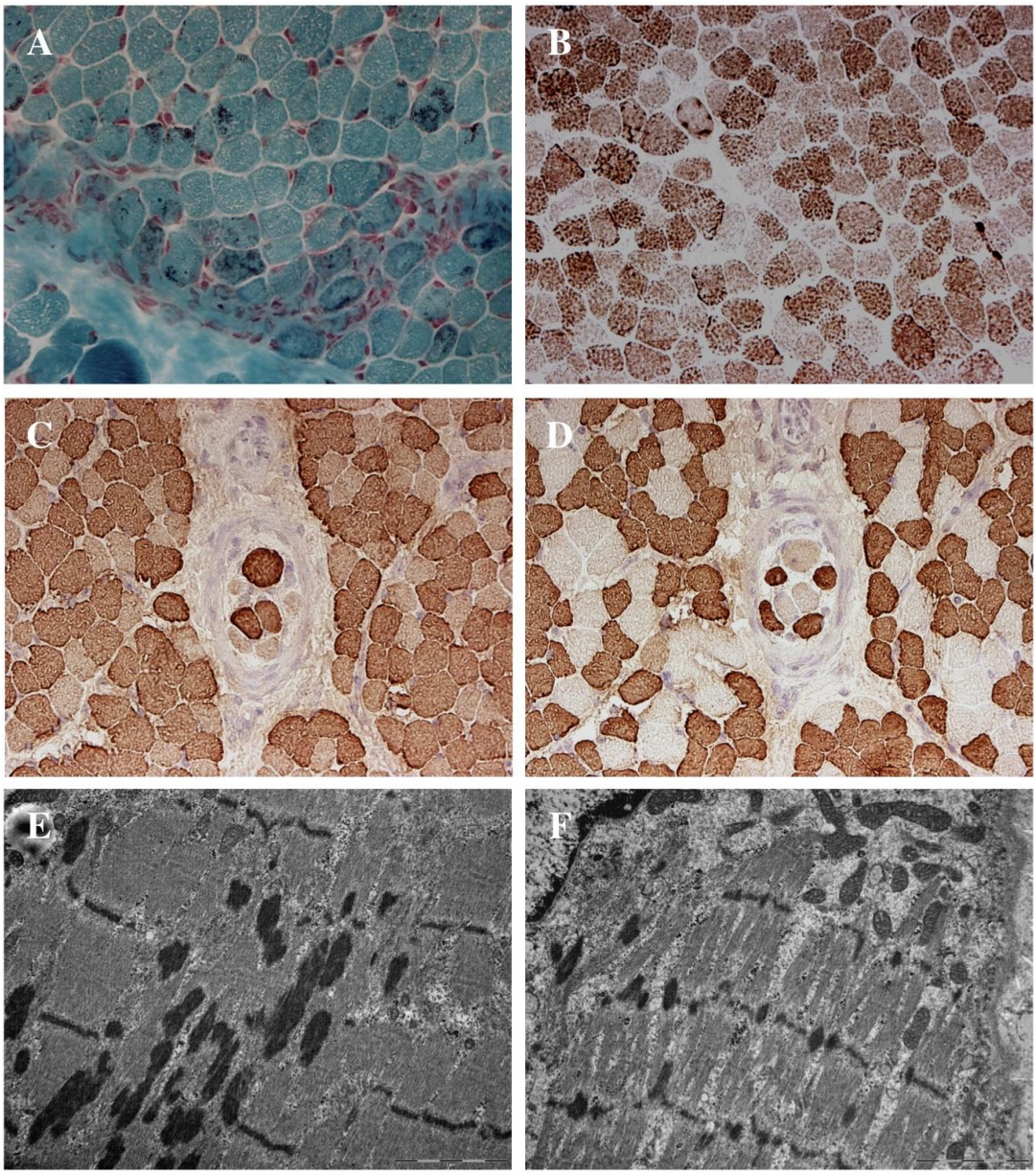
6.3.1 A Novel Molecular Phenotype

In this chapter I have described the molecular phenotype due to a unique gain-of-function mutation in actin. The child with 'stiff' muscles was treated in Dr Jain's clinic in Oxford. Genetic tests for the known neurological causes of a hypercontractile syndrome proved negative. Prof. N. Laing made the proposal that the causative mutation may be in a contractile protein, because histology showed the presence of nemaline bodies (made of extra-myofibrillar Z-disk material), shown in Figure 6.6; this work was done by Prof. C. Sewry's group. Prof. Laing's group subsequently identified the *ACTA1* K326N mutation in this patient.

Because of the novel mutation and unusual phenotype combined with the possibility of obtaining a biopsy from this patient, Prof. Laing encouraged us to investigate the actin mutation using the IVMA. We were provided with about 6 mg of patient tissue and an age matched control that was sufficient for a significant number of measurements.

Using the technique of isolating polymeric actin directly from thin filaments that was developed to study the *ACTC* E361G mutation (Song et al., 2010) described in Chapter 3, we were able to obtain actin filaments that contained 32% mutant actin.

Figure 6.6: Muscle biopsy from the quadriceps



A) Biopsy of quadricep tissue stained with modified Gomori trichrome showing abnormal variation in fibre; B) Combined staining for cytochrome oxidase and succinic dehydrogenase activity showing fibre type differentiation, some peripheral accumulation of cytochrome oxidase but no fibres lacking cytochrome oxidase activity; C) immunolabelling of serial areas with antibodies to slow and D) fast myosin showing two main fibre types and co-expression of both isoforms in some fibres. The central area is a spindle. Electron micrographs of the muscle biopsy showing E) rods orientated longitudinally and transversely; F) Z-lines in focal sarcomeres that are thickened and rod-like in shape. From "NEMALINE MYOPATHY WITH STIFFNESS AND HYPERTONIA ASSOCIATED WITH AN *ACTA1* MUTATION" (Neurology, in press, Rakesh K Jain, Sandeep Jayawant, W Squier, Francesco Muntoni, Caroline A Sewry, Adnan Y. Manzur, Ros Quinlivan,Suzanne Lillis, Heinz Jungbluth, John C. Sparrow, Gianina Ravenscroft, Kristen J. Nowak, Massimilano Memo, Steve B. Marston, and Nigel G. Laing).

My investigation showed that in fully reconstituted thin filaments this mutation caused increased sliding speed (not statistically significant) and a 7% increase in the percentage of filaments motile ($p = 0.008$). The major effect of the mutation, however, was a 2.5 fold increased Ca^{2+}-sensitivity ($p < 0.0001$). The prediction that this mutation would cause a gain-of-function was, thus, confirmed at the single filament level.

It is interesting to note that the molecular characteristics of the *ACTA1* K326N mutation are similar to what I found for the *TPM2* ΔK7 mutation (increased motile velocity and percentage motile in 3.9 μM Ca^{2+}, 2.4-fold increase in Ca^{2+}-sensitivity); that patient was not known to have congenitally 'stiff muscle' but showed contractures at a young age and thus did not correspond to the typical Nemaline myopathy diagnosis.

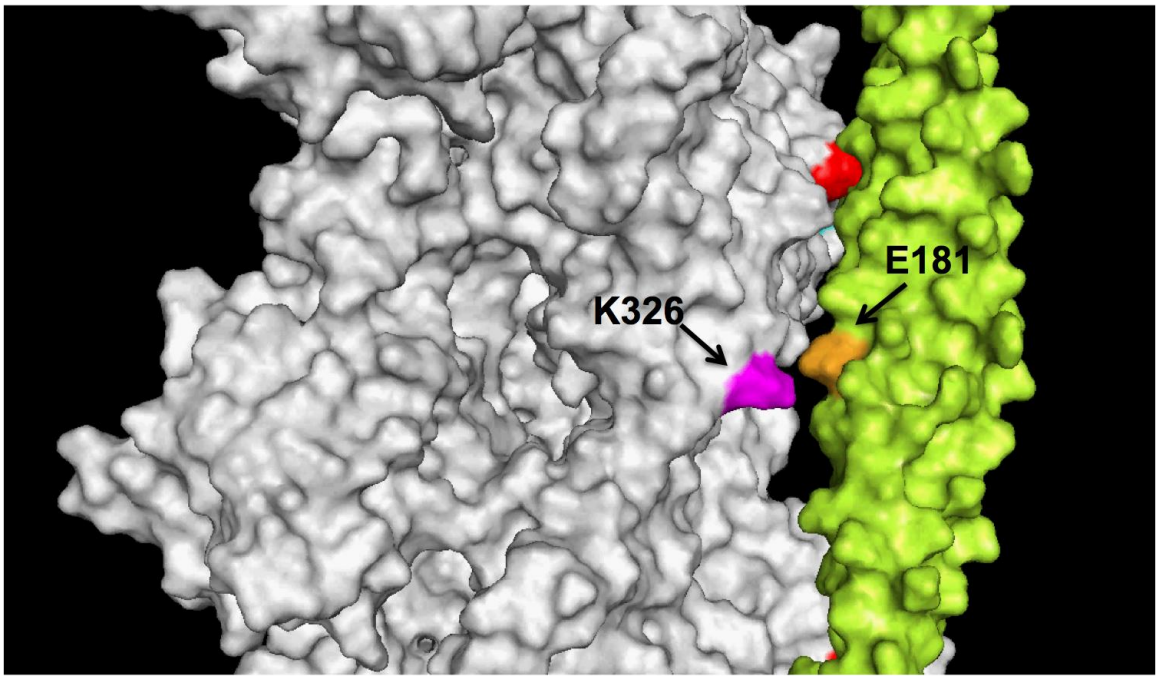
6.3.2 Structural Insights

The location of Lys326 in the mature protein is consistent with a mutation affecting Ca^{2+}-regulation. Accordingly to the three state model described in section 1.3.1.2, tropomyosin would change its position on the actin filament with the activation state of the thin filament. This would let myosin interact strongly, weakly or not interact at all. In the structural model proposed by Brown *et al.* (2005) and the molecular dynamics of Li *et al* (2010) for the actin-tropomyosin complex, Lys326 is part of the interface between the two proteins in the "closed" state (Figure 6.7) and is proposed to make an ionic bond with tropomyosin in 5 out of the 7 actins in the functional unit (with tropomyosin's D20, E104, E142, E181, E223). The positive charge neutralised by the mutation to Asn therefore could destabilise the "closed" state and change the equilibrium towards the "open" state. If this is the case, we would expect to observe the change in the *in vitro* motility assay, with higher Ca^{2+}-sensitivity, possibly higher percentage motile in activating conditions, and also an increase in the cooperativity. All of these changes were in fact observed in the experiments above with a striking 2.5 fold

increase in the Ca^{2+}-sensitivity. The molecular phenotype does correlate with the hypertonic clinical phenotype. The absence of an increase in the isometric force suggests that only the on/off equilibrium is involved without changes in other interactions.

In this context it is very interesting to consider another *ACTA1* mutation, D292V, which following the same structural model, is positioned on the same actin-tropomyosin interface. This mutation produces an opposite charge neutralisation and has, in fact, a completely different effect compared to K326N: it permanently switches off the thin filament with no possibility to rescue their motility, and hypotonia in the muscles (Clarke et al., 2007). It highlights the importance of these charged residues to maintain the equilibrium between states in normal condition.

Figure 6.7: Structural model showing the contact between actin K326 and tropomyosin E181 when the actin-tropomyosin complex is in the "closed" state



Structure of actin filament (grey), with highlighted in purple Lys326, tropomyosin, in green with Glu181 in yellow. In the 'closed' state these two residues are in direct contact forming an ionic bond. In red is actin Asp25 which is highly important for the 'closed' state binding as well. This residue is supposed to contact Lys6 on tropomyosin, just on the side of Lys7. The effects of the deletion of Lys7 have been described in Chapter 5 and are closely related to those of Lys326Asn in producing a hypercontractile phenotype. Actin-tropomyosin rendered in Pymol; coordinates used were those from Li *et al.* (2011).

7 General Discussion

7.1 DCM as a Result of Uncoupling Between Troponin I Phosphorylation and the Thin Filament Ca^{2+}-sensitivity

The study involving DCM mutations was triggered by previous work done in this lab. Until recently there had been a consensus that DCM-linked mutations cause lower crossbridge turnover rate and myofilament Ca^{2+}-sensitivity (Mirza et al., 2005, Carballo et al., 2009, Chang and Potter, 2005), but there were some recorded exceptions. All the DCM mutations studied to date (including mine) were tabulated by Marston (2011). Out of 14 mutations studied 6 did not reduce myofibrillar Ca^{2+}-sensitivity, therefore we have searched for an alternative mutation-induced dysfunction common to all DCM mutations. In the thesis of Dr E. Dyer and two papers (Dyer et al., 2009, Song et al., 2010), it was shown how previous theories developed by using recombinant proteins expressed in *E.coli* were limited by the absence of post-translational modifications, in particular TnI phosphorylation. Her pilot work showed how 2 mutations, cardiac actin E361G and cardiac troponin C G159D, affected the functional properties of the thin filaments in additional ways to what was reported by earlier studies. Her study indicated that an uncoupling between the level of TnI phosphorylation and the change in thin filament Ca^{2+}-sensitivity was found with both mutations, while neither caused a decrease in Ca^{2+}-sensitivity with troponin at a native phosphorylation level.

In addition, a study by Biesiadecki *et al.* (2007) showed, with the same TnC G159D mutant, a blunted response to TnI Ser22/23 phosphorylation. In that study, Ser22/23 were substituted by Asp residues to mimic phosphorylation and whole recombinant troponin was substituted

in rat skinned trabeculae. It was shown that the generation of tension did not change in Ca^{2+}-sensitivity with the Asp residues mimicking phosphorylation when compared with unphosphorylated troponin with the G159D mutation.

We therefore formulated a hypothesis that the common myofilament dysfunction causing familial DCM was the uncoupling of the relationship between TnI phosphorylation by PKA and change in myofilament Ca^{2+}-sensitivity, that is an important determinant of the lusitropic response. To investigate this I focused on reconstituting thin filaments using only troponin purified from human or mouse hearts, thus obtaining a phosphorylation level comparable to that present *in vivo* (Messer et al., 2009) and also the other native post-translational modifications potentially present. Also tropomyosin was purified from human donor heart tissue.

Firstly I confirmed Dr Dyer's work with E361G and G159D, then two troponin T mutants, all purified from transgenic mouse heart samples, and one troponin I mutant, purified from a patient explanted heart sample, were investigated. Two cardiac tropomyosin mutants were expressed recombinantly with a eukaryotic system to obtain N-terminal acetylation, which was reported to be very important for proper assembly of the whole thin filament regulatory machinery. This was used as the commonly used Ala-Ser N-terminal extension was not an adequate substitute for N-terminal acetylation (Palm et al., 2003, Monteiro et al., 1994, Mirza et al., 2007).

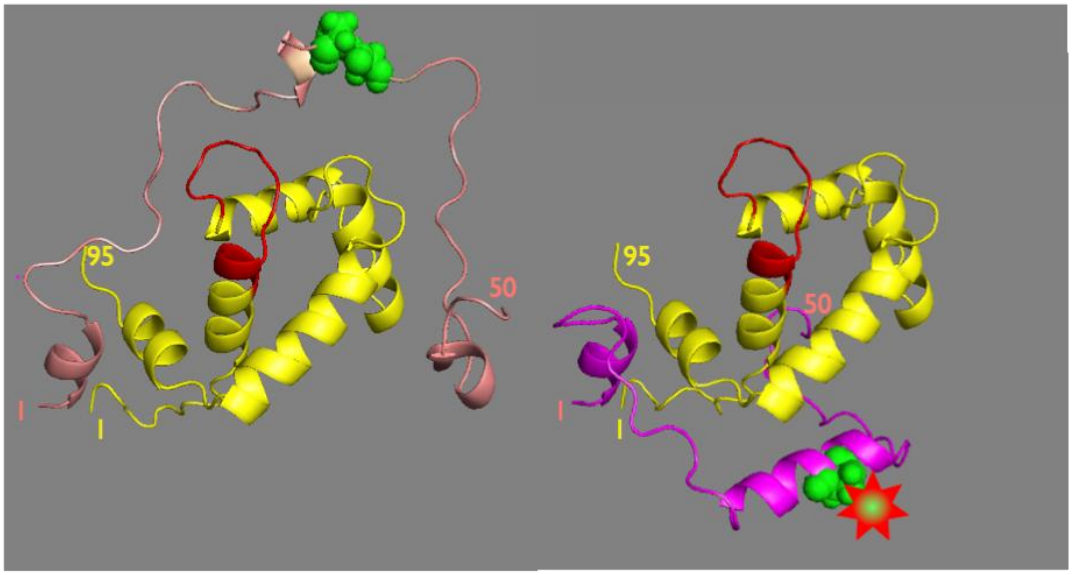
All of the 7 mutants investigated induced a loss-of-function in the thin filaments, but it was a quite subtle modification in their regulation and cardiac specific, since skeletal TnI does not have the N-terminal regulatory extension with phosphorylation sites 22/23. I demonstrated that the poison peptides were able to impair the regulation at sub-stoichiometric concentrations, meaning that they would cooperatively impair also the neighbouring

regulatory units. This is important since all DCM patients were heterozygous. Uncoupling has been recently reported also for three rare DCM TnC mutants (Pinto et al., 2011). These mutants were recombinantly expressed in *E.coli* and then reconstituted in endogenous troponin after depletion of the C subunit in pig skinned heart fibres. They all showed a blunted response to TnI phosphorylation when it was treated with PKA.

Our present understanding is that the absolute Ca^{2+}-sensitivity in the mutant filaments may determine the severity of the clinical symptoms but it does not directly induce DCM, as too many exceptions to the low Ca^{2+}-sensitivity rule have been described thus far. The uncoupling they produce in the fine regulation of the Ca^{2+}-sensitivity, on the other hand, is something that has been observed for all of the mutations tested.

A structural model of the interaction between the cardiac specific N-terminal extension of TnI and TnC shows that in the unphosphorylated (high Ca^{2+} sensitivity) state there is a weak ionic interaction between TnI amino acids 20-31 and the Ca^{2+} binding loop of TnC and that when Ser 22 and 23 are phosphorylated this interaction is absent, thus accounting for the lower Ca^{2+} sensitivity of phosphorylated troponin (as explained in section 1.3.2.1, Figure 7.1). In general we find that the Ca^{2+} sensitivity of unphosphorylated DCM mutant-containing thin filaments is the same as, or lower than, the Ca^{2+} sensitivity of natively phosphorylated wild-type thin filaments. On this basis, we propose a simple mechanistic hypothesis for uncoupling where the mutations allosterically destabilise the TnI N-terminus-TnC interaction resulting in a default state similar to phosphorylated wild-type troponin, independently from TnI phosphorylation.

Figure 7.1: Ribbon structures of the N-terminus of cTnC and the N-terminal extension of cTnI when phosphorylated and unphosphorylated



Troponin I N-terminus (pink) interaction with troponin C (yellow). The Ca^{2+}-binding loop (red) interacts with troponin I leading to modulation of Ca^{2+}-sensitivity. Serines 23 and 24 shown in green.

Phosphorylated troponin I N-terminus (magenta) interaction with troponin C N-terminus (yellow). The Ca^{2+}-binding loop (red) does not interact with troponin I. Serines 23 and 24 shown in green.

Drawn with Pymol by Prof. Steve Marston, based on structure from (Howarth et al., 2007)

It is interesting to note that uncoupling has also been reported in mutant cardiac α-actin and cTnI associated with a different inherited cardiomyopathy: hypertrophic cardiomyopathy (Song et al., 2011, Deng et al., 2003), and as a secondary abnormality in troponin isolated from interventricular septum of patients with hypertrophic obstructive cardiomyopathy, where it is not mutation-related (Jacques et al., 2009, Bayliss et al., 2011). This suggests that uncoupling may be a widespread phenomenon in pathological heart muscle. In the case of DCM mutations, however, uncoupling is the only abnormality consistently linked to the disease and shown to be a direct consequence of the disease-causing mutation. In hypertrophic cardiomyopathy it could be connected to the development of DCM at a late stage.

The PKA-dependent decrease in myofilament Ca^{2+} sensitivity and associated increase in the

rate of Ca^{2+} dissociation from TnC is a key component of the lusitropic response. Rapid relaxation (lusitropy) is a prerequisite for the faster heart rate and increased contractile force (inotropy) induced by β-adrenergic stimulation. Therefore it is likely that uncoupling caused by DCM mutation blunts the response to β-adrenergic stimulation, leading to a reduced cardiac reserve. The resulting contractile dysfunction under stress, predisposes the heart to dilated cardiomyopathy in the long term. This hypothesis is supported at the whole animal level by the observation of a significantly reduced response to acute β-adrenergic agonists in cardiac α-actin E361G, cTnT ΔK210 and α-tropomyosin E54K DCM mutant mice (Song et al., 2010, Du et al., 2007, Rajan et al., 2007). Mutation-dependent changes in absolute myofibrillar Ca^{2+} sensitivity may also contribute to the DCM phenotype, but the lack of a correlation indicates that they are not necessary for the DCM phenotype and in the cases of cardiac α-actin E361G and α-tropomyosin E54K mutations, uncoupling is the only functional difference between mutant and wild-type. We propose that the uncoupling blunts the response to β-adrenergic stimulation in the hearts of patients with familial DCM and that this causes reduced cardiac reserve that could be sufficient to trigger DCM in the long term.

7.2 The Hypercontractile Phenotype

Two mutations, one on skeletal actin, K326N, and one on β-tropomyosin, ΔK7, were initially classified as Nemaline myopathy causing. This evaluation was based only on the presence of nemaline bodies in the myofibers, but it did not correlate with the clinical features showed by the patients.

The case of actin K326N was more extreme, the patient was classified as 'stiff' and did not survive more than 9 months. The β-tropomyosin ΔK7 patients, instead, although showing the

same contractures when young in 5 different unrelated families, later developed generalised weakness, and therefore were diagnosed as Nemaline myopathy.

These two mutants, though, showed a very similar molecular phenotype, with enhanced Ca^{2+}-sensitivity to a similar level, representing a gain-of-function, and in the case of ΔK7 also an increased motile velocity. The changes with ΔK7 were found with 50% mutant protein, although the level of incorporation in the patients' sarcomeres was not successfully measured. My work on actin K326N provided a sufficient base to relate the 'stiff' phenotype to the hypercontractile phenotype found in actin from biopsy, since we also proved that it was expressed and incorporated into thin filaments through 2D electrophoresis.

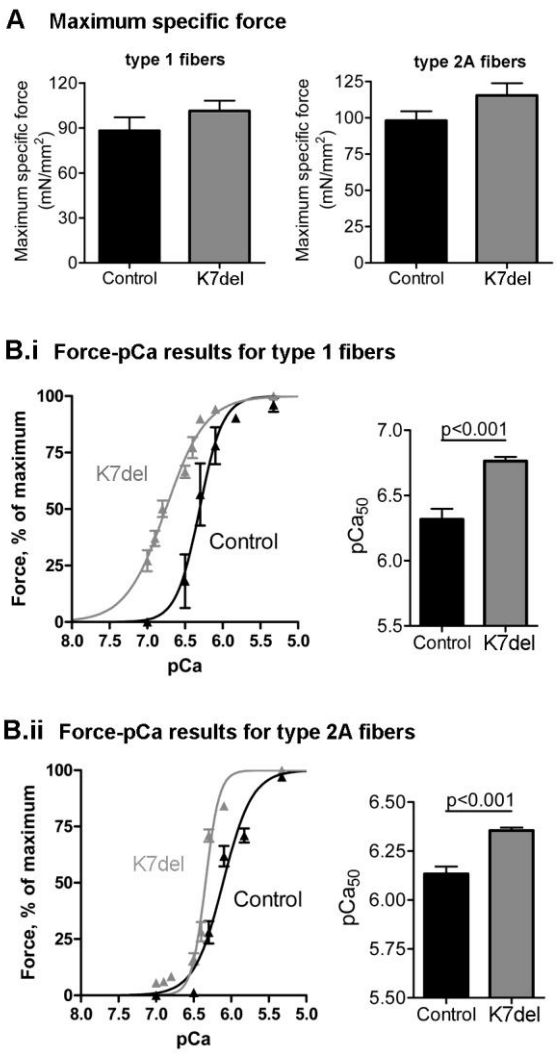
The considerations on ΔK7 are more complex. In other experiments performed in Dr N. Clarke's lab it was shown how β-tropomyosin ΔK7 was expressed and incorporated into high-molecular weight complexes in the biopsies. It was also present in a larger concentration than the WT, but they could not discern whether the mutant protein was mainly contained in the sarcomeres or the nemaline rods. When they performed the same experiments in primary cultured patient myotubes or with transfected cultured C2C12 cells, which were not developing any nemaline rods, it was seen that the mutant protein, even though present in high-molecular weight complexes, represented only a small fraction of the total.

Important experiments were performed by Dr C. Ottenheijm on single myofibers from patient biopsies. These confirmed the high Ca^{2+}-sensitivity phenotype (Figure 7.2). This indicates how the poison effect of the mutant can be seen with the native proportion. My work then indicated that the mutation is sufficient to express the phenotype seen in the myofibres in completely synthetic thin filaments.

These are unique findings for mutants correlated with muscle myopathies, which are usually associated with a loss-of-function inducing muscle weakness. It is interesting that, in both

cases, the initial diagnosis, based on histology was proven to be misleading and therefore emphasises the superiority of genetic and functional assays in establishing the true phenotype.

Figure 7.2: Force generation and Ca^{2+}-sensitivity of single myofibres dissected from ΔK7 patient muscle biopsy



These graphs were kindly supplied by Dr Ottenheijm. They represent his findings on the force generation and Ca^{2+}-sensitivity of the ΔK7 β-tropomyosin mutant fibres from a patient biopsy compared with donor fibres. His results agreed with mine on the description of a hypercontractile phenotype.

Other sarcomeric mutations associated with contractural phenotypes have been associated with increased Ca^{2+} sensitivity and hypercontractile phenotypes (Table 7.1), such as mutants

linked to distal arthrogryposes (Robinson et al., 2007). The patients described in this thesis, though, had generalised stiffness and contractures, unlike the prominent contractures of the distal limbs, and moreover had nemaline bodies, which have never been described in connection to that disease. This might be related also to the expression pattern of the gene mutated, for example *ACTA1* is expressed in all skeletal muscles.

Also in the heart, contractile proteins mutations have been described as causing hypercontractile phenotypes with increased Ca^{2+}-sensitivity, as the usual molecular phenotype in HCM (Table 7.1). Comparison of all the gain-of-function myopathies shows striking similarity: Ca^{2+}-sensitivity is increased 2-3 fold in every case, yet the patient phenotypes are very variable in severity.

Table 7.1: Examples of gain-of-function mutations in thin filaments proteins

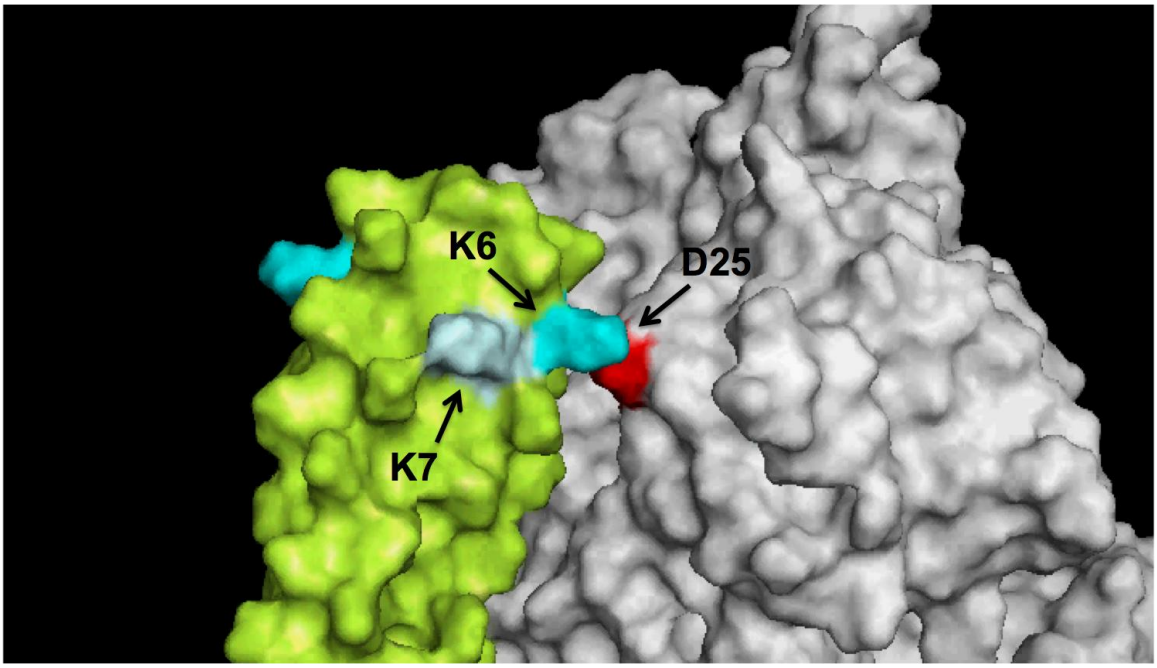
Diagnosis	Gene	Mutation	Ca^{2+} sensitivity	Reference
Stiff muscles	***ACTA1***	**K326N**	↑	Chapter 6
Infantile contractures	***TPM2***	**ΔK7**	↑	Chapter 5
Distal Arthrogryposes	***TPM2***	**R91G**	↑	Robinson *et al.*, 2007
	TNNI2	**R174Q**	↑	
		R156ter	↑	
	TNNT3	**R63H**	↑	
HCM	***ACTC***	**E99K**	↑	Song *et al., 2011*
	TPM1	**E180G**	↑	Bing *et al., 2000*
	TNNT2	**K280N**	↑	Messer, unpublished

↑ = higher than WT

Structurally K326 interacts with tropomyosin in the 'closed' state (as illustrated in Figure 6.7), therefore the mutation may destabilize that state, shifting the equilibrium towards the 'open' state. K7 instead is in a run of 3 Lys (K5-K7), in which K6 interacts with actin Asp25 in the 'closed' state again (Figure 7.3). The deletion of the neighbouring lysine would interfere with this interaction and alter the equilibrium away from the 'closed' state.

In conclusion, these two skeletal muscle mutations represent the first reported causes of hypercontractile phenotypes in the presence on nemaline bodies, which, so far, had only been connected with muscle weakness. This indicates that several different molecular mechanisms could lead to the formation of nemaline bodies and that they probably cannot be considered as markers of a congenital myopathy leading just to muscle weakness.

Figure 7.3: Structural model showing the contact between actin D25 and tropomyosin K6 when the actin-tropomyosin complex is in the "closed" state



Structure of actin filament (grey), with highlighted in red D25, tropomyosin (green) with K6 in blue and K7 in pale blue. In the 'closed' state D25 and K6 are in direct contact forming an ionic bond; just on the side is K7. The effects of the deletion of Arg7 may disrupt this interaction shifting the equilibrium to the 'open' state thus causing the hypercontractile phenotype. Molecules rendered in Pymol using pdb file from Li *et al.* (2011).

7.3 Tropomyosin Mutations and Skeletal Muscle Myopathy: An Undefined Situation

The investigation on β- and γ-tropomyosin mutations leading to one or more of the skeletal muscle diseases, Nemaline myopathy, Cap disease and CFTD, could not provide definitive results on the functional modifications inducing a pathway (Table 7.2). None of the two tropomyosin isoforms is expressed in the heart and in fact none of the mutations considered produced any cardiac complication in the patients.

It is clear, from the IVMA experiments, that all of the mutations considered provide negative modifications in the normal functioning of the thin filaments, therefore acting as poison peptides when incorporated, but there has not been a direct correlation between one contractile phenotype and the formation of a macromolecular structure or its absence.

Table 7.2: Summary of the findings on β- and γ-tropomyosin

Tm Isoform	Mutation	Ratio	Diagnosis	Actin Binding	Max Motile Velocity	Ca^{2+} sensitivity	Solid Data?
β	ΔK7	50%	Hypercontractile	=	↑	↑	YES
		100%		↓	↓	↑	NO
	E41K	100%	CD	=	↓	↓	YES
	ΔK49	100%	CD	↓	↓	↑	NO
	E117K	100%	CFTD	=	↓	↓	YES
	ΔE139	100%	CD	↓	↓	↑	NO
	Q147P	100%	NM	↓	↓	↓	NO
γ	A4V	100%	CFTD	Time dependent	=	↓	NO
	R91P	100%	CFTD	Time dependent	=	↓	NO
	L100M	100%	CFTD	Time dependent	↓	↓	NO
	R167C	100%	CFTD, CD	Time dependent	=	↓	NO
	R167H	100%	CFTD, CD, NM	Time dependent	=	↓	NO

↑ = higher than the WT; ↓ = lower than the WT; "=" = very similar to the WT.

The fact that these mutants would induce generalised muscle weakness, in most cases more severe than in cardiomyopathies, leads us to expect an evident molecular phenotype. This was not the case as most of the mutations only induced a shift in the Ca^{2+}-sensitivity of 2-3 fold, which is similar to what was observed with cardiac DCM and HCM mutations. The only exception to the rule was the mutation D292V on skeletal actin linked to CFTD, which completely switched off the thin filaments (Chapter 6). The patient had quite severe clinical features and we used his muscle biopsy tissue for the experiments (Laing et al., 2004).

The γ-tropomyosin mutations were all linked to CFTD and they all seemed to show a consistent phenotype of decreased Ca^{2+}-sensitivity. Because of the technical issues with isolating tropomyosin from the baculovirus pellets, those results cannot be considered as definitive data. Interestingly, the β-tropomyosin E117K mutation, which can be considered as CFTD linked based on a re-examination of the histology, also showed a decrease in the Ca^{2+}-sensitivity as its molecular phenotype. If more solid data could be gathered on the γ-tropomyosin mutations by obtaining well regulated thin filaments, these preliminary indications could be tested.

The other β-tropomyosin mutations showed a range of molecular phenotypes. Three of these mutations were linked to Cap disease, but two deletion mutations (ΔK49 and ΔE139) had a much lower affinity to actin associated with an increased Ca^{2+}-sensitivity, while the third one had a normal affinity to actin and a decreased Ca^{2+}-sensitivity. Neither of the two deletion mutations was reported to cause episodes of peculiar contractions or stiffness. This may exclude a hypercontractile phenotype and differentiates them from the phenotype of ΔK7, which, moreover, was reported to have nemaline bodies, not cap structures. In that case the discovery of the hypercontractile molecular phenotype prompted a reconsideration of the

profile of the patients with a final change in diagnosis. The last mutation, Q147P, which was linked to canonical Nemaline myopathy, showed a lower affinity to actin and a lower Ca^{2+}-sensitivity. Thus even this mutant, that shows the same histological features of ΔK7, does not share the same molecular phenotype.

It must be considered also that in all these patients there was a trend to have a higher percentage of slow-twitch muscle fibres than normal and for type 1 fibres to be smaller than expected. Both are findings that are common to most forms of congenital myopathy and likely represent long-term adaptations to pathological stimuli.

The general indication given by this study is that probably there is no direct correlation between the functional molecular phenotype induced by a mutation in tropomyosin and the formation of one of these supramolecular disorganised structures seen in histology. It is very likely that different causes can lead to the same effect and that therefore those structures are not a good marker to identify the dysfunctional process that caused them. It is also a possibility that other genetic factors would intervene as adaptations or compensations, leading to the formation of one or the other or none. This could explain the genetic overlap between diseases.

7.4 Future Work

Concerning the DCM investigation, the IVMA data were solid and thorough, with 7 mutants analysed and at least one on each of the thin filaments subunits. It could be interesting to test the uncoupling also with other experimental techniques involving single fibres or myofibrils from patients or transgenic mouse heart samples. This would require the development of procedures accomplishing total dephosphorylation of TnI directly in the fibres without any modification of their functions. Following the indications given by this study, new *in vivo*

experiments can be planned. To investigate the physiological consequences of uncoupling by studies involving β-adrenergic stimulation and the consequences of stress-induced pathways seems the best way to proceed. On animal models it could be done using drugs (acute dobutamine, chronic angiotensin), exercise or through surgery (aortic constriction).

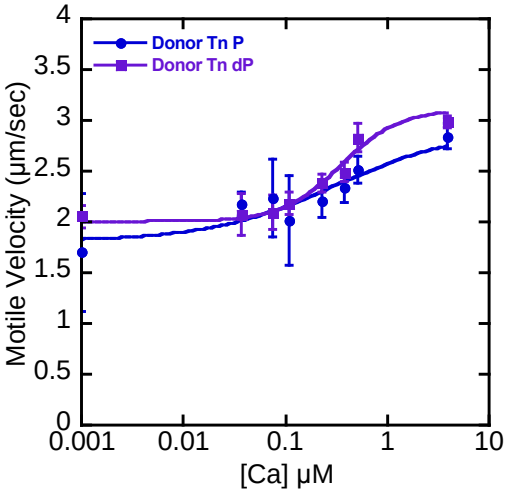
The β-tropomyosin mutations study was incomplete. Because of a lack of recombinant protein many of the experiments planned could not be performed. More repeats of the basic 100% mutant protein experiments should be performed to obtain statistical significance. Then experiments with 50:50 WT:mutant mixes should be performed and also with mixes of α- or γ-tropomyosin, so that the question about the differences between homo- and heteropolymers could be addressed. When in possession of biopsies of these mutations, coupled IVMA and single fibre experiments could be performed.

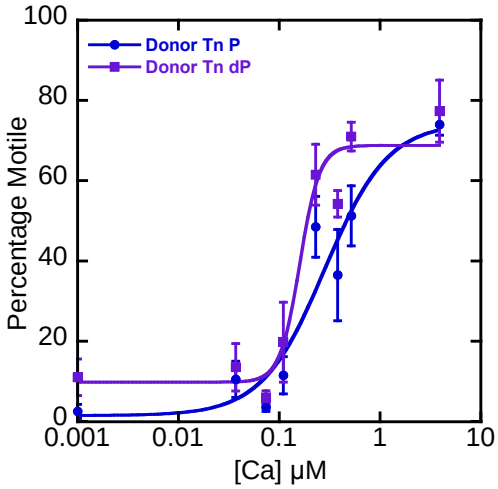
Finally, with the γ-tropomyosin mutants the most important problem to be overcome is to obtain pure monomeric tropomyosin and then test its ability to regulate the thin filaments in IVMA. Based on other workers experience, γ-tropomyosin is not different from α- and β-tropomyosin, so it seems likely that we were using a defective batch of γ-tropomyosin baculovirus/*sf9* expression pellets.

APPENDIX

From section 3.2.3.3

Donor human heart, P/dP 1





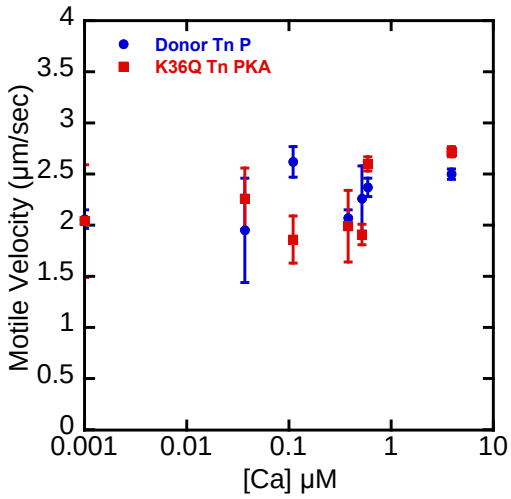
	Value	Error
Hill Coefficient	1.39	0.74
EC_{50}	0.28	0.12

	Value	Error
Hill COefficient	4.45	2.37
EC_{50}	0.16	0.03

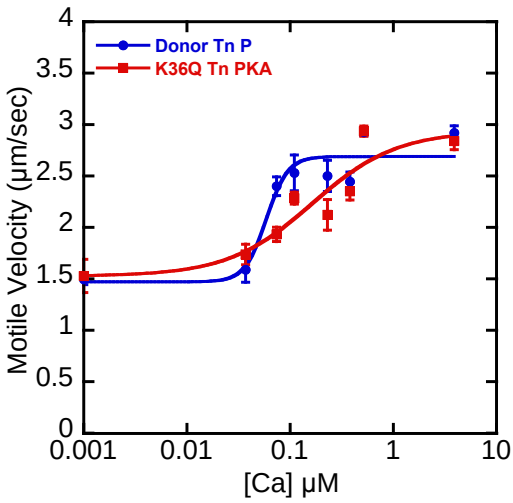
From section 4.1.3.1

Donor / K36Q , P/PKA

1

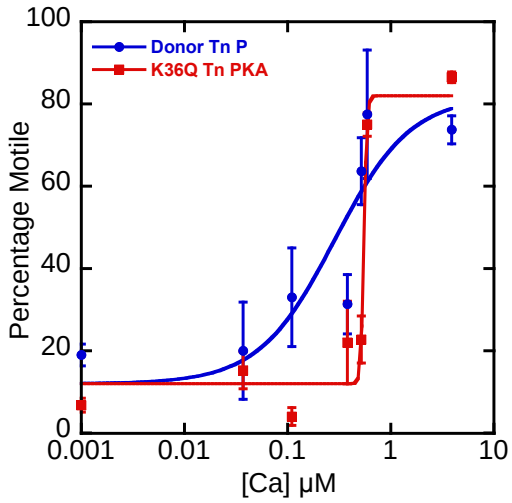


2



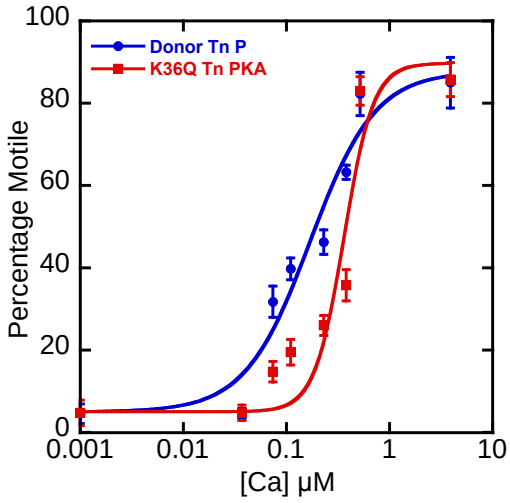
	Value	Error
Hill Coefficient	4.18	3.06
EC_{50}	0.06	0.02

	Value	Error
Hill Coefficient	1.06	0.65
EC_{50}	0.16	0.11



	Value	Error
Hill Coefficient	1.18	0.58
EC_{50}	0.29	0.11

	Value	Error
Hill Coefficient	30.91	10.18
EC_{50}	0.55	0.01

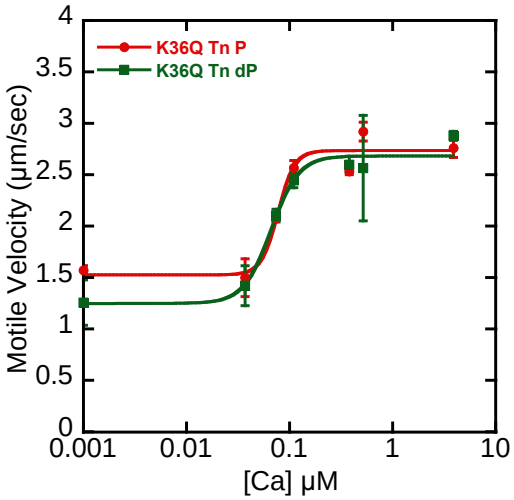


	Value	Error
Hill COefficient	1.38	0.38
EC_{50}	0.17	0.04

	Value	Error
Hill Coefficient	3.06	1.4
EC_{50}	0.36	0.06

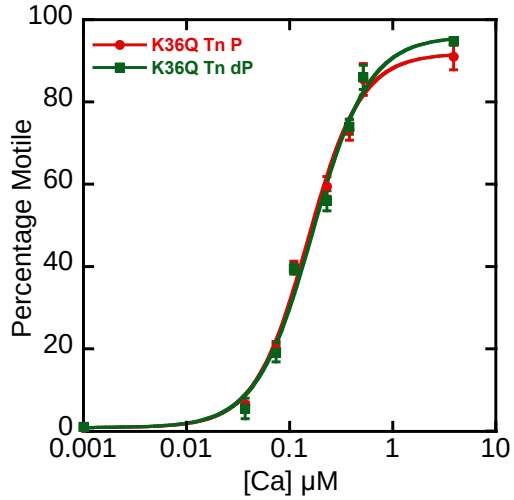
From section 4.1.3.2

K36Q, P/dP 2



	Value	Error
Hill Coefficient	5.39	3.5
EC_{50}	0.08	0.01

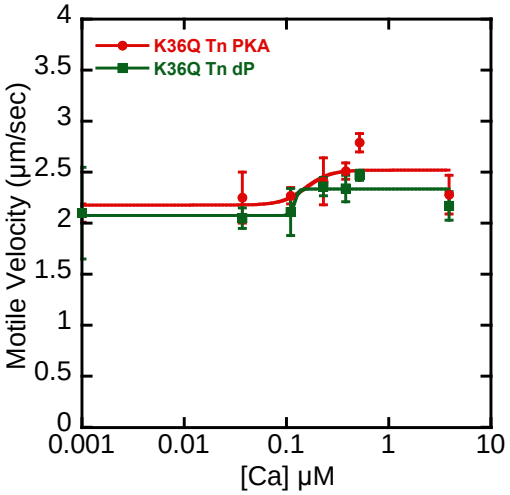
	Value	Error
Hill Coefficient	3.26	1.22
EC_{50}	0.07	0.01

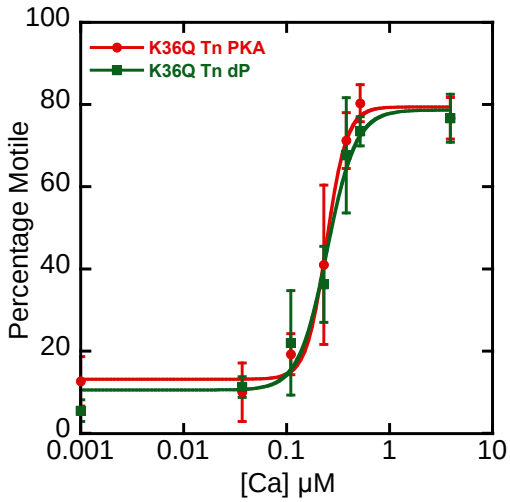


	Value	Error
Hill Coefficient	1.68	0.18
EC_{50}	0.15	0.01

	Value	Error
Hill Coefficient	1.59	0.19
EC_{50}	0.17	0.02

K36Q, PKA/dP
1

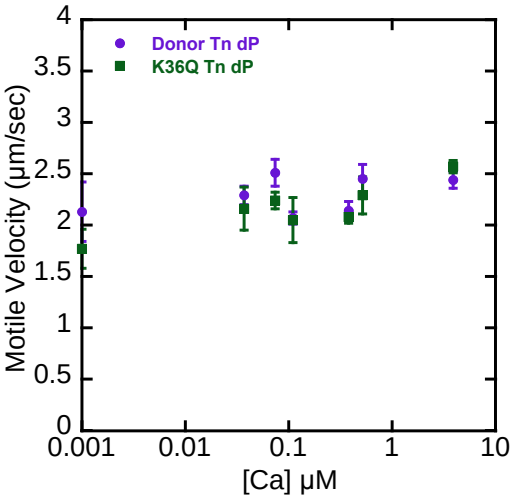


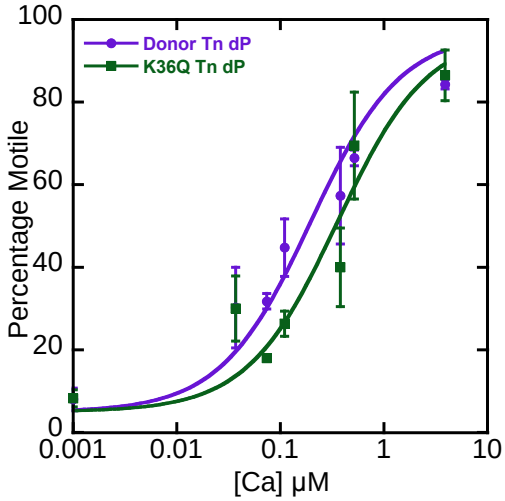


	Value	Error
Hill Coefficient	4.44	1.32
EC_{50}	0.24	0.02

	Value	Error
Hill Coefficient	3.14	1.04
EC_{50}	0.25	0.03

Donor / K36Q, dP
2



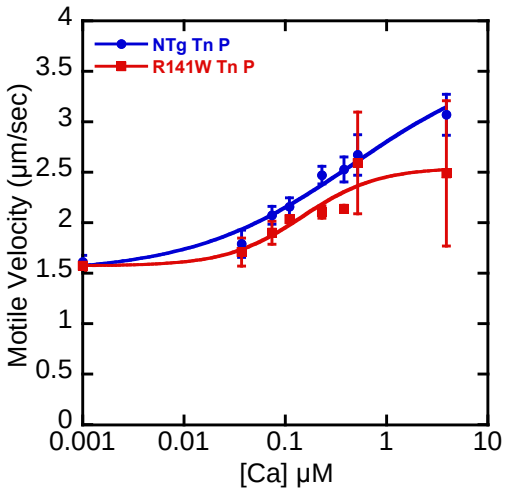


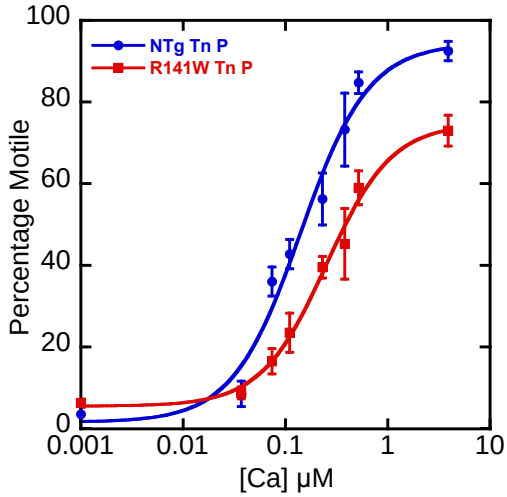
	Value	Error
Hill Coefficient	1	/
EC_{50}	0.2	0.04

	Value	Error
Hill Coefficient	1	/
EC_{50}	0.36	0.09

From section 4.2.2.1

NTg / R141W, P 3



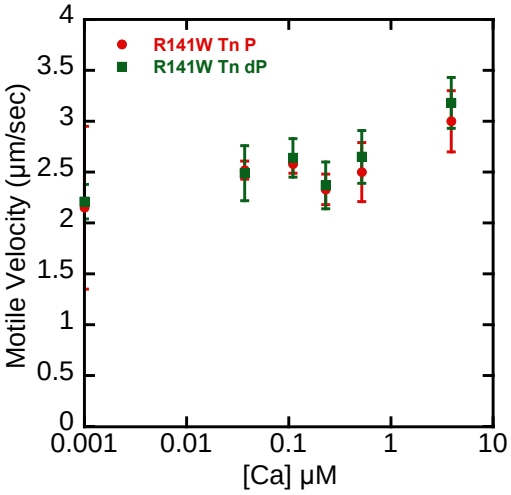


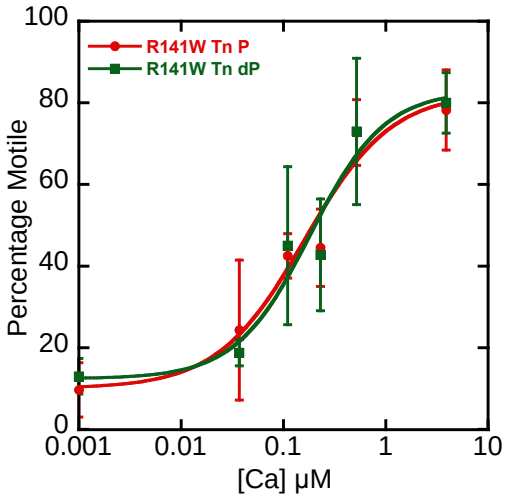
	Value	Error
Hill Coefficient	1.31	0.29
EC_{50}	0.14	0.03

	Value	Error
Hill Coefficient	1.36	0.2
EC_{50}	0.25	0.03

From section 4.2.2.2

R141W, P/dP 2

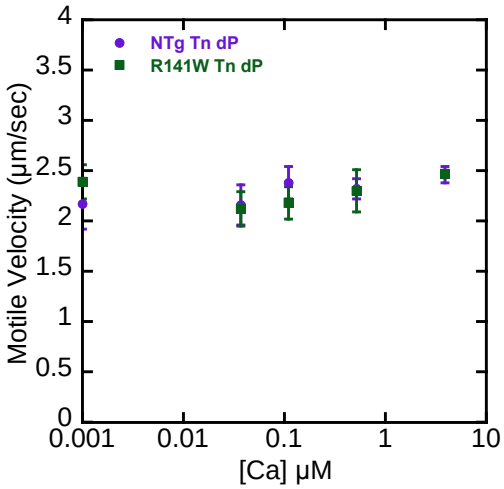


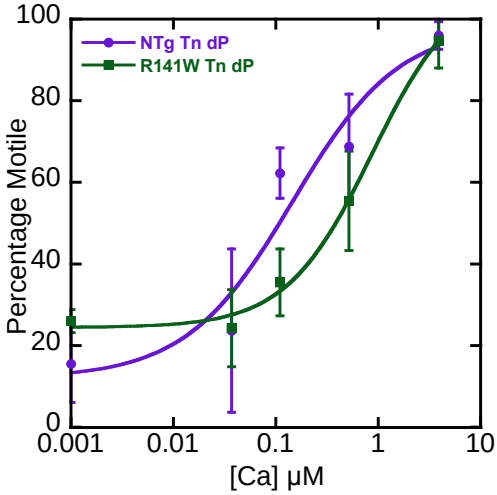


	Value	Error
Hill Coefficient	1.02	0.5
EC_{50}	0.16	0.08

	Value	Error
Hill COefficient	1.19	0.69
EC_{50}	0.18	0.1

NTg / R141W, dP
3





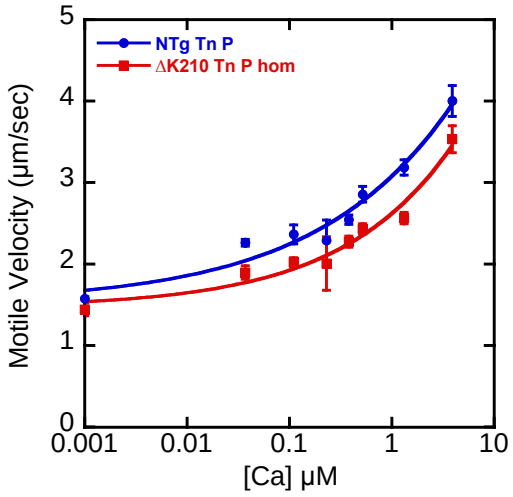
	Value	Error
Hill Coefficient	1	/
EC_{50}	0.15	0.2

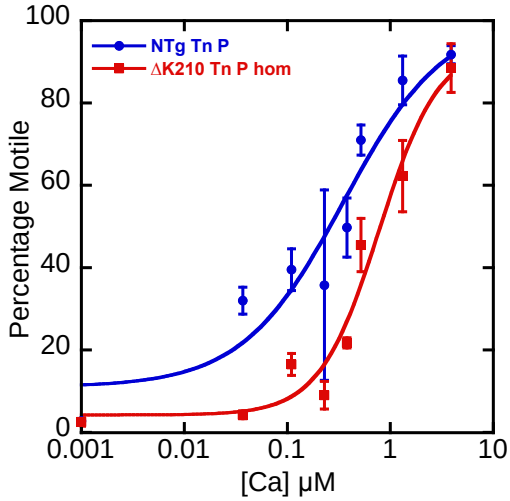
	Value	Error
Hill Coefficient	1.04	0.5
EC_{50}	0.87	0.61

From section 4.2.4.1

NTg / ΔK210 hom, P

2

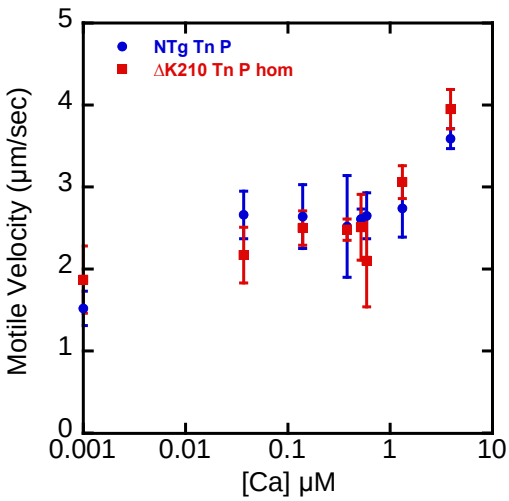


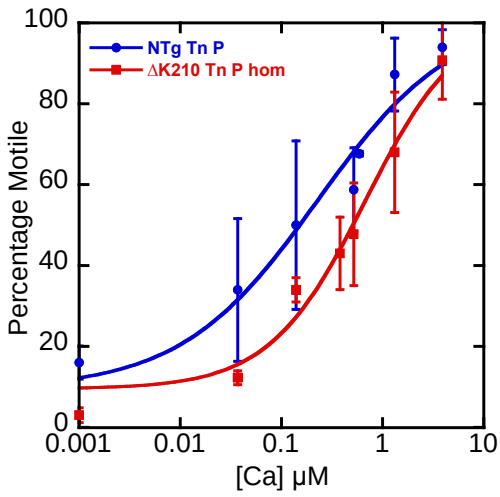


	Value	Error
Hill Coefficient	1	/
EC_{50}	0.35	0.19

	Value	Error
Hill Coefficient	1.5	0.29
EC_{50}	0.78	0.17

3

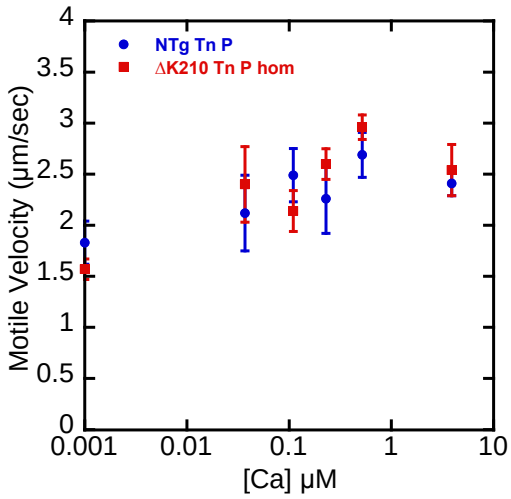


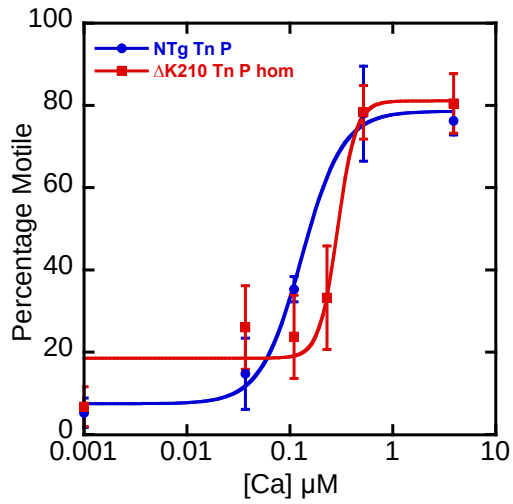


	Value	Error
Hill Coefficient	1	/
EC_{50}	0.22	0.05

	Value	Error
Hill Coefficient	1	/
EC_{50}	0.67	0.09

4

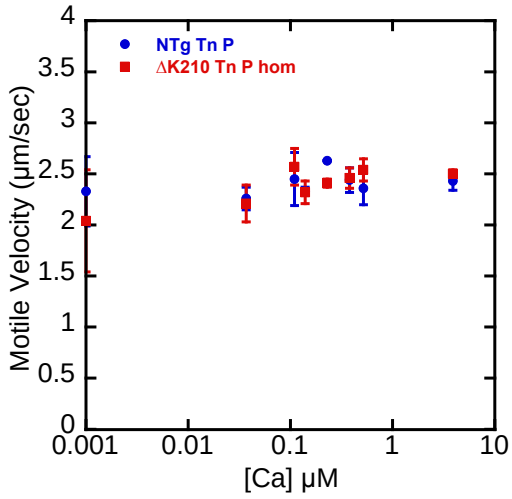


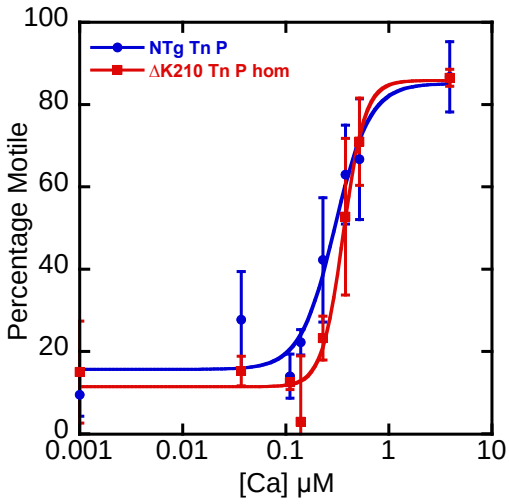


	Value	Error
Hill Coefficient	2.18	1.09
EC_{50}	0.13	0.02

	Value	Error
Hill Coefficient	4.87	5.27
EC_{50}	0.29	0.09

6



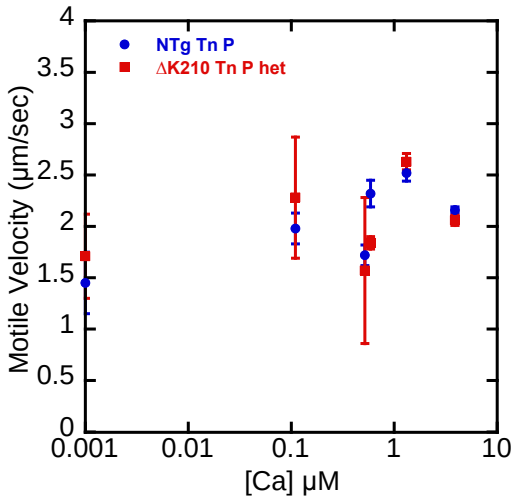


	Value	Error
Hill Coefficient	2.57	0.96
EC_{50}	0.3	0.06

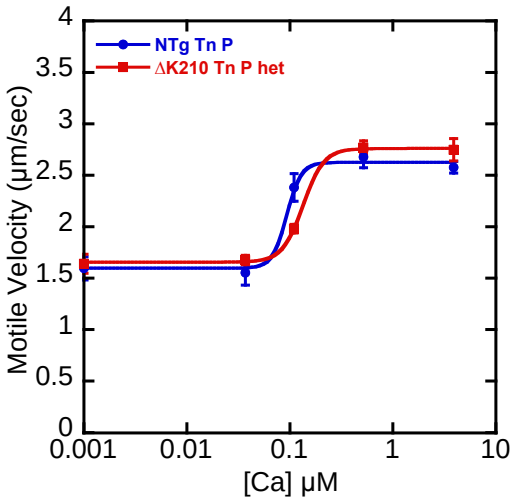
	Value	Error
Hill Coefficient	4.16	1.2
EC_{50}	0.36	0.03

NTg / ΔK210 het, P

1

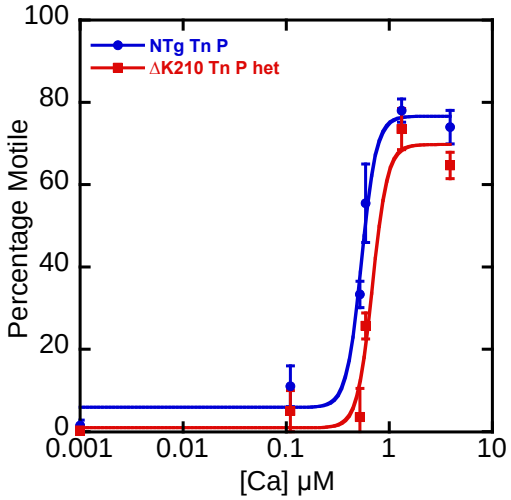


4



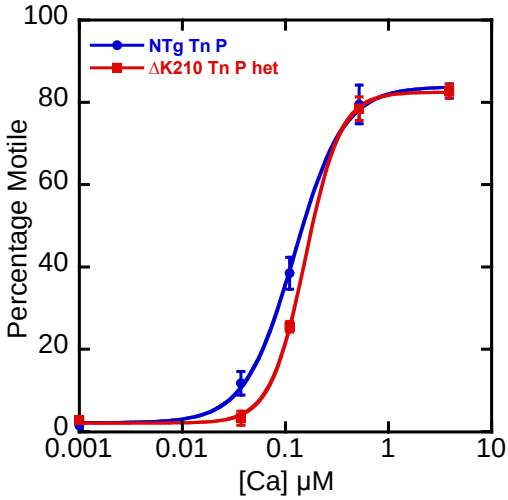
	Value	Error
Hill Coefficient	6.17	35.15
EC_{50}	0.09	0.09

	Value	Error
Hill Coefficient	4.29	5.96
EC_{50}	0.13	0.04



	Value	Error
Hill Coefficient	6	/
EC_{50}	0.54	0.03

	Value	Error
Hill Coefficient	6	/
EC_{50}	0.69	0.06



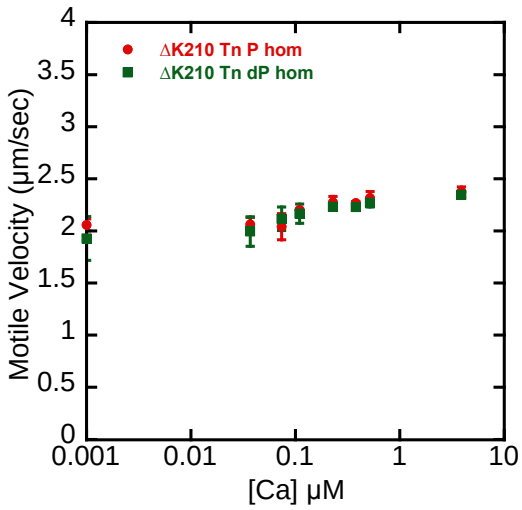
	Value	Error
Hill Coefficient	1.81	0.25
EC_{50}	0.12	0.01

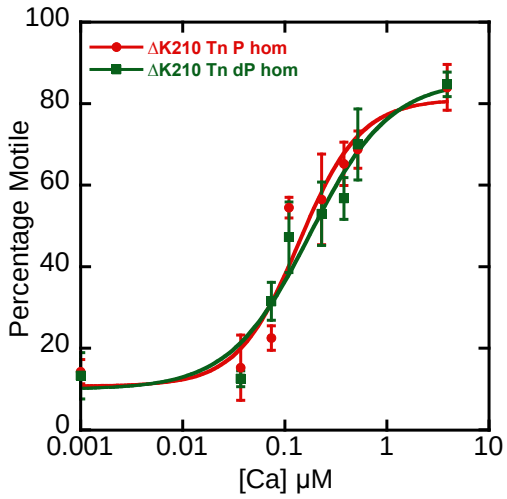
	Value	Error
Hill Coefficient	2.54	0.28
EC_{50}	0.16	0.01

From section 4.2.4.2

ΔK210 hom, P/dP

1

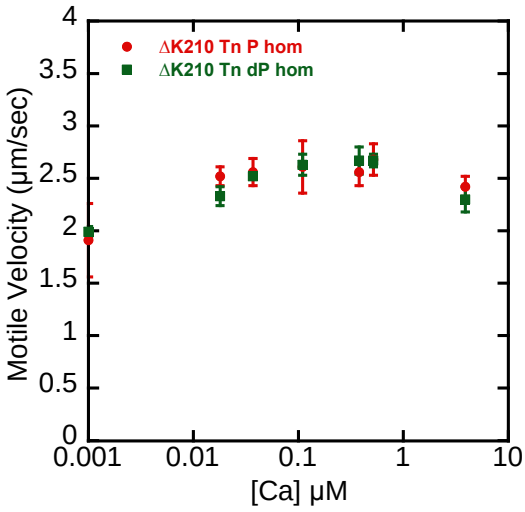


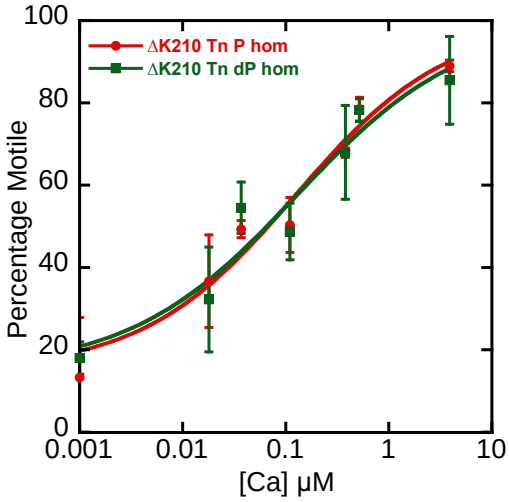


	Value	Error
Hill Coefficient	1.44	0.61
EC_{50}	0.14	0.05

	Value	Error
Hill Coefficient	1.11	0.38
EC_{50}	0.18	0.06

2



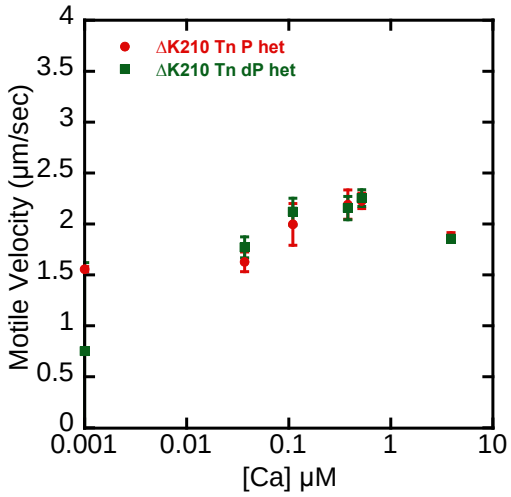


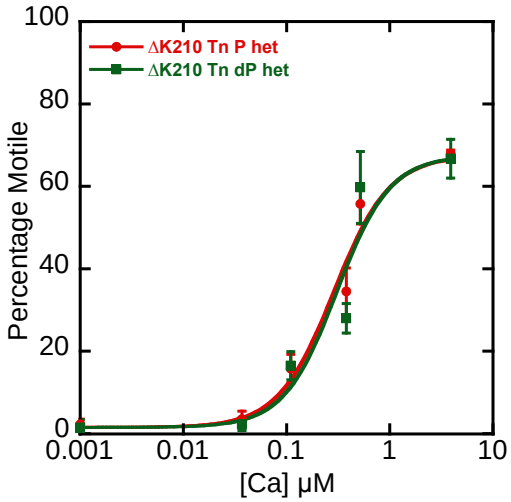
	Value	Error
Hill Coefficient	1	/
EC_{50}	0.12	0.03

	Value	Error
Hill Coefficient	1	/
EC_{50}	0.13	0.04

ΔK210 het, P/dP

1

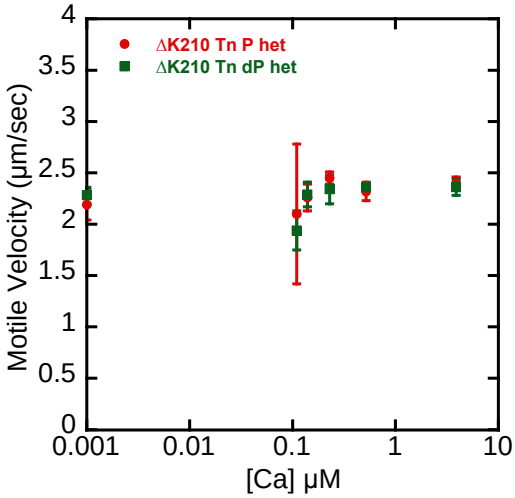


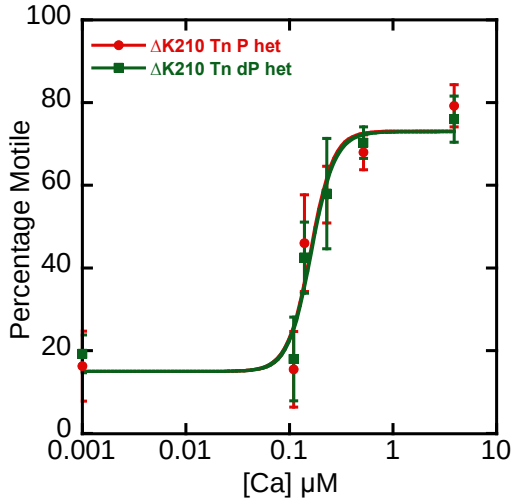


	Value	Error
Hill Coefficient	1.62	0.39
EC_{50}	0.29	0.04

	Value	Error
Hill Coefficient	1.69	0.73
EC_{50}	0.31	0.07

4

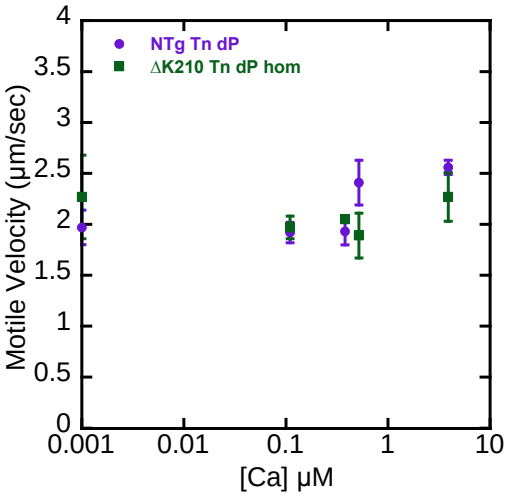


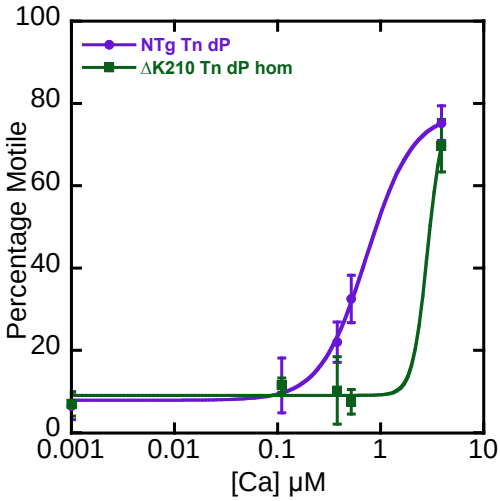


	Value	Error
Hill Coefficient	3.93	2.14
EC_{50}	0.16	0.03

	Value	Error
Hill Coefficient	3.87	1.5
EC_{50}	0.16	0.02

NTg / ΔK210 hom, dP
1



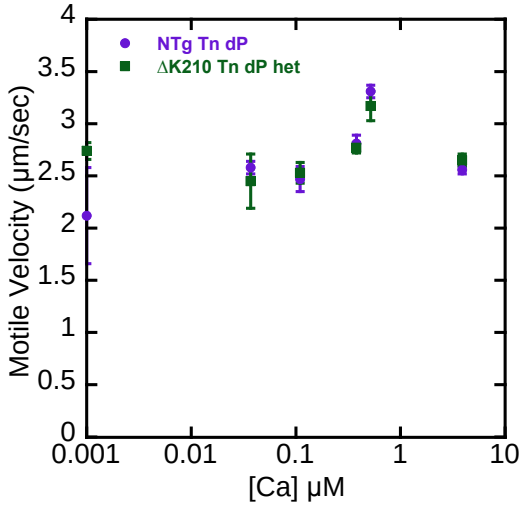


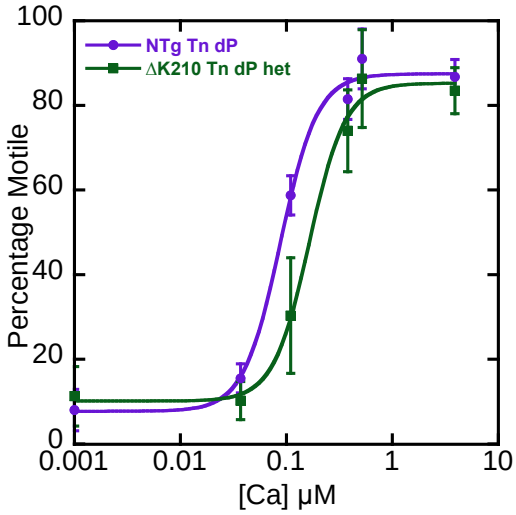
	Value	Error
Hill Coefficient	1.93	0.3
EC_{50}	0.73	0.08

	Value	Error
Hill Coefficient	6.02	653.88
EC_{50}	2.86	96.49

NTg / ΔK210 het, dP

1

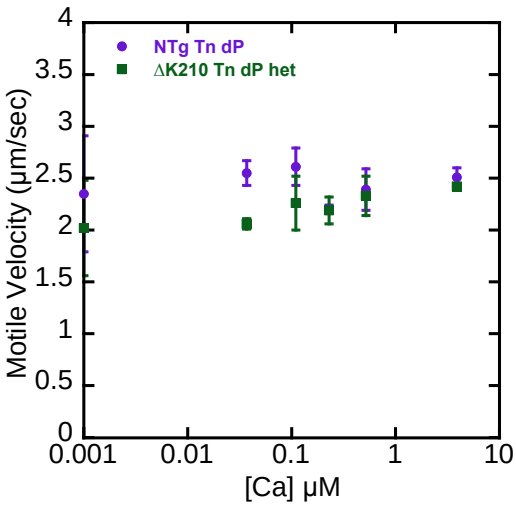


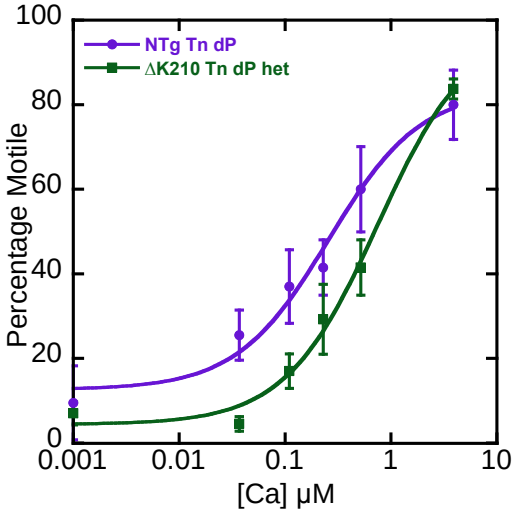


	Value	Error
Hill Coefficient	2.5	0.69
EC_{50}	0.09	0.01

	Value	Error
Hill Coefficient	2.56	0.7
EC_{50}	0.16	0.03

4





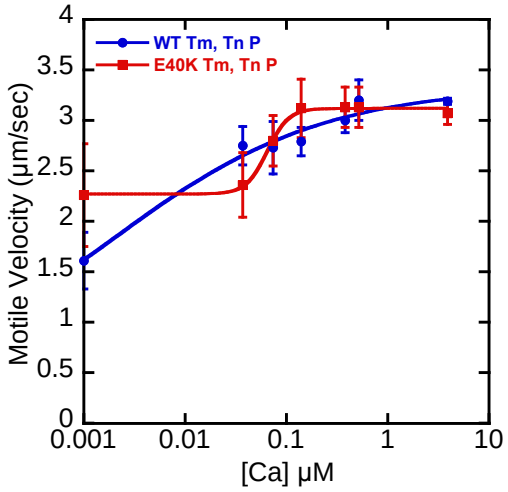
	Value	Error
HIll Coefficient	1	/
EC_{50}	0.26	0.07

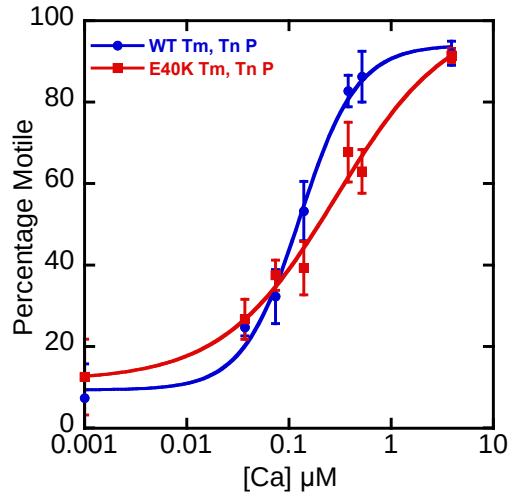
	Value	Error
Hill Coefficient	1	/
EC_{50}	0.75	0.16

From section 4.3.2.1

WT / E40K, P

1

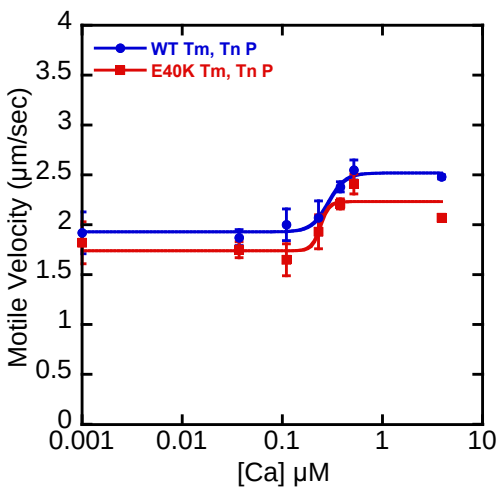


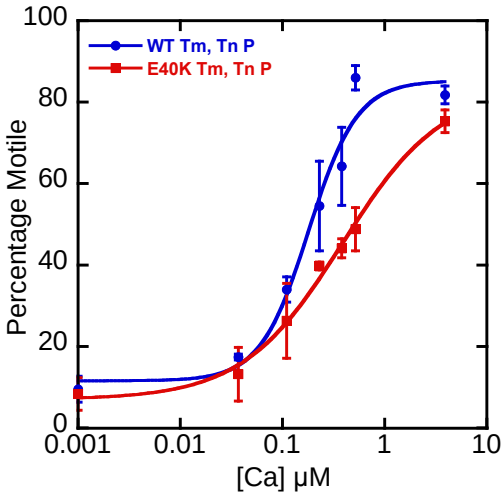


	Value	Error
Hill Coefficient	1.55	0.24
EC_{50}	0.13	0.02

	Value	Error
Hill Coefficient	0.78	0.25
EC_{50}	0.29	0.14

3





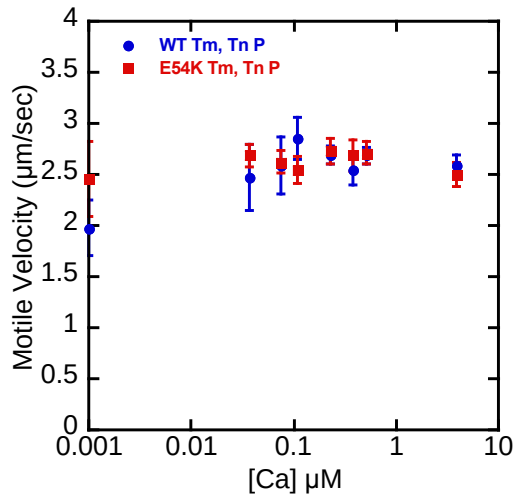
	Value	Error
Hill Coefficient	1.83	0.64
EC_{50}	0.18	0.04

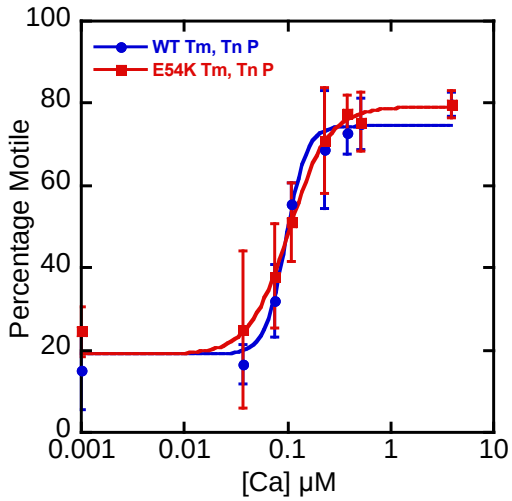
	Value	Error
Hill Coefficient	1	/
EC_{50}	0.39	0.09

From section 4.3.2.2

WT / E54K, P

1

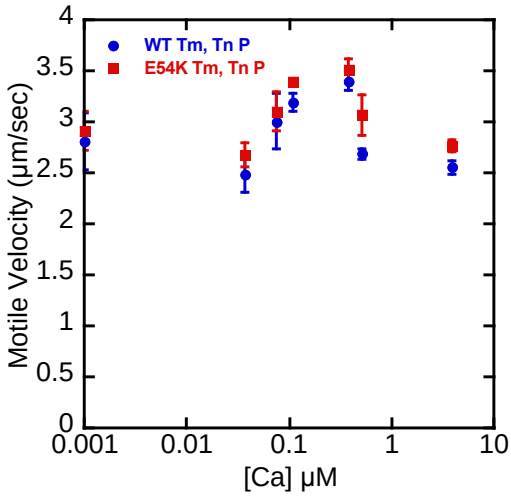


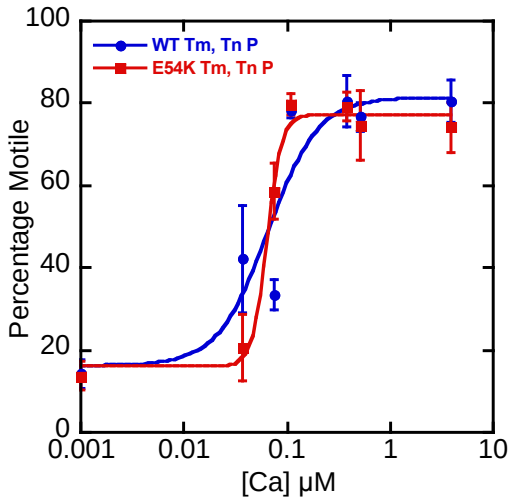


	Value	Error
Hill Coefficient	4.4	1.21
EC_{50}	0.1	0.01

	Value	Error
Hill Coefficient	2.25	0.34
EC_{50}	0.1	0.01

2

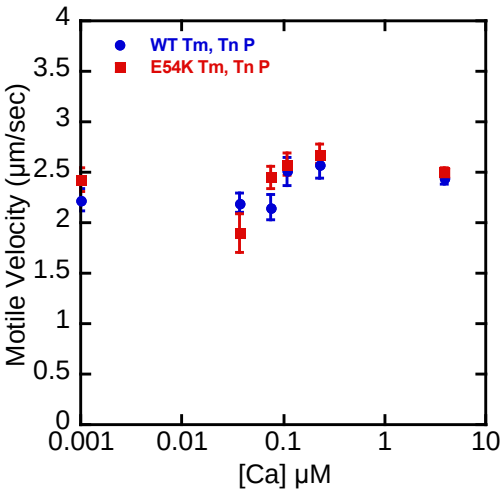


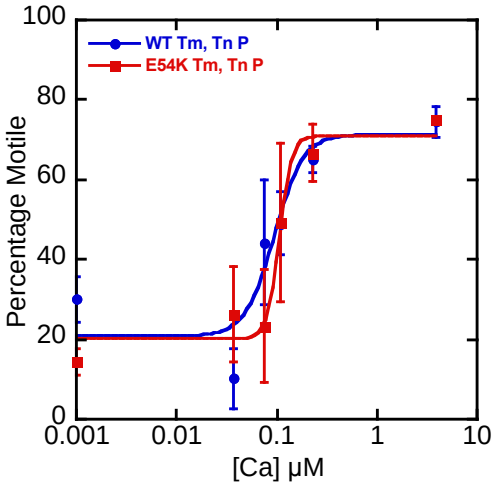


	Value	Error
Hill Coefficient	1.8	1.65
EC_{50}	0.07	0.03

	Value	Error
Hill Coefficient	6.18	3.51
EC_{50}	0.06	0.01

3





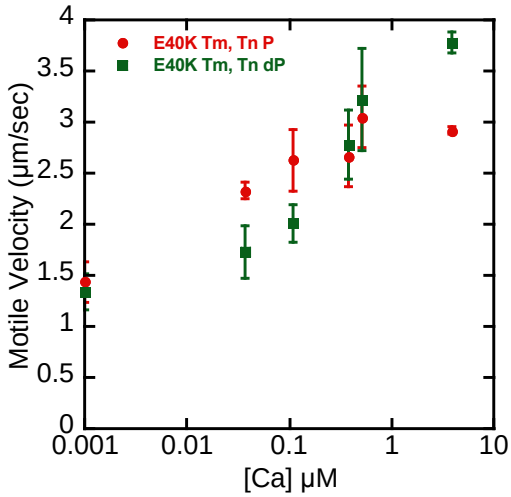
	Value	Error
Hill Coefficient	3.01	3.41
EC_{50}	0.09	0.03

	Value	Error
Hill Coefficient	7.1	6.24
EC_{50}	0.11	0.01

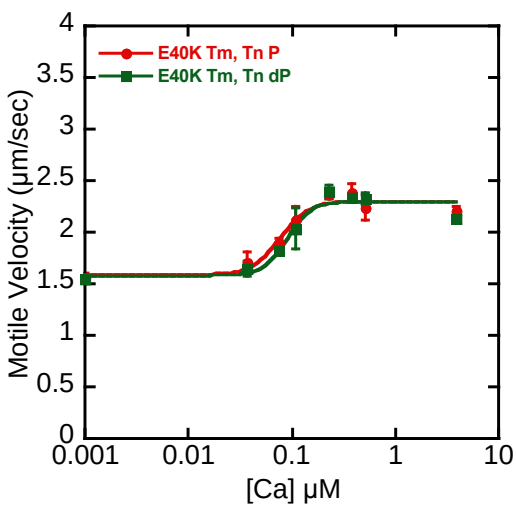
From section 4.3.2.3

E40K, P/dP

1

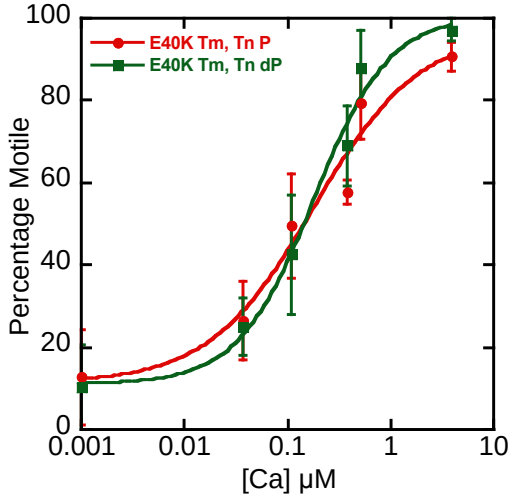


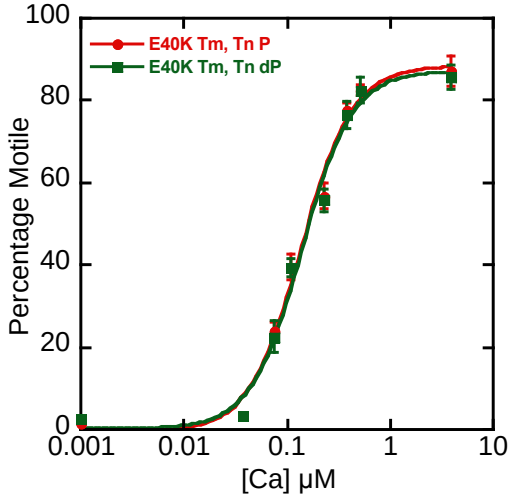
3



	Value	Error
Hill Coefficient	3.21	1.64
EC_{50}	0.08	0.01

	Value	Error
Hill Coefficient	3.79	2.56
EC_{50}	0.09	0.01





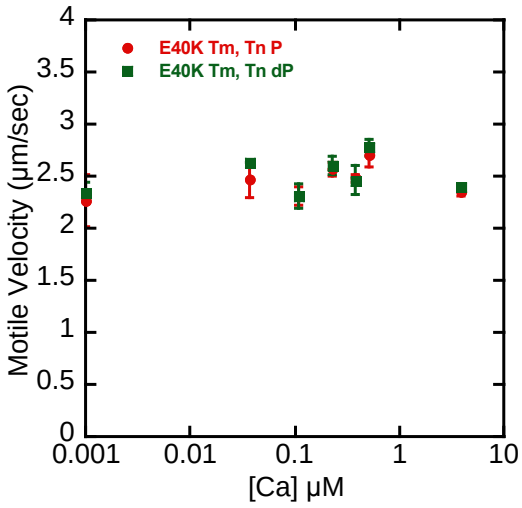
	Value	Error
Hill Coefficient	0.86	0.44
EC_{50}	0.18	0.12

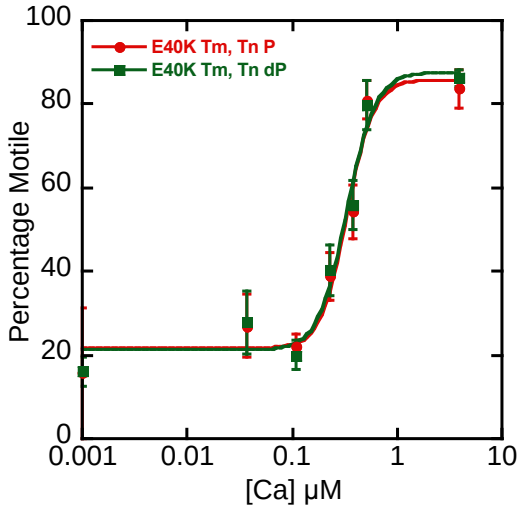
	Value	Error
Hill Coefficient	1.19	0.33
EC_{50}	0.18	0.05

	Value	Error
Hill Coefficient	1.79	0.29
EC_{50}	0.14	0.02

	Value	Error
Hill Coefficient	1.82	0.33
EC_{50}	0.14	0.02

5



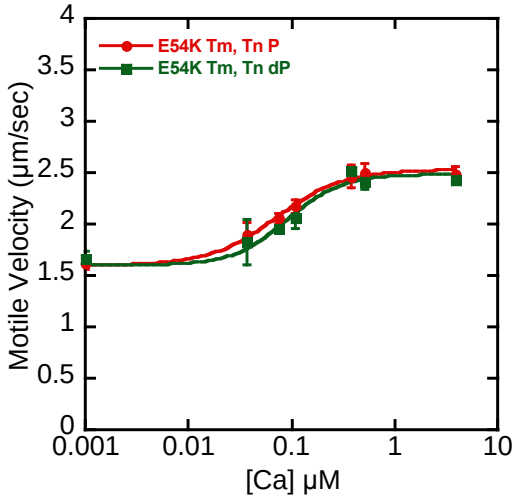


	Value	Error
Hill Coefficient	3.49	1.42
EC_{50}	0.33	0.05

	Value	Error
Hill Coefficient	3.22	1.19
EC_{50}	0.33	0.05

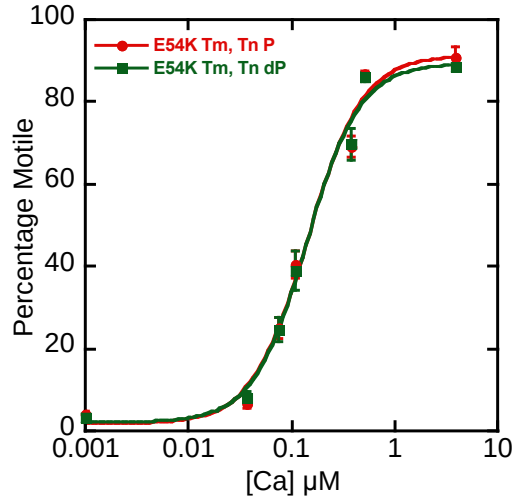
E54K, P/dP

2



	Value	Error
Hill Coefficient	1.34	0.21
EC_{50}	0.07	0.01

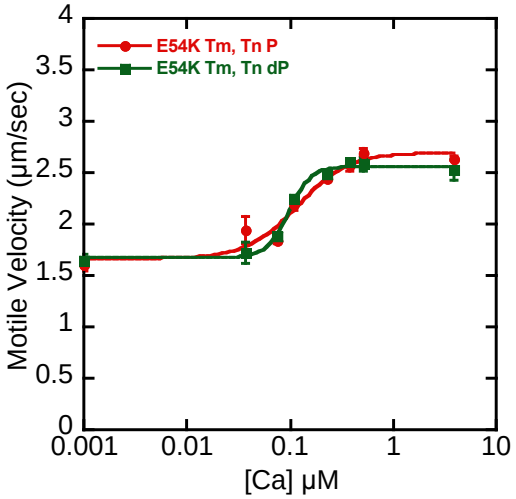
	Value	Error
Hill Coefficient	1.65	0.56
EC_{50}	0.09	0.02



	Value	Error
Hill Coefficient	1.62	0.38
EC_{50}	0.14	0.03

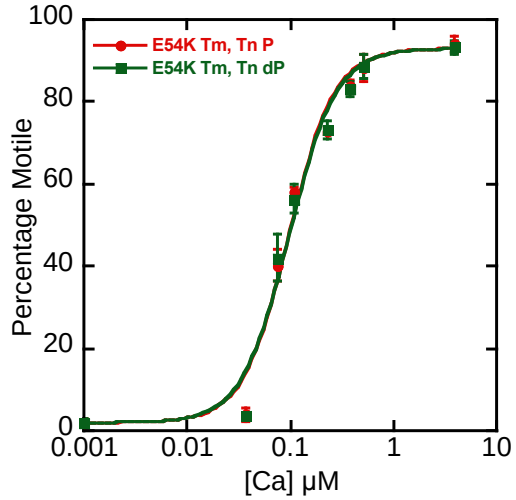
	Value	Error
Hill Coefficient	1.68	0.35
EC_{50}	0.14	0.02

3



	Value	Error
Hill Coefficient	1.76	0.69
EC_{50}	0.12	0.03

	Value	Error
Hill Coefficient	4.06	0.86
EC_{50}	0.1	0.01

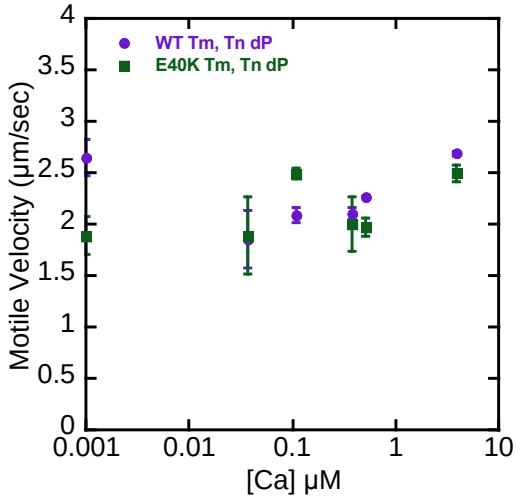


	Value	Error
Hill Coefficient	1.94	0.31
EC_{50}	0.1	0.01

	Value	Error
Hill Coefficient	1.91	0.31
EC_{50}	0.1	0.01

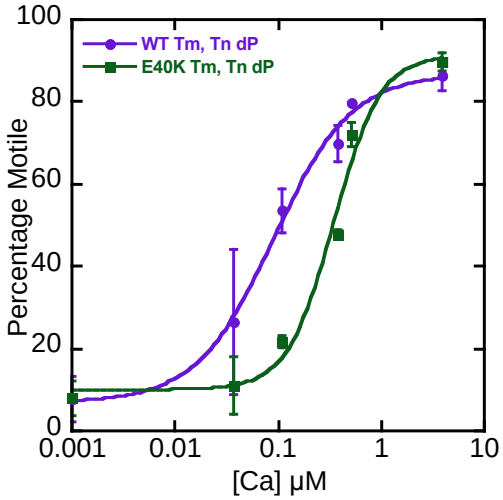
WT / E40K, dP

2



	Value	Error
Hill Coefficient	3	0.7
EC_{50}	0.05	0.01

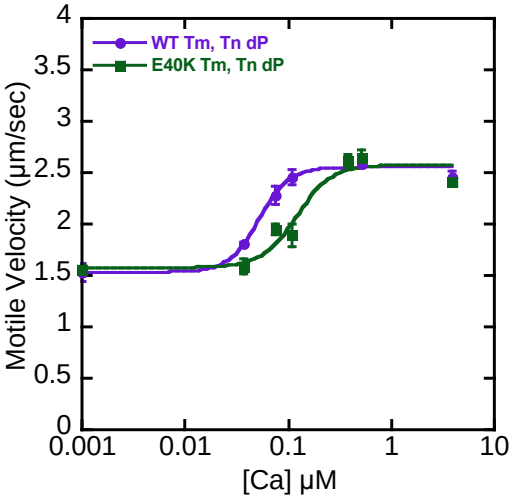
	Value	Error
Hill Coefficient	2.57	2.26
EC_{50}	0.12	0.04

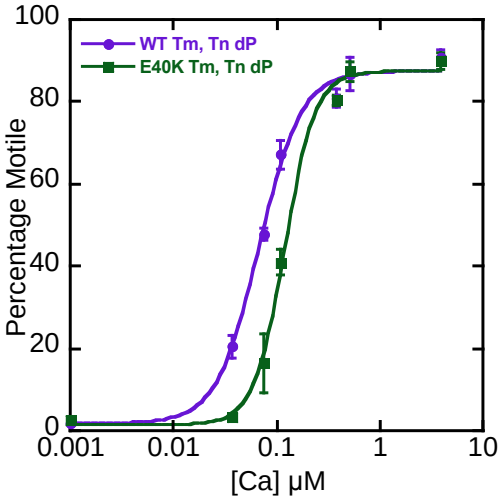


	Value	Error
Hill Coefficient	1.16	0.23
EC_{50}	0.09	0.02

	Value	Error
Hill Coefficient	1.94	0.85
EC_{50}	0.35	0.07

3



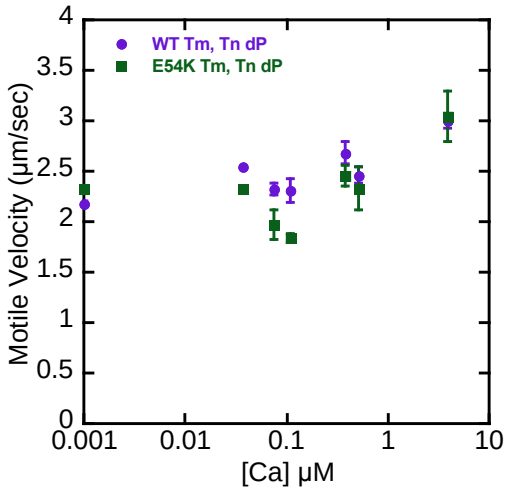


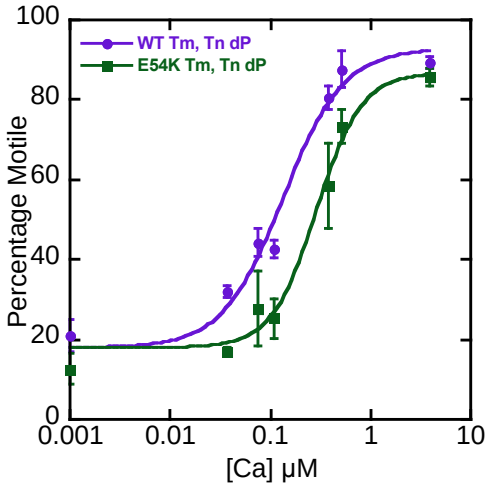
	Value	Error
Hill Coefficient	2.12	0.34
EC_{50}	0.07	0.01

	Value	Error
Hill Coefficient	2.93	0.68
EC_{50}	0.12	0.01

WT / E54K, dP

2

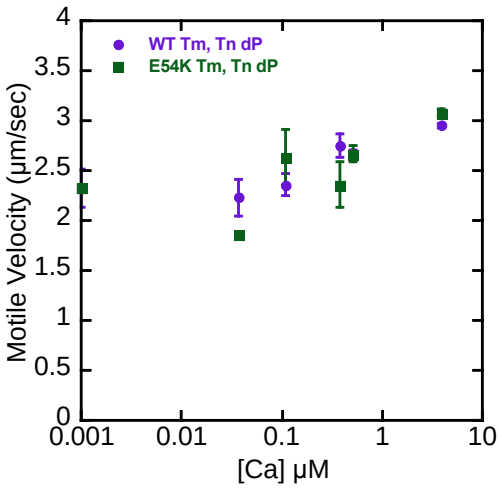


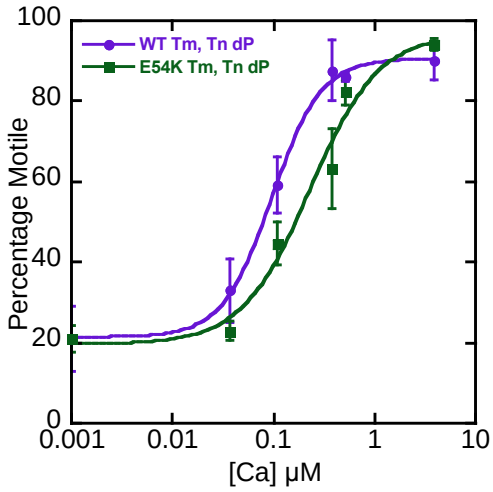


	Value	Error
Hill Coefficient	1.44	0.34
EC_{50}	0.13	0.03

	Value	Error
Hill Coefficient	1.94	0.38
EC_{50}	0.29	0.04

4





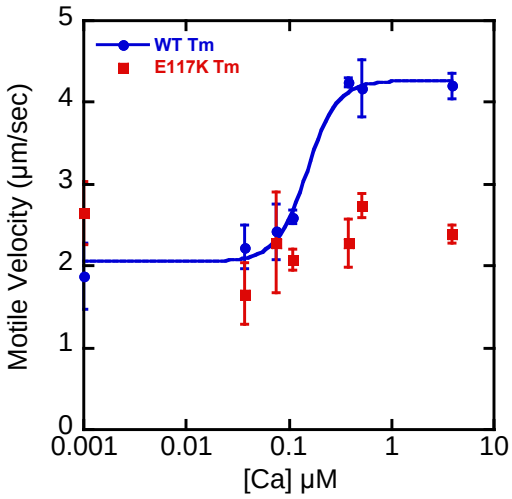
	Value	Error
Hill Coefficient	1.79	0.26
EC_{50}	0.1	0.01

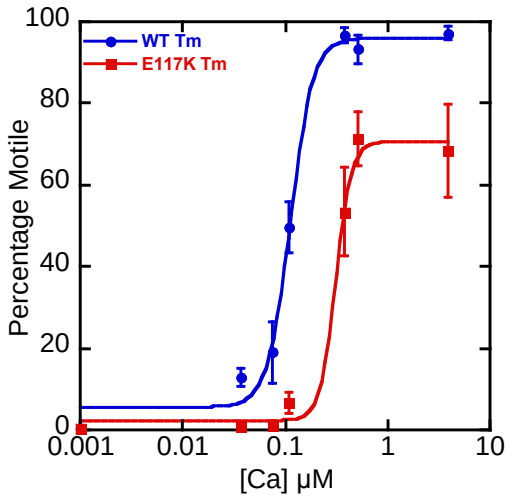
	Value	Error
Hill Coefficient	1.29	0.47
EC_{50}	0.23	0.08

From section 5.2.2

WT / E117K

2

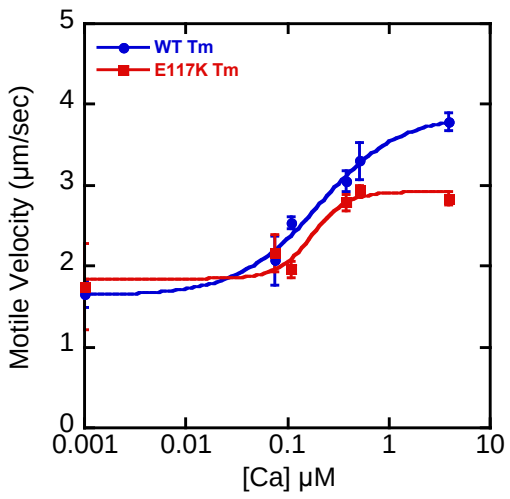


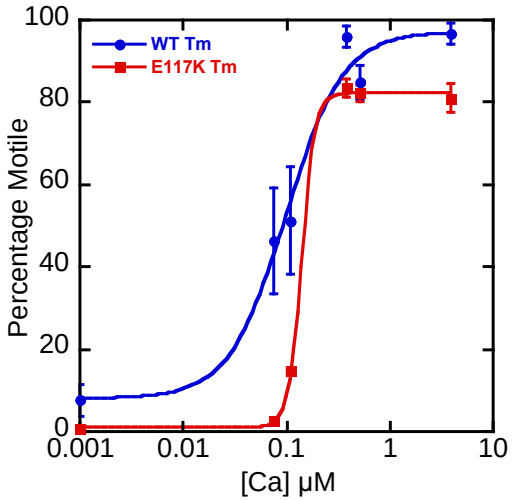


	Value	Error
Hill Coefficient	3.93	1.3
EC_{50}	0.11	0.01

	Value	Error
Hill Coefficient	5.78	4.89
EC_{50}	0.31	0.05

3





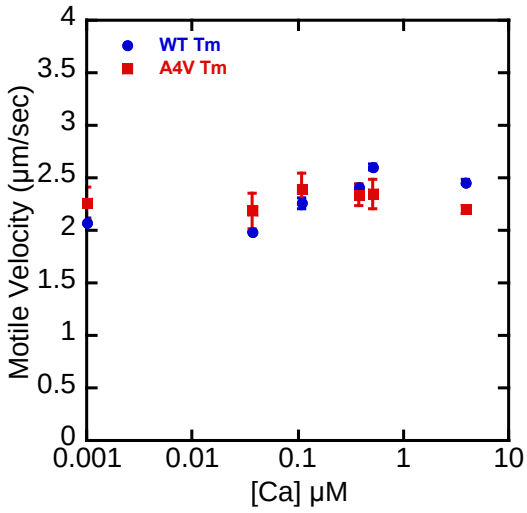
	Value	Error
Hill Coefficient	1.58	0.79
EC_{50}	0.1	0.03

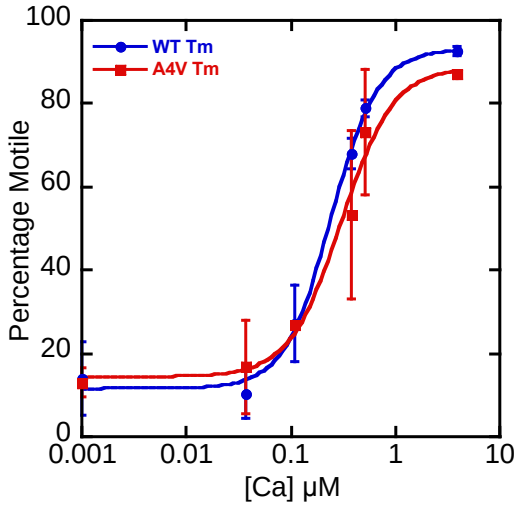
	Value	Error
Hill Coefficient	6.71	3.89
EC_{50}	0.14	0.02

From Chapter 5.3

WT / A4V

2

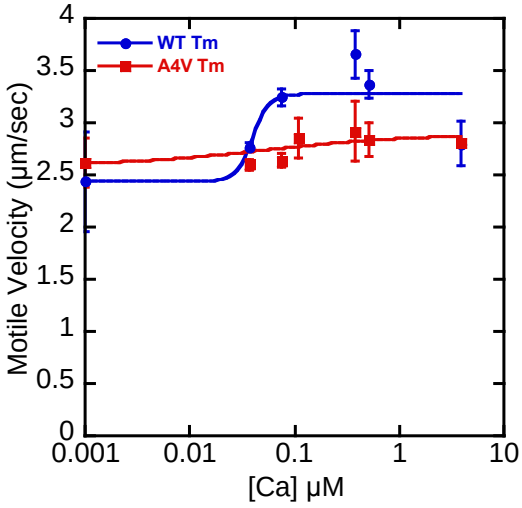


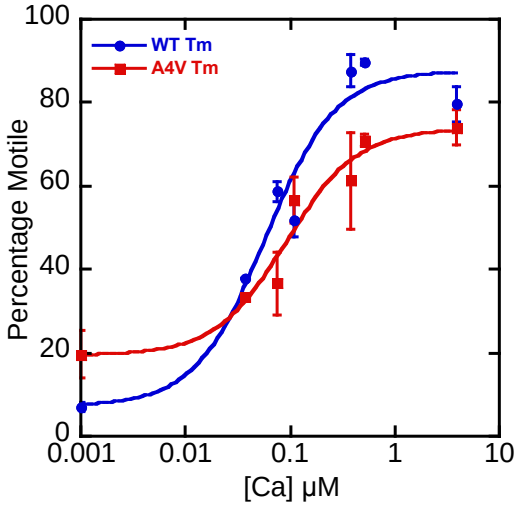


	Value	Error
Hill COefficient	1.95	0.28
EC_{50}	0.24	0.03

	Value	Error
Hill Coefficient	1.76	0.58
EC_{50}	0.3	0.06

3



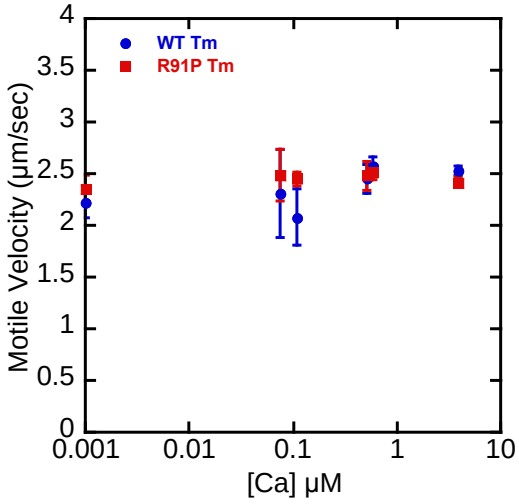


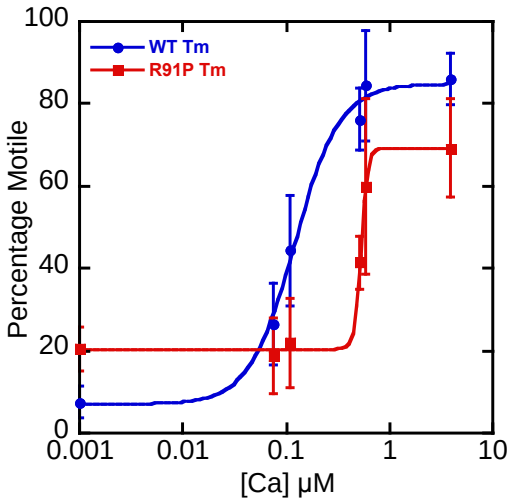
	Value	Error
Hill Coefficient	1.3	0.73
EC_{50}	0.06	0.02

	Value	Error
Hill Coefficient	1.29	0.59
EC_{50}	0.09	0.03

WT / R91P

1

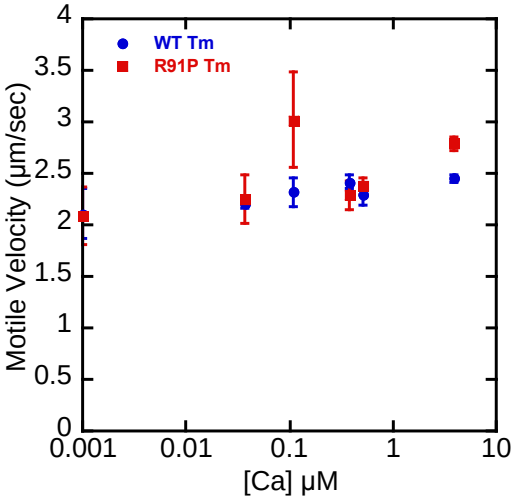


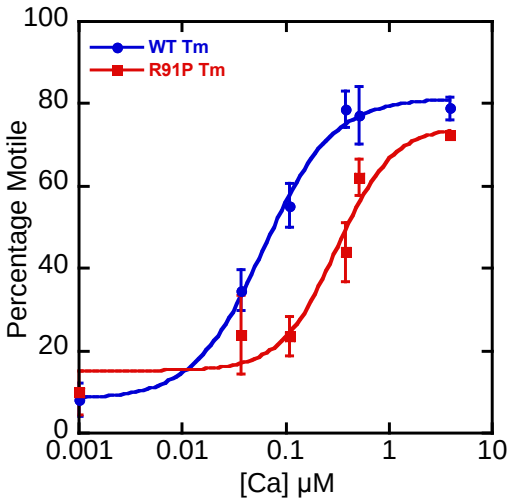


	Value	Error
Hill Coefficient	1.98	0.65
EC_{50}	0.12	0.02

	Value	Error
Hill Coefficient	13.66	2.23
EC_{50}	0.53	0.01

3



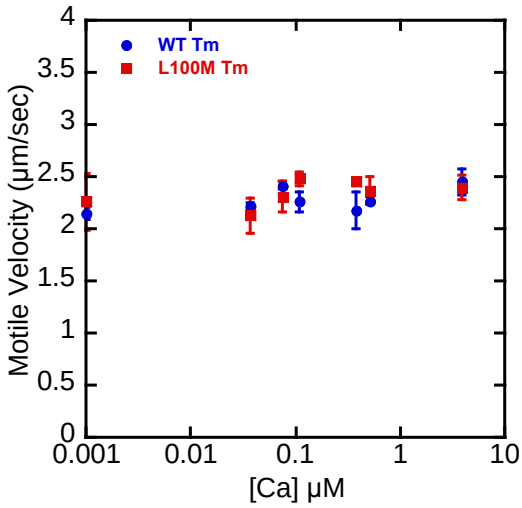


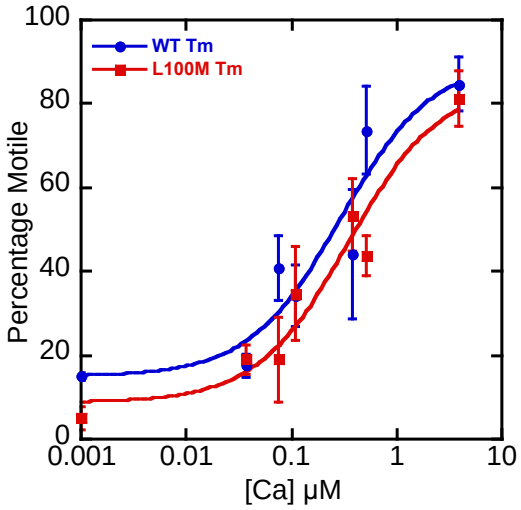
	Value	Error
Hill Coefficient	1.29	0.29
EC_{50}	0.06	0.01

	Value	Error
Hill Coefficient	1.61	1
EC_{50}	0.31	0.12

WT / L100M

1

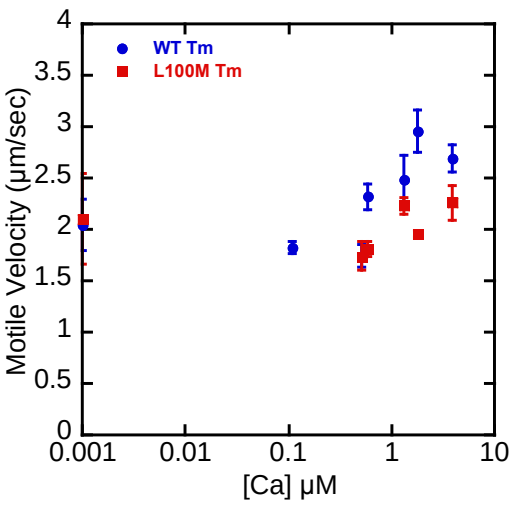


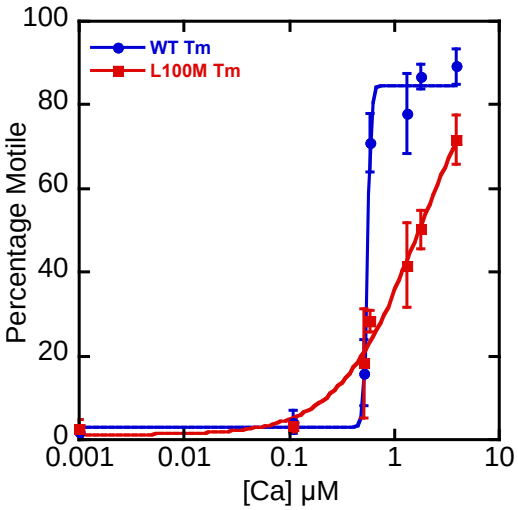


	Value	Error
Hill Coefficient	1	/
EC_{50}	0.29	0.19

	Value	Error
Hill Coefficient	1	/
EC_{50}	0.35	0.17

3



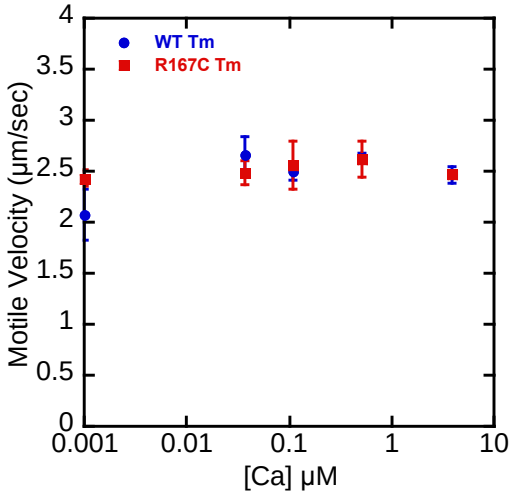


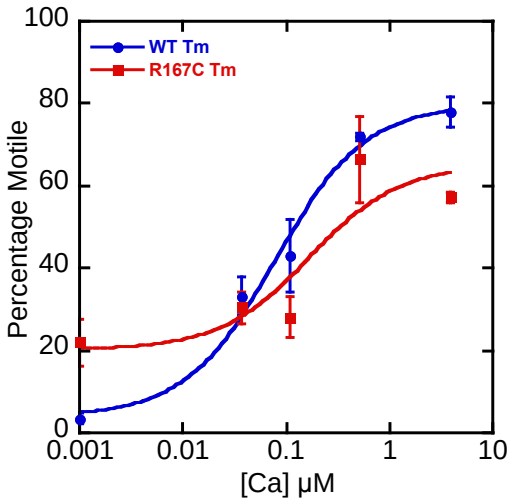
	Value	Error
Hill Coefficient	25.88	5.41
EC_{50}	0.55	0.01

	Value	Error
Hill Coefficient	1.13	0.33
EC_{50}	1.76	0.94

WT / R167C

1

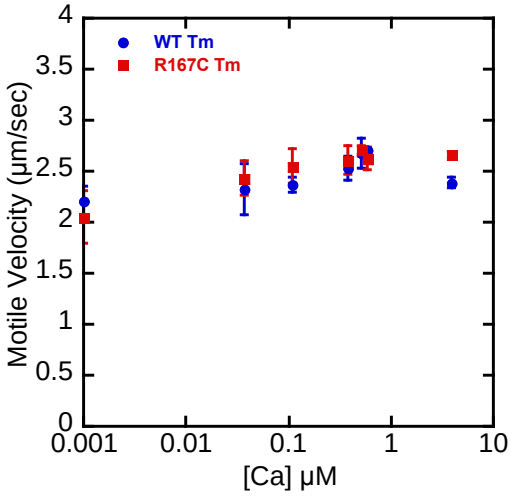


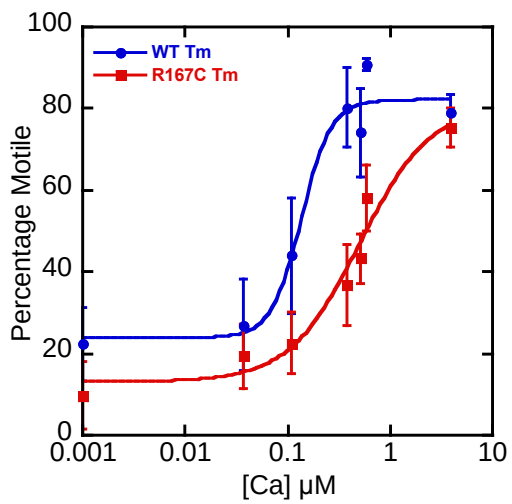


	Value	Error
Hill Coefficient	1	/
EC_{50}	0.08	0.03

	Value	Error
Hill Coefficient	1	/
EC_{50}	0.17	0.2

3





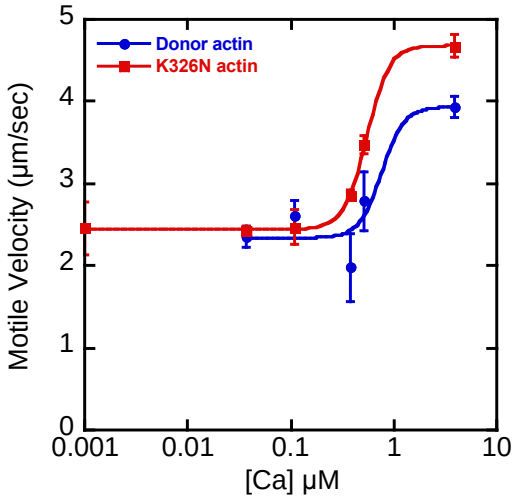
	Value	Error
Hill Coefficient	2.95	2.8
EC_{50}	0.14	0.04

	Value	Error
Hill Coefficient	1.26	0.72
EC_{50}	0.5	0.18

From section 6.2

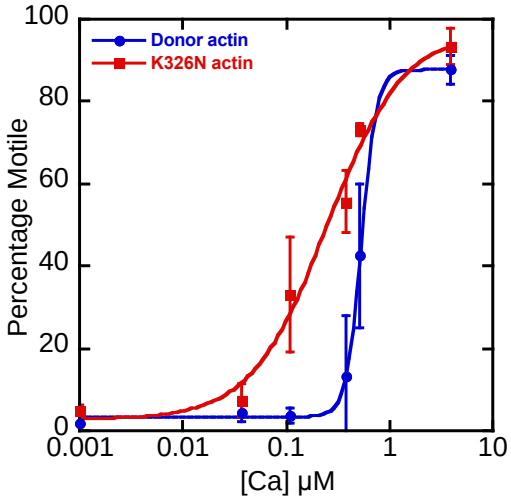
Donor / K326N

2



	Value	Error
Hill Coefficient	4	/
EC_{50}	0.76	0.38

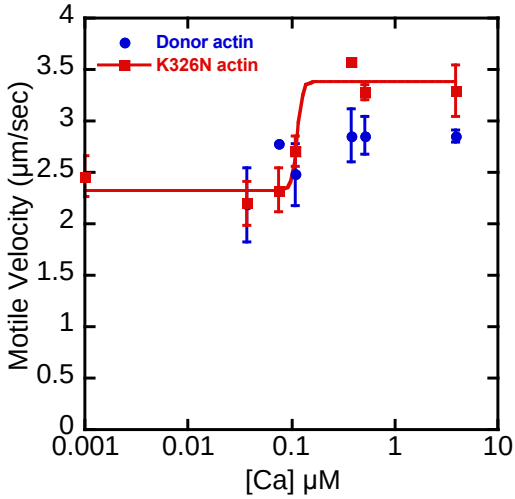
	Value	Error
Hill Coefficient	4.19	0.29
EC_{50}	0.54	0.01

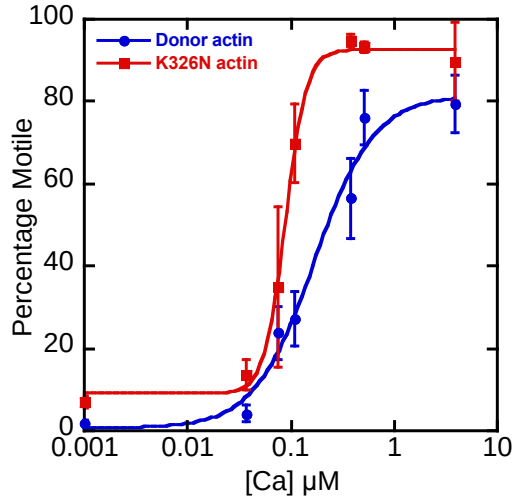


	Value	Error
Hill Coefficient	5.99	0.54
EC_{50}	0.53	0.01

	Value	Error
Hill Coefficient	1.19	0.35
EC_{50}	0.25	0.07

3

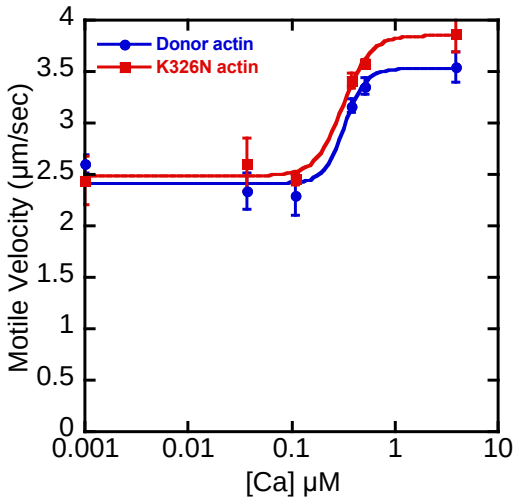




	Value	Error
Hill Coefficient	1.51	0.42
EC_{50}	0.17	0.05

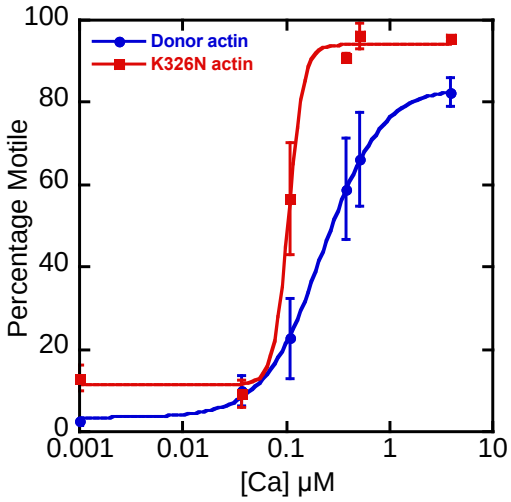
	Value	Error
Hill Coefficient	4.33	0.62
EC_{50}	0.09	0.01

4



	Value	Error
Hill Coefficient	4.39	5.83
EC_{50}	0.33	0.09

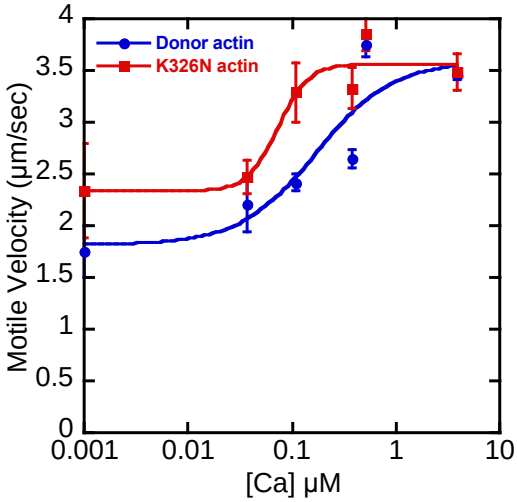
	Value	Error
Hill Coefficient	3.3	1.77
EC_{50}	0.32	0.06



	Value	Error
Hill Coefficient	1.52	0.11
EC_{50}	0.23	0.01

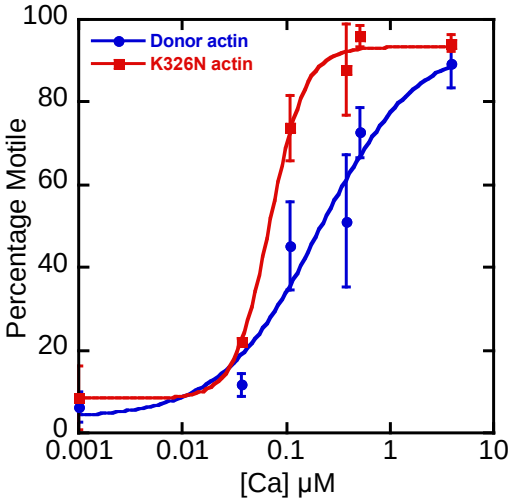
	Value	Error
Hill Coefficient	6.03	29.96
EC_{50}	0.11	0.02

6



	Value	Error
Hill Coefficient	1.19	1.3
EC_{50}	0.17	0.2

	Value	Error
Hill COefficient	2.99	2.74
EC_{50}	0.07	0.04



	Value	Error
Hill COefficient	0.93	0.55
EC_{50}	0.21	0.15

	Value	Error
Hill COefficient	2.58	0.44
EC_{50}	0.07	0.01

Bibliography

AGRAWAL, P. B., GREENLEAF, R. S., TOMCZAK, K. K., LEHTOKARI, V. L., WALLGREN-PETTERSSON, C., WALLEFELD, W., LAING, N. G., DARRAS, B. T., MACIVER, S. K., DORMITZER, P. R. & BEGGS, A. H. 2007. Nemaline myopathy with minicores caused by mutation of the CFL2 gene encoding the skeletal muscle actin-binding protein, cofilin-2. *Am J Hum Genet,* 80**,** 162-7.

AKKARI, P. A., SONG, Y., HITCHCOCK-DEGREGORI, S., BLECHYNDEN, L. & LAING, N. 2002. Expression and biological activity of Baculovirus generated wild-type human slow alpha tropomyosin and the Met9Arg mutant responsible for a dominant form of nemaline myopathy. *Biochem Biophys Res Commun,* 296**,** 300-4.

ALPERT, N. R., MULIERI, L. A. & WARSHAW, D. 2002. The failing human heart. *Cardiovasc Res,* 54**,** 1-10.

ANDERSON, P. A., MALOUF, N. N., OAKELEY, A. E., PAGANI, E. D. & ALLEN, P. D. 1991. Troponin T isoform expression in humans. A comparison among normal and failing adult heart, fetal heart, and adult and fetal skeletal muscle. *Circ Res,* 69**,** 1226-33.

AYAZ-GUNER, S., ZHANG, J., LI, L., WALKER, J. W. & GE, Y. 2009. In Vivo Phosphorylation Site Mapping in Mouse Cardiac Troponin I by High Resolution Top-Down Electron Capture Dissociation Mass Spectrometry: Ser22/23 Are the Only Sites Basally Phosphorylated. *Biochemistry,* 48**,** 8161-8170.

BARTON, P. J., TOWNSEND, P. J., BRAND, N. J. & YACOUB, M. H. 1997. Localization of the fast skeletal muscle troponin I gene (TNNI2) to 11p15.5: genes for troponin I and T are organized in pairs. *Ann Hum Genet,* 61**,** 519-23.

BAYLISS, C., MARSTON, S., MESSER AE. 2011. *Troponin I Phosphorylation Is Uncoupled From Myofibrillar Ca2+-sensitivity In Septal Myectomy Samples From Hocm Patients Due To An Abnormality In Troponin T. *Circulation,* 124.

BERS, D. M. 2001. *Excitation-contraction coupling and cardiac contractile force,* Dordrecht ; London, Kluwer Academic.

BERS, D. M. 2002. Cardiac excitation-contraction coupling. *Nature,* 415**,** 198-205.

BIESIADECKI, B. J., KOBAYASHI, T., WALKER, J. S., JOHN SOLARO, R. & DE TOMBE, P. P. 2007. The troponin C G159D mutation blunts myofilament desensitization induced by troponin I Ser23/24 phosphorylation. *Circ Res,* 100**,** 1486-93.

BING, W., FRASER, I. D. C. & MARSTON, S. B. 1997. Troponin I and troponin T interact with troponin C to produce different Ca2+-dependant effects on actin-tropomyosin filament motility. *Biochem. J.,* 327**,** 335-340.

BING, W., KNOTT, A. & MARSTON, S. 2000. A simple method for measuring the relative force exerted by myosin on actin filaments in the *in vitro* motility

assay: evidence that tropomyosin and troponin increase force in single filaments. *Biochem J,* 350**,** 693-699.

BRADFORD, M. M. 1976. A rapid and sensitive method for the quantitation of microgram quantities of protein utilizing the principle of protein-dye binding. *Anal Biochem,* 72**,** 248-54.

BRONSON, D. D. & SCHACHAT, F. H. 1982. Heterogeneity of contractile proteins. Differences in tropomyosin in fast, mixed, and slow skeletal muscles of the rabbit. *J Biol Chem,* 257**,** 3937-44.

BROOKE, M. 1973. Congenital Fibre Type Disproportion. *Experta Medica***,** 147-59.

BROWN, J. H., KIM, K. H., JUN, G., GREENFIELD, N. J., DOMINGUEZ, R., VOLKMANN, N., HITCHCOCK-DEGREGORI, S. E. & COHEN, C. 2001. Deciphering the design of the tropomyosin molecule. *Proc Natl Acad Sci,* 98**,** 8496-501.

BROWN, J. H., ZHOU, Z., RESHETNIKOVA, L., ROBINSON, H., YAMMANI, R. D., TOBACMAN, L. S. & COHEN, C. 2005. Structure of the mid-region of tropomyosin: bending and binding sites for actin. *Proc Natl Acad Sci U S A,* 102**,** 18878-83.

BURGOYNE, T., MUHAMAD, F. & LUTHER, P. K. 2008. Visualization of cardiac muscle thin filaments and measurement of their lengths by electron tomography. *Cardiovasc Res,* 77**,** 707-12.

CARBALLO, S., ROBINSON, P., OTWAY, R., FATKIN, D., JONGBLOED, J. D., DE JONGE, N., BLAIR, E., VAN TINTELEN, J. P., REDWOOD, C. & WATKINS, H. 2009. Identification and functional characterization of cardiac troponin I as a novel disease gene in autosomal dominant dilated cardiomyopathy. *Circ Res,* 105**,** 375-82.

CHANG, A. N. & POTTER, J. D. 2005. Sarcomeric protein mutations in dilated cardiomyopathy. *Heart Fail Rev,* 10**,** 225-35.

CLARKE, N. F., DOMAZETOVSKA, A., WADDELL, L., KORNBERG, A., MCLEAN, C. & NORTH, K. N. 2009. Cap disease due to mutation of the beta-tropomyosin gene (TPM2). *Neuromuscul Disord,* 19**,** 348-51.

CLARKE, N. F., ILKOVSKI, B., COOPER, S., VALOVA, V. A., ROBINSON, P. J., NONAKA, I., FENG, J. J., MARSTON, S. & NORTH, K. 2007. The pathogenesis of ACTA1-related congenital fiber type disproportion. *Ann Neurol,* 61**,** 552-561.

CLARKE, N. F., KIDSON, W., QUIJANO-ROY, S., ESTOURNET, B., FERREIRO, A., GUICHENEY, P., MANSON, J. I., KORNBERG, A. J., SHIELD, L. K. & NORTH, K. N. 2006. SEPN1: associated with congenital fiber-type disproportion and insulin resistance. *Ann Neurol,* 59**,** 546-52.

CLARKE, N. F., KOLSKI, H., DYE, D. E., LIM, E., SMITH, R. L., PATEL, R., FAHEY, M. C., BELLANCE, R., ROMERO, N. B., JOHNSON, E. S., LABARRE-VILA, A., MONNIER, N., LAING, N. G. & NORTH, K. N. 2008. Mutations in TPM3 are a common cause of congenital fiber type disproportion. *Ann Neurol.*

CLARKE, N. F. & NORTH, K. N. 2003. Congenital fiber type disproportion--30 years on. *J Neuropathol Exp Neurol,* 62**,** 977-89.

CLARKE, N. F., SMITH, R. L., BAHLO, M. & NORTH, K. N. 2005. A novel X-linked form of congenital fiber-type disproportion. *Ann Neurol,* 58**,** 767-72.

CLARKE, N. F., WADDELL, L. B., COOPER, S. T., PERRY, M., SMITH, R. L., KORNBERG, A. J., MUNTONI, F., LILLIS, S., STRAUB, V., BUSHBY, K., GUGLIERI, M., KING, M. D., FARRELL, M. A., MARTY, I., LUNARDI,

J., MONNIER, N. & NORTH, K. N. 2010. Recessive mutations in RYR1 are a common cause of congenital fiber type disproportion. *Hum Mutat,* 31**,** E1544-50.

COHN, J. N., BRISTOW, M. R., CHIEN, K. R., COLUCCI, W. S., FRAZIER, O. H., LEINWAND, L. A., LORELL, B. H., MOSS, A. J., SONNENBLICK, E. H., WALSH, R. A., MOCKRIN, S. C. & REINLIB, L. 1997. Report of the National Heart, Lung, and Blood Institute Special Emphasis Panel on Heart Failure Research. *Circulation,* 95**,** 766-70.

CONEN, P. E., MURPHY, E. G. & DONOHUE, W. L. 1963. Light and Electron Microscopic Studies of "Myogranules" in a Child with Hypotonia and Muscle Weakness. *Can Med Assoc J,* 89**,** 983-6.

COPELAND, O., SADAYAPPAN, S., MESSER, A. E., STIENEN, G. J., VELDEN, J. & MARSTON, S. B. 2010. Analysis of cardiac myosin binding protein-C phosphorylation in human heart muscle. *J Mol Cell Cardiol,* 49**,** 1003-1011.

CORBETT, M. A., AKKARI, P. A., DOMAZETOVSKA, A., COOPER, S. T., NORTH, K. N., LAING, N. G., GUNNING, P. W. & HARDEMAN, E. C. 2005. An alphaTropomyosin mutation alters dimer preference in nemaline myopathy. *Ann Neurol,* 57**,** 42-9.

CRAIG, S. W., LANCASHIRE, C. L. & COOPER, J. A. 1982. Preparation of smooth muscle a-actinin. *Methods in Enzymology.,* 85**,** 516-521.

CUISSET, J. M., MAURAGE, C. A., PELLISSIER, J. F., BAROIS, A., URTIZBEREA, J. A., LAING, N., TAJSHARGHI, H. & VALLEE, L. 2006. 'Cap myopathy': case report of a family. *Neuromuscul Disord,* 16**,** 277-81.

D'AMICO, A., GRAZIANO, C., PACILEO, G., PETRINI, S., NOWAK, K. J., BOLDRINI, R., JACQUES, A., FENG, J. J., PORFIRIO, B., SEWRY, C. A., SANTORELLI, F. M., LIMONGELLI, G., BERTINI, E., LAING, N. & MARSTON, S. B. 2006. Fatal hypertrophic cardiomyopathy and nemaline myopathy associated with ACTA1 K336E mutation. *Neuromuscul Disord,* 16**,** 548-552.

DAVIES, M. J. 2000. The cardiomyopathies: an overview. *Heart,* 83**,** 469-74.

DE PAULA, A. M., FRANQUES, J., FERNANDEZ, C., MONNIER, N., LUNARDI, J., PELLISSIER, J. F., FIGARELLA-BRANGER, D. & POUGET, J. 2009. A TPM3 mutation causing cap myopathy. *Neuromuscul Disord,* 19**,** 685-8.

DEBOLD, E. P., SABER, W., CHEEMA, Y., BOOKWALTER, C. S., TRYBUS, K. M., WARSHAW, D. M. & VANBUREN, P. 2010. Human actin mutations associated with hypertrophic and dilated cardiomyopathies demonstrate distinct thin filament regulatory properties in vitro. *J Mol Cell Cardiol,* 48**,** 286-292.

DENG, Y., SCHMIDTMANN, A., KRUSE, S., FILATOV, V., HEILMEYER, L. M., JR., JAQUET, K. & THIELECZEK, R. 2003. Phosphorylation of human cardiac troponin I G203S and K206Q linked to familial hypertrophic cardiomyopathy affects actomyosin interaction in different ways. *J Mol Cell Cardiol,* 35**,** 1365-74.

DONNER, K., OLLIKAINEN, M., RIDANPAA, M., CHRISTEN, H. J., GOEBEL, H. H., DE VISSER, M., PELIN, K. & WALLGREN-PETTERSSON, C. 2002. Mutations in the beta-tropomyosin (TPM2) gene--a rare cause of nemaline myopathy. *Neuromuscul Disord,* 12**,** 151-8.

DOS REMEDIOS, C. G. & MOENS, P. D. 1995. Actin and the actomyosin interface: a review. *Biochim Biophys Acta,* 1228**,** 99-124.

DU, C. K., MORIMOTO, S., NISHII, K., MINAKAMI, R., OHTA, M., TADANO, N., LU, Q. W., WANG, Y. Y., ZHAN, D. Y., MOCHIZUKI, M., KITA, S., MIWA, Y., TAKAHASHI-YANAGA, F., IWAMOTO, T., OHTSUKI, I. & SASAGURI, T. 2007. Knock-In Mouse Model of Dilated Cardiomyopathy Caused by Troponin Mutation. *Circ Res,* 101**,** 185-194.

DURAND, J. B., BACHINSKI, L. L., BIELING, L. C., CZERNUSZEWICZ, G. Z., ABCHEE, A. B., YU, Q. T., TAPSCOTT, T., HILL, R., IFEGWU, J., MARIAN, A. J. & ET AL. 1995. Localization of a gene responsible for familial dilated cardiomyopathy to chromosome 1q32. *Circulation,* 92**,** 3387-9.

DURLING, H. J., REILICH, P., MULLER-HOCKER, J., MENDEL, B., PONGRATZ, D., WALLGREN-PETTERSSON, C., GUNNING, P., LOCHMULLER, H. & LAING, N. G. 2002. De novo missense mutation in a constitutively expressed exon of the slow alpha-tropomyosin gene TPM3 associated with an atypical, sporadic case of nemaline myopathy. *Neuromuscul Disord,* 12**,** 947-51.

DYER, E., JACQUES, A., HOSKINS, A., WARD, D., GALLON, C., MESSER, A., KASKI, J., BURCH, M., KENTISH, J. & MARSTON, S. 2009. Functional Analysis of a Unique Troponin C Mutation, Gly159Asp that Causes Familial Dilated Cardiomyopathy, Studied in Explanted Heart Muscle. *Circulation: Heart Failure,* 2**,** 456-464.

EAST, D., SOUSA, D., LEHMAN, W. & MULVIHILL, D. P. 2010. Precise Modulation of Tropomyosin Polymer Length is Crucial for its Association with Actin and Ability to Regulate Myosin Function. *Biophys J,* 98**,** 156a-156a.

EISENBERG, E. & KIELLEY, W. W. 1974. Troponin-tropomyosin complex. Column chromatographic separation and activity of the three, active troponin components with and without tropomyosin present. *J Biol Chem,* 249**,** 4742-8.

EL-ARMOUCHE, A. & ESCHENHAGEN, T. 2009. Beta-adrenergic stimulation and myocardial function in the failing heart. *Heart Fail Rev,* 14**,** 225-41.

FENG, J. J. & MARSTON, S. 2009. Genotype-Phenotype Correlations in ACTA1 Mutations That Cause Congenital Myopathies. *Neuromusc Disord,* 19**,** 6-16.

FENTZKE, R. C., BUCK, S. H., PATEL, J. R., LIN, H., WOLSKA, B. M., STOJANOVIC, M. O., MARTIN, A. F., SOLARO, R. J., MOSS, R. L. & LEIDEN, J. M. 1999. Impaired cardiomyocyte relaxation and diastolic function in transgenic mice expressing slow skeletal troponin I in the heart. *J Physiol,* 517**,** 143-157.

FIDZIANSKA, A. 2002. "Cap disease"--a failure in the correct muscle fibre formation. *J Neurol Sci,* 201**,** 27-31.

FIDZIANSKA, A., BADURSKA, B., RYNIEWICZ, B. & DEMBEK, I. 1981. "Cap disease": new congenital myopathy. *Neurology,* 31**,** 1113-20.

FINLEY, N., ABBOTT, M. B., ABUSAMHADNEH, E., GAPONENKO, V., DONG, W., GASMI-SEABROOK, G., HOWARTH, J. W., RANCE, M., SOLARO, R. J., CHEUNG, H. C. & ROSEVEAR, P. R. 1999. NMR analysis of cardiac troponin C-troponin I complexes: effects of phosphorylation. *FEBS Lett,* 453**,** 107-12.

FLASHMAN, E., REDWOOD, C., MOOLMAN-SMOOK, J. & WATKINS, H. 2004. Cardiac myosin binding protein C: its role in physiology and disease. *Circ Res,* 94**,** 1279-89.

FRASER, I. D. & MARSTON, S. B. 1995. In vitro motility analysis of actin-tropomyosin regulation by troponin and calcium. The thin filament is switched as a single cooperative unit. *J Biol Chem,* 270**,** 7836-7841.

FRYE, J., KLENCHIN, V. A. & RAYMENT, I. 2010. Structure of the tropomyosin overlap complex from chicken smooth muscle: insight into the diversity of N-terminal recognition. *Biochemistry,* 49**,** 4908-20.

GEEVES, M. A., FEDOROV, R. & MANSTEIN, D. J. 2005. Molecular mechanism of actomyosin-based motility. *Cell Mol Life Sci,* 62**,** 1462-77.

GEEVES, M. A. & HOLMES, K. C. 1999. Structural mechanism of muscle contraction. *Annu. Rev. Biochem.,* 68**,** 687-728.

GEEVES, M. A. & HOLMES, K. C. 2005. The molecular mechanism of muscle contraction. *Adv Protein Chem,* 71**,** 161-93.

GORDON, A. M., HOMSHER, E. & REGNIER, M. 2000. Regulation of contraction in striated muscle. *Physiol Rev,* 80**,** 853-924.

GREASER, M. L. & GERGELY, J. 1973. Purification and properties of the components from tropinin. *J Biol Chem,* 248**,** 2125-33.

GREENFIELD, N. J., HUANG, Y. J., SWAPNA, G. V., BHATTACHARYA, A., RAPP, B., SINGH, A., MONTELIONE, G. T. & HITCHCOCK-DEGREGORI, S. E. 2006. Solution NMR structure of the junction between tropomyosin molecules: implications for actin binding and regulation. *J Mol Biol,* 364**,** 80-96.

GREGORIO, C. C. & ANTIN, P. B. 2000. To the heart of myofibril assembly. *Trends Cell Biol,* 10**,** 355-62.

GUNNING, P. W., SCHEVZOV, G., KEE, A. J. & HARDEMAN, E. C. 2005. Tropomyosin isoforms: divining rods for actin cytoskeleton function. *Trends Cell Biol,* 15**,** 333-41.

HAMDANI, N., KOOIJ, V., VAN DIJK, S., MERKUS, D., PAULUS, W. J., REMEDIOS, C. D., DUNCKER, D. J., STIENEN, G. J. & VAN DER VELDEN, J. 2008. Sarcomeric dysfunction in heart failure. *Cardiovasc Res,* 77**,** 649-58.

HERRON, T. J., KORTE, F. S. & MCDONALD, K. S. 2001. Power output is increased after phosphorylation of myofibrillar proteins in rat skinned cardiac myocytes. *Circ Res,* 89**,** 1184-90.

HERSHBERGER, R. E. & SIEGFRIED, J. D. 2011. Update 2011: clinical and genetic issues in familial dilated cardiomyopathy. *J Am Coll Cardiol,* 57**,** 1641-9.

HERZBERG, O. & JAMES, M. N. G. 1985. Structure of the calcium regulatory muscle protein troponin-C at 2.8Å resolution. *Nature,* 313**,** 653-659.

HILL, T. L., EISENBERG, E. & GREENE, L. E. 1980. Theoretical model for the cooperative equilibrium binding of myosin subfragment 1 to the actin-troponin-tropomyosin complex. *Proc.Natl.Acad.Sci.U.S.A.,* 77**,** 3186-3190.

HILL, T. L., EISENBERG, E. & GREENE, L. E. 1983. Alternate model for the cooperative equilibrium binding of myosin subfragment-1-nucleotide complex to actin-troponin-tropomyosin. *Proc Natl Acad Sci U S A,* 80**,** 60-4.

HITCHCOCK-DEGREGORI, S. E. & SINGH, A. 2010. What makes tropomyosin an actin binding protein? A perspective. *J Struct Biol,* 170**,** 319-24.

HODGKINSON, J. L. 2000. Actin and the smooth muscle regulatory proteins: a structural perspective. *J Muscle Res Cell Motil,* 21**,** 115-130.

HOH, J. F., ROSSMANITH, G. H., KWAN, L. J. & HAMILTON, A. M. 1988. Adrenaline increases the rate of cycling of crossbridges in rat cardiac muscle

as measured by pseudo-random binary noise-modulated perturbation analysis. *Circ Res,* 62**,** 452-61.
HOLMES, K. C. 1997. The swinging lever-arm hypothesis of muscle contraction. *Curr Biol,* 7**,** R112-8.
HOLMES, K. C., POPP, D., GEBHARD, W. & KABSCH, W. 1990. Atomic model of the actin filament. *Nature,* 347**,** 44-9.
HOLTHAUZEN, L. M., CORREA, F. & FARAH, C. S. 2004. Ca2+-induced rolling of tropomyosin in muscle thin filaments: the alpha- and beta-band hypothesis revisited. *J Biol Chem,* 279**,** 15204-13.
HOROWITS, R. 2006. Nebulin regulation of actin filament lengths: new angles. *Trends Cell Biol,* 16**,** 121-4.
HOUSER, S. R. & MARGULIES, K. B. 2003. Is depressed myocyte contractility centrally involved in heart failure? *Circ Res,* 92**,** 350-8.
HOWARTH, J. W., MELLER, J., SOLARO, R. J., TREWHELLA, J. & ROSEVEAR, P. R. 2007. Phosphorylation-dependent conformational transition of the cardiac specific N-extension of troponin I in cardiac troponin. *J Mol Biol,* 373**,** 706-22.
HUNG, R. M., HAWKINS, C. E., YOON, G., BIGGAR, D. & VAJSAR, J. 2009. Repeat muscle biopsy in the diagnosis of cap myopathy with ACTA1 gene mutation. *Neuromuscular Disord,* 19**,** 638-638.
HUXLEY, A. F. 1957. Muscle structure and theories of contraction. *Prog Biophys Biophys Chem,* 7**,** 255-318.
HUXLEY, A. F. & NIEDERGERKE, R. 1954. Measurement of muscle striations in stretch and contraction. *J Physiol,* 124**,** 46-7P.
HUXLEY, H. & HANSON, J. 1954. Changes in the cross-striations of muscle during contraction and stretch and their structural interpretation. *Nature,* 173**,** 973-6.
ILKOVSKI, B., MOKBEL, N., LEWIS, R. A., WALKER, K., NOWAK, K. J., DOMAZETOVSKA, A., LAING, N. G., FOWLER, V. M., NORTH, K. N. & COOPER, S. T. 2008. Disease severity and thin filament regulation in M9R TPM3 nemaline myopathy. *J Neuropathol Exp Neurol,* 67**,** 867-77.
JACQUES, A., HOSKINS, A., KENTISH, J. & MARSTON, S. B. 2009. From genotype to phenotype: a longitudinal study of a patient with hypertrophic cardiomyopathy due to a mutation in the MYBPC3 gene. *J Musc Res Cell Motil,* 29**,** 239-246.
JAENICKE, T., DIEDERICH, K. W., HAAS, W., SCHLEICH, J., LICHTER, P., PFORDT, M., BACH, A. & VOSBERG, H. P. 1990. The complete sequence of the human beta-myosin heavy chain gene and a comparative analysis of its product. *Genomics,* 8**,** 194-206.
JIN, J. P. & CHONG, S. M. 2010. Localization of the two tropomyosin-binding sites of troponin T. *Arch Biochem Biophys,* 500**,** 144-50.
JOHNSTON, J. J., KELLEY, R. I., CRAWFORD, T. O., MORTON, D. H., AGARWALA, R., KOCH, T., SCHAFFER, A. A., FRANCOMANO, C. A. & BIESECKER, L. G. 2000. A novel nemaline myopathy in the Amish caused by a mutation in troponin T1. *Am. J. Hum. Genet.,* 67**,** 814-821.
JUAN, F., WEI, D., XIONGZHI, Q., RAN, D., CHUNMEI, M., LAN, H., CHUAN, Q. & LIANFENG, Z. 2008. The changes of the cardiac structure and function in cTnTR141W transgenic mice. *Int J Cardiol,* 128**,** 83-90.
KAMISAGO, M., SHARMA, S. D., DEPALMA, S. R., SOLOMON, S., SHARMA, P., SMOOT, L., MULLEN, M. P., WOOLF, P. K., WIGLE, E. D., SEIDMAN, J. G., SEIDMAN, C. E., JARCHO, J. & SHAPIRO, L. R. 2000.

Mutations in Sarcomere Protein Genes as a Cause of Dilated Cardiomyopathy. *N Engl J Med,* 343**,** 1688-1696.

KASKI, J. P., BURCH, M. & ELLIOTT, P. M. 2007. Mutations in the cardiac Troponin C gene are a cause of idiopathic dilated cardiomyopathy in childhood. *Cardiol Young,* 17**,** 675-7.

KATRUKHA, A. G., BEREZNIKOVA, A. V., ESAKOVA, T. V., FILATOV, V. L., BULGARINA, T. V. & GUSEV, N. B. 1995. A new method of human cardiac troponin I and troponin T purification. *Biochem Mol Biol Int,* 36**,** 195-202.

KATZ, A. M. 2006. Physiology of the heart. *Philadelphia, Pa.,* London, Lippincott Williams & Wilkins.

KAWASAKI, H., NAKAYAMA, S. & KRETSINGER, R. H. 1998. Classification and evolution of EF-hand proteins. *Biometals,* 11**,** 277-95.

KAZMIERSKI, S. T., ANTIN, P. B., WITT, C. C., HUEBNER, N., MCELHINNY, A. S., LABEIT, S. & GREGORIO, C. C. 2003. The complete mouse nebulin gene sequence and the identification of cardiac nebulin. *J Mol Biol,* 328**,** 835-46.

KENTISH, J. C., MCCLOSKEY, D. T., LAYLAND, J., PALMER, S., LEIDEN, J. M., MARTIN, A. F. & SOLARO, R. J. 2001. Phosphorylation of troponin I by protein kinase A accelerates relaxation and crossbridge cycle kinetics in mouse ventricular muscle. *Circ Res,* 88**,** 1059-65.

KINOSHITA, E., KINOSHITA-KIKUTA, E., TAKIYAMA, K. & KOIKE, T. 2006. Phosphate-binding tag, a new tool to visualize phosphorylated proteins. *Mol Cell Proteomics,* 5**,** 749-57.

KINOSHITA-KIKUTA, E., AOKI, Y., KINOSHITA, E. & KOIKE, T. 2007. Label-free kinase profiling using phosphate affinity polyacrylamide gel electrophoresis. *Mol Cell Proteomics,* 6**,** 356-66.

KNOTT, A., PURCELL, I. F. & MARSTON, S. 2002. In vitro motility analysis of thin filaments from failing and non-failing human hearts induces slower filament sliding and higher Ca2+-sensitivity. *J Mol Cell Cardiol,* 34**,** 469–482.

KOBAYASHI, T. & SOLARO, R. J. 2005. Calcium, thin filaments, and the integrative biology of cardiac contractility. *Annu Rev Physiol,* 67**,** 39-67.

KOCICA, M. J., CORNO, A. F., CARRERAS-COSTA, F., BALLESTER-RODES, M., MOGHBEL, M. C., CUEVA, C. N., LACKOVIC, V., KANJUH, V. I. & TORRENT-GUASP, F. 2006. The helical ventricular myocardial band: global, three-dimensional, functional architecture of the ventricular myocardium. *Eur J Cardiothorac Surg,* 29 Suppl 1**,** S21-40.

KOOIJ, V., SAES, M., JAQUET, K., ZAREMBA, R., FOSTER, D. B., MURPHY, A. M., DOS REMEDIOS, C., VAN DER VELDEN, J. & STIENEN, G. J. 2010. Effect of troponin I Ser23/24 phosphorylation on Ca2+-sensitivity in human myocardium depends on the phosphorylation background. *J Mol Cell Cardiol,* 48**,** 954-63.

KORN, E. D., CARLIER, M. F. & PANTALONI, D. 1987. Actin polymerization and ATP hydrolysis. *Science,* 238**,** 638-44.

KOSTYUKOVA, A. S., HITCHCOCK-DEGREGORI, S. E. & GREENFIELD, N. J. 2007. Molecular basis of tropomyosin binding to tropomodulin, an actin-capping protein. *J Mol Biol,* 372**,** 608-18.

LAEMMLI, U. K. 1970. Cleavage of structural proteins during the assembly of the head of bacteriophage T4. *Nature,* 227**,** 680-5.

LAING, N. G., CLARKE, N. F., DYE, D. E., LIYANAGE, K., WALKER, K. R., KOBAYASHI, Y., SHIMAKAWA, S., HAGIWARA, T., OUVRIER, R., SPARROW, J. C., NISHINO, I., NORTH, K. N. & NONAKA, I. 2004. Actin mutations are one cause of congenital fibre type disproportion. *Ann Neurol,* 56**,** 689-94.

LAING, N. G., WILTON, S. D., AKKARI, P. A., DOROSZ, S., BOUNDRY, K., KNEEBONE, C., BLUMBERGS, P., WHITE, S., WATKINS, H., LOVE, D. R. & HAAN, E. 1995. A mutation in the a tropomyosin gene *TMP3* associated with autosomal dominant nemaline myopathy. *Nature Genetics,* 9**,** 75-79.

LAWLOR, M. W., DECHENE, E. T., ROUMM, E., GEGGEL, A. S., MOGHADASZADEH, B. & BEGGS, A. H. 2010. Mutations of tropomyosin 3 (TPM3) are common and associated with type 1 myofiber hypotrophy in congenital fiber type disproportion. *Hum Mutat,* 31**,** 176-83.

LAYLAND, J., SOLARO, R. J. & SHAH, A. M. 2005. Regulation of cardiac contractile function by troponin I phosphorylation. *Cardiovasc Res,* 66**,** 12-21.

LEGRICE, I. J., SMAILL, B. H., CHAI, L. Z., EDGAR, S. G., GAVIN, J. B. & HUNTER, P. J. 1995. Laminar structure of the heart: ventricular myocyte arrangement and connective tissue architecture in the dog. *Am J Physiol,* 269**,** H571-82.

LEHMAN, W. & CRAIG, R. 2008. Tropomyosin and the steric mechanism of muscle regulation. *Adv Exp Med Biol,* 644**,** 95-109.

LEHMAN, W., HATCH, V., KORMAN, V., ROSOL, M., THOMAS, L., MAYTUM, R., GEEVES, M. A., VAN EYK, J. E., TOBACMAN, L. S. & CRAIG, R. 2000. Tropomyosin and actin isoforms modulate the localization of tropomyosin strands on actin filaments. *J Mol Biol,* 302**,** 593-606.

LEHRER, S. S. & GEEVES, M. A. 1998. The muscle thin filament as a classical cooperative/allosteric regulatory system. *J Mol Biol,* 277**,** 1081-1089.

LEHTOKARI, V. L., CEUTERICK-DE GROOTE, C., DE JONGHE, P., MARTTILA, M., LAING, N. G., PELIN, K. & WALLGREN-PETTERSSON, C. 2007. Cap disease caused by heterozygous deletion of the beta-tropomyosin gene TPM2. *Neuromuscul Disord,* 17**,** 433-42.

LI, D., CZERNUSZEWICZ, G. Z., GONZALEZ, O., TAPSCOTT, T., KARIBE, A., DURAND, J. B., BRUGADA, R., HILL, R., GREGORITCH, J. M., ANDERSON, J. L., QUINONES, M., BACHINSKI, L. L. & ROBERTS, R. 2001. Novel cardiac troponin T mutation as a cause of familial dilated cardiomyopathy. *Circulation,* 104**,** 2188-93.

LI, M. X., WANG, X. & SYKES, B. D. 2004. Structural based insights into the role of troponin in cardiac muscle pathophysiology. *J Muscle Res Cell Motil,* 25**,** 559-79.

LI, X. E., HOLMES, K. C., LEHMAN, W., JUNG, H. & FISCHER, S. 2010. The shape and flexibility of tropomyosin coiled coils: implications for actin filament assembly and regulation. *J Mol Biol,* 395**,** 327-39.

LI, X. E., TOBACMAN, L. S., MUN, J. Y., CRAIG, R., FISCHER, S. & LEHMAN, W. 2011. Tropomyosin position on F-actin revealed by EM reconstruction and computational chemistry. *Biophys J,* 100**,** 1005-13.

LIONEL, H. O. 2005. Mechanism Of Cardiac Contraction and Relaxation. *Heart Disease: A Textbook Of Cardiovascular Medicine*.

LOWRY, O. H., ROSEBROUGH, N. J., FARR, A. L. & RANDALL, R. J. 1951. Protein measurement with the Folin phenol reagent. *J Biol Chem,* 193**,** 265-75.

LYMN, R. W. & TAYLOR, E. W. 1971. Mechanism of adenosine triphosphate hydrolysis by actomyosin. *Biochemistry,* 10**,** 4617-24.

MACLENNAN, D. H. & KRANIAS, E. G. 2003. Phospholamban: a crucial regulator of cardiac contractility. *Nat Rev Mol Cell Biol,* 4**,** 566-77.

MANNING, E. P., TARDIFF, J. C. & SCHWARTZ, S. D. 2011. A model of calcium activation of the cardiac thin filament. *Biochemistry,* 50**,** 7405-13.

MARGOSSIAN, S. S. & LOWEY, S. 1982. Preparation of myosin and its subfragments from rabbit skeletal muscle. *Methods Enzymol,* 85 Pt B**,** 55-71.

MARSTON, S. 2003. Random walks with thin filaments: application of in vitro motility assay to the study of actomyosin regulation. *J Musc Res Cell motil,* 24**,** 149-156.

MARSTON, S. 2008. How does genotype define phenotype? Microphysiology of a tropomyosin mutation in situ shows the limitations of reductionism. *J Physiol,* 586**,** 2821.

MARSTON, S., MIRZA, M., ABDULRAZZAK, H. & SEWRY, C. 2004. Functional characterisation of a mutant actin (Met132Val) from a patient with nemaline myopathy. *Neuromuscul Disord,* 14**,** 167-74.

MARSTON, S. B. 2011. How Do Mutations in Contractile Proteins Cause the Primary Familial Cardiomyopathies? *J Cardiovasc Transl Res,* 4**,** 245-255.

MARSTON, S. B., FRASER, I. D. C., WU, B. & ROPER, G. 1996. A simple method for automatic tracking of actin filaments in the motility assay. *J Musc Res Cell Motil,* 17**,** 497-506.

MARSTON, S. B. & WALKER, J. W. 2009. Back to the future: new techniques show that forgotten phosphorylation sites are present in contractile proteins of the heart whilst intensively studied sites appear to be absent. *J Muscle Res Cell Motil,* 30**,** 93-5.

MARTTILA, M., LEMOLA, E., WALLEFELD, W., MEMO, M., DONNER, K., LAING, N. G., MARSTON, S., GRONHOLM, M. & WALLGREN-PETTERSSON, C. 2012. Abnormal actin binding of aberrant beta-tropomyosins is a molecular cause of muscle weakness in TPM2-related nemaline and cap myopathy. *Biochem J,* 442**,** 231-9.

MASON, J. M. & ARNDT, K. M. 2004. Coiled coil domains: stability, specificity, and biological implications. *Chembiochem,* 5**,** 170-6.

MAYTUM, R., LEHRER, S. & GEEVES, M. 1999. Cooperativity and switching within the Three-state model of muscle regulation. *Biochemistry,* 38**,** 1102-1110.

MCGUIGAN, J. A., LUTHI, D. & BURI, A. 1991. Calcium buffer solutions and how to make them: a do it yourself guide. *Can J Physiol Pharmacol,* 69**,** 1733-49.

MCKILLOP, D. F. A. & GEEVES, M. A. 1993. Regulation of the interaction between actin and myosin subfragment-1: evidence for three states of the thin filament. *Biophys.J.,* 65**,** 693-701.

MERCIER, P., FERGUSON, R. E., IRVING, M., CORRIE, J. E., TRENTHAM, D. R. & SYKES, B. D. 2003. NMR structure of a bifunctional rhodamine labeled N-domain of troponin C complexed with the regulatory "switch" peptide from troponin I: implications for in situ fluorescence studies in muscle fibers. *Biochemistry,* 42**,** 4333-48.

MESSER, A., GALLON, C., MCKENNA, W., ELLIOTT, P., DOS REMEDIOS, C. & MARSTON, S. 2009. The use of phosphate-affinity SDS-PAGE to measure the troponin I phosphorylation site distribution in human heart muscle. *Proteomics Clin Appl,* 3**,** 1371-1382.

MESSER, A. E., JACQUES, A. M. & MARSTON, S. B. 2007. Troponin phosphorylation and regulatory function in human heart muscle: dephosphorylation of Ser23/24 on troponin I could account for the contractile defect in end-stage heart failure. *J Mol Cell Cardiol,* 42**,** 247-59.

METZGER, J. M. & WESTFALL, M. V. 2004. Covalent and noncovalent modification of thin filament action. The essential role of troponin in cardicac muscle regulation. *Circ Res,* 94**,** 146-158.

MIRZA, M., MARSTON, S., WILLOTT, R., ASHLEY, C., MOGENSEN, J., MCKENNA, W., ROBINSON, P., REDWOOD, C. & WATKINS, H. 2005. Dilated cardiomyopathy mutations in three thin filament regulatory proteins result in a common functional phenotype. *J Biol Chem,* 280**,** 28498-28506.

MIRZA, M., ROBINSON, P., KREMNEVA, E., COPELAND, O., NIKOLAEVA, O., WATKINS, H., LEVITSKY, D., REDWOOD, C., EL-MEZGUELDI, M. & MARSTON, S. 2007. The effect of mutations in alpha tropomyosin (E40K and E54K), that cause familial dilated cardiomyopathy, on the regulatory mechanism of cardiac muscle thin filaments. *J Biol Chem,* 282**,** 13487-13497.

MOGENSEN, J., MURPHY, R. T., SHAW, T., BAHL, A., REDWOOD, C., WATKINS, H., BURKE, M., ELLIOTT, P. M. & MCKENNA, W. J. 2004. Severe disease expression of cardiac troponin C and T mutations in patients with idiopathic dilated cardiomyopathy. *J Am Coll Cardiol,* 44**,** 2033-40.

MONTEIRO, P. B., LATARO, R. C., FERRO, J. A. & REINACH, F. 1994. Functional alpha-tropomyosin produced in Escherichia coli. A dipeptide extension can substitute the amino-terminal acetyl group. *J Biol Chem,* 269**,** 10461-10466.

MORACZEWSKA, J., GREENFIELD, N. J., LIU, Y. & HITCHCOCK-DEGREGORI, S. E. 2000. Alteration of Tropomyosin Function and Folding by a Nemaline Myopathy-Causing Mutation. *Biophys J,* 79**,** 3217-3225.

MUNOT, P., LASHLEY, D., JUNGBLUTH, H., FENG, L., PITT, M., ROBB, S. A., PALACE, J., JAYAWANT, S., KENNET, R., BEESON, D., CULLUP, T., ABBS, S., LAING, N., SEWRY, C. & MUNTONI, F. 2010. Congenital fibre type disproportion associated with mutations in the tropomyosin 3 (TPM3) gene mimicking congenital myasthenia. *Neuromuscul Disord,* 20**,** 796-800.

MUNTONI, F., CAU, M., GANAU, A., CONGIU, R., ARVEDI, G., MATEDDU, A., MARROSU, M. G., CIANCHETTI, C., REALDI, G., CAO, A. & ET AL. 1993. Brief report: deletion of the dystrophin muscle-promoter region associated with X-linked dilated cardiomyopathy. *N Engl J Med,* 329**,** 921-5.

NORTH, K. N., LAING, N. G. & WALLGREN-PETTERSSON, C. 1997. Nemaline myopathy: current concepts. The ENMC International Consortium and Nemaline Myopathy. *J Med Genet,* 34**,** 705-13.

NORTH, K. R., MM 2010. Nemaline Myopathy. *Gene review*.

NOWAK, K. J., WATTANASIRICHAIGOON, D., GOEBEL, H. H., WILCE, M., PELIN, K., DONNER, K., JACOB, R. L., HUBNER, C., OEXLE, K., ANDERSON, J. R., VERITY, C. M., NORTH, K. N., IANNACCONE, S. T., MULLER, C. R., NURNBERG, P., MUNTONI, F., SEWRY, C., HUGHES, I., SUTPHEN, R., LACSON, A. G., SWOBODA, K. J., VIGNERON, J., WALLGREN-PETTERSSON, C., BEGGS, A. H. & LAING, N. G. 1999. Mutations in the skeletal muscle alpha-actin gene in patients with actin myopathy and nemaline myopathy. *Nat Genet,* 23**,** 208-12.

OCHALA, J., LI, M., OHLSSON, M., OLDFORS, A. & LARSON, L. 2008. Defective regulation of contractile function in muscle fibres carrying an E41K β-tropomyosin mutation. *J Physiol,* 586, 2993-3004.

OHLSSON, M., FIDZIANSKA, A., TAJSHARGHI, H. & OLDFORS, A. 2009. TPM3 mutation in one of the original cases of cap disease. *Neurology,* 72**,** 1961-3.

OHLSSON, M., QUIJANO-ROY, S., DARIN, N., BROCHIER, G., LAC√®NE, E., AVILA-SMIRNOW, D., FARDEAU, M., OLDFORS, A. & TAJSHARGHI, H. 2008. New morphologic and genetic findings in cap disease associated with beta-tropomyosin (TPM2) mutations. *Neurology,* 71**,** 1896-901.

OKAMOTO, Y. & SEKINE, T. 1985. A streamlined method of subfragment one preparation from myosin. *J Biochem,* 98**,** 1143-5.

OLSON, T. M., KISHIMOTO, N. Y., WHITBY, F. G. & MICHELS, V. V. 2001. Mutations that Alter the Surface Charge of Alpha-tropomyosin are Associated with Dilated Cardiomyopathy. *J Mol Cell Cardiol,* 33**,** 723-32.

OLSON, T. M., MICHELS, V. V., THIBODEAU, S. N., TAI, Y. S. & KEATING, M. T. 1998. Actin mutations in dilated cardiomyopathy, a heritable form of heart failure. *Science,* 280**,** 750-2.

OTTENHEIJM, C. A., HEUNKS, L. M. & DEKHUIJZEN, R. P. 2008. Diaphragm adaptations in patients with COPD. *Respir Res,* 9**,** 12.

PAGANI, E., ALOUSI, A., GRANT, A., OLDER, T., DZIUBAN, S. & ALLEN, P. 1988. Changes in myofibrillar content and Mg-ATPase activity in ventricular tissues from patients with heart failure caused by coronary artery disease, cardiomyopathy, or mitral valve insufficiency. *Circ Res,* 63**,** 380-385.

PAGE, E. 1978. Quantitative ultrastructural analysis in cardiac membrane physiology. *Am J Physiol,* 235**,** C147-58.

PALM, T., GREENFIELD, N. J. & HITCHCOCK-DEGREGORI, S. E. 2003. Tropomyosin ends determine the stability and functionality of overlap and troponin T complexes. *Biophys J,* 84**,** 3181-9.

PELIN, K., HILPELA, P., DONNER, K., SEWRY, C., AKKARI, P. A., WILTON, S. D., WATTANASIRICHAIGOON, D., BANG, M. L., CENTNER, T., HANEFELD, F., ODENT, S., FARDEAU, M., URTIZBEREA, J. A., MUNTONI, F., DUBOWITZ, V., BEGGS, A. H., LAING, N. G., LABEIT, S., DE LA CHAPELLE, A. & WALLGREN-PETTERSSON, C. 1999. Mutations in the nebulin gene associated with autosomal recessive nemaline myopathy. *Proc Natl Acad Sci U S A,* 96**,** 2305-10.

PENISSON-BESNIER, I., MONNIER, N., TOUTAIN, A., DUBAS, F. & LAING, N. 2007. A second pedigree with autosomal dominant nemaline myopathy caused by TPM3 mutation: a clinical and pathological study. *Neuromuscul Disord,* 17**,** 330-7.

PERRY, S. V. 1998. Troponin T: genetics, properties and function. *J Muscle Res Cell Motil,* 19**,** 575-602.

PERRY, S. V. 1999. Troponin I: inhibitor or facilitator. *Mol Cell Biochem,* 190**,** 9-32.

PERRY, S. V. 2001. Vertebrate tropomyosin: distribution, properties and function. *J Muscle Res Cell Motil,* 22**,** 5-49.

PFUHL, M., WINDER, S. J. & PASTORE, A. 1994. Nebulin, a helical actin binding protein. *EMBO J,* 13**,** 1782-9.

PHILLIPS, G. N., JR., FILLERS, J. P. & COHEN, C. 1986. Tropomyosin crystal structure and muscle regulation. *J Mol Biol,* 192**,** 111-131.

PINTO, J. R., SIEGFRIED, J. D., PARVATIYAR, M. S., LI, D., NORTON, N., JONES, M. A., LIANG, J., POTTER, J. D. & HERSHBERGER, R. E. 2011. Functional characterization of TNNC1 rare variants identified in dilated cardiomyopathy. *J Biol Chem*.

POTTER, J. D. 1982. Preparation of troponin and its subunits. *Methods Enzymol,* 85 Pt B**,** 241-63.

PRONINA, O., ROBINSON, P., BORIVIKOV, Y. & REDWOOD, C. 2007. Alteration of the beta tropomyosin function by nemaline myopathy-causing mutations E117K and Q147P. *Biophys J,* 2007 Congress Proceedings**,** 625a.

RAJAN, S., AHMED, R. P., JAGATHEESAN, G., PETRASHEVSKAYA, N., BOIVIN, G. P., URBONIENE, D., ARTEAGA, G. M., WOLSKA, B. M., SOLARO, R. J., LIGGETT, S. B. & WIECZOREK, D. F. 2007. Dilated cardiomyopathy mutant tropomyosin mice develop cardiac dysfunction with significantly decreased fractional shortening and myofilament calcium sensitivity. *Circ Res,* 101**,** 205-14.

RAYMENT, I., RYPNIEWSKI, W. R., SCHMIDT-BASE, K., SMITH, R., TOMCHICK, D. R., BENNING, M. M., WINKELMANN, D. A., WESENBERG, G. & HOLDEN, H. M. 1993. Three-dimensional structure of myosin subfragment-1: a molecular motor. *Science,* 261**,** 50-8.

RAZZAQ, A., SCHMITZ, S., VEIGEL, C., MOLLOY, J. E., GEEVES, M. A. & SPARROW, J. C. 1999. Actin residue glu(93) is identified as an amino acid affecting myosin binding. *J Biol Chem,* 274**,** 28321-8.

ROBERTSON, S. P., JOHNSON, J. D., HOLROYDE, M. J., KRANIAS, E. G., POTTER, J. D. & SOLARO, R. J. 1982. The effect of troponin I phosphorylation on the Ca2+-binding properties of the Ca2+-regulatory site of bovine cardiac troponin. *J Biol Chem,* 257**,** 260-3.

ROBINSON, P., LIPSCOMB, S., PRESTON, L. C., ALTIN, E., WATKINS, H., ASHLEY, C. C. & REDWOOD, C. S. 2007. Mutations in fast skeletal troponin I, troponin T, and beta-tropomyosin that cause distal arthrogryposis all increase contractile function. *Faseb J,* 21**,** 896-905.

ROBINSON, P., MIRZA, M., KNOTT, A., ABDULRAZZAK, H., WILLOTT, R., MARSTON, S., WATKINS, H. & REDWOOD, C. 2002. Alterations in thin filament regulation induced by a human cardiac troponin T mutant that causes dilated cardiomyopathy are distinct from those induced by troponin T mutants that cause hypertrophic cardiomyopathy. *J Biol Chem,* 277**,** 40710-40716.

ROWLAND, L. P. 2011. HIV-related neuromuscular diseases: nemaline myopathy, amyotrophic lateral sclerosis and bibrachial amyotrophic diplegia. *Acta Myol,* 30**,** 29-31.

SADAYAPPAN, S., FINLEY, N., HOWARTH, J. W., OSINSKA, H., KLEVITSKY, R., LORENZ, J. N., ROSEVEAR, P. R. & ROBBINS, J. 2008. Role of the acidic N' region of cardiac troponin I in regulating myocardial function. *Faseb J,* 22**,** 1246-57.

SAEKI, Y., SHIOZAWA, K., YANAGISAWA, K. & SHIBATA, T. 1990. Adrenaline increases the rate of cross-bridge cycling in rat cardiac muscle. *J Mol Cell Cardiol,* 22**,** 453-60.

SAMBUUGHIN, N., YAU, K. S., OLIVE, M., DUFF, R. M., BAYARSAIKHAN, M., LU, S., GONZALEZ-MERA, L., SIVADORAI, P., NOWAK, K. J., RAVENSCROFT, G., MASTAGLIA, F. L., NORTH, K. N., ILKOVSKI, B., KREMER, H., LAMMENS, M., VAN ENGELEN, B. G., FABIAN, V., LAMONT, P., DAVIS, M. R., LAING, N. G. & GOLDFARB, L. G. 2010.

Dominant mutations in KBTBD13, a member of the BTB/Kelch family, cause nemaline myopathy with cores. *Am J Hum Genet,* 87**,** 842-7.

SANOUDOU, D. & BEGGS, A. H. 2001. Clinical and genetic heterogeneity in nemaline myopathy--a disease of skeletal muscle thin filaments. *Trends Mol Med,* 7**,** 362-8.

SCHAUB, M. C., HEFTI, M. A., ZUELLIG, R. A. & MORANA, I. 1998. Modulation of contractility in human cardiac hypertrophy by myosin essential light chain isoforms. *Cardiovasc Res,* 37**,** 381-404.

SCHIAFFINO, S. & REGGIANI, C. 2011. Fiber types in Mammalian skeletal muscles. *Physiol Rev,* 91**,** 1447-531.

SCHULENBERG, B., AGGELER, R., BEECHEM, J. M., CAPALDI, R. A. & PATTON, W. F. 2003. Analysis of steady-state protein phosphorylation in mitochondria using a novel fluorescent phosphosensor dye. *J Biol Chem,* 278**,** 27251-5.

SEIDMAN, J. G. & SEIDMAN, C. 2001. The genetic basis for cardiomyopathy: from mutation identification to mechanistic paradigms. *Cell,* 104**,** 557-67.

SHY, G. M., ENGEL, W. K., SOMERS, J. E. & WANKO, T. 1963. Nemaline Myopathy. A New Congenital Myopathy. *Brain,* 86**,** 793-810.

SMITH, C. A. & RAYMENT, I. 1996. Active site comparisons highlight structural similarities between myosin and other P-loop proteins. *Biophys J,* 70**,** 1590-602.

SOLARO, R. J. & RARICK, H. M. 1998. Troponin and tropomyosin: proteins that switch on and tune in the activity of cardiac myofilaments. *Circulation Research,* 83**,** 471-80.

SOLARO, R. J., ROSEVEAR, P. & KOBAYASHI, T. 2008. The unique functions of cardiac troponin I in the control of cardiac muscle contraction and relaxation. *Biochem Biophys Res Commun,* 369**,** 82-7.

SOLARO, R. J. & VAN DER VELDEN, J. 2010. Why does troponin I have so many phosphorylation sites? Fact and fancy. *J Mol Cell Cardiol,* 48**,** 810-6.

SONG, W., DYER, E., STUCKEY, D., COPELAND, O., LEUNG, M., BAYLISS, C., MESSER, A. E., WILKINSON, R., TREMOLEDA, J., SCHNEIDER, M., HARDING, S., REDWOOD, C., CLARKE, K., NOWAK, K., MONSERRAT, L., WELLS, D. & MARSTON, S. 2011. Molecular mechanism of the Glu99lys mutation in cardiac actin (ACTC gene) that causes apical hypertrophy in man and mouse. *J Biol Chem,* 286**,** 27582-27593.

SONG, W., DYER, E., STUCKEY, D., LEUNG, M.-C., MEMO, M., MANSFIELD, C., FERENCZI, M., LIU, K., REDWOOD, C., NOWAK, K., HARDING, S., CLARKE, K., WELLS, D. & MARSTON, S. 2010. Investigation of a transgenic mouse model of familial dilated cardiomyopathy. *J Mol Cell Cardiol,* 49**,** 380-389.

SONNENBLICK, E. H. & SKELTON, C. L. 1974. Reconsideration of the ultrastructural basis of cardiac length-tension relations. *Circ Res,* 35**,** 517-26.

SPRANG, S. R. 1997. G protein mechanisms: insights from structural analysis. *Annu Rev Biochem,* 66**,** 639-78.

SPUDICH, J. A. 2001. The myosin swinging cross-bridge model. *Nat Rev Mol Cell Biol,* 2**,** 387-92.

SPUDICH, J. A. & WATT, S. 1971. The regulation of rabbit skeletal muscle contraction. I. Biochemical studies of the interaction of the tropomyosin-troponin complex with actin and the proteolytic fragments of myosin. *J Biol Chem,* 246**,** 4866-71.

SQUIRE, J. M. & PARRY, D. A. 2005. Comparative motile mechanisms in cells. *Adv Protein Chem,* 71**,** 1-15.

STEINBERG, T. H., AGNEW, B. J., GEE, K. R., LEUNG, W. Y., GOODMAN, T., SCHULENBERG, B., HENDRICKSON, J., BEECHEM, J. M., HAUGLAND, R. P. & PATTON, W. F. 2003. Global quantitative phosphoprotein analysis using Multiplexed Proteomics technology. *Proteomics,* 3**,** 1128-44.

STRAUB, F. B. 1942. Actin. *Studies from the Institute of Medical Chemsitry, University of Szeged,* 2**,** 3-15.

SUGDEN, P., SEVERS, NJ, MACLEOD, KT, POOLE-WILSON, PA 2003. Biochemistry and cellular phisiology of heart muscle. *Oxford textbook of medicine***,** 809-820.

SUNDBERG, M., ROSENGREN, J. P., BUNK, R., LINDAHL, J., NICHOLLS, I. A., TAGERUD, S., OMLING, P., MONTELIUS, L. & MANSSON, A. 2003. Silanized surfaces for in vitro studies of actomyosin function and nanotechnology applications. *Anal Biochem,* 323**,** 127-38.

SWEENEY, H. L. 1995. Function of the N terminus of the myosin essential light chain of vertebrate striated muscle. *Biophys J,* 68**,** 112S-119S.

SWEENEY, H. L., BOWMAN, B. F. & STULL, J. T. 1993. Myosin light chain phosphorylation in vertebrate striated muscle: regulation and function. *Am J Physiol,* 264**,** C1085-C1095.

TAJSHARGHI, H., OHLSSON, M., LINDBERG, C. & OLDFORS, A. 2007. Congenital myopathy with nemaline rods and cap structures caused by a mutation in the beta-tropomyosin gene (TPM2). *Arch Neurol,* 64**,** 1334-8.

TAKEDA, N., YAMASHITA, A., MAEDA, K. & MAEDA, Y. 2003. Structure of the core domain of human cardiac troponin in the Ca2+-saturated form. *Nature,* 424**,** 35-41.

TIMSON, D. J., TRAYER, H. R. & TRAYER, I. P. 1998. The N-terminus of A1-type myosin essential light chains binds actin and modulates myosin motor function. *Eur J Biochem,* 255**,** 654-662.

TOBACMAN, L. S. 1996. Thin filament-mediated regulation of cardiac contraction. *Annu Rev Physiol,* 58**,** 447-81.

TOWBIN, J. A., HEJTMANCIK, J. F., BRINK, P., GELB, B., ZHU, X. M., CHAMBERLAIN, J. S., MCCABE, E. R. & SWIFT, M. 1993. X-linked dilated cardiomyopathy. Molecular genetic evidence of linkage to the Duchenne muscular dystrophy (dystrophin) gene at the Xp21 locus. *Circulation,* 87**,** 1854-65.

TOWNSEND, P. J., YACOUB, M. H. & BARTON, P. J. 1997a. Assignment of the human cardiac/slow skeletal muscle troponin C gene (TNNC1) between D3S3118 and GCT4B10 on the short arm of chromosome 3 by somatic cell hybrid analysis. *Ann Hum Genet,* 61**,** 375-7.

TOWNSEND, P. J., YACOUB, M. H. & BARTON, P. J. 1997b. Assignment of the human fast skeletal muscle troponin C gene (TNNC2) between D20S721 and GCT10F11 on chromosome 20 by somatic cell hybrid analysis. *Ann Hum Genet,* 61**,** 457-9.

TOYOSHIMA, C., ASAHI, M., SUGITA, Y., KHANNA, R., TSUDA, T. & MACLENNAN, D. H. 2003. Modeling of the inhibitory interaction of phospholamban with the Ca2+ ATPase. *Proc Natl Acad Sci U S A,* 100**,** 467-72.

TRAYER, I. P., TRAYER, H. R. & LEVINE, B. A. 1987. Evidence that the N-terminal region of A1-light chain of myosin interacts directly with the C-terminal region of actin. A proton magnetic resonance study. *Eur J Biochem,* 164**,** 259-66.

URBANCIKOVA, M. & HITCHCOCK DEGREGORI, S. E. 1994. Requirement of amino-terminal modification for striated muscle alpha-tropomyosin function. *J.Biol.Chem.,* 269**,** 24310-24315.

VAN DER VELDEN, J., PAPP, Z., ZAREMBA, R., BOONTJE, N. M., DE JONG, J. W., OWEN, V. J., BURTON, P. B., GOLDMANN, P., JAQUET, K. & STIENEN, G. J. 2003. Increased Ca2+-sensitivity of the contractile apparatus in end-stage human heart failure results from altered phosphorylation of contractile proteins. *Cardiovasc Res,* 57**,** 37-47.

VAN EERD, J. P. & TAKAHASHI, K. 1975. The amino acid sequence of bovine cardiac tamponin-C. Comparison with rabbit skeletal troponin-C. *Biochem Biophys Res Commun,* 64**,** 122-7.

VIBERT, P., CRAIG, R. & LEHMAN, W. 1997. Steric-model for activation of muscle thin filamnets. *J Mol Biol,* 266**,** 8-14.

VINOGRADOVA, M. V., STONE, D. B., MALANINA, G. G., KARATZAFERI, C., COOKE, R., MENDELSON, R. A. & FLETTERICK, R. J. 2005. Ca2+-regulated structural changes in troponin. *Proc Natl Acad Sci U S A,* 102**,** 5038-5045.

WADDELL, L. B., KREISSL, M., KORNBERG, A., KENNEDY, P., MCLEAN, C., LABARRE-VILA, A., MONNIER, N., NORTH, K. N. & CLARKE, N. F. 2010. Evidence for a dominant negative disease mechanism in cap myopathy due to TPM3. *Neuromuscul Disord,* 20**,** 464-6.

WALKER, J. S., LI, X. & BUTTRICK, P. M. 2010. Analysing force-pCa curves. *J Muscle Res Cell Motil,* 31**,** 59-69.

WALLGREN-PETTERSSON, C., JASANI, B., NEWMAN, G. R., MORRIS, G. E., JONES, S., SINGHRAO, S., CLARKE, A., VIRTANEN, I., HOLMBERG, C. & RAPOLA, J. 1995. Alpha-actinin in nemaline bodies in congenital nemaline myopathy: immunological confirmation by light and electron microscopy. *Neuromuscul Disord,* 5**,** 93-104.

WATTANASIRICHAIGOON, D., SWOBODA, K. J., TAKADA, F., TONG, H. Q., LIP, V., IANNACCONE, S. T., WALLGREN-PETTERSSON, C., LAING, N. G. & BEGGS, A. H. 2002. Mutations of the slow muscle alpha-tropomyosin gene, TPM3, are a rare cause of nemaline myopathy. *Neurology,* 59**,** 613-7.

WEBER, A., PENNISE, C. R., BABCOCK, G. G. & FOWLER, V. M. 1994. Tropomodulin caps the pointed ends of actin filaments. *J Cell Biol,* 127**,** 1627-35.

WEEDS, A. G. & TAYLOR, R. S. 1975. Separation of subfragment-1 isoenzymes from rabbit skeletal muscle myosin. *Nature,* 257**,** 54-56.

WOLFF, M., BUCK, S., STOKER, S., GREASER, M. & MENTZER, R. 1996. Myofibrillar calcium sensitivity of isometric tension is increased in human dilated cardiomyopathies. *J Clin Invest,* 98**,** 167-176.

XIE, X., HARRISON, D. H., SCHLICHTING, I., SWEET, R. M., KALABOKIS, V. N., SZENT-GYORGYI, A. G. & COHEN, C. 1994. Structure of the regulatory domain of scallop myosin at 2.8 A resolution. *Nature,* 368**,** 306-12.

XU, C., CRAIG, R., TOBACMAN, L., HOROWITZ, R. & LEHMAN, W. 1999. Tropomyosin positions in regulated thin filaments revealed by cryoelectron microscopy. *Biophys J,* 77**,** 985-92.

Journal of Molecular and Cellular Cardiology 49 (2010) 380–389

Contents lists available at ScienceDirect

Journal of Molecular and Cellular Cardiology

journal homepage: www.elsevier.com/locate/yjmcc

Original article

Investigation of a transgenic mouse model of familial dilated cardiomyopathy

Weihua Song [a,1], Emma Dyer [b,1], Daniel Stuckey [c], Man-Ching Leung [a], Massimiliano Memo [a], Catherine Mansfield [d], Michael Ferenczi [d], Ke Liu [e], Charles Redwood [f], Kristen Nowak [g], Sian Harding [a], Kieran Clarke [c], Dominic Wells [d], Steven Marston [a,*]

[a] Cardiovascular Medicine, NHLI, Imperial College London, SW3 6LY, UK
[b] MRC HRSU, Queen's Medical Research Institute, Edinburgh EH16 4TJ, UK
[c] Department of Physiology, Anatomy and Genetics, University of Oxford, OX1 3PT, UK
[d] Molecular Medicine, NHLI, Imperial College London, SW3 6LY, UK
[e] Division of Neuroscience and Mental Health, Imperial College London, W12 ONN, UK
[f] Department of Cardiovascular Medicine, University of Oxford, OX3 9DU, UK
[g] Western Australian Institute for Medical Research, Nedlands, WA 6009, Australia

ARTICLE INFO

Article history:
Received 2 November 2009
Received in revised form 17 May 2010
Accepted 18 May 2010
Available online 17 June 2010

ABSTRACT

We have investigated a transgenic mouse model of inherited dilated cardiomyopathy that stably expresses the *ACTC* E361G mutation at around 50% of total actin in the heart. F-actin isolated from *ACTC* E361G mouse hearts was incorporated into thin filaments with native human tropomyosin and troponin and compared with NTG mouse actin by *in vitro* motility assay. There was no significant difference in sliding speed, fraction of filaments motile or Ca^{2+}-sensitivity (ratio EC_{50} E361G/NTG = 0.95 ± 0.08). The Ca^{2+}-sensitivity of force in skinned trabeculae from *ACTC* E361G mice was slightly higher than NTG (EC_{50} E361G/NTG = 0.78 ± 0.04). The molecular phenotype was revealed when troponin was dephosphorylated; Ca^{2+}-sensitivity of E361G-containing thin filaments was now lower than NTG (EC_{50} $E361G_{dPTn}$/NTG_{dPTn} = 2.15 ± 0.09). We demonstrated that this was due to uncoupling of Ca^{2+}-sensitivity from troponin I phosphorylation by comparing Ca^{2+}-sensitivity of phosphorylated and dephosphorylated thin filaments. For NTG actin-containing thin filaments EC_{50} native/dPTn = 3.0 ± 0.3 but for E361G-containing thin filaments EC_{50} native/dPTn = 1.04 ± 0.07.We studied contractility in isolated myocytes and found no significant differences under basal conditions. We measured cardiac performance by cine-MRI, echocardiography and with a conductance catheter over a period of 4 to 18 months and found minimal systematic differences between NTG and *ACTC* E361G mice under basal conditions. However, the increase in septal thickening, ejection fraction, heart rate and cardiac output following dobutamine treatment was significantly less in ACTC E361G mice compared with NTG. We propose that the *ACTC* E361G mutation uncouples myofilament Ca^{2+}-sensitivity from Troponin I phosphorylation and blunts the response to adrenergic stimulation, leading to a reduced cardiac reserve with consequent contractile dysfunction under stress, leading to dilated cardiomyopathy.

© 2010 Elsevier Ltd. All rights reserved.

1. Introduction

Dilated cardiomyopathy is usually defined as left ventricular end-diastolic dimension >95th percentile for age and body surface area and shortening fraction <28% [1]. It is a common cause of heart failure and it is now established that 20–30% of cases of dilated cardiomyopathy are due to mutations [2]. Many mutations associated with familial DCM are in proteins of the sarcomere or cytoskeleton. In particular, cases of "pure" dilated cardiomyopathy that are not associated with other symptoms such as conduction disease are usually caused by mutations in the contractile proteins actin, myosin, tropomyosin and troponin I,C and T [2–4] and these have been intensively investigated using recombinant proteins *in vitro* [5–13]. To study the molecular mechanism of familial DCM at the whole animal level we have created a transgenic mouse model of DCM due to a mutation in a key component of the contractile apparatus, actin , *ACTC* E361G [1]. This mutation was associated with DCM in a single family; two individuals with the *ACTC* E361G mutation were diagnosed at ages 41 and 14 and the two other family members carrying the mutation were partially affected (one, aged 34, showed dilation only and the other, aged 9 showed borderline dilation, [14]). The charge neutralisation mutation is located on the surface of actin subdomain 1, potentially involved in weak binding of myosin.

In developing the *ACTC* E361G transgenic mouse, our guiding principal has been to approach as closely as possible the situation in human tissue. The major advantage of studying a DCM mutation in the *ACTC* gene is that the protein is highly conserved with no reported

* Corresponding author.
E-mail address: s.marston@imperial.ac.uk (S. Marston).
[1] Equal contribution.

0022-2828/$ – see front matter © 2010 Elsevier Ltd. All rights reserved.
doi:10.1016/j.yjmcc.2010.05.009

amino-acid polymorphisms. Uniquely amongst the contractile proteins, both skeletal and cardiac actin have an identical amino-acid sequence in man and mouse and an identical isoform distribution in heart (21% skeletal actin [*ACTA1*], 79% cardiac actin [*ACTC*]) [15,16]. We have expressed the *ACTC* E361G without any adduct that could alter function and at a level of 50%, which is the predicted level in heterozygotes. Furthermore it has been demonstrated that over-expression of actin in the heart does not lead to any alteration in the stoichiometry or structure of the myofibrils or any accumulation of actin in the cytoplasm [17]. These are important issues for faithfully reproducing disease, as has been highlighted by recent debates on the validity of transgenic mouse models [18,19].

Two published mouse models of DCM caused by mutations in other thin filament proteins have problems in this respect. The troponin T ΔK210 knock-in model [20] has mouse-sequence Troponin T as well as Troponin I and troponin C, which is likely to alter the response to the mutation compared with all-human components as we have demonstrated [21]; moreover this model was mainly studied in a homozygous form yet we know that 100% and 50% ΔK210 TnT behave differently *in vitro* when tested with human sequence TnI and TnC [5,6]. The α-tropomyosin E54K transgenic mouse model [22] has been reported to express mutant tropomyosin at up to 70% in myofibrils, but there is also a substantial quantity of free E54K tropomyosin in the cytoplasm of this model which may be more responsible for the phenotype than the mutation incorporated into thin filaments. Both of these models exhibit symptoms of severe heart failure from an early age. In contrast, we found that *ACTC* E361G transgenic mice show little or no overt disease phenotype when kept under normal conditions (at least up to 18 months old) but purified actin from the *ACTC* E361G mice exhibits a clear phenotype at the single filament level when investigated by *in vitro* motility assay. We found that the primary molecular defect caused by this mutation is that it renders the thin filament Ca^{2+}-sensitivity insensitive to the level of troponin I phosphorylation. We propose a novel mechanism for dilated cardiomyopathy: the uncoupling caused by the actin E361G mutation blunts the response to adrenergic stimulation, leading to a reduced cardiac reserve with consequent contractile dysfunction under stress, leading to dilated cardiomyopathy.

2. Methods

The generation of transgenic mice [23] and their phenotypic characterisation by magnetic resonance imaging (cine-MRI) [24], echocardiography, conductance catheter [25] and in isolated myocytes [26] and skinned papillary muscles [27] used established methodologies described in the data supplement. Troponin I and MyBP-C phosphorylation levels were measured in myofibrillar fractions [28,29]. Mutant actin was isolated and thin filaments were reconstituted with native human troponin and tropomyosin for study by *in vitro* motility assay as described [29,30]. Full details are presented in the data supplement.

3. Results

3.1. Production and characterisation of transgenic mice

We obtained two lines of mice (361.13 and 361.20) that expressed the *ACTC* E361G transgene. The presence of mutant protein in heart muscle could be detected by 2D electrophoresis since the single charge change of glutamic acid to glycine shifts the iso-electric point by 0.07 pI units (Supplementary data A). We found that mutant actin content was variable in PCR-positive hearts of line 361.13 but line 361.20 stably expressed mutant actin at close to 50% of total actin in the heart. All subsequent transgenic mice used in this study were heterozygotes bred from 361.20. Subsequently, random samples of mouse hearts (20% of total) were tested to confirm the continued presence of the mutant protein at around 50% in transgenic mouse hearts up to 18 months old.

The contractile protein composition of myofibrils from non-transgenic (NTG) and *ACTC* E361G hearts was indistinguishable (Fig. 1A) and comparison of phosphorylation levels of MyBP-C, troponin T, troponin I and MLC-2 in myofibrils showed no significant difference in phosphorylation between NTG and transgenic mouse irrespective of age (Fig. 1B). Separation of troponin I phosphospecies by phosphate affinity SDS-PAGE showed that 37–45% of troponin I was the bis-phosphorylated species and total phosphorylation was 1.3 molsPi/mol troponin I. These figures are similar to those measured in human donor heart samples [28]. Dobutamine treatment increased troponin I phosphorylation by 10–20% (Supplementary data B).

3.2. Cardiac phenotype of transgenic mice at 4–6 months old

The transgenic mice showed no overt signs of cardiac abnormality. Survival rate up to 21 months and heart/body weight ratio were indistinguishable from non-transgenic litter-mates. 4-month-old mice were examined by cine-MRI. This showed no abnormalities of size or morphology and no significant differences in end diastolic volume or end-systolic volume, nor in calculated peak ejection or filling rates (Fig. 2, Supplementary data C).

With 6-month-old mice, *in vivo* M-mode echocardiography measurements revealed significantly increased left ventricle internal diameter in *ACTC* E361G mice (3.95 ± 0.06 vs. 3.43 ± 0.10 mm, $p<0.01$) at the end of diastole with the same end-systolic ventricle diameter. The left ventricle posterior wall of *ACTC* E361G mice showed a trend to decreased thickness at both end of systole and diastole but this was not significantly different from NTG mice. Fractional shortening of the ventricle diameter appeared to be the same (Supplementary data D). Lead II ECG recording on the same groups of mice under anaesthesia revealed significantly decreased QRS amplitude in *ACTC* E361G mice (0.78 ± 0.06 vs. 1.11 ± 0.10 mV, $p = 0.01$).

The absence of cardiac dysfunction at rest was also apparent from measurements of pressure and volume of mouse hearts *in situ* using the conductance catheter technique on 6-month-old mice (4 *ACTC* E361G, 5 NTG). We did not observe any significant difference in either systolic or diastolic function or ventricle volume at the end of diastole (18.88 ± 1.12 in NTG and 20.25 ± 1.78 μl in *ACTC* E361G, $p = 0.5$ [31] (Supplementary data E)).

With echocardiography, we also compared the effect of a bolus injection of dobutamine on 6-month NTG and *ACTC* E361G mice. The dobutamine-induced increase in septum thickness at end of diastole and end of systole was significantly less in *ACTC* E361G mice (Table 1). There was no significant difference in the increase of heart rate but the calculated increase in cardiac output was significantly less in *ACTC* E361G mice.

We then examined contractility in individual myocytes from NTG and *ACTC* E361G mouse hearts (Fig. 3). Contractile responses to Ca^{2+}, isoprenaline or frequency were as predicted for mouse ventricular myocytes, and acceleration of relaxation with either frequency or isoprenaline stimulation was clearly observed, confirming the sensitivity of the measurements. In basal conditions (1 mM $CaCl_2$, 1 Hz, 0.2 mA stimulation, 37 °C), the cardiomyocytes from *ACTC* E361G mouse hearts did not perform differently compared with those from NTG mouse hearts in contraction amplitude (% shortening), contraction speed (time to peak contraction) or relaxation speed (time to 50% relaxation, time to 90% relaxation). Myocytes from *ACTC* E361G mice did not behave differently from NTG mouse cells in response to increases in Ca^{2+} concentration, or stimulation frequency, but EC_{50} for isoprenaline stimulation of contraction amplitude was increased two-fold in *ACTC* E361G mice, although the differences were not statistically significant (Fig. 3).

3.3. Cardiac phenotype of older transgenic mice

We investigated older mice to determine whether a DCM phenotype developed over time (Fig. 4). At 12 months, end-systolic

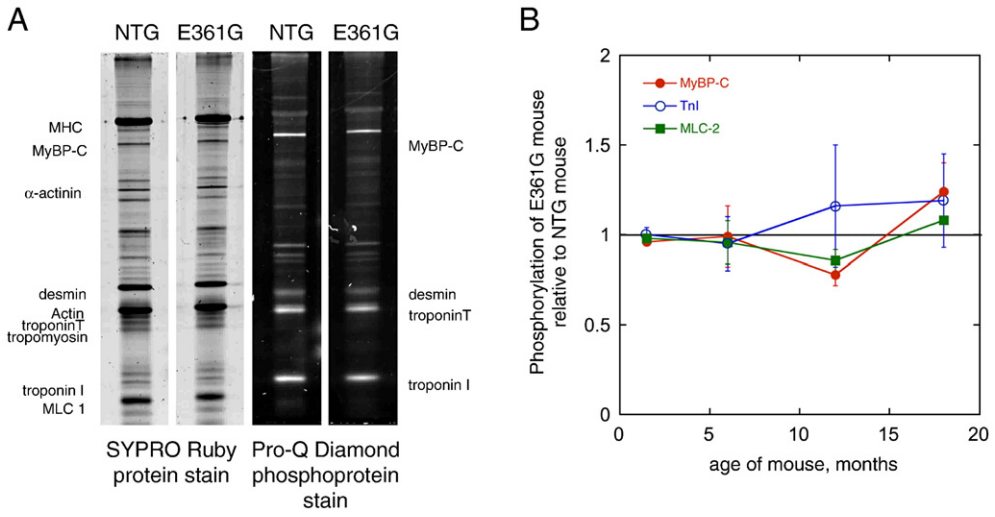


Fig. 1. Contractile protein phosphorylation in non-transgenic and *ACTC* E361G transgenic mouse hearts. (A) The myofibrillar fraction was separated by SDS-PAGE and stained successively with Pro-Q Diamond phosphoprotein stain and SYPRO Ruby total protein stain. The Pro-Q Diamond stain indicates phosphorylation of myosin binding protein C (MyBP-C), troponin T and troponin I. Phosphorylation levels in NTG and ACTC E361G mouse myofibrils are the same (1.30 and 1.33 molsPi/mol, respectively, measured by Phosphate affinity SDS-PAGE). (B) Relative levels of MyBP-C, troponin I and MLC-2 phosphorylation in NTG and ACTC E361G mouse hearts is plotted against the age of the mice. Each point is the mean and S.E.M. of 3–5 measurements using Pro-Q Diamond or phosphate affinity SDS-PAGE. There is no significant difference in contractile protein phosphorylation at any age.

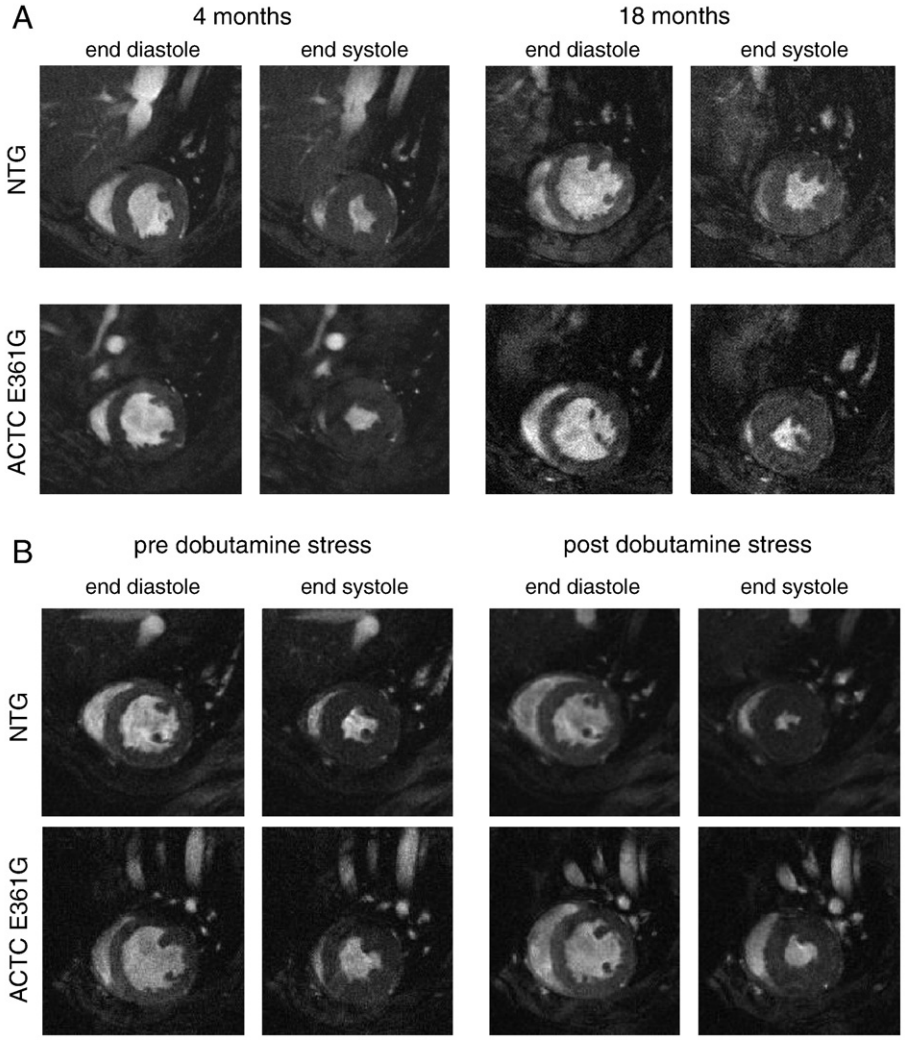


Fig. 2. Nontransgenic and *ACTC* E361G transgenic mouse hearts imaged by cine-MRI. (A) End-diastolic and end-systolic mid-papillary short-axis cine-MRI images acquired from 4-month-old and 18-month-old NTG and ACTC E361G mice. (B) End diastolic and end systolic cine-MR images acquired from 18-month-old NTG and *ACTC* E361G mice prior to, and 10 min after i.p. injection of 1.5 μg/g dobutamine. Cardiac parameters derived from cine-MRI are shown in Table 2 and Supplementary Data C and H.

Table 1
Response to β-adrenergic stimulation in 6-month-old mice measured by echocardiography. 6-month NTG ($n=7$) and *ACTC* E361G ($n=7$) mice were studied by *in vivo* dobutamine stress echocardiography. The parameters are given as mean ± SEM. NTG and *ACTC* E361G values are compared by *t* test.

Change post dobutamine		NTG ($n=7$)	*ACTC* E361G ($n=7$)	*p* value
Septum thickness diastole	mm	0.32 ± 0.08	0.05 ± 0.06	0.01
Septum thickness systole	mm	0.44 ± 0.10	0.20 ± 0.04	0.04
Posterior wall thickness diastole	mm	0.01 ± 0.10	0.14 ± 0.18	0.41
Posterior wall thickness systole	mm	0.29 ± 0.10	0.46 ± 0.20	0.45
LV diameter diastole	mm	−0.59 ± 0.15	−0.52 ± 0.16	0.76
LV diameter systole	mm	−1.01 ± 0.28	−1.00 ± 0.16	0.96
Heart rate	bpm	158.0 ± 7.61	136.9 ± 23.05	0.40
Cardiac output	ml/min	3.09 ± 0.86	0.05 ± 0.70	0.03

pressure of *ACTC* E361G mice was significantly lower than that of NTG mice (63 ± 3 vs. 72 ± 3 mm Hg, $p=0.05$), speed of ventricle contraction was decreased (−635 ± 63 vs. −840 ± 59 μl/s, $p=0.04$) but not the speed of pressure increase (dP/dt_{max}), which indicates a slower contraction in *ACTC* E361G hearts. Both $-dP/dt$ and Tau of *ACTC* E361G mice were significantly different from those of NTG mice indicating an impaired relaxation although overall cardiac function was not significantly weakened (Supplementary data F).

The mice were investigated again at around 18 months. The same groups of *ACTC* E361G and NTG mice were studied first by cine-MRI and then a week later with the conductance catheter. No statistically significant differences in standard MRI measurements of cardiac morphology and function between NTG and *ACTC* E361G were identified (Supplementary Data H). However, *ACTC* E361G mice had a reduced response to β-adrenergic stimulation; the dobutamine-mediated increases in heart rate, ejection fraction and cardiac output were significantly lower than those observed in the NTG mice (Fig. 2, Table 2).

Ejection fraction of *ACTC* E361G mice was significantly lower (72 ± 3 vs. 83 ± 2%, $p=0.01$) when studied with conductance catheter (Supplementary Data G). Despite the differences shown with conductance catheter at 12 months, both groups have shown similar function at 4 to 6 months and 18 months with no consistent trend as shown with both conductance catheter and MRI, indicating that cardiac function and

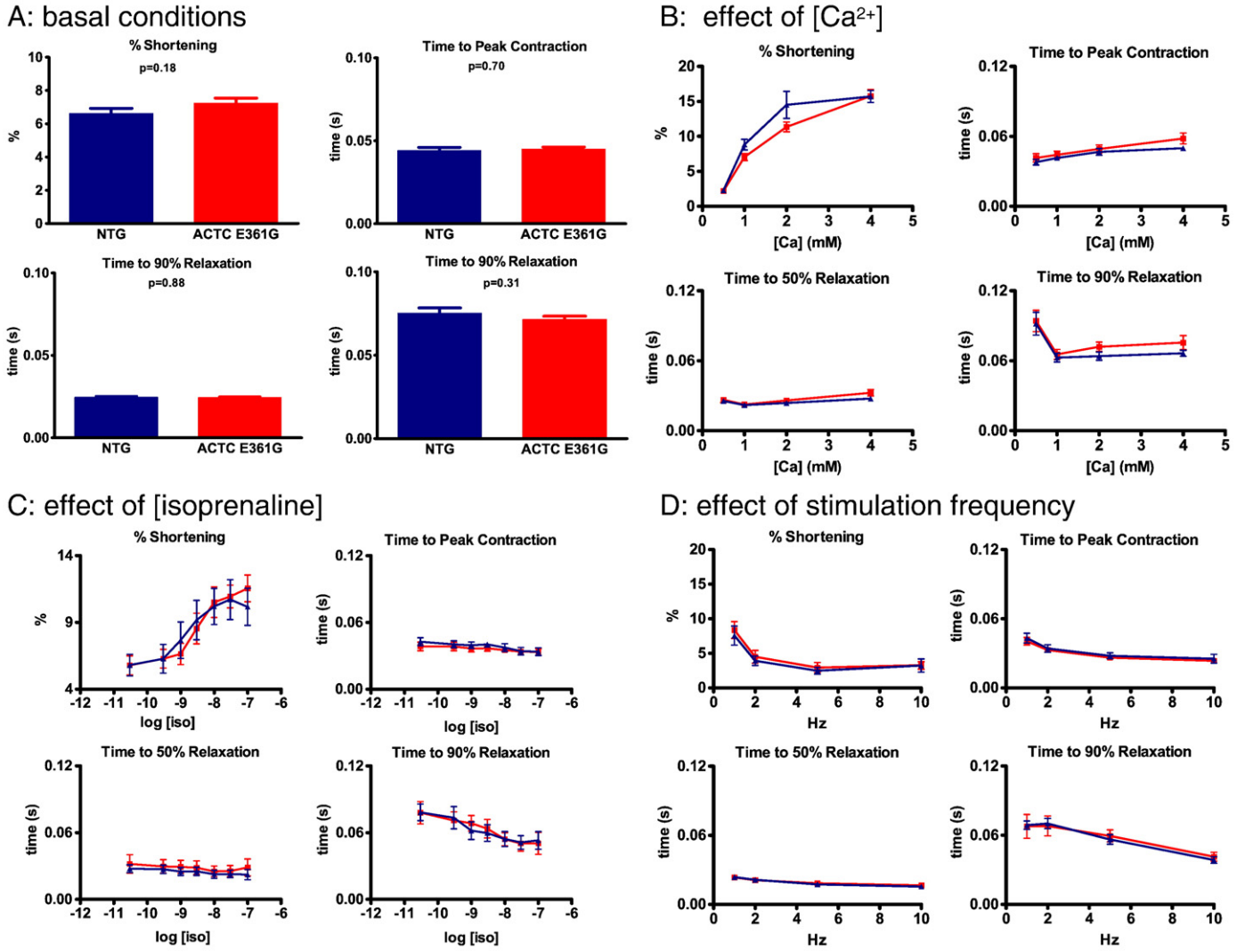


Fig. 3. Comparison of contractile properties of isolated myocytes from 5-month-old nontransgenic and *ACTC* E361G transgenic mouse hearts. (A) NTG (blue triangles) and ACTC E361G (red squares) mouse cells compared in basal conditions (1 Hz, 0.2 mA, 1 mM $CaCl_2$, 37 °C) show no significant differences. (B) The effect of increasing $CaCl_2$ concentration on myocyte contraction. Shortening amplitude is strongly dependent on $[Ca^{2+}]$, but there are no significant differences between NTG and ACTC E361G mouse heart myocytes. (C) The effect of isoprenaline. Contractile amplitude is increased and rates of shortening and relaxation are increased. The EC_{50} for increase in contractile amplitude was 3.7 ± 1.3 nM for NTG and 7.1 ± 1.9 nM for E361G mouse heart cells ($p=0.13$). (D) The effect of increasing stimulation frequency.

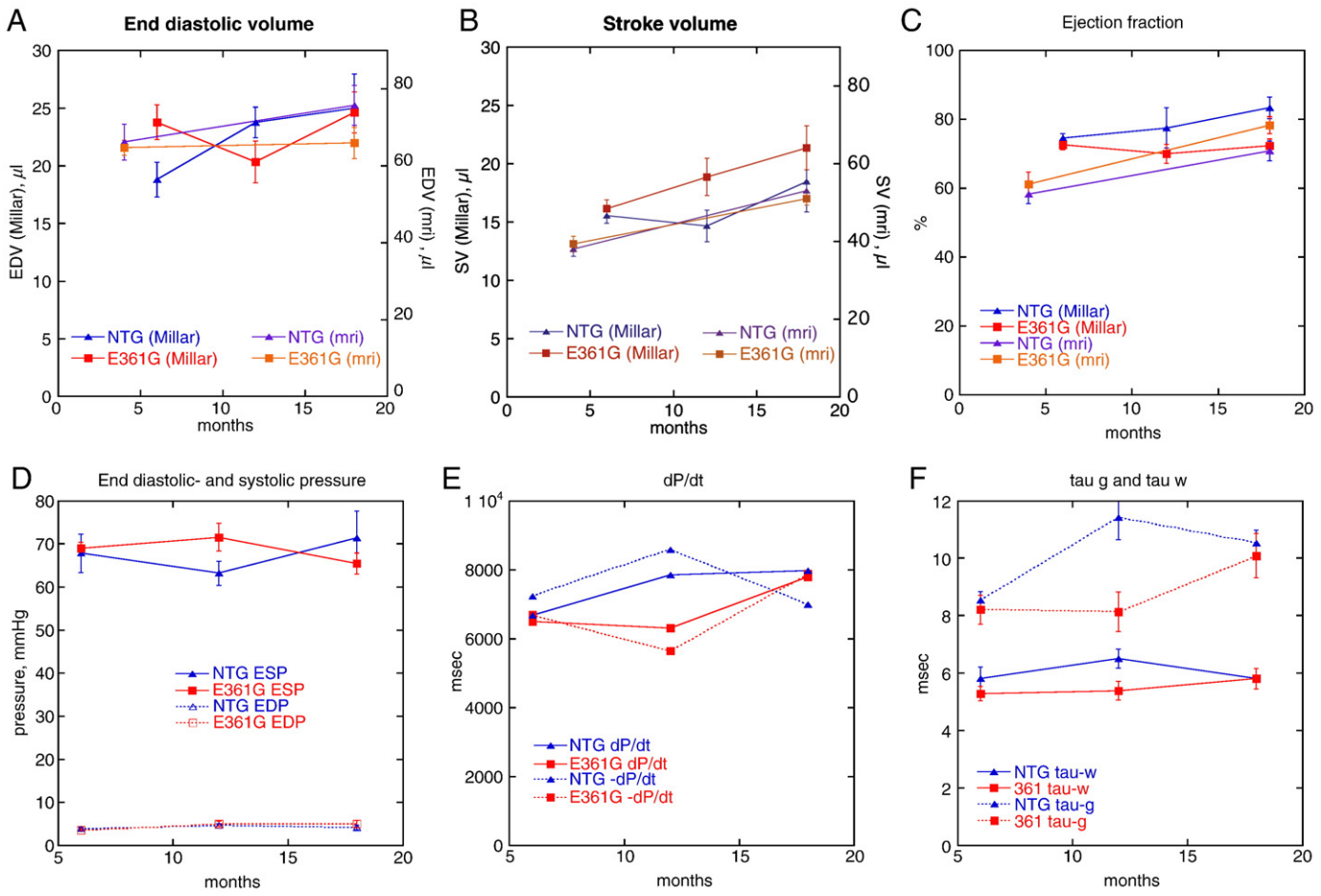


Fig. 4. Changes in contractile parameters with age in nontransgenic and *ACTC* E361G transgenic mouse hearts. The plots show MRI and conductance catheter measurements of the contractile parameters plotted against age. (A) End diastolic volume measured by both Millar catheter and cine-MRI; note the different *y* axes. (B) Stroke volume measured by both Millar catheter and cine-MRI; note the different *y* axes. (C) Ejection fraction; Millar catheter and cine-MRI data plotted on the same *y* axis. (D) End diastolic pressure and end-systolic pressure, measured by Millar catheter. (E) Rates of contraction (dP/dt) and relaxation ($-dP/dt$), measured by Millar catheter. (F) Rate constants Tau_g and Tau_w, measured by Millar catheter.

morphology of *ACTC* E361G mice do not show any significant differences from non-transgenic litter-mates at any age under normal husbandry.

We also measured the levels of contractile protein phosphorylation at 1, 6, 12 and 18 months but found no significant trend in phosphorylation level with age in the *ACTC* E361G or the non-transgenic mice (Fig. 1B).

3.4. Molecular phenotype of thin filaments containing mutated E361G

Since the mutational effects at the whole mouse level appeared to be compensated for, we next examined the properties of purified actin from *ACTC* E361G mouse. Initial attempts at isolating actin by the traditional acetone powder method indicated that the monomeric actin from *ACTC* E361G mouse hearts was unstable and readily aggregated so that subsequent polymerisation of actin produced polymeric actin containing only wild-type actin. We therefore isolated polymeric actin directly by isolating thin filaments and then stripping off the regulatory proteins (Supplementary data A). When we compared NTG and E361G actin in the *in vitro* motility assay we found that the sliding speed was 7% lower for the E361G actin ($n=30$, $p=0.02$) whilst the fraction of filaments motile was not different ($p=0.65$, see Fig. 5). When we compared the affinity of E361G and NTG actin for α-actinin we found reduced affinity in the E361G mice ($K_{dE361G}/K_{dNTG}=5.2\pm0.5$, $n=3$, Supplementary data I).

We reconstructed thin filaments using the mouse actin with tropomyosin and troponin isolated from human donor heart muscle. These thin filaments would be identical to native human thin filaments since the amino acid sequences of human and mouse cardiac actin are the same and troponin and tropomyosin have native post-translational modifications including N-terminal acetylation and phosphorylation. With the addition of 50nM human cardiac tropomyosin, the sliding speed of actin filaments increased slightly but E361G actin-containing filaments remained slower than NTG filaments ($n=30$, $p=0.001$). With the further addition of 50 nM human cardiac troponin, from donor heart, the thin filaments became Ca^{2+}-sensitive. At activating Ca^{2+} concentrations, at least 70% of thin filaments were motile and sliding speed was slightly higher than for actin-tropomyosin whilst at relaxing Ca^{2+} concentration (10^{-9} M),

Table 2
Response to β-adrenergic stimulation in 18-month-old mice measured by MRI. 18 month NTG ($n=7$) and *ACTC* E361G ($n=5$) mice were studied by *in vivo* dobutamine stress cine-MRI. Three slices (basal, mid-papillary and apical) were acquired and used to assess changes in LV volume. The derived parameters are given as mean ± S.E.M. NTG and *ACTC* E361G values are compared by *t* test.

Change post dobutamine		NTG ($n=7$)	*ACTC* E361G ($n=6$)	*p* value
End-diastolic volume	µl	−6.9 ± 5.0	−4.2 ± 4.7	0.36
End-systolic volume	µl	−6.9 ± 3.4	−3.0 ± 2.7	0.06
Stroke volume	µl	0.0 ± 2.5	−1.2 ± 2.6	0.43
Ejection fraction	%	15.7 ± 6.6	7.2 ± 6.2	0.05
Heart rate	bpm	169 ± 58	102 ± 35	0.04
Cardiac output	ml/min	4.3 ± 1.9	1.9 ± 1.1	0.03

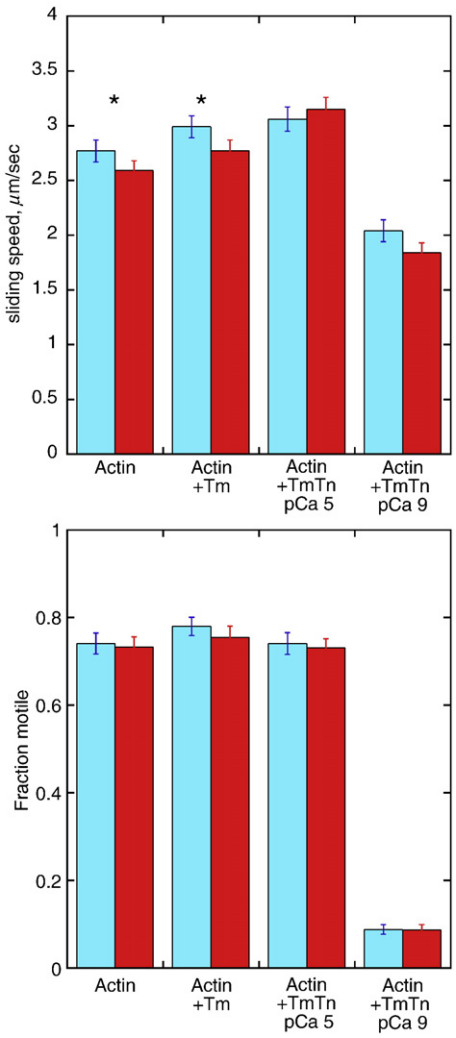


Fig. 5. *In vitro* motility measurements comparing NTG and E361G actin. The movement of actin filaments over immobilised heavy meromyosin was observed and the speed of movement and fraction of filaments motile were determined. Means and S.E.M. of 30–35 measurements using 7 pairs of mouse hearts are shown. Pale blue bars, NTG actin; red bars, E361G actin. E361G actin filaments moved significantly slower than NTG actin in the absence and presence of tropomyosin. Motility was Ca^{2+}-regulated in the presence of troponin but no differences between NTG and E361G actin were observed.

the fraction of filament motile was reduced to 8% and sliding speed was reduced by 35–40%, however, thin filaments containing NTG and E361G actin were indistinguishable in both activating and relaxing conditions (Fig. 5).

Measurements of the Ca^{2+}-dependence of *in vitro* motility using human-like reconstituted thin filaments showed that the Ca^{2+}-sensitivity of thin filaments containing E361G actin was slightly higher (5% lower EC_{50}) than NTG actin-containing thin filaments but the difference was not statistically significant (Table 3, Fig. 6). This was unexpected, since most DCM mutations previously studied caused a 2- to 3-fold reduced Ca^{2+}-sensitivity [6]. We therefore investigated Ca^{2+}-regulation of isometric force in chemically skinned mouse papillary muscle (Fig. 7, Table 3). We found that Ca^{2+}-sensitivity of the *ACTC* E361G mouse papillary muscle was significantly greater (37% lower EC_{50}) than NTG littermates (Fig. 7B), but there was no significant differences in Hill coefficient (Fig. 7C) or maximum isometric tension (Fig. 7D).

In further *in vitro* motility studies we noted that the Ca^{2+}-sensitivity of thin filaments containing E361G actin was significantly

Table 3
Ca^{2+}-sensitivity of skinned papillary muscle and thin filaments containing NTG and *ACTC* E361G actin. Values are mean ± S.E.M. for *n* separate measurements. EC_{50} values compared by paired *t*-test. Ratio is compared by single-value *t* test compared to 1.

	Method	EC_{50}, μM			
		NTG actin	E361G actin	*n*	Ratio EC_{50} E361G/NTG
Skinned mouse papillary muscle	Isometric tension	1.14 ± 0.03	0.90 ± 0.03 $p<0.0001$	8	0.78 ± 0.04 $p<0.0001$
Native human troponin	Thin filament motility	0.12 ± 0.029	0.109 ± 0.026 $p=0.20$	7	0.95 ± 0.08 $p=0.53$
Rabbit fast skeletal troponin	Thin filament motility	0.082 ± 0.025	0.38 ± 0.22	3	3.33
Dephosphorylated human troponin	Thin filament motility	0.26 ± 0.12	0.49 ± 0.17 $p=0.06$	4	2.15 ± 0.09 $p=0.01$

lower than NTG actin when fast skeletal muscle troponin was used in place of human cardiac troponin (3.3-fold higher EC_{50}, Table 3, Fig. 6). Skeletal muscle troponin I lacks the N-terminal peptide of cardiac troponin I that is phosphorylated by PKA, suggesting that the functional effect of the *ACTC* E361G DCM mutation may involve the phosphorylation-dependent change in Ca^{2+}-sensitivity rather than directly affecting the regulatory protein function. To test this hypothesis we dephosphorylated human cardiac troponin with acid phosphatase. We found that, using dephosphorylated troponin, the Ca^{2+}-sensitivity of E361G actin-containing thin filaments was now lower than NTG actin (Ratio EC_{50} E361G/NTG = 2.15 ± 0.09, $p=0.01$) (Table 3, Fig. 6).

The difference between thin filaments with E361G or native actin appeared because the Ca^{2+}-sensitivity of NTG thin filaments was higher when dephosphorylated whilst the Ca^{2+}-sensitivity of the E361G actin-containing thin filaments did not change. This was demonstrated directly by comparing native phosphorylated and dephosphorylated thin filaments (Fig. 8). These measurements showed clearly that the Ca^{2+}-sensitivity of E361G actin-containing thin filaments was not responsive to changes in troponin I phosphorylation levels in contrast to the NTG actin-containing thin filaments where the unphosphorylated troponin gave a 3 fold higher Ca^{2+}-sensitivity.

4. Discussion

We have generated and characterised transgenic mice that stably express the *ACTC* E361G mutation at around 50% of total actin in the heart and show a distinctive uncoupling of Ca^{2+}-sensitivity of thin filaments motility from the level of troponin I phosphorylation *in vitro* but do not exhibit a DCM-like phenotype under normal resting conditions *in vivo*. These findings highlight the key role of abnormal response to adrenergic stimulation in DCM and heart failure.

4.1. ACTC E361G transgenic mouse as a model of human DCM

This mouse model was planned to reproduce the human case of familial dilated cardiomyopathy (DCM) as closely as possible. Cardiac actin is the only contractile protein that has an identical amino acid sequence in man and mouse as well as an identical isoform distribution (79% cardiac actin and 21% skeletal actin [16,32,33]). This is an important property since we have found that the effect of HCM and DCM mutations on function *in vitro* can vary significantly depending on species, isoform and post-translational modifications [7,21,30]. Actin transgenes with the MHC promoter lead to substitution rather than overexpression of actin [17] and we observed that myofibrillar protein content is normal (Fig.1) and there is no unincorporated actin in the cytoplasm. Mutant actin is expressed consistently at around 50% of total actin in the *ACTC* E361G mouse

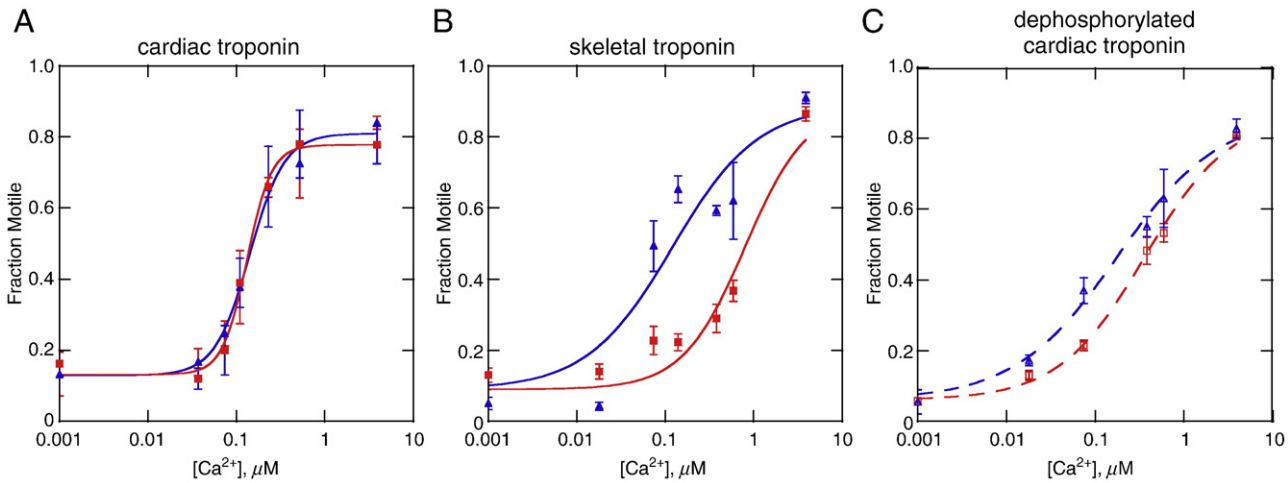


Fig. 6. *In vitro* motility analysis comparing Ca^{2+}-activation of motility of thin filaments reconstituted with NTG or E361G actin, tropomyosin and troponin. Representative experiments are shown. Points are mean and sem of 4 measurements made in the same motility cell. The lines are best fits to the Hill equation. Mean results of 3–7 experiments are summarised in Table 3. Solid lines, native troponin; dotted lines, dephosphorylated troponin; red squares and lines, E361G actin; blue triangles and lines, NTG actin. (A) Mouse actin, human cardiac tropomyosin and native human cardiac troponin (1.7 mols P/mol TnI): NTG and ACTC E361G are indistinguishable (see Data Supplement J). (B) Mouse actin, human cardiac tropomyosin and rabbit fast skeletal troponin: E361G actin Ca^{2+}-sensitivity is lower than NTG. (C) Mouse actin, human cardiac tropomyosin and dephosphorylated human cardiac troponin: E361G actin Ca^{2+}-sensitivity is lower than NTG.

heart. In common with most DCM-causing mutations, *ACTC* E361G is a dominant negative mutation [1]. Since the individual carrying the mutation is heterozygous, it would be expected to express the mutant protein at 50% or less.

The level of expression of disease-causing mutations in human heart is not often measured but the available data support this hypothesis [34,35]. No data are available about the expression of *ACTC* E361G in the patients with this mutation, however the HCM-causing mutation, *ACTC* E99K, showed 39% mutant actin in a patient heart biopsy sample (Monserrat, Marston, Leung, unpublished observation). Another DCM-causing mutation (*TNNC1* G159D) was shown to be expressed at 40–45% in the patient's heart [30] and other disease-causing mutations in actin were expressed at 50% or less (*ACTA1* mutations D292V, P302S, K336E [36,37]). It is therefore likely that the level of expression in our transgenic mouse is similar to that in the familial DCM patients with this mutation. It is important to study the functional effects of mutations at the same level of expression as found *in vivo*, since *in vitro* experiments show that the functional

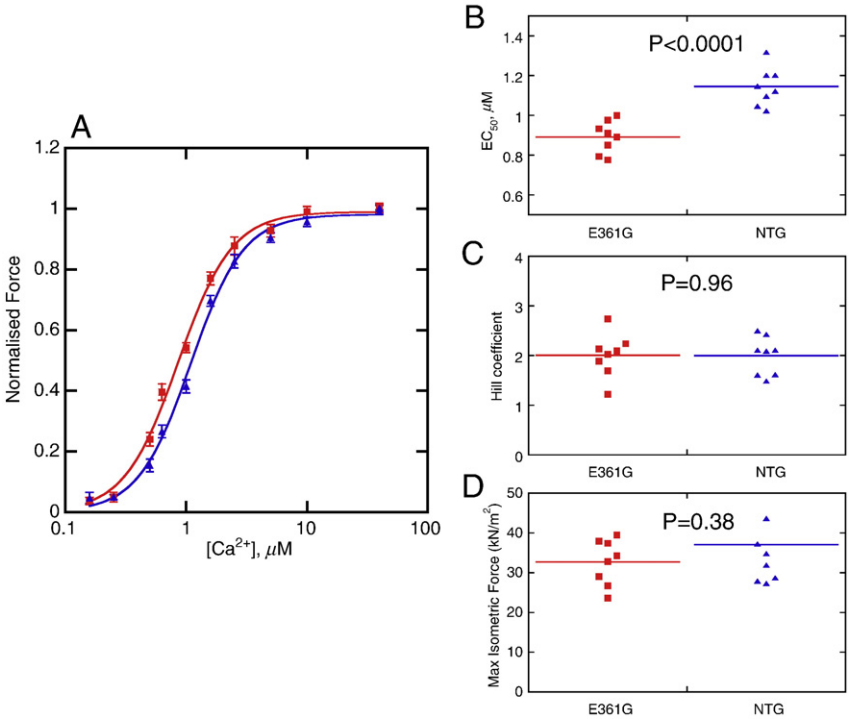
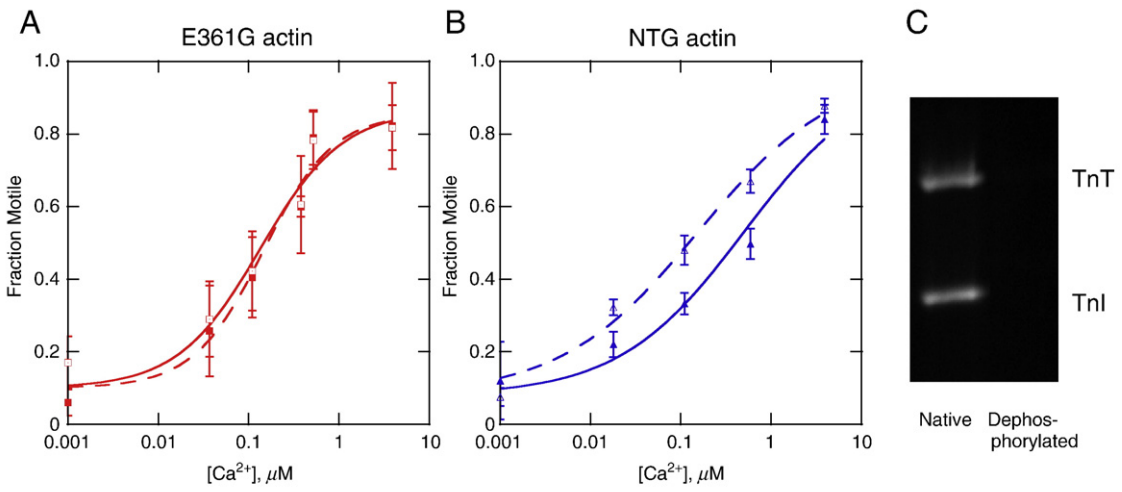


Fig. 7. Ca^{2+}-dependence of isometric force measured in skinned papillary muscle from ACTC E361G and NTG mice. (A) Dependence of normalised isometric force on Ca^{2+} concentration. The points are the means ± sem from Ca^{2+}-curves obtained with 8 papillary muscles each from NTG (blue triangles) or *ACTC* E361G mice (red squares). The lines are fits to the Hill equation: for NTG muscle $EC_{50} = 1.09 \pm 0.12$ μM and $n_H = 1.99 \pm 0.12$. For *ACTC* E361G muscle $EC_{50} = 0.86 \pm 0.03$ μM and $n_H = 1.94 \pm 0.13$. (B) EC_{50} values from individual muscle shown in a dot plot. Means are *ACTC* E361G muscle $EC_{50} = 0.90 \pm 0.03$ μM, NTG muscle $EC_{50} = 1.15 \pm 0.03$ μM, (C) Hill coefficients compared in a dot plot. Means are $n_H = 2.01 \pm 0.15$ for *ACTC* E361G and 2.00 ± 0.13 for NTG. (D) Maximum isometric force compared in a dot plot. Means are 33.4 ± 2.1 kN/m^2 for *ACTC* E361G and 37.1 ± 4.4 for NTG.



	EC50 for fraction motile			
	Native human troponin	Dephosphorylated human troponin	n	Ratio EC50 native/dP
NTG actin	0.24±0.07	0.08±0.02		3.0±0.3
		p=0.03 (paired)	5	p=0.003
E361G actin	0.31±0.08	0.31±0.09		1.04±0.07
		p=0.75 (paired)	5	p=0.58

Fig. 8. Effect of troponin dephosphorylation on Ca^{2+}-sensitivity of motility in thin filaments reconstituted with NTG or ACTC E361G actin. Representative experiments are shown. Points are mean and sem of 4 measurements made in the same motility cell. The lines are best fits to the Hill equation. Mean results are summarised in the table below. Solid lines, native troponin; dotted lines, dephosphorylated troponin; red squares and lines, E361G actin; blue triangles and lines, NTG actin. (A) Native and dephosphorylated human troponin compared with E361G actin. Complete results are shown in Data Supplement K. (B) Native and dephosphorylated human troponin compared with NTG actin. Complete results are shown in Data Supplement L. (C) Pro-Q Diamond stained SDS-PAGE of native and dephosphorylated troponin.

effects of mutations in thin filament proteins vary with the fraction of mutant protein present [8,21,29,38]. The most striking example is another DCM mutation, *TNNT2* ΔK210, which produced opposite effects when present at 50% or 100% of total troponin T [5].

4.2. Molecular phenotype of ACTC E361G thin filaments

By isolating the 50% E361G actin from transgenic mouse hearts and reconstituting thin filaments using tropomyosin and troponin extracted from human donor heart we were able to exactly reconstruct human thin filaments for functional assays. When isolated by the traditional acetone powder method the monomeric E361G actin was unstable and aggregated, therefore polymerisation of the mouse actin yielded only wild-type actin. However, the 50% E361G actin was readily prepared using a protocol for isolating native thin filaments, followed by the removal of the regulatory proteins [39].

The pure 50% E361G f-actin was measurably different from wild-type actin extracted from non-transgenic mouse hearts in sliding speed and affinity for α-actinin. The latter result agrees with the measurements of Wong et al. [40], using 100% E361G β-actin expressed in yeast.

When studied using recombinant proteins, DCM-causing mutations have consistently shown decreased Ca^{2+}-sensitivity and maximum crossbridge turnover rate [8,21,29,38]. Interestingly, when 50% E361G actin was incorporated into thin filaments, there was no significant difference in sliding speed, fraction of filaments motile or Ca^{2+}-sensitivity when measured with skeletal muscle HMM in the *in vitro* motility assay (Figs. 5, 6, Table 3). The human cardiac troponin used for these studies was phosphorylated. In particular, troponin I was phosphorylated at a level of 1.7 mols Pi/mole of which 1.1 mols/mole was shown to be at serines 22 and 23, the sites specifically phosphorylated by PKA [28,29]. The Ca^{2+}-sensitivity of skinned papillary muscle was actually slightly higher in the *ACTC* E361G mutant mouse (Fig. 7).

The molecular phenotype was revealed when troponin was dephosphorylated by treatment with phosphatase; Ca^{2+}-sensitivity of NTG actin-containing thin filaments increased 3-fold but with 50% E361G actin-containing thin filaments, Ca^{2+}-sensitivity did not change with phosphorylation level (Fig. 8). The previous *in vitro* studies of the functional effects of DCM-causing mutations in troponin T, troponin C and tropomyosin, using recombinant troponin subunits that were not phosphorylated, all showed reduced Ca^{2+}-sensitivity [6,8,11,12]. Thus the actin E361G mutation follows the same pattern as previously studied DCM mutations in thin filament proteins, but only when troponin is dephosphorylated (Fig. 6C, Table 3).

4.3. Uncoupling of Troponin I phosphorylation from the change in Ca^{2+}-sensitivity

Comparison of 50% E361G actin-containing thin filaments that were either normally phosphorylated or unphosphorylated has shown a new property of this DCM-causing mutation: Ca^{2+}-sensitivity is independent of the level of troponin phosphorylation in contrast to non-transgenic actin where, as has been observed using many functional assays, Ca^{2+}-sensitivity is lower in thin filaments when troponin I is phosphorylated at Ser 22 and 23 (Fig. 8, Table 3) [29,41,42]. In fact this insensitivity to TnI phosphorylation is probably a more important feature of the DCM phenotype than the change in the absolute Ca^{2+}-sensitivity as currently proposed [4,6,8]. Recent studies of the DCM mutation in troponin C, *TNNC3* G159D, which was studied in troponin extracted from a patient biopsy, reinforces this hypothesis [30]. The mutant troponin was phosphorylated at the same level as donor heart but the Ca^{2+}-sensitivity was actually significantly higher than donor heart troponin; on the other hand Ca^{2+}-sensitivity was virtually independent of troponin I phosphorylation.

Both studies that have used native human sequence proteins indicate that the DCM phenotype does not correlate with changed Ca^{2+}-sensitivity, but it does correlate with uncoupling of Ca^{2+}-sensitivity from troponin I phosphorylation. The PKA-dependent decrease in myofilament Ca^{2+}-sensitivity and associated increase in Ca^{2+} dissociation rate is a key component of the lusitropic response to adrenergic stimulation. Rapid relaxation (lusitropy) is a pre-requisite for the faster heart rate and increased contractile force (inotropy) induced by β-adrenergic stimulation. Thus, we propose that the uncoupling caused by the *ACTC* E361G mutation blunts the response to adrenergic stimulation, leading to a reduced cardiac reserve with consequent contractile dysfunction under stress, leading to dilated cardiomyopathy. Our observation of a significantly reduced response to acute dobutamine stimulation in *ACTC* E316G mice (Fig. 2, Tables 1, 2) supports the hypothesis at the whole animal level. This mechanism parallels the proposed role of troponin I phosphorylation in heart failure, where desensitisation of β-receptors is associated with reduced PKA activity and enhanced phosphatase activity leading to dephosphorylation of PLB, TnI, MyBP-C and blunting of the response to adrenergic stimulation [43–46].

4.4. Correlation of molecular phenotype and whole mouse phenotype

The *ACTC* E361G mutation is reported to be relatively benign. DCM was diagnosed on the basis of dilation (defined as end diastolic volume >95th percentile of the normal population) and ejection fraction <28%. In the family with the *ACTC* E361G mutation two individuals were diagnosed at ages 41 and 14 and the two other family members carrying the mutation were partially affected (one, aged 34, showed dilation only and the other, aged 9 showed borderline dilation, [14]). In our 50% ACTC E361G transgenic mice the only difference from non-transgenic littermates was a 15% higher left ventricle internal diameter (Supplementary data D). We could find no significant differences in the contractile behaviour of isolated myocytes that could be linked to the phenotype, and we could also not detect any differences in haemodynamic parameters of the whole mouse using both conductance catheter measurements (open chest) or MRI (intact mouse) (Fig. 4), however the response to stimulation by the β_1-adrenergic agonist, dobutamine, was blunted, consistent with uncoupling of TnI phosphorylation from altered myofibrillar Ca^{2+}-sensitivity (Tables 1, 2).

There are several reasons for the absence of an obvious whole animal phenotype, despite a clear molecular phenotype. Compensatory changes that minimise the effect of a mutation are frequently observed in transgenic mice, particularly if the mice are kept at rest. For cardiomyopathic mutations, examples include the *MYH7* R403Q mutation where no phenotype was observed until mice were subjected to intensive swimming exercise [47] and a heterozygous knock-in *MYBPC3* mutation where no symptoms were found until the mice were subjected to chronic catecholamine infusion [48]. In Morimoto's study of the *TNNT2* ΔK210 DCM-causing mutation it was found that the heterozygous mice exhibited no overt phenotype at rest and that there was an increase in the size and speed of the Ca^{2+}-transient that could compensate for the effect of the mutation [20].

We propose that the primary defect in familial DCM is in the lusitropic response to adrenergic stimulation, therefore we would expect that the disease phenotype is only manifested under stress, such as the acute dobutamine stress we applied to the *ACTC* E361G mice. The other molecular abnormality we observed was weaker binding of actin filaments to α-actinin. Since α-actinin forms the main connections between thin filaments and the Z-line it is possible that weak binding could lead to breakage of sarcomeres and loss of force transmission. However this, too, would only be manifested under mechanical stress.

Acknowledgments

We acknowledge the help of Alex Bauer, Kim Wells, Doug Lopes and O'neal Copeland at Imperial College London and Caroline Carr, Department of Physiology, Anatomy and Genetics, University of Oxford in undertaking these investigations. The work was funded by grants from the British Heart Foundation including a generous donation from The Dr E G J Olsen Charitable Fund.

Appendix A. Supplementary data

Supplementary data associated with this article can be found, in the online version, at doi:10.1016/j.yjmcc.2010.05.009.

References

[1] Olson TM, Michels VV, Thibodeau SN, Tai YS, Keating MT. Actin mutations in dilated cardiomyopathy, a heritable form of heart failure. Science 1998;280:750–2.
[2] Mogensen J, Murphy RT, Shaw T, Bahl A, Redwood C, Watkins H, et al. Severe disease expression of cardiac troponin C and T mutations in patients with idiopathic dilated cardiomyopathy. J Am Coll Cardiol 2004;44:2033–40.
[3] Kamisago M, Sharma SD, DePalma SR, Solomon S, Sharma P, Smoot L, et al. Mutations in sarcomere protein genes as a cause of dilated cardiomyopathy. N Engl J Med 2000;343:1688–96.
[4] Chang AN, Potter JD. Sarcomeric protein mutations in dilated cardiomyopathy. Heart Fail Rev 2005;10:225–35.
[5] Robinson P, Mirza M, Knott A, Abdulrazzak H, Willott R, Marston S, et al. Alterations in thin filament regulation induced by a human cardiac troponin T mutant that causes dilated cardiomyopathy are distinct from those induced by troponin T mutants that cause hypertrophic cardiomyopathy. J Biol Chem 2002;277:40710–6.
[6] Mirza M, Marston S, Willott R, Ashley C, Mogensen J, McKenna W, et al. Dilated cardiomyopathy mutations in three thin filament regulatory proteins result in a common functional phenotype. J Biol Chem 2005;280:28498–506.
[7] Mirza M, Robinson P, Kremneva E, Copeland O, Nikolaeva O, Watkins H, et al. The effect of mutations in alpha tropomyosin (E40K and E54K), that cause familial dilated cardiomyopathy, on the regulatory mechanism of cardiac muscle thin filaments. J Biol Chem 2007;282:13487–97.
[8] Robinson P, Griffiths PJ, Watkins H, Redwood CS. Dilated and hypertrophic cardiomyopathy mutations in troponin and alpha-tropomyosin have opposing effects on the calcium affinity of cardiac thin filaments. Circ Res 2007;101:1266–73.
[9] Carballo S, Robinson P, Otway R, Fatkin D, Jongbloed JD, de Jonge N, et al. Identification and functional characterization of cardiac troponin I as a novel disease gene in autosomal dominant dilated cardiomyopathy. Circ Res 2009;105:375–82.
[10] Venkatraman G, Harada K, Gomes AV, Kerrick GW, Potter JD. Different functional properties of Troponin T mutants that cause dilated cardiomyopathy. J Biol Chem 2003;278:41670–6.
[11] Chang AN, Harada K, Ackerman MJ, Potter JD. Functional consequences of hypertrophic and dilated cardiomyopathy-causing mutations in alpha-tropomyosin. J Biol Chem 2005;280:34343–9.
[12] Morimoto S, Lu Qw, Harada K, Takahashi-Yanaga F, Minakami R, Ohta M, et al. Ca2 + -desensitizing effect of a deletion mutation Delta K210 in cardiac troponin T that causes familial dilated cardiomyopathy. Proc Natl Acad Sci 2002;99:913–8.
[13] Lu QW, Morimoto S, Harada K, Du CK, Takahashi-Yanaga F, Miwa Y, et al. Cardiac troponin T mutation R141W found in dilated cardiomyopathy stabilizes the troponin T-tropomyosin interaction and causes a Ca(2+) desensitization. J Mol Cell Cardiol 2003;35:1421–7.
[14] Olson TM, Kishimoto NY, Whitby FG, Michels VV. Mutations that alter the surface charge of alpha-tropomyosin are associated with dilated cardiomyopathy. J Mol Cell Cardiol 2001;33:723–32.
[15] Suurmeijer AJ, Clement S, Francesconi A, Bocchi L, Angelini A, Van Veldhuisen DJ, et al. Alpha-actin isoform distribution in normal and failing human heart: a morphological, morphometric, and biochemical study. J Pathol 2003;199:387–97.
[16] Copeland O, Nowak KJ, Laing NG, Ravenscroft G, Marston S. * Quantitative assay of skeletal α-actin expression in normal and pathological human and mouse hearts. Biophys J 2009;96:499a.
[17] Kumar A, Crawford K, Flick R, Klevitsky R, Lorenz JN, Bove KE, et al. Transgenic overexpression of cardiac actin in the mouse heart suggests coregulation of cardiac, skeletal and vascular actin expression. Transgenic Res 2004;13:531–40.
[18] Cook S, Clerk A, Sugden P. Are transgenic mice the 'Älkahest' to understanding myocardial hypertrophy and failure? J Mol Cell Cardiol 2008;46:118–29.
[19] Molkentin JD, Robbins J. With great power comes great responsibility: using mouse genetics to study cardiac hypertrophy and failure. J Mol Cell Cardiol 2008;46:130–6.
[20] Du CK, Morimoto S, Nishii K, Minakami R, Ohta M, Tadano N, et al. Knock-in mouse model of dilated cardiomyopathy caused by troponin mutation. Circ Res 2007;101:185–94.
[21] Redwood C, Lohmann K, Bing W, Esoposito G, Elliott K, Abdulrazzak H, et al. Investigation of a truncated troponin T that causes familial hypertrophic cardiomyopathy: Ca2+ regulatory properties of reconstituted thin filaments depend on the ratio of mutant to wild-type peptide. Circ Res 2000;86:1146–52.
[22] Rajan S, Ahmed RP, Jagatheesan G, Petrashevskaya N, Boivin GP, Urboniene D, et al. Dilated cardiomyopathy mutant tropomyosin mice develop cardiac dysfunction

with significantly decreased fractional shortening and myofilament calcium sensitivity. Circ Res 2007;101:205–14.
[23] Davies JK, Wells DJ, Liu K, Whitrow HR, Daniel TD, Grignani R, et al. Characterization of the role of gamma2 R531G mutation in AMP-activated protein kinase in cardiac hypertrophy and Wolff–Parkinson–White syndrome. Am J Physiol Heart Circ Physiol 2006;290:H1942–51.
[24] Stuckey D, Carr C, Tyler DJ, Aasum E, Clarke K. Novel MRI method to detect altered left ventricular ejection and filling patterns in rodent models of disease. Magn Reson Med 2008;60:582–7.
[25] Nishio R, Sasayama S, Matsumori A. Left ventricular pressure–volume relationship in a murine model of congestive heart failure due to acute viral myocarditis. J Am Coll Cardiol 2002;40:1506–14.
[26] Davies CH, Davia K, Bennett JG, Pepper JR, Poole-Wilson PA, Harding SE. Reduced contraction and altered frequency response of isolated ventricular myocytes from patients with heart failure. Circulation 1995;92:2540–9.
[27] Palmer BM, Fishbaugher DE, Schmitt JP, Wang Y, Alpert NR, Seidman CE, et al. Differential cross-bridge kinetics of FHC myosin mutations R403Q and R453C in heterozygous mouse myocardium. Am J Physiol Heart Circ Physiol 2004;287:H91–9.
[28] Messer A, Gallon C, McKenna W, Elliott P, Dos Remedios C, Marston S. The use of phosphate-affinity SDS-PAGE to measure the troponin I phosphorylation site distribution in human heart muscle. Proteomics Clin Appl 2009;3:1371–82.
[29] Messer AE, Jacques AM, Marston SB. Troponin phosphorylation and regulatory function in human heart muscle: dephosphorylation of Ser23/24 on troponin I could account for the contractile defect in end-stage heart failure. J Mol Cell Cardiol 2007;42:247–59.
[30] Dyer E, Jacques A, Hoskins A, Ward D, Gallon C, Messer A, et al. Functional analysis of a unique troponin c mutation, Gly159Asp that causes familial dilated cardiomyopathy, studied in explanted heart muscle. Circulation: Heart Failure 2009;2:456–64.
[31] Jacoby C, Molojavyi A, Flögel U, Merx MW, Ding Z, Schrader J. Direct comparison of magnetic resonance imaging and conductance microcatheter in the evaluation of left ventricular function in mice. Basic Res Cardiol 2006;101:87–95.
[32] Vandekerckhove J, Bugaisky G, Buckingham M. Simultaneous expression of skeletal muscle and heart actin proteins in various striated muscle tissues and cells. A quantitative determination of the two actin isoforms. J Biol Chem 1986;261:1838–43.
[33] Alonso S, Garner I, Vandekerckhove J, Buckingham M. Genetic analysis of the interaction between cardiac and skeletal actin gene expression in striated muscle of the mouse. J Mol Biol 1990;211:727–38.
[34] Nier V, Schultz I, Brenner B, Forssmann W, Raida M. Variability in the ratio of mutant to wildtype myosin heavy chain present in the soleus muscle of patients with familial hypertrophic cardiomyopathy. A new approach for the quantification of mutant to wildtype protein. FEBS Lett 1999;461:246–52.
[35] Bottinelli R, Coviello DA, Redwood CS, Pellegrino MA, Maron BJ, Spirito P, et al. A mutant tropomyosin that causes hypertrophic cardiomyopathy is expressed in vivo and associated with an increased calcium sensitivity. Circ Res 1998;82:106–15.
[36] Clarke NF, Ilkovski B, Cooper S, Valova VA, Robinson PJ, Nonaka I, et al. The pathogenesis of ACTA1-related congenital fiber type disproportion. Ann Neurol 2007;61:552–61.
[37] D'Amico A, Graziano C, Pacileo G, Petrini S, Nowak KJ, Boldrini R, et al. Fatal hypertrophic cardiomyopathy and nemaline myopathy associated with ACTA1 K336E mutation. Neuromuscul Disord 2006;16:548–52.
[38] Elliott K, Watkins H, Redwood CS. Altered regulatory properties of human cardiac troponin I mutants that cause hypertrophic cardiomyopathy. J Biol Chem 2000;275:22069–74.
[39] Tobacman L, Sawyer D. Calcium binds cooperatively to the regulatory sites of the cardiac thin filament. J Biol Chem 1990;265:931–9.
[40] Wong WW, Doyle TC, Cheung P, Olson TM, Reisler E. Functional studies of yeast actin mutants corresponding to human cardiomyopathy mutations. J Musc Res Cell Motil 2002;22:665–74.
[41] van der Velden J, Papp Z, Zaremba R, Boontje NM, de Jong JW, Owen VJ, et al. Increased Ca2+-sensitivity of the contractile apparatus in end-stage human heart failure results from altered phosphorylation of contractile proteins. Cardiovasc Res 2003;57:37–47.
[42] Hamdani N, de Waard M, Messer AE, Boontje NM, Kooij V, van Dijk S, et al. Myofilament dysfunction in cardiac disease from mice to men. J Musc Res Cell Motil 2009;29:189–201.
[43] Houser SR, Margulies KB. Is depressed myocyte contractility centrally involved in heart failure? Circ Res 2003;92:350–8.
[44] A. Messer. Structural and functional polymorphisms of troponin in failing heart. PhD Thesis. London: London; 2007.
[45] Jacques A, Copeland O, Messer A, Gallon C, King C, McKenna W, et al. Myosin binding protein C phosphorylation in normal, hypertrophic and failing human heart muscle. J Mol Cell Cardiol 2008;45:209–16.
[46] Hamdani N, Kooij V, van Dijk S, Merkus D, Paulus WJ, Remedios CD, et al. Sarcomeric dysfunction in heart failure. Cardiovasc Res 2008;77:649–58.
[47] Geisterfer-Lowrance AA, Christe M, Conner DA, Ingwall JS, Schoen FJ, Seidman CE, et al. A mouse model of familial hypertrophic cardiomyopathy. Science 1996;272:731–4.
[48] Schuermann F, Schlossarek S, Mearini G, Geetz B, Eschenhagen T, Carrier L. Adrenergic stress unmasks exaggerated septal hypertrophy and proteasome impairment in heterozygous cMyBP-C mutant mice. Circulation 2008;118(Suppl 2):S521.

BJ www.biochemj.org

This is a data-enriched, interactive PDF that provides the gateway to a world of information when opened in Utopia Documents
Download FREE software now

BJ Disease

Biochem. J. (2012) **442**, 231–239 (Printed in Great Britain) doi:10.1042/BJ20111030

Abnormal actin binding of aberrant β-tropomyosins is a molecular cause of muscle weakness in *TPM2*-related nemaline and cap myopathy

Minttu MARTTILA*†, Elina LEMOLA*†, William WALLEFELD‡, Massimiliano MEMO§, Kati DONNER‖, Nigel G. LAING‡, Steven MARSTON§, Mikaela GRÖNHOLM¶ and Carina WALLGREN-PETTERSSON*†[1]

*The Folkhälsan Institute of Genetics, Biomedicum Helsinki, Finland, †Department of Medical Genetics, Haartman Institute, University of Helsinki, Biomedicum Helsinki, Finland, ‡Molecular Neurogenetics Laboratory, Centre for Medical Research, West Australian Institute for Medical Research, University of Western Australia, Queen Elizabeth II Medical Centre, Nedlands, WA, Australia, §National Heart and Lung Institute, Imperial College London, London SW3 6LY, U.K., ‖Department of Medicine, University of Helsinki, Helsinki, Finland, and ¶Division of Biochemistry and Biotechnology, Department of Biosciences, University of Helsinki, Helsinki, Finland

NM (nemaline myopathy) is a rare genetic muscle disorder defined on the basis of muscle weakness and the presence of structural abnormalities in the muscle fibres, i.e. nemaline bodies. The related disorder cap myopathy is defined by cap-like structures located peripherally in the muscle fibres. Both disorders may be caused by mutations in the *TPM2* gene encoding β-Tm (tropomyosin). Tm controls muscle contraction by inhibiting actin–myosin interaction in a calcium-sensitive manner. In the present study, we have investigated the pathogenetic mechanisms underlying five disease-causing mutations in Tm. We show that four of the mutations cause changes in affinity for actin, which may cause muscle weakness in these patients, whereas two show defective Ca^{2+} activation of contractility. We have also mapped the amino acids altered by the mutation to regions important for actin binding and note that two of the mutations cause altered protein conformation, which could account for impaired actin affinity.

Key words: actin binding, calcium-sensitivity, cap myopathy, circular dichroism (CD), nemaline myopathy (NM), β-tropomyosin (β-Tm).

INTRODUCTION

NM (nemaline myopathy) is a genetically heterogeneous congenital myopathy showing wide clinical variability, including different grades of severity and ages of onset [1]. It was described in two separate reports by Shy et al. [2] and Conen et al. [3] in 1963. The diagnostic criteria are muscle weakness and nemaline bodies present in skeletal muscle, with no other simultaneously occurring significant structural abnormalities. NM-causing mutations have been found in seven genes: nebulin (*NEB*) [4], α-actin (*ACTA1*) [5], α-Tm (tropomyosin) (*TPM3*) [6], β-Tm (*TPM2*) [7], troponin T1 (*TNNT1*) [8], cofilin-2 (*CFL2*) [9] and KBTBD13 (Kelch repeat and BTB domain-containing protein 13) [10].

Cap myopathy was first described in 1981 by Fidzianska et al. [11]. It is characterized by the presence of cap-like structures that are located peripherally under the sarcolemma and show abnormal accumulation of sarcomeric proteins [11]. The first genetic causes of cap disease were identified in the *TPM2* gene in 2007: a deletion of glutamic acid at position 139 [12] and a change at position 41 of glutamate to lysine [13].

Tms are encoded by four genes, *TPM1–4* (α, β, γ and δ), from which at least 20 different isoforms are expressed [14]. In skeletal muscle three Tm isoforms are expressed from the *TPM1* (α-Tm_{fast} or α-Tm), *TPM2* (β-Tm) and *TPM3* (α-Tm_{slow} or γ-Tm) genes [15]. Tms are fibrous molecules composed of two α-helices forming coiled-coil dimers. The dimers polymerize head-to-tail and overlap by eight to nine amino acids. Tm dimers are located in the grooves of F-actin (filamentous actin) filaments providing structural stability and modulating filament function [14]. These interactions are essential for the function of striated muscle. In order to investigate the molecular mechanisms causing NM and cap myopathy, we studied the effects of five patient mutations in β-Tm (the *TPM2* gene) on actin binding and thin filament Ca^{2+} regulation. In addition, protein modification and conformation were studied using MS and CD spectroscopy.

One of the mutations studied (Q147P) causes NM [7], two (K49del and E139del) cause cap myopathy [12,13,16] and one (E41K) is associated with a dominantly inherited myopathy that showed nemaline bodies in one of two biopsies of a mother and caps in her daughter's biopsy [12,13]. The last of the mutations studied (E117K) is associated with an unspecific congenital myopathy, first diagnosed as NM, but, on closer scrutiny, found not to show verifiable nemaline bodies [7].

MATERIALS AND METHODS

Constructs

TPM2 cDNA (GenBank® accession number NM_009416) cloned into pGEX4-1 (GE Healthcare) was used as a template for PCR. Forward 5′-GATCCATGGACGCCATCAAGAAGAAG-3′ and reverse 5′-TCGAGTCAGAGGGAAGTGATGTCAT-TG-3′ primers were designed to copy the *TPM2* sequence, but to exclude the GST tag. Fusion DNA polymerase (Thermo Fisher Scientific) was used under the following PCR conditions: denaturation at +98 °C for 30 s, denaturation at +98 °C for 10 s, annealing at +58 °C for 30 s, elongation at +72 °C for 30 s and final elongation at +72 °C for 7 min. The programme was cycled 34 times. Products were cloned into the Zero blunt TOPO vector using a PCR cloning kit (Invitrogen). Plasmids were extracted using QIAprep Spin Miniprep kit (Qiagen). The mutations (Table 1) were introduced into mouse cDNA using the QuikChange® Site-Directed Mutagenesis kit (Stratagene). Plasmids were sequenced using BigDye version 3.1

Abbreviations used: CFTD, congenital fibre type disproportion; DTT, dithiothreitol; F-actin, filamentous actin; HMM, heavy meromyosin; IVMA, *in vitro* motility assay; LC-MS/MS, liquid chromatography tandem MS; NM, nemaline myopathy; T_{melt}, melting temperature; Tm, tropomyosin; WT, wild-type.

[1] To whom correspondence should be addressed (email carina.wallgren@helsinki.fi).

© The Authors Journal compilation © 2012 Biochemical Society

Biochemical Journal

Table 1 Mutations in the *TPM2* gene used in the present study and summary of results

∼, values equal to WT Tm values; –, values lower than wt; +, values higher than WT; #, not measurable. Calculated WT and mutant Tm α-helical content is in percentage at 20 °C and 37 °C using Contin-LL software [24,25].

		α-Helical content (%)		Change in α-helical content (%)						
Tm2	Disease	20 °C	37 °C	20 °C	37 °C	T_m (°C)	ΔT_m (°C)	Actin binding	CD +20 °C/+37 °C	IVMA Ca^{2+}-sensitivity
WT	None	97.3 ± 2.8	80.8 ± 1.6			40.2 ± 0.0 °C				
E41K	NM cap	98.2 ± 2.6	79.4 ± 2.1	+0.9%	−1.4%	40.3 ± 0.3 °C	+0.1	∼	∼/∼	–
K49del	Cap	84.6 ± 3.1	65.0 ± 1.6	−12.7%*	−15.8%*	39.3 ± 0.2 °C	−0.9	–	–/–	#
E117K†	'NM'	99.8 ± 0.2	87.9 ± 4.3	+2.5%	+7.1%*	40.5 ± 0.3 °C	+0.3	+	+/+	–
E139del	Cap	79.5 ± 0.7	68.2 ± 1.2	−17.8%*	−12.6%*	40.8 ± 0.3 °C	+0.6	–	–/–	#
Q147P	NM	96.4 ± 3.6	88.0 ± 0.8	−0.9%	+7.2%*	41.7 ± 0.1 °C	+1.5	–	∼/+	#

*Significant difference from the WT ($P < 0.001$).
†Mutation E117K is associated with an unspecific congenital myopathy, first diagnosed as NM but on closer scruting found not to show verifiable nemaline bodies.

sequencing chemistry and an ABI 3730 DNA Analyzer (Applied Biosystems). The sequences were analysed using the Sequencher 4.5 software.

Production of WT (wild-type) and aberrant β-Tms

Recombinant β-Tms were produced using a Bac-to-Bac baculovirus expression system (Invitrogen) in *Sf9* insect cells. The insect cells were grown in supplemented Grace's Insect Medium (Invitrogen) containing 10 % fetal bovine serum (Gibco) and 1 % penicillin/streptomycin (Gibco) in 500 ml of medium at 27 °C.

Extraction of proteins

Proteins were extracted from *Sf9* cells using a modification of the method described by Akkari et al. [17]. Extraction was performed in a buffer containing 1 M NaCl, 50 mM imidazole (pH 7), 0.5 mM $MgCl_2$, 1 mM EDTA, 1 mM EGTA, 5 mM DTT (dithiothreitol) and 1× protease inhibitor (Roche). Proteins were boiled for 10 min in a water bath. The denatured proteins were spun at 9000 rev./min in a Sorval SS-34 rotor for 20 min at +4 °C and the supernatant saved. The proteins were precipitated in 70 % ammonium sulfate (Fluka) and incubated at room temperature (22 °C) in a mixer for 1 h. The samples were spun at 9000 rev./min in a Sorval SS-34 rotor for 20 min at 4 °C and the pellets saved. The pellets were dissolved into a buffer containing 400 mM NaCl, 5 mM Pipes and 1 M DTT, pH 7.1. Samples were transferred into Slide-A-Lyzer 10 kDa molecular-mass cut-off dialysis cassettes (Pierce). They were dialysed in 200–500 volumes of the same buffer overnight, with one buffer change. The buffer was changed to 50 mM Na_2HPO_4/NaH_2PO_4, 1 M NaCl and 5 mM DTT (pH 4.5), and the proteins were dialysed for 2.5 h in a mixer at 4 °C and the buffer changed after 1 h. The precipitated proteins were separated from the buffer by spinning in a Sorval SS-34 rotor at 16000 rev./min for 15 min at 4 °C. The pellets were dissolved in a buffer containing 400 mM NaCl, 5 mM Pipes and 1 M DTT (pH 7.1). The samples were dialysed in 200–500 volumes of the same buffer overnight, with one buffer change. The proteins were spun in an Eppendorf centrifuge at 14000 rev./min for 20 min at 4 °C. The supernatant contained the purified β-Tms.

Actin binding

Actin-binding assays were performed using Cytoskeleton's Actin Binding Protein Biochem Kit (Cytoskeleton). In a previous actin-binding assay 1.5 μM Tms and 5 μM F-actin were used [18]; however, in the present study we used 10.35 μM Tms and 23 μM F-actin to be able to detect more actin-binding mutants. Tms were allowed to bind to F-actin for 30 min at room temperature. Samples were run in a Beckman Coulter Optima MAX Ultracentrifuge at 60000 rev./min for 1.5 h at 24 °C. Pellet and supernatant fractions were separated, analysed by SDS/PAGE (12 % gels) and stained with Coomassie Blue. Pellet and supernatant bands were quantified from four experiments carried out in duplicate using ImageJ (NIH).

Mass spectrometry

In-gel digestion and LC-MS/MS (liquid chromatography tandem MS) analysis of the resulting peptides was done at the Protein Chemistry Research Group and Core Facility in the Institute of Biotechnology, University of Helsinki (Helsinki, Finland).

Three-dimensional models

The mutations E41K, K49del and E139del were made to the amino acid sequence of Tm2 (GenBank® accession number P58775.1). The probable secondary structure of the mutants were assigned by homology modelling using the crystal structure corresponding to PDB codes 1C1GA and 2B9CA as templates, following a standard method in Discovery Studio (Accelreys).

Circular dichroism

Tm samples were analysed by CD spectroscopy. Spectral CD measurements were obtained over the far UV wavelength range of 250–190 nm in a buffer containing 0.25 M NaF and 0.02 M Na_2HPO_4/NaH_2PO_4 at pH 7.0. CD analysis was done using a J-810 Spectropolarimeter (Jasco) equipped with a Peltier thermostatically controlled cuvette holder, controlled via a PC running Spectra Analysis (Jasco, version 1.53.04) software. One-way ANOVA was conducted for the percentage α-helical content and melting temperature data sets with a Newman–Keuls post-hoc test using GraphPad Prism Version 4. The threshold for significance was set at $P < 0.05$.

IVMA (*in vitro* motility assay) data acquisition and analysis

Flow cells were constructed from a microscope slide and siliconized coverslip (washed in 0.2 % dichloromethylsilane in chloroform). Fluorescently labelled F-actin, Tm and troponin were mixed and incubated at 10× working concentration for 15 min at 4 °C. HMM (heavy meromyosin; 100 μl of 0.2 mg/ml) was infused into the flow cell, followed by 100 μl of thin filament mixture (10 nM actin-Φ, troponin and Tm between 10 and 100 nM). The fraction of fluorescently labelled thin filaments moving and their corresponding velocity were analysed in 50 mM KCl, 25 mM imidazole, 4 mM $MgCl_2$, 1 mM EDTA, 5 mM DTT, 0.5 mg/ml BSA, 0.1 mg/ml glucose oxidase, 0.02 mg/ml catalase,

© The Authors Journal compilation © 2012 Biochemical Society

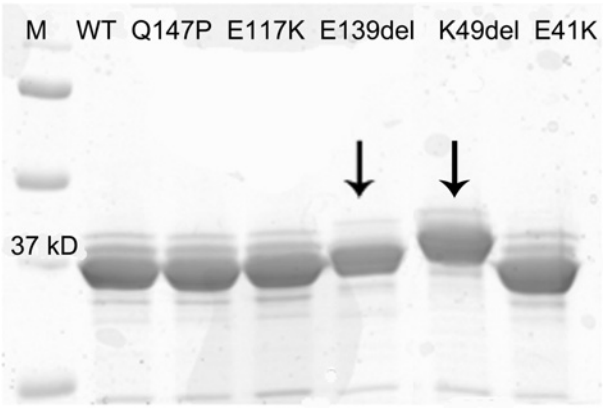


Figure 1 β-Tms produced in insect cells

SDS/PAGE of recombinant proteins stained with Coomassie Blue. Slower migrating samples are indicated with arrows. M, molecular mass standards (in kDa).

3 mg/ml glucose, 0.5 % methylcellulose, 5 mM Ca^{2+}/EGTA buffer, 1 mM MgATP and Tm at appropriate concentration. Filament movement was automatically tracked and recorded as described by Marston et al. [19]. The Ca^{2+}-concentration dependency data were fitted to the 4-parameter Hill equation: $y = a + X_{max}\,[Ca^{2+}]^n/(EC_{50} + [Ca^{2+}]^n)$.

RESULTS

Production and extraction of recombinant proteins

In order to study the functional differences between WT Tm and Tms containing known human disease-causing mutations, the mutations were introduced into WT β-Tm. Because post-translational modifications, especially N-terminal acetylation, are important for the function of β-Tms [20] we produced Tms in a baculovirus expression system in insect cells (*Sf9*) [17]. The purified proteins were run in SDS/PAGE, and differences in migration rate were found between the samples (Figure 1). The samples of mutations K49del and E139del run slower in SDS/PAGE.

Actin binding of WT and mutant Tms

The WT Tm and Tms with human disease-causing mutations were tested for actin binding (Figures 2A and 2B). Three samples, K49del, E139del and Q147P showed significantly weaker affinity for actin than WT. One sample, E117K, bound actin more strongly, whereas E41K did not show any significant change in actin binding (Figure 2C).

Functional analysis by IVMA

IVMA analyses the movement of fluorescently labelled thin filaments over a bed of immobilized HMM [21]. Thin filaments were reconstituted using rabbit skeletal actin and troponin, together with the baculovirus-expressed WT or mutant β-Tm homodimers. With WT thin filaments, we observed that both the speed of filament sliding over myosin and the fraction of filaments that are motile are regulated by Ca^{2+}. The troponin–Tm complex inhibits the movement of thin filaments under relaxing conditions ($Ca^{2+} \sim 10^{-9}$ M) so that the fraction motile is 10 % or less. At activating Ca^{2+} concentrations (3.5 μM) at least 80 % of filaments are motile, like actin alone. The sliding

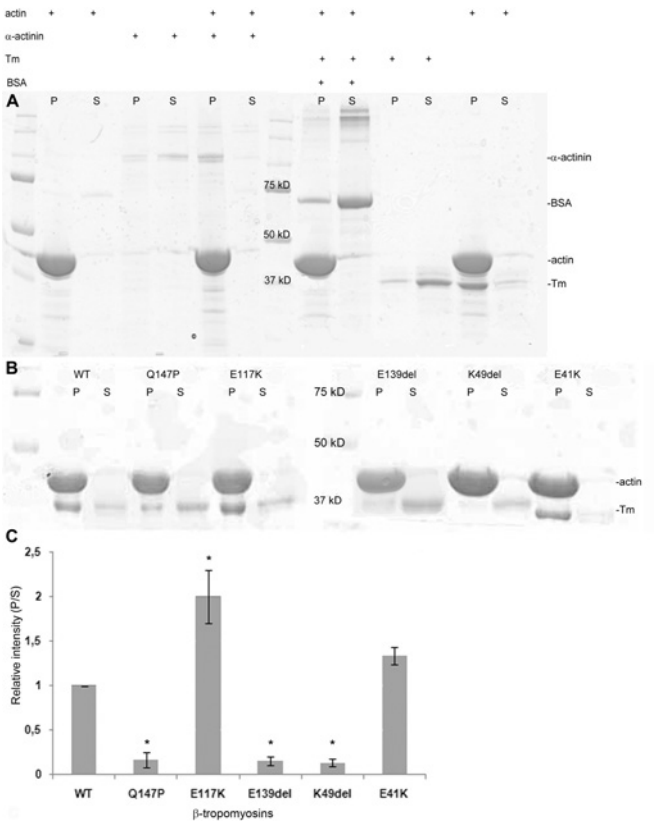


Figure 2 F-actin co-sedimentation assay

(**A**) Purified actin and Tm, BSA as a negative control or α-actinin as a positive control were incubated together and co-sedimented. The supernatants (S) and pellets (P) were separated, run on SDS/PAGE and Coomassie Blue stained. (**B**) F-actin co-sedimentation assay with WT Tm and Tm mutants performed as in (**A**). Molecular masses (in kDa) are given in the centre of each panel. (**C**) Quantification of actin–Tm co-sedimentation assay. Gels were quantified to determine the mean relative intensities of four independent actin co-sedimentation assays (P/P_{wt}:S/S_{wt}). Results are means $\pm$ S.D. of each sample. *P* values (WT compared with mutant) for the samples are 0.0007, 0.0392, 0.0001, 0.0029, 0.0013 and 0.2417 respectively using one-tailed distribution and the unpaired Student's *t* test. *Significant difference from the WT.

speed also increases 2-fold between relaxing and activating Ca^{2+} concentrations.

When mutant β-Tm K49del, E139del and Q147P were incorporated into thin filaments, it was found that motility was not switched off in low Ca^{2+} even with high Tm concentrations. Thin filaments with the WT β-Tm switched off at the standard Tm concentration (Figure 3) indicating that the abnormal function was due to the mutation in Tm. These mutants (K49del, E139del and Q147P) appear to have a lower affinity for actin compared with the WT, as indicated by the direct measurements. We hypothesize that these mutants could be washed away by the last buffers that are infused in the flow cell, leaving motility similar to actin alone. Therefore no curves could be recorded from with these constructs.

Thin filaments containing the β-Tm mutations E41K and E117K that bound strongly to actin were able to regulate the filaments, with low Ca^{2+} concentration causing a complete switch off of their motility.

Four Ca^{2+} curves were recorded from thin filaments containing E117K Tm (one represented in Figure 3A, lower panel). In comparison with WT thin filaments, motility was generally lower at high Ca^{2+} concentration (79.5 $\pm$ 4.1 % compared with 96.2 $\pm$ 0.5 % for WT, $P = 0.006$, unpaired *t* test). The speed of sliding increased slightly with increasing Ca^{2+} concentration,

© The Authors Journal compilation © 2012 Biochemical Society

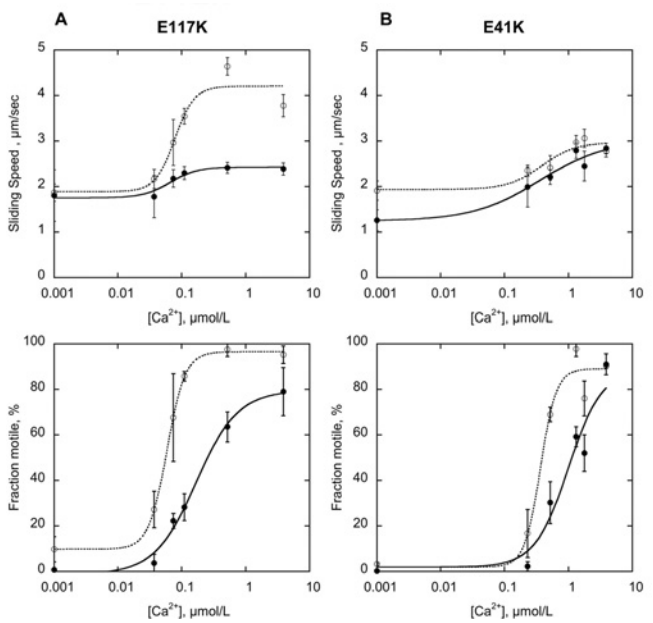


Figure 3 Tm Ca^{2+} sensitivity

The effect of β-Tm mutations E117K (**A**) and E41K (**B**) on Ca^{2+} regulation of thin filament motility. Ca^{2+}-dependence of sliding speed (upper panel) and fraction of filaments motile (lower panel) are plotted at different Ca^{2+} concentrations. Continuous lines and closed circles represent mutant Tm with skeletal muscle actin and troponin, broken lines and open circles represent WT Tm. Results are means $\pm$ S.E.M. of five replicate measurements in a single motility cell. The lines are fits to the Hill equation. Ca^{2+} sensitivity for the fraction motile parameter is $EC_{50} = 0.060 \pm 001$ μM for WT and $EC_{50} = 0.17 \pm 0.04$ μM for the E117K experiment, $EC_{50} = 0.36 \pm 04$ μM for WT and $EC_{50} = 1.00 \pm 0.18$ μM for the E41K experiment. EC_{50} of thin filaments is variable between different troponin preparations.

but it was significantly less than the WT Tm (sliding speed at 3.5 μM Ca^{2+}/sliding speed at 1 nM Ca^{2+} $= 1.34 \pm 0.16$ for E117K and 2.04 ± 0.15 for WT Tm, $P = 0.02$). In addition, the Ca^{2+} sensitivity of activation was much less (EC_{50} E117K/EC_{50} WT Tm $= 2.44 \pm 0.35$, $P = 0.03$) (Figure 3A, upper panel). Thus the E117K mutation is predicted to lead to reduced contractility. Two complete Ca^{2+} titration curves were recorded with the E41K Tm (Figure 3B). The results were similar to E117K, although maybe more marked in terms of reduced Ca^{2+} sensitivity (EC_{50} E41K/EC_{50} WT Tm $= 2.77$), but the increase in sliding speed was similar in E41K and WT.

MS and three-dimensional models

Purified β-Tm samples were run on SDS/PAGE gels. Two samples, K49del and E139del, showed slower migration than the WT and other mutant proteins. To find out whether the difference in migration could be due to post-transcriptional modifications, we used in-gel digestion of the proteins followed by LC-MS/MS analysis of the resulting peptides. The mass-spectrometric database (http://www.phosphosite.org) contains eight phosphorylation sites that have been found in mouse and human Tm. In addition to these we found in our analyses four novel phosphorylation sites. These were present in all samples including the WT. No other significant differences in peptide mass were found (results not shown). The protein modifications caused by the mutations and the N-terminal acetylation of the Tms were verified using LC-MS/MS. Post-transcriptional modifications were not found to be the reason for the difference in migration. Thus it may be due to a change in secondary structure conformation of the K49del and E139del mutants [22,23] as found

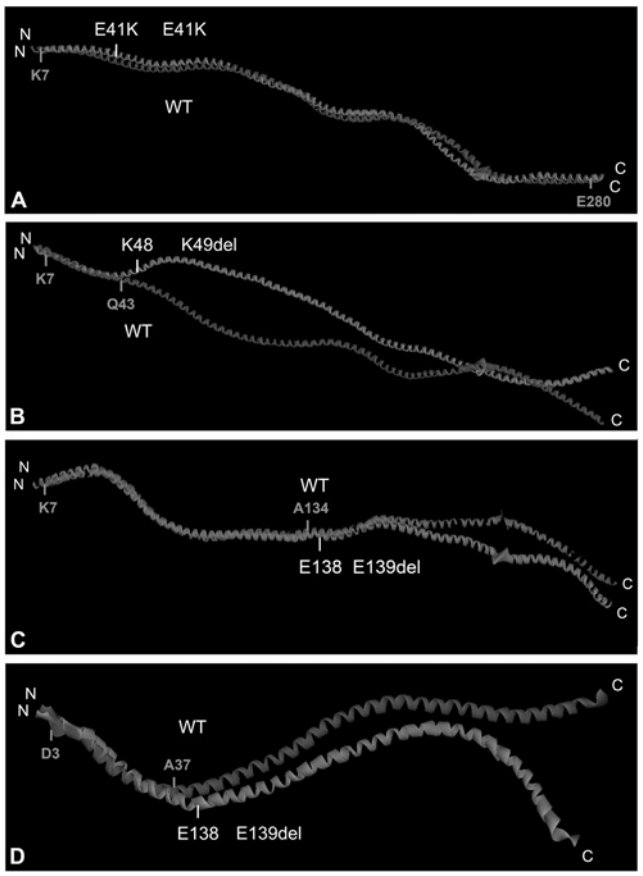


Figure 4 Structural alignments of Tms

Structural alignments of WT and mutant Tm using the Discovery Studio 2.1 program. The mutations K49del (**A**), E139del (**B** and **C**) and E41K (**D**) were made in rat Tm2 (P58775.1) and were superimposed over the WT structure 1C1GA (**A**, **C** and **D**) or 2B9CA (**B**). 2B9CA was used as it provided a better resolution. Amino acids before deletions are marked in deletion mutants and E41 in E41K. Amino acids used in comparison are shown.

with the D175N mutation in α-Tm [24]. To study this, three-dimensional models of the differentially migrating mutants were created (Figure 4). The α-helical conformation was changed in the K49del and E139del mutants.

CD spectra of Tm

Since three-dimensional models indicated that the structure may be affected in the mutants with aberrant migration pattern, to further study the structures of our mutant proteins, and the effect of disease causing mutations on overall secondary structure, CD spectra were produced. At 20 °C all recombinant Tm proteins showed CD spectra characteristic of α-helical proteins, featuring a minimum at 222 and 208 nm and a maximum at 190 nm (Figure 5). Table 1 shows the calculated α-helical content of each protein as determined by the Contin-LL method [25,26]. At 20 °C WT Tm had a calculated α-helical content of 97.3 ± 2.8 %. E117K displayed an α-helical content higher than that of the WT (99.8 ± 0.2 %). Two of the mutant proteins displayed lower calculated α-helical content: E139del (79.5 ± 0.7 %) and K49del (84.6 ± 3.1 %).

At 37 °C WT and mutant Tm proteins also displayed CD spectra characteristic of α-helical proteins (Figure 6). WT Tm was calculated to be 81.9 ± 1.8 % α-helical, whereas the Q147P and E117K showed the highest α-helical contents (88.3 ± 0.8 %

© The Authors Journal compilation © 2012 Biochemical Society

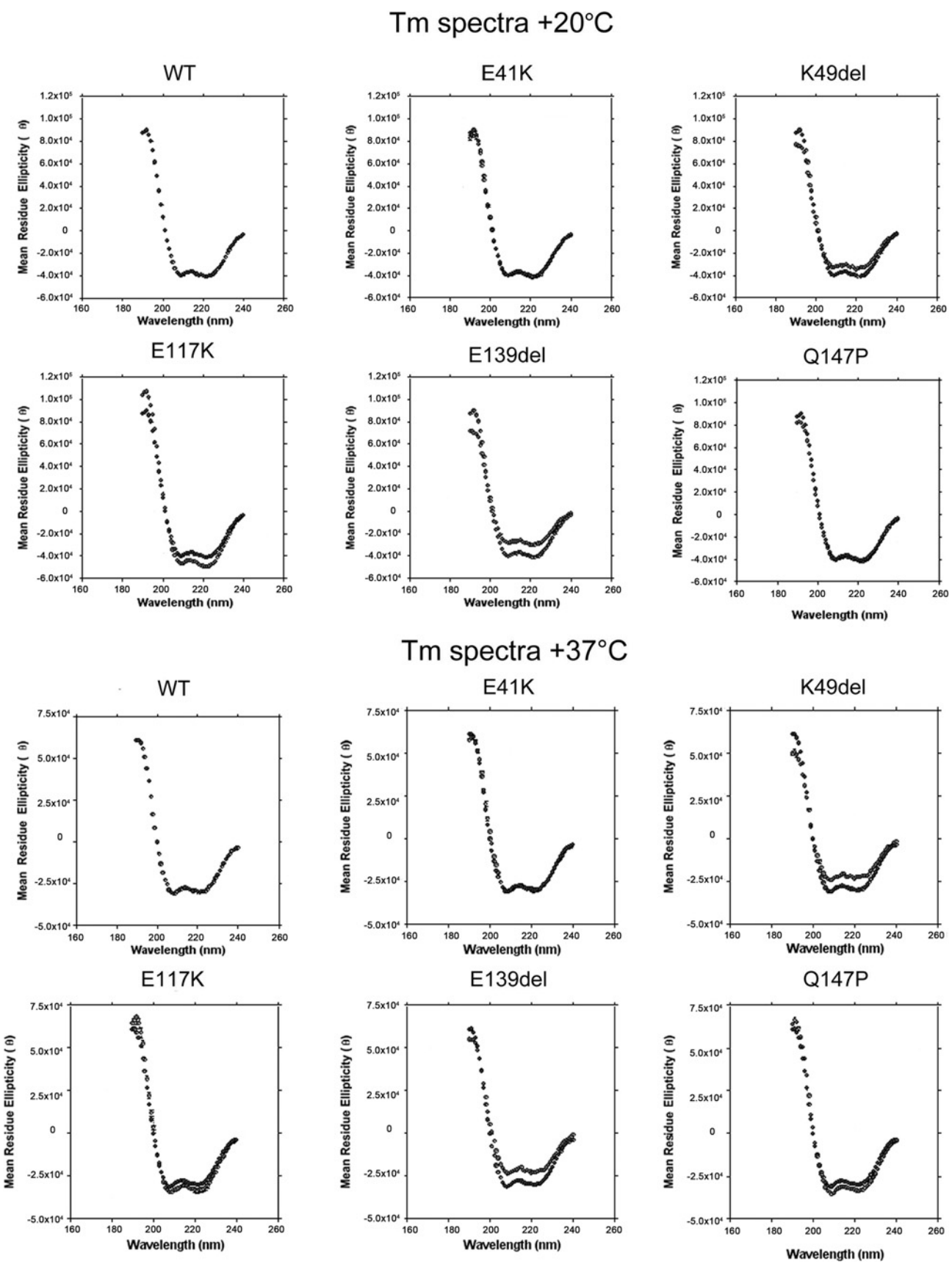


Figure 5 CD of Tms

CD spectra (250–190 nm) of Tm measured at 20 °C and 37 °C.

© The Authors Journal compilation © 2012 Biochemical Society

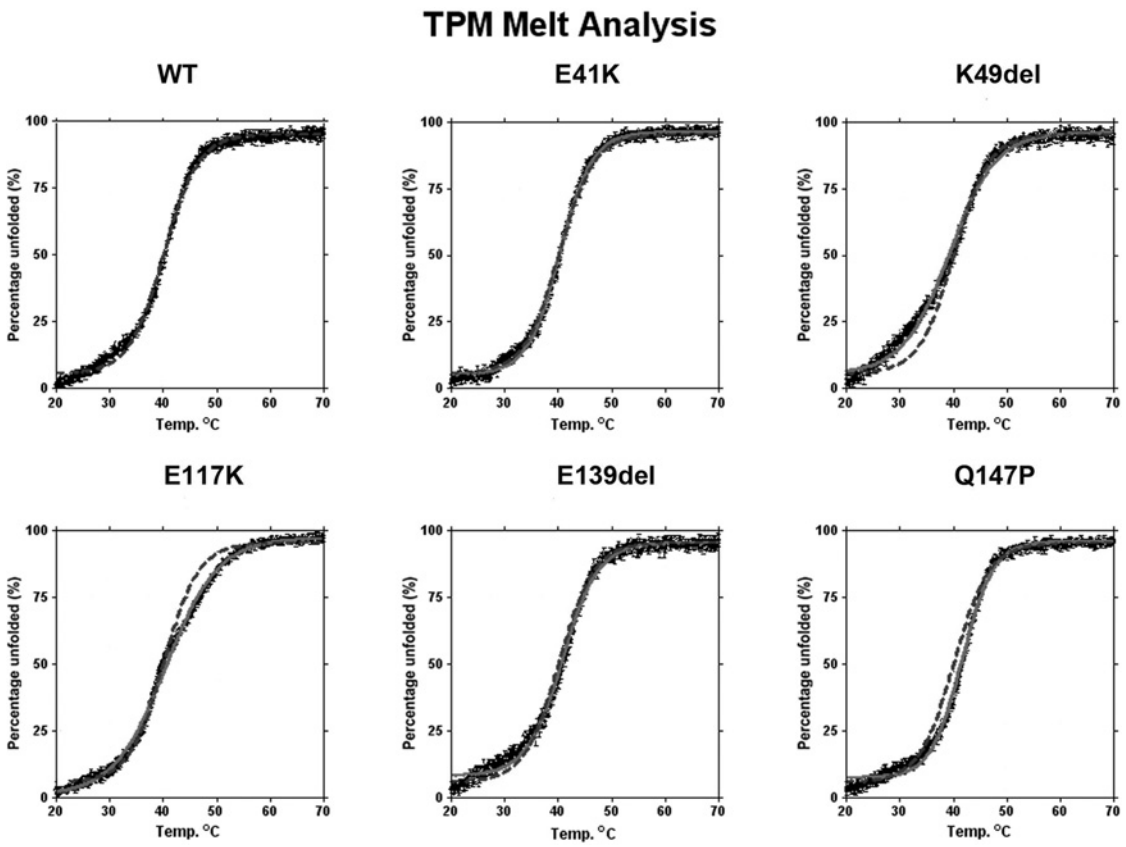


Figure 6 Thermodynamic analysis of Tms

For the Tm thermodynamic analysis, CD absorption was observed at 222 nm as the temperature was increased from 20 °C to 70 °C.

and 87.9 ± 4.3 % respectively). The lowest α-helical contents were seen with the K49del and E139del mutants (65.0 ± 1.6 % and 68.2 ± 1.2 % respectively). At both of the temperatures used, K49del and E139del displayed lower α-helical content than WT Tm. E117K showed higher α-helical content than WT at both temperatures and Q147P at 37 °C.

Thermodynamic analysis of β-Tm

To assess the thermodynamic properties of WT and mutant β-Tm the CD absorption was observed at 222 nm as the temperature was increased from 20 °C to 70 °C. This allowed observation of the protein from a completely folded state to a completely unfolded state and allowed the construction of a melt profile. WT and mutant proteins were modelled as a two-state transition from a fully folded (0 % unfolded) state to a fully unfolded state (100 % unfolded), and this was then plotted against temperature (Figure 6). A best-fit equation was generated from the data and the mid-point of the denaturation, taken as the T_{melt} (melting temperature) shown in Table 1. WT Tm was calculated to have a T_m of 40.2 ± 0.0 °C. The majority of mutant Tm proteins were calculated to have T_{melt} similar to or slightly higher than that of the WT. The K49del mutant was found to have the lowest T_{melt} of all samples studied (39.3 ± 0.2 °C). The denaturation profile of the E117K mutant appears to be quite different from both the WT and the other mutants, indicating that this may have a different unfolding profile, involving different sequential steps.

DISCUSSION

Altogether 11 mutations causing NM, cap myopathy or distal arthrogryposis have been described in the *TPM2* gene that codes for β-Tm [7,12,13,16,27–29]. Included in the present study were five of these, found to cause NM or cap myopathy. In striated muscle, β-Tm is present mainly as a heterodimer with α-Tm in fast muscles and γ-Tm in slow muscles [30]. Tm is almost completely α-helical and forms a parallel coiled-coil dimer. The Tm dimers polymerize with overlapping ends, forming a continuous strand that binds to actin in a slightly curved structure [31]. Tm, troponin and actin interactions regulate the contraction of muscle fibres in response to Ca^{2+} [14]. Therefore changes in the association with actin could be the cause of muscle weakness in muscle disorders, such as NM and cap myopathy, caused by Tm mutations. In the current models [32], it is proposed that Tm has a 7-fold repeated amino acid sequence motif, the heptad repeat that corresponds to the seven actin monomers covered by one Tm. Each motif is subdivided into α- and β-zones. In the relaxed state, Tm forms contacts with actin through positively charged residues in the N-terminal part of an α-zone and acidic residues on the C-terminal side of an α-zone (Figure 7). Ca^{2+} regulation is imposed on actin–Tm by the troponin complex that switches actin–Tm between the on and off conformational states. Thus mutations in Tm potentially can cause muscle dysfunction leading to myopathy through a variety of mechanisms, including effects on formation of dimers, end–end interactions, actin binding and the regulatory interaction with troponin.

© The Authors Journal compilation © 2012 Biochemical Society



Figure 7 Human β-Tm sequence

(**A**) Human β-Tm sequence with mutations (E41K, K49del, E117K, E139del and Q147P) used in the present study and α-zones. The corresponding heptad repeat positions are shown above the sequence. (**B**) Schematic presentation of the fifth α-zone. Sequence of rat striated muscle α-Tm with the positively charged residue followed by apolar residues marked that are found on the N-terminal side of each α-zone. On the C-terminal side, acidic residues found in each of the seven α-zones are proposed to form close contacts with subdomains 1 and 3 of actin. Corresponding heptad repeat positions are shown above the sequence. Based on data taken from [32].

The *a* and *d* residues of the Tm heptad repeat, as in all α-helix heptad repeats, are usually hydrophobic and packed at the interface of the α-helix. The *e* and *g* residues stabilize the coiled-coil through interchain electrostatic interactions and are often oppositely charged. Residues in the *b*, *c* and *f* positions bind other proteins [33]. The K49del, E117K and Q147P mutations are in *e* and *g* positions, probably affecting dimerization. The E139del and E41K mutations are in position *f*, and may affect the binding of other proteins: E139del the binding of actin and E41K a presumed other thin filament protein.

Defective formation of physiological dimers may affect the relative expression levels of the isoforms. Ochala et al. [34] have shown that the β/α ratio changes expressing the E41K β-Tm mutation and Corbett et al. [15] have shown altered Tm isoform ratios in muscle from M9R γ-Tm mutation patients and in the transgenic mouse model of this mutation.

It is well established that strong end–end interactions, integral αβ repeats and a continuous α-helix are essential for Tm binding to actin [15]. Three of the five β-Tm mutations investigated in the present study did not bind to actin in our assays: K49del, E139del and Q147P. The deletion mutants K49del and E139del shorten the α-zone of the second and fourth repeats respectively. Moreover, the deletions are close to proposed major actin contacts: Lys^{49} is located after a positively charged residue present in the N-terminal side of the α-zone proposed to form a direct contact with actin, whereas Glu^{39} is one of the acidic residues of the C-terminal half of the fourth α-zone proposed to form a contact with actin (Figure 7). All the deletion mutations change the heptad repeat sequence subsequent to the deleted amino acid that seems to have a profound effect upon the helical structure of the Tm dimer (Figure 4). In addition, the site-specific disruption of Tm–Tm and Tm–actin contacts and the long-range effect of shortening the α-zone would be expected to reduce the affinity of Tm for actin [35,36] as observed in the present study (Figure 2C). Interestingly, both the mutations that appeared to have caused the histological features of cap disease only (K49del and E139del), led to relatively large drops in α-helical content at both 20 °C and 37 °C, whereas those causing NM (or NM and cap disease) showed either a slight decrease or an increase in α-helical content (Table 1).

The mutant Q147P has been found to cause NM [7]. The Q147 residue is in position *g* of the heptad repeat and in the fourth β-zone just on the C-terminal side of the fourth α-zone. The non-polar proline introduced into the heptad repeat position *g*, normally occupied by a polar residue, should interfere with the local coiled-coil structure. Proline is not present in any WT Tm or in coiled-coil proteins in general, as it produces a kink in the coiled-coil helix [37]. Actin binding of the Q147P mutant was found to be significantly weaker than the binding of actin to WT Tm as might be expected with the disruption of the continuous α-helix [12,38,39].

Although actin–Tm affinity is much reduced in assays at sub-micromolar concentrations, it remains likely that mutant Tm can nevertheless bind to myofibrils in muscles where Tm concentration is approximately 100 μM. Moreover, it is well known that troponin greatly enhances the affinity of Tm for actin [18]. In fact, we were able to obtain some regulation of thin filaments in the motility assay with the weak-binding Tm mutants (K49del, E139del and Q147P) by raising the Tm and troponin concentrations. It remains to be seen whether the stoichiometry of Tm is deficient in the muscles of patients with these mutations.

E41K and E117K mutants bind to actin normally and both appear to directly affect the thin filament regulatory system. These mutations had profound effects upon Ca^{2+} regulation in thin filaments with a large reduction in Ca^{2+}-sensitivity and for E117K a much lower increase in sliding speed (i.e. cross-bridge turnover rate) due to troponin-inactivating conditions, which we have ascribed to the activity of troponin [39,40]. It is likely that the mutation can disrupt the delicate co-operative and allosteric interactions of the thin filament regulatory system. Although Glu^{17} is not in a region of Tm known to interact with troponin T, there is ample evidence for long-range propagation of structural and functional effects of mutations in Tm [41,42]. The mutation E117K is the one mutation to have stronger affinity for actin than WT Tm. We speculate that the higher affinity for actin might explain the absence of nemaline bodies in this patient. Tighter binding could result in the sarcomeric proteins remaining in the thin filaments and the Z disc, and not forming nemaline bodies. The contractile deficiency at the level of the troponin switch parallels that previously reported for CFTD (congenital fibre type disproportion) mutations, noted for muscle weakness without nemaline bodies [43,44].

Previous studies have addressed the pathogenic background of *TPM2* mutants that cause pathologies other than cap and nemaline body formation. Analysis of alterations in contractile properties due to a *TPM2* mutation, R133W, causing distal arthrogryposis in an affected mother and daughter [27], indicated slowing of cross-bridge attachment and acceleration of detachment. Thus the authors speculated that the alteration in myosin–actin kinetics induced by the mutation would cause fewer myosin molecules to be in the strong actin-binding state. This was suggested to be the cause of muscle weakness in the patients [45]. In another study using troponin-exchanged skinned fibres, the R91G mutant in *TPM2* caused a significant increase in Ca^{2+} sensitivity. R91G β-Tm was found to have a lower actin affinity than WT and form a less stable coiled coil [45]. In the related *TPM3* gene,

© The Authors Journal compilation © 2012 Biochemical Society

the M9R mutation causing NM was found to have a similar effect on actin binding [46]. In the present study, one of the mutants (E117K) showed stronger actin binding and higher α-helical content compared with the WT. This mutation caused neither cap formation nor any verifiable nemaline body formation and may be classified as CFTD. Three of the mutants causing nemaline body or cap formation showed weak actin binding, and two of these also had low α-helical content. Thus we speculate that a defective α-helical content and less effective actin binding might contribute to the formation of nemaline bodies and caps, possibly through the disorganization of interrelated sarcomeric proteins. In other cases, abnormal actin–Tm or troponin–Tm interactions may be the underlying cause of the patients' muscle weakness.

In summary, actin binding was weak in three of five mutants suggesting that abnormal binding between actin and aberrant Tm is the pathogenetic mechanism causing muscle weakness in these patients. Ca^{2+} activation of contractility was defective in the two other mutations, suggesting an alternative cause of contractile dysfunction. However, in view of the histological and clinical overlap described in previously published cases [13,27,47,48,50], these hypotheses need to be further explored.

AUTHOR CONTRIBUTION

Carina Wallgren-Pettersson was responsible for planning the project and for clinical correlations in the paper. Minttu Marttila performed actin-binding experiments, three-dimensional models and mass spectrometry and wrote the paper. Elina Lemola was responsible for protein production and actin-binding experiments. Kati Donner produced three tropomyosin constructs. Mikaela Grönholm, a senior protein expert, planned parts of the experimental work and wrote the paper. Nigel Laing and Steven Marston wrote the paper. William Wallefeld performed circular dichroism experiments and wrote the paper. Massimiliano Memo performed *in vitro* motility experiments and wrote the paper.

ACKNOWLEDGEMENTS

We thank Dr Nigel Clarke and Nancy Mokbel for helpful comments on the paper, Katarina Pelin for help on the project, Saara Ollila and Mari Korhonen for helping with the insect cell cultures, Jaakko Sarparanta for advice on the protein work, Pertteli Salmenperä for discussing the migration differences, Per Harald Jonson for help with the three-dimensional models and Tuula Nyman and Gunilla Rönnholm for MS data.

FUNDING

This work was supported by the Association Française contre les Myopathies, the Sigrid Jusélius Foundation, the Academy of Finland, the Finska Läkaresällskapet and the Medicinska understödsföreningen Liv och Hälsa r.f. (to M.M. and C.W.P.); an Australian National Health and Medical Research Council Fellowship [grant number 403904 (to N.G.L.)]; and the British Heart Foundation (to S.M. and M.M.). The University of Helsinki is a partner of TREAT-NMD (European Commission, 6th Framework Programme, proposal no. 036825; http://www.treat-nmd.eu).

REFERENCES

1 Wallgren-Pettersson, C., Pelin, K., Nowak, K. J., Muntoni, F., Romero, N. B., Goebel, H. H., North, K. N., Beggs, A. H. and Laing, N. G. (2004) Genotype–phenotype correlations in nemaline myopathy caused by mutations in the genes for nebulin and skeletal muscle α-actin. Neuromuscul. Disord. **14**, 461–470

2 Shy, G. M., Engel, W. K., Somers, J. E. and Wanko, T. (1963) Nemaline myopathy: a new congenital myopathy. Brain **86**, 793–810

3 Conen, P. E., Murphy, E. G. and Donohue, W. L. (1963) Light and electron microscopic studies of 'myogranules' in a child with hypotonia and muscle weakness. Can. Med. Assoc. J. **89**, 983–986

4 Pelin, K., Hilpela, P., Donner, K., Sewry, C., Akkari, P. A., Wilton, S. D., Wattanasirichaigoon, D., Bang, M. L., Centner, T., Hanefeld, F. et al. (1999) Mutations in the nebulin gene associated with autosomal recessive nemaline myopathy. Proc. Natl. Acad. Sci. U.S.A. **96**, 2305–2310

5 Nowak, K. J., Wattanasirichaigoon, D., Goebel, H. H., Wilce, M., Pelin, K., Donner, K., Jacob, R. L., Hübner, C., Oexlem, K. and Anderson, J. R. (1999) Mutations in the skeletal muscle α-actin gene in patients with actin myopathy and nemaline myopathy. Nat. Genet. **23**, 208–212

6 Laing, N. G., Wilton, S. D., Akkari, P. A., Dorosz, S., Boundy, K., Kneebone, C., Blumbergs, P., White, S., Watkins, H., Love, D. R. et al. (1995) A mutation in the α tropomyosin gene *TPM3* associated with autosomal dominant nemaline myopathy NEM1. Nat. Genet. **10**, 249

7 Donner, K., Ollikainen, M., Ridanpaa, M., Christen, H. J., Goebel, H. H., de Visser, M., Pelin, K. and Wallgren-Pettersson, C. (2002) Mutations in the β-tropomyosin (*TPM2*) gene: a rare cause of nemaline myopathy. Neuromuscul. Disord. **12**, 151–158

8 Johnston, J. J., Kelley, R. I., Crawford, T. O., Morton, D. H., Agarwala, R., Koch, T., Schäffer, A. A., Francomano, C. A. and Biesecker, L. G. (2000) A novel nemaline myopathy in the amish caused by a mutation in troponin T1. Am. J. Hum. Genet. **67**, 814–821

9 Agrawal, P. B., Greenleaf, R. S., Tomczak, K. K., Lehtokari, V. L., Wallgren-Pettersson, C., Wallefeld, W., Laing, N. G., Darras, B. T., Maciver, S. K., Dormitzer, P. R. et al. (2007) Nemaline myopathy with minicores caused by mutation of the *CFL2* gene encoding the skeletal muscle actin-binding protein, cofilin-2. Am. J. Hum. Genet. **80**, 162–167

10 Sambuughin, N., Yau, K. S., Olive, M., Duff, R. M., Bayarsaikhan, M., Lu, S., Gonzalez-Mera, L., Sivadorai, P., Nowak, K. J., Ravenscroft, G. et al. (2010) Dominant mutations in KBTBD13, a member of the BTB/Kelch family, cause nemaline myopathy with cores. Am. J. Hum. Genet. **87**, 842–847

11 Fidzianska, A., Badurska, B., Ryniewicz, B. and Dembek, I. (1981) 'Cap disease': new congenital myopathy. Neurology **31**, 1113–1120

12 Lehtokari, V. L., Ceuterick-de Groote, C., de Jonghe, P., Marttila, M., Laing, N. G., Pelin, K. and Wallgren-Pettersson, C. (2007) Cap disease caused by heterozygous deletion of the β-tropomyosin gene *TPM2*. Neuromuscul. Disord. **17**, 433–442

13 Tajsharghi, H., Ohlsson, M., Lindberg, C. and Oldfors, A. (2007) Congenital myopathy with nemaline rods and cap structures caused by a mutation in the β-tropomyosin gene (*TPM2*). Arch. Neurol. **64**, 1334–1338

14 Perry, S. V. (2001) Vertebrate tropomyosin: distribution, properties and function. J. Muscle Res. Cell. Motil. **22**, 5–49

15 Corbett, M. A., Akkari, P. A., Domazetovska, A., Cooper, S. T., North, K. N., Laing, N. G., Gunning, P. W. and Hardeman, E. C. (2005) An alphatropomyosin mutation alters dimer preference in nemaline myopathy. Ann. Neurol. **57**, 42–49

16 Ohlsson, M., Quijano-Roy, S., Darin, N., Brochier, G., Lacene, E., Avila-Smirnow, D., Fardeau, M., Oldfors, A. and Tajsharghi, H. (2008) New morphologic and genetic findings in cap disease associated with β-tropomyosin (*TPM2*) mutations. Neurology **71**, 1896–1901

17 Akkari, P. A., Song, Y., Hitchcock-DeGregori, S., Blechynden, L. and Laing, N. (2002) Expression and biological activity of baculovirus generated wild-type human slow α tropomyosin and the Met9Arg mutant responsible for a dominant form of nemaline myopathy. Biochem. Biophys. Res. Commun. **16**, 300–304

18 Hitchcock-DeGregori, S. E. and Heald, R. W. (1987) Altered actin and troponin binding of amino-terminal variants of chicken striated muscle α-tropomyosin expressed in *Escherichia coli*. J. Biol. Chem. **262**, 9730–9735

19 Marston, S. B., Fraser, I. D., Bing, W. and Roper, G. (1996) A simple method for automatic tracking of actin filaments in the motility assay. J. Muscle Res. Cell Motil. **17**, 497–506

20 Gunning, P., O'Neillm, G. and Hardeman, E. (2008) Tropomyosin-based regulation of the actin cytoskeleton in time and space. Physiol. Rev. **88**, 1–35

21 Fraser, I. D. and Marston, S. B. (1995) *In vitro* motility analysis of actin–tropomyosin regulation by troponin and calcium. The thin filament is switched as a single cooperative unit. J. Biol. Chem. **270**, 7836–7841

22 Mukherjee, S., Sharma, S., Kumar, S. and Guptasarma, P. (2005) Slow irreversible unfolding of *Pyrococcus furiosus* triosephosphate isomerase: separation and quantitation of conformers through a novel electrophoretic approach. Anal. Biochem. **347**, 49–59

23 Rath, A., Glibowicka, M., Nadeau, V. G., Chen, G. and Deber, C. M. (2009) Detergent binding explains anomalous SDS/PAGE migration of membrane proteins. Proc. Natl. Acad. Sci. U.S.A. **106**, 1760–1765

24 Bottinelli, R., Coviello, D. A., Redwood, C. S., Pellegrino, M. A., Maron, B. J., Spirito, P., Watkins, H. and Reggiani, C. (1998) A mutant tropomyosin that causes hypertrophic cardiomyopathy is expressed *in vivo* and associated with an increased calcium sensitivity. Circ. Res. **82**, 106–115

25 Whitmore, L. and Wallace, B. A. (2004) DICHROWEB, an online server for protein secondary structure analyses from circular dichroism spectroscopic data. Nucleic Acids. Res. **32** (Suppl. 2), W668–W673

26 Whitmore, L. and Wallace, B. A. (2008) Protein secondary structure analyses from circular dichroism spectroscopy: methods and reference databases. Biopolymers **89**, 392–400

27 Tajsharghi, H., Kimber, E., Holmgren, D., Tulinius, M. and Oldfors, A. (2007) Distal arthrogryposis and muscle weakness associated with a β-tropomyosin mutation. Neurology **68**, 772–775

© The Authors Journal compilation © 2012 Biochemical Society

28 Sung, S. S., Brassington, A. M., Grannatt, K., Rutherford, A., Whitby, F. G., Krakowiak, P. A., Jorde, L. B., Carey, J. C. and Bamshad, M. (2003) Mutations in genes encoding fast-twitch contractile proteins cause distal arthrogryposis syndromes. Am. J. Hum. Genet. **72**, 681–690

29 Monnier, N., Lunardi, J., Marty, I., Mezin, P., Labarre-Vila, A., Dieterich, K. and Jouk, P. S. (2009) Absence of β-tropomyosin is a new cause of escobar syndrome associated with nemaline myopathy. Neuromuscul. Disord. **19**, 118–123

30 Heeley, D. H., Dhoot, G. K. and Perry, S. V. (1985) Factors determining the subunit composition of tropomyosin in mammalian skeletal muscle. Biochem. J. **226**, 461–468

31 Li, X. E., Holmes, K. C., Lehman, W., Jung, H. and Fischer, S. (2010) The shape and flexibility of tropomyosin coiled coils: implications for actin filament assembly and regulation. J. Mol. Biol. **395**, 327–339

32 Brown, J. H., Zhou, Z., Reshetnikova, L., Robinson, H., Yammani, R. D., Tobacman, L. S. and Cohen, C. (2005) Structure of the mid-region of tropomyosin: bending and binding sites for actin. Proc. Natl. Acad. Sci. U.S.A. **102**, 18878–18883

33 Singh, A. and Hitchcock-Degregori, S. E. (2009) A peek into tropomyosin binding and unfolding on the actin filament. PLoS ONE **24**, 6336

34 Ochala, J., Li, M., Ohlsson, M., Oldfors, A. and Larsson, L. (2008) Defective regulation of contractile function in muscle fibres carrying an E41K β-tropomyosin mutation. J. Physiol. **586**, 2993–3004

35 Hitchcock-DeGregori, S. E. and An, Y. (1996) Integral repeats and a continuous coiled coil are required for binding of striated muscle tropomyosin to the regulated actin filament. J. Biol. Chem. **271**, 3600–3603

36 Hitchcock-DeGregori, S. E. (2008) Tropomyosin: function follows structure. Adv. Exp. Med. Biol. **644**, 60–72

37 East, D., Sousa, D., Lehman, W. and Mulvihill, D. P. (2010) Precise modulation of tropomyosin polymer length is crucial for its association with actin and ability to regulate myosin function. Biophys. J. **98**, 156–158

38 Chang, D. K., Cheng, S. F., Trivedi, V. D. and Lin, K. L. (1999) Proline affects oligomerization of a coiled coil by inducing a kink in a long helix. J. Struct. Biol. **128**, 270–279

39 Pronina, O. (2008) Alteration of β-tropomyosin function by nemaline myopathy-causing mutations E117K and Q147P. Biophys. J. Biophys. Soc. Abstr., 625

40 Bing, W., Razzaq, A., Sparrow, J. and Marston, S. (1998) Tropomyosin and troponin regulation of wt and E93K mutant actin filaments from *Drosophila* flight muscle: charge reversal on actin changes actin–tropomyosin from on to off state. J. Biol. Chem. **273**, 15016–15021

41 Bing, W., Fraser, I. D. and Marston, S. B. (1997) Troponin I and troponin T interact with troponin C to produce different Ca^{2+}-dependent effects on actin–tropomyosin filament motility. Biochem. J. **327**, 335–340

42 Farah, C. S. and Reinach, F. C. (1999) Regulatory properties of recombinant tropomyosins containing 5-hydroxytryptophan: Ca^{2+}-binding to troponin results in a conformational change in a region of tropomyosin outside the troponin binding site. Biochemistry **38**, 10543–10551

43 Nirody, J., Li, X., Sousa, D., Sumida, J., Fischer, S. and Lehrer, S. S. (2010) Electron microscopy and molecular dynamics on a D137L mutant of tropomyosin. Biophys. J. **98**, 414a

44 Clarke, N. F., Ilkovski, B., Cooper, S., Valova, V. A., Robinson, P. J., Nonaka, I., Feng, J. J., Marston, S. and North, K. (2007) The pathogenesis of ACTA1-related congenital fiber type disproportion. Ann. Neurol. **61**, 552–561

45 Ochala, J., Li, M., Tajsharghi, H., Kimber, E., Tulinius, M., Oldfors, A. and Larsson, L. (2007) Effects of a R133W β-tropomyosin mutation on regulation of muscle contraction in single human muscle fibres. J. Physiol. **581**, 1283–1292

46 Robinson, P., Lipscomb, S., Preston, L. C., Altin, E., Watkins, H., Ashley, C. C. and Redwood, C. S. (2007) Mutations in fast skeletal troponin I, troponin T, and β-tropomyosin that cause distal arthrogryposis all increase contractile function. FASEB J. **21**, 896–905

47 Moraczewska, J., Greenfield, N. J., Liu, Y. and Hitchcock-DeGregori, S. E. (2000) Alteration of tropomyosin function and folding by a nemaline myopathy-causing mutation. Biophys. J. **79**, 3217–3225

48 Cuisset, J. M., Maurage, C. A., Pellissier, J. F., Barois, A., Urtizberea, J. A., Laing, N., Tajsharghi, H. and Vallée, L. (2006) 'Cap myopathy': case report of a family. Neuromuscul. Disord. **16**, 277–281

49 Ohlsson, M., Fidzianska, A., Tajsharghi, H. and Oldfors, A. (2009) *TPM3* mutation in one of the original cases of cap disease. Neurology **72**, 1961–1963

50 Feng, J.-J. and Marston, S. B. (2009) Genotype–phenotype correlations in ACTA1 mutations that cause congenital myopathies. Neuromuscul. Disord. **19**, 6–16

Received 10 June 2011/15 November 2011; accepted 16 November 2011
Published as BJ Immediate Publication 16 November 2011, doi:10.1042/BJ20111030

© The Authors Journal compilation © 2012 Biochemical Society

Neurology®

Nemaline myopathy with stiffness and hypertonia associated with an *ACTA1* mutation

R.K. Jain, S. Jayawant, W. Squier, et al.

Neurology 2012;78;1100; Published online before print March 21, 2012;
DOI 10.1212/WNL.0b013e31824e8ebe

This information is current as of June 27, 2012

The online version of this article, along with updated information and services, is located on the World Wide Web at:
http://www.neurology.org/content/78/14/1100.full.html

Neurology ® is the official journal of the American Academy of Neurology. Published continuously since 1951, it is now a weekly with 48 issues per year. Copyright © 2012 by AAN Enterprises, Inc. All rights reserved. Print ISSN: 0028-3878. Online ISSN: 1526-632X.

AMERICAN ACADEMY OF NEUROLOGY®

R.K. Jain, MRCPCH
S. Jayawant, MD
W. Squier, MB, ChB
F. Muntoni, MD
C.A. Sewry, FRCPath
A. Manzur, FRCPCH
R. Quinlivan, FRCPCH
S. Lillis, MSc
H. Jungbluth, MD
J.C. Sparrow, PhD
G. Ravenscroft, PhD
K.J. Nowak, PhD
M. Memo, BSc
S.B. Marston, PhD
N.G. Laing, PhD

NEMALINE MYOPATHY WITH STIFFNESS AND HYPERTONIA ASSOCIATED WITH AN *ACTA1* MUTATION

Nemaline myopathy, known to be caused by mutations in 7 genes, including skeletal muscle α-actin (*ACTA1*),[1] is characterized by muscle weakness, hypotonia, and nemaline rods in muscle biopsy. Here we report a patient with nemaline rods but the opposite phenotype of hypercontractility.

Case report. The John Radcliffe Hospital ethics review board approved the study. The first child of nonconsanguineous European parents presented at 6 weeks of age with an apneic episode thought due to bilateral strangulated inguinal hernias and an umbilical hernia. However, after herniotomy, rigidity and recurrent apneas requiring mechanical ventilation continued.

The patient was born by elective Caesarean section at 39 weeks, with no perinatal complications, although the mother, with hindsight, thought there might have been stiffness in the weeks after birth as she had difficulty clothing him. Polyhydramnios had been noted.

On examination, he had very stiff and hypertrophic abdominal and proximal limb muscles and elbow and knee contractures. Deep tendon reflexes showed brisk contraction and slow relaxation and percussion myotonia could be elicited. However, EMG in multiple muscles showed no evidence of myotonia. He also had normal nerve conduction studies, MRI, EEG, and cardiac assessment, including echocardiography. Neurometabolic investigations were also normal including serum and CSF lactate, CSF neurotransmitters, urinary catecholamines, carnitine profile, white cell enzymes, and screening for mucopolysaccharidosis. Serum creatine kinase was slightly raised (370 IU, range 24–195). A sleep study showed hypoventilation and carbon dioxide retention.

Hyperekplexia, paroxysmal episodic pain disorder, neuromyotonia, and episodic ataxia were considered, though none exactly matched the phenotype because of the underlying stiffness, but relevant testing (*ARX*, *FRAXA*, *GLRA1*, *KCN1A*, *POLG*, *SCN9A*, anti GAD, and VGKC antibody studies) was negative. Pharmacologic treatment including phenytoin, carbamazepine, flecainide, baclofen, dantrolene, and acetazolamide was ineffective.

He continued having recurrent episodes of stiffness, where he stopped breathing and became apneic. Some episodes, despite ventilation, would progress to desaturation, bradycardia, and occasionally asystole requiring resuscitation. He needed invasive and noninvasive ventilation all his life, apart from a brief period of self-ventilating when he transiently improved on clonazepam.

Biopsy of the quadriceps demonstrated nemaline bodies (figure), leading to a pathologic diagnosis of nemaline myopathy. Molecular diagnosis identified a novel de novo mutation c.984G>C, p.Lys328Asn (Lys328Asn in the mature protein), in *ACTA1*.

At 10 weeks, he was transferred to Great Ormond Street Hospital. Hypertonia, with predominantly extensor tone in the arms, legs, and trunk, and a tendency for extensor posturing on stimulation were noted. Episodic stiffness was observed, which started for example as soon as he strained to initiate stooling.

The patient died in an asystolic episode aged 9 months.

We investigated whether the actin mutation produced any functional change that might explain the phenotype. Two-dimensional protein analysis[2] showed 32% mutant actin in the patient biopsy, demonstrating the mutation was not a null mutation (data not shown).

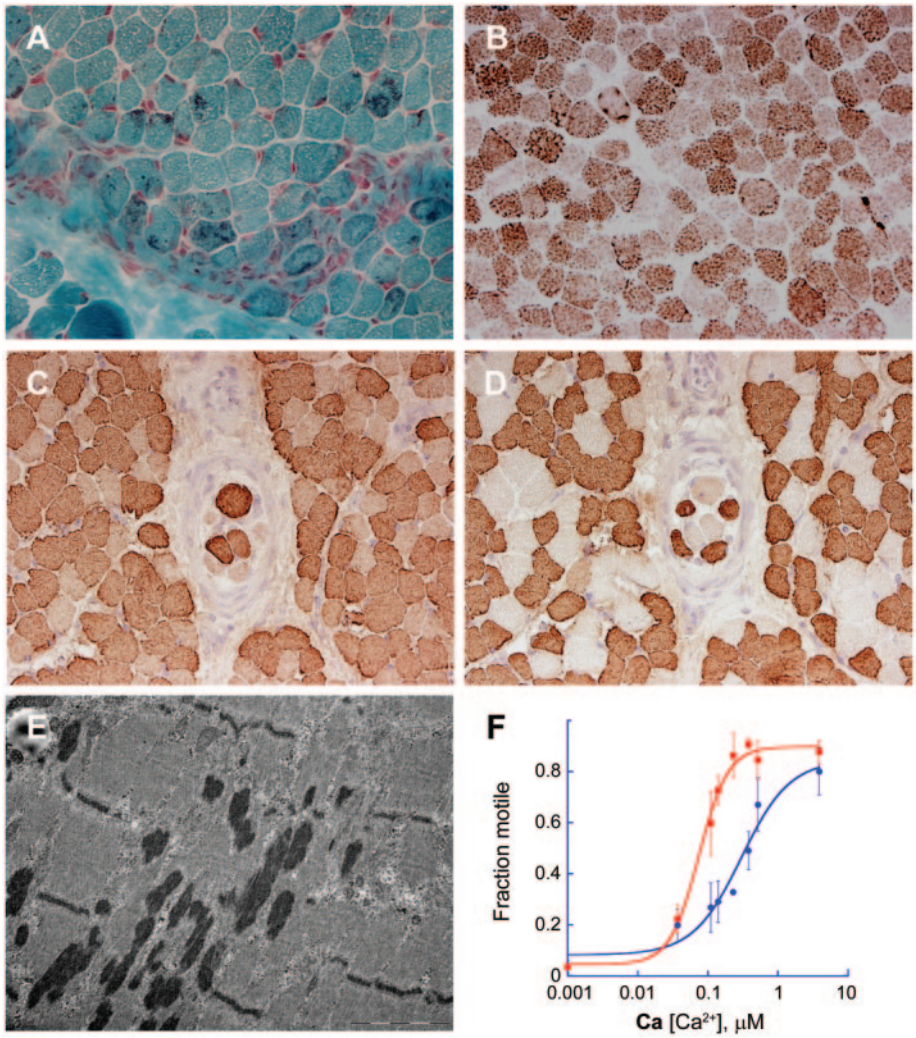
In vitro motility analysis of thin filaments reconstituted from actin isolated from the patient's muscle biopsy[2,3] showed increased sensitivity to Ca^{2+} (figure, G) demonstrating the p.Lys328Asn *ACTA1* mutation increases the activated states of the thin filament.

Unlike results for other *ACTA1* mutations,[3] expression of the p.Lys328Asn mutant in C2C12 tissue culture showed no evidence of rod-like structures (data not shown).

Discussion. This patient differs from previous descriptions of nemaline myopathy in having muscle stiffness, hypertrophic abdominal and proximal limb muscles, and elbow and knee contractures along with

Copyright © by AAN Enterprises, Inc. Unauthorized reproduction of this article is prohibited.

Figure Pathologic features of the patient muscle biopsy and calcium sensitivity of the p.Lys328Asn actin mutant



Muscle biopsy from the quadriceps: (A) Gomori trichrome shows abnormal variation in fiber size ranging from 5 to 20 μm and red staining rods in several fibers; (B) combined staining for cytochrome oxidase and succinic dehydrogenase activity shows fiber type differentiation, some peripheral accumulation of cytochrome oxidase, but no fibers lacking cytochrome oxidase activity; (C, D) immunolabeling of serial areas with antibodies to (C) slow and (D) fast myosin shows 2 main fiber types and coexpression of both isoforms in some fibers. The central area contains a muscle spindle. Electron micrographs of the muscle biopsy show (E) rods orientated longitudinally and transversely. (F) Comparative Ca^{2+} activation curves for thin filaments reconstituted with patient (red) or control (blue) actin and rabbit skeletal troponin and tropomyosin. Points are mean ± SE for fraction of filaments motile recorded in 4–6 randomly selected regions in each motility cell. Lines are best fit of mean data points to the Hill equation.

features of myotonia clinically but not electrophysiologically. The nemaline myopathy pathology and presence of an *ACTA1* mutation were at odds with the clinical picture, which was not that of a weak infant or a congenital myopathy. Mutations in other actins demonstrate a similar molecular phenotype of increased Ca^{2+} sensitivity,[2] or hypercontraction.[4] In addition, we had previously shown that an opposite charge change mutation, p.Asp294Val, in the same actin-tropomyosin interface as the p.Lys328Asn mutation,[5] causes permanent switching off of the thin filament and hypotonia.[3] Thus, we hypothesized that the p.Lys328Asn mutation might result in a higher Ca^{2+} sensitivity, which we demonstrated directly by in vitro motility assay. The molecular pathophysiology of the mutation explains the clinical phenotype in our patient and suggests a different mechanism of nemaline body formation for this mutation, compared with other *ACTA1* mutations, which is supported by the absence of rod structures in C2C12 culture. Our results expand the differential diagnosis of nemaline myopathy, and, along with muscle stiffness phenotypes in cytoplasmic body,[6] and myofibrillar[7] myopathies, indicate that a muscle biopsy should be considered in infants with unexplained stiffness and hypertonicity.

Copyright © by AAN Enterprises, Inc. Unauthorized reproduction of this article is prohibited.

From the Departments of Paediatric Neurology (R.K.J., S.J.) and Neuropathology (W.S.), John Radcliffe Hospital, Oxford; Dubowitz Neuromuscular Centre (F.M., C.A.S., A.M.), UCL Institute of Child Health and Great Ormond Street Hospital, London; Wolfson Centre for Inherited Neuromuscular Diseases (C.A.S., R.Q.), Robert Jones and Agnes Hunt Orthopaedic Hospital NHS Trust, Oswestry; Diagnostic DNA Laboratory (S.L.), GSTT Pathology, Guy's Hospital, London; Department of Paediatric Neurology–Neuromuscular Service (H.J.), Evelina Children's Hospital, Guy's and Thomas' NHS Foundation Trust, and Clinical Neuroscience Division, IOP, King's College, London; Department of Biology (Area 10) (J.C.S.), University of York, UK; Centre for Medical Research (G.R., K.J.N., N.G.L.), University of Western Australia and Western Australian Institute for Medical Research, Nedlands, Western Australia; and National Heart and Lung Institute (M.M., S.B.M.), Imperial College London, UK.

Author contributions: Dr. Jain was clinician in charge of the patient, led the initial investigations into the patient, contributed to the drafting and revision of the manuscript, drafting/revising the manuscript for content, including medical writing for content, study concept or design, analysis or interpretation of data. Dr. Jayawant was clinician in charge of the patient, led the initial investigations into the patient, contributed to the drafting of the manuscript, drafting/revising the manuscript for content, including medical writing for content analysis or interpretation of data. Dr. Squier performed pathology analysis for the patient, contributed to writing the pathology section of the manuscript, drafting/revising the manuscript for content, including medical writing for content, analysis or interpretation of data. Dr. Muntoni contributed to the clinical analysis of the patient, oversaw the review of the clinical information on the patient, had overall responsibility for the patient in London, contributed to the drafting and revision of the manuscript, drafting/revising the manuscript for content, including medical writing for content, study concept or design, analysis or interpretation of data. Dr. Sewry has performed and overseen the pathology analysis on the patient, contributed to drafting and revision of the manuscript, drafting/revising the manuscript for content, including medical writing for content, analysis or interpretation of data. Dr. Manzur contributed to the clinical analysis of the patient in London, analysis or interpretation of data. Dr. Quinlivan contributed to the clinical analysis of the patient, analysis or interpretation of data. S. Lillis performed the molecular analysis of the patient, contributed to drafting the manuscript, drafting/revising the manuscript for content, including medical writing for content, analysis or interpretation of data. Dr. Jungbluth had oversight of the molecular analysis of the patient, contributed to writing the manuscript, drafting/revising the manuscript for content, including medical writing for content, analysis or interpretation of data. Dr. Sparrow performed the theoretical analysis of the effect of the mutation on actin function, analyzed the effect in relation to known Drosophila mutations, study concept or design, analysis or interpretation of data. Dr. Ravenscroft performed the in vitro expression of the mutant actin protein, contributed to the drafting and revision of the manuscript, drafting/revising the manuscript for content, including medical writing for content, study concept or design, analysis or interpretation of data. Dr. Nowak has overseen the in vitro expression of the mutant actin protein and analysis, contributed to the drafting and revision of the manuscript, drafting/revising the manuscript for content, including medical writing for content, study concept or design, analysis or interpretation of data. M. Memo performed the in vitro motility analysis of the mutant actin protein, contributed to drafting the manuscript, drafting/revising the manuscript for content, including medical writing for content, analysis or interpretation of data. Dr. Marston assisted in conceptualizing the study, has overseen the in vitro motility analysis of the mutant actin protein, contributed to drafting and revision of the manuscript, drafting/revising the manuscript for content, including medical writing for content, study concept or design, analysis or interpretation of data. Dr. Laing conceptualized the study, had overall responsibility for coordinating the study, assisted with drafting and revision of the manuscript and analysis of data, drafting/revising the manuscript for content, including medical writing for content, study concept or design, analysis or interpretation of data.

*Contributors: Dr. Man-Ching Leung (National Heart and Lung Institute, London) (2-dimensional protein electrophoresis); Dr. Wilbert Peters, Radboud University Medical Centre, Nijmegen (*SCN9A *analysis); Prof. Mark Rees, Institute of Life Sciences, Swansea, Wales (*GLRA1 *analysis); Dr. Angela Vincent, Neurosciences Group, Weatherall Institute Oxford (anti-VGKC antibody); Prof. N.W. Wood, Institute of Neurology, London (*KCN1A *analysis).*

*Acknowledgment: The authors thank the Genetic Lab, Oxford (fragile X analysis); Immunology Department, Oxford (anti-GAD antibody); Institute of Medical Genetics, University Hospital of Wales, Cardiff (*ARX *analysis); and Oxford Molecular Genetic Department (*POLG *analysis).*

Study funding: Supported by Australian National Health and Medical Research Council (NH&MRC) Principal Research Fellowship 403904 (N.G.L.); NH&MRC grant 403941 (N.G.L., K.J.N., G.R.); EU-funded Framework 6 Network of Excellence 'Myores' (J.C.S.); British Heart Foundation (S.B.M., M.M.); UK National Commissioning Group to the Dubowitz Neuromuscular Centre (F.M., C.A.S., H.J.); Great Ormond Street Children's Charity (F.M.); Guy's & St Thomas Charitable Foundation (G70404) (S.L. and H.J.).

Disclosure: Dr. Jain, Dr. Jayawant, and Dr. Squier report no disclosures. Dr. Muntoni serves on scientific advisory boards for AVI BioPharma, Inc., Summit, PTC Therapeutics, Inc., and GlaxoSmithKline; serves on the editorial boards of Neuromuscular Disorders *and* Neuropaediatrics*; is listed as an author on a pending patent re: Tailed antisense nucleotides to redirect splicing; receives publishing royalties for* Duchenne Muscular Dystrophy *(Oxford University Press, 2003); and receives research support from AVI BioPharma, Inc., PTC Therapeutics, Inc., GlaxoSmithKline, Trophos, Wellcome Trust, the European Union, Medical Research Council UK, Muscular Dystrophy Campaign, Muscular Dystrophy Association USA, Gavriel Meier Trust, Spinal Muscular Atrophy Foundation, the NIH, the Association Française contre les myopathies (AFM), the NIHR, the Great Ormond Street Hospital Children's Charity, and the UK National Commissioning Group. Dr. Sewry serves on the editorial advisory boards of* Neuromuscular Disorders, Muscle & Nerve, *and* Neuropathology & Applied Neuropathology*; receives publishing royalties for* Muscle Biopsy: A Practical Approach *(Elsevier, 2007); and receives research support from the UK National Commissioning Group (funding to the Dubowitz Neuromuscular Centre, London). Dr. Manzur reports no disclosures. Dr. Quinlivan has received speaker honoraria from Genzyme Corporation and receives research support from the Muscular Dystrophy Campaign. S. Lillis received support from Guy's & St Thomas Charitable Foundation (G70404). Dr. Jungbluth received support from the UK National Commissioning Group funding to the Dubowitz Neuromuscular Centre and from the Guy's & St Thomas Charitable Foundation (G70404). Dr. Sparrow receives publishing royalties for* Enterprise for Life Scientists: Developing Innovation and Entrepreneurship in the Biosciences *(Scion Publishing Ltd, 2008) and has received research support from EU-funded Framework 6 Network of Excellence 'Myores'. Dr. Ravenscroft reports no disclosures. Dr. Nowak has received support from the Association Française contre les Myopathies, the Foundation Building Strength for Nemaline Myopathy, the Muscular Dystrophy Association (USA), Australian National Health and Medical Research Council (NH&MRC) project grant 403941, Australian Research Council Future Fellowship, and West Australian Medical and Health Research Infrastructure Fund. M. Memo has received support from the British Heart Foundation. Dr. Marston receives support from the British Heart Foundation. Dr. Laing serves as Associate Editor and on the editorial board of* Neuromuscular Disorders*; receives publishing royalties for* The Sarcomere and Skeletal Muscle Disease *(Springer, 2008); has received funding to attend conferences from the Danish Muscular Dystrophy Association and the Asian and Oceanian Myology Centre; receives/has received research support from the Association Française contre les Myopathies, the Foundation Building Strength for Nemaline Myopathy, Motor Neuron Disease Research*

Copyright © by AAN Enterprises, Inc. Unauthorized reproduction of this article is prohibited.

Institute of Australia, the Muscular Dystrophy Association (USA), the Australian National Health and Medical Research Council (NH&MRC), and the West Australian Medical and Health Research Infrastructure Fund.

Received April 25, 2011. Accepted in final form November 14, 2011.

Correspondence & reprint requests to Dr. Laing: nlaing@cyllene.uwa.edu.au

Copyright © 2012 by AAN Enterprises, Inc.

1. Sambuughin N, Yau KS, Olive M, et al. Dominant mutations in KBTBD13, a member of the BTB/Kelch family, cause nemaline myopathy with cores. Am J Hum Genet 2010;87:842–847.
2. Song W, Dyer E, Stuckey DJ, et al. Molecular mechanism of the E99K mutation in cardiac actin (ACTC gene) that causes apical hypertrophy in man and mouse. J Biol Chem 2011;286:27582–27593.
3. Clarke NF, Ilkovski B, Cooper S, et al. The pathogenesis of ACTA1-related congenital fiber type disproportion. Ann Neurol 2007;61:552–561.
4. Nongthomba U, Cummins M, Clark S, Vigoreaux JO, Sparrow JC. Suppression of muscle hypercontraction by mutations in the myosin heavy chain gene of Drosophila melanogaster. Genetics 2003;164:209–222.
5. Li XE, Tobacman LS, Mun JY, Craig R, Fischer S, Lehman W. Tropomyosin position on F-actin revealed by EM reconstruction and computational chemistry. Biophys J 2011;100:1005–1013.
6. Chen YD, Chen CH, Mak SC, Chi CS. Stiff-baby: an unusual manifestation of cytoplasmic body myopathy: report of one case. Acta Paediatr Taiwan 2001;42: 367–369.
7. Forrest KM, Al-Sarraj S, Sewry C, et al. Infantile onset myofibrillar myopathy due to recessive CRYAB mutations. Neuromuscul Disord 2011;21:37–40.

Refresh Your Annual Meeting Experience with New 2012 AAN On Demand

- More than 600 hours of cutting-edge educational content and breakthrough scientific research
- Online access within 24 hours of end of program
- Mobile streaming for most iPad®, iPhone®, and Android® devices
- USB Flash Drive offers convenient offline access (shipped after the Annual Meeting)
- Enhanced browser, search, and improved interface for better overall experience

Get a great value with special pricing on AAN On Demand *and* the Syllabi on CD. Pre-order and save up to $1,200! Learn more at *www.aan.com/view/ondemand2.*

Copyright © by AAN Enterprises, Inc. Unauthorized reproduction of this article is prohibited.

and validation of new prognostic models. Stroke 2002;33:1041–1047.
5. Weimar C, König IR, Kraywinkel K, Ziegler A, Diener HC, German Stroke Study Collaboration. Age and National Institutes of Health Stroke Scale Score within 6 hours after onset are accurate predictors of outcome after cerebral ischemia: development and external validation of prognostic models. Stroke 2004;35:158–162.

Ziad M.K. El-Zammar, Syracuse, NY; Steven R. Levine, Brooklyn, NY: Park et al.[1] suggest asymptomatic hemorrhagic transformation (AsxHT) may worsen outcome, as did Kimura et al.[2] Libman et al.[3] did not find this relationship. There may be several explanations.

The definition of AsxHT by Park et al. used different radiologic and clinical criteria.[4] Gradient echo MRI is more sensitive for deoxyhemoglobin than conventional MRI or CT. Cardiac embolism causes more severe stroke and frequent hemorrhagic transformation (HT) and is more commonly associated with worse outcomes. Perhaps adjusted analyses could not account for this. The adjusted odds ratio (OR) was 1.9 in all 6 cases of comparing modified Rankin Scale (mRS) scores, suggesting an identical contribution of AsxHT to each notch of worsening mRS across the full spectrum of mRS.

This is difficult to understand, especially since clinical judgment decided the contribution of HT to symptoms. The rate of thrombolysis based on the 3-month mRS—26% with mRS = 5 were thrombolyzed, vs 8% for each of mRS 0, 1, and 2, and 11%, 13%, and 15% for mRS = 3, 4, and 6—is notable. There may also be bias in who received thrombolysis based on baseline NIHSS. Controlling these prognostic factors is challenging, leaving this important issue open to further investigation.

Author Response: Hee-Joon Bae, Gyeonggi-Dong, Korea; Jung Hyun Park, Gyeongju, Korea; Juneyoung Lee, Seoul, Korea; Philip B. Gorelick, Chicago: We thank El-Zammar et al. for their comments. A key point for the interpretation of table 3 is to focus on change of the adjusted ORs for explanatory variables with different cutoff values of the mRS score.[1] We used an ordinal logistic regression model to reflect the ordinal nature of the mRS in our analysis. The ordinal logistic regression model assumes that the odds of having higher mRS scores with AsxHT to those without AsxHT are constant across all cutoff values of the mRS.[5–6] In our dataset, the proportional odds assumption was not satisfied for all variables. Therefore, the partial proportional odds model was employed and, as a result, the estimated ORs for variables not satisfying the assumption were varied according to a cutoff value of the mRS. The adjusted OR of 1.9 for AsxHT means that AsxHT was associated with a 1.9 times higher odds of resultant higher mRS scores than without AsxHT regardless of cutoff values of the mRS. Finally, in our study the rate of thrombolysis increased as the 3-month mRS score worsened. As mentioned in the article, we admit the possibility of residual confounding although we adjusted both variables in the model.

Copyright © 2012 by AAN Enterprises, Inc.

1. Park JH, Ko Y, Kim W-J, et al. Is asymptomatic hemorrhagic transformation really innocuous? Neurology 2012;78:421–426.
2. Kimura K, Iguchi Y, Shibazaki K, Aoki J, Terasawa Y. Hemorrhagic transformation of ischemic brain tissue after t-PA thrombolysis as detected by MRI may be asymptomatic, but impair neurological recovery. J Neurol Sci 2008;15:136–142.
3. Libman R, Kwiakowski T, Lyden P, et al. Asymptomatic hemorrhagic transformation of cerebral infarction does not worsen long-term outcome. J Stroke Cerebrovasc Dis 2005;14:50–54.
4. Hacke W, Donnan G, Fieschi C, et al. Association of outcome with early stroke treatment: pooled analysis of ATLANTIS, ECASS, and NINDS rt-PA stroke trials. Lancet 2004;363:768–774.
5. Peterson B, Harrell FE. Partial proportional odds models for ordinal response variables. J R Stat Soc Ser C Appl Stat 1990;39:205–217.
6. Williams, R. Generalized ordered logit/partial proportional odds models for ordinal dependent variables. Stata J 2006;6:58–82.

CORRECTION

Nemaline myopathy with stiffness and hypertonia associated with an *ACTA1* mutation

In the Clinical/Scientific Note "Nemaline myopathy with stiffness and hypertonia associated with an *ACTA1* mutation" by R.K. Jain et al. (*Neurology*® 2012;78:1100–1103), there are 2 errors on page 1100. In the right-hand column, paragraph 3 should read "(Lys326Asn in the mature protein)" and paragraph 7 should read ". . . increased sensitivity to Ca^{2+} (figure, F)." The authors regret the errors.

Author disclosures are available upon request (journal@neurology.org).

Copyright © by AAN Enterprises, Inc. Unauthorized reproduction of this article is prohibited.

Nemaline myopathy with stiffness and hypertonia associated with an *ACTA1* mutation
R.K. Jain, S. Jayawant, W. Squier, et al.
Neurology 2012;78;1100; Published online before print March 21, 2012;
DOI 10.1212/WNL.0b013e31824e8ebe

This information is current as of June 27, 2012

Updated Information & Services	including high resolution figures, can be found at: http://www.neurology.org/content/78/14/1100.full.html
References	This article cites 7 articles, 1 of which can be accessed free at: http://www.neurology.org/content/78/14/1100.full.html#ref-list-1
Subspecialty Collections	This article, along with others on similar topics, appears in the following collection(s): **All Genetics** http://www.neurology.org/cgi/collection/all_genetics **All Neuromuscular Disease** http://www.neurology.org/cgi/collection/all_neuromuscular_disease
Errata	http://www.neurology.org/content/78/21/1704.full.html
Permissions & Licensing	Information about reproducing this article in parts (figures, tables) or in its entirety can be found online at: http://www.neurology.org/misc/about.xhtml#permissions
Reprints	Information about ordering reprints can be found online: http://www.neurology.org/misc/addir.xhtml#reprintsus

AMERICAN ACADEMY OF NEUROLOGY®